NASA Conference Publication 2447
Part 1

NASA/DOD Control/Structures Interaction Technology 1986

Proceedings of a conference held in
Norfolk, Virginia
November 18-21, 1986

NASA

FIRST NASA/DOD CSI TECHNOLOGY CONFERENCE

ERRATA TO CONFERENCE PROCEEDINGS, NASA CP-2447, PART 1

INSERTS

PAGES 75,76 INSERT NEW PAGES FOR DELETED PAGES

PAGES 79,80 INSERT NEW PAGES FRO DELETED PAGES

PEN AND INK CORRECTIONS

PAGE 422, PARA 1, LINE 10 - SHOULD READ "DESIRABLE" VICE "DESIREABLE"

PAGE 424, FIGURE - MODE 3 SKETCH HEADING SHOULD READ "0.172 Hz" VICE "1.172 Hz"

PAGE 429, REFERENCE 2 - SHOULD READ "MODAL" VICE "MODEL"

NASA Conference Publication 2447
Part 1

NASA/DOD Control/Structures Interaction Technology 1986

Compiled by
Robert L. Wright
NASA Langley Research Center
Hampton, Virginia

Proceedings of a conference sponsored by NASA Langley Research Center, Hampton, Virginia, and Air Force Wright Aeronautical Laboratories, Wright-Patterson AFB, Ohio, and held in Norfolk, Virginia November 18-21, 1986

NASA
National Aeronautics and Space Administration

Scientific and Technical Information Branch

1986

PREFACE

The National Aeronautics and Space Administration (NASA) and the Department of Defense (DOD) are actively involved in the development of a validated technology data base in the areas of control/structures interaction, deployment dynamics and system performance for large flexible spacecraft. The generation of these technologies is essential to the efficient and confident development of this new class of spacecraft to meet stringent goals in safety, performance and cost. As a major element of this technology effort, the NASA Office of Aeronautics and Space Technology (OAST) has initiated the Control of Flexible Structures (COFS) Program which provides a major focus for the Research and Technology base activities in structural dynamics and controls and complements long range development programs at the Air Force Wright Aeronautical Laboratories (AFWAL). These activities provide a systematic approach to address technology voids through development and validation of analytical tools, extensive ground testing of representative structures, and in-space experiments for verification of analysis and ground test methods.

In order to promote timely dissemination of technical information acquired in these programs, the NASA Langley Research Center and the AFWAL will alternately sponsor an annual conference to report to industry, academia and government agencies on the current status of control/structures interaction technology. The First NASA/DOD CSI Technology Conference is the beginning of this series.

This publicatic is a compilation of the papers presented at the conference and is divided into two parts. Part I is to be distributed at the conference and Part II will be distributed after the conference.

This publication was expedited and enhanced through the efforts of the Research Information and Applications Division, Langley Research Center.

The use of trade names or names of manufacturers in this publication does not constitute an official endorsement of such products or manufacturers, either expressed or implied, by the National Aeronautics and Space Administration.

H. L. Bohon
General Chairman

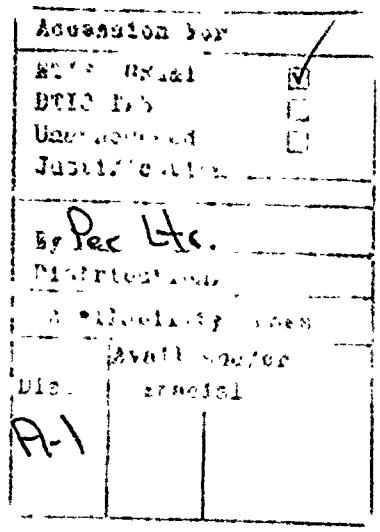

CONTENTS

CONTROL OF FLEXIBLE STRUCTURES (COFS)

SELECTED NASA RESEARCH IN CONTROL/STRUCTURES INTERACTIONS

ADVANCED COMPOSITES FOR LARGE NAVY SPACECRAFT

William E. Davis
Ametek, Inc.
Composite Materials and Applications Division
Anaheim, California

First NASA/DOD CSI Technology Conference
Norfolk, Virginia
November 18-21, 1986

CONTRACT SUMMARY

Future spacecraft will be an essential part of the US defense system and ensuring survivability is critical to the spacecraft design. Potential threats to the spacecraft include space-based laser, ground-based laser, and direct ascent nuclear and KEW (pellet) weapon systems. Many of these systems will be large in comparison to conventional spacecraft and the requirements for precision static and dynamic dimensional control are very severe. Payloads such as IR sensors, RF antennas, etc. must be pointed very accurately, which requires dimensionally stable support structures that also have inherent passive damping thus resulting in precise alignment under static, dynamic and thermal disturbances.

This paper is an overview of work conducted on contract for the Naval Sea Systems Command. The objective of this contract was to provide direction for the development of high modulus graphite reinforced metal matrix composites. These advanced materials can have a significant effect on the performance of a spacecraft before, during and after an evasive maneuver.

The information contained in this paper is based on a paper entitled "Spacecraft Survivability by Maneuvering-KEW Environment" (Reference 1) and the contract final report "Effects of Materials and Structures on Spacecraft Controls", N00024-83-C-5353 (Reference 2).

TITLE:	EFFECTS OF MATERIALS ON SPACECRAFT CONTROL AND MANEUVERABILITY
OBJECTIVE:	ASSESS THE IMPACT OF MMC ON SPACECRAFT MANEUVERING
CONTRACT MONITOR:	MARLIN KINNA
PERIOD OF CONTRACT:	SEPTEMBER 1983-MARCH 1985

Figure 1

SUMMARY OF PROGRAM TASKS

The work conducted on this program was organized into seven technical tasks; Figure 2 provides an overview of the program. Task 1 was development of a generic Navy spacecraft model. Finite element models of candidate structural designs were developed. In Task 2, the finite-element model(s) of the structure were used to conduct analytical assessments involving conventional materials, resin matrix composites and metal matrix composites. In Task 3 and 4, MMC material design, fabrication and evaluation was conducted. This consisted of generating material designs and developing a data base for a broad range of graphite reinforced MMC materials. All material was procured according to specifications which set material quality and material property standards. In Task 5, a set of evasive maneuvering requirements were derived and used in Task 6 to conduct analytical simulations. These analytical simulations used current SOA material properties and projected material properties to provide an indication of key payoffs for material development. In Task 7, a set of material development recommendations was generated.

CONTRACT OVERVIEW

- DEFINE GENERIC ITSS SPACECRAFT MODEL
- ANALYTICAL ASSESSMENT TO IDENTIFY KEY MATERIAL VARIABLES AND INITIAL PROPERTY GOALS
- DESIGN, PROCURE, TEST AND EVALUATE STATE-OF-THE-ART METAL MATRIX COMPOSITE MATERIALS
- DETERMINE THE EFFECT OF MATERIAL VARIABLES ON MANEUVERING SPACECRAFT PERFORMANCE
- RECOMMEND DEVELOPMENT PROGRAMS TO OPTIMIZE MANEUVERING SPACECRAFT DESIGN
- MAJOR PROGRAM ACHIEVEMENTS

Figure 2

GENERIC ITSS SPACECRAFT

ITSS was selected for developing a generic spacecraft model for analytical assessments. A finite-element model of a generic spacecraft and performance requirements that incorporate characteristics of the ITSS spacecraft concepts were defined. The ITSS will be a combination of IR and RF payloads assembled on one spacecraft. The RF system will be relatively large and flexible and the IR system will be comparatively rigid. The combined spacecraft was modeled as an RF antenna with slewing, pointing, and maneuvering requirements and the IR payload was assumed to be a rigid mass lumped at the spacecraft bus. Specific numerical performance requirements and distrubances for the spacecraft were defined in this task.

Figure 3 illustrates the generic spacecraft model. The primary components which impact its dynamic behavior are the antenna dish, the antenna feed, the feed boom, and the spacecraft bus. The rigid IR payload must meet stringent pointing requirements while mounted to these flexible components. The generic model was defined around the flexible part of the spacecraft, i.e., the RF antenna. Based on the results of previous space-based surveillance studies, an RF dish diameter (antenna aperture) of 30 meters and an operational wavelength of 3 cm were chosen. The IR payload is treated as a rigid mass and part of the spacecraft bus. A polar orbit with an altitude of 5600 nautical miles was also specified. The nominal generic spacecraft weighs approximately 4000 kg.

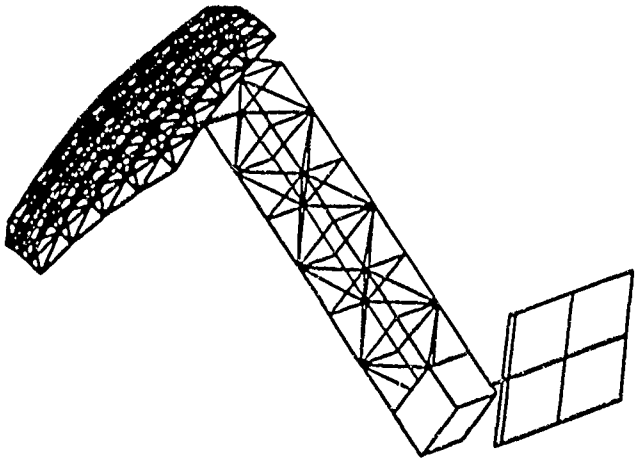

REQUIRED OPERATIONS

- EVASIVE MANEUVER — 150 NMI, 25 MINUTES
- SCANNING — 22°, 33 SEC
- STEP-STARE — 45°, 15 SEC

- 30 METER DISH DIAMETER
- 30 METER FEED MAST LENGTH
- ≅4000 KG MASS

Figure 3

MATERIAL EVALUATION

Material design and fabrication development tasks were conducted wherein a broad range of MMC material variables were used to develop specimen designs using graphite fibers in aluminum and magnesium matrices. The materials evaluated in this program are shown in Figure 4. Two sets of material designs were evaluated in this program. The initial set of materials were designed based on data developed in previous work. Material test data developed in Task 4, was used to design the second set of materials. Materials were procured in flat plate and tube form and specifications were imposed for all of the fabrication activities. Batch acceptance tests were performed on the precursor wire material prior to proceeding with fabrication processes. Diffusion bonding, pultrusion and Rapipress processes were used to fabricate the material designs evaluated in this program. A comprehensive fabrication quality assessment task was conducted where all parts were tested by ultrasonic inspection methods (C-scan) and photomicrographs were taken.

SUMMARY OF FABRICATED PANELS

Material	Foil	Layup	Size	Manufacturer
Round 1				
P100/6061	Al	$(0)_2$	8 in. × 8 in.	DWA
P55/6061	Al	$(0)_2$	8 in. × 8 in.	DWA
P55/6061	Al	$(0)_4$	8 in. × 8 in.	DWA
P55/6061	Al	$(\pm 16)_S$	8 in. × 8 in.	DWA
P100/AZ91C	Ti	$(0)_2$	8 in. × 8 in.	DWA
P100/AZ91C	Mg	$(0)_2$	8 in. × 8 in.	DWA
P55/AZ91C	Mg	$(0)_2$	8 in. × 8 in.	DWA
P55/6061	Al	$(0)_2$	16 in. × 6 in.	MCI
P55/6061	Al	$(0)_4$	16 in. × 6 in.	MCI
P100/6061	Al	$(0)_2$	16 in. × 6 in.	MCI
P100/6061	Al	$(0)_2$	16 in. × 6 in.	MCI
P55/6061	Al	$(\pm 16)_S$	16 in. × 6 in.	MCI
Round 2				
P120/6061	Al	$(0)_2$	8 in. × 8 in.	DWA
P120/AZ91C	Mg	$(0)_2$	8 in. × 8 in.	DWA
P120/AZ91C	Ti	$(0)_2$	8 in. × 8 in.	DWA

SUMMARY OF FABRICATED TUBES

Length	Material	Foil	Layup	Size (Dia. × Wall Thick.)	Manufacturer
42 in.	P100/Al	Al	$(0)_2$	1.071 in. × 0.048 in.	MCI
42 in.	P100/Mg	Mg	$(0)_2$	1.067 in. × 0.048 in.	MCI
42 in.	P120/Al	Al	$(0)_2$	1.068 in. × 0.046 in.	MCI
42 in.	P120/Mg	Mg	$(0)_2$	1.071 in. × 0.047 in.	MCI
18 in.	P100/Al	Ti	$(0)_2$	1.501 in. × 0.047 in.	DWA

Figure 4

SUMMARY OF MATERIAL
PROPERTY TEST DATA

A test matrix was designed to satisfy two objectives. The first objective was to obtain the necessary data for conducting analytical performance assessments using the generic spacecraft. These tests include longitudinal tensile modulus, shear modulus, coefficient of thermal expansion and material density. The second objective was to enhance the material design data base by obtaining relevant properties essential to conducting a complete structural design. These properties include longitudinal tensile, transverse tensile and shear properties. A summary of the longitudinal tensile testing is summarized in Figure 5.

P100 COMPOSITE MATERIAL PROPERTIES SUMMARY

MATERIAL PROPERTY	MEASURED PROPERTIES							
	P100/AZ91C Ti FOIL		P100/AZ91C Mg FOIL		P100/6061 Al FOIL		P100/6061 GROUND WIRE Al FOIL	
	CALC.	MEASURED	CALC.	MEASURED	CALC.	MEASURED	CALC.	MEASURED
LONGITUDINAL MODULUS (MSI)	49.4	53.8	47.2	52.2	49.6	47.5	50.4	48.6
LONGITUDINAL STRENGTH (KSI)	155.8	103.8	154.6	116.8	147.5	119.9	150.3	120.2
CTE (IN/IN-°F)	+0.207	TBD	+0.254	TBD	+0.624	TBD	+0.575	TBD
V_F%	—	43.9	—	43.6	—	44.0	—	44.9
DENSITY (PCI)	0.0807	0 0783	0.0706	0.0719	0.0892	0.0901	0.0890	0.0889

Figure 5

ANTENNA PAYOFFS FOR
SPACECRAFT MANEUVERING

Development of high specific modulus and high inherent damping materials can have a significant effect on the performance of a spacecraft before, during and after an evasive maneuver. The major effects are illustrated in Figure 6. High specific modulus reduces the peak amplitude dynamic distortions and also minimizes total static deformation. High damping properties result in faster settling time for structural vibrations. In both cases, the time required to reach operational capability after a maneuvering disturbance is imposed will be minimized by increasing these material parameters. As part of this contract, the effects of high specific modulus and damping loss factor on maneuvering capability were assessed.

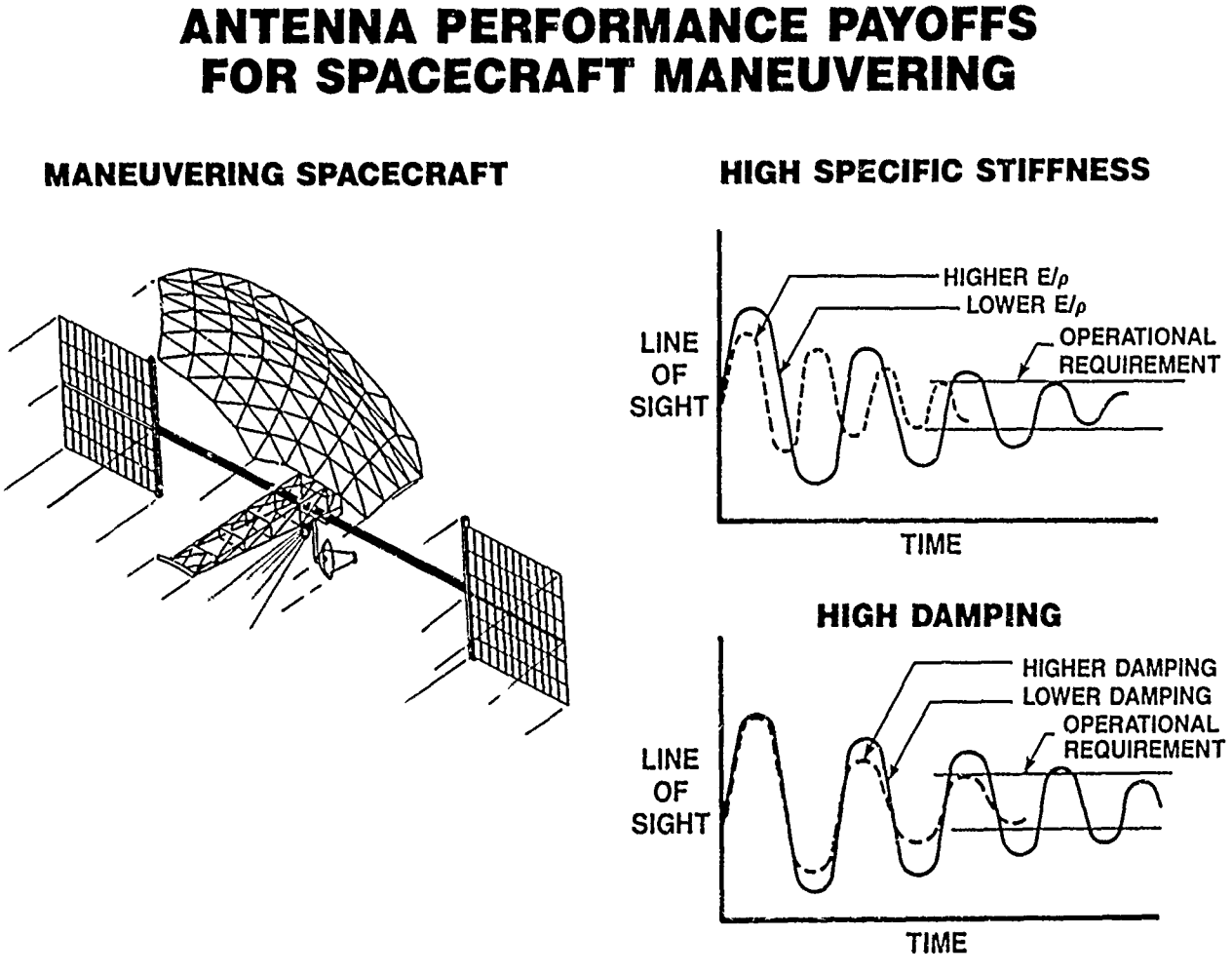

Figure 6

SPACECRAFT STRUCTURAL MASS VS. FIBER MODULUS
(EQUIVALENT PERFORMANCE DESIGNS)

Maneuvering simulations were conducted using the generic spacecraft design where a large combination of material designs were evaluated. These simulations are conducted by imposing disturbances on the finite-element model of the generic spacecraft and then analyzing the resulting response.

Figure 7 shows the effects of improving the fiber modulus on reducing the structural mass of the vehicle. P100 Gr/Al with 50% fiber volume (zero CTE) is approximately the state of the art in graphite reinforced metal matrix composites. Developing Gr/Mg capability and increasing the fiber modulus to 100 MSI can significantly improve the structural mass characteristics of the vehicle. This results in reduction in launch weight, added payload capability, reduced mass on-orbit, etc.

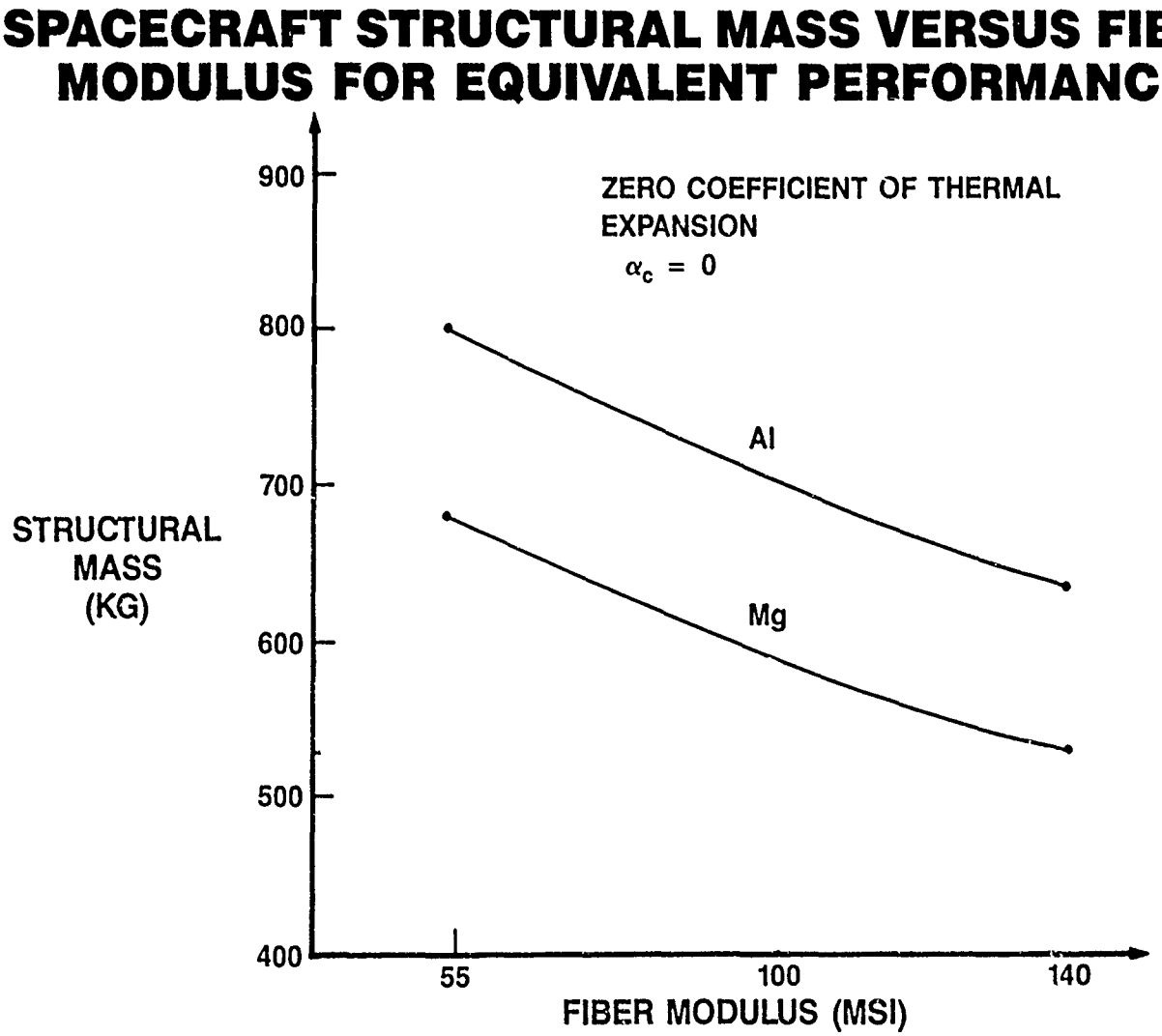

Figure 7

MATERIAL EFFECTS ON SPACECRAFT SCAN TORQUE

Reductions in the structural mass of large area structures results in lower mass moments of inertia. This, in turn, reduces the scan torque requirements for the vehicle. If P55 Gr/Al material were used in this design the scan torque requirements are 6000 N-M which is pushing the state-of-the-art capability in CMG torque capacity. P100 Gr/Mg would require 4700 N-M torque which is well within the capability of todays state-of-the-art actuator torque capacity. This would result in less risk, lower power requirements, higher reliability and reduced ACS weight.

SPACECRAFT SCAN TORQUE versus FIBER MODULUS FOR EQUIVALENT PERFORMANCE

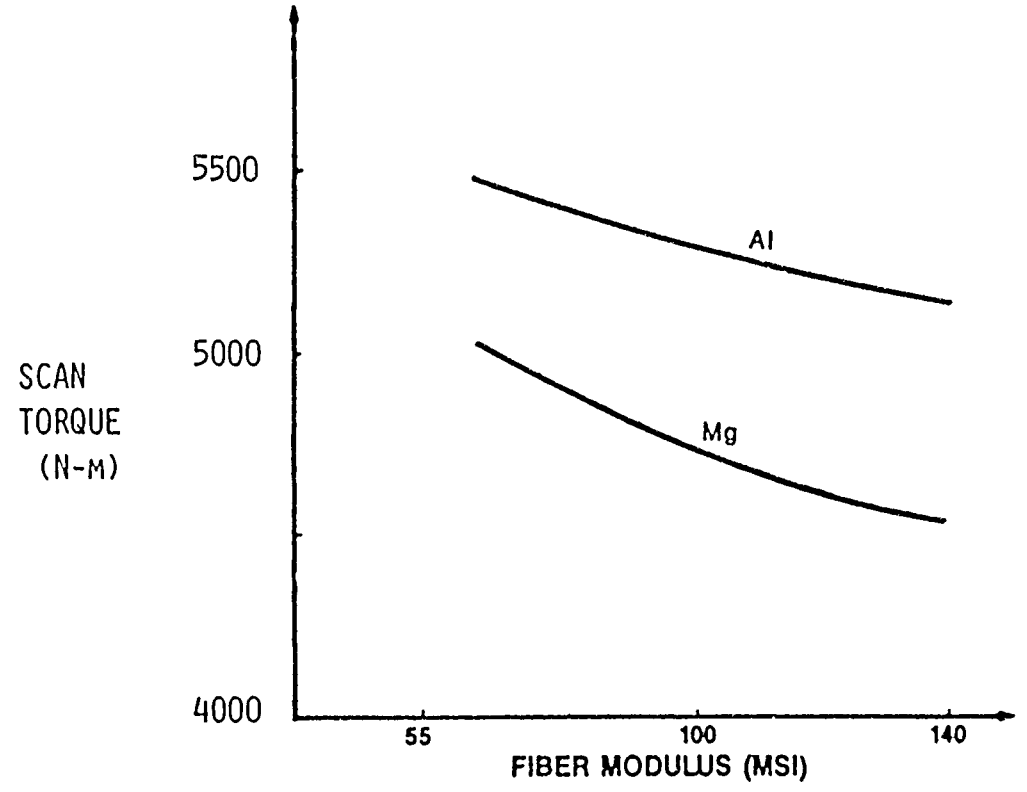

Figure 8

SUMMARY

Unidirectionally reinforced metal matrix composites are ideal for application to large truss structures in space. They are attractive for use when thermal distortions are critical, and in addition, their extremely high stiffness to weight ratio suits them for use in dynamic environments. Structural designs based on the use of very high modulus MMC will be lightweight and may enable operation during an evasive maneuver without the need for structural control systems. The use of metal matrix composites can reduce structural mass and inertia, requiring smaller maneuvering thrusts and scanning torques, and resulting in additional fuel and actuator weight savings.

REFERENCES

1. Davis, William E.; Levin, Richard N.; and Lesieutre, George A.: Spacecraft Survivability by Maneuvering - KEW Environment, Sixth Metal Matrix Composites Technology Conference (Monterey, CA.) May, 1985

2. Effects of Materials and Structures on Spacecraft Controls. HR Textron SED CR 850001 (NSSC Contract No. N00024-83-C-5353), Apr. 1985.

N-ROSS: THE DYNAMICS AND CONTROL ISSUES

Robert E. Lindberg
Naval Research Laboratory
Washington, DC

First NASA/DOD CSI Technology Conference
Norfolk, Virginia
November 18-21, 1986

MISSION AND APPROACH

The Navy Remote Ocean Sensing System (N-ROSS) satellite will be launched in 1990 to provide the Navy with the operational capability to measure sea surface parameters on a worldwide year-round basis in all weather conditions. The satellite will carry four primary instruments, two active and two passive, in a low-earth sun-synchronous orbit. The radar altimeter, similar to the instrument currently flying on GEOSAT, will measure absolute altitude above the geoid and will contribute to the determination of wave height. The scatterometer, an evolutionary design derivative of the SEASAT instrument, will be capable of both wind speed and wind direction measurement. The microwave imager (or SSM/I) and the Low Frequency Microwave Radiometer are passive scanning instruments, the first operating at 19.3, 22.2, 37.0 and 85.5 GHz, and the second at 5.2 and 10.4 GHz. The SSM/I, currently under development for the DMSP program, will measure water vapor and map sea ice edges. The LFMR is a new instrument design that will measure sea surface temperature to better than $1^{o}C$, to contribute to the mapping of currents, fronts and eddies in the ocean surface structure.

THE N-ROSS SATELLITE MISSION:

MEASURE SEA SURFACE PARAMETERS OVER 95% OR MORE OF THE WORLD'S OCEANS UNDER ALL WEATHER CONDITIONS

THE APPROACH:

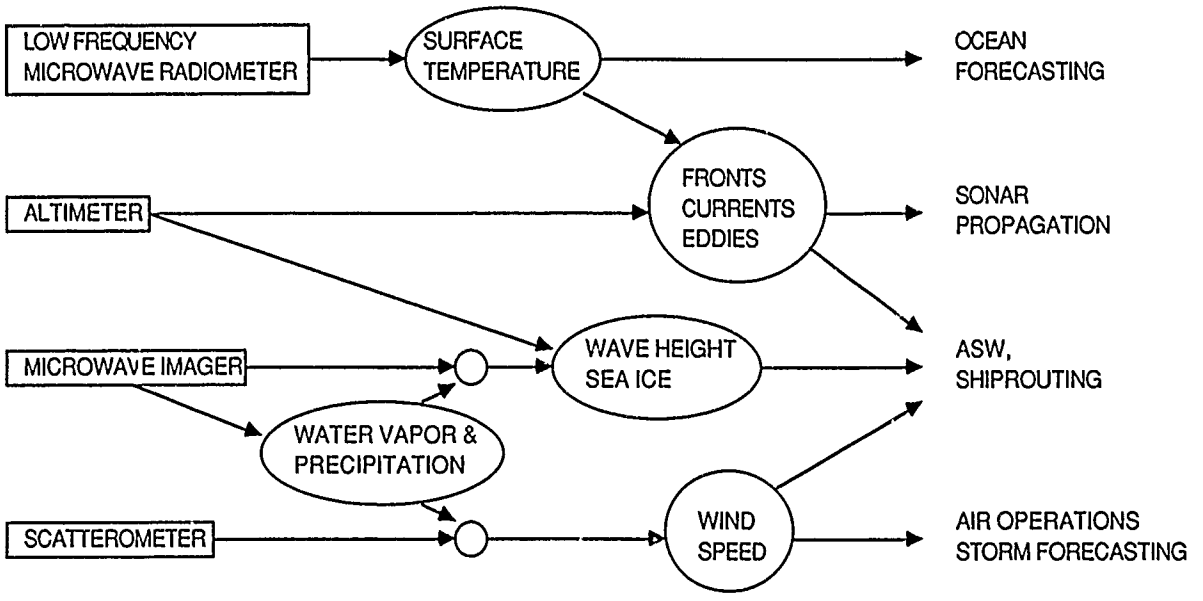

Figure 1

BASELINE N-ROSS CONFIGURATION

To evaluate the feasibility of the N-ROSS mission, a baseline vehicle design was developed during 1984 and 1985 as a derivative of the DMSP satellite design. An end view of this design, shown in Fig. 2, includes a fixed solar array attached to the far end, the SSM/I mounted on the top of the main structure, the altimeter (and a Doppler beacon antenna) on the bottom or earth-facing surface, and the scatterometer antennas to the right of the main structure. Clearly the most mechanically complex instrument is the LFMR, incorporating a nearly 22 ft. deployable truss structure (DTS) antenna, two deployed support booms and a radiometer electronics package all spinning at 15.8 rpm. The spin drive motor is mounted at the outboard end of an 8 ft. deployed spacecraft boom, required to provide non-interfering fields-of-view for all four sensors on the three-axis-stabilized vehicle.

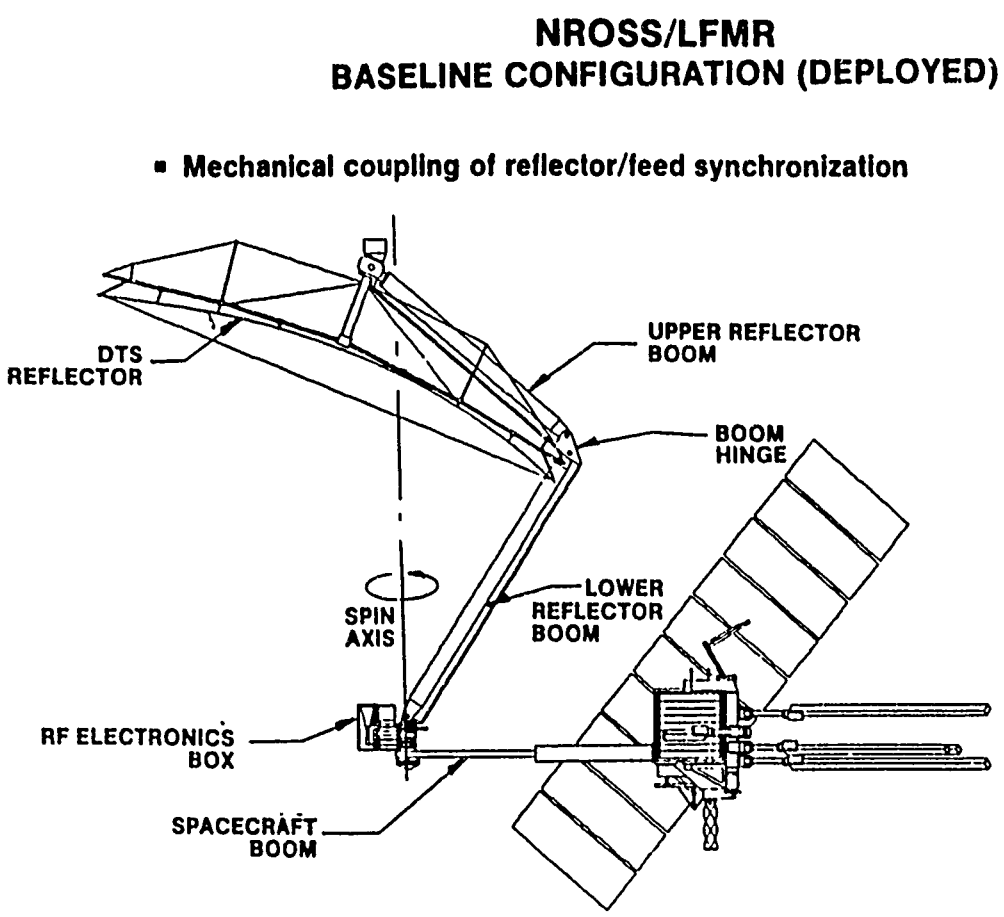

Figure 2

DYNAMICS AND CONTROL CONCERNS

The flexibility of the LFMR and the other appendage structures, together with the active spin drive system and the 0.05 deg pointing knowledge requirement for the LFMR sensor boresight, combine to immediately identify control-structure interaction as a technology issue in the N-ROSS baseline design. Figure 3 highlights some fundamental concerns involving the dynamics and control performance of flexible satellites. These issues are common to most satellite concepts incorporating large lightweight flexible components, even those which do not spin, and they were considered significant in the baseline N-ROSS design.

FUNDAMENTAL CONCERNS WITH THE DYNAMICS AND CONTROL OF FLEXIBLE SPACECRAFT

MOTION OF THE FLEXIBLE STRUCTURES CAN DESTABILIZE ATTITUDE CONTROL SYSTEM

ATTITUDE CONTROL SYSTEM CAN EXCITE STRUCTURAL RESONANCES

EXTERNAL DISTURBANCES CAN EXCITE STRUCTURAL RESONANCES

STRUCTURAL FLEXIBILITY ALONG WITH INHERENT ERROR SOURCES CAN DEGRADE POINTING PERFORMANCE BEYOND THE SPECIFIED VALUE

Figure 3

ADDITIONAL N-ROSS ISSUES

The design and concept of operations for the baseline N-ROSS design raises several specific issues, related to control-structure interaction, but not typically addressed in the development of technologies for the control of large space structures. While the LFMR is designed to operate at a constant spin rate, the initial spin up (and contingency despin) of the sensor raises concern that it might act as a frequency sweep disturbance input to the spacecraft, with the potential to excite structural resonances up to 0.26 Hz (15.8 rpm). Additionally, the LFMR antenna and support booms are expected to deform measurably under centrifugal forces when spinning (which is taken into account in the design, so that the deformed configuration has the desired geometry). The deformation will result in a change in mass properties, thereby inducing both a static and a dynamic imbalance. This then is expected to lead to a requirement for an on-orbit balance mechanism. Finally, the momentum of the LFMR and the SSM/I are each proposed to be compensated by a separate momentum wheel controlled independent of the reaction-wheel-based attitude control system. These separate control loops, all coupled through the vehicle rigid body dynamics, can lead to a system which cannot be guaranteed to be stable for all inputs.

ADDITIONAL CONCERNS SPECIFIC TO N-ROSS

SPIN-UP OPERATIONS MAY SWEEP STRUCTURAL RESONANCES

LFMR MAY REQUIRE ON-ORBIT BALANCE TO COMPENSATE FOR STATIC DEFLECTIONS UNDER SPIN

MOMENTUM COMPENSATION REQUIRES SEPARATE CONTROL LOOP

Figure 4

DYNAMICS AND CONTROL CONTRIBUTORS

Many aspects of the N-ROSS baseline design have the potential to contribute to a control-structure interaction problem for this vehicle. Figure 5 summarizes the most significant of these. They include interacting flexible structures and rotating instruments and devices on the vehicle, independently designed and implemented control systems that are coupled through either vehicle dynamics or structural dynamics, and external disturbances that have the potential to degrade pointing performance and even destabilize the attitude of the satellite.

CONTRIBUTING SOURCES

FLEXIBLE STRUCTURES

- LFMR Reflector and Booms
- LFMR Deployment Boom
- NSCAT Antennas
- Solar Array

ROTATING COMPONENTS

- LFMR
- SSM/I
- Momentum Compensation Assemblies
- Reaction Wheels

CONTROL SYSTEMS

- Attitude Control
- LFMR Drive System
- SSM/I Drive System
- MCA Drives

OTHER DYNAMICS

- Thruster firing
- Deployment sequences
- External torques

Figure 5

STATIC AND DYNAMIC BALANCE

The static and dynamic balance of a deformable spinning instrument such as the LFMR warrants special examination. In balancing a rigid spinning device (such as the SSM/I), the static and dynamic balance can be performed sequentially. In a nonspinning state, the center of mass can be adjusted to lie on the spin axis. The dynamic balance can then be achieved by spinning the sensor, and symmetrically adjusting ballast mass to eliminate (or reduce) the cross-products of inertia with respect to the spin axis. For the SSM/I, this will be accomplished in ground test prior to integration with the satellite.

For an asymmetric flexible structure such as the LFMR, the center of mass and inertias of the structure will change with spin rate, and the alignment of both the center of mass and the principal inertia axis can only be accomplished after the instrument is spinning. These same mass properties also vary between a one-g and a zero-g environment, and between atmosphere and vacuum. This leads to a requirement for either extensive testing coupled with simulation to extrapolate to on-orbit conditions, or an active method of achieving instrument balance once the vehicle is in orbit.

FOR A RIGID STRUCTURE

STATIC - PLACE C.G. ON THE SPIN AXIS

DYNAMIC - ALIGN THE PRINCIPAL INERTIA AXIS WITH SPIN AXIS

FOR A FLEXIBLE STRUCTURE

C.G. AND INERTIA AXES WILL MOVE AS INSTRUMENT IS SPUN UP

BOTH "STATIC" AND "DYNAMIC" BALANCE MUST BE ACHIEVED AT FULL SPIN RATE

Figure 6

DYNAMIC STABILITY STUDY

In response to the recognition that control structure interaction was a technology driver for the N-ROSS baseline satellite design, the Naval Research Laboratory was commissioned in September 1985 to lead a six month effort to evaluate the N-ROSS/LFMR configuration. A Dynamic Stability Study would focus on the baseline configuration, assuming a design frozen to that detailed in the April 1985 conceptual design review. The study objectives are recounted in Fig. 7.

OBJECTIVES:

DEVELOP INTEGRATED FLEXIBLE BODY STRUCTURAL DYNAMICS AND CONTROL SIMULATION OF THE ON-ORBIT N-ROSS CONFIGURATION

DETERMINE ATTITUDE STABILITY IN SPIN-UP AND STEADY-STATE OPERATION OF THE LFMR

ASSESS THE CONTRIBUTION OF STRUCTURE AND CONTROL INTERACTIONS TO LFMR BORESIGHT POINTING

EXAMINE OFF-NOMINAL CONDITIONS TO DETERMINE CONTROL MARGINS AND PARAMETER SENSITIVITIES INHERENT IN THE BASELINE DESIGN

Figure 7

DYNAMIC STABILITY STUDY PARTICIPANTS

The original organization of the study called for two independent teams of investigators, using software tools and simulation techniques of their own choosing but considering a common design database, to each assemble an integrated simulation capable of addressing the four study objectives. The original teaming arrangements paired RCA with Aerospace Corp. and Harris with Cambridge Research. During the course of the study the government announced its intention to competitively procure the N-ROSS satellite; at that point Harris and RCA chose to voluntarily cease further participation in the study. Using control system and structural models previously developed by these two participants, the two remaining team members continued to develop the integrated simulations. The MULTIFLEX code was developed internally at Aerospace for this purpose, while Cambridge Research employed the DISCOS code originally developed at Martin Marietta for NASA Goddard Space Flight Center.

RCA ASTROELECTRONICS

- Provided vehicle structural models
- Provided attitude control system model

HARRIS GASD

- Provided LFMR structural model
- Provided drive motor and MCA control models

AEROSPACE CORP.

- Developed integrated simulation using MULTIFLEX

CAMBRIDGE RESEARCH

- Developed integrated simulation using DISCOS

Figure 8

COMMON ASSUMPTIONS AND GROUND RULES

The two remaining study participants continued their work independently, with the Naval Research Laboratory maintaining a common and consistent set of model data to be used by both parties. NRL also provided resolution of modeling issues raised by the participants and defined the scope and limitations of the simulations and analyses to be performed.

Figure 9 lists the principal modeling assumptions. The number of structural modes included for each of the flexible components, together with the total number of states in the simulation, are listed to the right. These are taken from the Aerospace simulation; Cambridge Research employed two models - the first with 63 states modeled only the LFMR as flexible, the second included all flexible appendages and contained 109 states.

	(modes included)
Rigid spacecraft bus	
Detailed attitude determination and control subsystem model - reaction wheel control loops, sensor dynamics, etc	
Flexible scatterometer antenna model	6 modes
Flexible LFMR support boom models	2 modes
Flexible LFMR antenna model	5 modes
LFMR momentum compensation assembly model	
Fixed flexible solar array model	5 modes
Fixed rigid SSM/I model	
Orbital pitch rate included in dynamics	
	51 vehicle states
	15 control states
	66 total states

Figure 9

FREQUENCY CHARACTERISTICS

The frequency characteristics of the April 1985 baseline design are summarized in Fig. 10. The most significant concerns, and those which received careful examination during the course of the study, were the coupling of the LFMR spin frequency and the lower solar array modes with the attitude control loop, specifically the digital filter. Since the spin rate is well below the vehicle rate determination sampling frequency, it was anticipated as well that an imbalance of the LFMR would be observable as an attitude disturbance by the attitude determination software.

CONTROL/STRUCTURES FREQUENCY CHARACTERISTICS

ACS BANDWIDTHS

GYRO	F < 2.244 HZ
DIGITAL FILTER	F < 0.5 HZ
RATE DETERMINATION SOFTWARE	F < 5 HZ
REACTION WHEEL	F > 0.000265 HZ

SYSTEM MODE FREQUENCIES

LFMR SPIN RATE	0.26 HZ
SOLAR ARRAY MODE FREQS.	0.397, 0.576, 0.723, 1.08, 1.37
LFMR MODE FREQS.	1.67, 1.89, 2.72, 5.03, 6.05
SCATTEROMETER MODE FREQS.	4.98, 5.08, 36.5, 43.9, 75.4
SUPPORT BOOM MODE FREQS.	14.1, 15.1

Figure 10

ISSUES CONSIDERED

The development of extensive integrated control-structure simulations provided the opportunity to examine a wide range of issues of concern in the baseline design. The list of issues examined, summarized in Fig. 11, attests to the capacity of such simulations to go far beyond the relatively straightforward task of demonstrating stability and determining overall steady-state structure and control performance. Such simulations can be used effectively to refine the design for a particular concept. Results of the N-ROSS simulations led directly to recommendations for revised LFMR imbalance specifications and improved values for attitude control subsystem loop gains.

INDIVIDUAL ISSUES EXAMINED USING INTEGRATED SIMULATIONS

STEADY - STATE VEHICLE AND SENSOR POINTING PERFORMANCE

EFFECT OF STATIC AND DYNAMIC IMBALANCE ON ATTITUDE STABILITY

EFFECT OF SPIN RATE ON STATIC AND DYNAMIC IMBALANCE

SENSITIVITY OF BALANCE TO BALANCE WEIGHT MOVEMENT

LFMR, SCATTEROMETER AND SOLAR ARRAY DEFORMATION

MOMENTUM MISMATCH EFFECTS

SPIN AXIS MISALIGNMENT EFFECTS

THRUSTER DISTURBANCE EFFECTS

SPIN-UP DYNAMIC PERFORMANCE

Figure 11

CONCLUSIONS AND OPEN ISSUES

As a result of these efforts, the N-ROSS Dynamic Stability Study team concluded by consensus that the frozen April 1985 design was viable and contained no "show stoppers", although it was also clear from the study results that the configuration required further optimization. While the frozen N-ROSS configuration used has since been superceded, and the vehicle is now under competitive procurement, several other results remain from the study that will have lasting value to the N-ROSS program. The importance of constructing an integrated simulation, to serve as a design and verification aid, has been clearly established. The two team approach to the study afforded the Navy a higher degree of confidence in the results than could have been accomplished by a single simulation, and the approach led to results that highlighted subtleties in the model and simulation development that surely would have been overlooked without the benefit of an independent companion simulation with which to compare.

CONCLUSIONS

N-ROSS APRIL 1985 BASELINE DESIGN EXHIBITS NO SHOW-STOPPERS WITH RESPECT TO DYNAMIC STABILITY OR CONTROL STRUCTURE INTERACTION

ALL ISSUES UNCOVERED DURING THE STUDY CAN BE RESOLVED THROUGH APPLICATION OF GOOD ENGINEERING DESIGN PRACTICES

OPEN ISSUES

DEPLOYMENT DYNAMICS AND STABILITY

DEPLOYMENT MECHANISM DESIGN AND JOINT STIFFNESS

THERMALLY INDUCED EXCITATIONS

SPIN-UP / SPIN-DOWN SCENARIOS INCLUDING TORQUE SHAPING

ON - ORBIT BALANCE MECHANISM DESIGN

BALANCE ALGORITHM DEVELOPMENT

Figure 12

ACKNOWLEDGEMENTS

Some of the material presented here is excerpted from the final reports of the studies conducted by Aerospace Corp. and Cambridge Research Division of Photon Research Associates. The authors of those reports are: at Aerospace - P. Mak, M. Tong, A. Jenkin and A. Compito, and at Cambridge Research - J. Turner, H. Chun, and K. Soosaar. S. Fisher of NRL maintained the database models for the study. F. Diederich commissioned the study and provided general guidance.

SPACECRAFT DYNAMICS AND CONTROL PROGRAM AT AFRPL

A. Das
L. K. S. Slimak
W. T. Schlaegel

Interdisciplinary Space Technology Branch
Air Force Rocket Propulsion Laboratory
Edwards AFB, California

First NASA/DOD CSI Technology Conference
November 18-21, 1986

INTRODUCTION

A number of future DOD and NASA spacecraft such as the space based radar will be not only an order of magnitude larger in dimension than the current spacecraft, but will exhibit extreme structural flexibility with very low structural vibration frequencies. Another class of spacecraft (such as the space defense platforms) will combine large physical size with extremely precise pointing requirement. Such problems require a total departure from the traditional methods of modeling and control system design of spacecraft where structural flexibility is treated as a secondary effect. With these problems in mind, the Air Force Rocket Propulsion Laboratory (AFRPL) initiated research to develop dynamics and control technology so as to enable the future large space structures (LSS).

AFRPL's effort in this area can be subdivided into the following three overlapping areas: (a) Ground Experiments, (b) Spacecraft Modeling and Control, and (c) Sensors and Actuators. This paper summarizes both the in-house and contractual efforts of the AFRPL in LSS. However, only Air Force funded programs are discussed, ongoing Strategic Defense Initiative Office funded efforts are not covered in this paper.

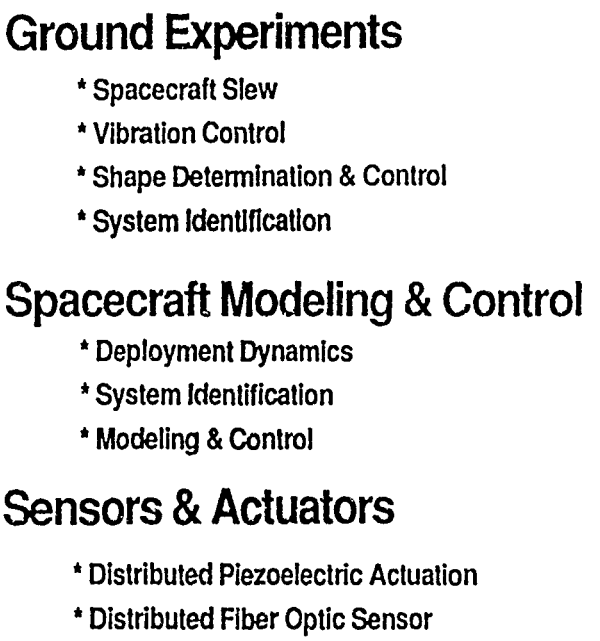

Figure 1.

SLEWING AND VIBRATION SUPPRESSION FOR FLEXIBLE STRUCTURES

A number of future DOD and NASA space systems will require rapid slewing (retargeting) of the spacecraft. The large moment of inertia of such spacecraft coupled with rapid retargeting requirement results in slew torque requirement of 10^5 - 10^6 Nm. Currently only ON-OFF reaction control system thrusters can provide the large torque required, however, ON-OFF thrusters by their very nature have the tendency of significantly vibrating the structure. The objective of this project was to develop control laws using thrusters for spacecraft slew which minimize structural vibration and demonstrate the theory on a ground experiment.

The experimental set-up consists of a rigid hub on which four flexible appendages are mounted. The hub is mounted on an air bearing table, thus allowing it to rotate freely about the vertical axis. ½lb control thrusters are mounted in pairs on the ends of two arms. Sensors consist of a hub angle resolver and 4 accelerometers, one on each arm (fig. 2).

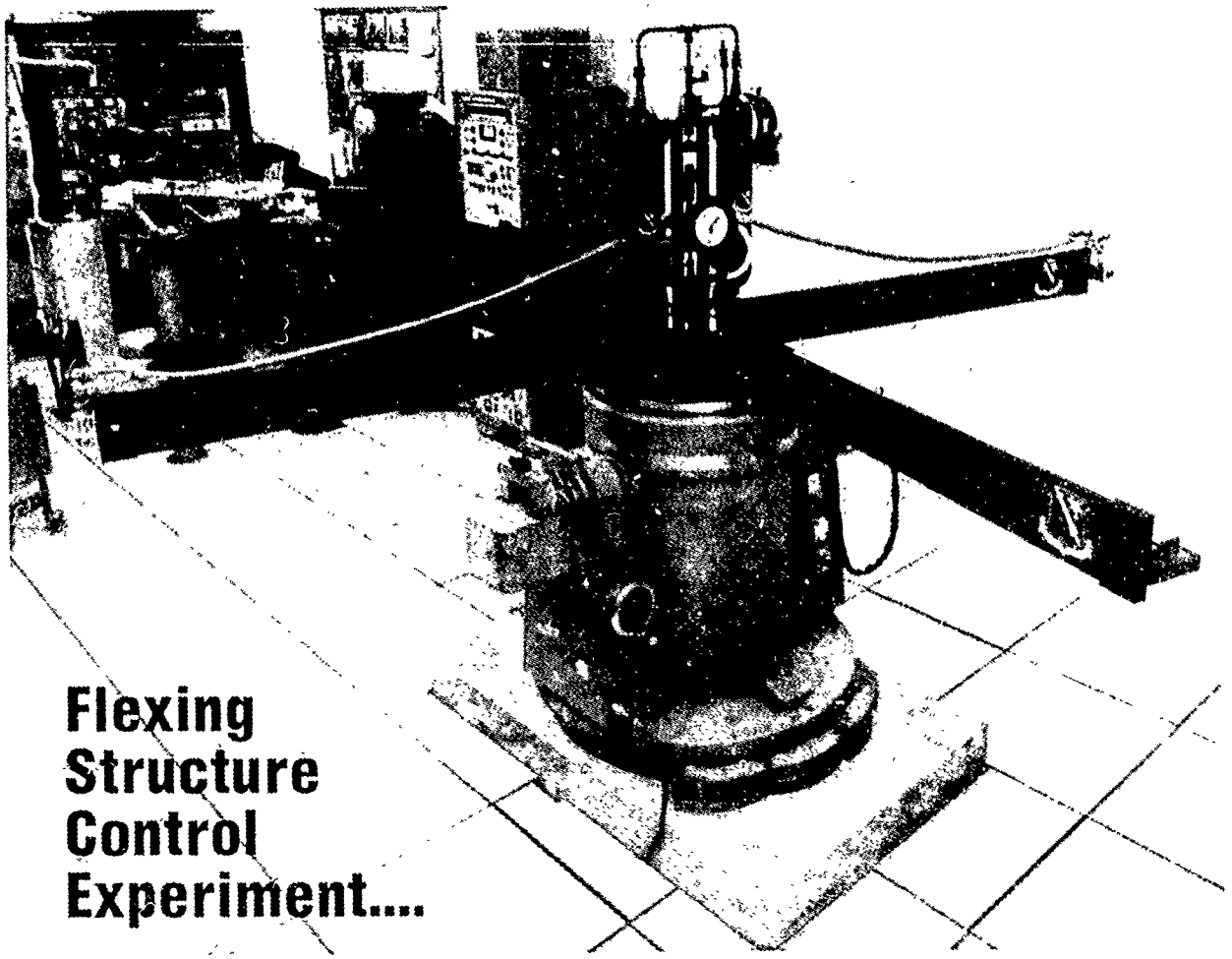

Figure 2.

SLEWING AND VIBRATION SUPPRESSION USING ON-OFF THRUSTERS

In the initial set of experiments, the thrusters were used to perform 15-degree slew maneuvers. A computer simulation program was developed to predict the performance of the control system. Fig. 3 shows the performance of the controller for one of the tests (ref. 1). The solid lines correspond to the simulation results whereas the dots are the experimental results. The figure gives the response of the first three modes (Y1 - hub rotation in degrees; Y2, Y3 - amplitude of first and second vibration modes in milli g, respectively).

The experiment demonstrated that ON-OFF thrusters can be used for rapid slew of flexible space structures while minimizing structural vibration. However, the exclusive use of thrusters limits the performance of the control system in the terminal phase of the slew maneuver. This is because of the minimum impulse bit of the thruster system, thus any attempt to dampen structural vibrations below a particular energy level throws the control system into limit cycles. One way of overcoming this problem is to include small linear actuators in the control system. This was confirmed by computer simulations.

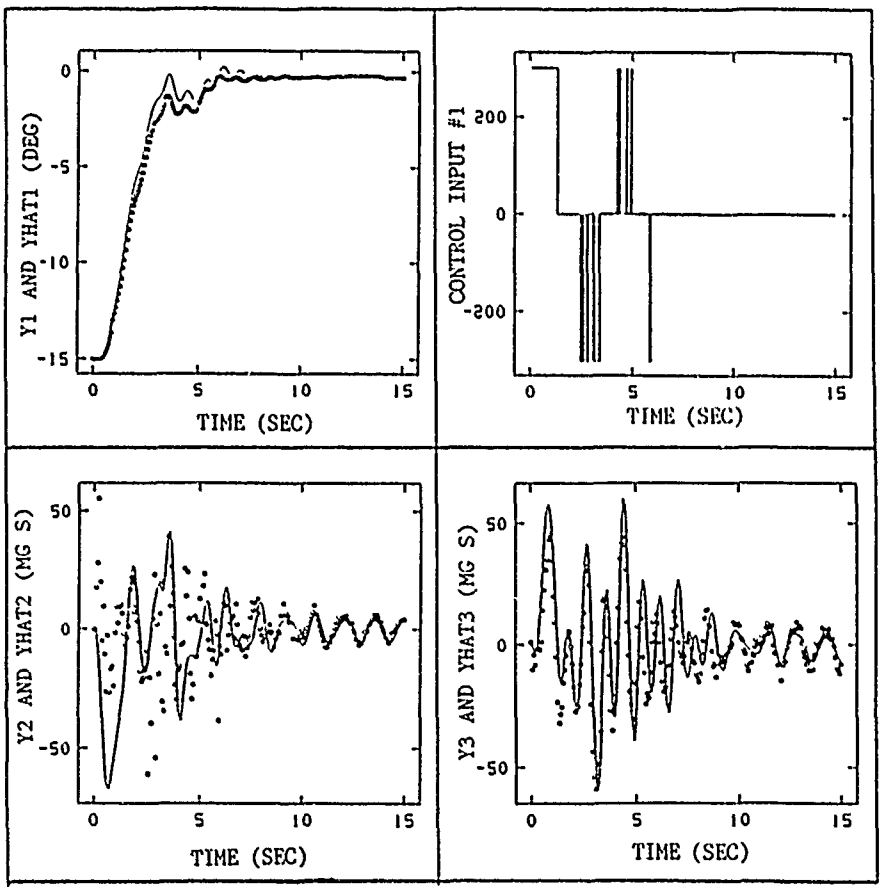

TEST #141

- 15° Slew, Rapid Maneuver
- R = 9.69 X 10^{-8}
- Undershoot Caused by :
  - Damping of Rigid Body Mode by Colomb Friction
  - 2nd Flexible Mode's Substantial Hub Rotation

Figure 3.

SLEWING AND VIBRATION SUPPRESSION FOR FLEXIBLE STRUCTURES

One of the conclusions of the earlier study was that vibration control of the flexible spacecraft structure during slew can be significantly improved when linear actuation devices are used in combination with thrusters. In the current effort both lumped and distributed linear actuators will be used. Control laws are currently being developed which use, along with ON-OFF thrusters, the hub motor, four bi-directional proof mass actuators (one on the tip of each flexible arm) and piezoelectric film as a distributed vibration suppression actuator on all four arms.

Flexing Structure Slew Control

* Generalized Slew Control
* Verified Controller Design Methods Using the AFRPL/CSDL Experimental Structure
* Suggested Using Linear Actuators Combined with On-Off Thrusters

Linear Torquer Slew Control

* Develop Theory for Combining Linear Actuation Devices Such as Proof-Mass Actuators and CMG's With On-Off Thrusters
* Demonstrate Hybrid Controller Theory Through Analysis and Simulation
* Validate Controller Theory Using AFRPL/CSDL Experimental Structure

Piezoelectric Distributed Actuator

* Develop Theory for Employing a Piezoelectric Film as a Vibration Controller
* Combine Piezoelectric Film for Vibration Control with On-Off Thrusters, Proof-Mass Actuators and CMG's for Slew Control
* Validate Theory on AFRPL/CSDL Experimental Structure

Figure 4.

ADVANCED DISTRIBUTED PIEZOELECTRIC ACTUATOR

One of the most exciting concepts for structural vibration control is the use of a piezoelectric film as a distributed actuator. The concept consists of a thin ($\sim 3 \times 10^{-2}$mm in thickness) polyvinylidene floride film polarized in one direction. The film elongates or contracts in the polarized direction depending on the magnitude and polarity of the voltage applied across its nickel plated faces (fig. 5). The strain occurs over the entire length of the film, thus making it a truely distributed actuator. This actuator provides the possibility of controlling all the modes of the system, thus avoiding the problem of spillover of the uncontrolled modes (ref. 2).

Preliminary testing of the actuator concept were done on a 15cm long cantilevered steel beam. Fig. 5 compares the performance of two active control logics with the open loop decay of the vibrations. The constant-amplitude controller (a nonlinear controller) provided double the damping of the uncontrolled system for large vibrations. For small vibrations the controller performed extremely well, increasing the damping by a factor of 40 over the uncontrolled system for small vibrations.

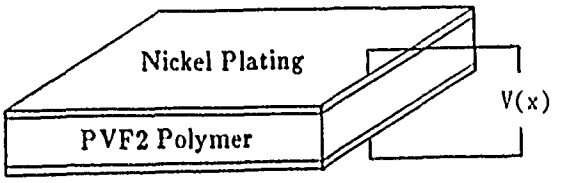

PVF_2 Properties

Thickness	28×10^{-3} mm
Modulus, E	2.0×10^{9} Nm^2
Density	1800 kgm^{-3}

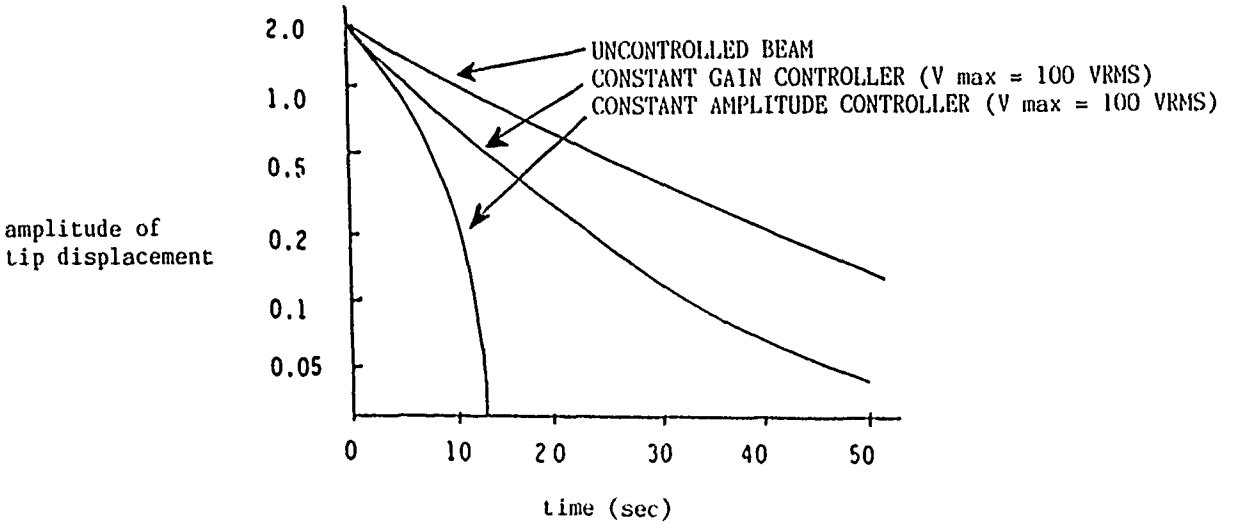

Figure 5.

Another concept which has the potential of high payoff is the possibility of using a fiber optic waveguide as a lightweight distributed sensor. A short and intense pulse of laser light is injected into one end of the fiber. The forward traveling pulse is continuously backscattered towards the source due to Rayleigh scattering. Observation of the Rayleigh backscattered energy is made by placing a beam splitter between the fiber and the source and directing the returned energy at a high speed detector. The fiber is bonded to the structure whose deformation is to be monitored. The fiber is made to pass through a small transducer (see fig. 6) at the locations in the structure where the bending is to be determined. The transducer pinches the fiber thus reducing the return signal from that point. The reduction in the return signal is proportional to the structural bending. Currently the AFRPL is funding a proof of concept demonstration of the lightweight distributed sensor.

- **Demonstrate Feasibility of Distributed Fiber Optic Deflection Sensor**

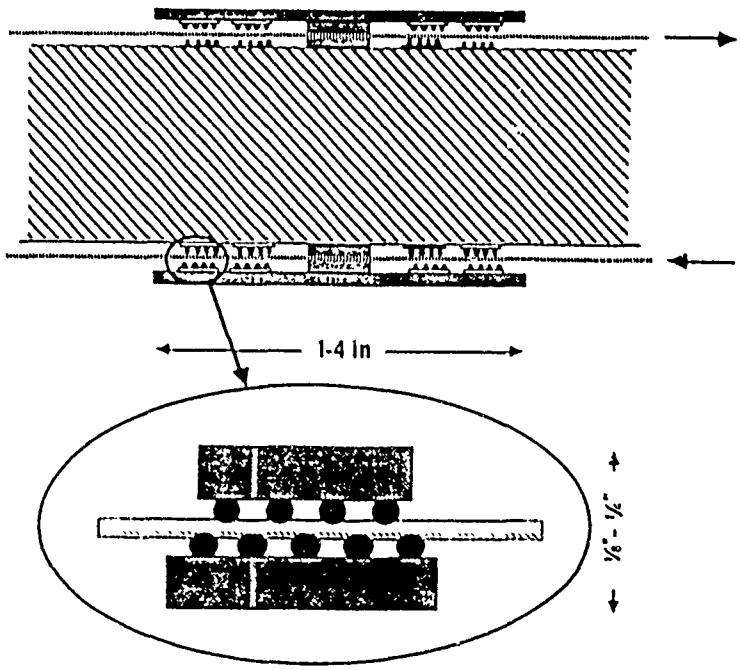

- **Lightweight Distributed Sensor**

Figure 6.

3-DIMENSIONAL SHAPE CONTROL EXPERIMENT

The objective of this effort is the demonstration of selected shape determination and control technology for future flexible structures using a physical structure in a laboratory environment.

The test article consists of an umbrella-like structure with 10ft long ribs and a 12ft long boom. The neighboring ribs are connected to each other through a pair of tension wires so as to provide coupling. The article is rigidly supported at the center to the backup structure, also each rib is levitated to offset the effects of gravity. The levitation system allows the ribs to freely flex in a vertical plane. An excitor in the feed will be used to introduce noise in the structure. Multiple sensors and actuators such as the SHAPES sensor under development at the Jet Propulsion Laboratory, rib control force actuator, 2-directional displacement sensor on the feed, etc., will be attached to the structure. The experiments to be conducted under this effort include (a) static shape determination, (b) dynamic model identification, (c) transient regulation by distributed control, and (d) parameter error and model truncation compensation using adaptive control techniques.

- **Demonstrate Sensing and Control of a Lightweight Antenna Structure**
- **Establish Standard Test Bed for 3D Structure Control**

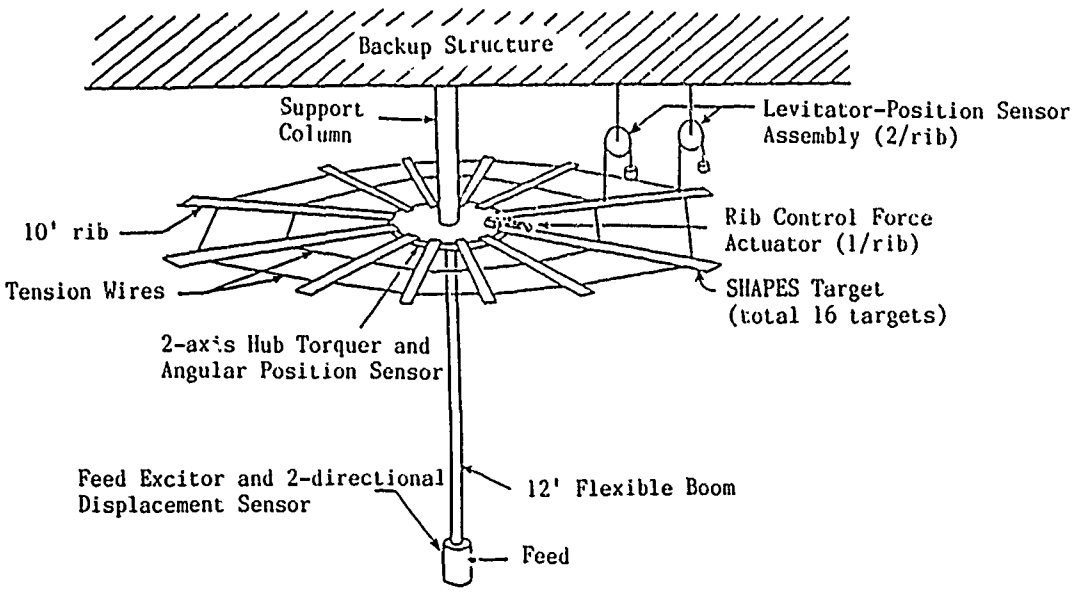

- **Reduce Risk for Space-based Radar**

Figure 7.

IN-HOUSE EXPERIMENTS IN CONTROL AND IDENTIFICATION

The objective of the recently initiated in-house experimental effort is to provide the AFRPL with the capability of (a) verifying new parameter identification and control methods being developed and (b) performing a quick feasibility check on new innovative ideas prior to substantial investment in that area. Most importantly, this facility will be made available to university faculty and DOD contractors for conducting experiments. The details of the means through which the facility can be made available are currently being worked on.

The approach involves designing the control system on a control design software package (e.g., MATRIX$_X$) and then directly implementing it on a desktop real-time controller. In this approach, the control system is down loaded to the controller and implemented in a matter of minutes without the engineer having to program the controller.

In the immediate future, the plan calls for testing the optimal sensor location logic for unique identification (being developed under a separate effort) on a 2-dimensional grid structure. Also work has just begun on a new facility with a test stand which is anchored directly to the bedrock and isolated from the rest of the structure to minimize vibrations. This facility should be available for use in roughly one year. In addition, AFRPL has a number of vacuum chambers of various sizes, the largest one being 30 ft in diameter.

WHY:

* **Provide Feasibility Check on New Ideas**
* **Provide Test Bed for Control & Identification Logic Developed for AFRPL**
* **Provide an Equipped Facility for University Faculty/Students**

HOW:

* **Use Simple 1, 2, & 3-D Structures**
* **Use Design Software Coupled with Real-Time Control/System Identification Hardware for Rapid Turnaround**
* **Up to 30ft Diameter Vacuum Chambers Available**

CURRENT PLAN:

* **Cantilevered Beam & Grid Structure**
* **Use MATRIX$_X$ + Real-Time Controller**
* **Experiments**
  - **System Identification , Vibration Suppression , New Sensor & Actuator , ...**

Figure 8.

DEPLOYMENT DYNAMICS OF LARGE SPACE STRUCTURES

A number of future spacecraft such as Space Based Radar (SBR) will be packaged into a compact structurally dense form for launch, and the spacecraft will automatically unfold to the operational state once in orbit. The anticipated large structural size (> 30 meters) coupled with extreme structural flexibility precludes extensive ground testing of the deploying process. An alternate approach to obtain confidence in the spacecraft deployment is to simulate the dynamics on a computer.

None of the currently available computer programs can simulate the deployment of a large class of spacecraft. For deployment studies, DISCOS has proven to be computationally inefficient and requires significant modifications for each application. Since 1982, AFRPL has made significant investments for the development of a general purpose spacecraft deployment prediction code.

State-of-the-Art

- Analysis
  - Dynamic Interactive Simulation of Controls and Structures (DISCOS)
    - Requires Significant Modification for Each Application
    - Computationally Inefficient
- Experiments
  - Ground
    - Mostly Limited to Simple Structures/Elements (by Size)
    - Terrestrial Effects also Limit Utility
  - Space Experiments from Shuttle in FY89

Technology

- Deployment Simulation of Large Space Systems

Payoff

- Reliable and Accurate Computer Simulation of Large Space Systems to Minimize Number of Tests Required on any Given Structure

Transition Target

- Space Based Radar

Figure 9.

LARGE SPACE STRUCTURE DEPLOYMENT DYNAMICS

AFRPL's initial study in the development of a deployment dynamics computer program consisted of two major tasks. In Task 1, a new mathematical formulation for simulating the deploying process was developed and a preliminary design of the software architecture was laid out. In Task 2, a pilot computer program was developed to test the mathematical formulations. The computer program is not a general purpose code and is set up to simulate the deployment of the Grumman bicycle wheel SBR concept only (see ref. 3 for details). In its present form, the code is fairly computer intensive, requiring four hours of CPU time on a VAX 11-750 computer for a 4310 second deployment simulation. The spacecraft was modeled as consisting of eight tubes and eight bridges. The deployed portion of each gore (the radar reflector) was replaced by two cables. Eight stays (four each connected to the upper and lower ends of the hub) provide stiffness to the structure and can stabilize the deployment. In the current version of the code, torsional springs between the bridges and tubes are the source of energy for deployment. An alternate approach is to use motors instead of springs.

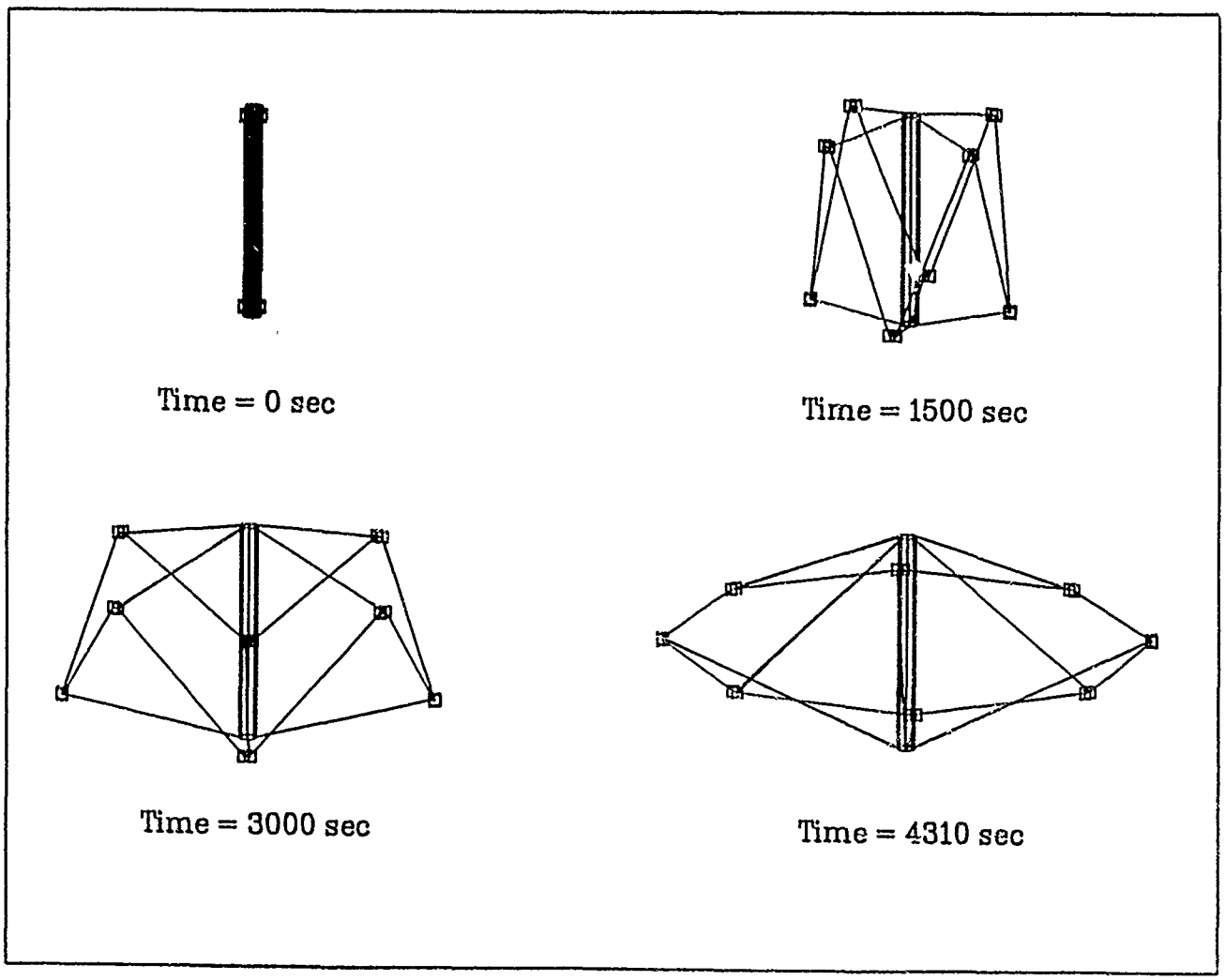

Figure 10.

DEPLOYMENT DYNAMICS SOFTWARE DEVELOPMENT

The objective of the ongoing program is to develop a general purpose computer code for simulating the deployment dynamics of a large class of future space structures. The effort consists of 5 major tasks. In Task 1, future DOD and NASA missions will be reviewed for their deployment needs. Also an assessment of the state of the art in deployment technologies will be made. In Task 2, which is the heart of the effort, extended modeling capability such as active hinge point control and mass flow modeling will be incorporated in the code. The program will have the capability of evaluating the impact of distributed environmental disturbances such as gravity gradient, magnetic field torques, etc., on the deployment process. The capability of linearizing the nonlinear system about an operating point of interest so as to study the system stability will be provided. Also an entanglement indicator in the form of a post processor shall be developed. A host of extended software features will be incorporated in the code under Task 3. This is to include common I-O structure, restart capability, CAD interfaces and graphics outputs, etc. Task 4 shall investigate the impact of nonlinear structures effects. Techniques for generating open and closed loop deployment sequences shall be developed under Task 5. Also under this task the closed loop response of a number of test examples will be generated.

Deployment State-of-the-Art Assessment

Extended Analysis and Modeling

* Active Hinge Point Control
* Mass Flow Modeling Capability
* Distributed External Environment Effects
* Entanglement Indication
* Stability Analysis

Extended Software Features

Nonlinear Structure

Control of Deployment

* Open & Closed Loop Deployment
* Test Examples

Figure 11.

ON-ORBIT SYSTEM IDENTIFICATION

The design of high precision vibration and pointing control systems for future large space structures will require an accurate mathematical model of the plant. Currently mathematical models are obtained using either distributed or lumped parameter methods. In the latter category, finite element modeling codes (e.g., NASTRAN) have become very popular. However, unmodeled variations in the physical/material properties and unmodeled nonlinearities such as joints result in large errors in the frequency and shape of the higher modes. For the current class of spacecraft, extensive ground based modal testing can be done to validate/update the mathematical model. However, for future large space structures, the large physical size coupled with in some cases extreme structural flexibility will preclude accurate ground based parameter identification tests. A solution to this problem, which has gained popularity, is to perform on orbit system identification. Currently there are available a large class of methods which have been used for ground based parameter identification of diverse plants. It is, however, not clear which of these methods, if any, could be adapted to perform on-orbit system identification. With this in mind, AFRPL funded a study with the American Society of Civil Engineers. This study (being performed by a committee of experts in the area of system identification) will identify areas requiring future effort.

Need: Accurate System Model a Must for Precise Pointing and Control of LSS

Problems in Structural Modeling

- No Information on Modal Damping
- Higher Modal Frequencies in Substantial Error
- Unmodeled Variations in Physical and Material Properties
- Unmodeled Nonlinearities Such as Joints

Problems in Ground Testing

- Difficult/Impossible to Test Flexible LSS on Ground
- Gravity Bias
- Atmospheric Effects

A Solution: On Orbit System Identification

Figure 12.

NONUNIQUENESS IN IDENTIFICATION

Mathematical modeling of dynamic systems involves the creation of a model by the analyst and prediction of the response of the system to given excitations. The idea is to measure the dynamic responses for the same inputs and update the model so as to minimize the difference between the predicted and measured responses. However, contrary to expectations, it was found that elimination of the mismatch in the time histories was not sufficient to guarantee unique identification (ref. 4). Also a preliminary study revealed that by properly locating the sensors, one can obtain unique identification.

The objective of this effort is to develop and test by computer simulations a methodology for optimally locating sensors in a large space structure so as to enable unique identification of its structural model.

Problems With Current Techniques

* Identification Problem is in General ill Posed
* Large Number of Sensors Required
* Large Amount of Data Generated

Issues Addressed in Current Effort

* Optimal Sensor Location for Unique Identification
* Minimum Number of Sensors Required
* Data Compression Techniques to Alleviate Data Handling
* Numerical Studies to Assess the Efficacy of Methods Proposed

Figure 13.

MODELING AND CONTROL OF FLEXIBLE STRUCTURES

Recent research in control system theory showed that in feedback systems with a time delay in the feedback loop (regardless of how small the delay may be), there is a potential of instability in the system (ref. 5). Since the delay in the feedback loop could be caused by sensors, actuators or control electronics, this is of concern in many control systems. Another question which has currently received a lot of attention is at what stage of the control system design process a truncated model of the distributed system adequate. Numerous examples are available to demonstrate that a truncated finite element model which is fully adequate for determining the open loop system response is inadequate for control system design.

This program is addressing the issue of modeling and control of distributed systems with delay and inherent structural damping. The modeling approach involves starting out with the necessary partial differential equations without modal truncation. The control problem is then formulated and its "solution" determined without introducing any approximations. The system is then truncated so as to numerically calculate the time varying gains (for details of the method see ref. 5). This effort will also address the question of the feasibility of developing a general purpose computer program which can implement the methodology.

Issue

Potential of Instability in Feedback Systems Due to Time Delay in Sensors & Actuators

* **Potential of Instability Regardless of the Magnitude of Delay**
* **Addition of Damping Tends to Reduce Instability**

Current Program

* **Investigate Modeling & Control of Distributed System with Delay and Structural Damping**
* **Develop Damping Models for Adequately Modeling Joints**
* **Feasibility of a General Purpose Computer Program**

Figure 14.

REFERENCES

1. Floyd, M. A.; and Vander Velde, W. E.: Verification of RCS Controller Methods for Flexible Spacecraft. AFRPL TR-84-092, December 1984.

2. Bailey, T.; and Hubbard, J. E.: Distributed Piezoelectric-Ploymer Active Vibration Control of a Cantilever Beam. Journal of Guidance, Control, and Dynamics, Vol. 8, Sept.-Oct. 1985.

3. Keat, J.; and Turner, J.: Large Space Structure Deployment Dynamics. AFRPL TR-86-020, March 1986.

4. Udwadia, F. E.; and Sharma, D. K.: Some Uniqueness Results Related to Building Structural Identification. SIAM Journal of Applied Mathematics, Vol. 34, January 1978.

5. Burns, J. A. et al.: Modeling and Control of Flexible Structures. AFRPL TR-85-030, May 1985.

FLIGHT DYNAMICS LABORATORY OVERVIEW

Colonel Thaddeus Sandford
Air Force Wright Aeronautical Laboratories
Wright-Patterson Air Force Base, Ohio

First NASA/DOD CSI Technology Conference
Norfolk, Virginia
November 18-21, 1986

Divisions of the Flight Dynamics Laboratory

The Flight Dynamics Laboratory (FDL) is one of four Air Force Wright Aeronautical Laboratories (AFWAL) and part of the Aeronautical Systems Division located at Wright-Patterson AFB, Ohio. The FDL is responsible for the planning and execution of research and development programs in the areas of structures and dynamics, flight controls, vehicle equipment/subsystems, and aeromechanics. Some of the areas being researched in the four FDL divisions are as follows: large space structures (LSS) materials and controls; advanced cockpit designs; bird-strike-tolerant windshields; and hypersonic interceptor system studies. Two of the FDL divisions are actively involved in programs that deal directly with LSS control/structures interaction: the Flight Controls Division and the Structures and Dynamics Division.

Flight Controls Division Areas of Research

The Flight Controls Division has several programs that address control/structures interaction technology for large space structures. These programs include pointing and shape control studies for large (100-meter) radar systems and robust control systems development. Research is performed in advanced controls/fighter technology integration, attitude and trajectory control for hypersonic vehicles, advanced cockpit designs, and flight simulator technology.

Structures and Dynamics Division Areas of Research

Some of the technology areas being developed in the Structures and Dynamics Division are advanced composite aircraft and spacecraft structures, cast aluminum structures technology, stores/aircraft flutter testing, and structures/dynamics/controls interaction. Programs have also been developed to research LSS control hardware, passive and active vibration control, suspension systems, and design optimization.

Large Space Structure Concept

Many defense systems have been proposed that incorporate space based structures an order of magnitude larger than those in orbit today. With the tremendous size and adverse environment associated with these systems come many challenges to the design and test engineers. Weight limitations imposed on LSS designs have made them much less rigid. This high flexibility combined with low damping results in structures very sensitive to disturbance forces. The structural precision required by many proposed missions creates the need for passive and active control systems. In the figure below is a space-based laser system concept whose flexibility, required precision, and size (approx. 15-m dia.) necessitate the use of combined passive and active control systems and specialized ground test procedures.

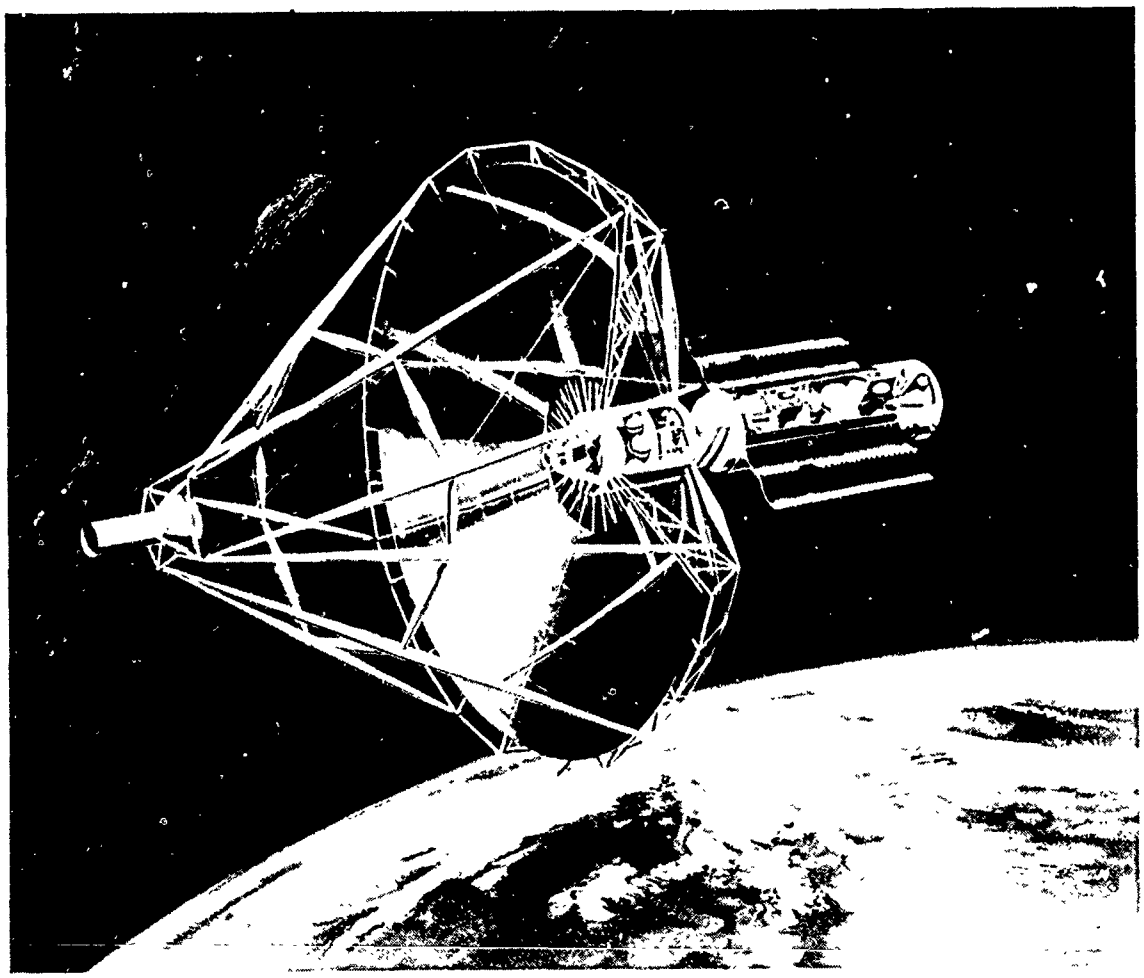

Technology Drivers

Development of large space structure control systems is hampered by the difficulty of the necessary performance validation ground tests. While some systems are too large for full-scale testing and/or do not lend themselves well to scaling techniques, the dynamics of a system on the ground may be radically changed when placed in orbit. The microgravity, low atmospheric pressure, thermal cycling environment of earth orbit produce material property changes and unique structural loads that may degrade control system performance. What is needed are technologies that allow earth-bound development and testing of LSS control systems to ensure reliable on-orbit system performance. The figure below illustrates some of the LSS technology drivers.

LARGE SIZE

- SCALING LAWS
- GROUND TEST TECHNIQUES

FLEXIBILITY

- ACTIVE & PASSIVE CONTROL

HIGH PERFORMANCE

- CONTROL / STRUCTURE OPTIMIZATION

ENVIRONMENT

- ADVANCED MATERIALS
- UNIQUE CONTROL HARDWARE
- GROUND TEST FACILITIES

Technical Issues Addressed by Flight Dynamics Laboratory

The Flight Dynamics Laboratory has developed several programs that address the challenging dynamics issues presented above. In the figure below is a chart illustrating the application of FDL programs to the development of the required technology areas.

PROGRAMS / ISSUES	BASIC RESEARCH	POINTING & SHAPE CONTROL	ROBUST CONTROL	LSS ACTIVE VIBRATION CONTROL	VIBRATION CONTROL OF SPACE STRUC	ACTIVE CONTROL EVALUATION FOR SPACECRAFT	LSS TECHNOLOGY PROGRAM	PASSIVE & ACTIVE CONT OF SPACE STRUCTURES	PRECISION STRUCTURAL JOINTS
THEORETICAL CONTROLS DEVELOPMENT	X		X						
OPTIMIZATION	X	X							
SCALE MODELING				X				X	
ACTIVE CONTROL IMPLEMENTATION						X	X	X	
PASSIVE DAMPING				X			X	X	
GROUND TEST TECHNIQUES				X	X	X	X		
HARDWARE					X		X		X

Basic Research Objectives

Several basic research programs are underway in the areas of optimization, analysis, and control algorithm development. Optimal control and estimation methods for discrete structural systems and modeling errors and their effect on the robustness of control/structures interaction are being studied and the structural dynamics and controls disciplines are being integrated for optimum structures in the space environment. Algorithms for structural optimization, precision pointing, shape control, and vibration suppression are being developed as well. The figure below summarizes the objectives for these programs.

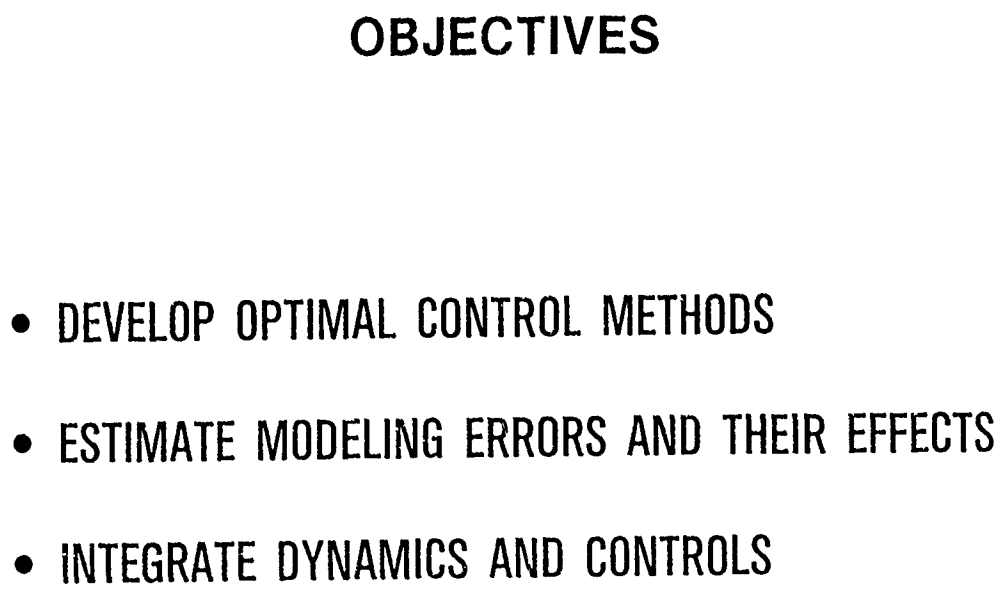

Basic Research Spacecraft Model

Many analytical spacecraft models have been used in the basic research programs. Shown in the figure below is one such model, the Draper Model #2. This model was developed for the Defense Advanced Research Projects Agency (DARPA) Active Control of Space Structures (ACOSS) program. In this model a flexible metering truss, approximately 22 x 20 meters, supports primary, secondary, and tertiary mirrors and the focal plane array. Attached to this structure is an equipment platform with solar arrays. The primary objective was to meet stringent line-of-sight and jitter control requirements by applying modern control techniques and state-of-the art hardware concepts.

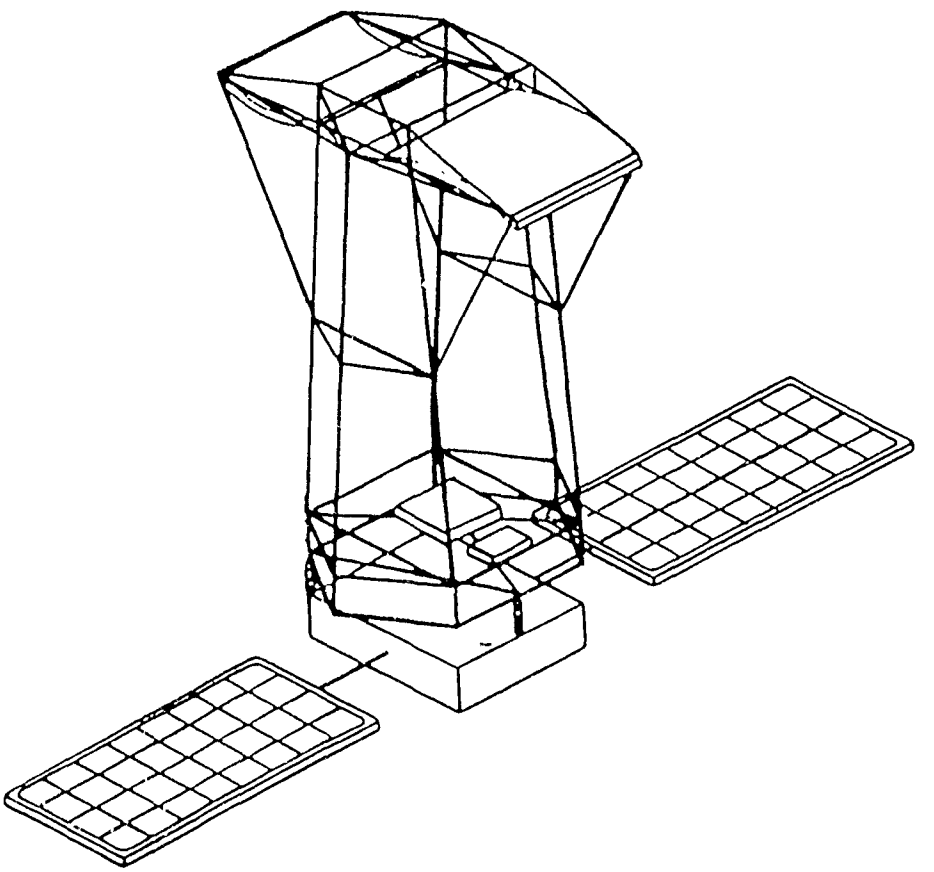

Large Spacecraft Pointing and Shape Control

The objective of the Large Spacecraft Pointing and Shape Control program is to develop an integrated control system for a realistic large (100-meter) space antenna for controlling slewing, pointing, shaping, and vibration of the structure. General Dynamics, Convair Division, has defined mission drivers and environmental factors, performed control trade-off studies, and developed control algorithms for a realistic large flexible space antenna. The figure below summarizes the objective, approach, and payoffs of this program.

OBJECTIVE:

- DEVELOP INTEGRATED CONTROL SYSTEM FOR REALISTIC SPACE ANTENNA CONTROL SLEWING, POINTING, SHAPING AND VIBRATION

APPROACH:

- MODEL REALISTIC ANTENNA AND ACTUATOR / SENSORS
  - STRUCTURE-LIMITED ANTENNA MODEL
- DEVELOP CONTROL ALGORITHMS
- PERFORM CONTROL TRADE-OFFS

PAYOFF:

- SHAPE CONTROL OF ANTENNA VERIFIED
- OPTIMIZED SUPPORTING TRUSS

Antenna Configuration

The figure below shows the configuration of the antenna model used in the Large Spacecraft Pointing and Shape Control program. The antenna dish is over 100 meters in diameter with a 110 meter support mast. Lengthy trade studies were performed to determine the optimal mix of the system parameters.

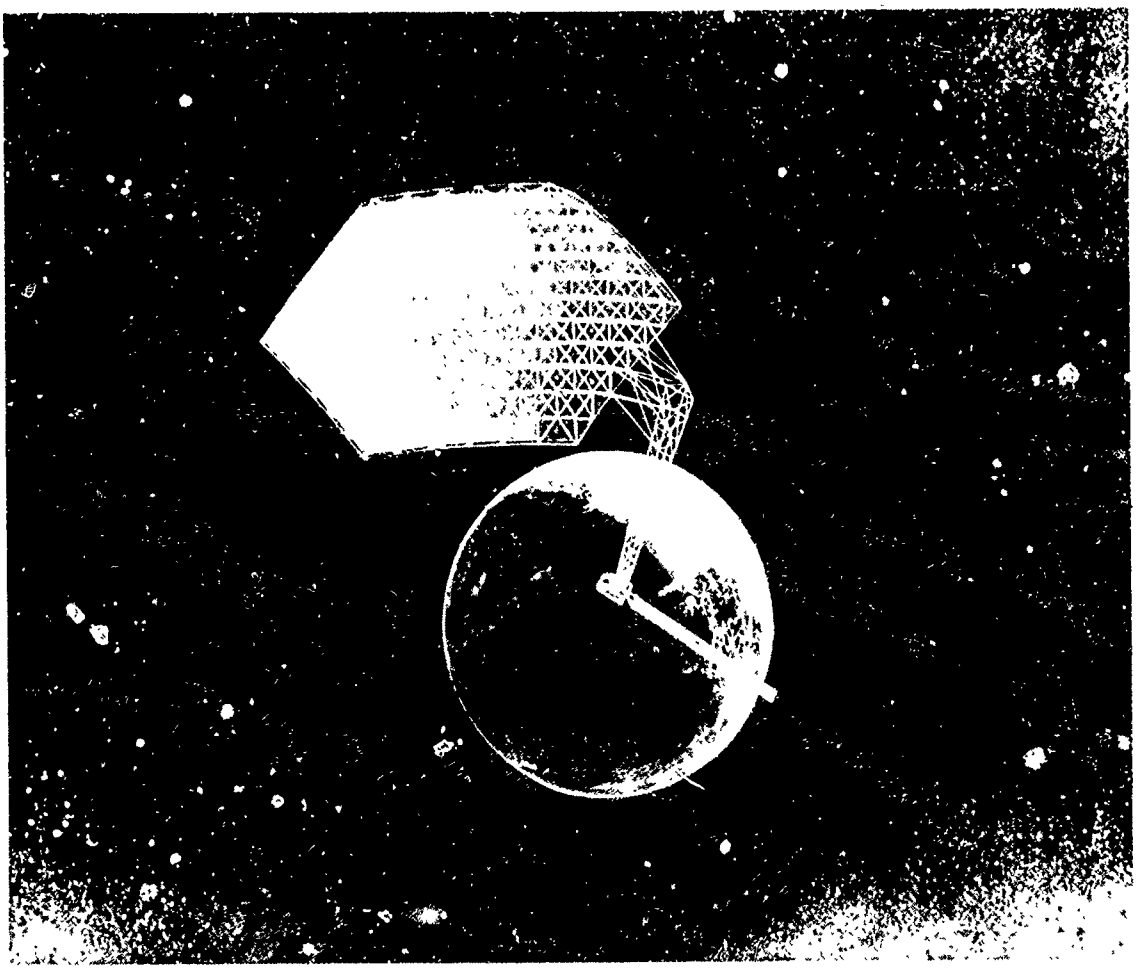

Robust Control for Large Space Antennas

Robust Control for Large Space Antennas is a two-year effort contracted to Honeywell Systems Research Center to assess the benefits of robust control design for pointing and shape control of large space antennas for both structured and unstructured uncertainty. Using the 100-meter geodetic truss reflector developed in the Large Spacecraft Pointing and Shape Control program as the baseline antenna configuration, performance/robustness measures were developed. A Linear Quadratic Gaussian/Loop Transfer Recovery (LQG/LTR) control algorithm was designed and the performance/robustness was analytically verified. The figure below gives a brief description of the objectives, approach, and payoffs of this program.

OBJECTIVES:

- ASSESS BENEFITS OF ROBUST CONTROL DESIGN
- EVALUATE CONTROLLER PERFORMANCE

APPROACH:

- USE REALISTIC SPACE ANTENNA DESIGN
- DEVELOP PERFORMANCE / ROBUSTNESS MEASURES

PAYOFFS:

- IMPROVED POINTING AND SHAPE CONTROL
- GUIDELINES FOR ACHIEVING PERFORMANCE / STABILITY ROBUSTNESS

Antenna Design

The figure below illustrates the antenna design used in the Robust Control for Large Space Antennas program. Given in the figure are some of the major dimensions.

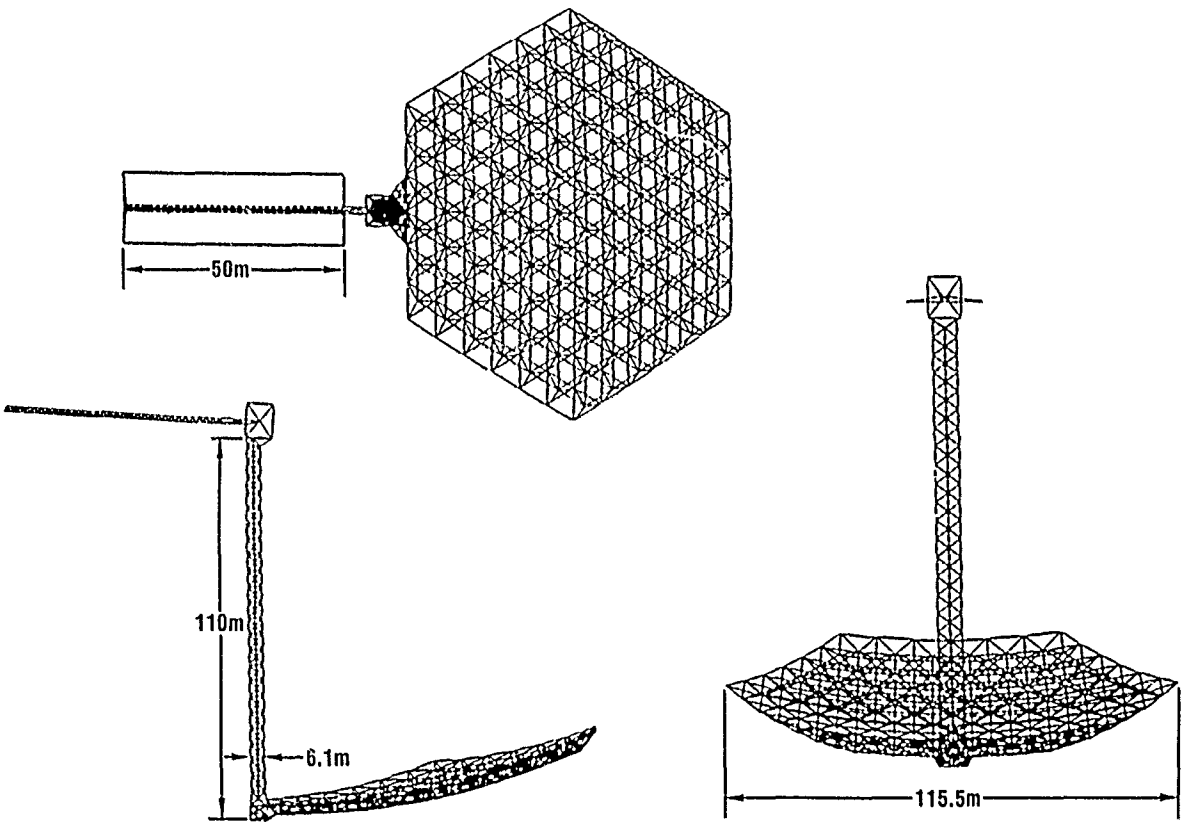

Large Space Structures Technology Program

The Large Space Structures Technology Program (LSSTP) was created to address many of the LSS control challenges and develop an in-house capability for LSS test and analysis. The objectives, approach, and payoff of the LSSTP are given in the figure below.

OBJECTIVES:

- DEVELOP TEST AND ANALYSIS CAPABILITY

APPROACH:

- CONTROLS-DESIGNED STRUCTURES TESTS
  - PASSIVE DAMPING STUDIES
  - ACTIVE VIBRATION CONTROL TESTS
- HARDWARE DEVELOPMENT
  - LIGHTWEIGHT PROOF MASS ACTUATORS
  - NONINTERFERING SENSORS

PAYOFFS:

- VERIFY ANALYTICAL ALGORITHMS
- VERIFY GROUND TEST TECHNIQUES
- EVALUATION OF ACTUATORS AND SENSORS

Program Schedule

The figure below illustrates the time schedule for the various activities associated with the Large Space Structures Technology Program beginning with the facility development started in FY 85. Within the program are subtasks to develop the LSS testing capabilities of the facility, develop low-restraint suspension systems, and perform controls experiments on a set of structures that progress in complexity. Tests of active vibration control have been completed for a simple cantilever beam and will progress to a more complex and realistic large space structure test article. Intermediate complexity test articles are now being tested which include a cantilever beam with rotary inertia and a set of two 12-meter damped and undamped truss structures. Fifth-scale models of the NASA-Langley Control of Flexible Structures program (COFS) 60-meter Mast beam will also be tested.

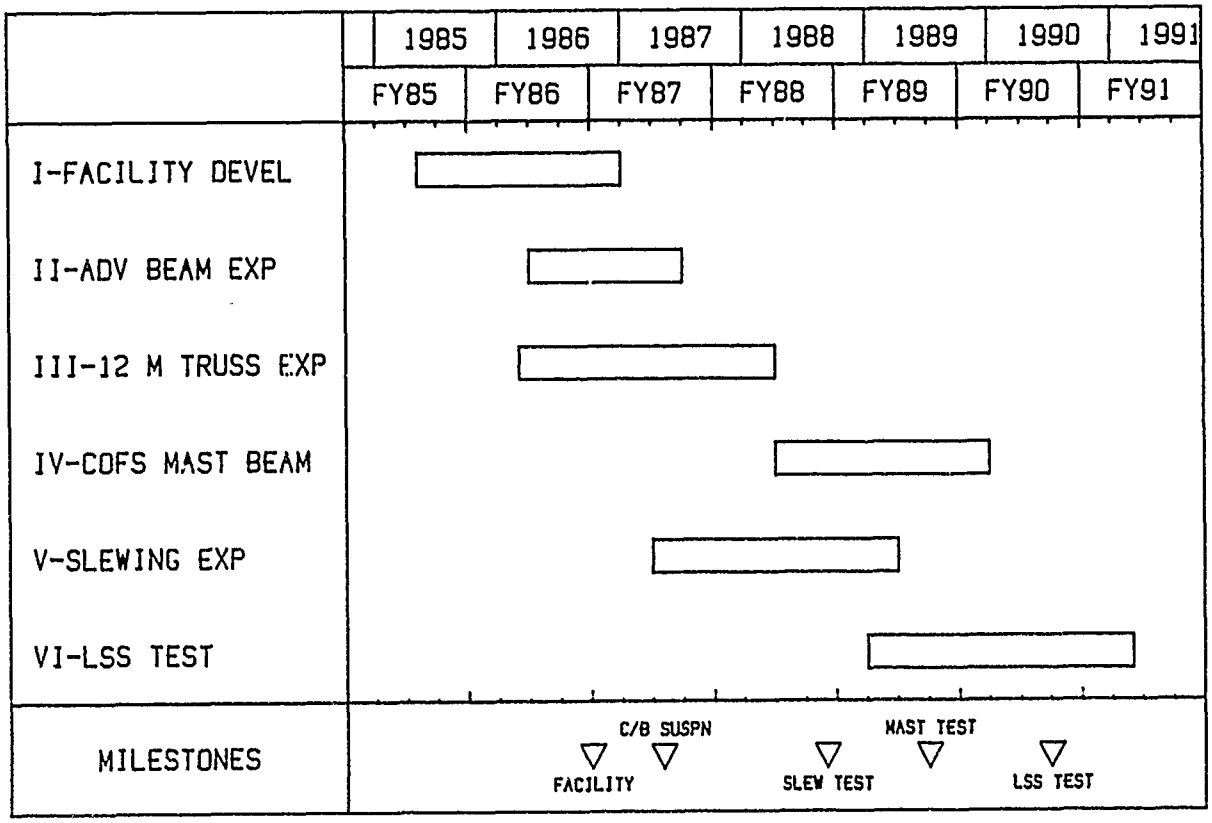

Dynamics Testbed Structure

The figure below shows a forty-foot truss structure fabricated from PVC tubing used in the facility development portion of the LSSTP. The structure was used to test and develop sensing, actuation, and data analysis equipment and methods. The 40-foot truss testbed is shown located in the large chamber of the Flight Dynamics Laboratory Sonic Fatigue Facility. Designed for the vibration and acoustic testing of large aircraft and missiles, the chamber is over 12 meters high, 17 meters wide, and 21 meters long. With its large size and excellent data gathering and analysis equipment, the facility is ideal for large space structures testing.

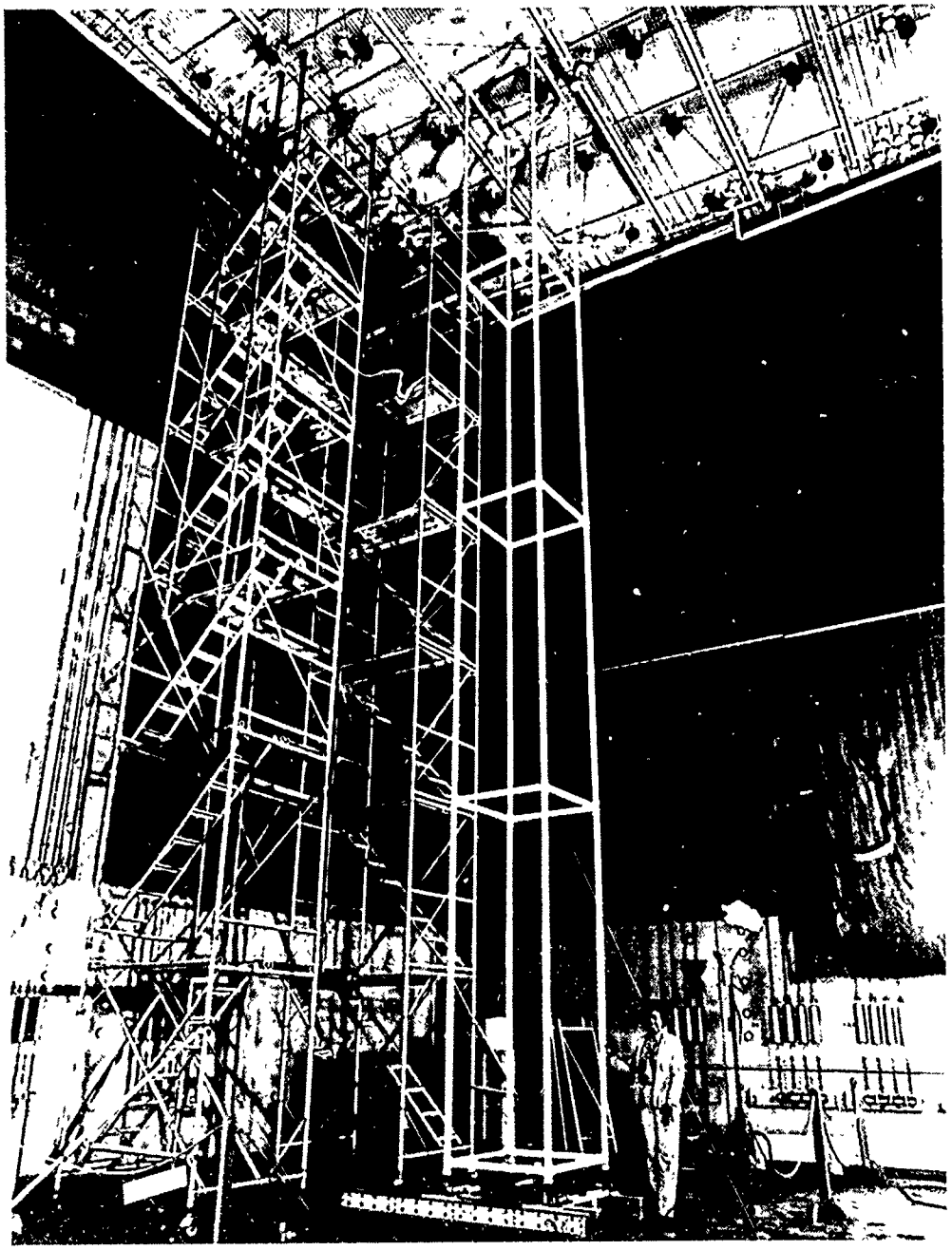

Large Space Structures Active Vibration Control

The objectives of Large Space Structures Active Vibration Control program are to verify and extend the results of laboratory control tests. Through ground tests of a fifth-scale version of the NASA-Langley Control of Flexible Structures (COFS) 60-meter deployable beam, one-g test procedures will be developed and verified. Active and passive control techniques will be tested on the scale beam in the AFWAL test facilities and the results will be validated with data from the shuttle flight tests of the full-scale hardware. The figure below summarizes the objectives, approach, and payoffs of this program.

OBJECTIVE:

- VERIFY AND EXTEND LABORATORY CONTROL TESTS

APPROACH:

- COOPERATIVE EFFORT WITH NASA-LANGLEY SPACE TEST PROGRAM
  1/5-SCALE MAST MODEL TESTED IN AFWAL LABORATORY

PAYOFFS:

- OBTAIN LOW-COST SPACE TEST EXPERIENCE AND DATA
- VERIFY 1-g, 1 ATMOSPHERE LABORATORY TEST RESULTS

Deployable Space Beam

The figure below shows a truss structure being deployed from the space shuttle cargo bay as will the 60-meter Mast beam in the NASA-Langley Control of Flexible Structures program. The Large Space Structures Active Vibration Control Program will perform ground tests of active and passive control of damped and undamped fifth-scale Mast beams and validate the tests through comparison with the space test data.

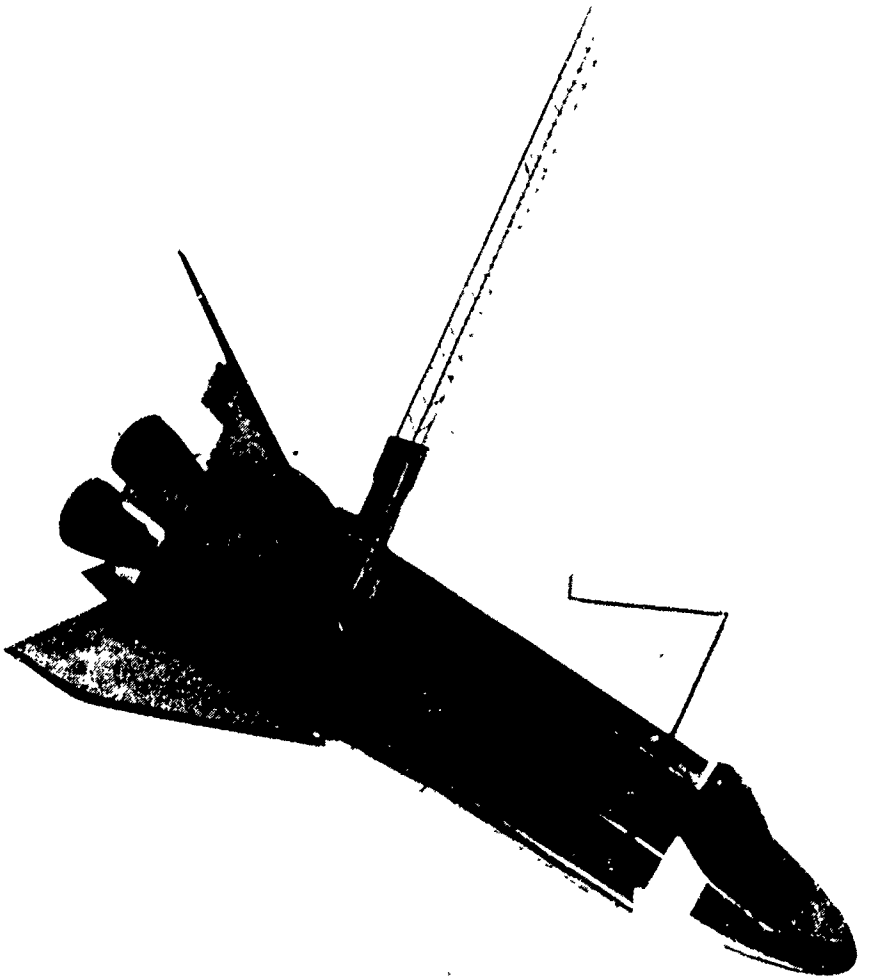

Vibration Control of Space Structures (VCOSS II)

Vibration Control of Space Structures (VCOSS II) is a cooperative program between the Structures and Dynamics Division and the NASA Marshall Space Flight Center to develop and demonstrate actuator and sensor hardware for flexible-mode control of a space structure in the presence of dynamic disturbances. In this 28-month contract, TRW developed a set of linear proof-mass actuators and optical position sensors to control a 45-foot Astromast space structure suspended vertically in the NASA-Marshall Ground Test Verification Facility. The Astromast is a spare magnetometer boom identical to the ones used on the Voyager and Mariner spacecraft. The objectives, approach, and payoffs of the VCOSS II program are listed in the figure below.

OBJECTIVES:

- DEVELOP LAB HARDWARE TEST TECHNIQUES
- OPTIMIZE CONTROLS / STRUCTURE INTERACTION

APPROACH:

- DESIGN AND BUILD IMPROVED SENSORS AND ACTUATORS
  - 2.1 POUND FORCE PROOF-ACTUATORS
  - LASER-OPTIC SENSOR SYSTEM
- TEST CONTROL SYSTEM ON 40-FOOT ASTROMAST STRUCTURE

PAYOFFS:

- DEVELOPMENT OF IMPROVED ACTUATOR / SENSOR HARDWARE
- LIGHTWEIGHT ACTIVELY CONTROLLED STRUCTURES

Linear Proof-Mass Actuators

Linear proof-mass actuators and optical sensors were developed in the Vibration Control of Space Structures program. Shown in the figure below is one of the linear proof-mass actuators with attached mounting bracket and LVDT compensation sensor.

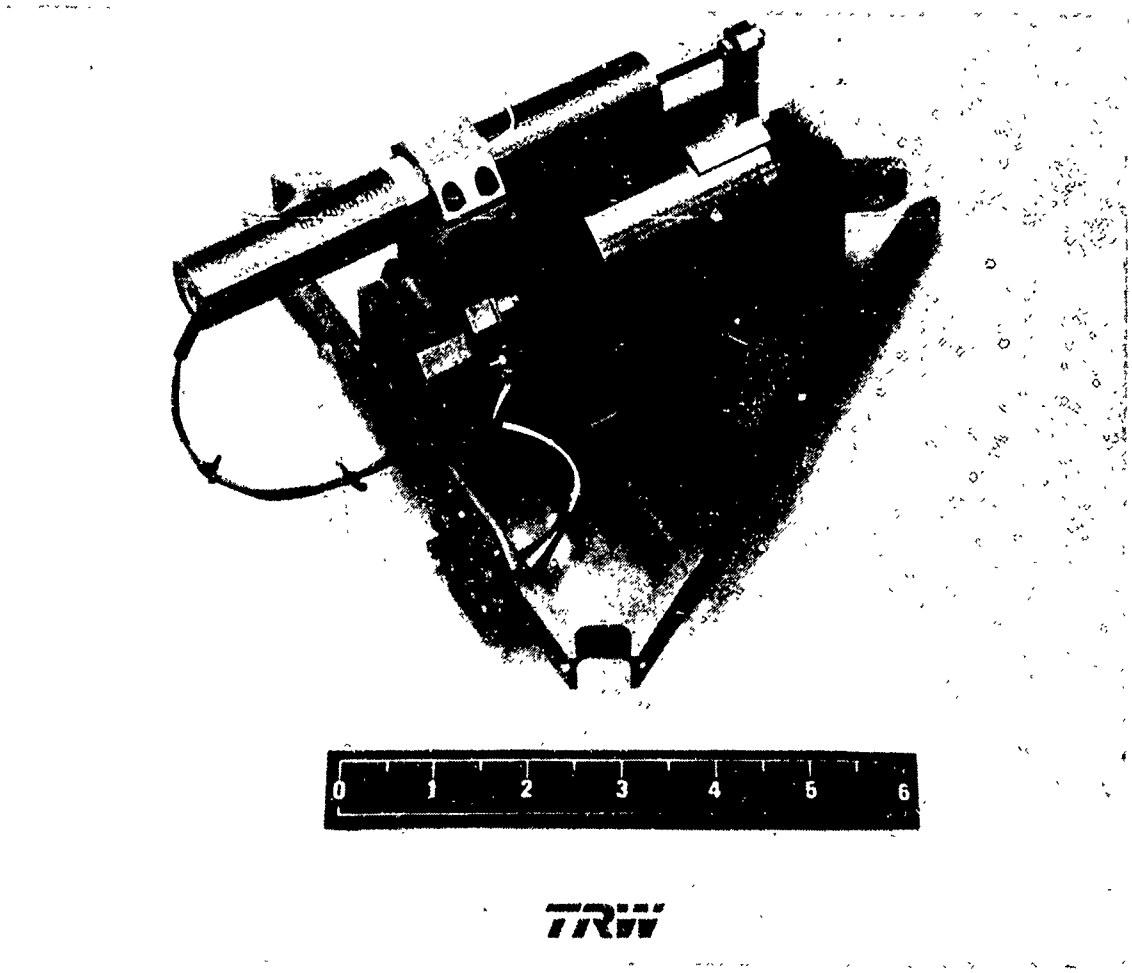

Active Control Evaluation for Spacecraft (ACES)

Active Control Evaluation for Spacecraft (ACES) is a DOD and NASA funded, cooperative AFWAL/Air Force Weapons Laboratory and Marshall Space Flight Center program to assess leading techniques for LSS flexible mode control. The control testing will be performed in the NASA-Marshall test facility using the Astromast structure and the VCOSS II actuator and sensor hardware. The control techniques to be tested are Harris' Maximum Entropy/Optimal Projection (ME/OP), Lockheed's High Authority/Low Authority Control (HAC/LAC), and TRW's Positivity. Below are the program objective, approach, and payoff.

OBJECTIVE:

- ASSESS LEADING TECHNIQUES FOR FLEXIBLE MODE CONTROL

APPROACH:

- USE VCOSS II DEVELOPED CONTROL HARDWARE
- IMPLEMENT AND TEST ON SPACECRAFT ANTENNA AND FEED MAST

PAYOFF:

- SELECTION OF OPTIMAL CONTROL TECHNIQUE

Modified Astromast Structure

The flexible spacecraft model used in the Active Control Evaluation for Spacecraft program is the Astromast structure used in the VCOSS II program with added offset antenna dish and feed. An artist's rendering of the test structure is shown in the figure below.

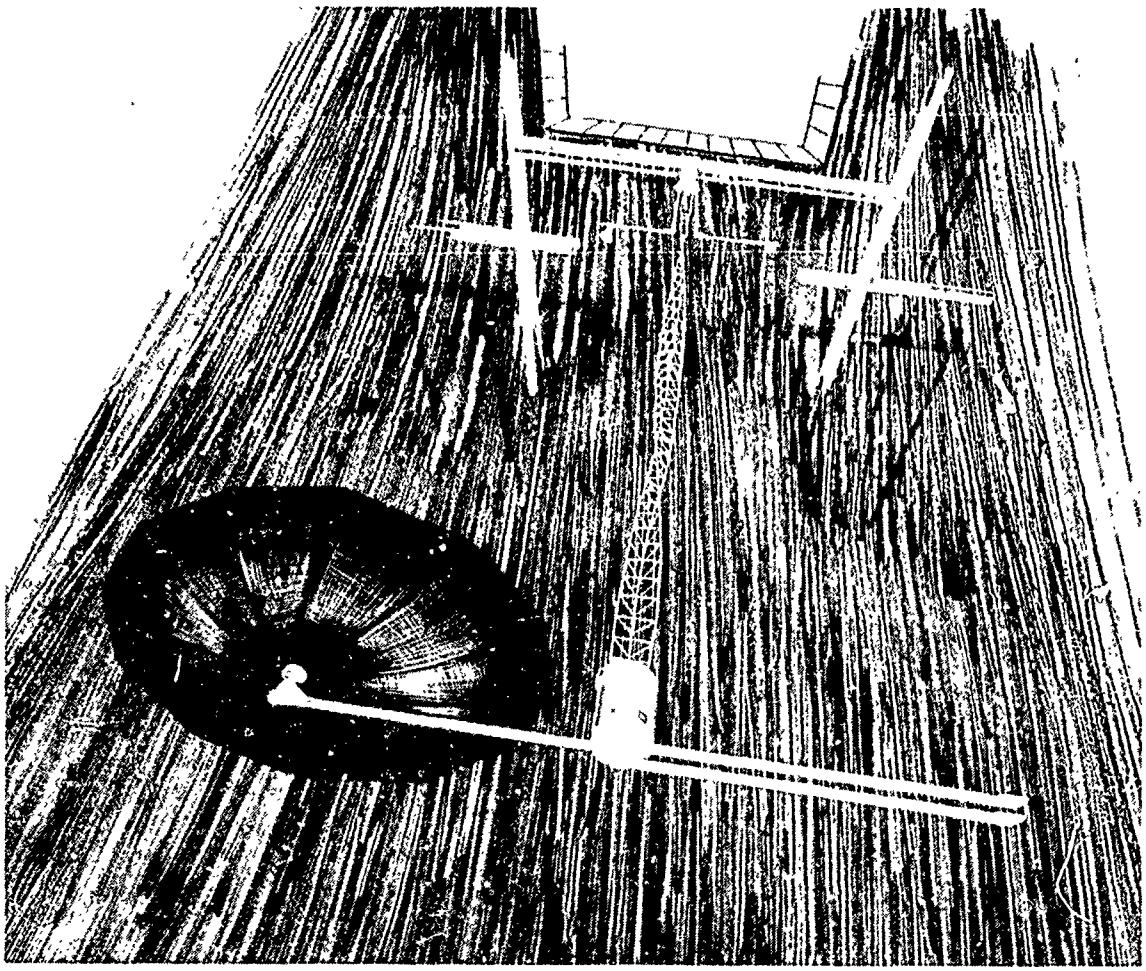

Development of Precision Structural Joints for Large Space Structures

Development of Precision Structural Joints for Large Space Structures is a program contracted to General Dynamics Convair Division for the development of design data on dimensionally stable, zero free-play, enhanced high energy laser survivable joints for large space structures. Innovative designs of low thermal response materials (composites) will be developed and joint strength/stiffness, free-play, thermal response, and dimensional precision will be validated. The objective, approach, and payoff of this program are shown in the figure below.

OBJECTIVE:

- DEMONSTRATE LIGHTWEIGHT, THERMALLY STABLE JOINTS

APPROACH:

- HARDWARE DESIGN
  - 2 JOINT DESIGNS
  - 2 MATERIAL COMBINATIONS
  - MULTIPLE MEMBER JOINTS
- HARDWARE TESTS
  - LOADS
  - THERMAL STABILITY
  - FREE PLAY

PAYOFF:

- DESIGN CRITERIA DEVELOPED FOR SPACE STRUCTURE JOINTS

Joint Installed on SADE Beam

Development of Precision Structural Joints for Large Space Structures program baselines for joint design development are the contractor's GEO-truss antenna fitting and three joints from the NASA Marshall Structural Assembly Demonstration Experiment (SADE) linear beam. Two designs, a graphite/aluminum GEO-truss antenna fitting and a carbon-carbon nodal fitting from the SADE beam, were selected for fabrication. The SADE beam is shown deployed in the figure below. In the left foreground is one of the joints developed in this program.

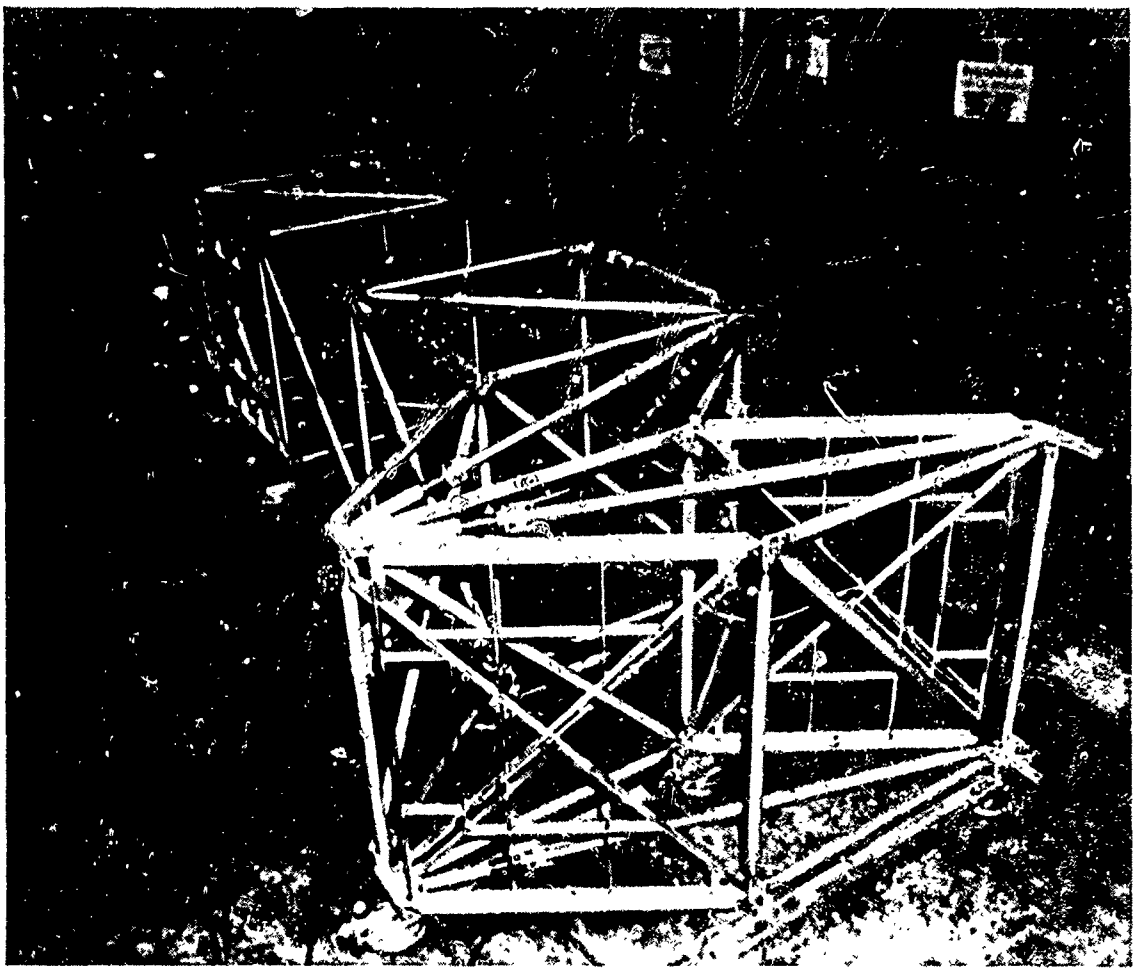

Passive and Active Control of Space Structures (PACOSS)

Passive and Active Control of Space Structures (PACOSS) is an advanced development program being conducted by Martin Marietta Denver Aerospace under sponsorship by the Flight Dynamics Laboratory and the Strategic Defense Initiative Organization. The program approach is to determine the dynamic challenges of future large precision space systems, develop structural concepts which incorporate and integrate passive damping with the active control system, and fabricate and test a dynamic test article which incorporates the damping technology. The PACOSS objectives and goals are to demonstrate the benefits of passive structural damping technology to the dynamic performance of large precision space structures, achieve 50% reduction in settling time following retargeting, 90% reduction in line of sight jitter, and significant reduction in cost and complexity of active vibration control systems. The figure below summarizes the program objective, approach, and payoffs.

OBJECTIVE:

- DIMENSIONAL PRECISION THROUGH PASSIVE DAMPING

APPROACH:

- DESIGN, FABRICATE AND TEST A REPRESENTATIVE SPACE STRUCTURE

PAYOFFS:

- 90% REDUCTION IN LINE-OF-SIGHT JITTER
- 50% REDUCTION IN SETTLING TIME AFTER MANEUVER
- SYNERGISTIC EFFECT ON ACTIVE CONTROL SYSTEM

Dynamic Test Article

One of the PACOSS dynamic test articles consists of a large box and ring truss with attached solar arrays and tripod secondary support which represent structural components from a variety of proposed large space structures. This structure is shown in the artist's concept in the figure below.

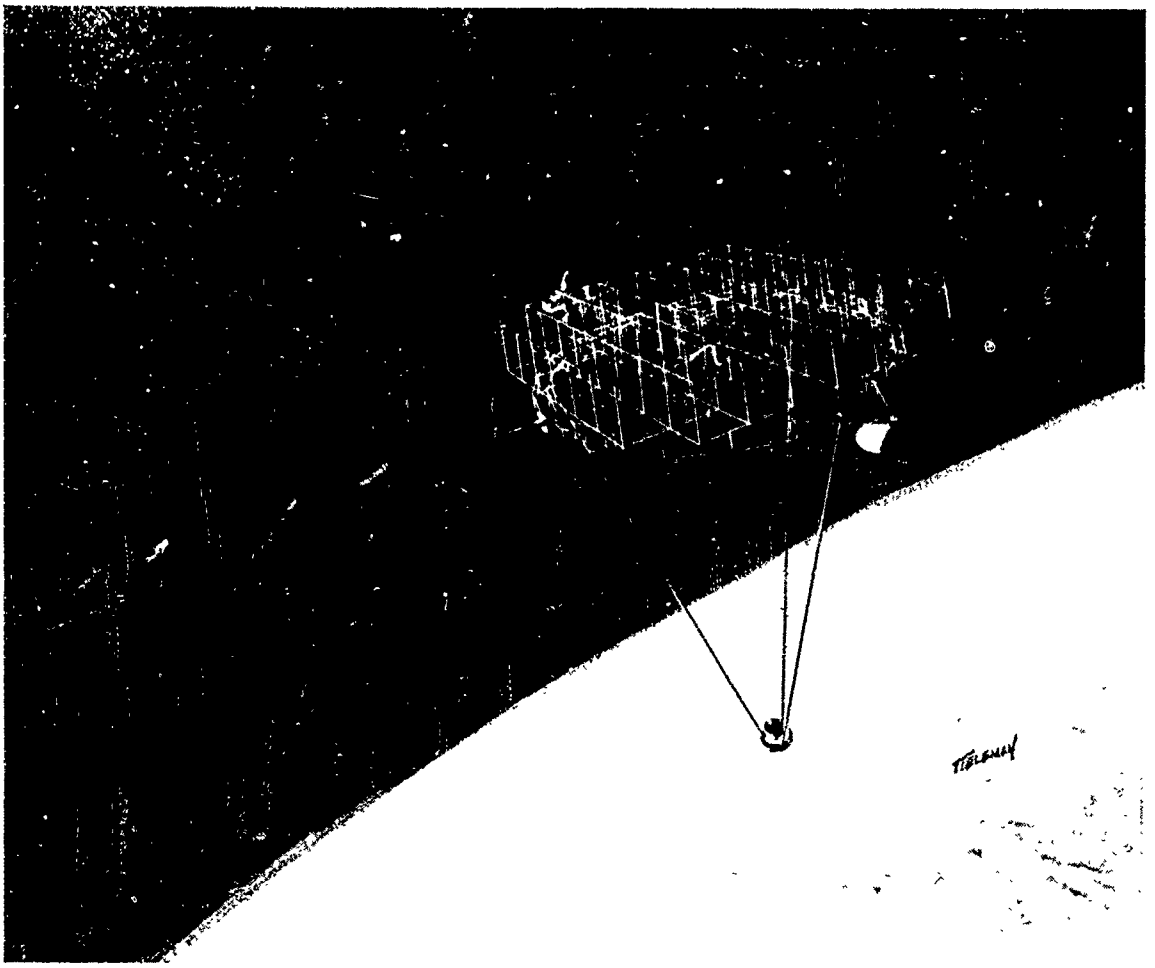

Technology Needs

Experience in applying active control to large flexible space structures has indicated that there are several technology needs that must be addressed. Listed in the figure below, these needs are high force low mass actuators; lightweight, high sensitivity sensors; efficient, robust controllers; lightweight structures; and space test experience. Future developmental programs should be focused on these issues.

- HIGH FORCE / LOW MASS ACTUATORS
- LIGHTWEIGHT, WIDEBAND SENSORS
- EFFICIENT, ROBUST CONTROLLERS
- LIGHTWEIGHT STRUCTURES
- SPACE TEST EXPERIENCE

ACTIVE CONTROL EVALUATION FOR SPACECRAFT (ACES)

J. Pearson and W. Yuen
Air Force Wright Aeronautical Laboratories
Wright-Patterson AFB, OH

First NASA/DOD CSI Technology Conference
November 18-21, 1986

THE LARGE SPACE STRUCTURE CONTROL PROBLEM

Historically, spacecraft have been relatively small and stiff, with alignment and pointing performed by rigid-body techniques. Because of new requirements for large space structures (high-resolution radars and antennas, large optics, and lasers) requiring accurate pointing and tracking, flexible-body control methods must be used. Figure 1 is an artist's illustration of a representative spacecraft with an offset-feed antenna that will require active control of the alignment of the feed mast. The Air Force goal is to develop vibration control techniques for large flexible spacecraft by addressing sensor, actuator, and control hardware and dynamic testing. The Active Control Evaluation for Spacecraft (ACES) program will address the Air Force goal by looking at two leading control techniques and implementing them on a structural model of a flexible spacecraft under laboratory testing.

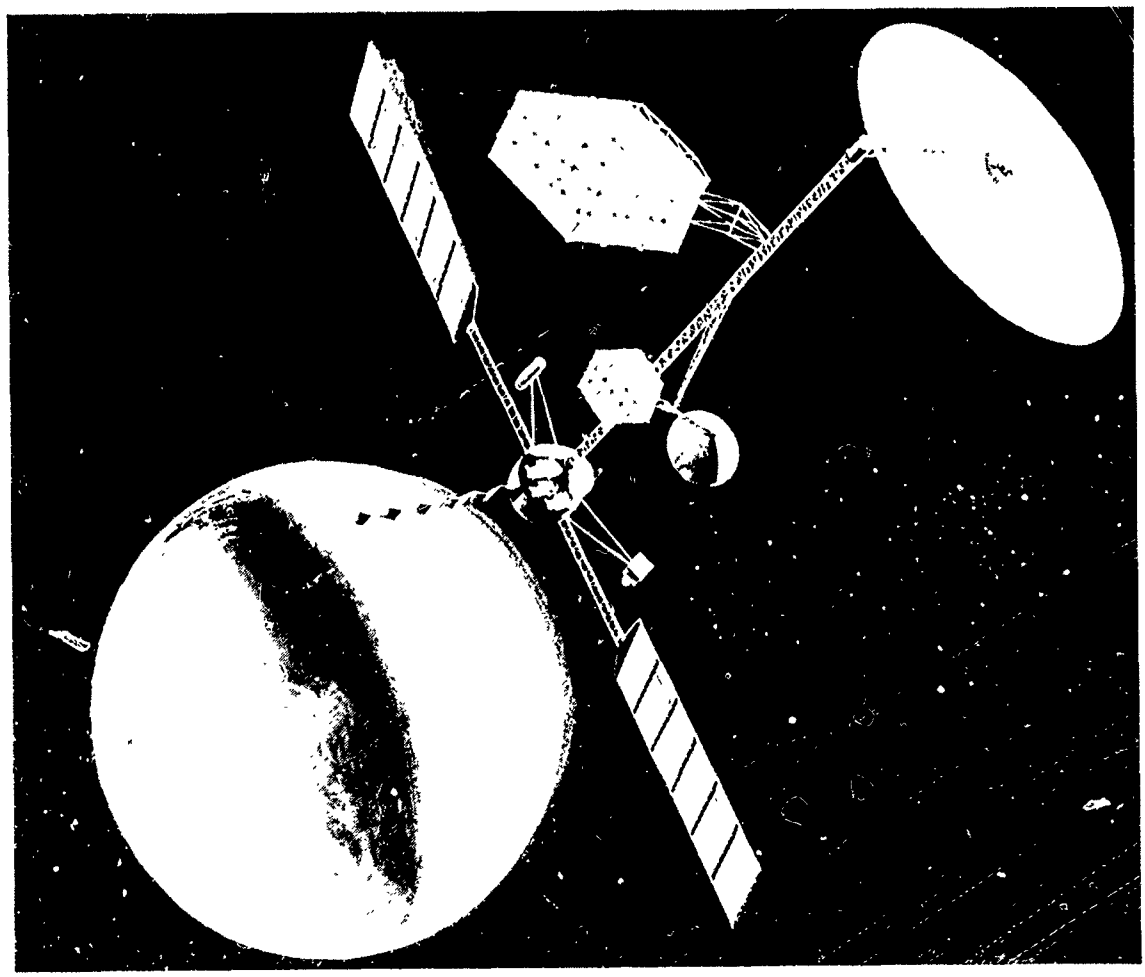

Figure 1

ACTIVE CONTROL OF SPACE STRUCTURES (ACOSS) STUDIES

The control techniques that will be studied in this program were initially investigated in the Active Control Of Space Structures (ACOSS) program sponsored by Defense Advanced Research Projects Agency (DARPA). The ACOSS program started in 1978; in six years it involved eighteen contracts and seven major contractors to develop and demonstrate the technology to suppress vibration in large space structures. The control goal was to meet the stringent line-of-sight and jitter control requirements of representative spacecraft. Various experiments with beams, plates, trusses, and frame structures were conducted using damping augmentation and elastic mode control. Disturbance models were developed, sensors and actuators were surveyed, and system identification studies were performed (Figure 2). The ACOSS studies were chiefly analytical, with limited laboratory testing. The leading techniques resulting from this program were High Authority Control/Low Authority Control (HAC/LAC), Positivity, and Filter Accomodated Model Error Sensitivity Suppression (FAMESS).

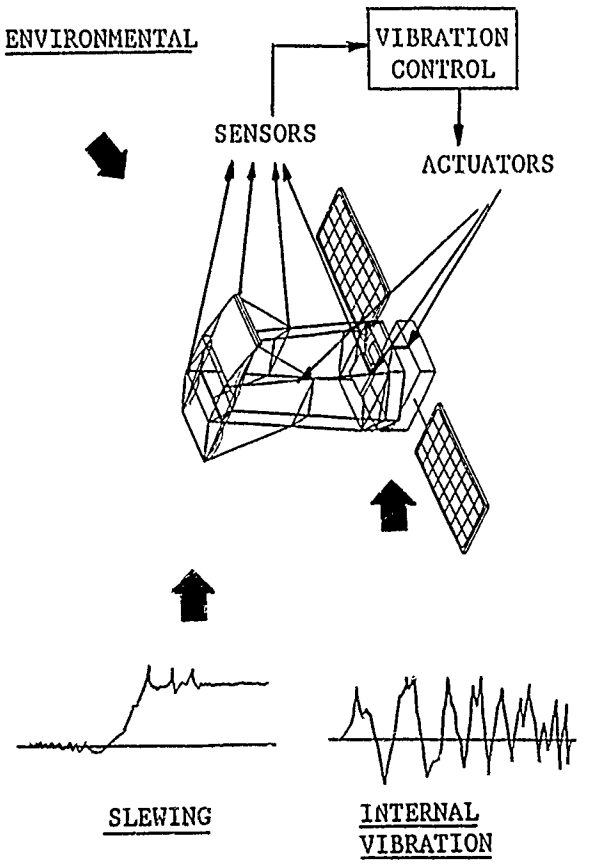

- ANALYTICAL DEVELOP ACTIVE CONTROL CONCEPTS
  - LOW FREQUENCIES
  - SPACECRAFT MODELS
  - CONTROL ALGORITHM
- SLEWING AND ENVIRONMENTAL DISTURBANCES
- QUANTIFYING POINTING PERFORMANCE

Figure 2

VIBRATION CONTROL OF SPACE STRUCTURE (VCOSS) HARDWARE

The VCOSS I program extended the ACOSS program by applying modern control techniques and state-of-the-art hardware concepts to the Draper Model two structure developed under ACOSS. The VCOSS II program was a cooperative effort between the NASA Marshall Space Flight Center (NASA-MSFC) and the Air Force Wright Aeronautical Laboratories (AFWAL) to build state-of-the-art control hardware (optical sensors and linear proof mass actuators) and apply it to a laboratory test structure consisting of a modified Astromast (Figure 3). The hardware was tested at the NASA-MSFC Ground Test Verification Facility. TRW developed the control hardware and Control Dynamics Company developed the test structure for the VCOSS II program (Refs. 1-3).

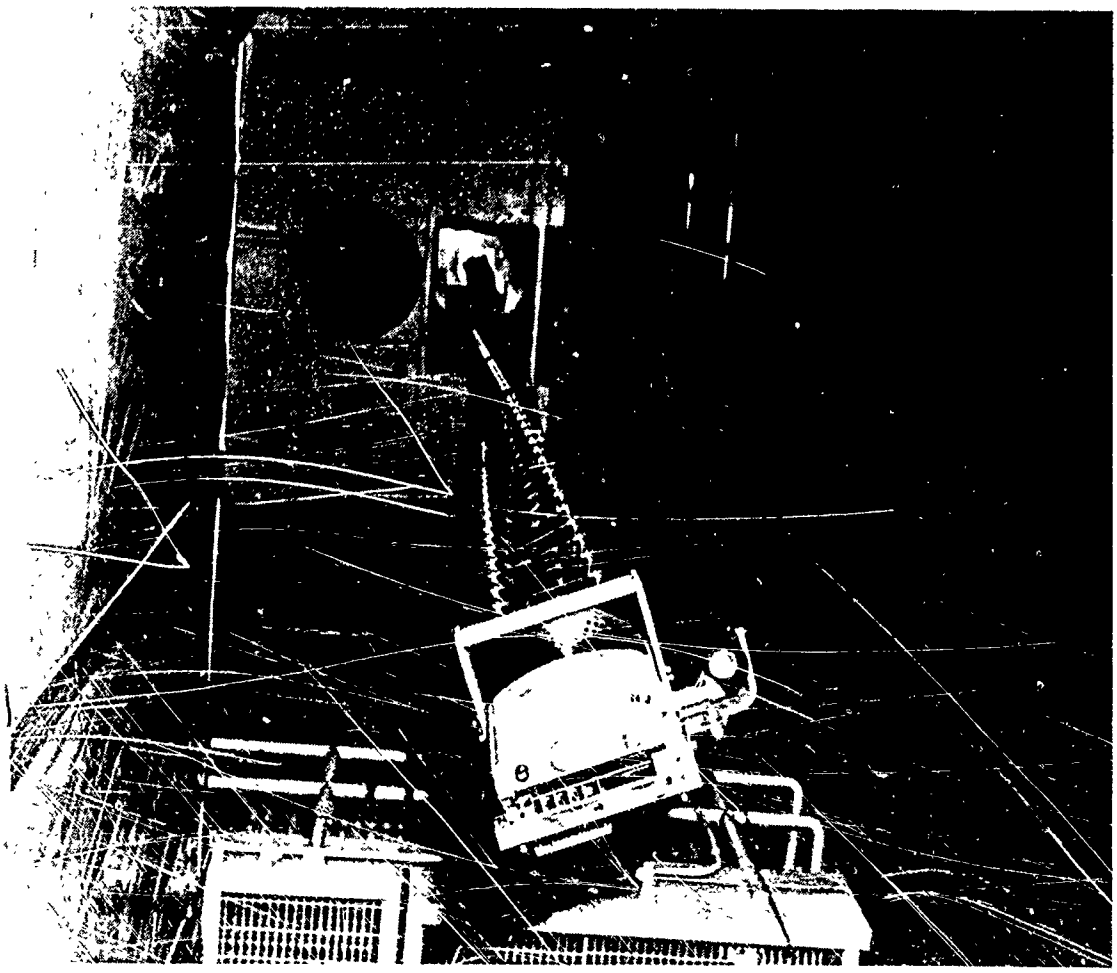

Figure 3

ACES PROGRAM DEVELOPMENT

With the analytical work and control hardware development completed under ACOSS and VCOSS, the next step was to utilize the available structure and hardware for comparing the control techniques. The Strategic Defense Initiative Organization (SDIO) was interested in evaluating the relative control performance of the techniques on the same structure and sensor/actuator hardware. The Active Control Evaluation for Spacecraft (ACES) program is designed to carry out this evaluation in a cooperative DOD/NASA effort (Figure 4). A portion of the ACES work will be contracted to Control Dynamics Company, who will prepare the structural hardware and control algorithms for testing in the Marshall facility.

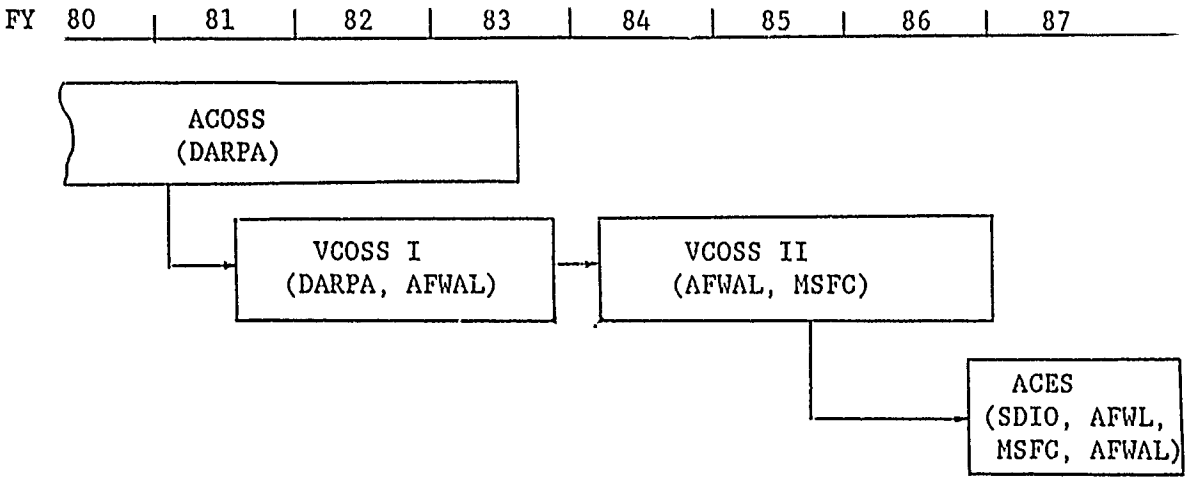

Figure 4

PROGRAM OBJECTIVES

The objective of ACES is to assess leading control techniques for large space structure vibration control (Figure 5) using a common structure and fixed configuration of sensors and actuators. These control techniques will be implemented in hardware and tested on the modified VCOSS structure with optical position sensors and proof mass actuators. The control objective is to minimize a line-of-sight pointing error between the structure's offset antenna and the end of the feed mast structure.

- IMPLEMENT AND ASSESS LARGE SPACE STRUCTURE CONTROL DESIGN TECHNIQUES
- TEST THE CONTROLLERS IN THE NASA-MSFC LSS GROUND TEST VERIFICATION (GTV) FACILITY
- MINIMIZE LINE-OF-SIGHT POINTING ERROR BETWEEN STRUCTURE'S ANTENNA AND FEED MAST

Figure 5

ACES STRUCTURE

For the ACES program, the VCOSS structure is configured with an offset antenna and counterbalance arm weights (Figure 6). The 13-meter truss structure is cantilevered vertically from a hydraulic shaker table and gimbal motors. Truss members are made from fiberglass and are connected such that a helical triangular cross section truss is created; the truss supports only tension loads. There are two bays, located at the midpoint and free end of the structure, for placement of control actuators. A laser source is mounted at the top of the structure and aimed at a mirror on the offset antenna; the reflected beam will be used as feedback by the controller to reduce the jitter to less than a specified line-of-sight error between the antenna and the end of the feed mast.

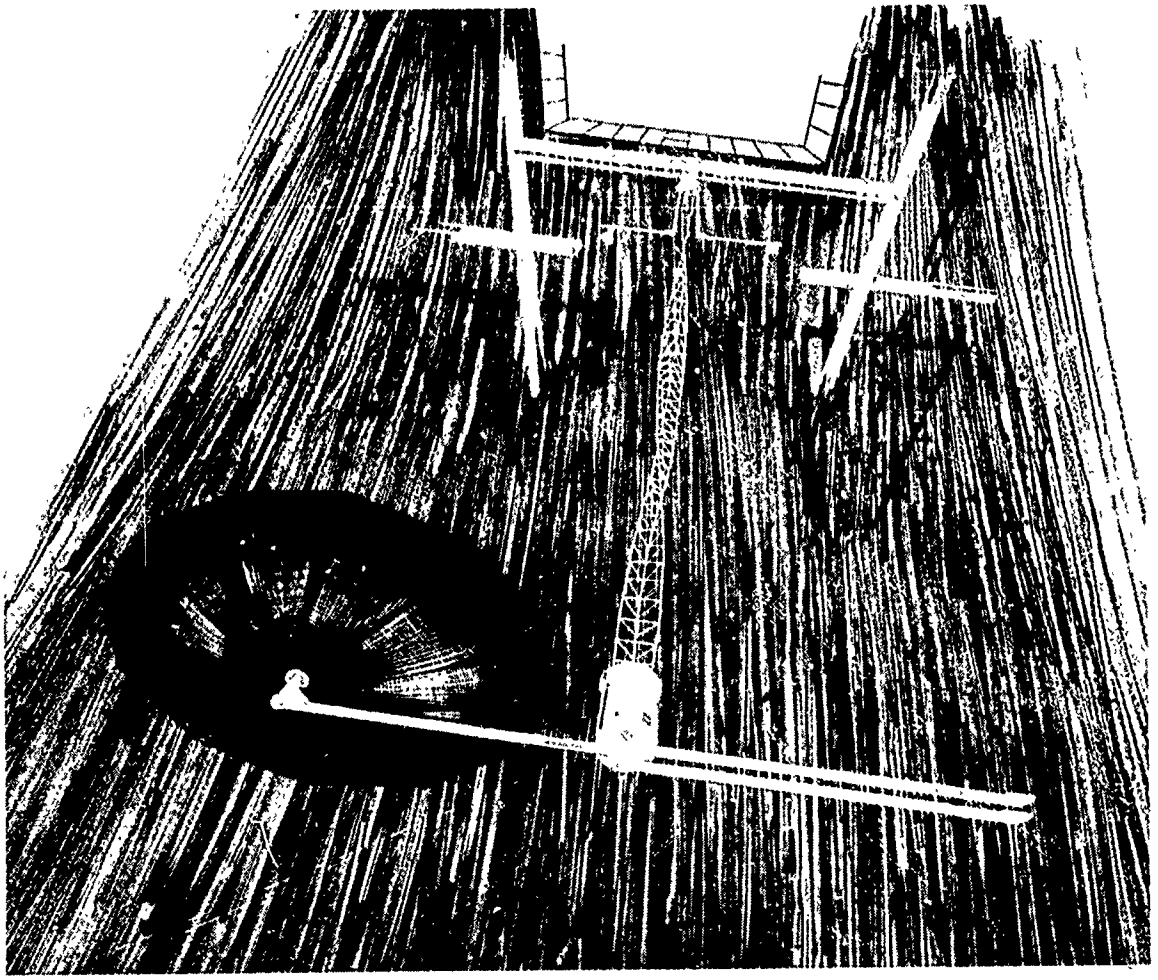

Figure 6

PROGRAM APPROACH

The first phase in the ACES program is to review and to assess the HAC/LAC and FAMESS control techniques for testing on the modified VCOSS structure (Figure 7). Appropriate sensors and actuators will be available for use with both techniques; locations will be the same for both techniques. The control actuators will be positioned at the midpoint and free end of the structure. The laser source for the optical sensor is mounted on the feed mast. The beam will be reflected from a mirror on the offset antenna onto the detectors mounted above the shaker table bay. The next phase is to develop an analysis simulation with the control algorithms implemented for dynamics verification. The third phase is to convert the control laws into high level computer language and test them in the NASA-MSFC facility. The final phase is to compile all analytical and test results for performance comparisons.

- REVIEW AND ASSESS PROPOSED TECHNIQUES FOR TESTING ON VCOSS II STRUCTURE
- SUPPORT DESIGN, FABRICATION, AND INSTALLATION OF NECESSARY HARDWARE
- APPLY TECHNIQUES TO STRUCTURAL MODEL USING VCOSS II SENSORS AND ACTUATORS
- DEVELOP A GENERIC SIMULATION TO EVALUATE PERFORMANCE OF CONTROL LAWS
- COMPILE ALL ANALYTICAL AND TEST RESULTS FOR PERFORMANCE COMPARISON

Figure 7

ACES SENSORS

The optical displacement sensors were developed in the VCOSS program and consist of two components: the laser source and the two-axis decenter receiver (Figure 8)

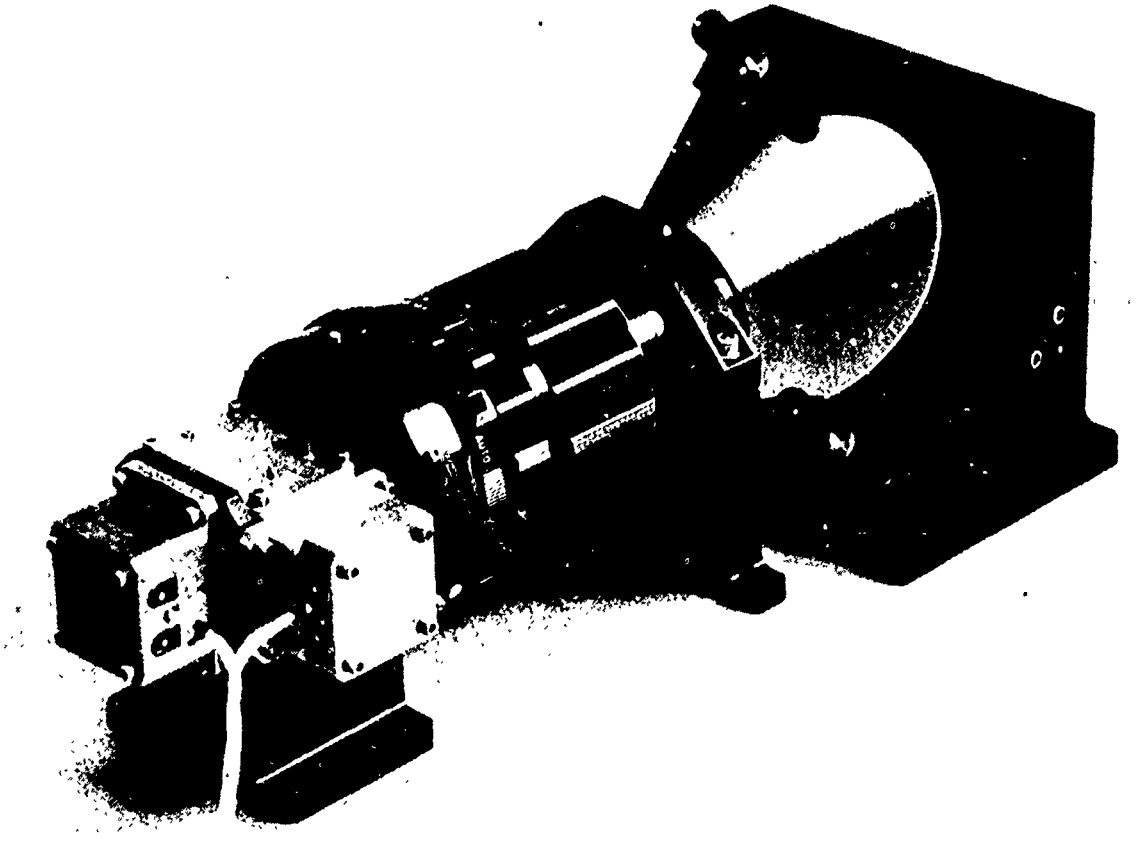

Figure 8

ACES ACTUATORS

The actuators were also developed under the VCOSS program. Each unit consists of a modified linear motor with the coil anchored on the structure and the magnet supported on a shaft and allowed to slide freely (Figure 9).

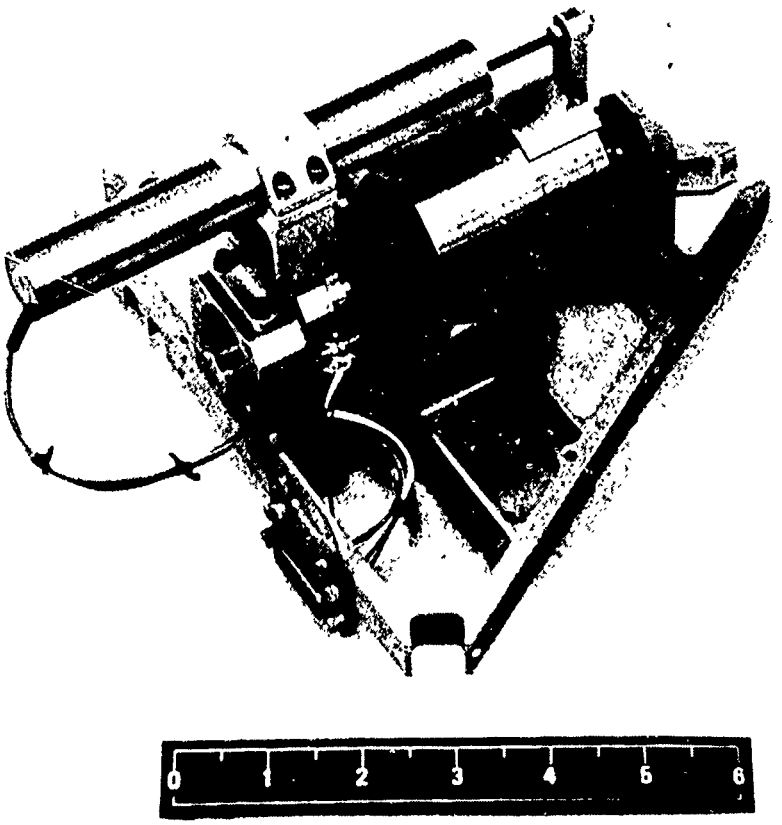

Figure 9

ACES CONTROL HARDWARE

Major components of the control hardware will be provided by NASA-MSFC. Existing hardware set up at the NASA facility for the testing includes a shaker table from which the structure is suspended, three-axis base accelerometers and gyros, and three-axis tip accelerometer and rate gyros (Figure 10). The base shaker table will be used to apply the two disturbance spectra to the ACES configured structure. A disturbance signal generator, gimbal torque amplifiers, and a system health monitor will be tied into a Hewlett Packard 9020 computer that is dedicated to control. The HP 9020 is also linked with NASA's mainframe COMSEC computer. Additional equipment to be added are bidirectional cold gas thrusters, an optical detector system, and two gimbal systems.

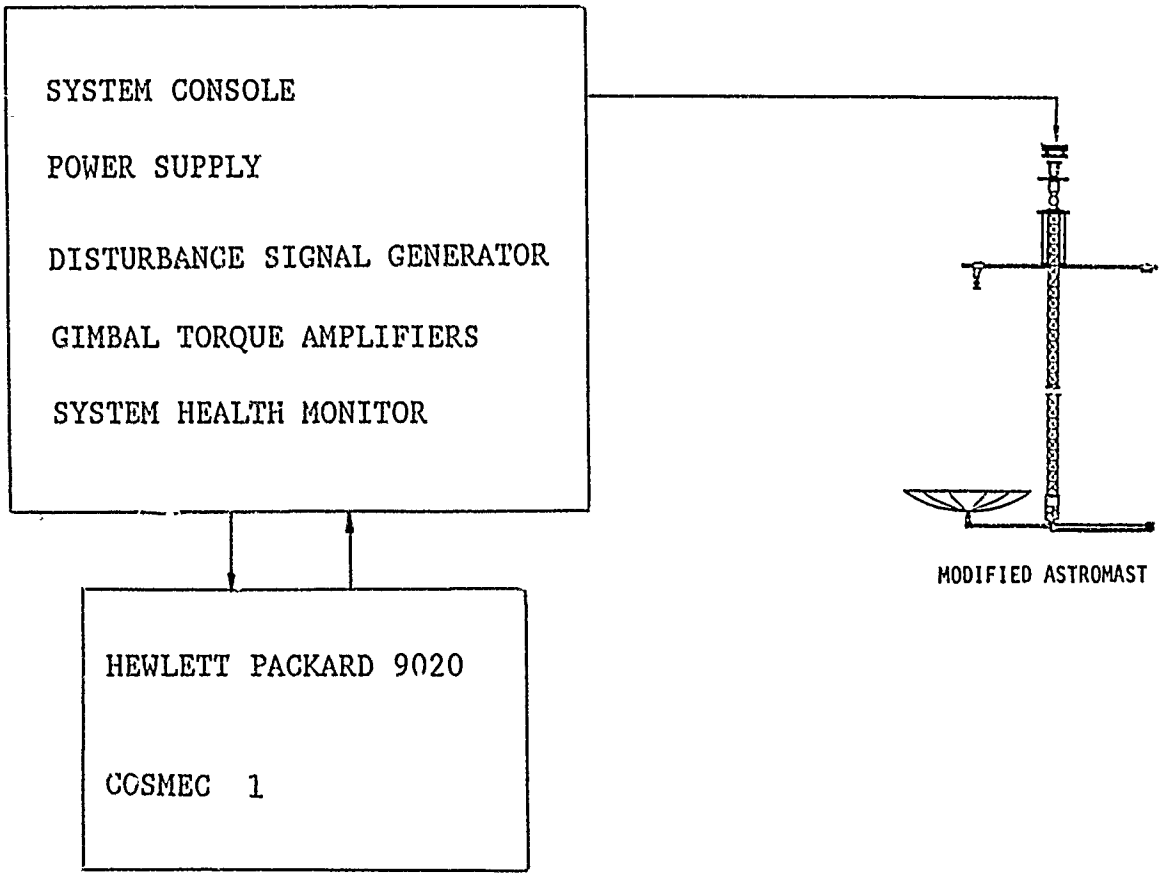

Figure 10

HIGH-AUTHORITY/LOW-AUTHORITY CONTROL TECHNIQUE

The HAC/LAC control technique, developed by Lockheed, addresses the particular problem of instabilities in the system created by spillover (Figure 11). Spillover is the interaction of the controller with unmodeled modes. The control design must not destabilize poorly known high frequency modes while controlling the low frequency modes. HAC/LAC approaches this problem on two levels. The HAC design incorporates high damping over a low bandwidth to meet performance goals; this is a frequency-shaped extension of LQG methods. The second level, the LAC design, incorporates low damping over a high bandwidth to eliminate spillover-induced instabilities (Ref. 4).

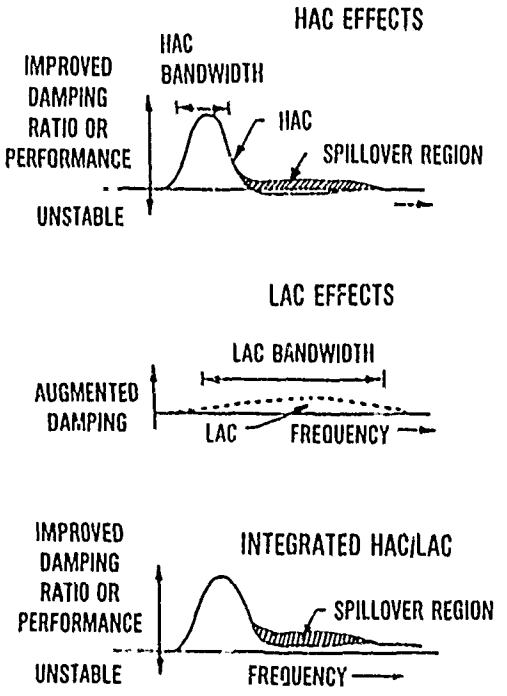

HIGH AUTHORITY

- LARGE DAMPING RATIO CHANGES
- EIGENVECTOR CHANGES
- LQG SYNTHESIS WITH FREQUENCY SHAPING
- ENHANCED CONVENTIONAL LQG ROBUSTNESS

LOW AUTHORITY

- BROADBAND DAMPING AUGMENTATION
- ROBUST AGAINST MODELING ERROR
- SIMPLIFIED SYNTHESIS (LEAST SQUARES, JACOBI'S PERTURBATION)

Figure 11

POSITIVITY CONTROL TECHNIQUE

The Positivity method, developed by TRW, addresses the stability of control system designs based on inaccurate structural models (Figure 12). The Positivity theorem requires that the plant matrix be positive real and the controller matrix be strictly positive real for a stable system. To be positive real, the real part of a transfer function as a function of frequency is always greater than or equal to zero. To be strictly positive real, the real part is always greater than zero. The positivity of a system is determined either in the time or frequency domain. The time domain test uses B.D.O. Anderson's positivity criterion. Application of this test results in the observation that the transfer matrix of the plant is positive real if ideal colocated sensors and actuators are used. Actuator and sensor dynamics are difficult to include with this test, unless a frequency domain test is used. If the plant matrix is determined to be non-positive, an embedding operator must be incorporated to make the plant matrix positive (Ref. 4).

DESIGN STEPS:
1. ENSURE PLANT MATRIX IS POSITIVE REAL
2. DESIGN CONTROLLER MATRIX THAT IS STRICTLY POSITIVE REAL

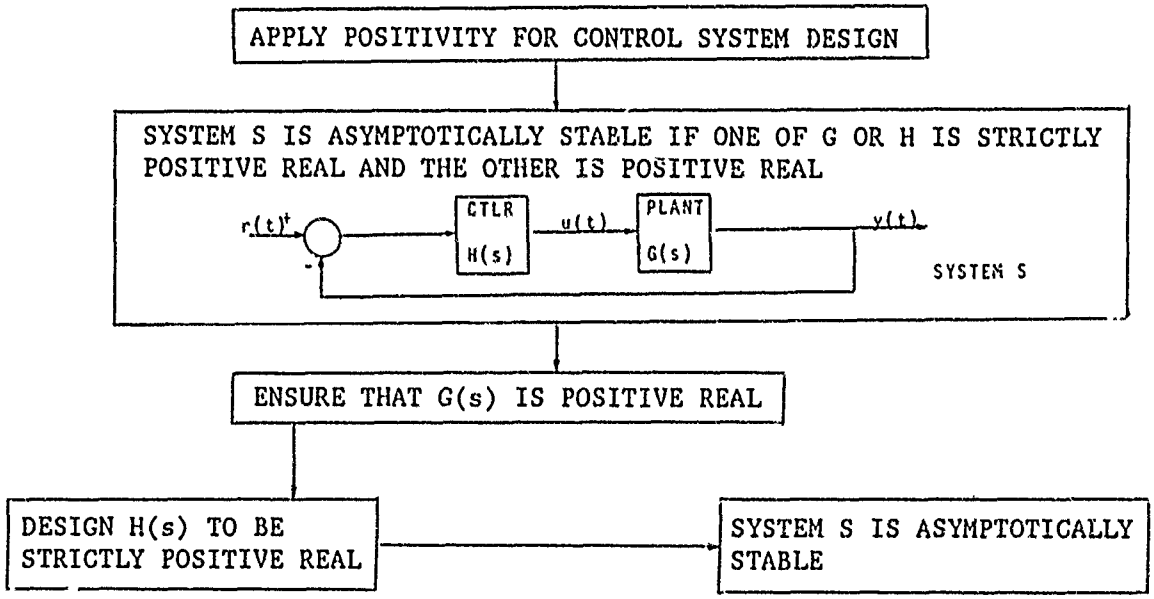

Figure 12

DISTURBANCE SPECTRUM

A disturbance spectrum that would excite all the vibration modes of interest was developed in the ACOSS program and will be used in the ACES effort (Figure 13).

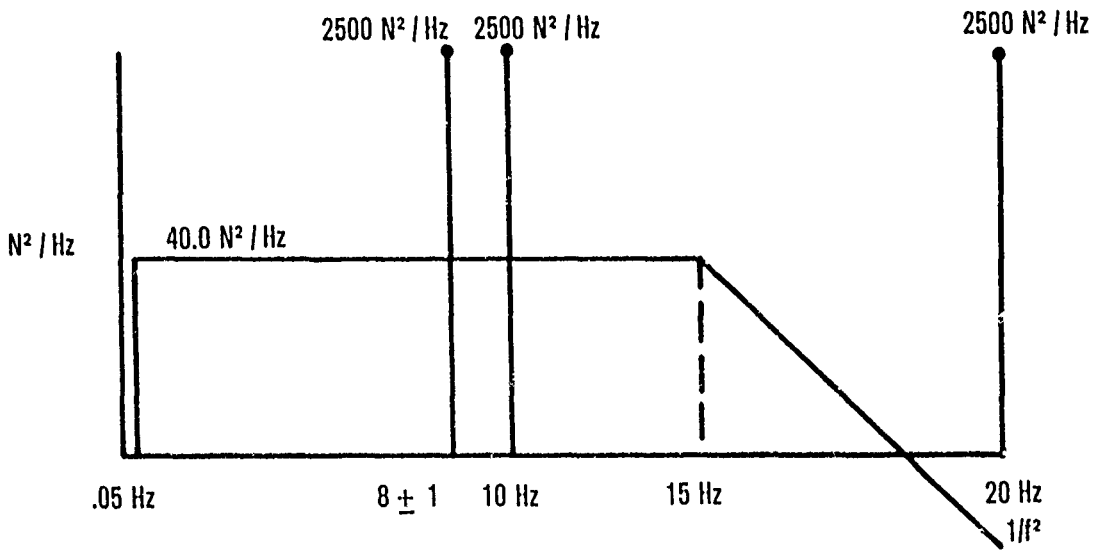

Figure 13

CONTROL CRITERIA

The goal of this test is to have the controller minimize line-of-sight error between the antenna and the feed mast (Figure 14). In minimizing this error, several criteria will be considered in evaluating each technique's performance. These will include total reduction of line-of-sight error, computational efficiency (meeting the speed and memory requirements of the available digital system), and robustness (controller performance for off-optimum structural parameters). These criteria will be applied to both disturbance spectra.

- MINIMIZE ANTENNA/FEED MAST LINE-OF-SIGHT POINTING ERROR
- DETERMINE PERFORMANCE OF CONTROL TECHNIQUES:
  - ROBUSTNESS
  - COMPUTATIONAL EFFICIENCY

Figure 14

PROGRAM RESULTS

The results of this evaluation will give a better understanding of the trade-offs involved with each control technique (Figure 15). With the number and location of sensors and actuators fixed and the control goal specified, a good evaluation of the techniques can be performed. By eliminating particular sensors or actuators and observing how well the control techniques respond to this change in the system, robustness will be determined. The control design must meet the requirements of the digital system in terms of computational speed and memory capacity. The effects of sampling and computational lags should also be accounted for by the control technique. The degree of line-of-sight error correction will determine the limits of control technique capability with the available hardware.

- BETTER UNDERSTANDING OF CONTROL TECHNIQUE TRADE-OFFS
- ROBUSTNESS, COMPUTATIONAL EFFICIENCY, AND PERFORMANCE OF TECHNIQUES DETERMINED
- A COMPARISON OF THE TECHNIQUES PERFORMED

Figure 15

PROGRAM APPLICATIONS

The payoff from this program will be twofold. Capabilities of these control techniques will be better understood, and these techniques may then be applied to specific control problems in other programs (Figure 16). The Air Force Weapons Laboratory plans to use the results of this program in determining a control technique for their Joint Optics/Structures Experiment (JOSE) program. AFWAL plans to incorporate one of the ACES techniques into the Large Space Structure Active Vibration Control program and into their in-house Large Space Structure Technology Program. The results from the ACES evaluation will also increase the confidence in each technique.

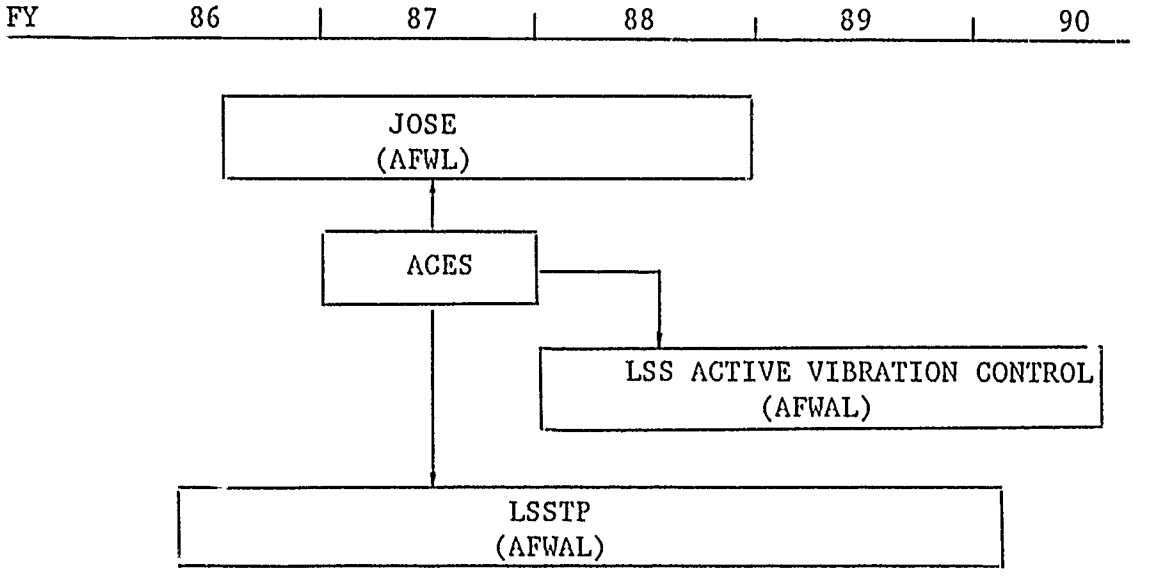

Figure 16

REFERENCES

1. Lockheed Missiles & Space Company, Inc: Vibration Control of Space Structures VCOSS A: High and Low-Authority Hardware Implementation. AFWAL-TR-83-3074, July 1983.

2. TRW Space and Technology Group: Vibration Control of Space Structures VCOSS B: Momentum Exchange and Truss Damping. AFWAL-TR-83-3075, July 1983.

3. TRW : Vibration Control of Space Structures (VCOSS II). AFWAL-TR-86-3073, 1986.

4. Control Dynamics Company: ACOSS Seventeen (Active Control of Space Structures). RADC-TR-84-186, Sept. 1984.

PACOSS PROGRAM OVERVIEW AND STATUS

L. C. ROGERS
AIR FORCE WRIGHT AERONAUTICAL LABORATORIES

and

K. E. RICHARDS, JR.
MARTIN MARIETTA DENVER AEROSPACE
DENVER, COLORADO

NASA/DOD CSI TECHNOLOGY CONFERENCE
NOVEMBER 18-21, 1986

INTRODUCTION

Many future civilian and military large space structures (LSS) will have as performance objectives stringent pointing accuracies, short settling times, relatively fast response requirements, or combinations thereof. Many of these structures will be large, light weight, and will exhibit high structural modal density at low frequency and within the control bandwidth. The attainment of the performance objectives will be a challenge to the controls engineer.

Although it is possible in principle to achieve structural vibration control through purely active means, experience with complex structures has shown that the realities of plant model inaccuracies and sensor/actuator dynamics frequently combine to produce substandard performance.

A more desirable approach is to apply passive damping technology to reduce the active control burden. Development of the technology to apply this strategy is the objective of the PACOSS (Passive and Active Control Of Space Structures) program (Figure 1).

- FUTURE LARGE SPACE STRUCTURES (LSS) WILL REQUIRE STRUCTURAL VIBRATION CONTROL TO ACHIEVE PERFORMANCE GOALS

- VIBRATION DAMPING MAY BE ACHIEVED BY PASSIVE OR ACTIVE MEANS, OR BOTH

- MAJOR GOALS OF PACOSS PROGRAM
  - DEMONSTRATE ROLES OF PASSIVE AND ACTIVE CONTROL FOR FUTURE LSS
  - DEVELOP MEANS OF PASSIVE VIBRATION CONTROL
  - EXPERIMENTALLY VERIFY DAMPING PREDICTIONS AND CONTROL ALGORITHMS

Figure 1

OUTLINE

A key element in the PACOSS program is the Representative System Article (RSA). The RSA is a generic "paper" system that serves as a testbed for damping and controls studies. It also serves as a basis for design of the smaller Dynamic Test Article (DTA), a hardware testbed for the laboratory validation of analysis and design practices developed under PACOSS. These topics will be discussed in greater detail (Figure 2).

- PACOSS REPRESENTATIVE SYSTEM ARTICLE (RSA)
- PASSIVE/ACTIVE CONTROL STUDY
- PACOSS DYNAMIC TEST ARTICLE (DTA)
- DTA TEST PLAN AND STATUS
- CONCLUSIONS

Figure 2

RSA PURPOSE

The PACOSS program is generic in nature in that the damping technology being developed applies to a broad spectrum of future LSS. The RSA must contain the dynamic characteristics to be found in future systems, including the dense modal spectrum. It should contain substructures found in future LSS concepts to permit direct application of damping treatments and devices developed under PACOSS to real future systems.

The RSA also serves as the link between the DTA, the hardware test article, and future LSS. Concepts tested and validated under 1-g conditions can be evaluated under on-orbit conditions by applying proven designs to the analytic RSA model (Figure 3).

- TRACEABLE TO REAL FUTURE SPACE SYSTEMS
  - CONTAINS SUBSTRUCTURES FOUND ON FUTURE LSS
  - CONTAINS HIGH MODAL DENSITY AND ASSOCIATED DYNAMICS PROBLEMS OF FUTURE LSS
- GENERIC STRUCTURE FOR ANALYTIC DEMONSTRATION OF VARIOUS CONTROL APPROACHES
- SERVES AS A LINK BETWEEN FUTURE LSS AND THE DYNAMIC TEST ARTICLE (HARDWARE)

Figure 3

REPRESENTATIVE SYSTEM ARTICLE (RSA) DESIGN

The utility of the RSA concept is in direct proportion to the number of future systems that it represents. To obtain a broad base for the design, the Military Space Systems Technology Model (MSSTM) and the corresponding NASA document (NSSTM) were examined to determine which structures and missions would benefit from passive damping technology (Reference 1). In all, it was determined that 13 future military systems and six future NASA systems would benefit from the application of passive augmentation (Figure 4).

- REVIEW MILITARY SPACE SYSTEMS TECHNOLOGY MODEL AND NASA EQUIVALENT
- DETERMINE SYSTEMS REQUIRING STRUCTURAL VIBRATION CONTROL
- DETERMINE WHICH DYNAMIC CHARACTERISTICS ARE GENERIC AND IMPORTANT FOR FUTURE LSS
- INCORPORATE THESE DYNAMIC CHARACTERISTICS INTO RSA DESIGN

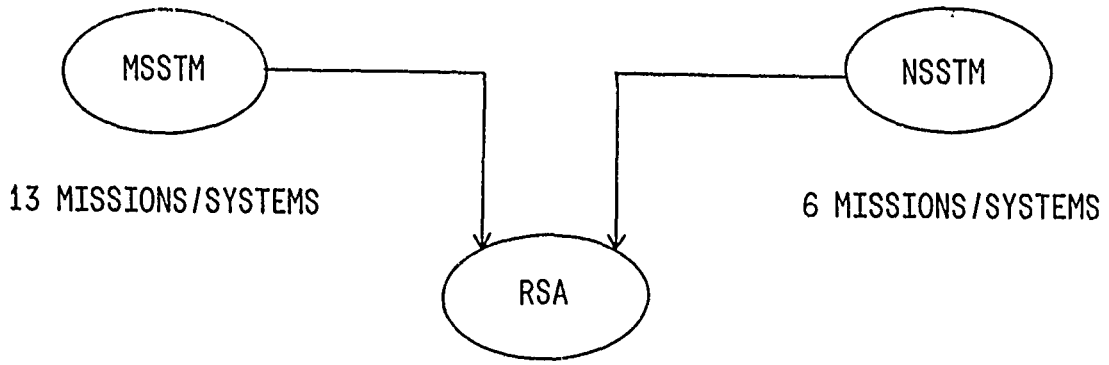

Figure 4

RSA COMPONENT SUMMARY

The substructures comprising the RSA and their respective sizes are shown in Figure 5, as well as some of the applicable future systems. It should be noted that the ring truss is the "hardback" for the system, and as such was not considered for passive damping treatments.

Each of the other components is a candidate for passive damping treatments and devices. The damping design is done at the component or substructure level, and thus is applicable to the parent real system. Naturally, the damping achieved in the overall system modes is determined by the damping in the substructure modes as well as the degree of participation of the substructure modes in the system modes.

COMPONENT	DIMENSIONS, M	APPLICABLE SYSTEMS
BOX TRUSS	20 x 20 x 2.5	SPACE-BASED RADAR LARGE EARTH OBSERVING SYSTEM SPACE STATION
RING TRUSS	DIA: 22.4	GENERIC TRUSS STRUCTURE
TRIPOD	DIA AT BASE: 20 HEIGHT: 20	SPACE-BASED LASER LARGE DEPLOYABLE DEFLECTOR
EQUIPMENT PLATFORM	LENGTH: 10	SPACE STATION
ANTENNA	DIA: 5	SPACE-BASED RADAR SPACE STATION
SOLAR ARRAYS	LENGTH: 20	SPACE-BASED RADAR SPACE STATION

Figure 5

REPRESENTATIVE SYSTEM ARTICLE (RSA)

Figure 6 is an artist's concept of the on-orbit RSA. All seven substructures are shown. The overall largest dimension is approximately 60 meters.

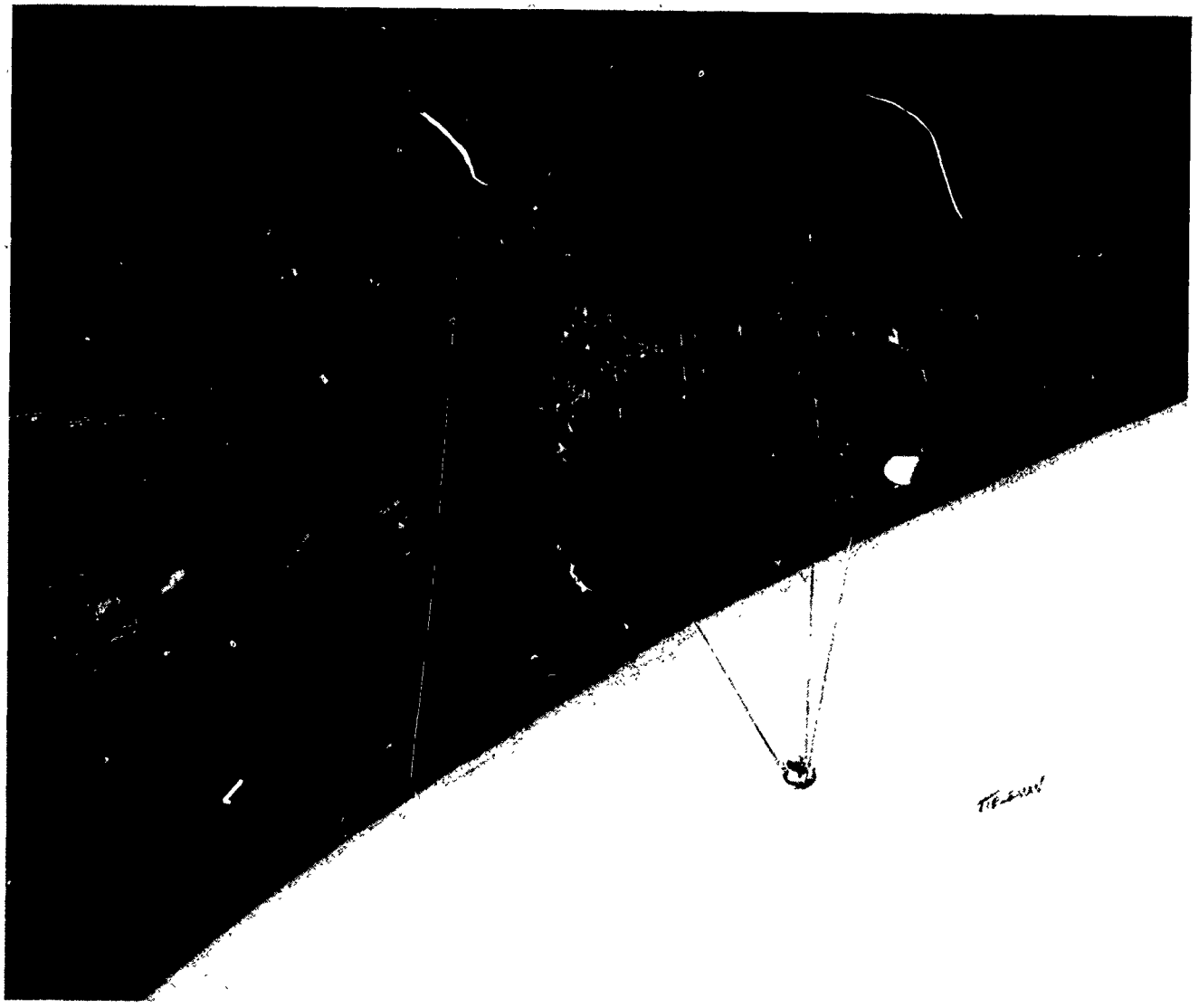

Figure 6

COUPLED SYSTEM ANALYSIS

The system normal modes were calculated with the Craig-Bampton technique. Substructure normal modes below 15 Hz and all constraint modes were used in the synthesis.

The results of the coupling produced in excess of 200 modes below 10 Hz. Many of the modes are local in nature, but there are still 34 global modes with significant modal strain energy contained in two or more substructures (Figure 7).

- CRAIG-BAMPTON COUPLING (FREQUENCY CUTOFF 15 Hz)
- 210 SYSTEM MODES BELOW 10 Hz
- 34 "GLOBAL" SYSTEM MODES

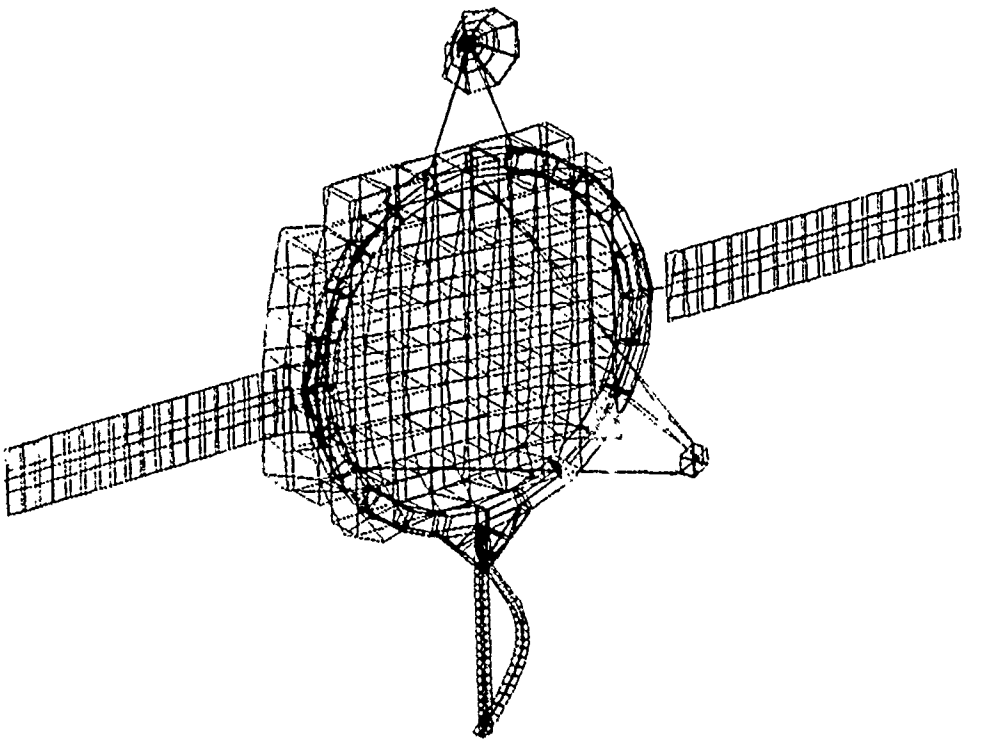

Figure 7

CONTROL SYSTEM/PASSIVE DAMPING STUDY

To demonstrate the benefits of passive damping on RSA performance and to select target levels for passive damping design, a simple control study was undertaken (Figure 8 and Reference 2).

The controlled variables were system line of sight (LOS), which will be defined on a later chart, and attitude. A 0.01 radian slew maneuver was commanded, and the system was considered to have settled when LOS excursions remained in a 100-microradian (zero-peak) band.

The RSA is not a real system, and selection of the desired settling time is somewhat arbitrary. It was decided to select rigid-body control torque levels producing reasonable settling times of 3.25 seconds for the pitch (about the solar arrays) axis and 5.0 seconds about the yaw (perpendicular to pitch and LOS) axis for the rigid RSA. These times then became performance requirements for the flexible system.

Various realizable levels of passive damping were designed into the system, and active modal control was utilized as required to achieve the performance goals. Total control energy for the maneuver was calculated for each passive/active combination.

- CONTROL LINE OF SIGHT DURING SLEW
- SELECT DESIRED PERFORMANCE FROM RIGID-BODY RESPONSE
- FOR VARIOUS LEVELS OF REALIZABLE PASSIVE DAMPING, DETERMINE CONTROL ENERGY REQUIRED TO ACHIEVE DESIRED PERFORMANCE
- USE ACTIVE MODAL CONTROL ONLY AS REQUIRED

Figure 8

LINE-OF-SIGHT DEFINITION

Figure 9 defines the LOS as used in this study. Note that the LOS response due to primary reflecting surface deformation is approximated by an average of selected rotations on the box truss.

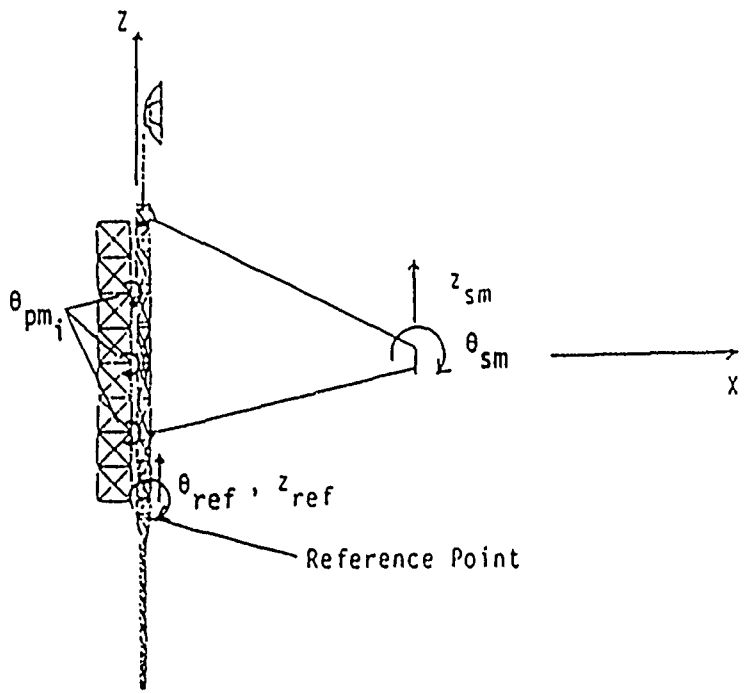

$$LOS_y = \left(2\frac{f_s}{f_p} - 1\right)\theta_{ref} + \frac{2}{13}\sum_{i=1}^{13}\theta_{pm_i} - 2\frac{f_s}{f_p}\theta_{sm} - \frac{1}{f_p}(z_{ref} - z_{sm})_{flex}$$

Where

f_s = Focal length of secondary mirror

f_p = Focal length of primary mirror

$(z_{ref} - z_{sm})_{flex}$ = Relative z deflection of secondary mirror to reference point due to structural deformation

Figure 9

SENSOR/ACTUATOR LOCATIONS (PITCH DYNAMICS MODEL)

Figure 10 shows the sensor/actuator locations and the selection criterion for their location. Symmetry of the structure results in pitch and yaw dynamics being uncoupled. The ten symmetric modes with the highest gain into LOS were retained for the pitch study, and the nine antisymmetric modes with highest gain into LOS were retained for the yaw-axis simulation.

A nominal modal damping level of 0.2% viscous was assumed to represent the untreated structure. It should be noted that, without additional active augmentation, this system exhibited a mild instability due to the presence of a low pass filter in the attitude control system, which had a 1-Hz cutoff frequency.

In the pitch case, it was determined that for low levels of passive damping, modal control was required for six modes. As the amount of passive augmentation was increased, the number of modes requiring active augmentation was reduced to two.

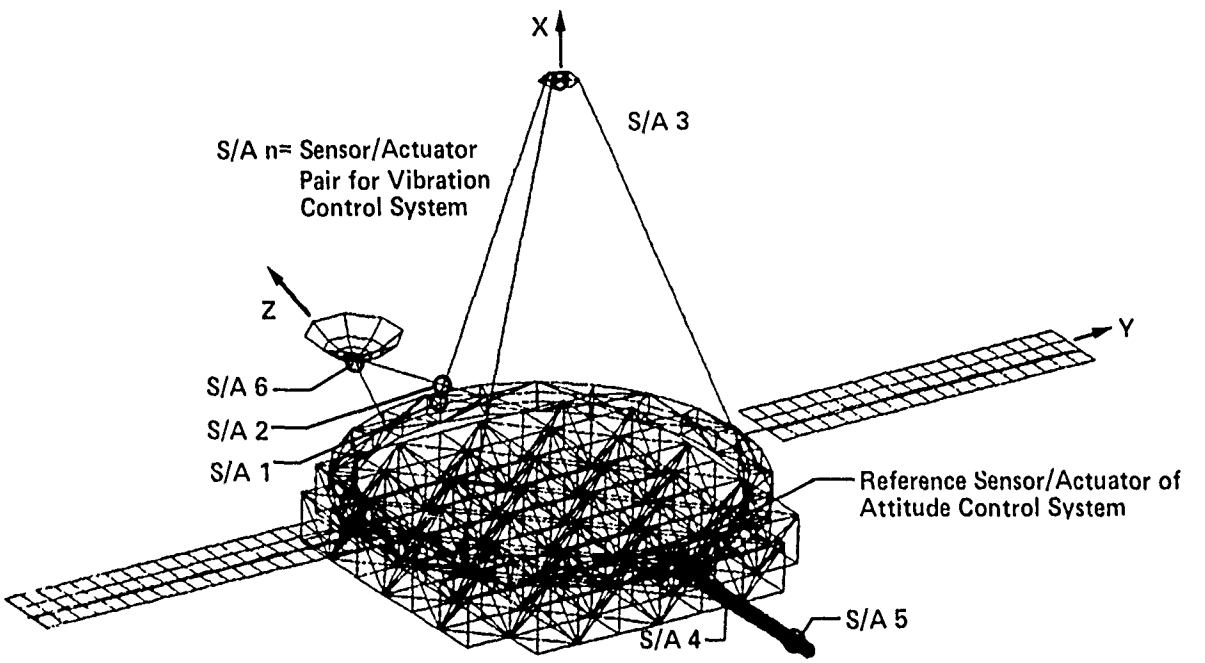

- IDEAL ANGULAR RATE SENSORS AND TORQUE WHEELS
- LOCATIONS SELECTED TO GIVE $(\phi_{REL})_C$ THE LARGEST DETERMINANT
- 6 S/A PAIRS REQUIRED FOR ACTIVE DAMPING ALONE
- 2 S/A PAIRS USED FOR PASSIVE + ACTIVE DAMPING ABOVE CERTAIN LEVELS

Figure 10

LOS RESPONSE TO 0.01 rad SLEW

When designing damping treatments, the analyst utilizes the modal strain energy (MSE) method to design a damping treatment to produce the desired amount of damping in a target mode. There is "damping spillover" into other modes, wherein non-target modes also receive some damping. Thus, each mode will receive in general a different level of damping.

Figure 11 shows the LOS response for different levels of average modal damping for the modes included in the simulation. Note that, for low levels of average passive damping, six-mode active control was used. Higher levels required active control of only two modes. It is obvious that the settling times for all systems are virtually identical.

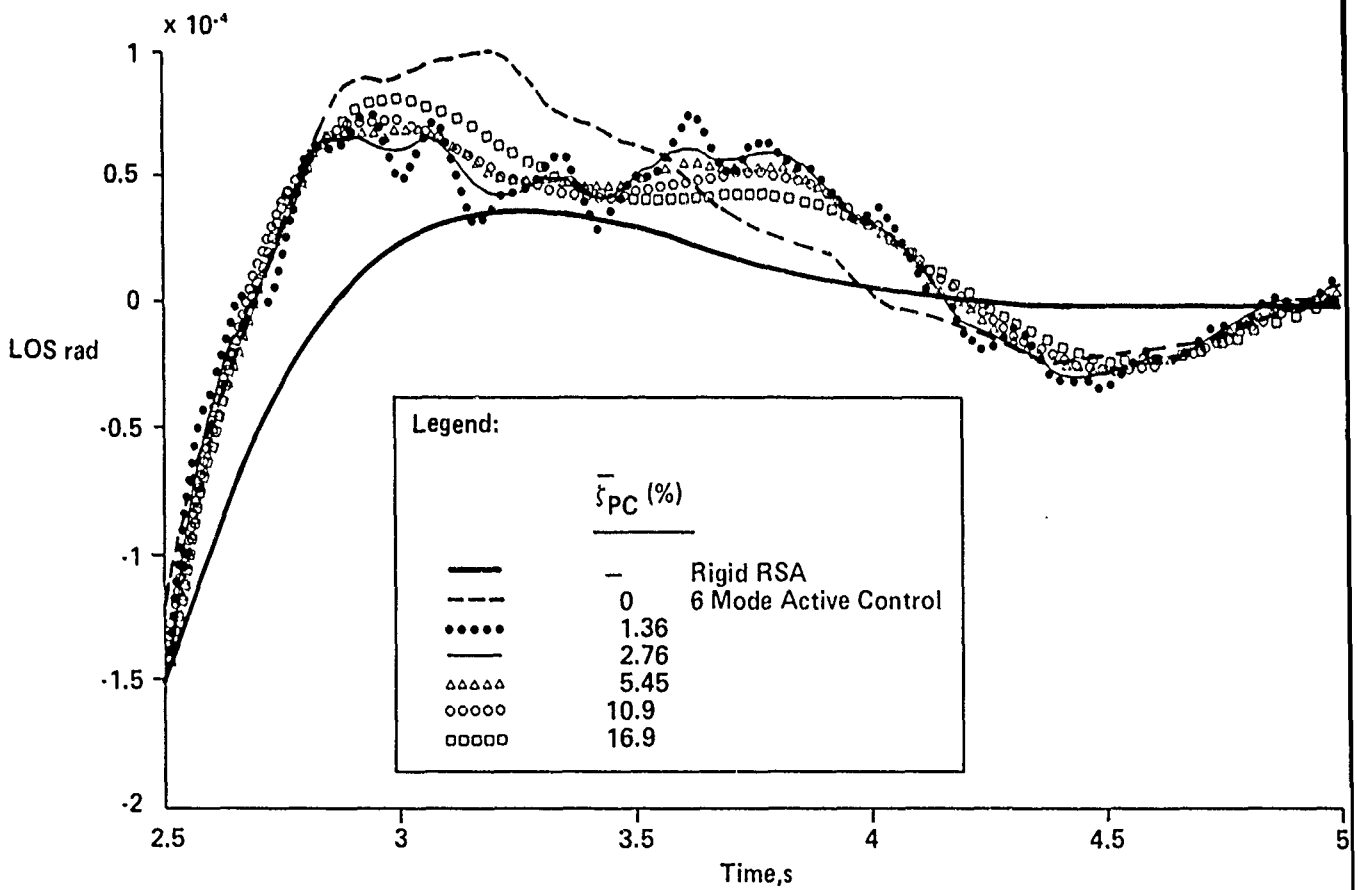

Figure 11

The control energy requirements for the pitch-axis simulation are shown in Figure 12, where the energy has been normalized to the value required for the 0.2% nominally damped (untreated) system.

Two horizontal scales have been furnished. The lower scale is the average level of passive damping for all modes in the system. This scale is of interest for low levels of passive damping in which active augmentation is required for six modes.

The upper scale is the average level of passive damping for the first two modes. Above the level of passive damping for which two-mode active control is sufficient, the response is dominated by these modes, and increasing the damping level on the passively controlled modes produces little effect on system performance.

The PACOSS DTA design goal was selected to be an average damping value of 5%. At this level, the RSA requires only one third of the control energy of the untreated system for pitch-axis control. A similar study for the yaw axis resulted in an even greater reduction.

Active Control Energy Expenditure

vs

Passive Damping Augmentation

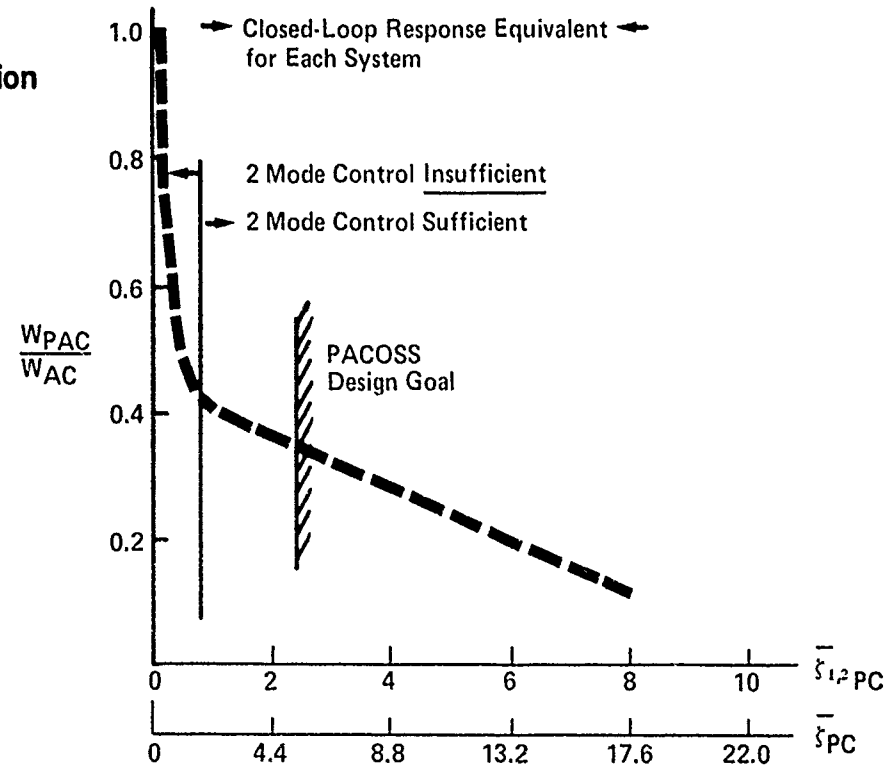

Figure 12

BENEFITS

The benefits of the passive/active control strategy on the system level are obvious (Figure 13). With reduced sensor/actuator requirements, the system becomes simpler, less expensive, and more reliable. Reduction in control system complexity results in weight savings, both for the control components as well as reduced structural strength because of the lower control torque levels. These savings, together with increased robustness and reliability will compensate for, if not totally offset, the weight of the viscoelastic damping treatments.

It is essential, however, that the structure be designed for passive damping augmentation. It is inefficient to post-treat an existing structure.

- PASSIVE + ACTIVE DAMPING GIVES DESIRED PERFORMANCE WHILE
  - REDUCING NUMBER OF ACTIVE CONTROL COMPONENTS
  - REDUCING ENERGY AND POWER REQUIREMENTS
- THIS CAN LEAD TO
  - MORE ROBUST AND RELIABLE SYSTEMS
  - LESS EXPENSIVE SYSTEMS
- FUTURE LSS SHOULD BE DESIGNED TO FACILITATE PASSIVE DAMPING TECHNOLOGY

Figure 13

DYNAMIC TEST ARTICLE (DTA) REQUIREMENTS

The DTA design was chosen to be dynamically similar to the RSA and will serve as a hardware validation of design and analysis techniques for passive damping treatments. The requirements shown in Figure 14 have been selected to assure traceability to the RSA within the realities of the test environment and budgetary constraints. In addition, a program requirement is that the DTA be space-qualifiable. Among other implications, delivery in a single Shuttle flight was assumed.

- VALIDATION OF DAMPING TREATMENT DESIGN AND ANALYSIS TECHNIQUES
- DYNAMICALLY SIMILAR TO RSA
- DELIVERABLE TO ORBIT AS SINGLE SHUTTLE PAYLOAD
- NEGLIGIBLE UNPREDICTED DAMPING
- SUITABLE FOR 1-G TEST
- EASILY AND INEXPENSIVELY FABRICATED

Figure 14

DTA DESIGN APPROACH

The DTA was designed to be essentially a scaled-down version of the RSA. Because of the 1-g test environment, it was necessary to shift the fundamental frequency upward by approximately 2 Hz. This will provide for a structure that can withstand the 1-g test environment, but will not compromise the control interaction aspects of the dynamics because the control bandwidth will be shifted accordingly.

Low-cost materials are being used to the maximum extent possible, but careful fabrication techniques are being utilized to assure that the structure is well known. In addition, the design is such that inadvertent sources of damping are avoided (Figure 15).

- ACHIEVE SIMILAR DYNAMIC CHARACTERISTICS ON COMPONENT LEVEL IN CONSTRAINED MODES
- GEOMETRIC SCALE FACTOR OF 1:7.72
- FREQUENCY SHIFT OF 2 Hz FOR DENSE BANDWIDTH
- USE SCALED-DOWN MEMBER CROSS SECTION
- ELIMINATE PIN JOINTS
- MINIMIZE AIR RESISTANCE
- ACCURATELY MODEL SUSPENSION MECHANISM AND INCLUDE EFFECTS OF GRAVITY ON COUPLED SYSTEM
- LOW-COST MATERIALS IN STANDARD SIZES
- STANDARD FABRICATION PROCESSES

Figure 15

SUMMARY OF FINAL DTA DIMENSIONS

The status of the DTA design at the time of this writing is shown in Figure 16, together with the component sizes and weights.

The ring truss has been fabricated and tested, and results are presented herein. This structure, as mentioned previously, was designed to have very low damping. Bonded joints were used extensively to simulate more expensive, precision hardware.

The tripod was designed to be heavily damped, with both constrained-layer damping treatments on the legs and novel viscoelastic rotational dampers for the secondary mirror. At the time of this writing, testing has not been completed.

COMPONENT	DIMENSION (M)	MASS (KG)
1) BOX TRUSS	2.59 x 2.59 x 0.324	180.5
*2) RING TRUSS	DIAMETER: 2.9	59.7
**3) TRIPOD	DIAMETER AT BASE: 2.59 HEIGHT: 2.59	29.9
4) EQUIPMENT PLATFORM	LENGTH: 1.295	7.04
5) ANTENNA	DIAMETER: 0.648	4.52
6,7) SOLAR ARRAYS	LENGTH: 2.59	12.0

* FABRICATED AND TESTED
** FABRICATED

Figure 16

DTA FINITE ELEMENT MODEL

The DTA finite element model is shown in Figure 17. Note that the extremely soft solar arrays have been rotated to lie in the plane of the gravity vector in the test configuration. This compromise was necessary to avoid buckling during test.

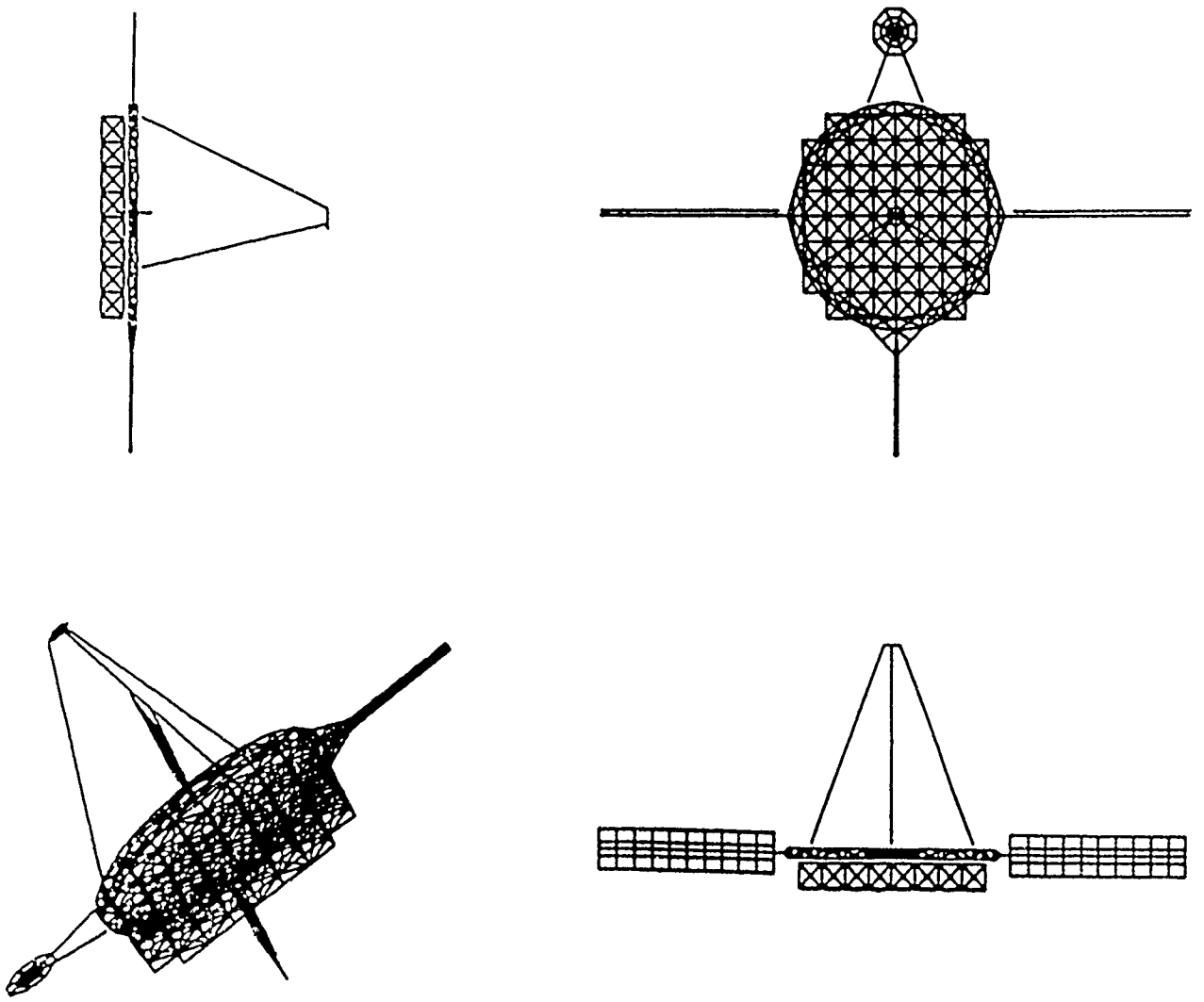

Figure 17

DTA TEST PROGRAM

An extensive test program is planned for the DTA, beginning at the component level (Figure 18). Each component will undergo a modal survey. As mentioned previously, the Craig-Bampton technique is used for system synthesis. For this reason, fixed-interface boundary conditions will be used for the appendage modal surveys.

The ring truss modal survey has been completed, and was done with the ring truss interfaces loaded with mass simulators. The ring truss response is critical to the overall system, and this approach was deemed most suitable to check the critical interface modeling.

In addition, the ring truss survey served to verify that inadvertent damping can be avoided with careful fabrication techniques. This test also served as a check on the suspension system, which will be described later.

After the component modal surveys are completed and analytic models refined as necessary, the DTA will be assembled and a system-level modal survey will be accomplished. Finally, a control system will be installed and closed-loop dynamic response tests will be performed.

- MODAL SURVEY OF EACH INDIVIDUAL COMPONENT
  - RING TRUSS "FREE-FREE" WITH MASS LOADING AT INTERFACES
  - APPENDAGES WITH FIXED INTERFACES
- MODAL SURVEY OF ASSEMBLED DTA
- CLOSED-LOOP TRANSIENT RESPONSE TESTS

Figure 18

DTA RING TRUSS MODAL SURVEY

The ring truss modal survey was completed in August. For the test, the truss was mass loaded and suspended by a zero spring rate mechanism (ZSRM) from long cables. This system resulted in three virtually zero frequency rigid-body modes and three approximately 0.20-Hz pendulum modes. The ZSRM suspension produced very little restraint in the vertical direction, effectively simulating a free condition for vertical motion.

Three separate excitation points were choser to assure that good data were obtained for all modes of interest. In addition, tuned decay tests were undertaken to achieve accurate damping data.

- SUSPENDED FROM THREE ZERO SPRING RATE DEVICES
  - VIRTUALLY NO RESTRAINT IN VERTICAL DIRECTION
  - THREE PENDULUM MODES OF APPROXIMATELY 0.25 Hz
- APPENDAGES REPLACED WITH MASS SIMULATORS TO LOAD INTERFACES
- SINGLE-POINT RANDOM EXCITATION AT THREE DIFFERENT DRIVE POINTS
- TUNED DECAY TESTS TO BETTER ESTIMATE DAMPING

Figure 19

The ring truss modal survey was performed in the Martin Marietta Reverberant Acoustic Lab (RAL). This chamber (Figure 20) provides a quiet temperature-controlled environment. Temperature control is essential for future tests where viscoelastic damping treatments are to be used.

Note the suspension system with the ZSRMs on the overhead beams.

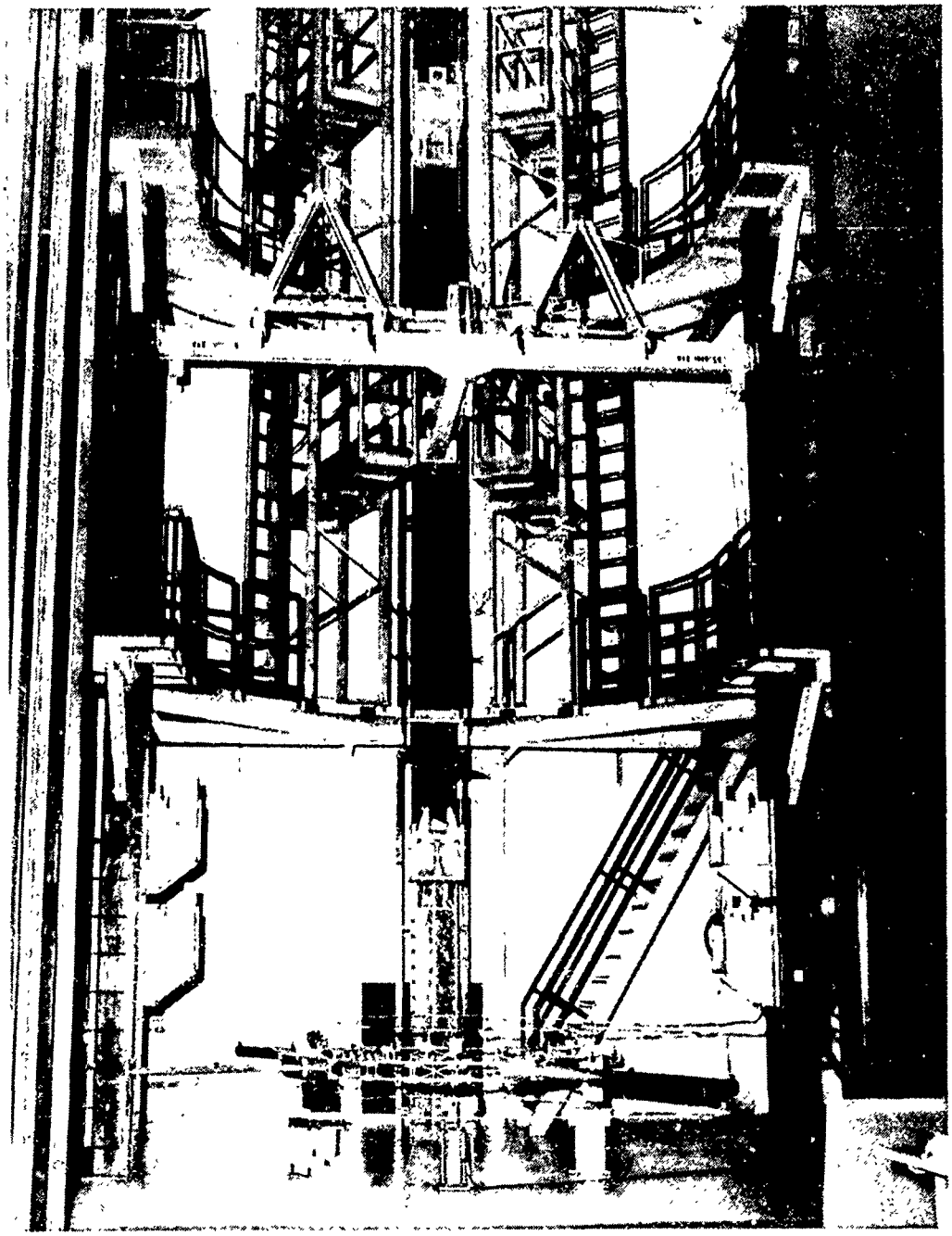

Figure 20

ZERO SPRING RATE DEVICE

Figure 21 is a closeup of one ZSRM. The spring constants for all three springs are chosen based on the weight to be supported. In the equilibrium position, the mechanism is adjusted so that the side spring rods are in the horizontal position. The side springs are preloaded in compression in this position.

With proper spring sizing and adjustment, the additional force in the vertical spring due to a downward motion of the cable is offset by the component of the compressive loads in the initially horizontal springs in the vertical direction due to a downward rotation of the horizontal springs.

For this particular test, each ZSRM supported about 200 lb. The effective spring rate of the mechanism was approximately 0.4 lb/in. at a 1/2-inch deflection in the vertical direction.

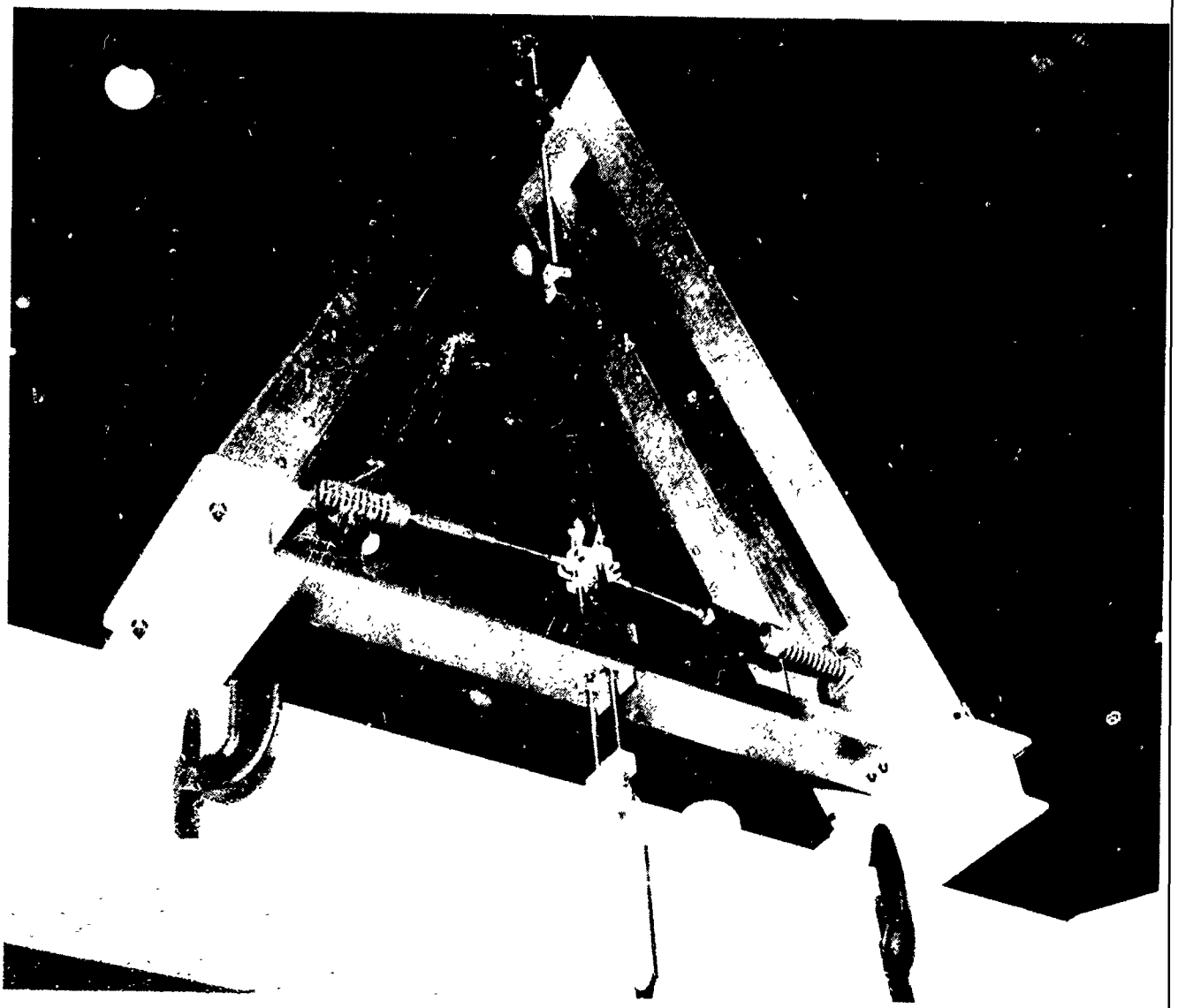

Figure 21

DTA RING TRUSS MODAL SURVEY RESULTS

The results of the ring truss modal survey are shown in Figure 22. The first two modal frequencies agreed very closely with predicted values. These modes are characterized by large motions at suspension points, and the agreement indicates that the ZSRMs were contributing negligible stiffness. The first mode, a symmetric mode, had large motion of the centerline suspension point and very little at the other two supports. The second mode, an antisymmetric mode, had virtually no motion on the centerline suspension point and large out-of-phase motions at the remaining two suspension points.

The higher damping ratios of these modes relative to modes involving small suspension point motion is indicative of slight friction in the ZSRMs.

Notice the very low damping in the remaining modes. For those modes that could be tuned separately, the decay traces provide more accurate damping values than the curve fits from the single-point random tests. For those modes where a range of values or no value for the tuned decay tests is given, satisfactory tuning was not achieved.

The uniformly low damping in the higher modes deserves emphasis. It is often assumed that higher modes have more inherent damping. This is not always the case in precision structures.

FREQUENCY (Hz)	MODAL (VISCOUS) DAMPING (PERCENT)			
	TUNED DECAY	TEST 1	TEST 2	TEST 3
3.24	0.30	0.80	0.42	
6.36	0.70	1.06	0.98	
8.78	0.14	0.21		
9.28	0.17	0.20	0.20	
12.47	0.2-0.3	0.33		
12.68	0.2-0.3	0.22	0.27	
13.05	0.16			0.25
13.22		0.18		
15.10	0.15	0.22	0.14	
16.2	0.17	0.20		

Figure 22

CONCLUSIONS

Although much of the research in the PACOSS program lies ahead, several conclusions can be drawn at this point in time (Figure 23). First, the best control strategy will result from the combined efforts of structural designers, control engineers, and damping designers working together early in the design phase, when sufficient latitude in the design exists to permit trades among the disciplines. Second, the common assumption that damping values increase with frequency does not always hold true with precision structures, and the implications on system performance, should such assumptions prove invalid, must be determined.

- BEST CONTROL STRATEGY FOR FUTURE LSS IS A COMBINATION OF PASSIVE DAMPING AND ACTIVE CONTROLS
- HIGHER MODES OF PRECISE STRUCTURES DO NOT NECESSARILY HAVE SIGNIFICANT INHERENT DAMPING
- OPTIMUM SYSTEMS WILL RESUL. FROM INTERACTION BETWEEN STRUCTURAL DESIGNERS. CONTROL ENGINEERS. AND DAMPING DESIGNERS EARLY IN THE DESIGN PHASE

Figure 23

REFERENCES

1. Morgenthaler, Daniel R.; and Gehling, Russell N.: Design and Analysis of the PACOSS Representative System. Damping 1986 Proceedings, May 1986 (AFWAL TR 86-3059).

2. Gehling, Russell N.: Active Augmentation of a Passively Damped Representative Large Space System. Damping 1986 Proceedings, May 1986 (AFWAL TR 86-3059).

DEPLOYABLE TRUSS STRUCTURE ADVANCED TECHNOLOGY

J.E. Dyer and M.P. Dudeck
General Dynamics Space Systems Division
San Diego, California

First NASA/DoD CSI Technology Conference
November 18-21, 1986

FUTURE SPACE ANTENNA REQUIREMENTS DRIVE DEPLOYABLE STRUCTURE TECHNOLOGY

Deployable space structures can be divided into three classes: linear support members, platforms, and antennas. Although each class has unique technology issues, future large, space antenna systems, with severe stiffness, stability, weight, and packaging requirements, are the major drivers of deployable structures technology (Figure 1).

Commercial and military communication, radiometric, and surveillance satellites increasingly require reflector antennas with RF apertures 5 meters or larger to satisfy future mission requirements. Due to launch vehicle payload envelope constraints, reflectors that can be deployed in space are required for the 5-meter or larger aperture antenna.

Typically, deployable reflectors use a flexible RF reflective surface supported by a deployable back structure. Deviation of a reflector surface from that of an ideal paraboloid results in degradation of its radiation pattern. Several factors contribute to on-orbit surface error, including surface geometry approximations, fabrication and adjustment tolerances, thermal and dynamic distortion due to the orbital environment, gravity effects, and deployment repeatability.

Current large, deployable RF reflectors are typically designed to operate at low frequencies where large surface errors can be tolerated without significant performance loss. However, the trend of future advanced space applications is toward the utilization of frequencies above 14 GHz where sidelobe degradation and gain loss due to surface error can severely penalize antenna performance. To meet future requirements, the large deployable reflector will be required to achieve on-orbit surface error approaching that of a solid-surface reflector (3-10 mils rms).

In addition, requirements to maximize gain performance and radiation pattern purity are dictating the use of offset reflector geometry to eliminate blockage by the feed array and support structure. Collectively, these requirements drive future antenna systems toward high stiffness and thermal stability. These characteristics are best provided by deployable composite truss structures.

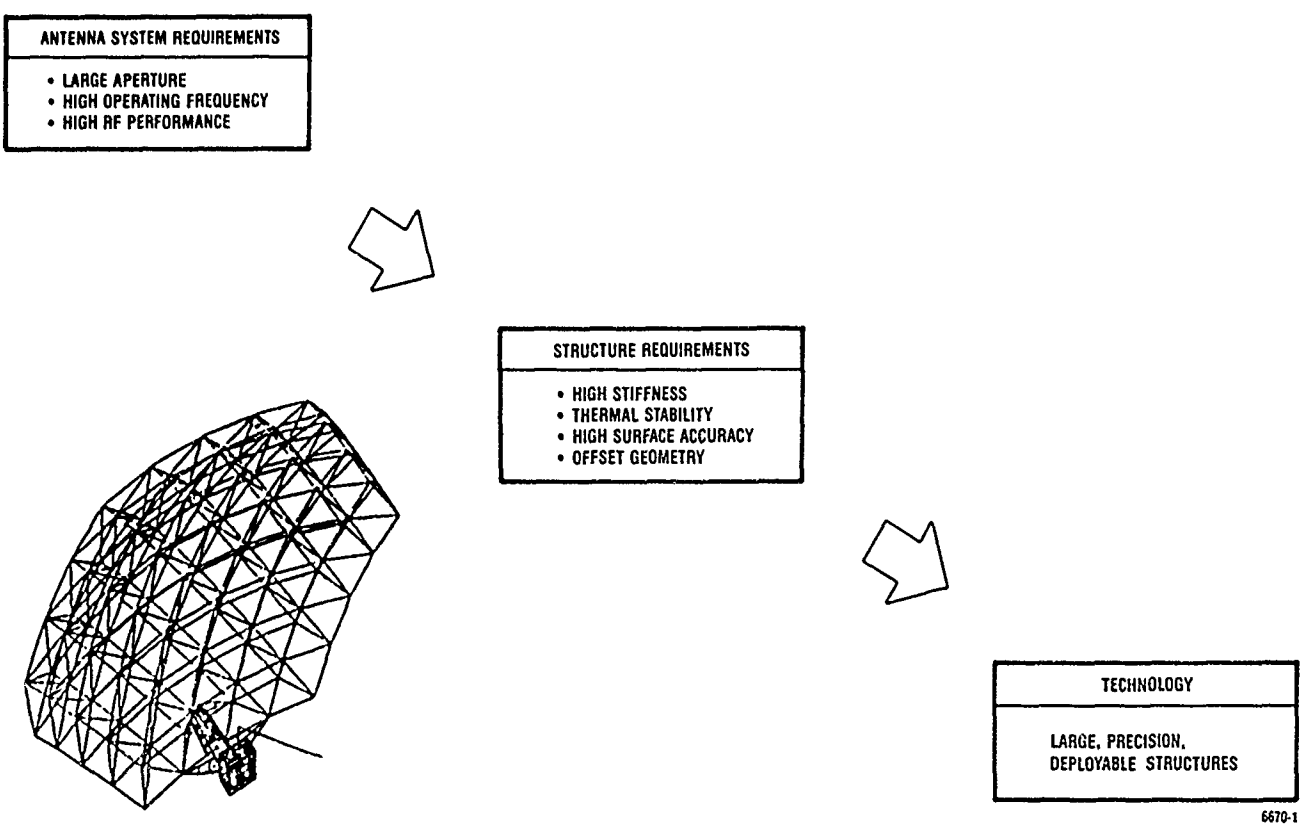

Figure 1.

DEPLOYABLE TRUSS STRUCTURES FOR FUTURE SPACE ANTENNAS

The deployable truss structure, when integrated with a precisely contoured mesh reflective surface, possesses the features needed to meet future space antenna requirements. Truss characteristics shown in Figure 2 that provide enhanced performance capabilities include:

- High Specific Stiffness — High inherent truss stiffness permits structure and control system frequency separation and minimizes active control needed to suppress structural vibrations excited by slewing torques and other dynamic disturbances. High stiffness also reduces deflections and reflector surface contour errors due to gravity effects during manufacture, adjustment, and ground test.
- Low Thermal Deformations — Low thermal deformations result from the use of simple axial truss structural members in an array manufactured from low-expansion, advanced composite materials.
- Good Packaging Efficiency — Folding tetrahedral building blocks provide an efficient structural package. This repeating modular truss design provides versatility by permitting simple scaling to accommodate varying geometric requirements.
- Edge-Mount Capability — For offset reflector applications, the tetrahedral truss reflector and feed structure are both deployed from one, simple edge mount thereby simplifying deployment, reducing weight, and improving system stiffness.

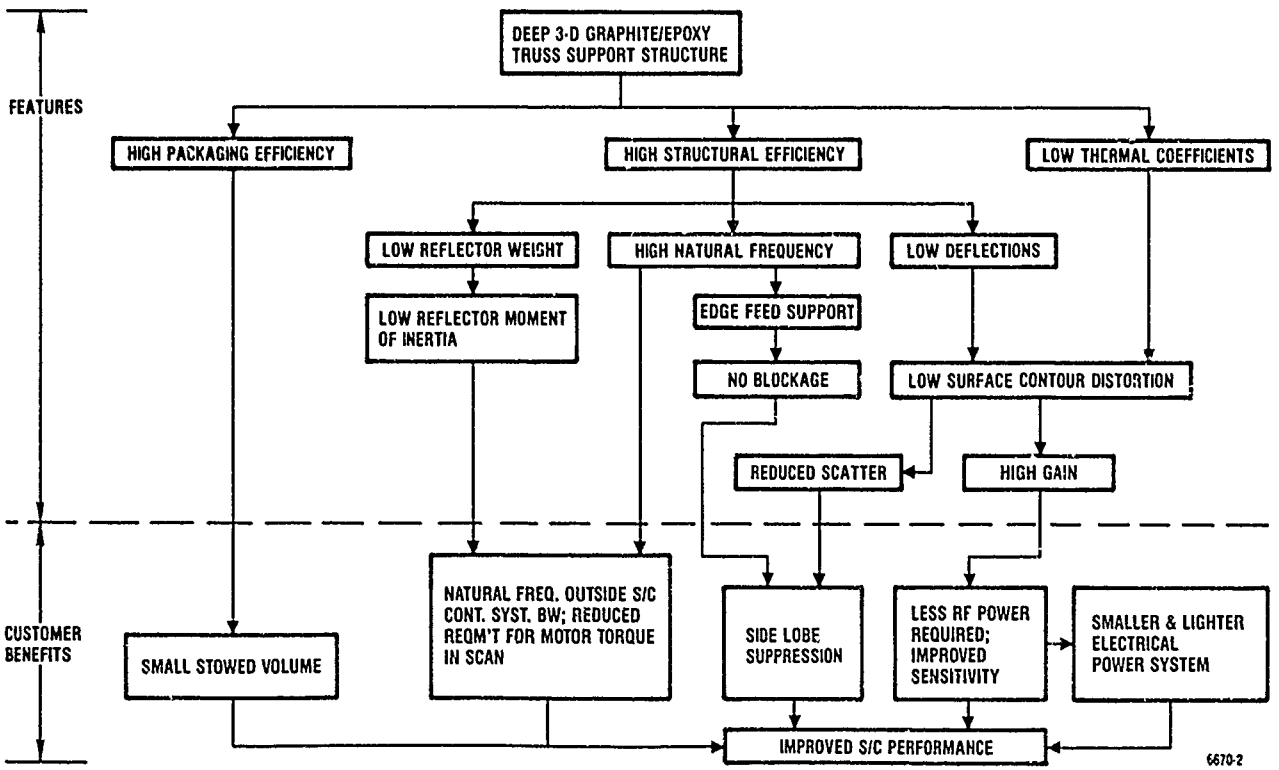

Figure 2.

TECHNOLOGY DEMONSTRATION ANTENNA

A 5-meter antenna (Figure 3) was recently fabricated by General Dynamics Space Systems to demonstrate precision deployable, tetrahedral truss reflector technology. Design requirements representative of a space-borne communications antenna operating over a frequency range up to 30 GHz included a 5-meter projected aperture with an F/D ratio of 1.3, an offset of 2.13 meters and manufacturing rss surface tolerance of 7.7 mils, and total on-orbit rss surface tolerance of 11 mils.

On-orbit errors are created by thermal, dynamic hygroscopic, and visco-elastic effects. Thermal distortion is minimized by setting an overall thermal expansion coefficient goal (near zero), and then designing the individual structural elements to meet this overall goal.

The deployable truss was fabricated from graphite/epoxy composites for high stiffness and low thermal expansion. The reflective surface was fabricated from gold-plated molybdenum wire knit into a tight mesh for low transmission losses.

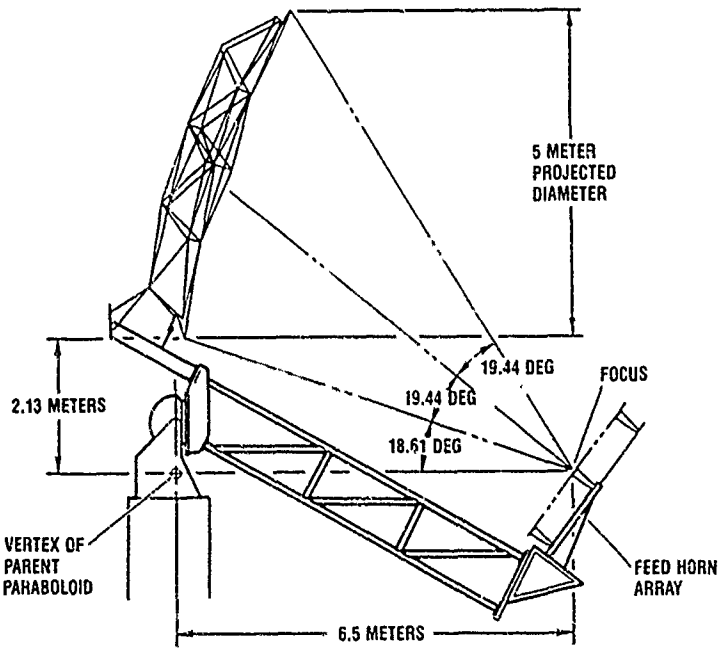

- DEPLOYABLE GRAPHITE/EPOXY TRUSS STRUCTURE
- PRECISION MESH SURFACE
- EDGE MOUNT

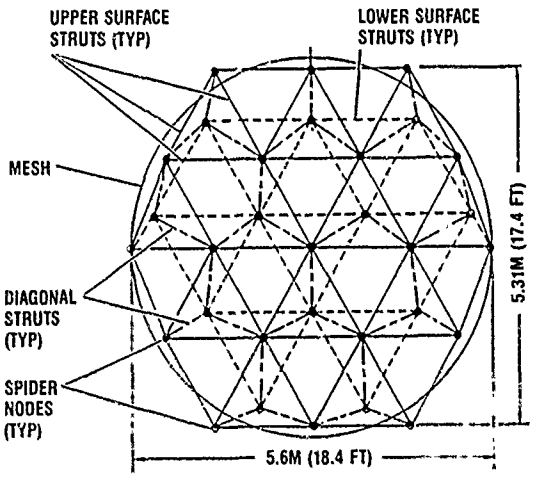

ERROR BUDGET FOR 5M DEPLOYABLE REFLECTOR

ERROR SOURCE	RMS SURFACE (MM)	ERROR MIL
FABRICATION SOURCES		
PROBE POSITION	0.054	(2.10)
PROBE GEOMETRY	0.064	(2.50)
MESH MEASUREMENT	0.051	(2.00)
MESH ADJUSTMENT	0.064	(2.50)
GRAVITY PREDICTION	0.051	(2.00)
DEPLOYMENT REPEATABILITY	0.076	(3.00)
SURFACE APPROXIMATIONS	0.114	(4.50)
ALIGNMENT	0.051	(2.00)
RSS TOTAL	0.194	(7.63)
ON-ORBIT SOURCES		
THERMAL DISTORTION	0.0787	(3.10)
DYNAMIC DISTORTION	0.0025	(0.10)
HYGROSCOPIC EFFECTS	0.0051	(0.20)
VISCOELASTIC CREEP	0.0127	(0.50)
RSS TOTAL	0.0800	(3.15)
TOTAL	0.255	(10.87)

6670 3

Figure 3.

TRUSS STRUCTURE DESIGN

The truss structure design was based on the deployable tetrahedral truss configuration with geometry and members selected to meet stiffness and surface precision requirements. A computerized tetrahedral truss analysis program (Figure 4) was used to generate the complete three-dimensional truss geometry and define the required truss element properties.

All structural elements, including tubular truss members and node fittings, used graphite/epoxy laminates designed to have an overall coefficient of thermal expansion (CTE) near zero. Zero tolerance titanium carpenter tape hinges were used to fold the truss members for packaging and to provide stored spring energy for deployment. The large, positive CTE of the titanium hinges was considered in the strut design so that when combined with the negative CTE graphite/epoxy tubes, the overall CTE of the member was near zero.

TRUSS PARAMETER: 4 BAY 30.00 DEG AN 5M (16.0 FT) RF DIAMETER
0.00 EF 283 L-RHO ROUND .400 F/D 20.0% CONTINGENCY

COMPONENTS	UNIT WEIGHT KILOGRAMS	(POUNDS)	NUMBER REQUIRED	WEIGHT KILOGRAMS	(POUNDS)
STRUTS	0.138	(0.305)	102	14.1	(31.1)
UPPER SURFACE	0.167	(0.369)	42	7.0	(15.5)
TUBES	0.099	(0.218)	42	4.1	(9.1)
HINGE	0.015	(0.032)	42	0.6	(1.4)
END FITTING+PINS	0.027	(0.060)	84	2.3	(5.0)
DIAGONALS	0.076	(0.167)	36	2.7	(6.0)
TUBES	0.073	(0.161)	36	2.6	(5.0)
END FITTING+PINS	0.001	(0.003)	72	0.1	(0.2)
LOWER SURFACE	0.182	(0.402)	24	4.4	(9.6)
TUBES	0.112	(0.247)	24	2.7	(5.9)
HINGE	0.015	(0.032)	24	0.4	(0.8)
END FITTINGS+PINS	0.028	(0.061)	48	1.3	(2.9)
SPIDER ASSEMBLY	0.125	(0.275)	31	3.9	(8.5)
MESH INSTALLATION	2.241	(4.941)	1	2.2	(4.9)
CONTINGENCY				4.0	(8.9)
REFLECTOR WEIGHT				24.3	(53.5)

X-C.G. CENTIMETERS (INCHES)	0.00000	(0.00000)
Y-C.G. CENTIMETERS (INCHES)	0.00000	(0.00000)
Z-C.G. CENTIMETERS (INCHES)	17.60790	(6.93223)
Ixx KILOGRAM METER SQ. (SLUG FT2)	56.98889	(42.00081)
Iyy KILOGRAM METER SQ. (SLUG FT2)	56.98889	(42.00081)
Izz KILOGRAM METER SQ. (SLUG FT2)	105.50880	(77.75999)
Ixy KILOGRAM METER SQ. (SLUG FT2)	0.00000	(0.00000)
Ixz KILOGRAM METER SQ. (SLUG FT2)	0.00000	(0.00000)
Iyz KILOGRAM METER SQ. (SLUG FT2)	0.00000	(0.00000)

NOTE - MOI ABOUT CENTER OF GRAVITY

MISCELLANEOUS GEOMETRY DATA	UPPER SUR		DIAGONAL		LOWER SUR	
LOAD (PCR) NEWTONS (LB)	896.0	(200.0)	1013.0	(226.0)	784.6	(175.0)
DIAMETER CM (IN.) STRUT	1.69	(0.67)	1.27	(0.50)	1.72	(0.68)
THICKNESS CM (IN.) STRUT	0.051	(0.020)	0.051	(0.020)	0.051	(0.020)
DES STRUT LENGTH CM (IN.)	154.4	(60.8)	102.3	(40.3)	169.3	(66.7)
HINGE LENGTH CM (IN.)	12.8	(5.0)	0.0	(0.0)	12.8	(5.0)

STANDOFF LH CM (IN.)	20.2	(8.0)	SPIDER DIA CM (IN.)	13.1	(5.2)
MESH AREA M2 (FT2)	22.5	(242.2)	TRUSS DEPTH M (FT)	0.2	(0.8)
PACKAGE DIA CM (IN.)	61.2	(24.1)	HEIGHT CM (IN.)	170.2	(67.0)

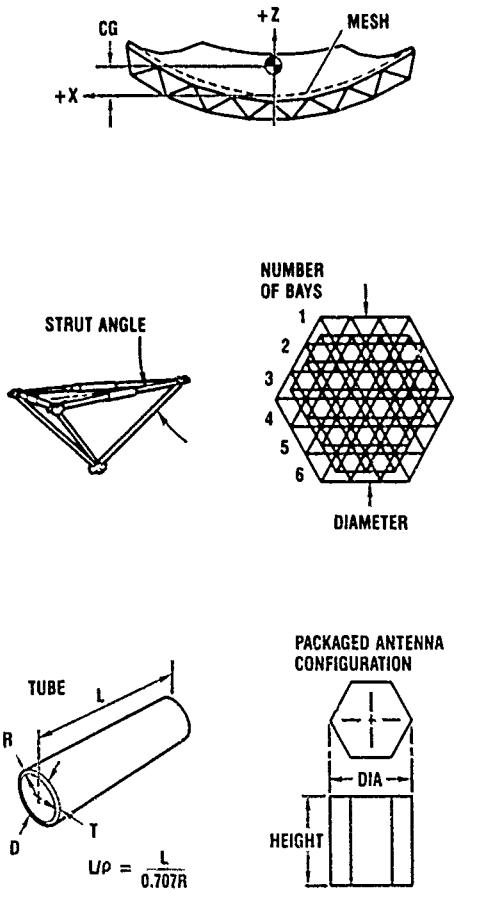

Figure 4.

Mesh system design used a computerized geometry analysis that optimally subdivided the mesh surface into small, triangular facets whose positions are controlled by lines attached to the truss structure node fitting (Figure 5). Consideration of illumination taper permits facet geometry to be varied so that the facet sizes progressively increase from the center to the periphery. This non-periodic geometry reduces grating lobes that may result from an equally subdivided surface. To meet the high precision required, the 5-meter diameter surface was divided into 1,944 facets varying in size from three to six inches on a side.

MESH GRID LINES

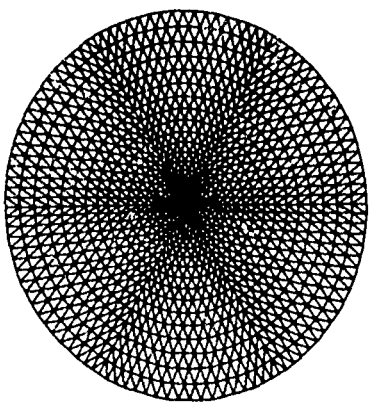

DROPLINES

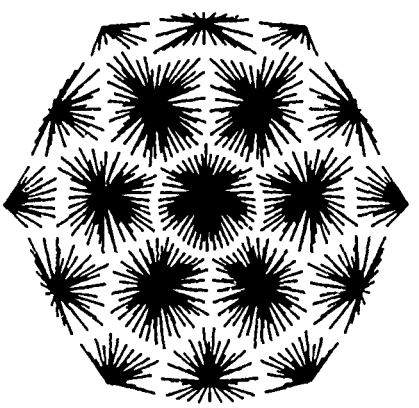

MESH SYSTEM WEIGHT SUMMARY

ITEM	NO. REQ	WEIGHT
MESH TRIANGLES	1944	2.975
GRID LINE SEGMENTS	2970	1.194
DROP LINES	1027	1.369
BUTTONS	1027	1.046
CLIPS	1027	0.136
MESH SYSTEM TOTAL		6.719
MESH AREA (SQ YDS)		25.1
TOTAL LINE LENGTH (FT)		3749.0

MESH DIA (FT)	16.404
NO. OF BAYS	4
F/D	1.309000
NO. OF DIV./BAY	9
X OFF SET - % DIA.	0.000000
Y OFFSET - % DIA.	0.426000
HOLE RADIUS (IN.)	0.0000
DB TAPER	10.00000
WEIGHTING	
0-NONE, 1-AR, 2-ILL, 3-BOTH	3
MESH LOAD LB/IN.	0.06000
GRID LINE LOAD LB	1.50000
GROSS WEIGHT LB	6.719
X-ARM	−0.022
Y-ARM	183.383
Z-ARM	36.337
I_{XX}-SLUG FT2	3.763
I_{YY}-SLUG FT2	3.768
I_{ZZ}-SLUG FT2	4.006
I_{XZ}-SLUG FT2	0.000
I_{XY}-SLUG FT2	0.000
I_{ZY}-SLUG FT2	1.183

NUMBER OF POINTS	65124
NORMAL RMS	0.00451
HALF PATH L RMS	0.00453
X DEFLECTION	−0.16197
Y DEFLECTION	−0.07396
Z DEFLECTION	0.04038
DELTA FOCAL LENGTH	0.33303
ROTATION ABOUT X-X	−0.00063
ROTATION ABOUT Y-Y	0.00031

6670-5

Figure 5.

TRUSS STRUCTURE FABRICATION

A simple but highly precise modular approach was used to fabricate the truss structure. Assembly was accomplished with the aid of 19 tooling stanchions (Figure 6) that precisely located the truss node fittings. Individual truss members and fittings were assembled on this tool so that any tolerances were removed by simple, on-assembly length adjustments.

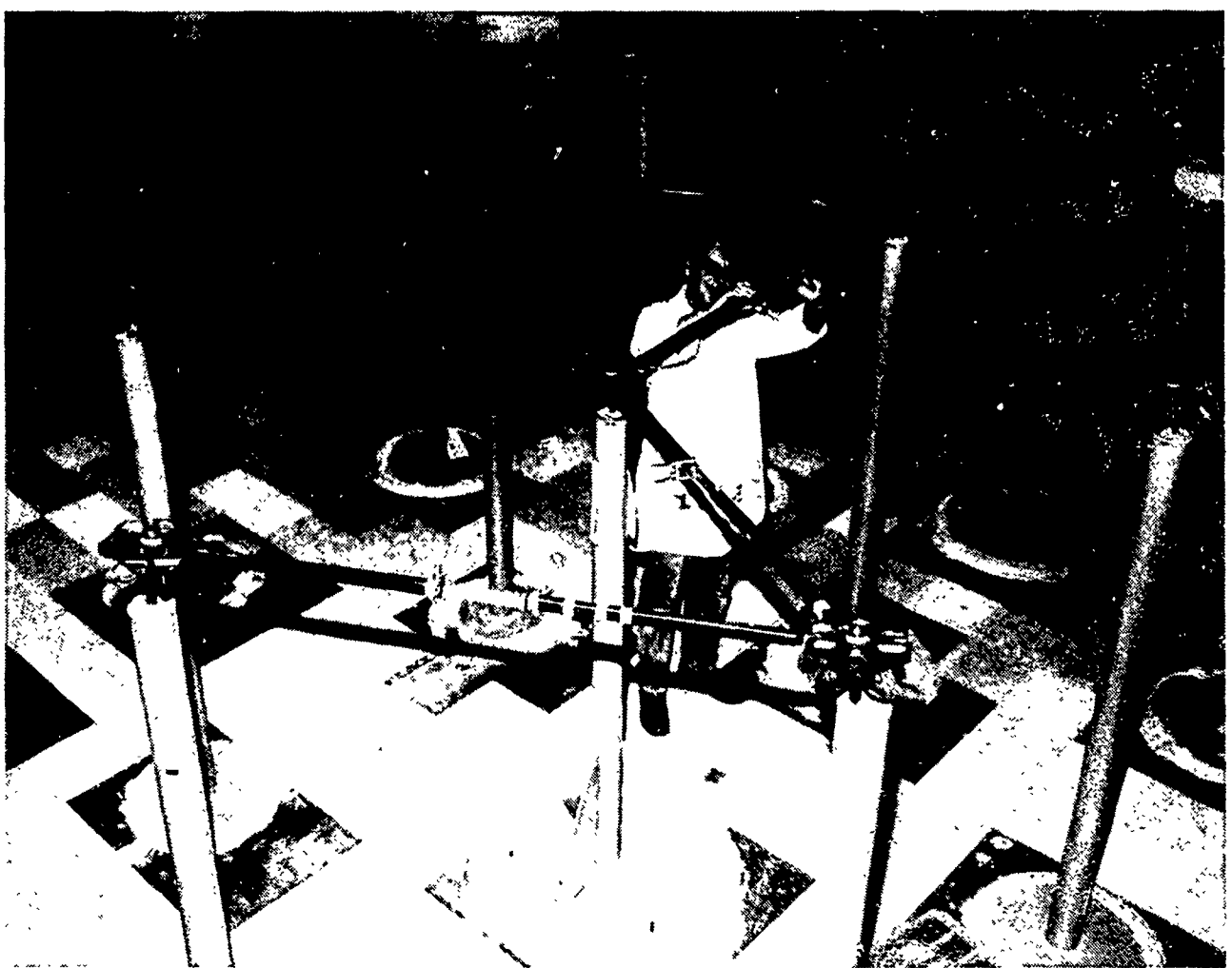

Figure 6.

MESH SURFACE FABRICATION

The mesh surface was fabricated using 20-gauge, two-bar tricot knit fabric. The pattern results in a 0.045-inch maximum dimension hole size, which extends RF performance into K-band and reduces cross-polarization response significantly. The fabric is knit from 1.2-mil, gold-plated molybdenum monofilament wire.

The mesh assembly is formed to the parabolic contour of a precision plaster mold (Figure 7). The initial contour of the mesh is maintained by a system of grid lines interconnected to buttons located at each apex of the triangular facets subdividing the mesh. The buttons, which are attached and bonded to the mesh, also provide the attach points for the 1,027 mesh control lines. These lines run from the truss node fittings to the mesh and are used to adjust the mesh surface.

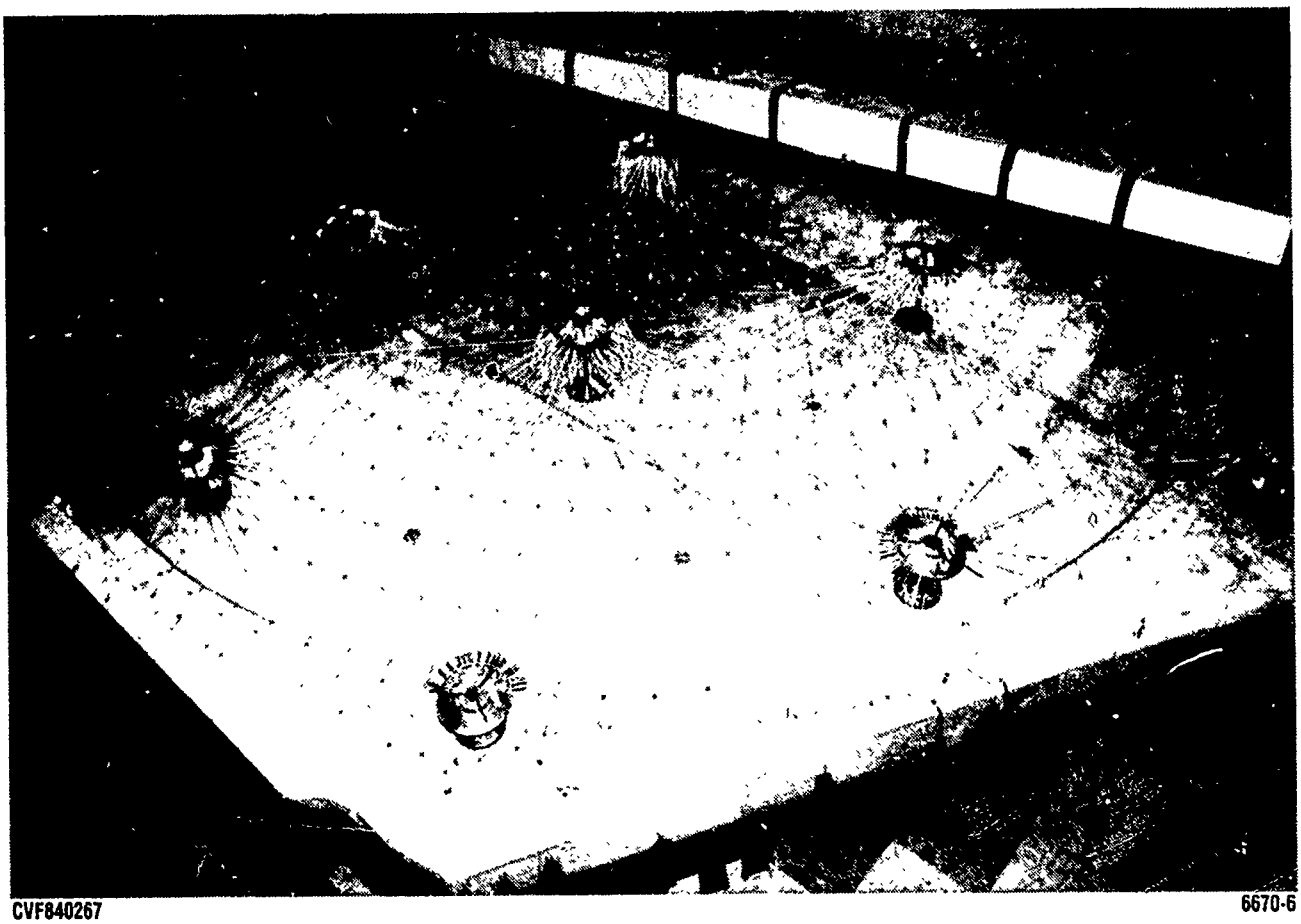

CVF840267 6670-6

Figure 7.

CONTOUR MEASUREMENT AND ADJUSTMENT

A computer-controlled profilometer contour measurement system incorporating a non-contact sensing probe (Figure 8) was used for measurement and adjustment of the reflective, mesh surface. The probe uses a digitally driven, capacitive transducer accurate to $\pm 1/2$ mil for proximity detection of the mesh surface. The 1,027 control lines between the mesh surface and the truss structure were loosened or tightened to adjust the mesh surface. Four iterations were required to complete adjustment of the mesh surface to the required accuracy. After the surface was set, the mesh control lines were locked out and the adjustment devices removed.

Photogrammetric measurements of 315 random targets on the surface were used to independently verify contour accuracy. After four adjustment cycles, the measured normal surface error was 8.3 mils rms using the profilometer and 8.6 mils using photogrammetric results.

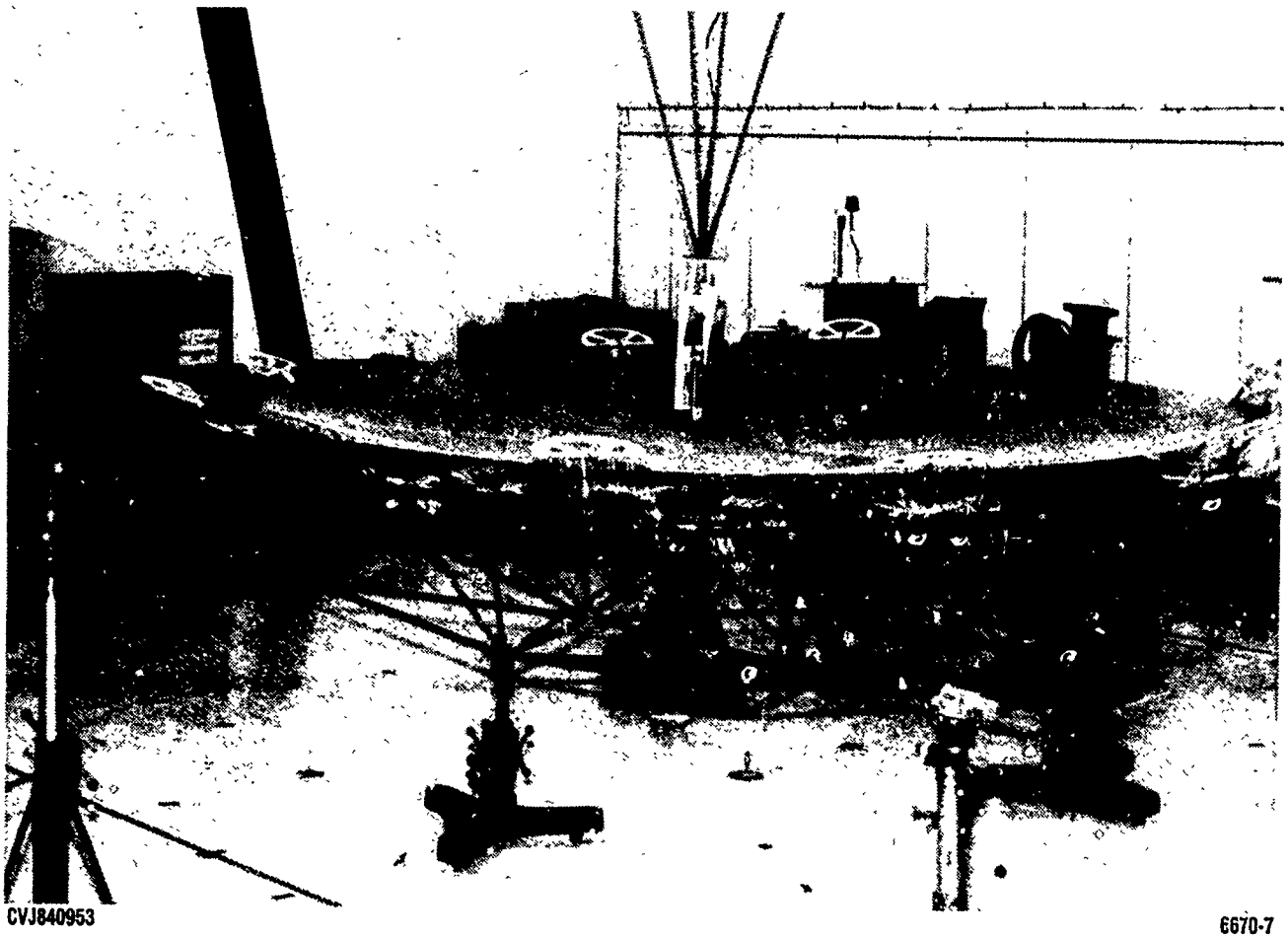

Figure 8.

PACKAGED REFLECTOR

When folded, the truss reflector forms a compact package whose dimensions are overall height - 1.8 meter, truss height - 1.1 meters, mesh diameter - 1.4 meters, and truss diameter - 0.9 meter. Packaged diameter is set by the number and size of node fittings used, and height is set by the length of the truss diagonal struts. The packaged reflector shown in Figure 9 shows one of three alternate packaging approaches, i.e., with all surface struts folded in. The other two approaches are with top struts folded out and with both top and bottom struts folded outward, which produces a longer, smaller-diameter package.

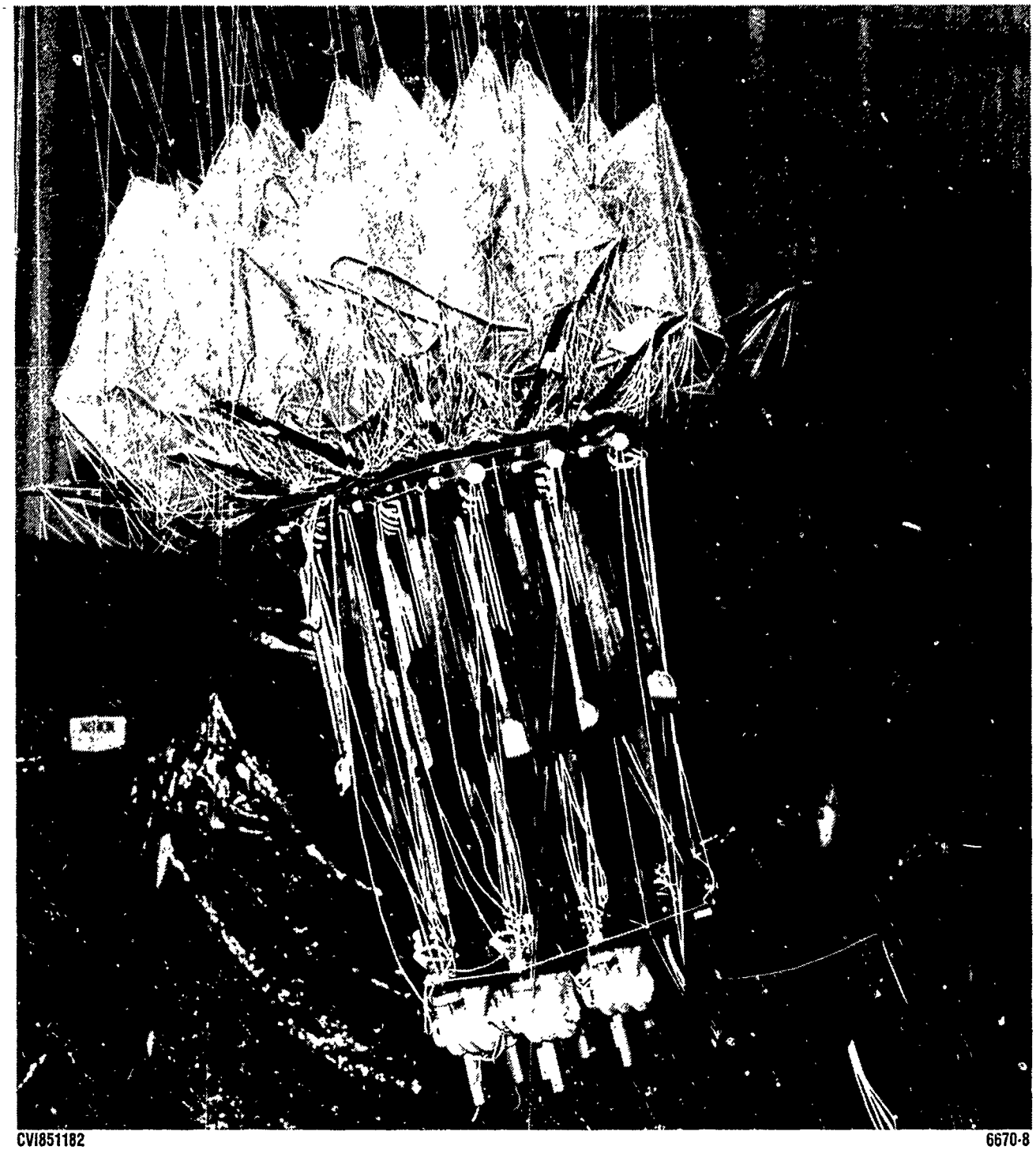

CVI851182 6670-8

Figure 9.

REFLECTOR DEPLOYMENT

Three deployments of the reflector were performed as shown in Figure 10. The truss reflector is normally a freely deploying system employing stored energy in folded spring hinges (carpenter tape hinges). These hinges are incorporated in all truss strut members of the geotruss structure supporting the reflector surface. When the package restraints are released, each strut begins to unfold. This action automatically drives the node fittings apart until the surface struts lock in their deployed position. The hinge provides a nearly constant deployment force until just before lock-up. At that point, the hinge force increases sharply to lock the truss member into its final position. This final lock-up force also ensures that the antenna surface mesh is stretched into its desired configuration.

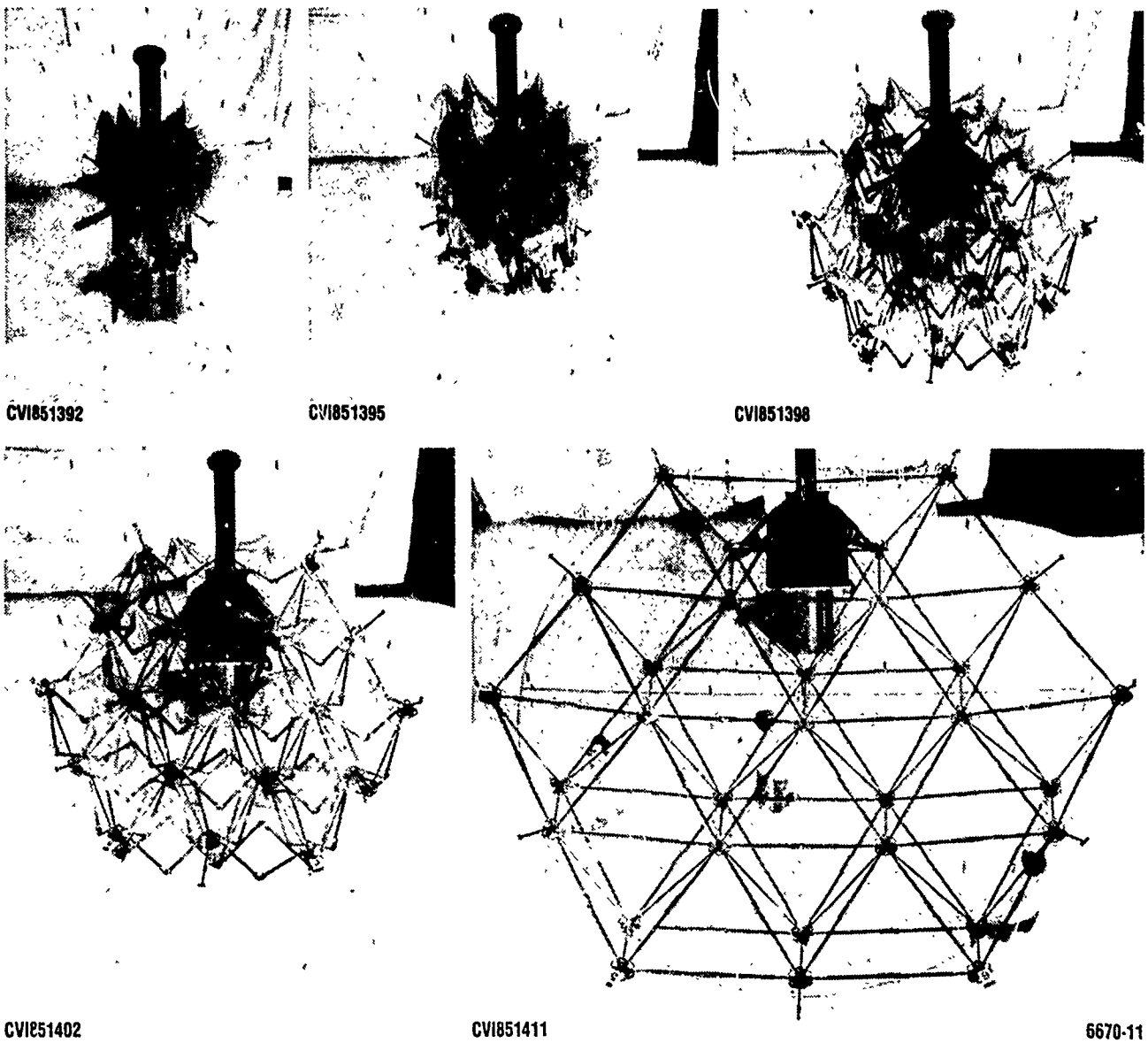

Figure 10.

ELECTROMAGNETIC (RF) TESTING

RF performance tests of the 5-meter tetrahedral truss reflector were performed at the Martin Marrietta Near Field Measurement Laboratory in Denver, Colorado. Linearly polarized on-focus feeds supplied by NASA LaRC were used to measure gain, far field patterns and cross-polarization at 2.27, 4.26, 7.73, and 11.6 GHz. Installation of the reflector on a 20-foot tower in the near field facility is shown in Figure 11. Results of these tests are being evaluated at NASA LaRC and General Dynamics Space Systems. Preliminary results indicate good RF performance that correlated well with analytical predictions. Typical results at 4.26 GHz are shown in the plot in Figure 11.

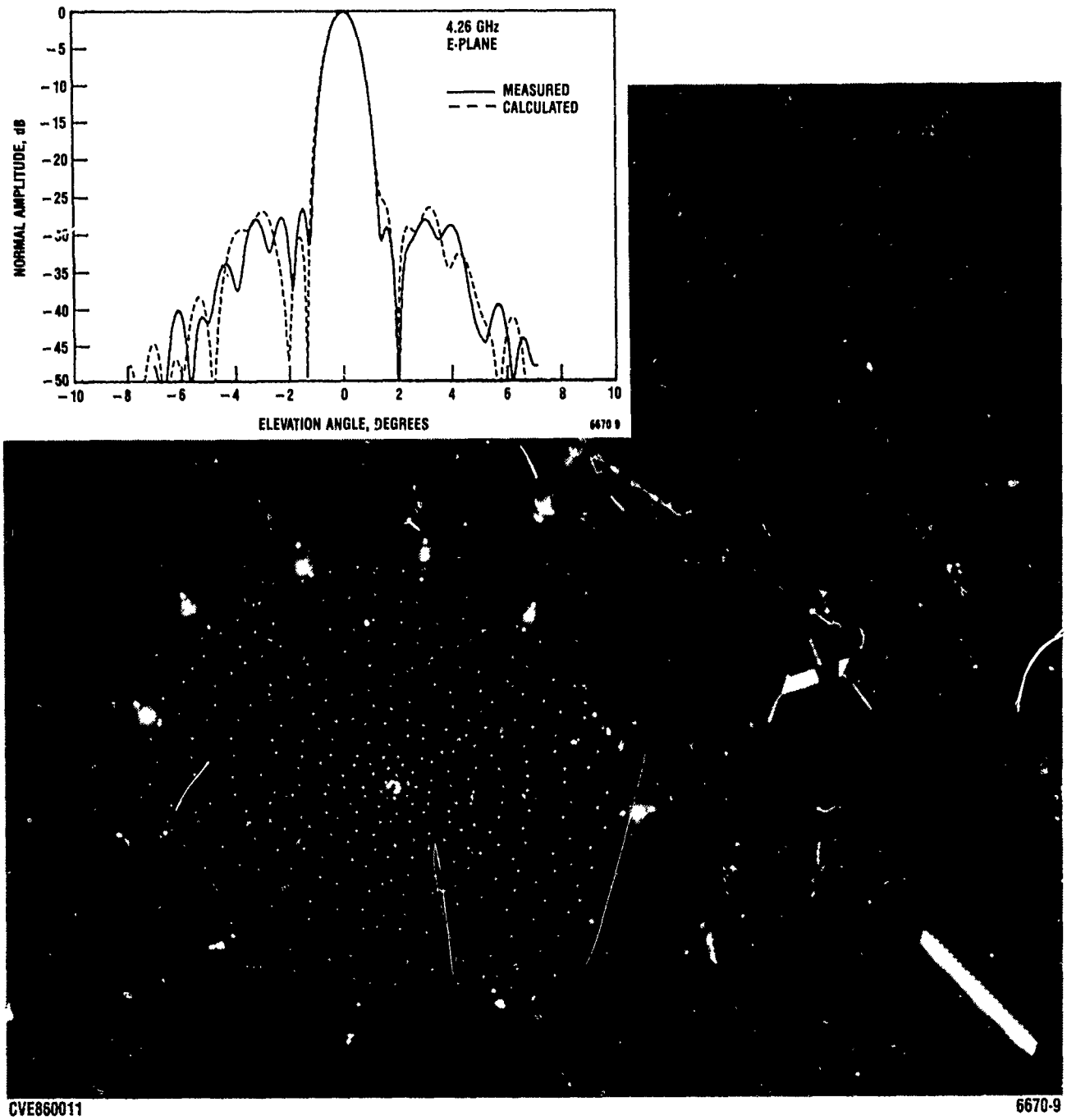

Figure 11.

DEPLOYABLE TRUSS TECHNOLOGY VERIFICATION PROGRAM

The 5-meter technology antenna program demonstrated the capability to successfully fabricate and test a precision deployable truss antenna. Deployable truss structure technology issues associated with on-orbit performance requirements need to be verified next by an integrated program of analysis and ground and flight testing. These technologies can be divided into five general categories: structural dynamics, active control, thermodynamics, electromagnetics, and structure/mechanisms design.

A 5-meter deployable truss reflector integrated with a deployable truss beam (Figure 12) can serve as a low-cost testbed for initial technology verification testing. Subsequent testing of a larger 15- to 20-meter article could be used to verify scaling-sensitive technology issues.

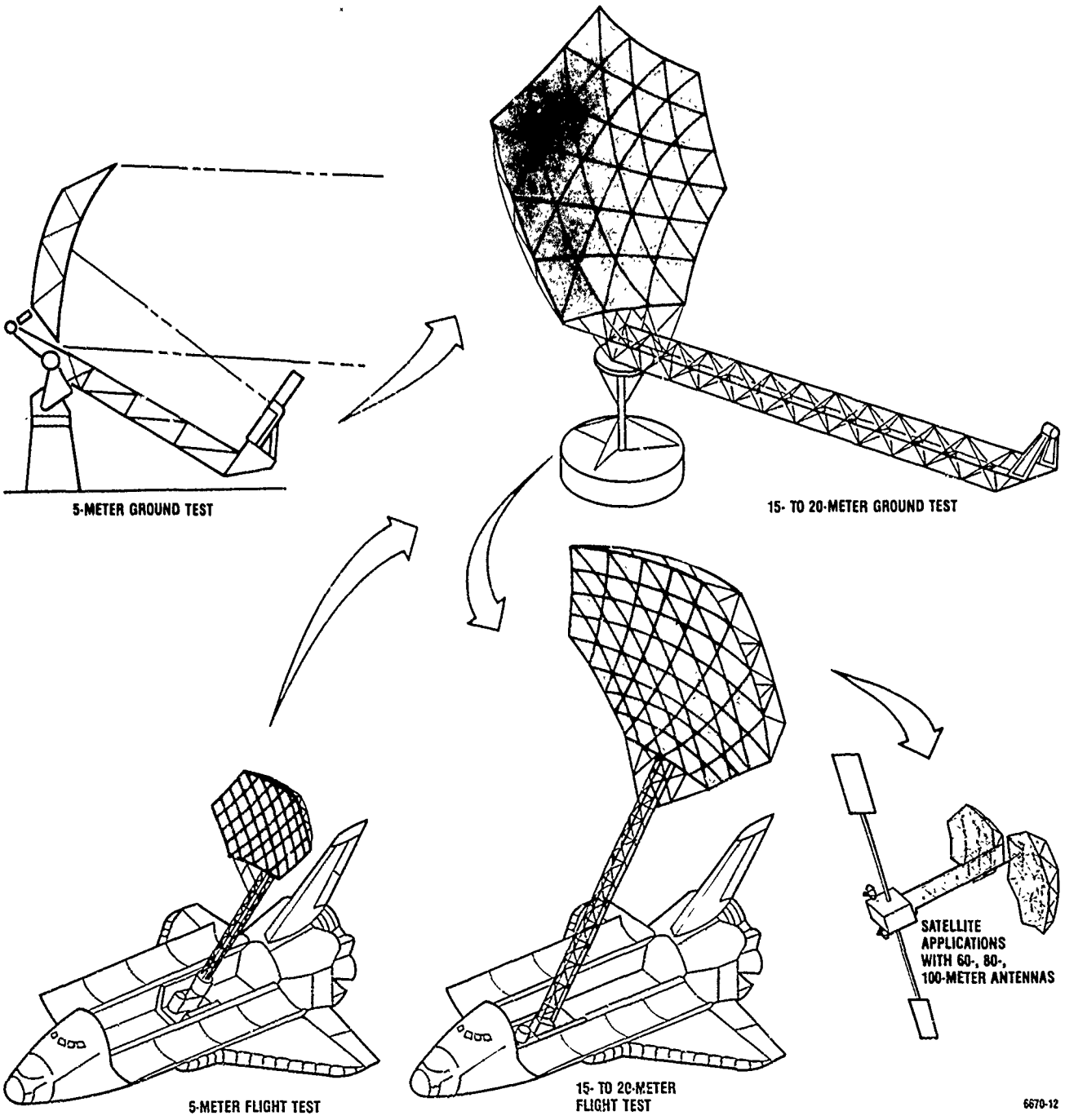

Figure 12.

CONCLUSIONS

The 5-meter technology antenna program demonstrated the overall feasibility of integrating a mesh reflector surface with a deployable truss structure to achieve a precision surface contour compatible with future, high-performance antenna requirements. Specifically, the program demonstrated:

- The feasibility of fabricating a precision, edge-mounted, deployable, tetrahedral truss structure.
- The feasibility of adjusting a truss-supported mesh reflector contour to a surface error less than 10 mils rms.
- Good RF test performance, which correlated well with analytical predictions.

Further analysis and testing (including flight testing) programs are needed to fully verify all the technology issues, including structural dynamics, thermodynamics, control, and on-orbit RF performance, which are associated with large, deployable, truss antenna structures.

DEVELOPMENT OF THE LENS ANTENNA DEPLOYMENT DEMONSTRATION (LADD) SHUTTLE-ATTACHED FLIGHT EXPERIMENT

H. Hill, Manager - Experiments Office/JA53
NASA George C. Marshall Space Flight Center
Huntsville, Alabama

D. Johnston, Project Manager/JA53
NASA George C. Marshall Space Flight Center
Huntsville, Alabama

H. Frauenberger, Program Manager
Space Systems Division; Grumman Corporation
Bethpage, New York

First NASA/DOD CSI Technology Conference
November 18-21, 1986

OPERATIONAL SPACE-FED SPACE BASED RADAR SATELLITE ON-ORBIT

Studies conducted over the past decade have shown that Space-Based Radar (SBR) will be a critical element of the U.S. surveillance system by the late 1990's. These studies have narrowed the choice to SBR systems employing space-fed or corporate-fed phased arrays. It is apparent that as stealth technology improves and defense against missile systems becomes viable, the SBR configuration must have growth potential and the capability of being deployed with large apertures to provide surveillance of dim targets. In order to enhance its survivability, it must be flown at high altitudes. It is equally apparent that in order to satisfy these requirements, a lightweight deployable aperture is required.

The Rome Air Development Center (RADC) and the Strategic Defense Initiative Organization (SDIO) have teamed together to provide technology for a deployable lens concept. These studies have addressed the various radar frequencies required for both atmospheric (L-Band; 1.0 - 2.0 GHz) and space (X-Band; 8.2 - 12.4 GHz) surveillance. As a result of these studies lightweight membrane apertures of the various radar frequencies are being developed along with an associated roll-out deployment technique. Figure 1 shows a typical large aperture operational space fed satellite. Utilizing the experience gained from the Solar Array Flight Experiment (SAFE), NASA's Marshall Space Flight Center (MSFC) will manage the development of a space flight demonstration of several of the applicable technologies.

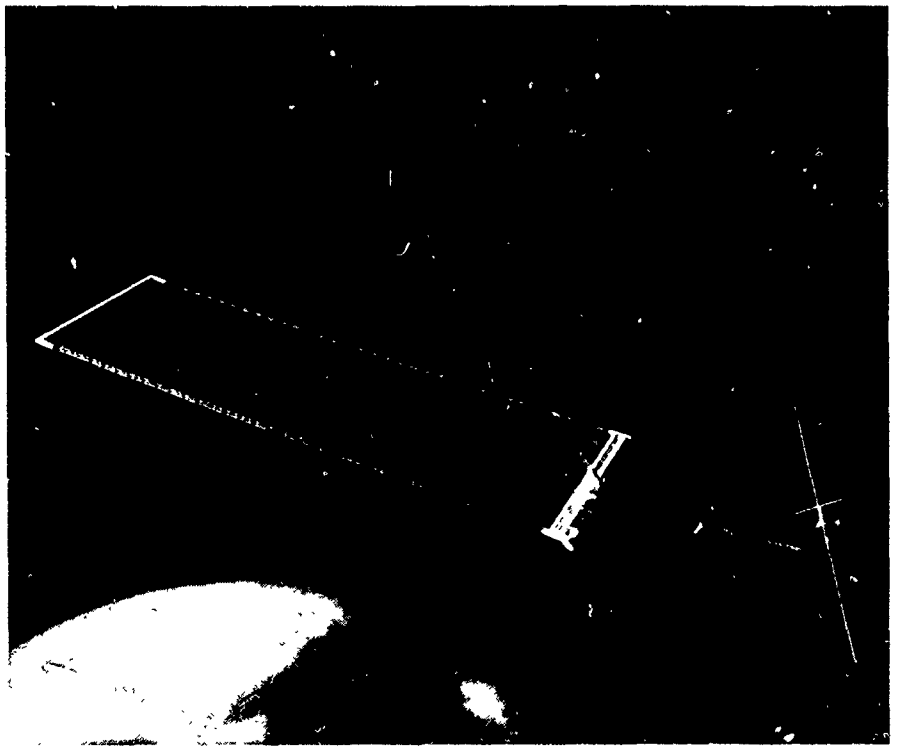

FIGURE 1

DEPLOYMENT CONCEPT FOR LARGE SPACE-FED SPACE BASED RADAR SATELLITE

The deployment sequence of the satellite is illustrated in Figure 2. The satellite is launched in its fully stowed configuration ("A") mounted lengthwise in the shuttle payload bay. Once in low earth orbit it is lifted out of the payload bay and transferred to the appropriate higher orbit via independent booster or space tug. After achieving the appropriate orbit, the satellite is unfolded ("B"), and locked ("C"), and the membrane is deployed by the extension of deployable masts ("D"). Although evident in Figure 1 but not illustrated in Figure 2, deployable masts also erect the feed used to illuminate the aperture and the solar panels which would be used on satellites of certain radar frequencies. As the two halves of the membrane are deployed a center seam which serves as an RF barrier is automatically formed unifying the ground plane into a single large aperture. When fully deployed ("E") the satellite is stabilized by small ion thrusters located at its corners. These control inputs are extremely small and do not cause structural or membrane responses that significantly affect radar operation. The need for large and accurate control inputs to repoint the aperture is eliminated by the inherent electronic beam steering of a phased array radar.

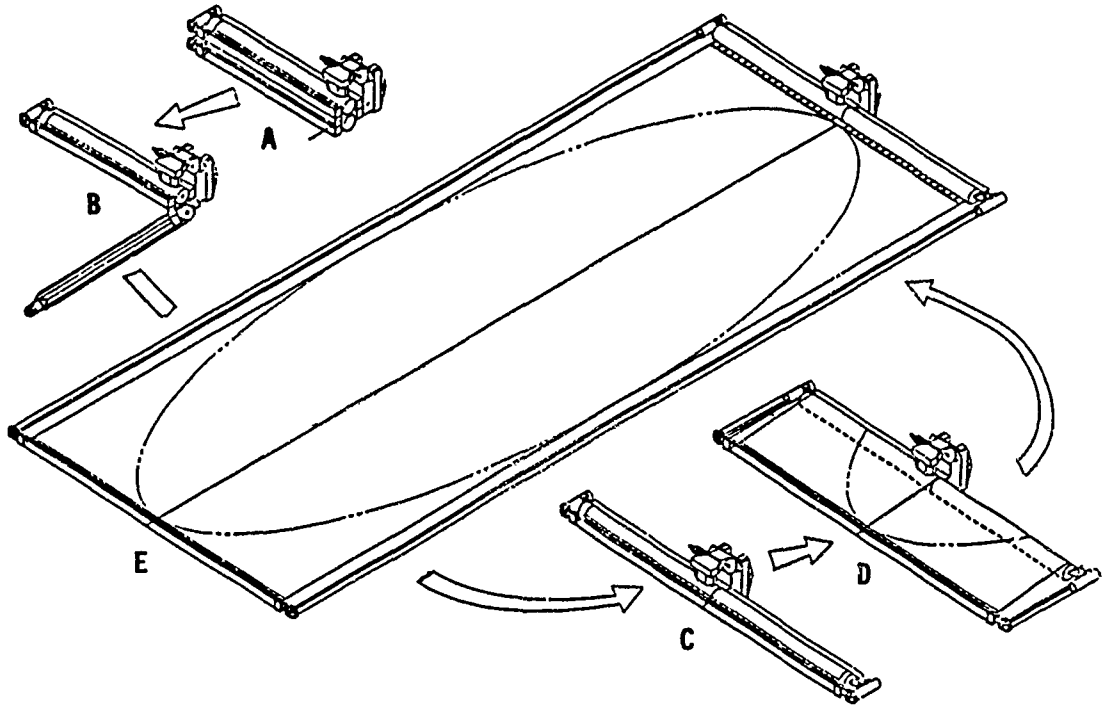

FIGURE 2

LADD EXPERIMENT DEPLOYED IN THE SHUTTLE CARGO BAY

An essential and significant early step towards making these large space-fed SBR satellites a reality is the Lens Antenna Deployment Demonstration (LADD) project that is being sponsored by the Strategic Defense Initiative Organization (SDIO) and NASA, managed by RADC and MSFC and developed under contract by the Space Systems Division of Grumman Corporation. The LADD is a scaled version of the operational satellite which will be mounted on a standard Material Science Laboratory (MSL) pallet, carried into orbit aboard the shuttle and deployed in the orbiter bay (see Figure 3). It is to be heavily instrumented to provide appropriate thermal and dynamics data on critical components. LADD is a single axis roll-out deployable/ retractable test article with a membrane which is representative of an X-band antenna. Its structural and mechanical concepts are, however, equally applicable to membranes tailored to other radar frequencies. The primary elements of LADD are a drum, two deployable side-masts/ canisters, an end beam and an 8 ft. x 20 ft. membrane populated by approximately 5000 dummy radar modules. The membrane dimensions were established by the width of the shuttle cargo bay and the lateral mounting of the LADD experiment.

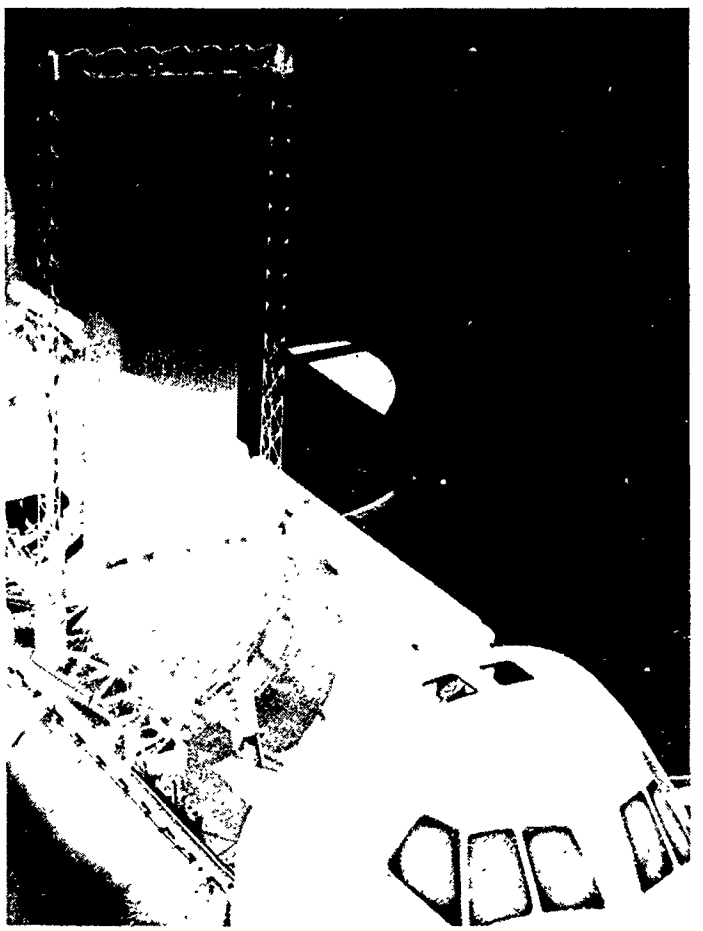

FIGURE 3

LADD STOWED CONFIGURATION (VIEW LOOKING FORWARD)

In the stowed (lift off and landing) configuration the membrane is rolled up on the drum and the side-masts are retracted into their canisters as shown in Figure 4. The experiment has been designed to fit within a 6 inch shuttle bay dynamic envelope.

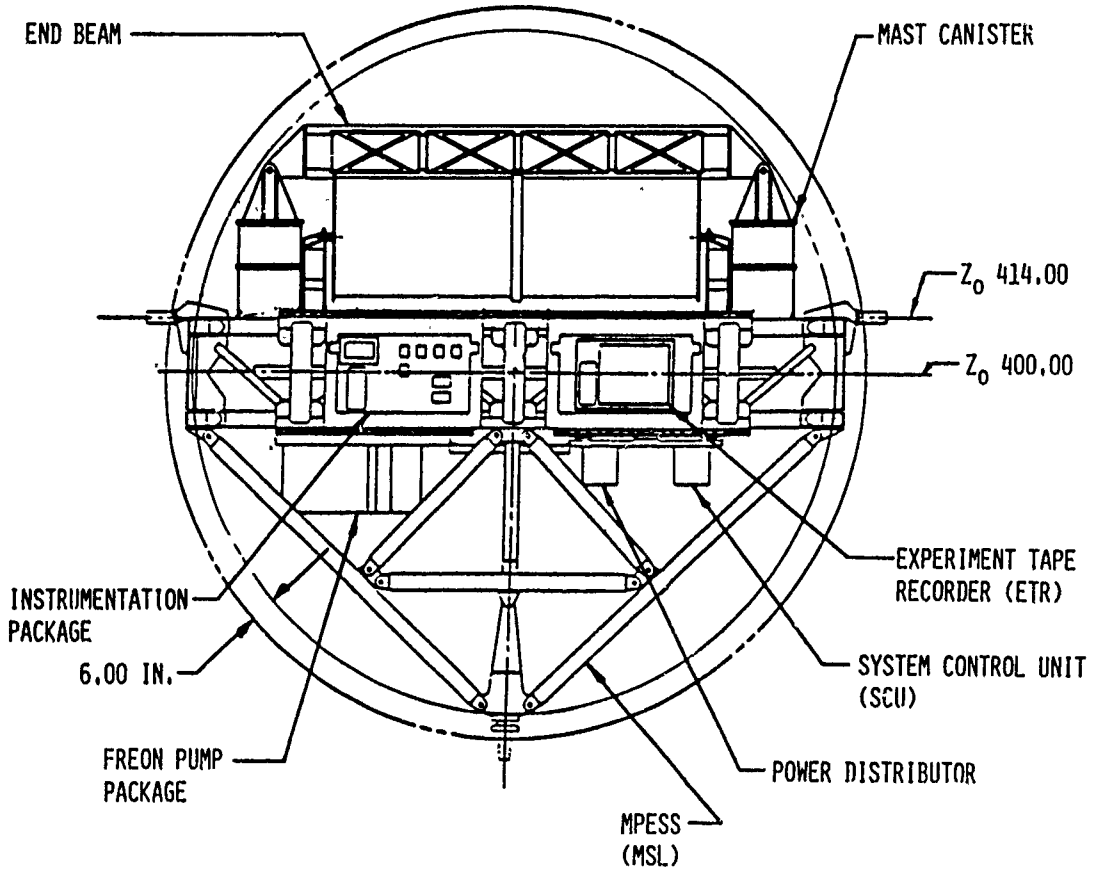

FIGURE 4

LADD DEPLOYED CONFIGURATION (VIEW LOOKING AFT)

In the deployed configuration the side-masts and aperture are extended out of the canisters and off of the drum respectively (Reference Figure 5).

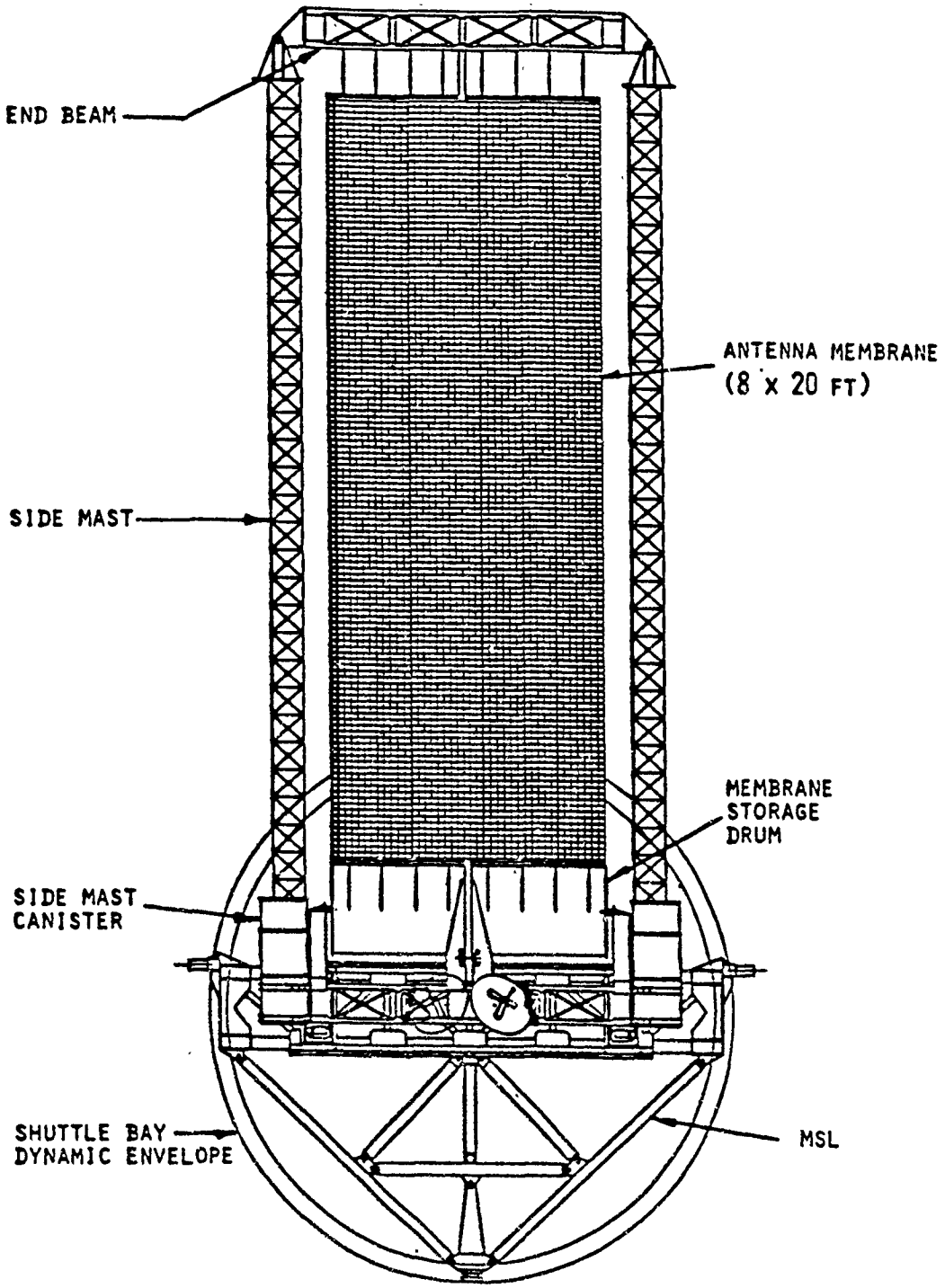

FIGURE 5

OBJECTIVES OF THE LADD PROGRAM

The primary objective of the LADD Program is to develop a technology demonstration test article that can be used for both ground and flight tests to demonstrate the structural and mechanical feasibility and reliability of the single-axis roll-out SBR approach. As designed, the LADD will essentially be a generic structural experiment which incorporates all critical technology elements of the operational satellite and is applicable to a number of future antenna systems. However, to fully determine its design integrity for meeting the lens flatness and constant geometry requirements in a zero "g" environment under extreme thermal conditions, the LADD must be space flight tested. By accurately surveying the structure under varying conditions the membrane tolerance-holding capabilities of the structure will be demonstrated. The flight test will provide data to verify analytical tools used to predict thermal and structural behavior. Most important, the experiment will provide an initial indication of structural damping in a zero "g" vacuum environment. The recently completed Solar Array Flight Experiment (SAFE) showed orbital damping greater than that experienced during ground testing. From the experience and the information obtained from LADD it is hoped that designs can be confidently extrapolated to operational satellites with apertures in the 20 m by 60 m size range.

The specific objectives to be achieved during the flight test include:

- Demonstration of system reliability through the repeated full deployment and retraction of the membrane at temperature extremes representative of an operational satellite.

- Demonstration of the membrane center seam integrity and reliability through its repeated formation and separation and the firing of orbiter primary control system thrusters during dynamic tests with the membrane deployed.

- Measurement of membrane flatness in a static mode and at temperature extremes representative of an operational satellite to verify compliance with radar system requirements.

- Verification of the integrity of the membrane launch support system (stowed mode) for sustaining launch and landing loads.

- Verification of dynamic and thermodynamic models and analyses of LADD to provide confidence in their extrapolation to, and use on large structures associated with operational satellites.

- Determination of structural and membrane damping coefficients on-orbit for use in future analyses.

OBJECTIVES OF THE LADD PROGRAM

OVERALL: DEVELOP TECHNOLOGY DEMONSTRATION TEST ARTICLE INCORPORATING KEY ELEMENTS OF SINGLE AXIS ROLL-OUT DEPLOYMENT APPROACH

SPECIFIC:

- DEMONSTRATE DEPLOYMENT/RETRACTION SYSTEM RELIABILITY
- DEMONSTRATE CENTER SEAM INTEGRITY AND RELIABILITY
- MEASURE DEPLOYED MEMBRANE FLATNESS (STATIC TEST)
- VERIFY INTEGRITY OF MEMBRANE LAUNCH SUPPORT SYSTEM
- OBTAIN DATA TO VERIFY DYNAMIC AND THERMODYNAMIC MODELS AND ANALYSES
- DETERMINE STRUCTURAL AND MEMBRANE DAMPING ON-ORBIT

FIGURE 6

ENGINEERING APPROACH

The LADD is being developed essentially as a protoflight system. A single article is being developed for both functional ground test and checkout and the flight experiment. All significant structural and mechanical features of the operational single axis roll-out antenna concept will be incorporated in the LADD design and ground tested. No changes in the design or hardware are envisioned between the ground and flight tests except those, if any, that might be dictated by the results of the ground tests.

In the engineering approach taken a number of design studies and analyses are being conducted prior to the completion of the design phase. These studies and analyses, which include a shuttle integration compatibility assessment and orbiter coupled loads analysis, are intended to ensure that the configuration selected will be shuttle compatible and that it will have the desired natural frequency to prevent cross coupling with orbiter frequencies and meet the lift-off, on orbit and landing loads criteria with adequate margins of safety.

- UTILIZE PROTOFLIGHT SYSTEM DEVELOPMENT CONCEPT
  (SINGLE TEST ARTICLE FOR GROUND AND FLIGHT TESTS)
- INCORPORATE ALL SIGNIFICANT FEATURES OF OPERATIONAL SATELLITE
- CONDUCT ALL ESSENTIAL STUDIES AND ANALYSES EARLY IN DESIGN PHASE TO:
  - ENSURE SHUTTLE COMPATIBILITY
  - PROVIDE ACCURATE DESIGN LOADS
  - GUARANTEE SUBSTANTIAL MARGINS OF SAFETY ARE ACHIEVED
- CONDUCT EXTENSIVE GROUND TESTS TO THOROUGHLY QUALIFY HARDWARE
- MODIFY HARDWARE ONLY WHEN DEEMED NECESSARY BY GROUND TEST RESULTS

FIGURE 7

LADD DUMMY MODULES AND SIMULATED X-BAND MEMBRANE

The LADD primary structural and mechanical components are identified in Figure 5. The LADD membrane, which is approximately 20 ft. long and 8 ft. wide, has a single layer laminated ground plane which is made of two panels, one on each side of the centerline. Each panel is made from two 2-ft wide sections that are permanently connected by thin metallized strips. The two panels are automatically mated during deployment by a center seam. These panels form the aperture that contains approximately 5,000 dummy transmitter/receiver (T/R) modules. The dummy modules (Figure 8) are designed and appropriately coated so that through passive solar heating their surface temperatures approximate those predicted for "live" x-band modules. Each module is mounted to the ground plane with two hollow rivets.

The ground plane Power Distribution System (PDS) for providing power to each T/R module will be simulated by a method that is similar to that which will be used in a live radar. In the LADD experiment the PDS will be used to transmit instrumentation signals about the membrane. The membrane is supported from the end beam by lanyards and from the drum by a series of constant force springs. These springs impart a constant pretension to the membrane at all times in the deployed state.

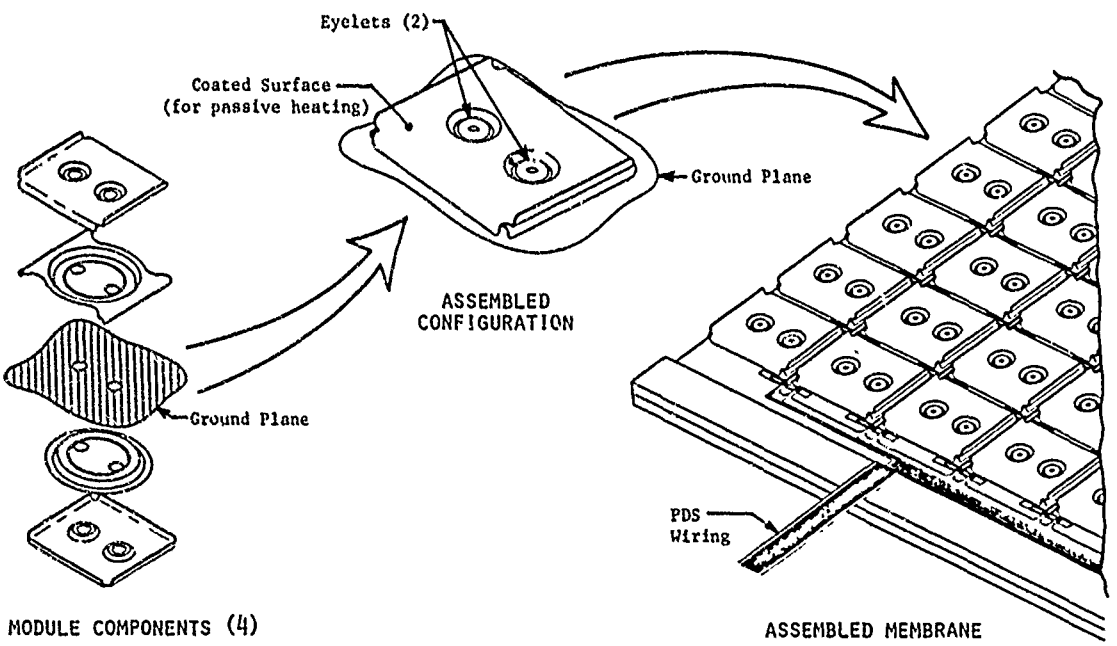

FIGURE 8

LADD END BEAM CONFIGURATION

The end beam that supports the membrane is constructed of 1 in. square boxed aluminum extrusions and is the common link or bridge structure between two coilable (deployable/retractable) fiberglass masts. These masts are similar to the one that was successfully flown on the Solar Array Flight Experiment (SAFE) on the space shuttle Discovery in September 1984.

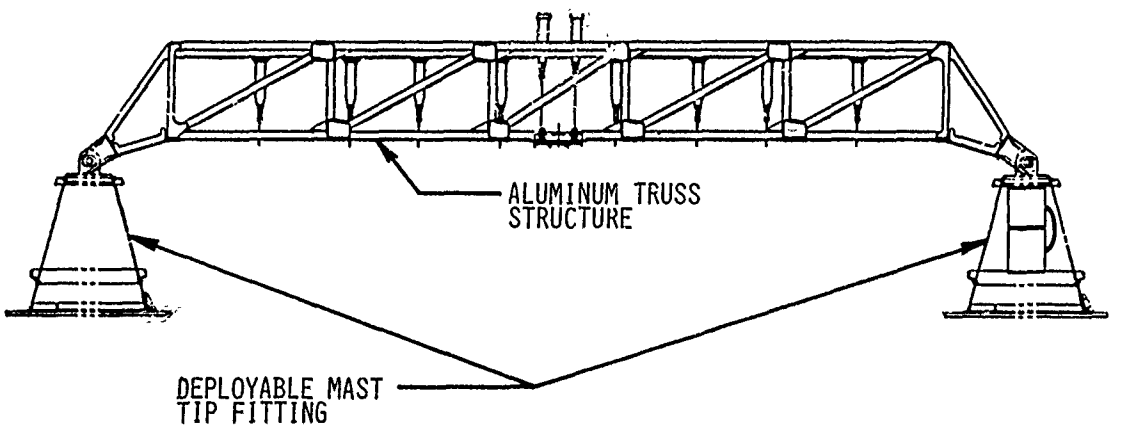

FIGURE 9

DEPLOYABLE SIDE MASTS

The deployment of the membrane is accomplished through the extension of the side masts. Each mast consists of three continuous fiberglass longeron members connected by a triangle of fiberglass batten members at specific, equally spaced locations along the longerons (see Figure 10). The region between the battens is called a "bay". The bay length is a significant factor in determining the mast local buckling strength. The LADD masts have been selected with sufficient strength to allow vertical deployment in a 1 "g" environment. Three pairs of fiberglass rods or stranded stainless steel wire diagonals connect the intersections of the battens and longerons between adjacent bays. Rollers are located at the outside of all three longerons at each batten location. The rollers are part of apex fittings that are permanently attached to the longerons and support the battens and diagonals. Detail "A" of Figure 10 shows the geometrical relationship between the longerons, battens and diagonals at a typical apex fitting.

The masts are retracted by coiling the longerons in torsion and stowing them in the bottom of the canisters. Deployment is accomplished by allowing the coiled (stowed) longerons to uncoil and straighten in a controlled manner. Both deployment and retraction is accomplished by rotating an elevating nut which has internal threads that simultaneously engage the rollers on each of the three longeron apex fittings associated with a batten attachment. During deployment, as the elevating nut rotates the rollers are pulled up through the threads and the coils of longeron are allowed to straighten. Reversing the direction of elevating nut rotation drives the rollers back into the canisters and forces the longerons to resume their coiled/retracted configuration. In the LADD experiment the deployment and retraction of the two masts will be synchronized to prevent asymmetry.

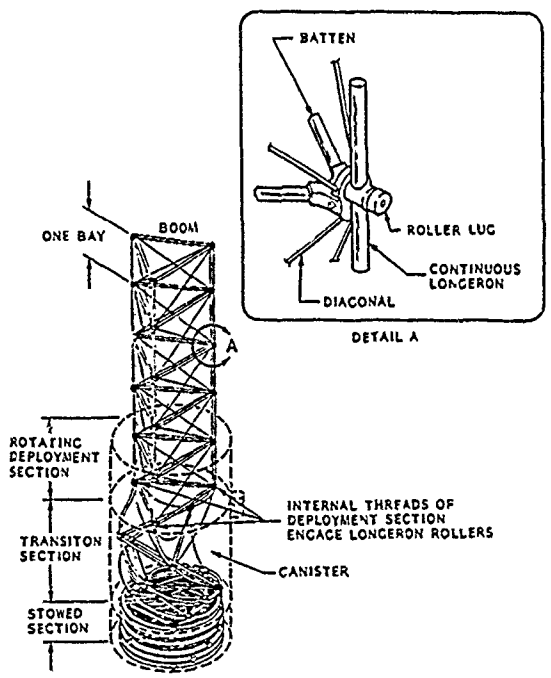

FIGURE 10

DRUM AND DRUM SUPPORT TRUNNIONS

During the deployment and retraction of the masts the LADD membrane is being unwound and rewound respectively from a 29-inch diameter, continuous 8 ft. long drum. The drum has an aluminum skin supported internally by stringers and ring frames. There is a flange at the center of the drum that duplicates the end rims of a folding drum envisioned in an operational system. The membrane launch support system is built into the drum skins to support the first layer of modules and the membrane during launch and landing. Each subsequent layer of membrane is supported by the modules of the previous wrap and, when fully stowed, an additional torque is applied to the drum and the drum is locked.

The drum is supported by trunnion fittings at each end that are fitted with rolling element and spherical bearings. The trunnions are tapered aluminum beams that are, in turn, connected to the drum support beam which is similar in construction to the end beam. The drum support beam has four "bathtub" fittings at each end that attach to the sides of the mast canisters. The drum support beam also supports the center seam mechanism.

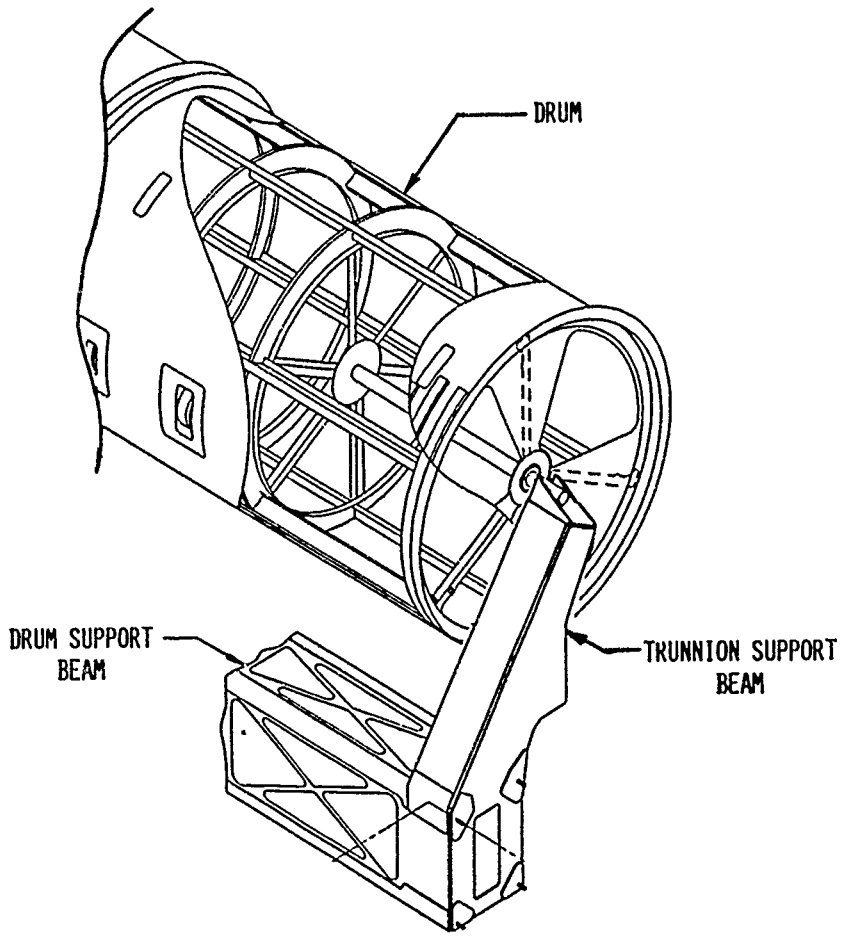

FIGURE 11

MEMBRANE CENTER SEAM ENGINEERING DEVELOPMENT TEST FIXTURE

The center seam, although not required on the 8 ft. wide LADD membrane, is being incorporated and is a key element of the technology demonstration. The center seam must provide structural integrity, an effective RF barrier, durability and appropriate life in terms of formation/separation cycles and yet fit within the limited space available (approximately 1/4 in.) between modules in the densely populated x-band membrane. A center seam configuration possessing all of these characteristics has been developed and tested. Figure 12 shows an engineering development test rig with an abbreviated width (5 module wide) membrane which forms two parallel center seams 20 ft. long. Center seams of virtually unlimited length can be fabricated using the processes developed by Grumman.

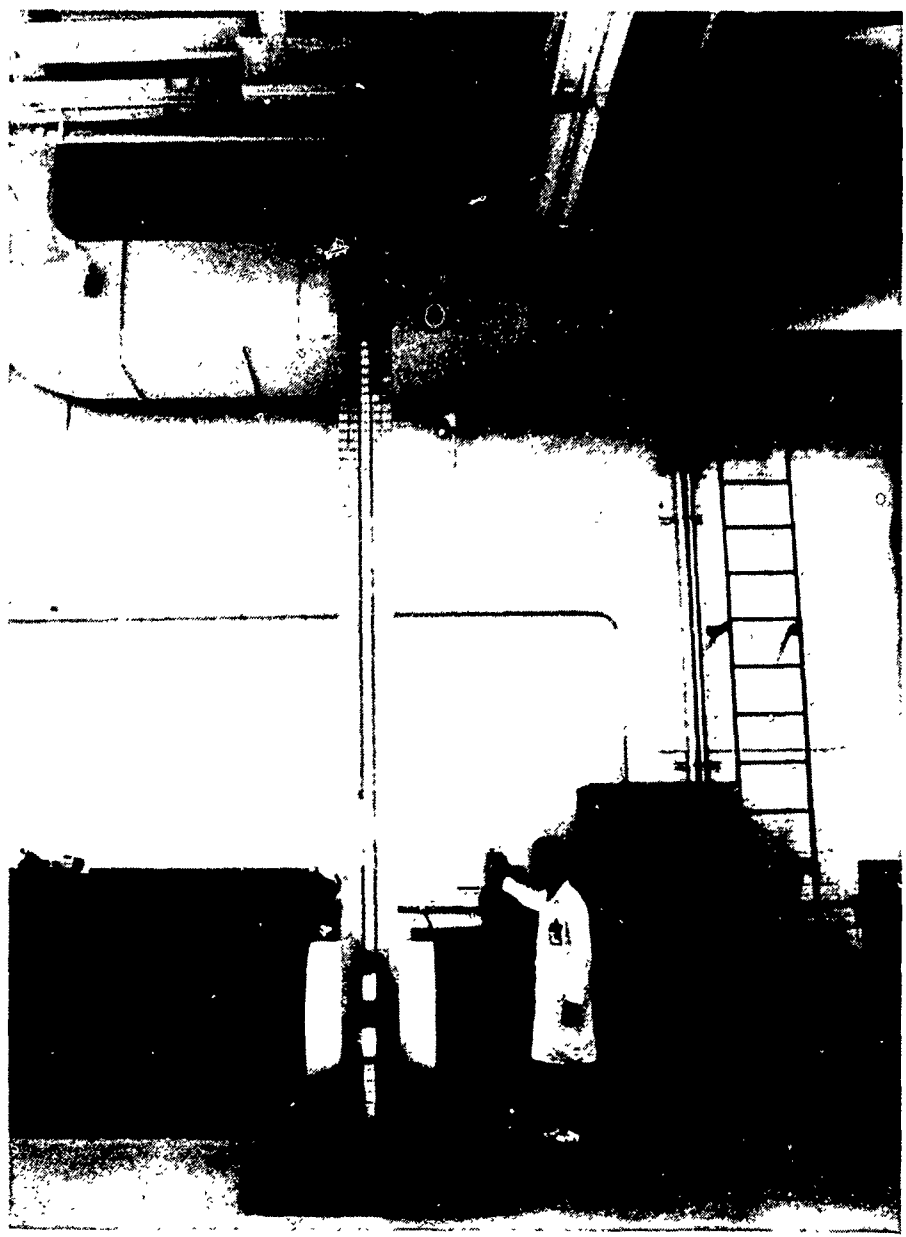

FIGURE 12

SEPARATION SYSTEM MECHANISM

The LADD structure is mounted to an adapter plate which is itself mounted to the MSL pallet. At the interface between the LADD drum support beam and adapter plate on both the port and starboard sides are redundant, two failure tolerant separation mechanisms (see Figure 13). These separation systems would be activated in the unlikely event that a failure of LADD or shuttle equipment prevents the retraction of safe stowage of the experiment. Should such an event present a flight safety problem, the Remote Manipulator System (RMS) would lift the experiment out of the payload bay and jettison it prior to re-entry.

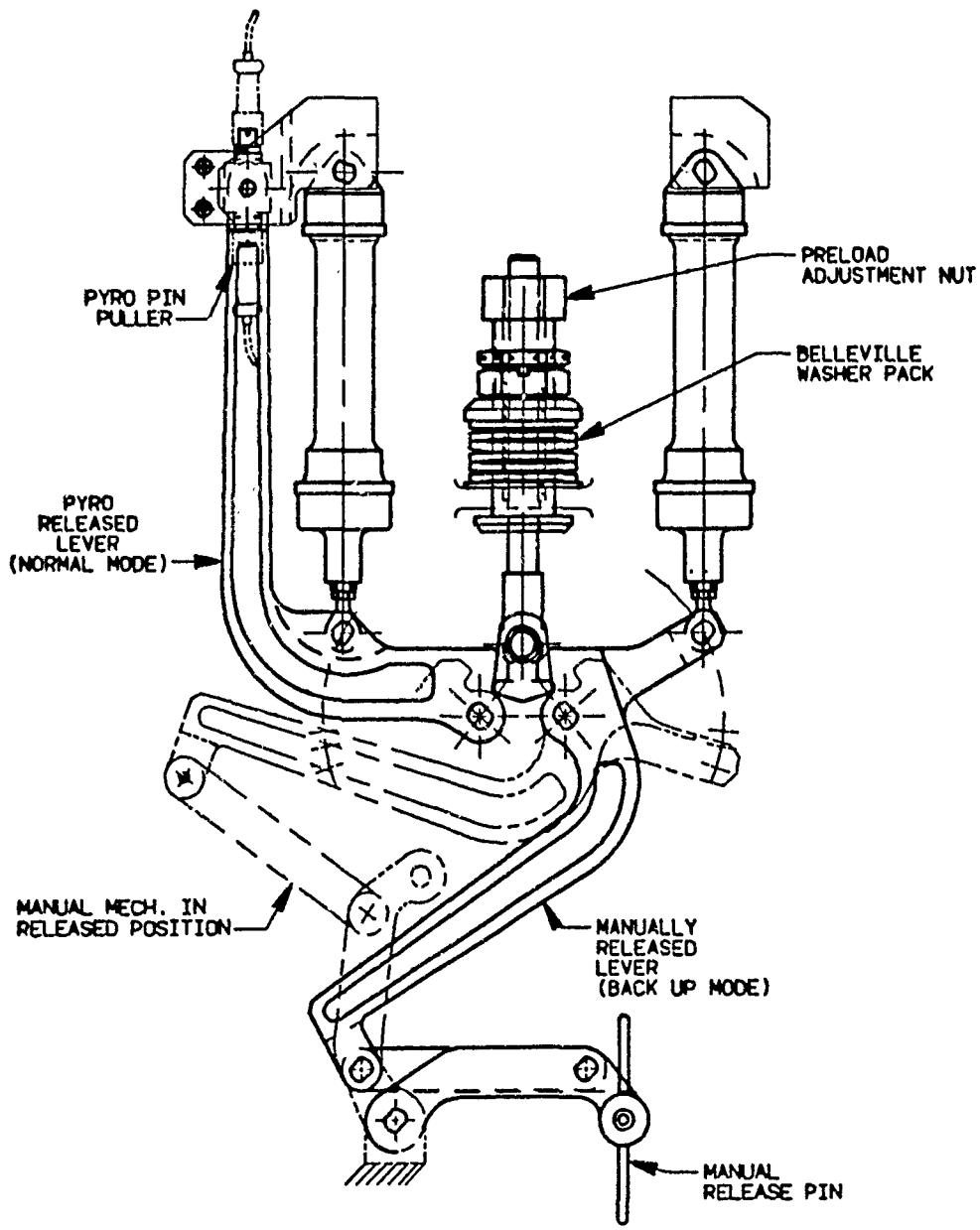

FIGURE 13

VERIFICATION OF DYNAMIC ANALYSES

Detailed finite element models of the LADD have been developed and comprehensive finite element analyses (FEA's) are being conducted for the ground test configuration attached to the MSL. The opportunity to perform meaningful correlation studies will be afforded when modal surveys are performed, at both Grumman and MSFC. These tests will also provide significant modal damping information that will be useful in final planning of the flight test program.

Flight testing will provide the opportunity to perform correlation studies to ultimately determine if the FEA's can accurately predict behavior of a single-axis roll-out satellite membrane. During flight testing membrane modal shapes will be recorded with the shuttle CCTV cameras. Dynamic inputs will be provided by firing specific orbiter primary RCS engines in a predetermined sequence. Determination of modal damping will provide important information with regard to the design of an SBR control system. Comparison of flight and ground test results for the LADD structure could also be helpful in resolving any anomalies.

- DETAILED FINITE ELEMENT MODELS OF STOWED LADD/MSL DEVELOPED
- BASE DRIVE AND COUPLED LOADS ANALYSES CONDUCTED FOR CRITICAL CONDITIONS
- MODAL SURVEYS OF LADD AND LADD/MSL COMBINATION WILL PROVIDE DATA FOR CORRELATION OF MODELS AND ANALYSES
- BASIC MODEL OF DEPLOYED MEMBRANE ALSO DEVELOPED
- DEPLOYED MODEL USED TO DEFINE ORBITER RCS FIRINGS FOR ON-ORBIT MODE SURVEYS
- ON-ORBIT DYNAMIC TESTS WILL PROVIDE ESSENTIAL MODAL DAMPING INFORMATION FOR FUTURE SBR SATELLITE DESIGNS

FIGURE 14

GSI CAMERA AND GAS CAN CONFIGURATION

The LADD is designed to meet the tolerances imposed by radar system requirements. The in-plane thermally-induced deflections can amount to a change in length of up to .04% for the long lens aperture. In an operational satellite this motion will be compensated for electronically. The out-of-plane flatness requirement for an x-band 8 ft. by 20 ft. membrane has also been determined. The membrane will be measured in the as-built configuration to establish baseline dimensions. After repeated deployments and retractions, measurement data will be collected for the membrane while on-orbit to determine if any permanent distortions have occurred.

The measurement of the membrane flatness and geometric stability will be determined with the use of three Geodetic Services Incorporated (GSI) photogrammetric cameras. Since existing cameras were not designed to be operated in a vacuum they will be contained in Get Away Special (GAS) cans (Figure 15) filled with presurized nitrogen.

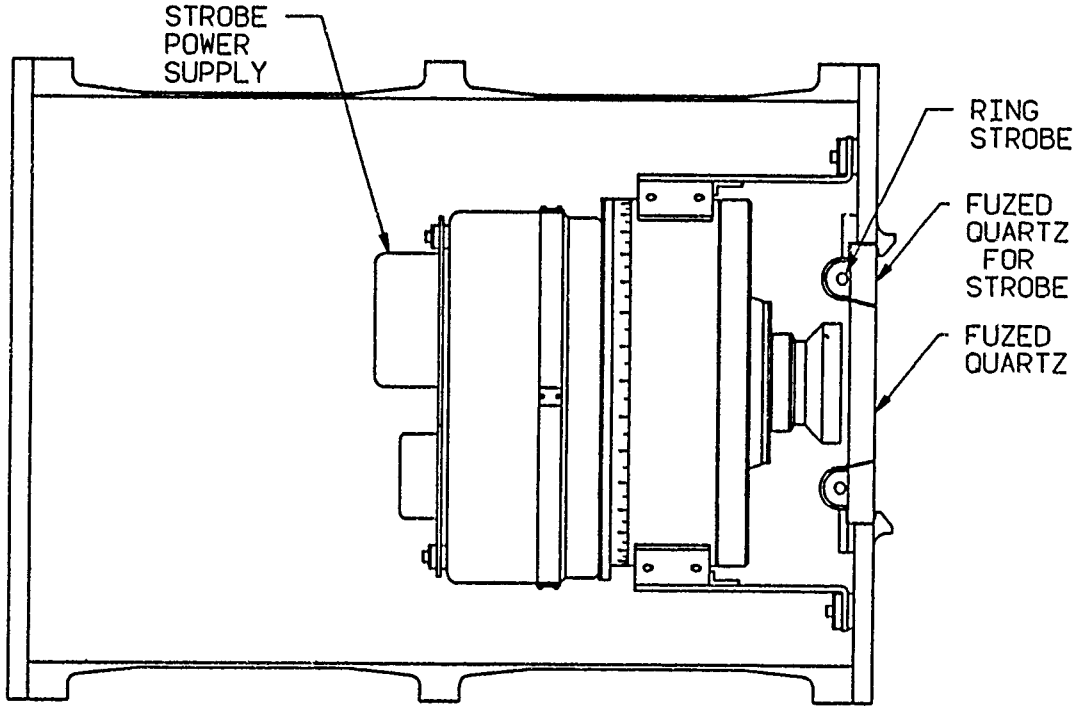

FIGURE 15

GENERAL CONFIGURATION - LADD MPESS CAMERA PALLET

The three cameras are carried in the shuttle on a Mission Peculiar Experiment Support Structure (MPESS) mounted forward of the LADD MSL pallet in the payload bay (Figure 16). Two of the cameras will be attached to the MPESS, and the third will be mounted on the previously flown Release/Engage Mechanism (REM) which is being furnished by MSFC.

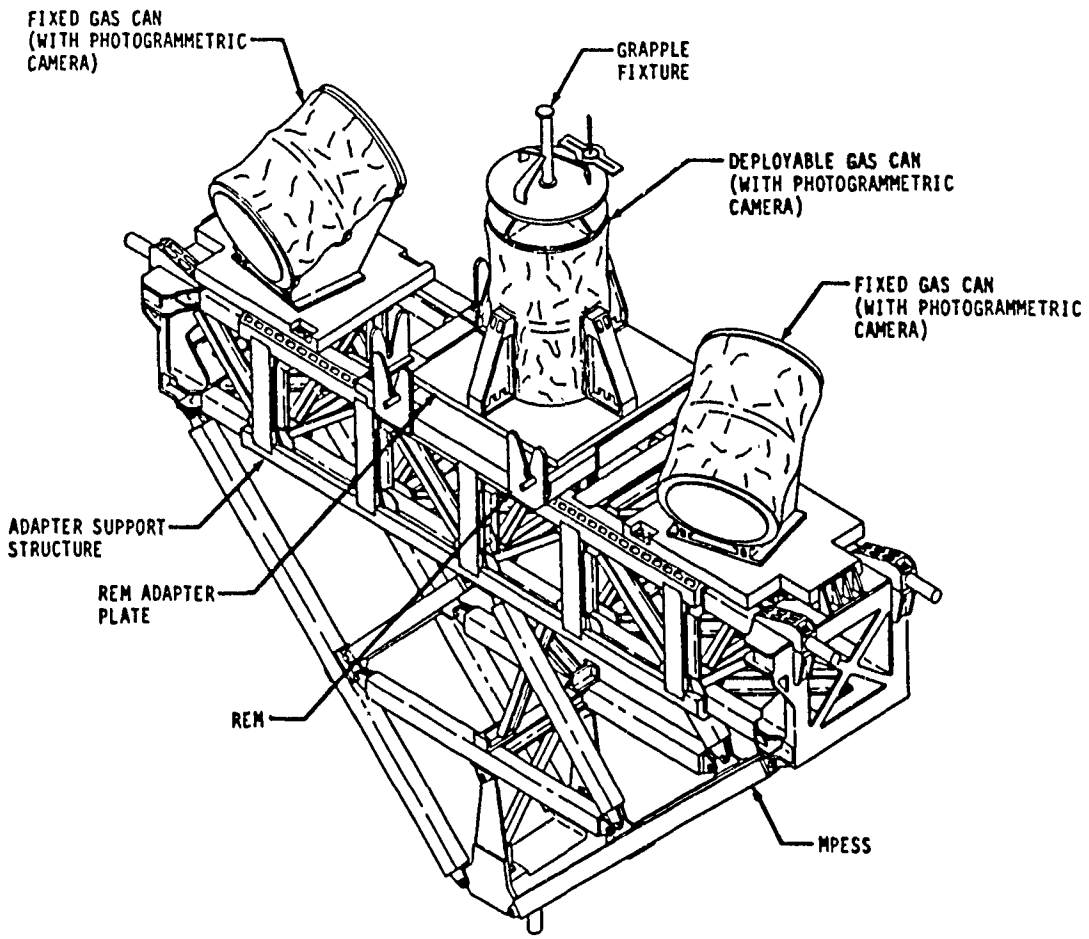

FIGURE 16

PHOTOGRAMMETRIC CAMERA TRIANGULATION

For photogrammetric measurement the REM mounted camera will be deployed and held by the RMS in such a position as to provide triangular viewing coverage of the membrane (Figure 17). Small photogrammetric targets will be mounted on the modules at specific locations on the membrane. Using analytic photogrammetry and calibration procedures that have been sucessfully employed in ground tests membrane flatness and geometric stability will be determined.

The deployment/retraction of the LADD and the activation of the three photogrammetric cameras will be commanded through hardwire control from the Payload Specialist station in the aft cabin of the shuttle.

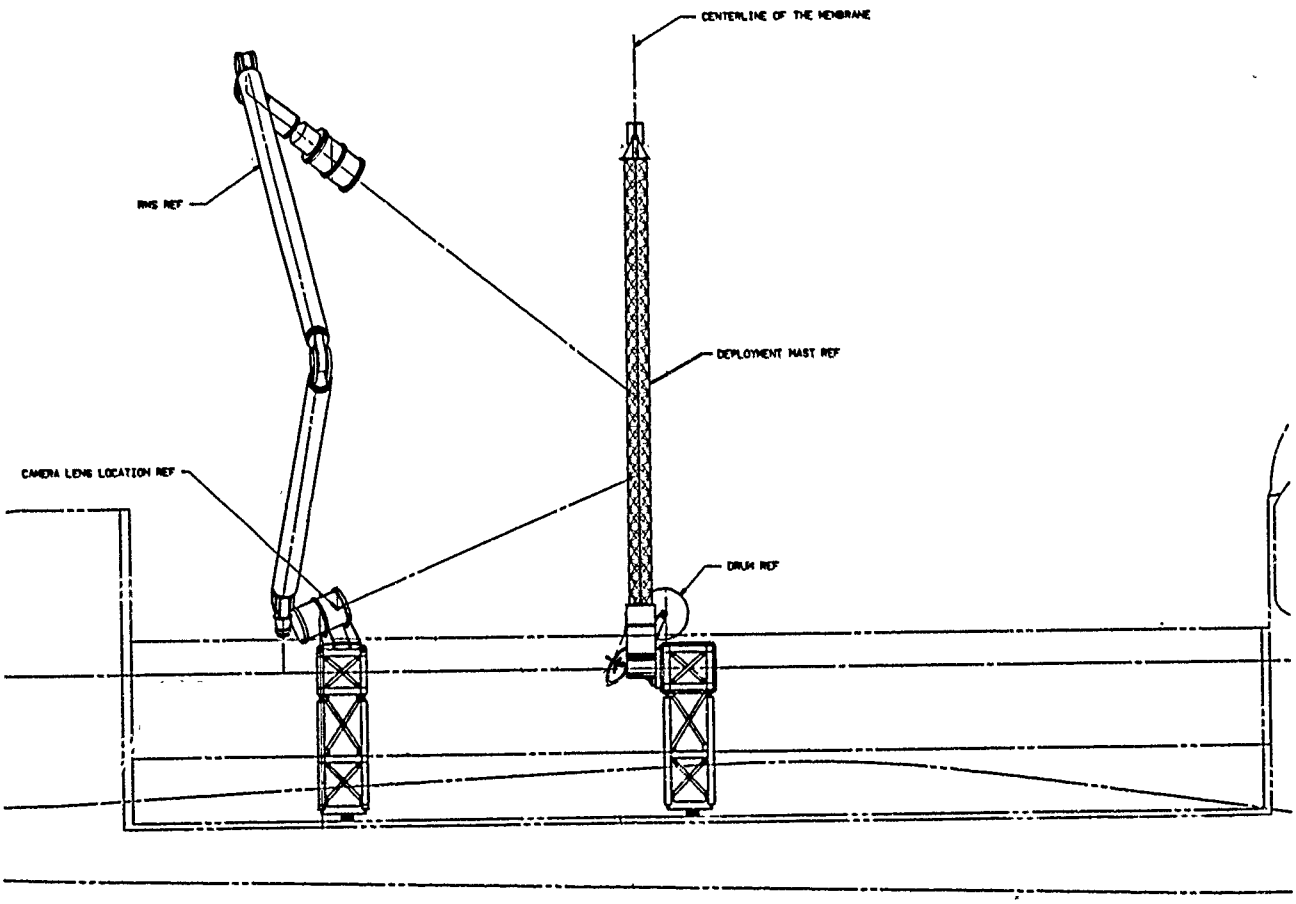

FIGURE 17

LADD PROGRAM MILESTONES

The specific experiment objectives have been published in the LADD Experiment Requirements Document and are currently being converted to a mission time line.

The LADD project recently completed its Preliminary Design Review and is progressing toward a Critical Design Review in early 1987. Figure 18 presents some program milestones as currently scheduled. Phase II of this program including the preflight testing, shuttle integration, flight support and post flight data reduction is currently in the planning stage. The flight date is, of course, not firm as the full impact of the shuttle booster redesign is as yet unknown and the new flight schedule and manifests have not been finalized.

ACCOMPLISHED	
PHASE I CONTRACT AWARD	OCTOBER 1985
PRELIMINARY REQUIREMENTS REVIEW (PRR)	JANUARY 1986
PRELIMINARY DESIGN REVIEW (PDR)	SEPTEMBER 1986
PLANNED	
CRITICAL DESIGN REVIEW (CDR)	JANUARY/FEBRUARY 1987
FABRICATION/INSTRUMENTATION COMPLETED	JANUARY 1988
TESTS/QUALIFICATION COMPLETED	APRIL 1989
DELIVERY TO KSC FOR CHECKOUT AND SHUTTLE INTEGRATION	APRIL 1989
FLIGHT READINESS REVIEW	4TH QUARTER 1989
FLIGHT	4TH QUARTER 1989/ 1ST QUARTER 1990

FIGURE 18

BOX TRUSS ANTENNA TECHNOLOGY STATUS

J.V. Coyner
E.E. Bachtell

Martin Marietta Denver Aerospace
Denver, Colorado

First NASA/DOD CSI Technology Conference
November 18-21, 1986

ABSTRACT

This paper summarizes recent technology development activities for box truss structures and box truss antennas. Three primary activities will be reported: the development of an integrated analysis system for box truss mesh antennae; dynamic testing to characterize the effect of joint free play on the dynamic behavior of box truss structures; the fabrication of a 4.5 meter diameter offset fed mesh reflector integrated to an all graphite epoxy box truss cube.

Analysis of Box Truss Mesh Antennas

An integrated analysis system has been developed to model, analyze, and predict RF performance of box truss antennas with reflective mesh surfaces. This analysis system is unique in that it integrates custom-written programs for cord-tied mesh surfaces, thereby drastically reducing both the man-hours and computer-dollars required to design and analyze mesh antennas. The program can be used to analyze the effects of (1) on-orbit thermal environments, (2) solar pressure, (3) on-orbit calibration or continuous adjustment of the mesh tie system to improve surface accuracy, and (4) gravity distortions during setting.

The analysis system uses nonlinear finite-element, surface topography and interpolation, and RF aperture integration techniques. The system provides a quick and cost-effective final link in the design process for box truss antennas.

Dynamic Testing of Box Truss Space Structures

Testing was performed to quantify the effect of joint free play on a multi-bay statically determinate truss, and then assess the effects when the structure is modified to incorporate pretensioned diagonals producing a statically indeterminate truss. Also evaluated were the effects of levels of dynamic load on the dynamic performance of the truss. Testing of four truss configurations was performed:

1. Truss with tight joints

2. Truss with joints having normal free play

3. Truss with joints having excessive free play (three times or more than normal free play)

4. Truss with normal free play and cross-tension diagonals

The effect of magnitude of dynamic load was assessed for each test.

A test article for this purpose was designed and built. The test article consisted of ten bays of planar truss, each measuring 2 meters per side, suspended by long wires at each joint. Each side was made of square aluminum tubing, and all corner fittings were made of cast aluminum. Pins of varying size were used to assemble the truss thereby simulating various joint free play conditions. All joints could be shimmed and bolted tight to assure a no free play condition. Single, unloaded tube diagonals were interchangeable with dual, tensioned steel rod diagonals. Modal analyses of the suspended tube diagonal configuration were conducted and used to calculate frequency response functions simulating proposed test conditions for the purpose of evaluating the suspension system.

Fabrication of a 4.5m Box Truss Antenna

A 4.5 meter diameter offset mesh reflector was fabricated and integrated to an all graphite epoxy box truss cube. The reflector surface was designed to operate at X-Band (10 GHz) with a surface accuracy of $\lambda/20$ where λ = wavelength (30 mm). Four objectives were achieved during the fabrication, setting and testing of the antenna. They were: 1) demonstrated fabrication methods for both mesh and tie system, 2) demonstrated performance of modular tie system to precisely position and hold mesh surface, 3) verified nonlinear stress stiffened finite element analysis of the tie system.

SOLAR DYNAMIC POWER SYSTEMS FOR SPACE STATION

THOMAS B. IRVINE
MARSHA M. NALL
ROBERT C. SEIDEL

NASA LEWIS RESEARCH CENTER
CLEVELAND, OHIO

First NASA/DOD CSI Technology Conference
Norfolk, Virginia
November 18-21, 1986

OBJECTIVE

Solar dynamic systems studies and development are currently being performed by NASA Lewis Research Center and their Space Station Program Phase B and Advanced Development Program Contractors to complete preliminary design of a viable solar dynamic power module. This design must be compatible with a Space Shuttle launch and with on-orbit assembly aboard the Space Station.

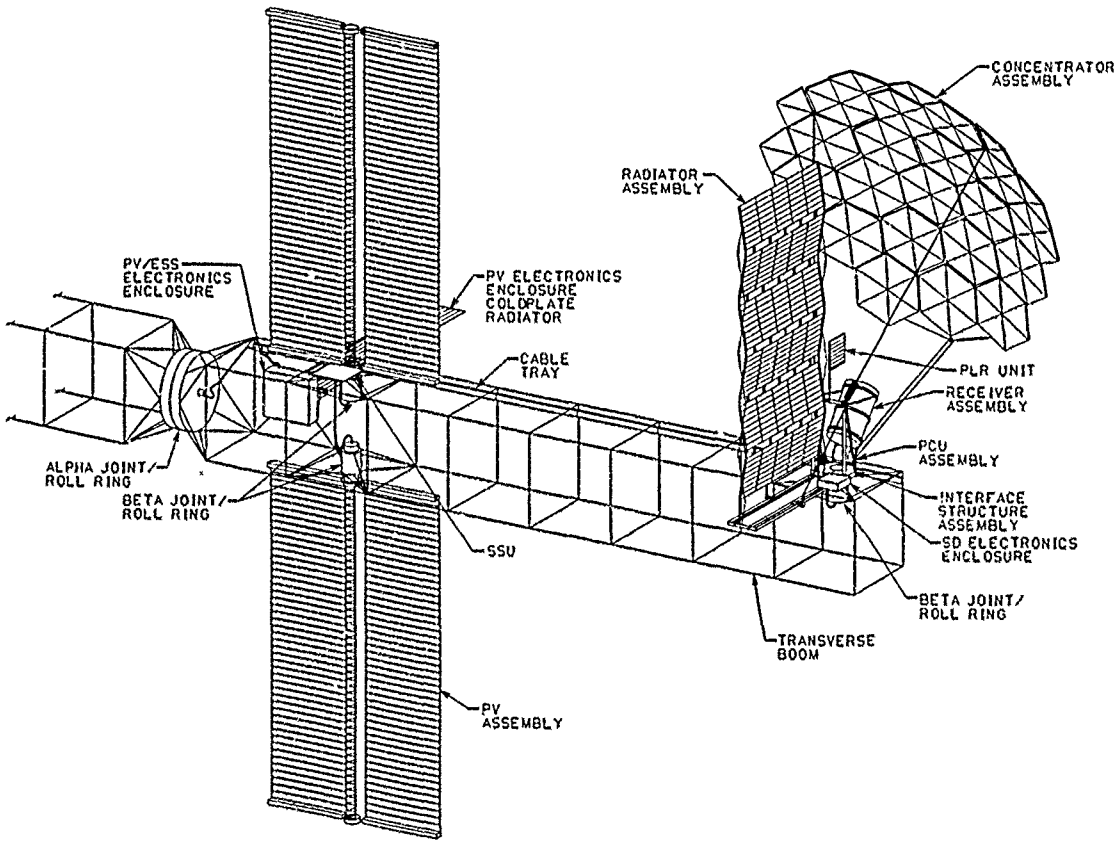

BACKGROUND

Solar dynamic power systems work by accurately pointing a reflector (concentrator towards the sun and focusing the reflected energy into a heat receiver where a working fluid is heated. This heated fluid is used to drive a turbine in a power conversion unit. Coupled to the turbine is an alternator which generates electricity thus completing the conversion of thermal to mechanical to electrical energy. The working fluid is cooled by a dedicated thermal control system (heat exchanger/radiator) in order to maintain proper thermodynamic state points. Both Organic Rankine Cycle and Closed Brayton Cycle heat engines are under consideration as potential "power plants" of the solar dynamic system.

Two solar dynamic power modules are utilized on the IOC Space Station. Each module is capable of delivering to the user's load converter an average of 25 kWe over the 90 to 95 minute Space Station orbit. During the 34.18 to 35.47 minute eclipse portion of the orbit, a thermal energy storage (TES) medium is required to heat the working fluid. A TES medium integral to the receiver has been proposed and is being pursued during preliminary design.

In order to achieve the appropriate flux distribution in the receiver cavity, concentrator mirror surface accuracy and pointing accuracy tolerances are tightly controlled. Structural integrity is required in the Space Station truss system, solar dynamic module interface and support structures and the concentrator substrate. To achieve required concentrator surface accuracies, very stringent manufacturing tolerances must be applied to the reflector design. In addition, active control of the vernier pointing capability is necessary to provide the required pointing accuracy.

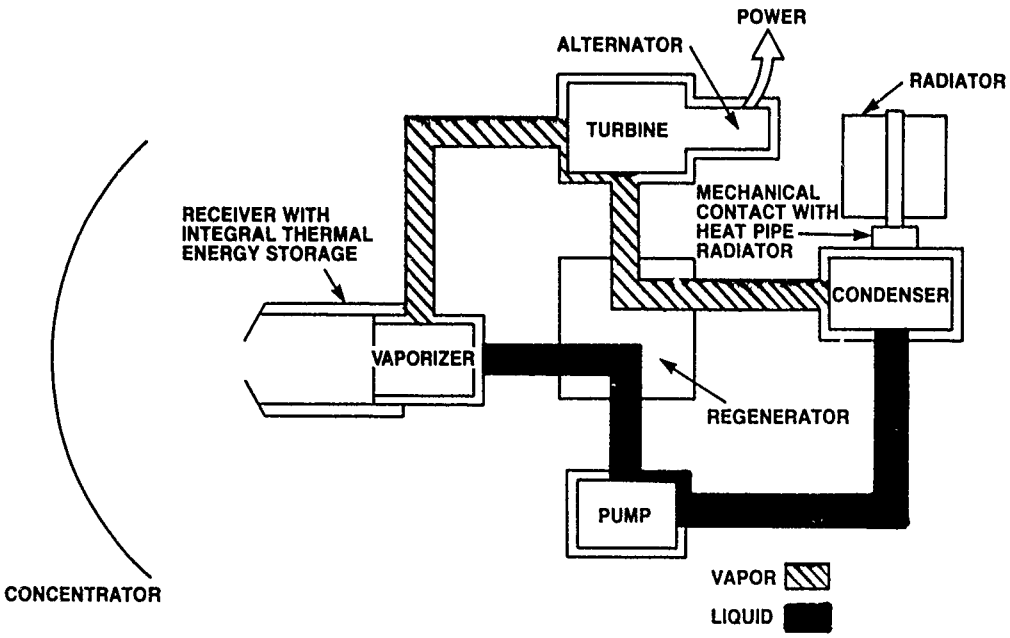

- Solar Dynamic ORC Is a Simple Energy Conversion Cycle

SCOPE AND APPROACH

A solar dynamic module conceptual design was generated during the Space Station Program WP-04 Phase B: Space Station Definition and Preliminary Design. Preliminary design based upon this conceptual design, discussed later, is currently being conducted.

Structural and control issues were among the many discriminators included in trade studies used to arrive at a baseline conceptual design. Finite element method static and dynamic analyses and control theory calculations were used to assess the structural characteristics of competing design concepts. Normal mode analysis was used to determine structural frequencies of the Space Station transverse boom given different solar dynamic module designs. Control theory was then used to predict system instabilities given the structural and controller bandwidths.

Presented herein is a summary of the structures and controls studies used to aid in the selection of a Space Station solar dynamic module design.

- Solar Dynamic Module Conceptual Design Trade Studies
  - Controls/Structures Interaction Discriminator
    - * Normal modes analysis of solar dynamic module conceptual designs using MSC/NASTRAN
    - * Classical control theory used to evaluate solar concentrator coarse and vernier pointing system
    - * Static and dynamic finite element analysis used to evaluate module support and transition structures

OUTLINE

Several different classes of solar concentrators were considered during the early stages of Phase B: Definition and Preliminary Design Studies. These options included single and multiple reflection systems and refraction systems. Simple and offset parabolic reflectors, selected as the best candidate designs, were studied by using structural normal modes analysis to determine the coupled solar dynamic module - transverse boom natural frequencies. The Space Station was modelled as a lumped parameter system to determine the control system stability.

The Parabolic Offset Linearly Actuated Reflector (POLAR) concept was chosen as the concept with which to go forward into preliminary design. The interface and support structure for this concept are currently being studied.

- Conceptual Designs
- Normal Modes Analysis
- Pointing Control and Coupling Analysis
- The Parabolic Offset Linearly Actuated Reflector
- Support Structure Design and Analysis
- Summary

CONCEPTUAL DESIGNS

A number of concentrator optical systems were considered during trade studies. These included, but were not limited to, symmetric Newtonian (parabolic), offset Newtonian, Cassegrainian, Fresnel refractor, and point focus trough designs. Key discriminators in determining the optical system included mass, drag, mass moment of inertia about the transverse boom, launch cost, development cost, annual cost, life-cycle cost, maintainability, logistics, safety, technology readiness, and IOC schedule/cost risk. Based primarily upon technology readiness and IOC schedule/cost risk, all but the symmetric and offset Newtonian concentrator designs were eliminated.

Three proposed design concepts studied in detail and shown in the figure are the modified sunflower deployable concentrator (simple Newtonian), the Offset U-Truss configuration (simple Newtonian), and the Parabolic Offset Linearly Actuated Reflector (POLAR) system (offset Newtonian).

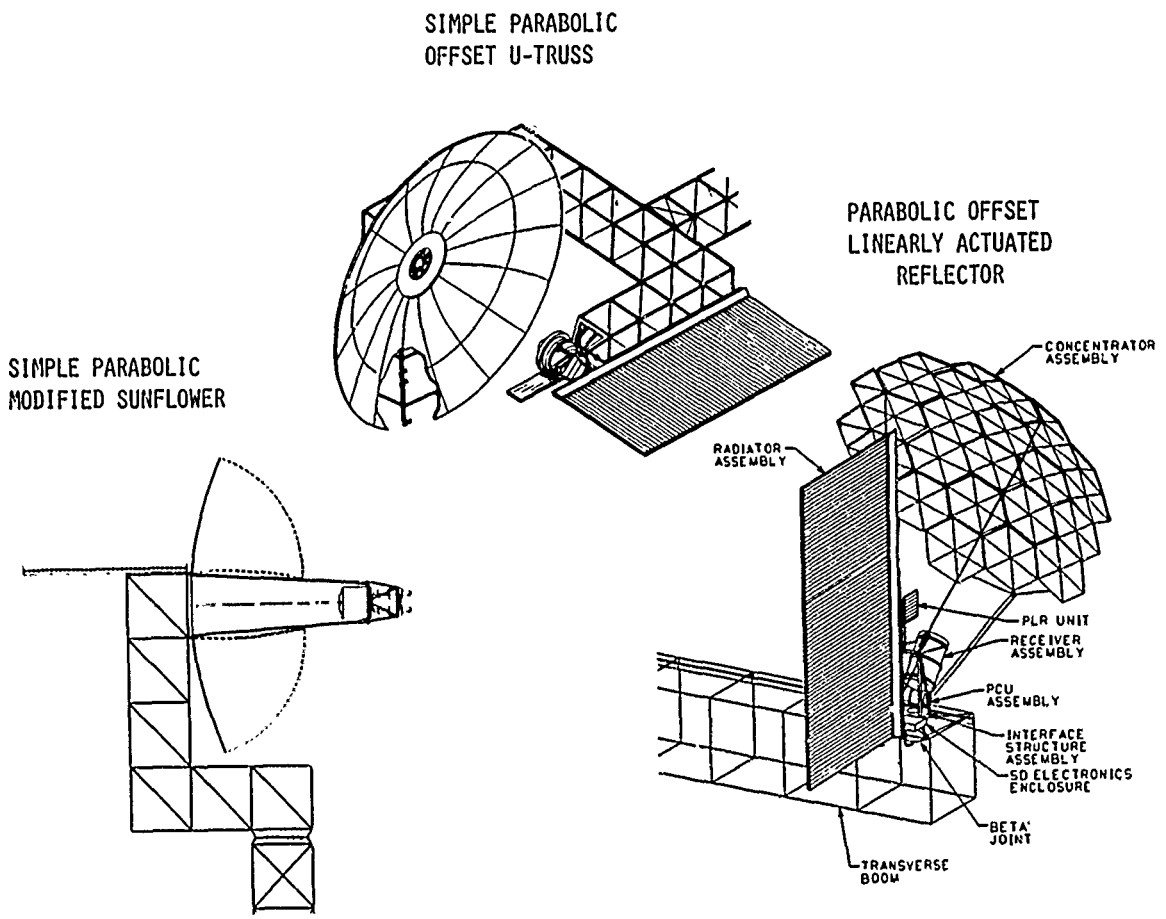

NORMAL MODES ANALYSIS

The finite element method (Ref. 1) was used to model the three solar dynamic module concepts under consideration, the modified sunflower, the POLAR, and the offset U-Truss. Continuous beam representations of the truss work (Ref. 2) and concentrated mass representations of the major components of the solar dynamic module were employed. Masses and dimensions of representative Closed Brayton Cycle solar dynamic module major components were used in this analysis and are listed below.

The length of the transverse boom was determined by shadowing considerations. The required spacing between the solar dynamic module and the vertical keel or between adjacent solar dynamic modules is set by the width of the solar concentrator and the maximum beta angle. Maximum beta is the addition of the orbit inclination and the seasonal rotation of the earth. For the analysis performed, the distance between the transverse boom/vertical keel intersection and solar dynamic module center line was 63 ft. The distance between adjacent solar dynamic modules for the growth configurations was 107.36 ft. This spacing was based upon a maximum beta joint of 55°.

Closed Brayton Cycle (25 kWe SD Module)

Component	Mass (lbs.)	On-Orbit Dimensions (ft)
Concentrator	1684	43.32 equiv dia
Receiver Including Eclipse TES	2860	6.67 dia × 7.92 length
PCU	1075	2.19 dia × 2.52 length
Radiator	3400	req'd area = 1000 sq ft
Panels (40 req'd)		width - 1. , thickness - .125 , length - 28.
Heat Exchanger		width - 3. , height - 2. , length - 45.
TOTAL	9019	

NORMAL MODES ANALYSIS (CONT'D)

Normal modes analysis was performed on each Closed Brayton Cycle solar dynamic module concept for three different cases. These cases were 100 kWe, 200 kWe, and 300 kWe Space Station models using replications of 25 kWe solar dynamic modules. The cases run were of the half transverse boom where the transverse boom/vertical keel interface was assumed fixed in all translations and rotations.

This simplified the problem significantly by reducing a substantial number of degrees of freedom that would ordinarily be assigned to define the entire dual-keel Space Station. It also allowed for the isolation of the transverse boom and its natural frequencies. The transverse boom torsional mode frequency is of particular interest because it is the structural frequency that could potentially couple with the alpha joint controller.

The natural frequencies and corresponding mode shapes for the fundamental torsional mode are shown in the figure below.

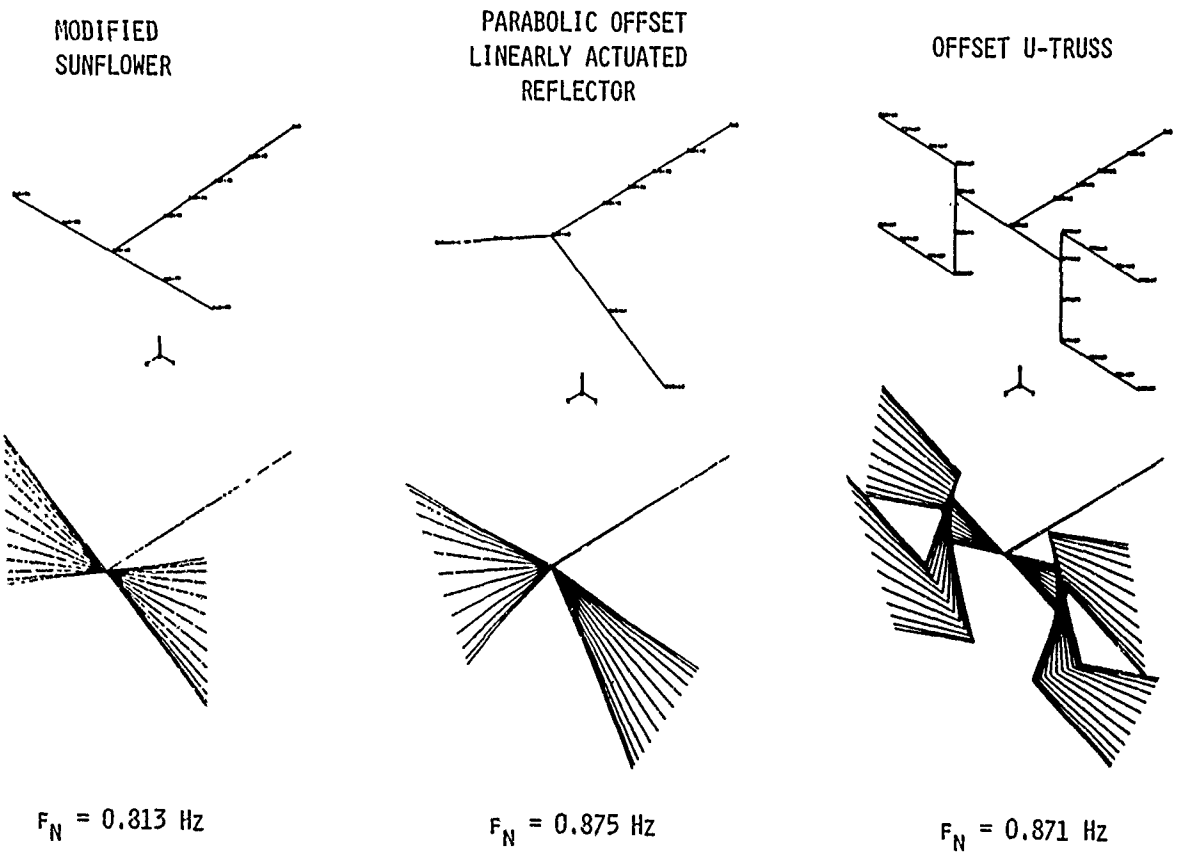

LOWEST TRANSVERSE BOOM TORSIONAL MODE NATURAL FREQUENCY
(ALL SD IOC CONFIGURATION)

Results of the transverse boom fundamental torsional mode natural frequency dependency on solar dynamic module design are summarized in the figure. All SD module designs exhibit the same general trend of frequency reduction in transverse boom torsion as the station power level increases. This frequency reduction is due to the increase in the mass of the system as the transverse boom is lengthened and the additional power modules are added. The actual frequency values of the POLAR conceptual design were found to be quite close to the values of the modified sunflower design at the power levels of 100 kWe, 200 kWe, and 300 kWe. The transverse boom fundamental torsional mode natural frequencies determined for both of these concepts appear to have adequate separation (ten times or greater) between the structural and controller bandwidth frequencies for all power levels studied. The U-Truss design concept, however, provided much lower transverse boom torsional natural frequencies. Whereas an IOC Space Station utilizing this design would not experience any structures and controls interaction, the same cannot be said for the growth power level. The 300 kWe system does not provide the desired decade of separation between the transverse boom natural frequency and the frequency of the rotary alpha joint controller bandwidth. The separation, in fact, is only half of the design goal.

TRANSVERSE BOOM FUNDAMENTAL TORSIONAL MODE FREQUENCY AS A FUNCTION OF POWER LEVEL

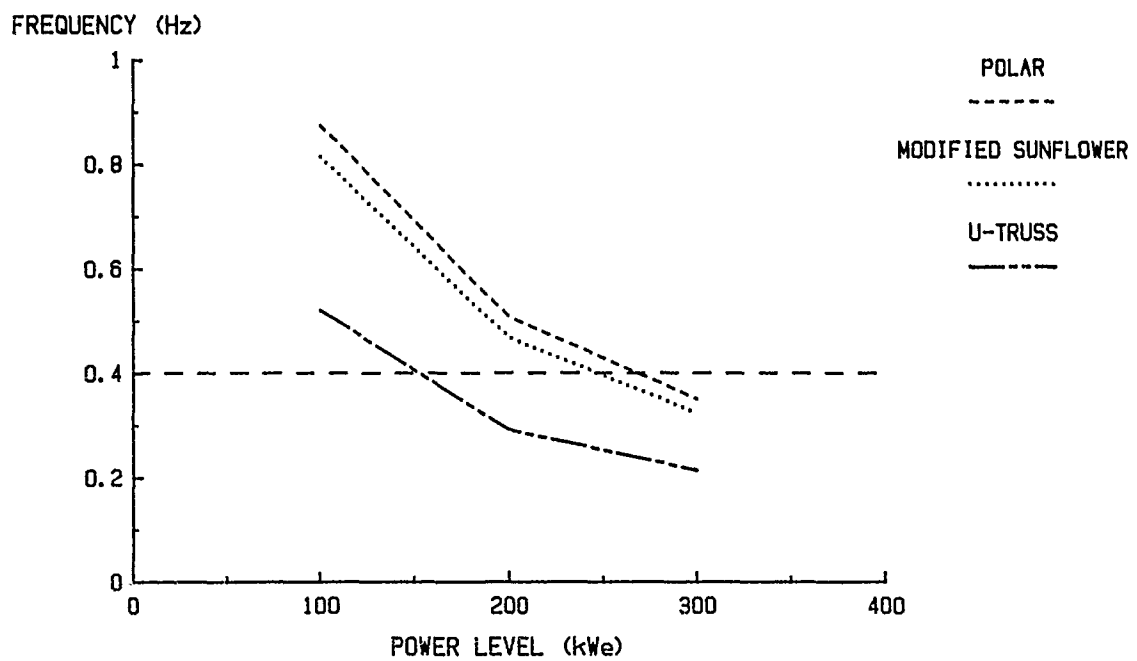

- RESULTS BASED ON 25 kWe MODULE SIZE
- 9 FT TRUSS SIZE USED AS POWER MODULE SUPPORT WHERE APPLICABLE

CONTROL OF CONCENTRATOR

The solar concentrator is to be pointed toward the sun with a wide angle of adjustment for each axis of rotation. The alpha joint provides continuous 360° tracking of the sun, and the fine pointing mechanism accounts for the 2° tolerance of the alpha joint. The concentration ratio at the receiver aperture can be several thousand suns and the concentrator focal point needs to be pointed accurately within 0.1 degree.

The vernier pointing control may operate in a high bandwidth near structural natural frequencies. A rule of thumb holds that controls should be well below structural frequencies to avoid oscillations. However, that rule applies for controls which "lock" a joint.

Stability and interactions of the vernier and coarse pointing controls are analyzed with a simplified torsional model of the station. The problem is simplified to consider only rotations about the alpha axis of rotation. Note that similar results are expected for the orthogonal beta axis.

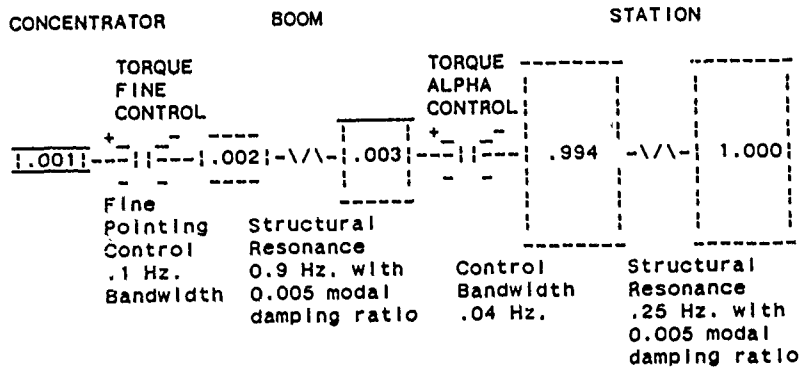

CONTROL IS SIMPLIFIED PURE PROPORTIONAL PLUS DERIVATIVE

CONTROL TORQUE = PROPORTIONAL GAIN * (COMMAND - ANGLE) + DERIVATIVE GAIN * (INBOARD VELOCITY * M1 - OUTBOARD VELOCITY)

IF M1 = 0 ONLY VELOCITY OUTBOARD OF ALPHA JOINT ENTERS

M1 = 1 VELOCITY IS DIFFERENCE ACROSS THE ALPHA JOINT

COMMAND SIGNAL FOR ALPHA AND VERNIER POINTING IS FROM CONCENTRATOR CONTROL COMPUTER

ALTERNATIVE COMMAND SIGNAL FOR ALPHA JOINT IS FROM STATION GUIDANCE

IF CONTROL GAINS AND ADJUSTED HIGH, JOINT APPEARS "LOCKED"

IF CONTROL GAINS AND ADJUSTED LOW, JOINT APPEARS "NON LOCKED"

Based upon the simplified model several observations are made. Results may motivate undertaking more detailed analysis to verify their accuracy.

Comments on the results shown in the figure below are listed here. The control law derivative gain operates on the relative velocity across the joint, i.e., "M1" = 1.

1. The pointing controls can be a beneficial (although unintended) source of system damping. The increase in damping, above the small .005 assumed structural damping, is a result of the active control.

2. The pointing controls may operate in bandwidths near system structural frequencies. The boom need not be designed stiff to avoid control instabilities.

3. If the pointing control gain is too high, the control tends to "lock" the joint and beneficial damping is lost. In the worst case, the system is unstable.

BOOM MODAL DAMPING RATIO INTERACTIONS WITH CONTROL GAIN OF ALPHA GIMBAL

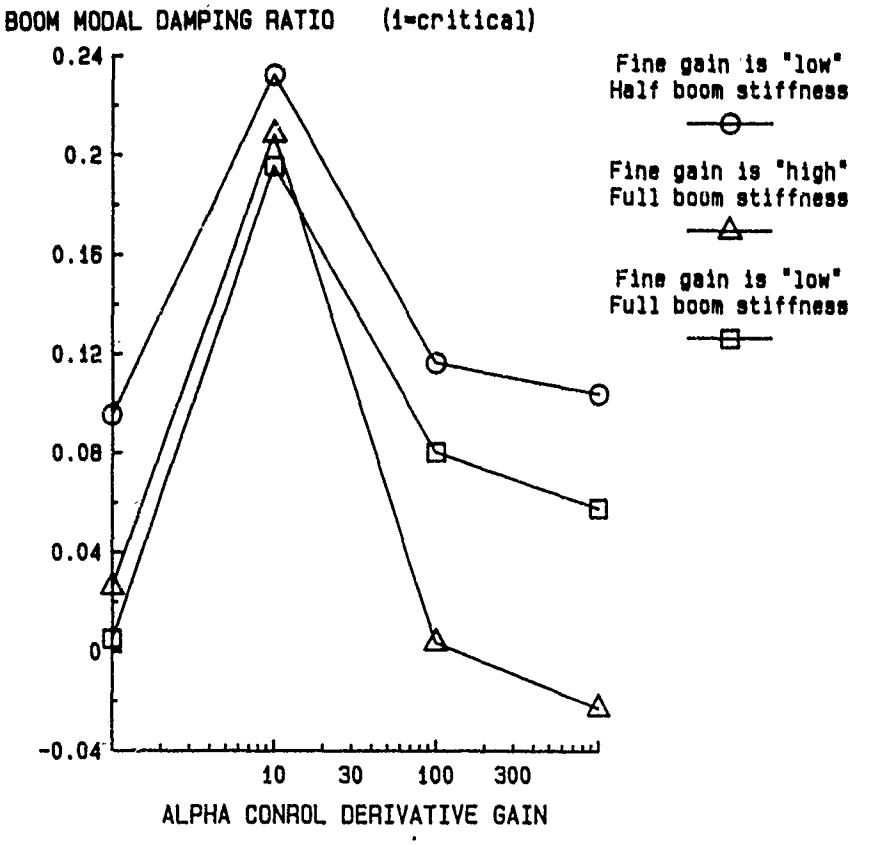

Derivative gain is normalized to 1 at low gain.

Less error crosses the alpha joint: a) if both joints work to reduce the same fine pointing error, and b) if disturbances can back drive the joints. Back drive joints can be natural vibration isolators, passively reducing disturbances from the station to the concentrator, removing the need for fast controls, and eliminating the potential for structural instabilities that can occur with too high gain.

The curves in the figure demonstrate control that eliminates the transmission of disturbances across the alpha joint. No error passes if:

1. The joint control uses derivative gain for outboard velocity only, i.e., (M1 = 0).

2. The COMMAND to the alpha joint is the fine pointing error and not a signal from station guidance.

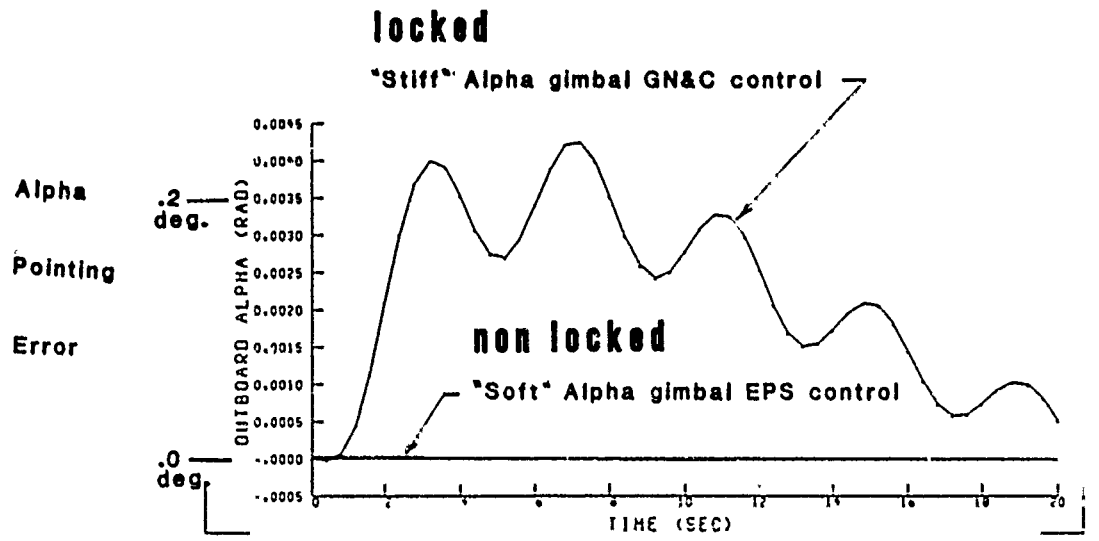

Response outboard Alpha gimbal to .0034 rps torsional disturbance to station

THE PARABOLIC OFFSET LINEARLY ACTUATED REFLECTOR

The conceptual design chosen as the baseline from the trade studies is the Parabolic Offset Linearly Actuated Reflector (POLAR) solar dynamic module.

The solar dynamic system consists of five major assemblies: concentrator, receiver, power conversion unit (PCU), radiator and interface structure assembly. The figure below reflects changes in the current design from the concept considered during trade studies. This includes most noticeably the utilization of a pumped loop radiator system instead of a heat pipe radiator. The module attaches to the Space Station structure outboard of the beta joint flange which mounts to the interface structure. The solar dynamic system interface with the power management and distribution system is outboard of the solar dynamic power module frequency converter and remote bus isolators.

The offset Newtonian concentrator consists of a segment of a parent parabola with a focal length to diameter ratio of 0.25 mounted offset from the parent parabolic axis of revolution. The receiver is tilted 53° with respect to the parent parabolic axis of revolution to achieve a nearly symmetric receiver cavity flux distribution. The offset configuration, used successfully in RF applications has a low mass moment of inertia about the transverse boom. In addition, there are no serious primary or secondary blockage problems. The offset reflector does cause larger cosine losses than a symmetric Newtonian concept. The desirable symmetric flux distributions are also more difficult to achieve.

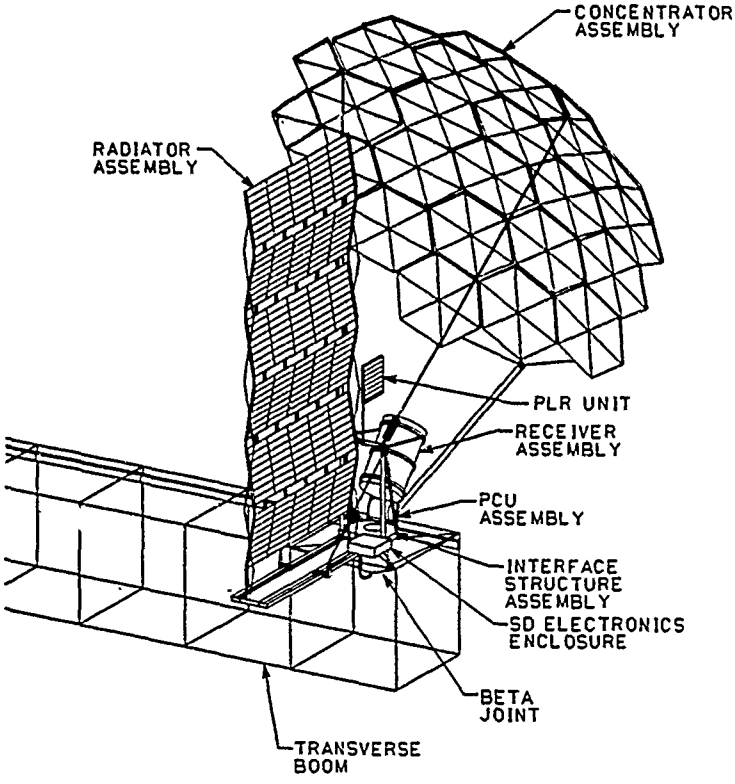

CHARACTERISTICS

MASS (CONCENTRATOR ONLY)
2418 LBS

DRAG (CONCENTRATOR ONLY)
2957 FT^2

MASS MOMENT OF INTERTIA (MODULE ABOUT TRANSVERSE BOOM)
0.5 $(10)^6$ LB.FT.S

SHUTTLE ORBITER PAYLOAD MANIFESTING
2 MODULES/LAUNCH

SOLAR CONCENTRATOR DESIGN

The solar concentrator is made up of an assemblage of 19 hexagonal panels. The panels are attached to each other with hinges and latches that are designed to perform two functions. The hinges and latches are first an assembly aid designed for either automated deployment or EVA assisted erection. After assembly of the 19 hexagonal panels into a single unit, the hinges and latches provide structural integrity. The hinges and latches are fabricated from aluminum.

The hexagonal panels are an assembly of I-beams and corner shear fittings to which triangular facets are attached. The hexagonal panel superstructure is entirely graphite/epoxy composite construction with the exception of the adjustment screws. The triangular facets are each approximately 3 ft. on a side. Constructed with a honeycomb core, graphite/epoxy composite facesheets, and a vapor deposited reflective surface, the facets weigh approximately 0.8 lbs./sq. ft. A protective coating applied over the reflective surface is required to reduce surface degradation. Focusing of the triangular facets is accomplished on the ground prior to packaging by means of the adjustment screws.

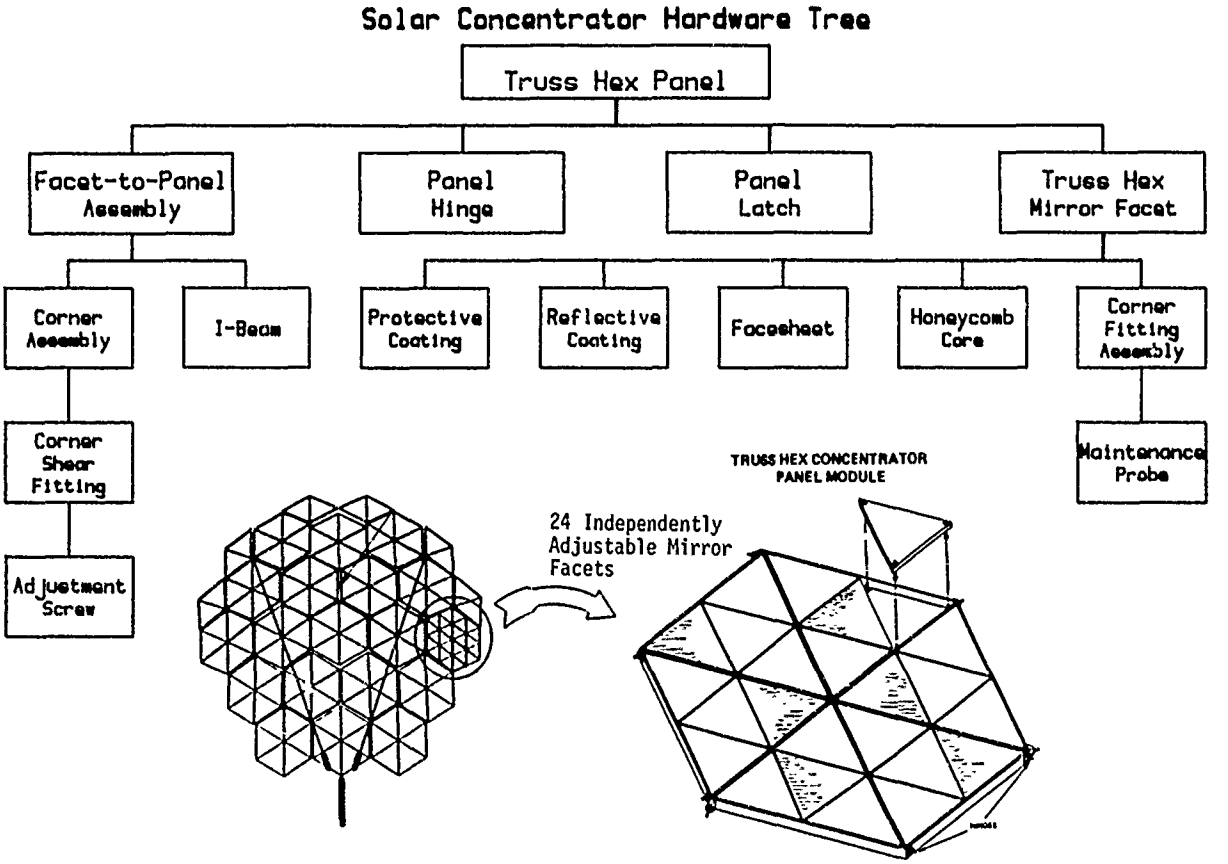

CONCENTRATOR SUPPORT STRUCTURE DESIGN AND ANALYSIS

The three strut solar concentrator support structure provides three degree of freedom vernier pointing capability by incorporation of linear actuators into two of the three tripod struts. This allows for solar vernier tracking by articulation of the concentrator. This also reduces the inertia that the actuator motor must overcome by requiring movement of only the concentrator. The drawback of the three strut tripod concentrator support system is the relatively poor structural dynamic characteristics exhibited by such a structure. Should one of the struts fail, there would exist no structure to support the concentrator in a stable manner.

An alternative to the three strut tripod concentrator support is the six strut tripod support system shown below. Static and dynamic structural analyses were performed to investigate the structural integrity of the three strut and six strut tripod support structures.

Pictorials of both concepts and their fundamental frequencies are shown below. The inside diameter and wall thickness of the three strut support structure were taken to be 3.0 in. and 0.15 in., respectively. The equivalent dimensions for the six strut support structure were 1.5 in. and 0.075 in.

3-STRUT TRIPOD CONCENTRATOR SUPPORT STRUCTURE

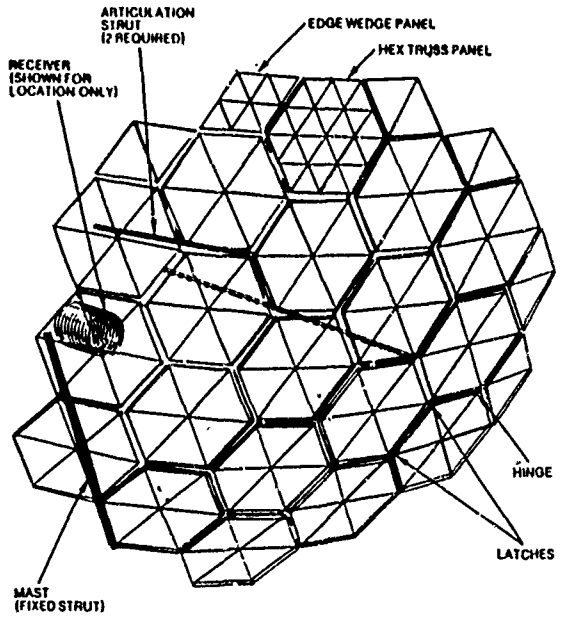

F_N = 0.271 Hz

6-STRUT TRIPOD CONCENTRATOR SUPPORT STRUCTURE

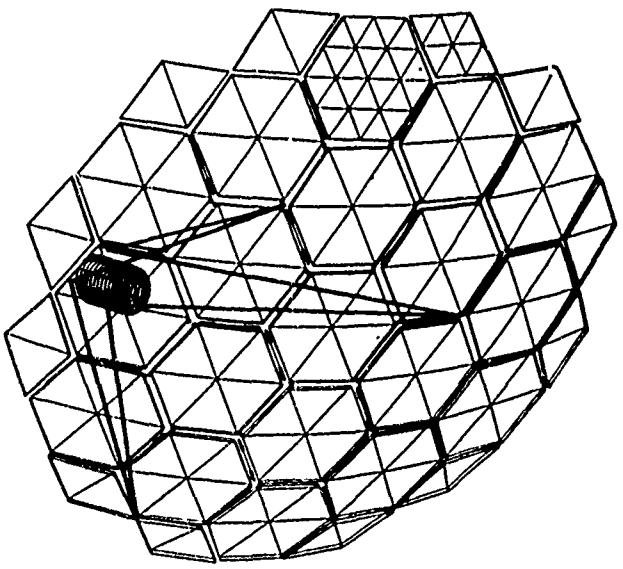

F_N = 1.46 Hz

A parametric linear static analysis of the candidate support structures were performed to determine their response to various load cases. By assuming the concentrator to be a rigid body relative to the support struts the structural performance of the two options was determined. Load cases where 1 lb. forces and 1 ft*lb moments were applied at the concentrator center of gravity were investigated. The results shown here are for the case where a 1 lb. force is applied parallel to the transverse boom axis with an inboard direction vector. Displacements, forces at the constraints, forces including axial, bending, and shear in the struts, and stresses in the struts were determined.

The worst case bending moments in the struts of the three and six strut tripods are shown plotted below. As seen, much lower bending moments are transferred through the six strut support structure. Moments transferred to the solar dynamic module mounting platform by the six strut support structure are calculated to be three orders of magnitude lower for the identical load case.

CONCENTRATOR SUPPORT BENDING MOMENTS

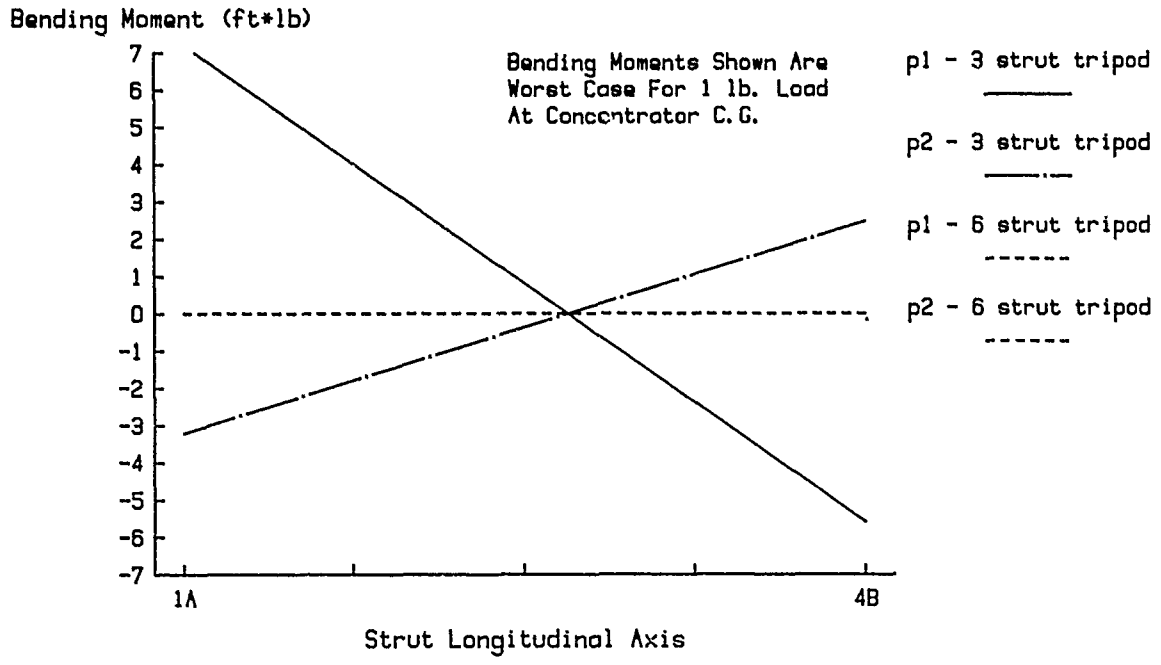

1A - Fixed End
4B - Concentrator Attach Pt.
p1 - plane 1 p2 - plane 2

The figure below shows the worst case shear stresses in the concentrator support structure struts (for the three and six strut tripods) for the 1 lb. force load case described previously. Not shown are the tensile and compressive forces in the struts which are in general an order of magnitude greater in the six strut tripod support system. These results along with the bending moments shown previously indicate that the six strut support structure is far more resistant to bending than the three strut tripod support. Hence, the six strut design, stiffer in bending, would minimize receiver spillage losses due to accelerations transmitted from the Space Station structure to the solar dynamic module.

The vernier pointing system design for the six strut tripod support still needs to be resolved. Solutions ranging from articulation of only the concentrator to articulation of the receiver/concentrator assembly are being investigated.

CONCENTRATOR SUPPORT SHEAR STRESSES

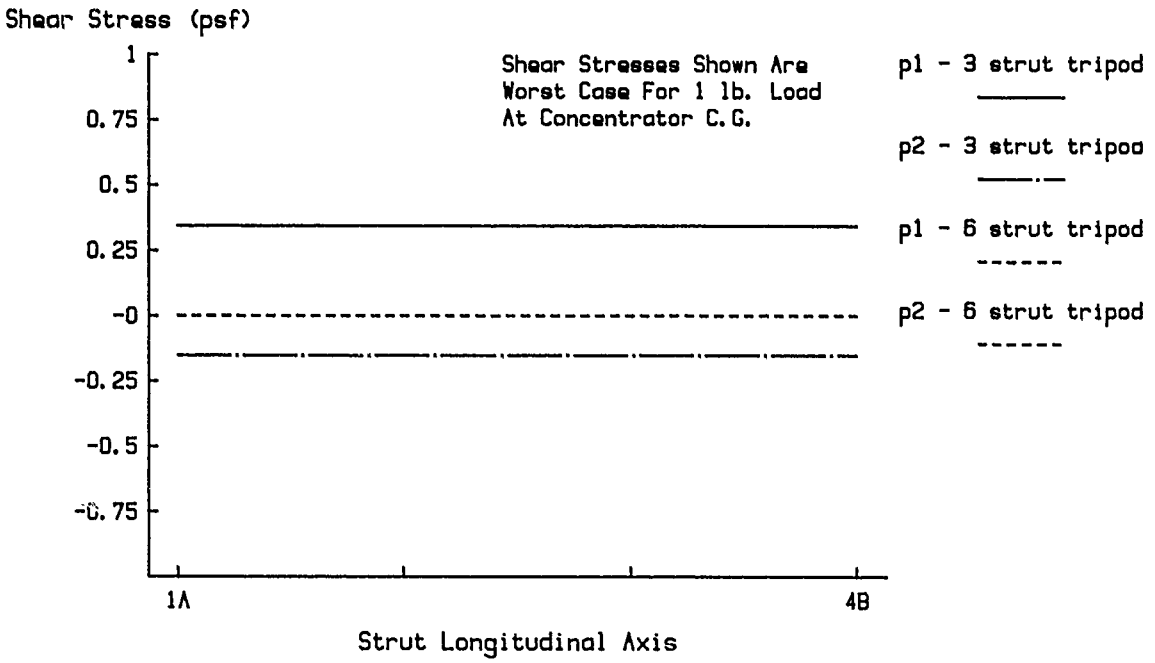

1A - Fixed End
4B - Concentrator Attach Pt.
p1 - Plane 1 p2 - Plane 2

SUMMARY

The Parabolic Offset Linearly Actuated Reflector (POLAR) solar dynamic module was selected as the baseline design for a solar dynamic power system aboard the Space Station. The POLAR concept was chosen over other candidate designs after extensive trade studies. The primary advantages of the POLAR concept are the low mass moment of inertia of the module about the transverse boom and the compactness of the stowed module which enables packaging of two complete modules in the Shuttle orbiter payload bay.

The fine pointing control system required for the solar dynamic module has been studied and initial results indicate that if disturbances from the station are allowed to back drive the rotary alpha joint, pointing errors caused by transient loads on the Space Station can be minimized. This would allow pointing controls to operate in bandwidths near system structural frequencies.

The incorporation of the fine pointing control system into the solar dynamic module is fairly straightforward for the three strut concentrator support structure. However, results of structural analyses indicate that this three strut support is not optimum. Incorporation of a vernier pointing system into the proposed six strut support structure is being studied.

REFERENCES

1. McCormick, C. W., ed., "MSC/NASTRAN User's Manual", (Version 63) May 1983.

2. Housner, J. M., "Structural Dynamics Model and Response of the Deployable Reference Configuration Space Station", NASA TM 86386, May 1985.

15 METER HOOP-COLUMN ANTENNA DYNAMICS: TEST AND ANALYSIS

W. Keith Belvin
NASA Langley Research Center
Hampton, VA 23665

and

Harold H. Edighoffer
Edighoffer Inc.
Newport News, VA 23602

First NASA/DOD CSI Technology Conference
Norfolk, Virginia
November 18-21, 1986

INTRODUCTION

Large Space Antennas (LSA) proposed for communication and remote sensing missions will require accurate dynamic analyses to predict structural vibration behavior and to assess the need for active vibration control. Of the numerous LSA concepts that have been proposed (see for example Refs. 1, 2 and 3), one concept, referred to as the Hoop-Column concept, has been fabricated (Ref. 2). A 15 meter diameter model has been constructed for deployment, electromagnetic and structural testing. The model, shown below, was designed and fabricated jointly by government and industry (Ref. 4). As part of the test program, static and dynamic tests have been performed in the Langley 16 Meter Vacuum Chamber. Results from these tests and comparisons with predicted structural behavior will be described.

15 METER DIAMETER HOOP-COLUMN ANTENNA

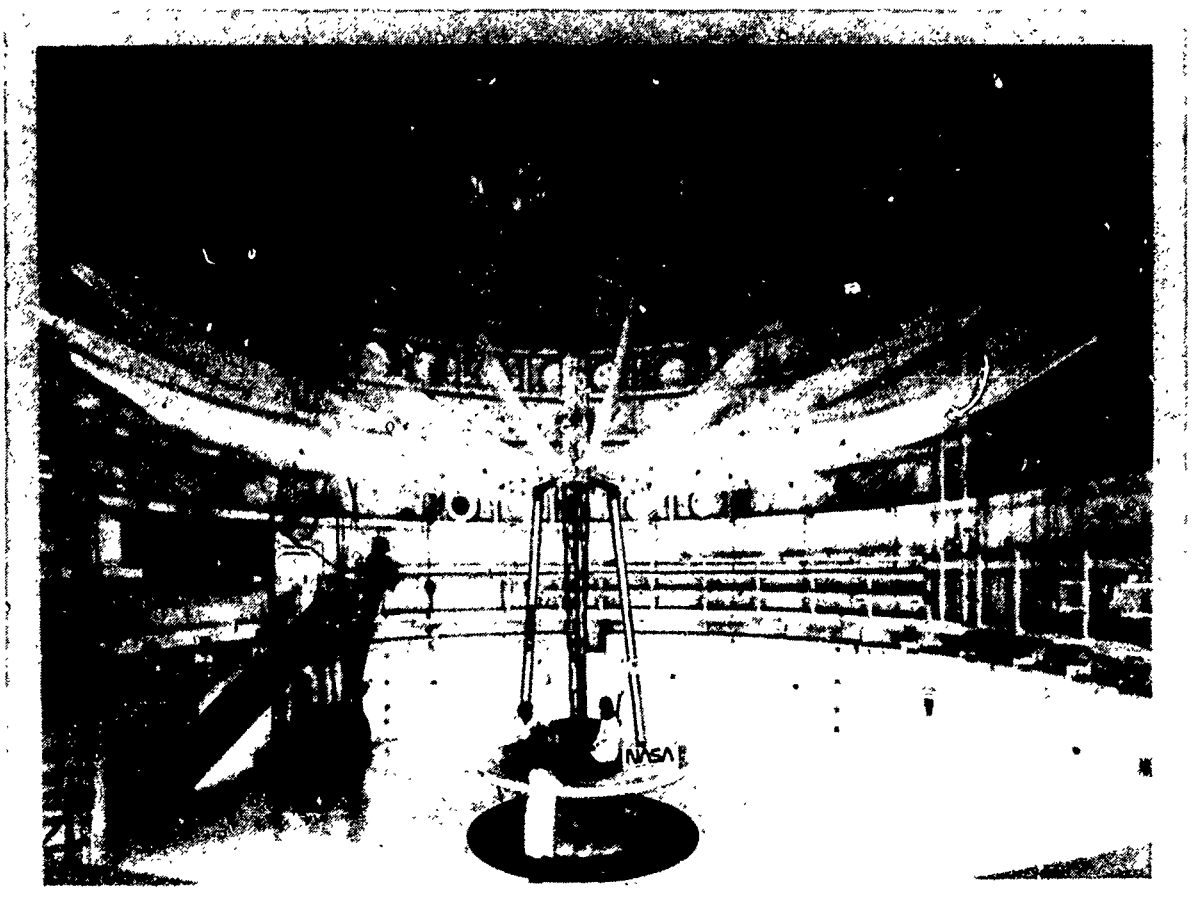

OUTLINE

A number of structural tests and analyses have been performed on the 15 meter antenna model. This paper will concentrate on vibration test and analysis results. As indicated in the outline below, a description of the experimental and analytical models will be presented first. Second, test and analysis results will be presented for the antenna mounted on a tripod support. Vibration results have been divided into three areas: global modes which are dominated by overall column bending and hoop motion; hoop modes which are dominated by inplane and out-of-plane hoop (ring) bending; and mesh modes which are localized surface mesh distortions. Results from a simplified analytical model will be presented followed by a description of the antenna vibrations when supported by a pendulum cable.

Description of:

- 15 meter hoop column antenna
- Antenna vibration tests
- Antenna analysis models
- Vibration modes with tripod support
  - global, hoop and mesh
- Reduced analytical model
- Global vibration modes
  - Cable suspension
- Summary

ANTENNA DEPLOYMENT

The figure below shows the antenna deployment sequence. First, the antenna is mounted on a tripod support in a stowed configuration. Next, the column is deployed by a motor driven cable system enclosed in the column longerons. The column telescopes outward simultaneously from top and bottom. After the column is deployed, the hoop is deployed by eight motors which are mounted in eight of the twenty-four hoop joints. Synchronizing rods are used to maintain uniform deployment of each hoop section. The final deployment step is the actuation of a preload segment at the bottom of the column. This segment extends outward to pretension all of the cables and mesh, thus providing a stable structural configuration. The antenna deploys from a volume of approximately 1 m by 3 m to a deployed size of 15 m in diameter by 9.5 m in height. The feed and feed mast were manually attached after the antenna was deployed.

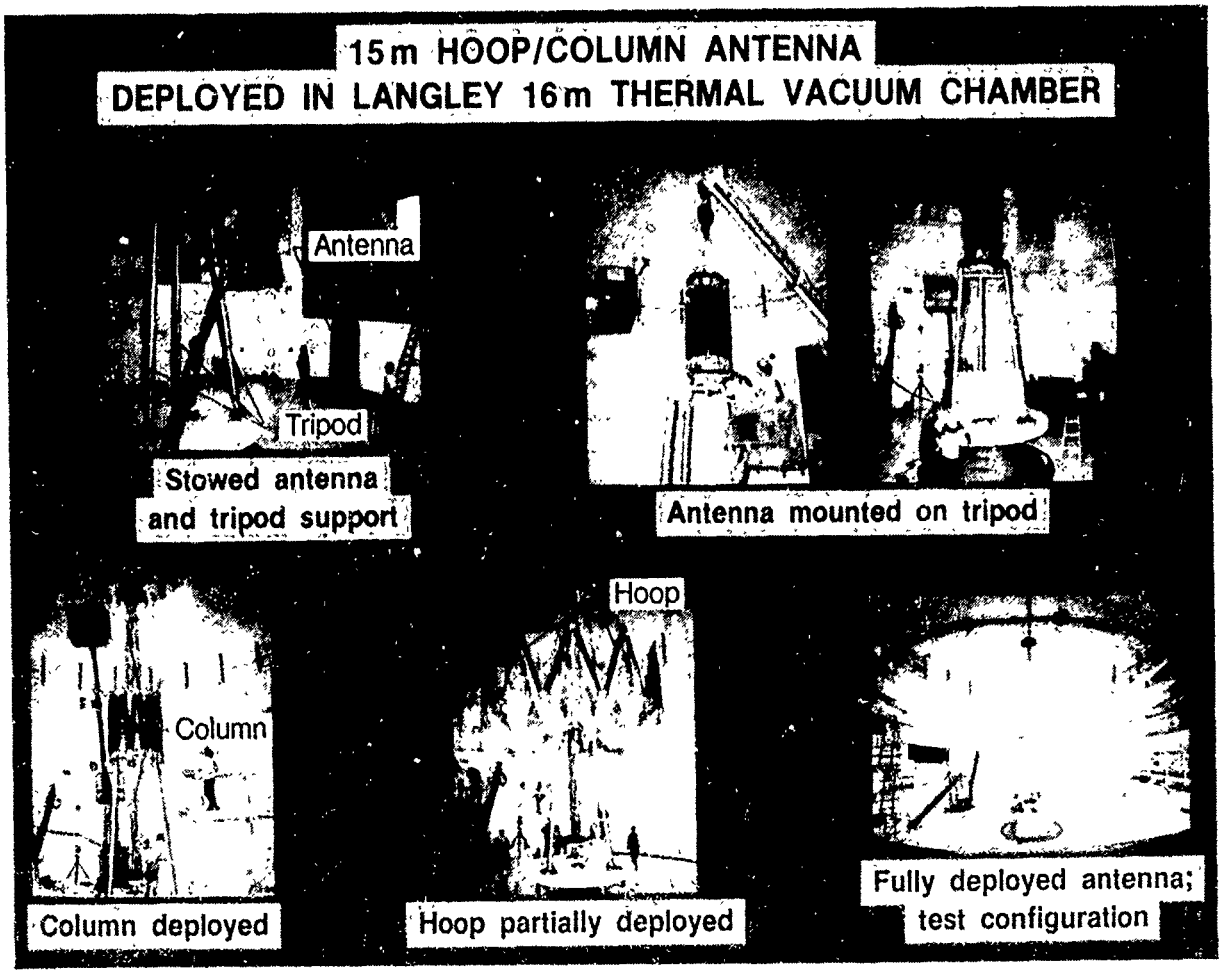

ANTENNA EXPERIMENTAL SETUP

The antenna was deployed inside a vacuum chamber as shown in the schematic diagram below. The deployment was stopped on several occasions to enable accelerometers and strain gages to be mounted on the column and hoop. A total of 58 servo accelerometers were used to measure the acceleration response of the antenna due to small random and sinusoidal disturbances. In addition, displacement measuring proximity probes were used to measure static deflections and surface mesh vibrations. The total mass of the antenna is 400.1 kg (880.5 lbs) with the center of gravity located at 1.85 m above the hoop. The rotational inertias of the antenna are $I_x = I_y = 11500$ kg-m^2 (101800 lb-s^2-in) and $I_z = 8160$ kg- m^2 (72200 lb-s^2-in).

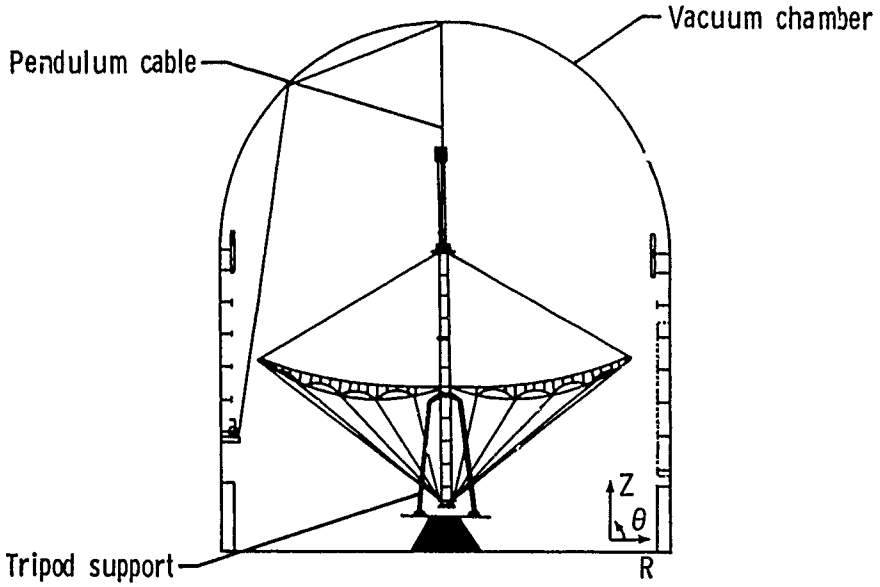

Antenna properties

Overall dimensions:

Diameter = 15 M (590.5 in.)

Height = 12.8 M (504 in.)

Elements	Mass (weight)
Hoop (graphite)	131.8 kg (290.1 lbs)
Column (graphite)	135.8 kg (298.7 lbs)
Surface mesh (gold plated molybdenum wire)	10.7 kg (23.6 lbs)
Cables (graphite and quartz)	2.1 kg (4.7 lbs)
Feed mast (steel)	11.5 kg (25.4 lbs)
Simulated feed weight	108.2 kg (238 lbs)
Total	400.1 kg (880.5 lbs)

ANTENNA FINITE ELEMENT MODEL: WITHOUT SURFACE

The antenna has been modeled with the Engineering Analysis Language finite element program described in Ref. 5. The hoop, column and hoop support cables were modeled first. The model shown below includes the flexibility of the tripod support. Preliminary vibration tests were performed prior to surface mesh installation to verify the antenna analytical model without the surface. These preliminary tests showed the need for modeling the tripod and including the rotational inertia of the column. The differential stiffness due to tension/compression loads in the members was included an all analyses. In addition, gravity loading was modeled to correlate with ground vibration test results.

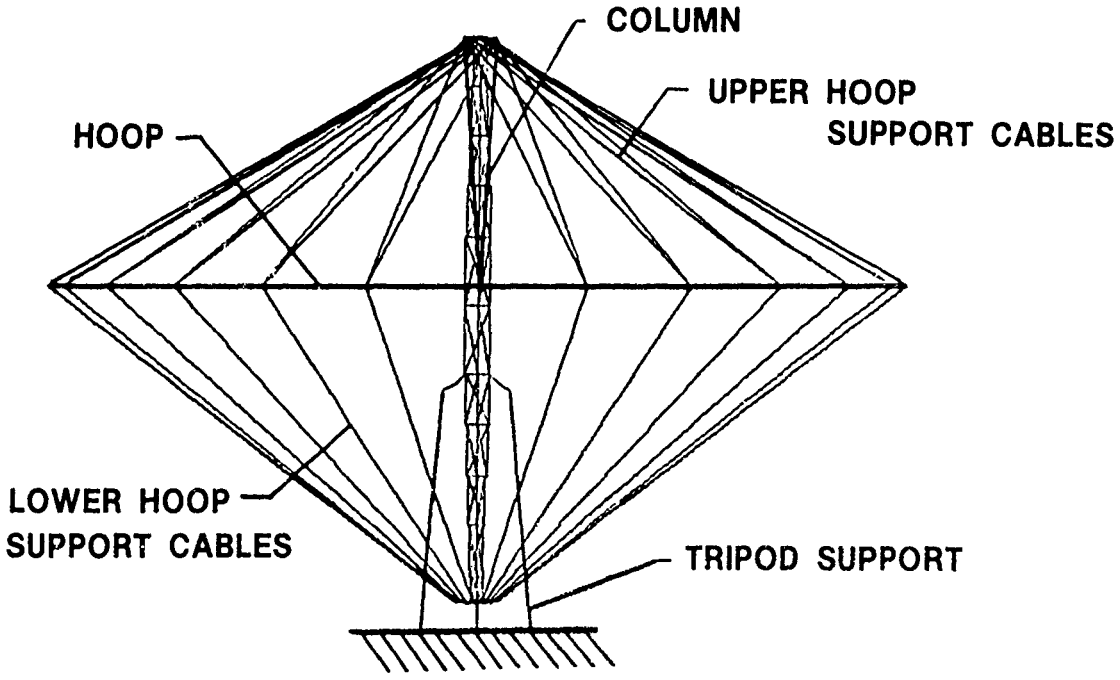

ANTENNA FINITE ELEMENT SURFACE MODEL

The antenna surface consists of four paraboloidal apertures shaped by pretensioned cables and mesh. Since twenty-four gores are present, the smallest representative element of the antenna surface is a three gore model as shown in the upper left of the figure below. Reflective symmetry permits one full aperture to be modeled as shown in the upper right six gore model. Repeated application of rotational symmetry yields the full surface model shown in the bottom figure. (Only mesh elements are shown for clarity.) The surface model was merged with the hoop and column model shown previously to permit analysis of the full antenna. The analytical model without the feed and feed mast contained 286 beam elements, 4664 rod elements and 2880 triangular mesh elements. A total of 2096 grid points and 8816 degrees of freedom were used in the analysis.

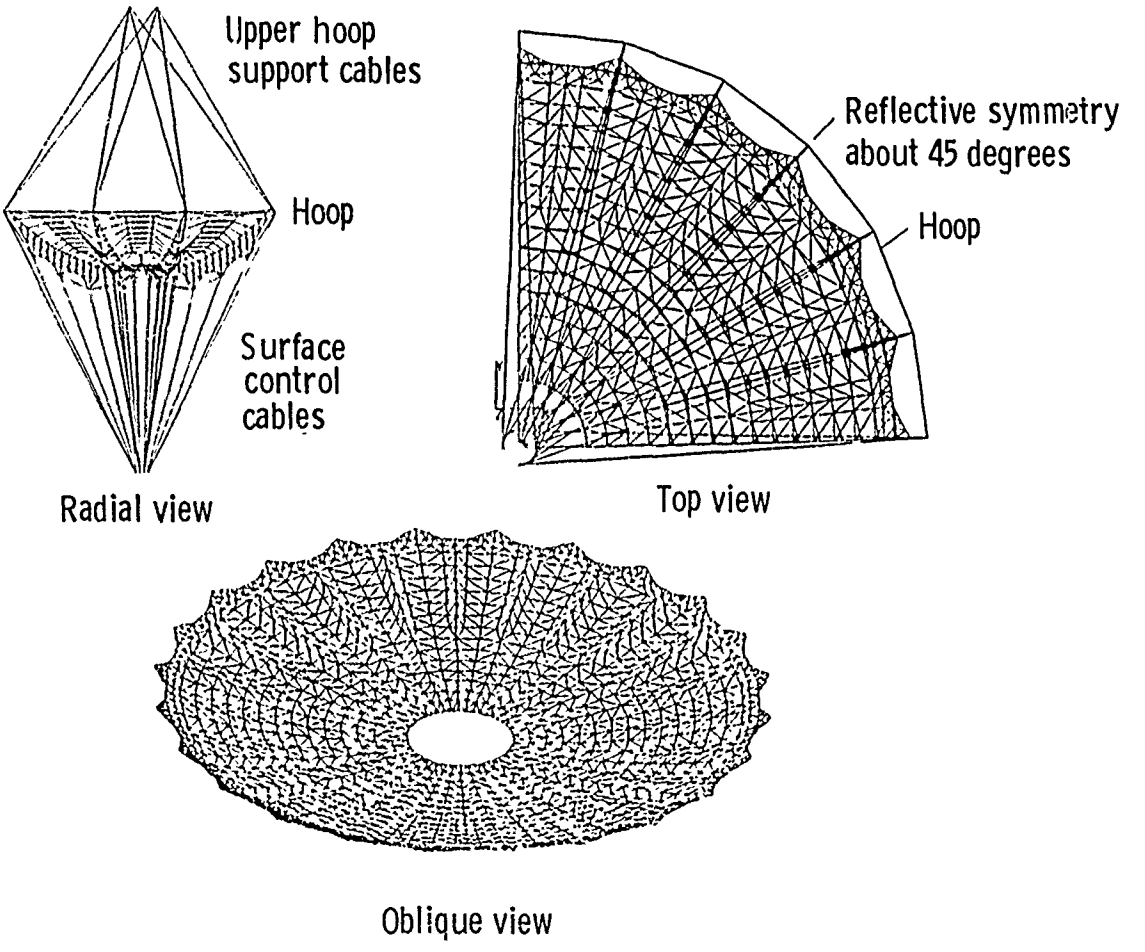

FREQUENCIES OF FIRST FOUR VIBRATION MODES

Test results showed the fundamental frequency of the antenna was 0.077 Hz when supported on the tripod. This mode was dominated by torsion of the hoop. As indicated in the table below, the second mode shape occurred at 0.704 Hz and consisted of hoop rocking and column bending. The number of modes at this frequency is indicated in parenthesis to be two since this mode shape can occur in two orthogonal planes. Although fabrication asymmetries usually yield two distinct frequencies, test results indicated no measurable difference in frequency when excited in different planes of vibration. The next mode shape was dominated by hoop inplane translation and column bending. Again two modes occur at the frequency of 1.76 Hz. The last mode indicated below is characterized by torsional motion of the lower column at 3.06 Hz. These four modes were found to be the dominant global modes when supported on the tripod. Initial analysis results showed significant errors in frequency when compared to the test data. The properties in the initial analysis were based on fabrication drawings, which can often lead to overestimates of member stiffnesses by neglecting the joints used in the assembly process. Thus, static tests of the assembled antenna were used to measure the effective stiffness of the hoop and column for refinement of the analytical model.

ANALYTICAL MODE SHAPES

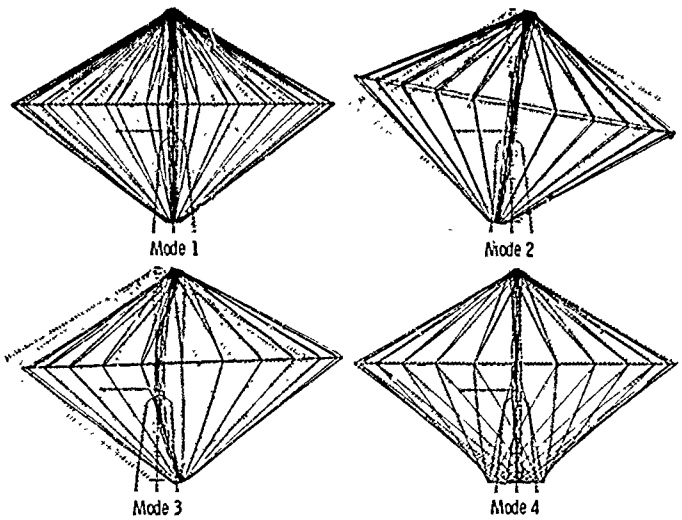

ORIGINAL ANALYSIS FREQUENCIES

Mode	Original analysis	Test	Mode shape
	Frequency (HZ)		
1	0.092	0.077	Hoop torsion
2 (2)	1.60	0.704	Hoop rocking/column bending
3 (2)	2.80	1.76	Hoop inplane/column bending
4	3.20	3.06	Lower column trosion

STATIC TESTS FOR ANALYTICAL MODEL REFINEMENT

Since component and subassembly tests of joints and other antenna parts could not be performed, the entire antenna was loaded to measure the effective member stiffnesses. The figure below indicates locations where point loads were applied to the antenna. Vertical, torsion and radial loads were applied to the hoop whereas only radial and torsional loads were applied to the base of the column. The deflection of the antenna was measured at the point of loading and computed using the analytical model. Comparisons between test and analysis indicated the analysis overestimated the stiffness by 17 percent for column bending and 10 percent for hoop torsion. Mass measurements of the antenna were also performed and used to update the analytical model. The analytical model was modified by adjusting the stiffness of column longeron and diagonal members and by adjusting the stiffness of the column to tripod attachment. The analytical model, refined using the static test data, was then used to recompute the first four vibration modes of the antenna.

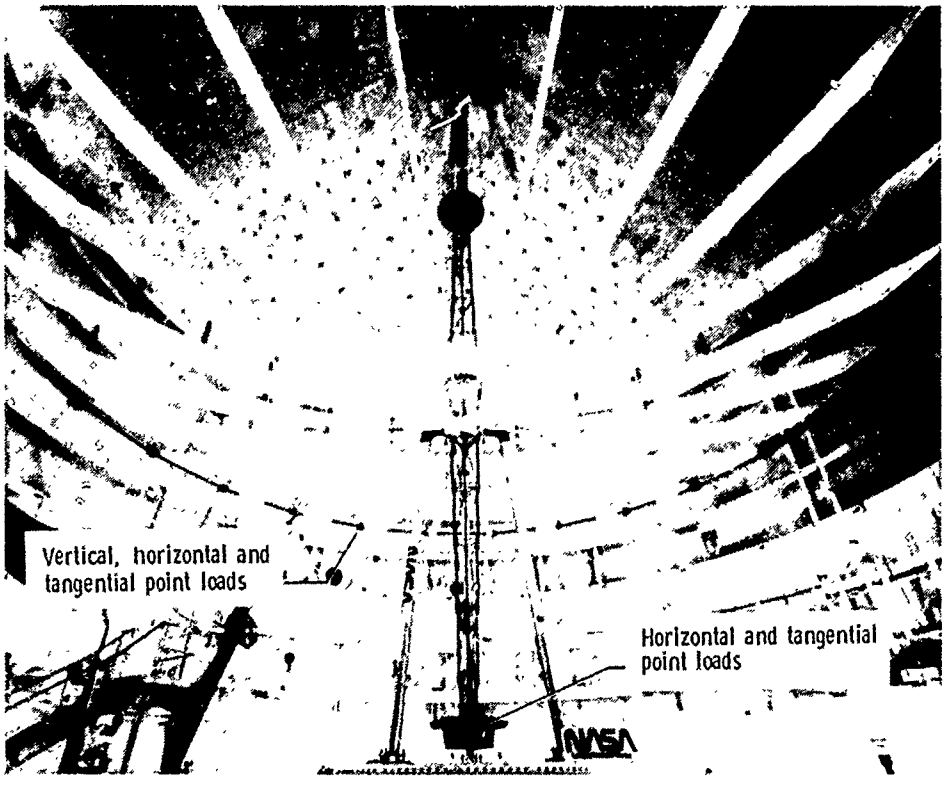

REFINED ANALYTICAL MODEL RESULTS

The table below lists the analysis and test frequencies after the antenna model was refined. Good frequency agreement was obtained. This indicates static test data should be used to refine the analytical models of large space structures particularly since the accuracy of static data increases as the flexibility of the structure increases. Also listed in the table are the measured frequencies and damping of the first four modes of the antenna. The damping is somewhat higher than usually found in spacecraft perhaps due to the deployable joints and the tripod interface. The damping increases when tested in ambient air. Unlike panel structures, the antenna shows very small decreases in frequency when tested in ambient air. This indicates large lattice structures can be tested in ambient air without significant changes in vibration frequencies of the global modes.

Mode	Refined analysis	Test			
		Vacuum		Ambient air	
	F (HZ)	F (HZ)	C/CR (%)	F (HZ)	C/CR (%)
1	0.077	0.077	1.9	0.076	3.8
2 (2)	0.697	0.704	3.8	0.700	4.3
3(2)	1.73	1.76	3.2	1.75	3.3
4	3.18	3.06	0.84	3.10	1.3

HOOP VIBRATION MODES

Although the antenna vibration is dominated by the global modes shown previously, a number of more localized modes exist. Out-of-plane ring bending of the hoop produces 12 modes from 6.3 to 10.1 Hz in the analysis. In addition, another 14 inplane ring bending modes occur from 10.7 to 14.4 Hz. As shown in the figure below, the modes shapes of the hoop modes involve rotation of the hoop joints. Since these hoop joints have some unknown effective rotational stiffness, mode for mode comparisons between test and analysis is almost impossible. Nevertheless, modeling the joints as being pinned in the out-of-plane direction and being rigid in the inplane direction, has yielded a frequency spectrum which agrees quite well with the test data. Some nonlinearity in the hoop modes has been found when testing at different force levels. It is felt that a mechanical locking mechanism to secure the joint in the deployed configuration or a method to completely pin the hoop joints would be useful in reducing nonlinearities and thus, permit better simulation of the hoop response.

Out-of-plane bending

12 modes From 6.3 to 10.1 HZ

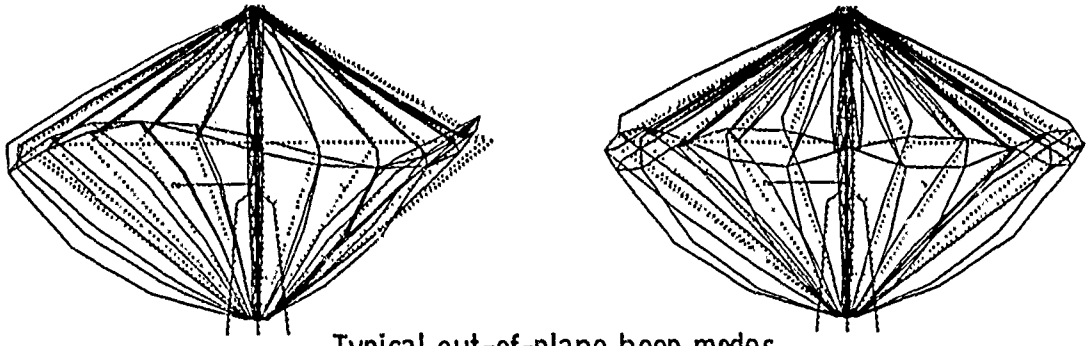

Typical out-of-plane hoop modes

Inplane bending

14 modes From 10.7 to 14.4 HZ

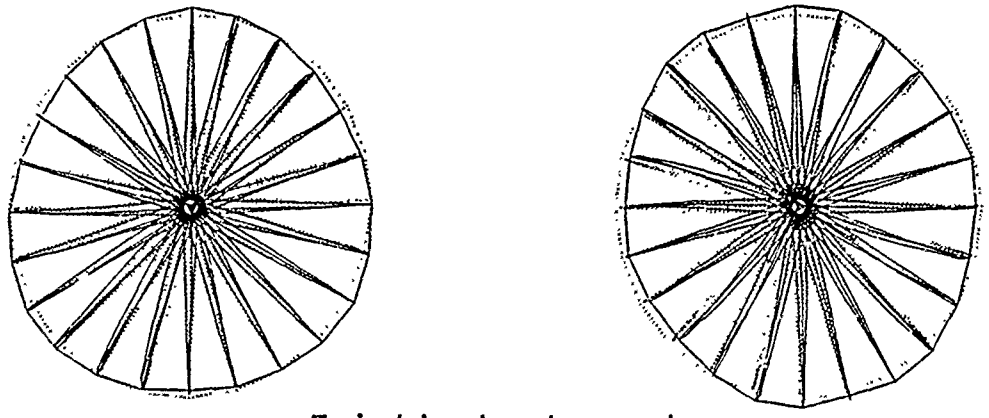

Typical in-plane hoop modes

MESH VIBRATION MODES

The analytical model predicts 70 vibration modes dominated by surface mesh displacements from 4.1 to 6.2 Hz. Shown below are typical mode shapes predicted by the analysis. Experimentally, these modes have been found to be highly damped and coupled. Although a frequency spectrum in this range can be found by testing the antenna, the data has not been successfully reduced into a set of recognizable mode shapes. The high damping of the knit mesh results in rapid dissipation of the excitation energy. Since the input energy did not propagate long distances, it was extremely difficult to produce a standing wave (vibration mode) in the surface mesh. To insure that membrane theory was adequate to model the mesh, a 1.22 m square knit mesh model was constructed for vibration testing.

70 modes from 4.1 to 6.2 HZ

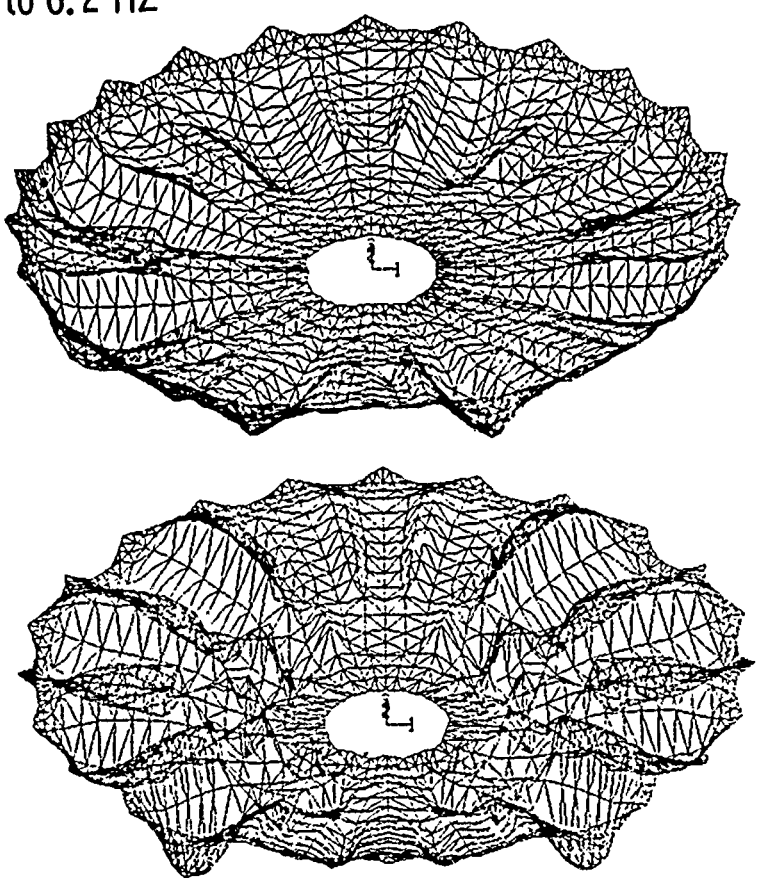

Typical mesh modes

1.22 METER SQUARE MESH VIBRATION MODEL

The figure below shows a 1.22 m square sample of the gold plated molybdenum mesh used for the reflector surface on the 15 m antenna model. The model was mounted in an 2.5 m vacuum sphere to permit testing at near vacuum conditions. An electrodynamic shaker was attached to the mesh for excitation and a proximity sensor mounted on a survey system was used to measure the response displacements. The mesh was pretensioned uniformly by lead weights which hung over circular rods. Tests were performed at two different tension levels to study tension effects; 3.01 N/m (0.0172 lbs/in.) and 6.02 N/m (0.0344 lbs/in.). The mesh density was measured to be 0.06284 g/m^2 (8.938×10^{-8} lbm/in^2). A differential equation for solution of a two dimensional membrane was used to predict the vibration frequencies.

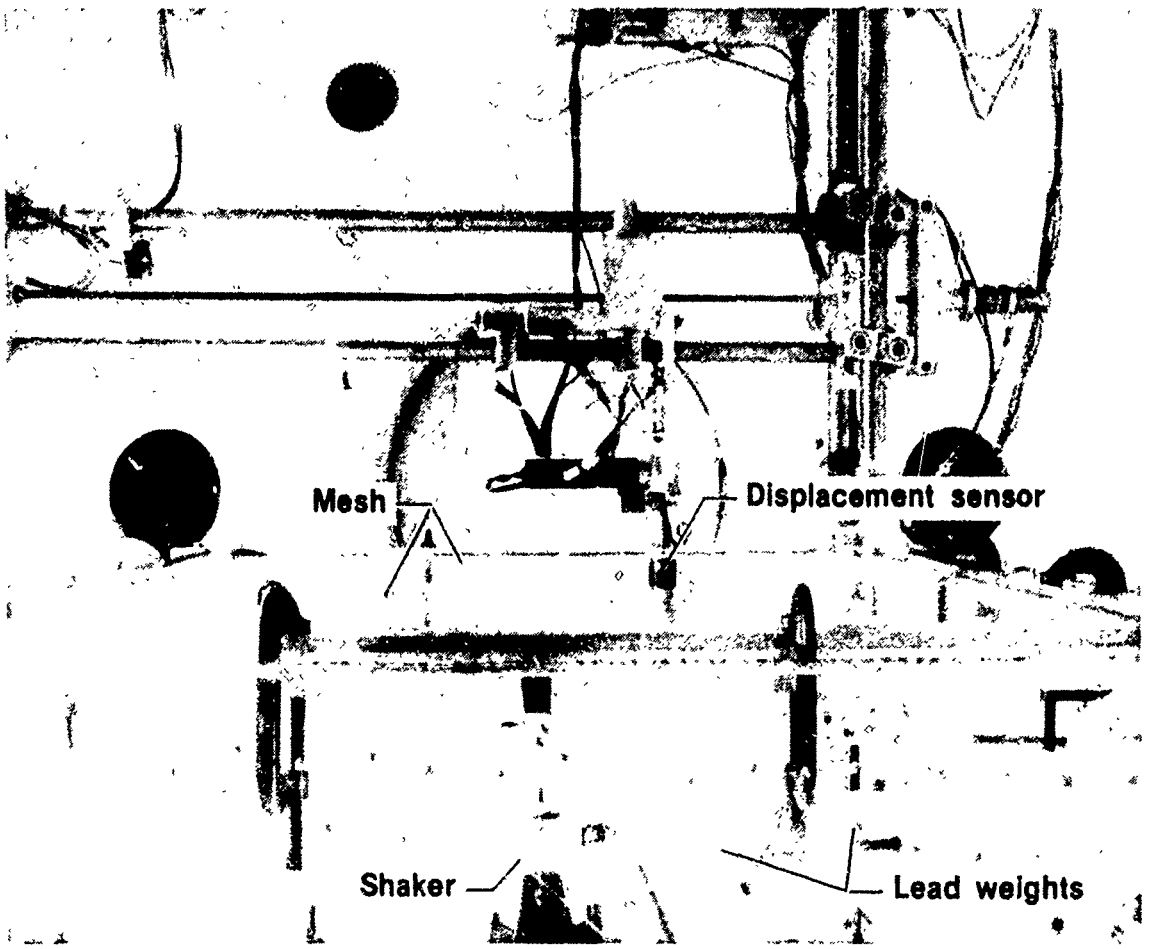

1.22 METER SQUARE MESH DYNAMICS

The table below lists frequencies and damping for selected vibration modes of the 1.22 m surface mesh model. The analytical frequencies are high perhaps due to the manner in which the lead weights were used to pretension the mesh. Since the lead weights hung over a circular rod, friction could reduce the amount of tension that is applied to the mesh. Nevertheless, the frequencies increase by the square root of the tension increase which indicates that the mesh can be modeled with membrane theory for prediction of out-of-plane vibration modes. The damping of the mesh is quite high, for example, 6.9 percent of critical damping in the first mode. Ambient air significantly increases the damping of the mesh. The frequencies of vibration are slightly lower at near vacuum pressure than at ambient air pressure. This is unusual since ambient air generally has an apparent mass effect and thus lowers vibration frequencies. One additional point to be made is that the damping tends to decrease as the tension level increases.

	Analysis	Test			
$N_X = N_Y = 3.01$ N/M (0.0172 lbs/in)		Vacuum		Ambient air	
Mode	F (HZ)	F (HZ)	C/CR (%)	F (HZ)	C/CR (%)
1	6.48	5.80	6.9	5.98	9.2
2 (2)	10.24	9.21	4.0	9.35	6.9
3	12.95	13.04	3.3	13.22	4.2
5 (2)	16.51	14.96	3.1	15.17	4.2
$N_X = N_Y = 6.02$ N/M (0.0344 lbs/in)					
1	9.16	8.26	5.0	8.43	7.1
2 (2)	14.48	12.89	4.3	12.96	4.7
3	18.31	16.64	3.1	16.79	3.7
5 (2)	23.35	20.93	2.3	21.13	3.3

SIMPLIFIED ANALYTICAL MODELS

The dominant modes contributing to antenna vibrations are the global modes described previously. Since these modes are not significantly affected by the surface mesh, a reduced analytical model was developed. The reduced model used a very crude representation of the surface mesh which resulted in only 996 degrees of freedom in the analysis. This model predicted the first four global modes quite accurately as shown in the table below. The mode shapes, also shown below, are similar to those shown previously. The column has been reduced using continuum beam theory (Ref. 6) which makes mode shape plots more difficult to visualize. The good accuracy obtained with the reduced model indicates that relatively crude representations of the surface are adequate to predict the global modes of the antenna.

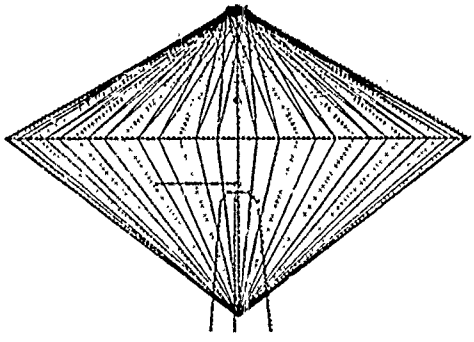

Mode 1

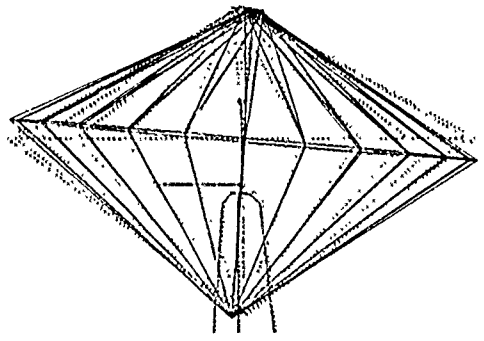

Mode 2

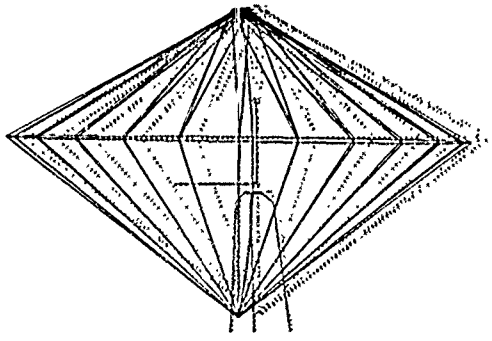

Mode 3

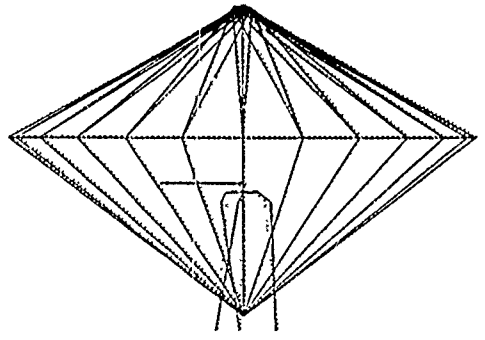

Mode 4

Mode	Full model	Reduced model
	Frequency (HZ)	
1	0.077	0.077
2 (2)	0.697	0.697
3 (2)	1.73	1.84
4	3.20	3.25

ANTENNA MODES WITH CABLE SUSPENSION AND FEED MAST

The reduced model was used to predict the global modes of the antenna when supported by a pendulum cable. A simulated feed weight and feed mast were also attached. The analytical model predicted the cable suspended frequencies shown below. A comparison of the test and analysis results show good agreement. Except for the first two pendulum modes, the cable suspended modes closely agree with the frequencies predicted for free-free boundary conditions. The fundamental flexible antenna frequency increases to 1.47 Hz for cable suspended or free-free vibrations. The test data which was acquired in ambient air shows the damping to be near 1 percent of critical for most modes. Antenna support systems can greatly influence the frequency and mode shapes of the global antenna modes. The hoop and mesh modes are not strongly affected by column support systems thus the hoop and mesh results shown previously are still valid when the antenna is cable suspended or free-free.

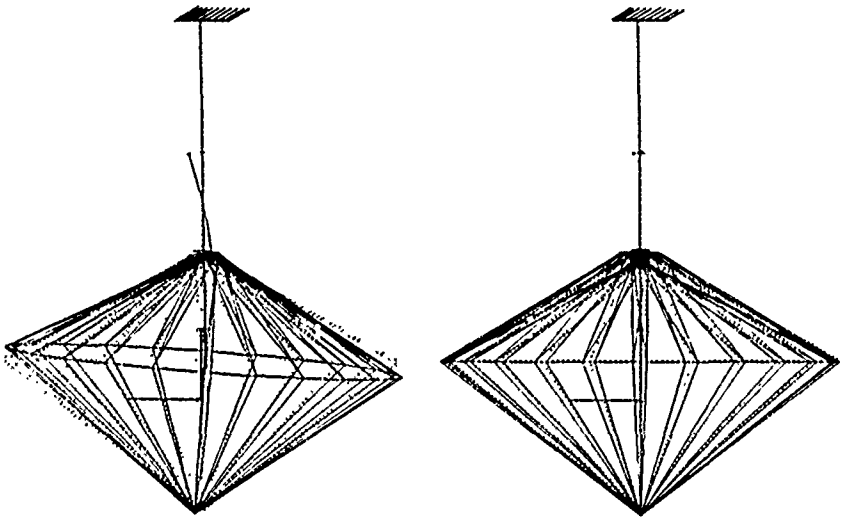

Mode 3 Mode 4

Mode	Analysis (reduced model)	Test		Mode shape
	F (HZ)	F (HZ)	C/CR (%)	
1 (2)	0.132	0.138	3.1	First pendulum
2 (2)	0.283	0.284	1.2	Second pendulum
3 (2)	1.47	1.47	1.3	Hoop rocking/column and feed mast bending
4	2.20	2.19	1.1	Column/hoop torsion
5 (2)	4.37	4.09	1.9	Second column and feed mast bending
6	5.40	5.42	0.94	Feed mast torsion

PROPOSED COFS II ANTENNA FLIGHT EXPERIMENT

The 15 meter hoop-column antenna has been tested for deployment, electromagnetic performance and structural behavior. Quasi-static shape control (Ref. 7) has shown the antenna is amenable to active surface shaping. Due to its demonstrated performance and interesting vibration behavior, the antenna is a candidate for flight experiments in the Control of Flexible Structures (COFS) program. The antenna structural behavior has been characterized with two suspension systems, however, the COFS II experiment illustrated below will require further structural analysis and testing. For example, more research is needed to fully understand the interaction between surface shape control and global antenna vibrations.

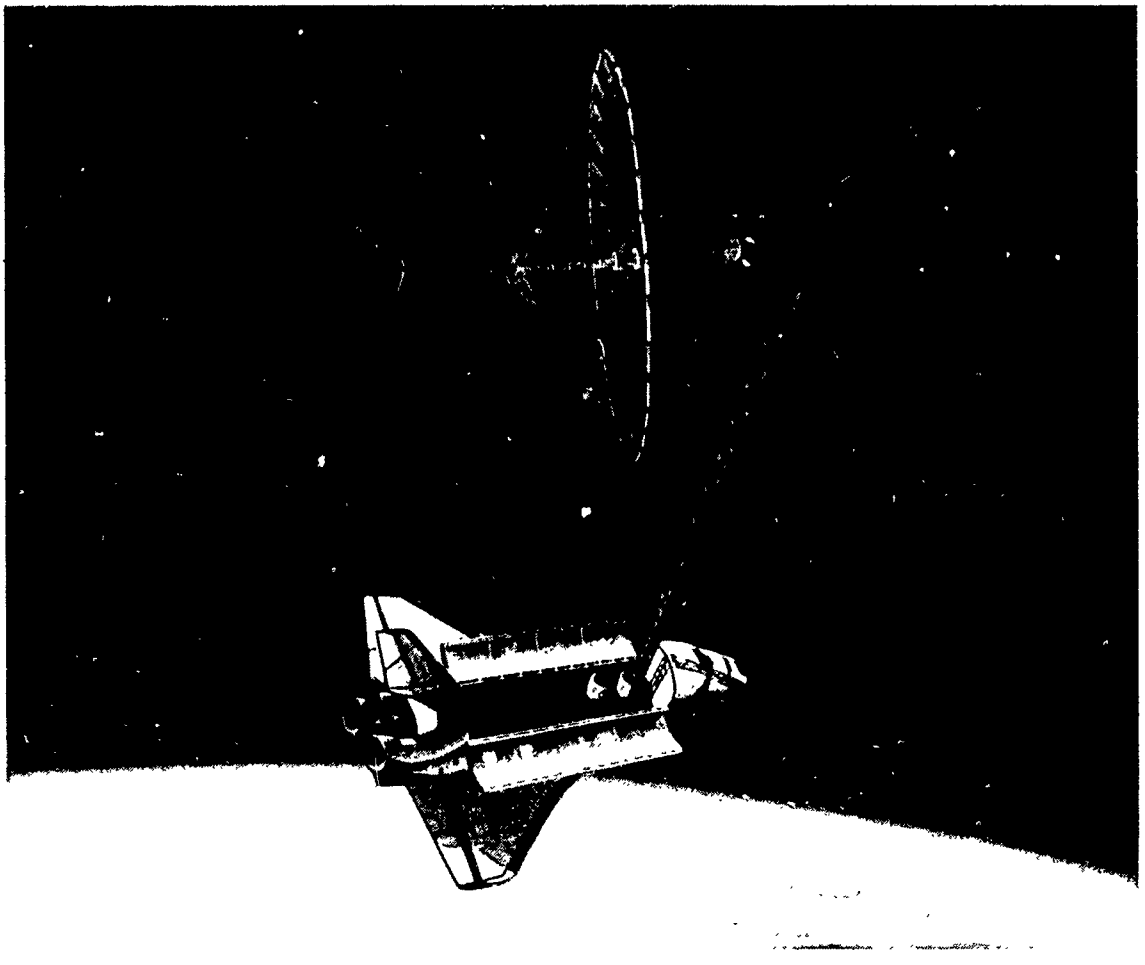

SUMMARY

A 15 meter model of the hoop-column antenna concept has been vibration tested for model characterization and analytical model verification. Linear finite element analysis predicted the global vibration frequencies accurately, however, good agreement between analysis and test data was obtained only after the analytical model was refined using static test data. As structures become more flexible, structural properties determined from static data become more accurate and should be used to update analytical models. Global vibration modes are not significantly affected by the surface mesh which permits simplified analytical models to be used for prediction of global behavior. These reduced models are believed sufficient for preliminary design and controls simulations where only global behavior is desired. The mesh modes were highly damped due to the knit mesh used for the reflector surface. These modes were also highly coupled and very difficult to measure in the laboratory. The inability to fully characterize the antenna mesh modes in the laboratory indicates robust methods for active surface vibration suppression will be needed. Fortunately, the surface mesh exhibits high passive damping which should be beneficial to active control systems.

- Static tests are needed to refine analytical models
- Mesh modes are highly damped (coupled)
- Reduced analytical models are adequate to predict global vibration modes
- The effect of cable and mesh modes on active control systems needs further investigation

REFERENCES

1. Freeland, R. E.; Garcia, N. F. and Iwamoto, H.: "Wrap-Rib Antenna Technology Development," NASA CP-2368, pp 139-166, Presented at the Large Space Antenna Systems Technology Conference, Dec. 4-6, 1984, Hampton VA.

2. Campbell, T. G.; Butler, D. H.; Belvin, W. K. and Allen B.: "Development of the 15-Meter Hoop/Column Antenna Concept," NASA CP-2368, pp 167-212, Presented at the Large Space Antenna Systems Technology Conference, Dec. 4-6, 1984, Hampton VA.

3. Coyner, J. V.: "Box Truss Development and Its Applications," NASA CP-2368, pp 213-236, Presented at the Large Space Antenna Systems Technology Conference, Dec. 4-6, 1984, Hampton VA.

4. Harris Corporation: "15 Meter Diameter Hoop Column Antenna", Final Report, NASA Contract No. NAS1-15763, June 1986.

5. Whetstone, W. D.: "EISI-EAL Engineering Analysis Language Reference Manual," EISI-EAL System Level 2091, Vols. 1 and 2, Engineering Information Systems, Inc. San Jose, CA, July, 1983.

6. Noor, A. K.; Anderson, M. S. and Greene, W. H.: "Continuum Models for Beam- and Platelike Lattice Structures," AIAA Journal, Vol. 16, No. 12, Dec. 1978, pp. 1219-1228.

7. Belvin W. K., Edighoffer H. E.and Herstrom, C. L. :"Quasi-Static Shape Control of a 15 Meter Hoop Column Antenna", To be Presented at the AIAA/ASME/ASCE/AHS 28th Structures, Structural Dynamics and Materials Conference, Monterey, California, April 6-8, 1987.

Application of Physical Parameter Identification to Finite Element Models

Allen J. Bronowicki*
Michael S. Lukich† Steven P. Kuritz†

TRW Space & Technology Group
Redondo Beach CA 90278

First NASA/DOD CSI Technology Conference
Norfolk, Virginia
November 18-21, 1986

*Staff Engineer
†Members of the Technical Staff

Abstract

A time domain technique for matching response predictions of a structural dynamic model to test measurements is developed. Significance is attached to prior estimates of physical model parameters and to experimental data. The Bayesian estimation procedure allows confidence levels in predicted physical and modal parameters to be obtained. Structural optimization procedures are employed to minimize an error functional with physical model parameters describing the finite element model as design variables.The number of complete FEM analyses are reduced using approximation concepts, including the recently developed convoluted Taylor series approach. The error function is represented in closed form by converting free decay test data to a time series model using Prony's method. The technique is demonstrated on simulated response of a simple truss structure.

1 Introduction

This work is motivated by the need to have at hand accurate structural dynamic models for the design of robust vibration suppression control systems. Knowledge of modal properties is of course necessary for control system design. Possession of an accurate physical model of the structure can also be beneficial. Such an instance is when one anticipates making modifications to the structure to incorporate control actuators in primary load paths for the purpose of reducing dynamic response. The physical model will allow one to predict the new modal properties of the perturbed structure. A modal model alone or even a mass and stiffness representation would not allow this.

A second motivation is the possibility of performing "on-orbit" structural system identification where the only test equipment available is the control system actuators and sensors. The number of sensors will necessarily be limited, nowhere near the scores or hundreds of accelerometers which are commonly used to saturate modal survey test articles. A prior structural model can provide valuable information which may then be supplemented by data acquired from the control system to provide response predictions more accurate than available from either analysis or test alone.

A beneficial side effect of the Bayesian parameter estimation approach is the availability of uncertainty estimates on both physical parameters and modal quantities such as frequencies and mode shapes. Variances on derived response quantities such as gain factors may also be obtained. These statistical estimates provide mean values and ranges which may be used to design the control system and test it for stability and robustness across the range of possible physical and modal parameter values.

1.1 Background

Previous work at TRW on system identification for the design of vibration suppression control systems has focused on the Maximum Likelihood approach. In the Maximum Likelihood approach no weight is given to prior parameter estimates nor is uncertainty assigned to the measurement data. Model parameters are adjusted so as to best fit the experimental data. This estimation procedure has been applied in the frequency domain to a flat plate experiment [1] and in the time domain to the Large Space Structure Truss Experiment (LSSTE) [2]. As applied in the time domain, the test article was excited by the control actuators using a fast sine sweep or "chirp" across the frequency range of interest. Motion was then allowed to decay. Physical parameter estimation was implemented by minimizing the error

residual between observed and predicted response at the control sensors. This error residual was defined as the integral over the duration of the test, both forced and unforced, of the square of the difference between measured and predicted response. As reported, the perturbation of physical parameters allowed the accurate matching of response in amplitude, frequency and phase over the duration of the experiment. The structural model was a set of discrete equations of motion and was not represented directly in the estimation procedure as a finite element model. The parameters which could be identified were as a result limited to inertia properties of the top plate, the modulus of elasticity and modal damping ratios.

Recent advances in the state of the practice of structural optimization techniques make it possible to consider the extension of physical parameter estimation to finite element models of at least moderate size. In particular, linking MSC/NASTRAN Design Sensitivity Analysis [3] with the Automated Design Synthesis (ADS) code [4] has enabled structural optimization to proceed on a production basis. Approximation concepts [5, 6] have allowed the reduction of the number of full structural analyses required for a model optimization to single digit levels. At TRW, structural models having up to 10,000 static and 400 dynamic degrees of freedom have been weight-optimized with minimum frequency constraints using up to 200 design variables. The availability of eigenvector derivatives [7] has enabled the prediction and minimization of vibratory response using the approximation concepts approach [8]. Physical parameter identification can be implemented using these proven methods by employing uncertain parameters as design variables and minimizing an appropriate error functional.

It was found in Reference 2 that a significant portion of the computation time was spent integrating the equations of motion for each trial design and for each perturbed design required for finite difference gradient calculations. A closed form representation for the error functional would increase the computational efficiency of the estimation process while enhancing numerical stability. Recognizing that linear models predict free decay response as a sum of exponentially damped sinusoids and that one can extract these same components from free decay test data employing Prony's method, such a closed form error functional has now been derived. The prior filtering of the test data using Prony's method has the advantage that frequency, mode shape and damping data are available to some extent and may be compared to prior model predictions even before the estimation procedure formally begins.

1.2 System Identification Methods

The system identification field is vast and the options one encounters in choosing an approach are numerous. Perhaps the greatest advantage of the approach adopted

herein is its ability to go directly from test data to an improved analytical model. This approach is by no means advocated as superior in all respects to others. It is one more tentative step in the direction of physical parameter identification and, in fact, some valuable lessons have been learned in its implementation. Some discussion of where this approach falls in the larger framework of system identification is in order.

The common starting point for system identification and model verification for most aerospace structures is the modal survey. This procedure is used to determine the system's normal modes, frequencies and modal damping ratios. This effort is undertaken independent of any prior knowledge of the model other than in the selection of instrumentation type and location and choice of modal identification procedure. Numerous modal identification techniques are available in either the frequency or the time domain [9]. Having a set of test modes, these are frequently corrected to enforce orthogonality to an analytic mass matrix using a technique such as Gram-Schmidt orthogonalization, or the Targoff method [10]. In this approach the analytic mass matrix is assumed perfect and the corrected modes are taken as linear combinations of test modes.

A procedure which might be labelled the Baruch–Berman method [11, 12] may also be employed to generate an improved analytic stiffness and mass matrix which exactly reproduces the measured mode shapes and frequencies while producing minimal changes to the analytic model in a weighted least squares sense. This procedure has been applied numerous times with considerable success. The predicted changes to the analytic mass and stiffness matrices have been used to guide the improvement of the physical finite element model in a heuristic manner. One criticism of the Baruch–Berman method is the generation of stiffness matrices with coupling between degrees of freedom which appear to be physically unconnected. Unrealistic mass changes have also been observed. Although the method generates a mass and stiffness model which generates the test modes, additional modes within the test bandwidth can also arise from the model.

A promising answer to the infeasible coupling problem has been provided by Kabe [13]. Assuming the test modes have been orthogonalized to the analytic mass matrix, an improved stiffness matrix is formed which preserves the topology of and minimizes the perturbation to the original analytic matrix, while exactly matching the test frequencies and modes supplied to the algorithm. The technique has not seen application in practice due to very large computational requirements.

Having in one's possession an improved stiffness and mass representation of a structure is not in all cases sufficient to allow the analysis process to proceed. In many cases the test configuration is not the field configuration. The structure in

question may be altered or coupled to other components, which would make a test verified physical finite element model valuable. The Bayesian technique [14, 15] is a general framework which allows one to match the analytic predictions of a model to test data while minimizing the changes to the original model. Uncertainties in the form of standard deviations may be assigned to one's original parameter estimates and to the measurement data. The resulting set of revised parameters will be provided with a statistical estimate of confidence given the additional knowledge provided by the test. The changes in estimated parameters vis-a-vis the original estimates can be used to infer the adequacy of the test and or the functional form of the analytic representation [16]. This method has been applied successfully to estimate a small bi-linear model using transient test data [17]. It is the intent of this work to extend the Bayesian technique in an efficient manner to finite element model estimation.

2 Estimation Procedure

An overview of the estimation procedure is given in the flow chart of Figure 1. The process consists of: 1) Test; 2) Prony analysis; 3) Finite Element Analysis; 4) Construction of an approximate problem; 5) Optimization; and 6) Bayesian statistical analysis. Steps 3–5 are repeated iteratively until the approximate problem converges to closely resemble the actual problem.

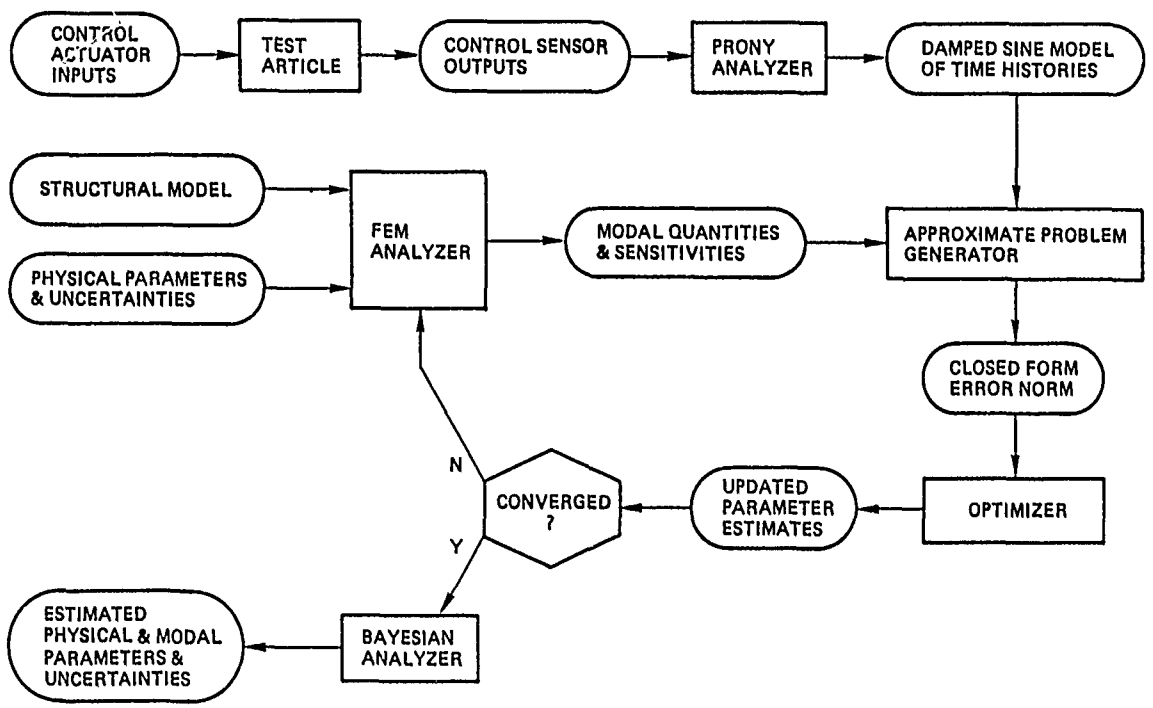

Figure 1: Parameter Estimation Using Structural Optimization Techniques

The test portion of the structural parameter estimation procedure is implemented by subjecting the test article to a series of force load events $\{F_k(t)\}$, $k = 1, \ldots, N_{lc}$ using combinations of control actuators. Free decay time histories $u^e_{jk}(t)$, $j = 1, \ldots, N_s$; $k = 1, \ldots, N_{lc}$ are measured at each of the N_s control sensors in each of the N_{lc} load conditions. This experimental data serves as the basis for the estimation procedure. Assuming that the structure behaves in a linear fashion, each of the recorded time histories can be represented as the sum of a finite number of

significant damped sinusoidal components as follows:

$$u^e_{jk}(t) \simeq \bar{u}_{jk}(t) \equiv \sum_{m=1}^{M_{jk}} \bar{A}_{mjk} \cos(\bar{\omega}_{mjk_d} t + \bar{\theta}_{mjk}) e^{-\bar{\zeta}_{mjk}\bar{\omega}_{mjk}t} \tag{1}$$

Zero time is assumed to occur at the end of the excitation process and at the beginning of the free decay. The subscript d denotes damped frequency as defined in Equation 2. The barred quantities are meant to represent the result of filtering experimental data. In this work Prony's method of extracting damped sinusoidal components was employed [18]. The particular implementation of this algorithm [19] has been found to operate quite well in the presence of considerable noise. The choice of the number of components in the time series model is done interactively until the user feels a good fit has been obtained. Pre-test analysis using the prior analytic model can serve as a guide to what frequency components may be expected at each sensor due to each load condition. Non-linearities and noise will in some sense be removed from the data in this process. One could of course employ the actual time history data in the optimization procedure. This would remove the necessity of making an assumption on the form of the time series model. It would also allow the data recorded during the excitation process to be fit to the analytic structural model. However, the computational burden is greatly increased by having to filter the data literally thousands of times during the optimization process. The insight gained through the estimated Prony model components will also be lost.

The linear analytic model is formed as a function of the variable parameter set $\mathbf{D}$. This model will also predict response at the sensors in the form of damped sinusoids. The response will be at the N damped natural frequencies of the system which are given in terms of the undamped natural frequencies ω_n and the modal damping ratios ς_n as follows:

$$\omega_{n_d} \equiv \omega_n \sqrt{1 - \varsigma_n^2} \tag{2}$$

The predicted response at each of the sensors j in each of the load conditions k as a function of parameters $\mathbf{D}$ is thus

$$u_{jk}(t;\mathbf{D}) = \sum_{n=1}^{N} A_{njk} \cos(\omega_{njk_d} t + \theta_{njk}) e^{-\varsigma_{njk}\omega_{njk}t} \tag{3}$$

We note that the amplitude, frequency, phase and damping ratio are all functions of the design variables and that the amplitude and phase are also functions of the excitations applied prior to time zero.

The Bayesian estimation procedure requires an error residual set $\mathbf{E}$ which is defined here as the root mean square difference between predicted and observed response over the duration of the experiment T, i.e.

$$E_{jk} \equiv \sqrt{\frac{1}{T}\int_0^T [\bar{u}_{jk}(t) - u_{jk}(t;\mathbf{D})]^2 \, dt} \tag{4}$$

Given the representation of both experimental and analytic response as sums of damped sinusoids, this error functional can be written in closed form. The algebra and the test process will be considerably simplified if the excitations applied to the structure are simple static loads applied at the actuators and released at time zero. Assuming the structural model is described adequately by a set of N real normal modes, $\{\phi_n\}$, the amplitude components in the damped sinusoidal representation will be

$$A_{njk} = \phi_{jn}\frac{1}{\omega_n^2}\{\phi_n\}^T\{F_k\} \tag{5}$$

and the phase angles θ_{njk} will be identically zero. Using pre-test predictions the input into expected modes of interest could be maximized by choosing the force vectors in proportion to modal response at the actuators. The number of independent combinations of force vectors is limited to the number of actuators, and additional modes may also be excited in each twang test. More load cases than actuators can nevertheless be employed as this will merely over-determine the test. One might hope that the phase components identified from the test, $\bar{\theta}_{mjk}$, will also be identically zero. This will invariably not be the case. These phase components may be discarded if their magnitude is small. Large measured phase components will indicate a problem in the test procedure, errors in the Prony analysis, or perhaps non-linearities in the test article.

2.1 Bayesian Estimation

The Bayesian estimation procedure may most easily be understood as the minimization of a performance index represented as the weighted sum square of error residuals between observed and predicted response plus a weighted sum square of error residuals between prior and adjusted parameter values, as defined in Equation 6. One is thus seeking to minimize a combination of measurement error and parameter error. If one weights measurements more heavily by assigning greater confidence (i.e. a smaller variance) to them , the design will then tend to match the measurements more strongly. If one weights one's initial estimates of the parameters more heavily by assigning them a smaller uncertainty then the adjusted parameters will tend to move less from the prior estimates.

The observation weighting function may be a full matrix if separate measurements are statistically correlated. The usual assumption is that the measurements are uncorrelated, resulting in a diagonal observation weight matrix. The parameter weighting matrix may also be full if the prior parameter estimates are correlated. This situation will present itself when data sets are considered sequentially, with the adjusted parameter set arising from one batch of data used as the prior model for the next batch. The prior model for the subsequent estimations will then usually exhibit a full covariance matrix. Allowing for the full statistical correlation of both measurements and parameters the problem is defined: Find that $\mathbf{D}^*$ which minimizes the performance index

$$\Upsilon(\mathbf{D}) \equiv \mathbf{E}(\mathbf{D})^T \mathbf{W}_e \mathbf{E}(\mathbf{D}) + (\mathbf{D} - \mathbf{D}^o)^T \mathbf{W}_{D^o} (\mathbf{D} - \mathbf{D}^o) \tag{6}$$

The subscript e denotes experimental data and the superscript o denotes original or prior parameter estimate. The weighting matrices $\mathbf{W}$ are the inverse of the covariance matrices $\mathbf{S}$. Thus the larger the uncertainty in a given measurement or a given parameter estimate, the smaller will be its assigned weight in the estimation procedure. The test covariance $\mathbf{S}_e$ and the prior parameter covariance $\mathbf{S}_{D^o}$ are usually assumed to be diagonal matrices with diagonal elements equal to the square of the standard deviation of the measurement or parameter in question. Thus the weight assigned will be $W_{ii} = 1/\sigma_i^2$ where σ is the standard deviation. The covariance of the final best fit parameter estimate will be

$$\mathbf{S}_{D^*} = \left[\mathbf{W}_{D^o} + \mathbf{T}^T \mathbf{W}_e \mathbf{T}\right]^{-1} = \left[\mathbf{S}_{D^o}^{-1} + \mathbf{T}^T \mathbf{S}_e^{-1} \mathbf{T}\right]^{-1} \tag{7}$$

In this case, $\mathbf{T}$ is a sensitivity matrix representing the rate of change of the error residuals with respect to the variable parameter set, i.e.

$$\mathbf{T} \equiv \left.\frac{\partial \mathbf{E}}{\partial \mathbf{D}}\right|_{\mathbf{D}^*}$$

The sensitivities must be evaluated for the optimum parameter set. The standard deviation of an improved estimated parameter can be derived from the diagonal elements of the covariance matrix as follows: $\sigma_{D_i^*} = \sqrt{S_{D_{ii}^*}}$.

A useful feature of the Bayesian approach is its ability to provide variance, or uncertainty, estimates of modal parameters such as frequency or mode shape [20]. The uncertainty bounds placed on the initial parameter estimates and the measurement data were propagated through the estimation procedure to provide uncertainties on the estimated parameter set as given in Equation 7. The optimum estimated parameter set $\mathbf{D}^*$ can in turn be used to provide estimates of expected

response quantities and their uncertainties. These expected response quantities will be obtained by evaluating the system's describing equations using the estimated parameter set. For example, expected natural frequencies, ω_n^*, and mode shapes, $\{\phi_n\}^*$, may be derived by performing an eigensolution on the matrix equations of motion using the optimum parameter set. Variance estimates may be obtained using the sensitivities of the response quantities in question with respect to parameters evaluated at the optimum. Using natural frequency as an example, its variance would be:

$$S_{\omega_n} = \left\{\frac{\partial \omega_n}{\partial \mathbf{D}}\right\}^T [S_D] \left\{\frac{\partial \omega_n}{\partial \mathbf{D}}\right\} \tag{8}$$

The ability to predict a range of natural frequencies due to uncertainties in model parameters could prove beneficial, especially in the design of control systems for on-orbit structures which cannot be fully tested on the ground.

2.2 Approximation Concepts

The ability to match the response of the structural model to the measured test data hinges on one's ability to efficiently compute the response for a large number of varied parameter combinations. Simply performing a complete eigensolution at each design iteration becomes excessively costly for all but the smallest systems. The approximation concepts approach [5] which has evolved in the structural optimization field solves the problem by defining an approximate problem based on solution of one structural eigenproblem, which is then submitted to the optimization process (see Figure 1). Having an optimum design (parameter set) for the approximate problem, the structure is re-analyzed, and the process continues until the approximate problem, and hence the design, converges. The number of complete structural analyses is thus minimized. The key to implementation is the construction of a highly accurate approximate problem.

In this work, the natural frequencies and mode shapes were modeled as approximate functions of the design variables using analytic gradient infromation. Eigenvector derivative calculations are the most costly portion of the design process. Nelson's method [21] was implemented here using over 200 lines of Direct Matrix Abstraction Programming (DMAP) [7]. This is the most efficient of the exact methods, but it still requires a full matrix decomposition for each eigenvector and a back-substitution for each design parameter. Given approximate eigenvalue and eigenvector functional relationships, $\tilde{\omega}_n(\mathbf{D})$ and $\{\tilde{\phi}_n(\mathbf{D})\}$, respectively, the objective function Υ was computed in closed form for all design perturbations. The objective function has a complex algebraic form, which makes computation of its

sensitivities by finite difference attractive from both computational and programming standpoints. The objective is also a highly non-linear function of frequency and mode shapes, so use of a quasi-linear approximation would degrade the approximate problem. The convoluted first order Taylor series expansion, derived by Woo [6], is used to approximate the eigen-parameters. This approximation, for any given function f, is

$$f(\mathbf{D}) \approx \tilde{f}(\mathbf{D}) \equiv f(\mathbf{D}_o) + \nabla f(\mathbf{D}_o)(\mathbf{D} - \mathbf{D}_o)\left(\frac{\mathbf{D}}{\mathbf{D}_o}\right)^p \tag{9}$$

The choice of the parameter p is obviously important in determining the character of the approximation. A choice of $p = 0$ is simply a linear Taylor series approximation. A choice of $p = -1$ turns out to be the same as linear Taylor series with respect to reciprocal design variables $1/D_i$. Schmit first proposed reciprocal design variables as providing a high-quality linearization of structural response quantities. Choosing the sign of p as shown below results in an approximation which consistently either under-predicts or over-predicts a linear approximation.

$$\text{sign}(p) = \begin{cases} -\text{sign}(\nabla f) & ; \quad \text{underpredictor} \\ +\text{sign}(\nabla f) & ; \quad \text{overpredictor} \end{cases}$$

Choosing the sign of p in this fashion one can guarantee conservativism in the design process, always over-predicting response and under-predicting stiffness. Woo has shown that an approximate problem may be constructed which is always convex, possessing no local minima, and with the attendant increases in efficiency to be gained using optimizers tailored to convex problems.

This is not our intent here. The parameter identification process is not one of conservatism, but of making a best estimate. The value of p chosen here in the extrapolation of eigenvalues was thus chosen to reflect the general law of diminishing returns (under-prediction vis-a-vis a linear extrapolation) and to fall somewhere between the linear and reciprocal variable assumptions. The value $p = -\frac{1}{2}\text{sign}(\nabla\omega_n^2)$ was found to accelerate the convergence of the approximate problems quite well. A value of $p = 0$ was used for eigenvector extrapolation as it is not at all clear whether one should over or under predict mode shape quantities.

3 Simulation Results

A simple ten-bar truss structure as shown in Figure 2 was chosen to test the performance of the estimation procedure. This structure was chosen to represent an optical pointer in some sense. The motions of the top element, axial, lateral and rotational, are taken to represent optical sensors. An attempt to perform parameter identification using just these sensors was made. An initial design was chosen to represent an analysts best estimate of the structure's characteristics. This design was perturbed to obtain a baseline design which represents the actual structure in the field. The baseline structure was excited and it's Prony characteristics were identified. Using the initial design as a starting point, the estimation procedure was used to match the response of the model to the "measured" response of the baseline model. The estimated parameter set was found to be significantly closer to the baseline parameter set for parameters which had response sensitivity. Parameters which did not produce significant response sensitivity were found to move in the right direction slightly. It may be noted that the difference from the baseline of all parameters was well within the final estimate of their standard deviations. Thus some parameters' estimates were significantly improved, while none were degraded.

The initial design was chosen such that all members had the same area of 0.1 in^2. Damping ratios in the lowest six modes were assumed to be 1%. The baseline model was then constructed by perturbing the initial design as follows: upper legs were decreased 10% in area, lower legs increased 20%, diagonals increased 10% and horizontals decreased 40%; damping in the first lateral mode remained at 1%, damping in the first axial and second lateral modes was increased to 1.5% and damping in higher modes was increased to 2%. Parameter values for the initial, the perturbed baseline and the final estimated designs are presented in Table 1. Initial assumed standard deviations and final estimated standard deviations are also given. The initial standard deviations were arrived at by assuming stiffness estimates were accurate to $\pm 40\%$ and damping estimates were accurate to only $\pm 400\%$.

Two separate "twang tests" were run on the perturbed model by applying and suddenly releasing 1,000 pound axial and lateral forces on the top element. Time histories of axial and lateral displacement and rotational response were recorded at the top of the truss. Axial motions were found to be de-coupled from lateral and rotational motions. The Prony components identified from the simulated tests are summarized in Table 2. The first axial and lateral modes were the only strong signals in the time histories, causing the parameter estimation process to be dominated by matching these components. The second and third lateral modes were clearly identified but had such small amplitudes that the estimation process all but ignored

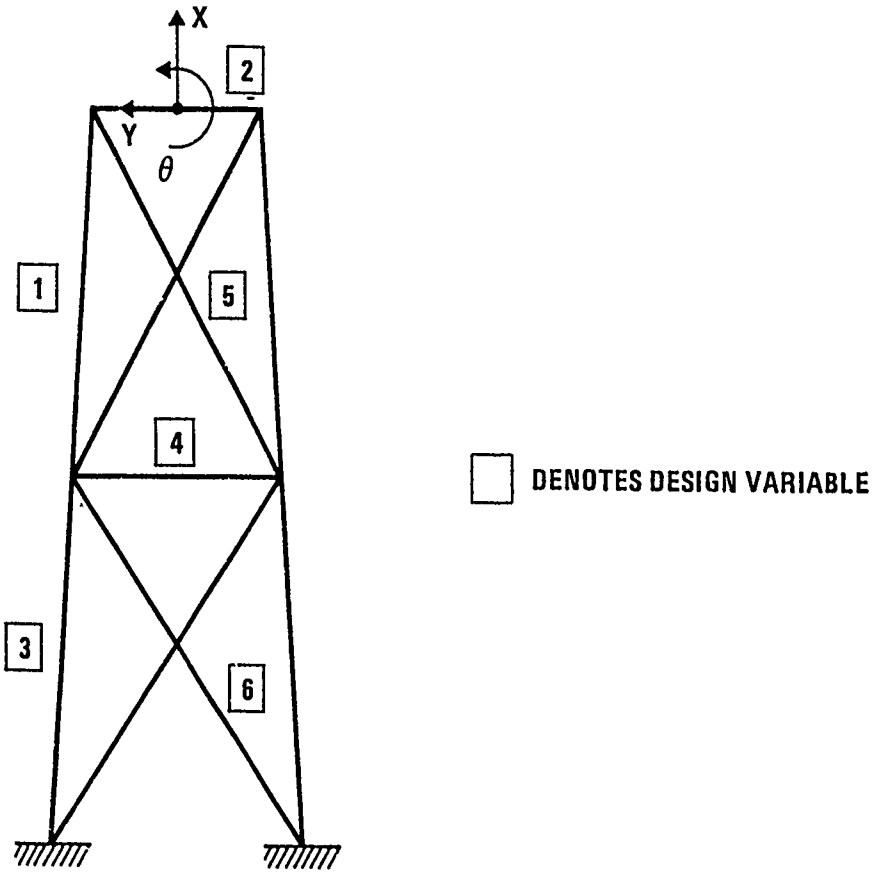

Figure 2: Ten Bar Truss Model

their presence. The Prony analyzer did not always identify the exact damping ratio as may be seen in the second component of measurement 2 which should have had $\varsigma = 1.5\%$. The higher than actual damping estimate was compensated for by the estimation of an amplitude greater than actual. The resultant integral of amplitude over the 2 second duration of the experiment was thus similar. The phase components of the identified signals were close enough to zero or π that they were ignored.

The three measurements were assigned initial standard deviations of approximately 5% of their peak values. The initial RMS error residuals and the final RMS error residuals for the estimated model are given in Table 3. The parameter estimation process came very close to eliminating the errors between observed and predicted response. A comparison of baseline, initial and estimated modal frequencies is given in Table 4. The first axial and lateral modes were matched quite well in frequency to the baseline. Their standard deviations were also reduced significantly. The second and third lateral modes, which were weakly present in the signals due to the lateral load case, were not estimated as strongly. As was seen in Table 1, the damping ratios for these weakly present modes were not estimated strongly either.

Table 1: Initial, Baseline and Estimated Parameter Sets for Ten Bar Truss

Parameter	Description	Initial Design	Baseline Design	Estimated Design	Initial σ_{D°	Estimated σ_{D^*}
A_1 (in^2)	Upper Legs	.1	.08	.0756	.04	.0332
A_2	Upper Horiz.	.1	.06	.0975	.04	.0400
A_3	Lower Legs	.1	.12	.1245	.04	.0244
A_4	Lower Horiz.	.1	.06	.0652	.04	.0287
A_5	Upper Diags.	.1	.11	.1023	.04	.0342
A_6	Lower Diags.	.1	.11	.1001	.04	.0328
ς_1 (%)	1st Lateral	1.0	1.0	1.0005	4.0	2.58
ς_2	2nd Lateral	1.0	1.5	1.175	4.0	3.88
ς_3	1st Axial	1.0	1.5	1.537	4.0	3.96
ς_{4+}	Higher Modes	1.0	2.0	1.024	4.0	3.99

The optimization process converged in four NASTRAN finite element analyses. An iteration history of frequencies in the first axial and lateral modes is given in Table 5. The frequencies actually computed in the FEM analyzer are contrasted with those predicted from the previous iteration by the convoluted Taylor series. Also shown are the portions of the objective function Υ due to the measurement error residuals and that due to the deviation of the parameter estimates from the initial parameter values. These are the square root of the first term in Equation 6 (measurement error) and the square root of the second term (parameter error). Note that the parameter error does not involve prediction error and hence is not extrapolated using convoluted Taylor series. Measurement error is an implicit function of modal quantities and hence it is also extrapolated indirectly. Note that the measurement errors were not predicted nearly as well as the frequencies. This is due to the non-linear nature of the objective. A small frequency or phase shift can produce large differences in error residuals. In any case, convergence to the optimum in only four finite element analyses must be considered extraordinary.

Table 2: Identified Prony Components

Time History	Sensor	Load Case	Amplitude	Frequency (Hz)	Damping %	Phase (Radians)
1	Axial (in)	Axial	.03149	15.292	1.521	-3.03
2	Lateral (in)	Lateral	.063791	3.664	1.002	.0142
			.0041	12.67	3.475	.1255
			.000886	26.267	2.54	.169
3	Rotation (rad)	Lateral	.008759	3.664	1.002	.0148
			.000360	12.655	1.224	.0961
			.000260	26.245	1.978	-2.975

Table 3: RMS Error Residuals

Time History	Initial Error	Final Error	Improvement %
1	.00685	.000192	97.2
2	.4547	.00232	99.5
3	.00595	.000189	96.8

Table 4: Model Frequencies in Hz

Mode	Description	Initial Design	Baseline Design	Estimated Design	Estimated σ^*
1	1st Lateral	3.448	3.664	3.663	0.142
2	2nd Lateral	12.49	12.67	12.21	1.242
3	1st Axial	15.09	15.31	15.30	0.102
4	3rd Lateral	26.60	26.25	25.39	2.778

Table 5: Iteration History

FEM Analysis	Computation Type	Lateral Frequency	Axial Frequency	Measurement Error	Parameter Error
1	Actual	3.4479	12.492	19.78	0.0
2	Actual	3.6440	11.489	2.524	1.062
	Convoluted	3.6615	11.432	.6676	
3	Actual	3.6563	12.125	.9369	1.238
	Convoluted	3.6614	12.096	.5015	
4	Actual	3.6631	12.206	.4067	1.240
	Convoluted	3.6631	12.206	.4068	

4 Conclusions

The parameter identification procedure outlined here has been shown to work quite well on a small test case. A limited amount of displacement data was used to back out physical parameters which one might not expect to be identifiable. Use of acceleration data would be expected to be more beneficial as it would allow higher modes than the first to be identified strongly, thus providing more data to the estimation procedure. Application to larger models and actual test data is in progress. It is expected that the largest difficulties will arise in three areas. First is the Prony process itself. Problems in separating closely spaced modes have been encountered. Close modes sometimes appear as one mode with a higher or lower damping ratio than is actually present. Sorting actual modes from noise modes is also a difficulty. The second problem is computation time for the eigenvector derivatives. This may be overcome using more approximate methods and by selective computation for only those modes contributing heavily to response. The third difficulty is encountered by the analyst in choosing an appropriate model of the system and in choosing the appropriate parameters in that model to vary. The appropriate parameters in this simulated test case were self-evident. Experience will certainly be the major determinant in solving this last problem.

The time domain estimation procedure is applicable to forcing functions other than step functions. However computation of amplitude and phase would be considerably more difficult for more complex force time histories. Impulse loading would however be simple to analyze and would excite higher modes more than twang tests. The use of impulses should be explored as an alternative to twang tests.

The use of a frequency domain procedure analogous to the current time domain procedure should also be explored. One could identify the poles and zeroes of a structure excited by white noise using an Auto Regressive-Moving Average (ARMA) time series model. Efficient lattice filter algorithms have been developed to do this. The power spectral density of this measured model could be matched to the PSD of the predicted model by integrating the square of the difference over the frequency domain. The integration can be performed in closed form using residue theory. This frequency domain scheme may be able to more strongly estimate the higher frequency modes and thus extract more information about the physical model.

References:

1. Bauer, R. D. and Tung, F. C., "Application of Maximum Likelihood Estimation of Modal Parameters", AIAA Guidance and Control Conference, Seattle WA, August 1984.

2. Lukich, M. S., and Tung, F. C., "Experimental Verification of Control and System Identification Techniques for a Flexible Truss Structure", American Control Conference, Seattle, June 1986.

3. "Design Sensitivity Analysis", MSC/NASTRAN Application Manual, Section 3.4, April 1983.

4. Vanderplaats, G. N., and Sprague, C. M., "ADS-1: A New General-Purpose Optimization Program", 24th AIAA Structures, Dynamics and Materials Conference, Lake Tahoe CA, May 1983.

5. Schmit, L. A., "Structural Optimization - Some Key Ideas and Insights", International Symposium on Optimum Structural Design, October 1984.

6. Woo, T. H., "Space Frame Optimization Subject to Frequency Constraints", 27th AIAA Structures, Dynamics and Materials Conference, San Antonio TX, 1986.

7. Wallenstein, D. V., "Calculation of Eigenvector Derivatives in Design Sensitivity Analysis", MSC/NASTRAN Application Note, January 1986.

8. Bronowicki, A. J., "Structural Modification to Minimize Response to Random Excitation", to be presented at Optoelectronics and Laser Applications Conference, Los Angeles CA, January 1987.

9. Ibrahim, S. R., "Modal Identification Techniques, Assessment and Comparison", Journal of Sound and Vibration, pp. 10-15, August 1985.

10. Targoff, W. P., "Orthogonality Check and Correction of Measured Modes", *AIAA Journal*, Vol. 14, pp.164-167, February 1976.

11. Baruch, M., "Optimization Procedure to Correct Stiffness and Flexibility Matrices Using Vibration Tests", *AIAA Journal*, Vol. 16, pp. 1208-1210, November 1978.

12. Berman, A. and Nagy, E. J.,"Improvement of a Large Analytical Model Using Test Data", *AIAA Journal*, Vol. 21, pp. 1168-1173, August 1983.

13. Kabe, A. M., "Stiffness Matrix Adjustment Using Mode Data", *AIAA Journal*, pp. 1431–1436, September 1985.

14. Collins, J. D., Hart, G. C., Hasselman, T. K. and Kennedy, B., "Statistical Identification of Structures", *AIAA Journal*, Vol. 12, pp. 185–190, February 1974.

15. Isenberg, J., "Progressing from Least Squares to Bayesian Estimation", ASME Winter Annual Meeting, Paper 79–WA/DSC–16, December 1979.

16. Hasselman, T. K. and Chrostowski, J. D., "Dynamic Model Verification of a Multi–Component System", SAE Aerospace Conference, Paper No. 841585, October 1984.

17. Evensen, D. A. and Bronowicki, A. J., "Modeling the Dynamic Response of Slabs to Overpressure", Defense Nuclear Agency Report No. 4535F, December 1977.

18. Auton, J. R. and Van Blaricu, M. L., "Translation of Prony's Original Paper and Bibliography of Prony's Method", ADA No. 104532, General Research Corporation, August 1981.

19. Burkhard, P. M., "Modifications of the Prony Spectral Line Estimator, with Applicati to Vasomotion," Ph.D. dissertation, University of California at San Dieg 1983.

20. Hasselman, T. K. and Hart, G. C., "Modal Analysis of Random Structural Systems", ASCE Journal of Engineering Mechanics, Vol. EM–3, pp. 561–579, June 1972.

21. Nelson, R. B., "Simplified Calculation of Eigenvector Derivatives", *AIAA Journal*, Vol. 14, No. 9, pp. 1201–1205, 1976.

SENSOR TECHNOLOGY FOR ADVANCED SPACE MISSIONS

N.M. Nerheim
R.P. De Paula

Jet Propulsion Laboratory
Pasadena, California

FIRST NASA/DOD CSI TECHNOLOGY CONFERENCE
NORFOLK, VIRGINIA
NOVEMBER 18-21, 1986

INTRODUCTION

Control systems of large space structures will require new capabilities in rapid and accurate sensing of numerous critical points on the structure in order to manage complex space operations. This paper presents a summary of the development of two sensors able to provide this capability. The first to be discussed is SHAPES, which stands for Spatial, High-Accuracy, Position-Encoding Sensor. SHAPES is an electro-optic sensor that combines optical angular position measurement with multiple light-pulse time-of-flight range measurements to provide three-dimensional position measurements. The unique characteristic of SHAPES is the capability to track multiple targets with precision at a data rate sufficient for control purposes.

The second sensor we will discuss is FORS, an acronym for Fiber Optics Rotation Sensor. FORS is a new type of gyro that utilizes semiconductor lasers and fiber optic waveguides, together with a unique integrated optics (IO) multifunction optical circuit design for optical signal processing. One of the most significant characteristics of FORS is the capability of very long life provided by solid-state components. Additional advantages are low weight and cost. In addition to its application as a precision navigation-grade gyro, FORS can be configured for monitoring many points of a large space structure by using miniature remote gyro heads connected with optical fiber to a central FORS signal processor.

SHAPES

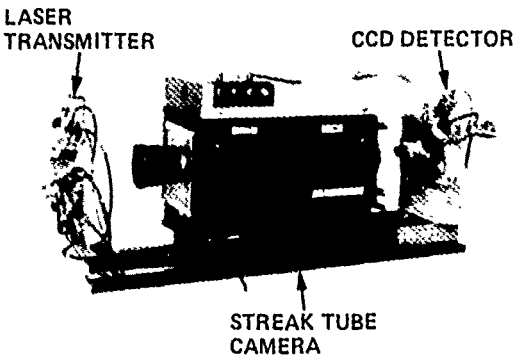

- 3-DIMENSIONAL POSITION MEASUREMENTS
- MULTIPLE TARGETS
- 10 MEASUREMENTS/SEC
- SUBMILLIMETER ACCURACY

FORS

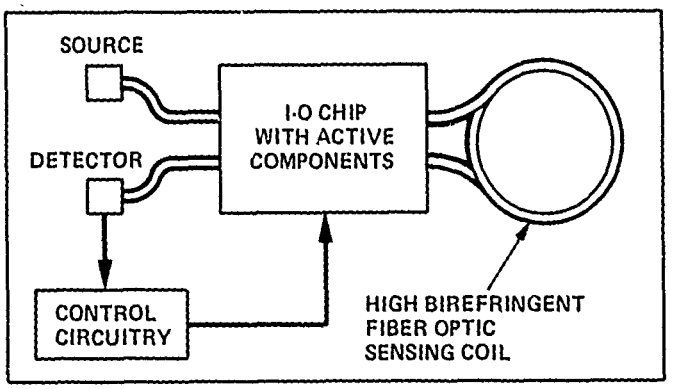

- LONG LIFE (ALL SOLID-STATE)
- LOW COST
- LIGHT WEIGHT

SHAPES OPERATING PRINCIPLE

The SHAPES operating principle is illustrated below. A continuous stream of optical pulses is directed to the target area and illuminates a number of points designated by retroreflectors. The return pulses are imaged onto the streak tube range detector. Time resolution is provided by the streak tube deflection plates as in an oscilloscope, and range is determined by correlation of the time-of-flight of the laser pulses with the deflection plate voltage. Angular position of each point will be obtained by imaging part of the returned light onto a CCD array detector. The well established CCD star tracker technology will be used for the angular position measurement.

Very short laser pulses are required for accurate range measurement. The present experiment utilizes 780 nm laser diodes which are driven by short (80 ps) current pulses to produce 30 ps optical pulses. When operated at 100 MHz, the average output power of each laser is about 0.25 mw and the light pulses are separated by 3 m as indicated below.

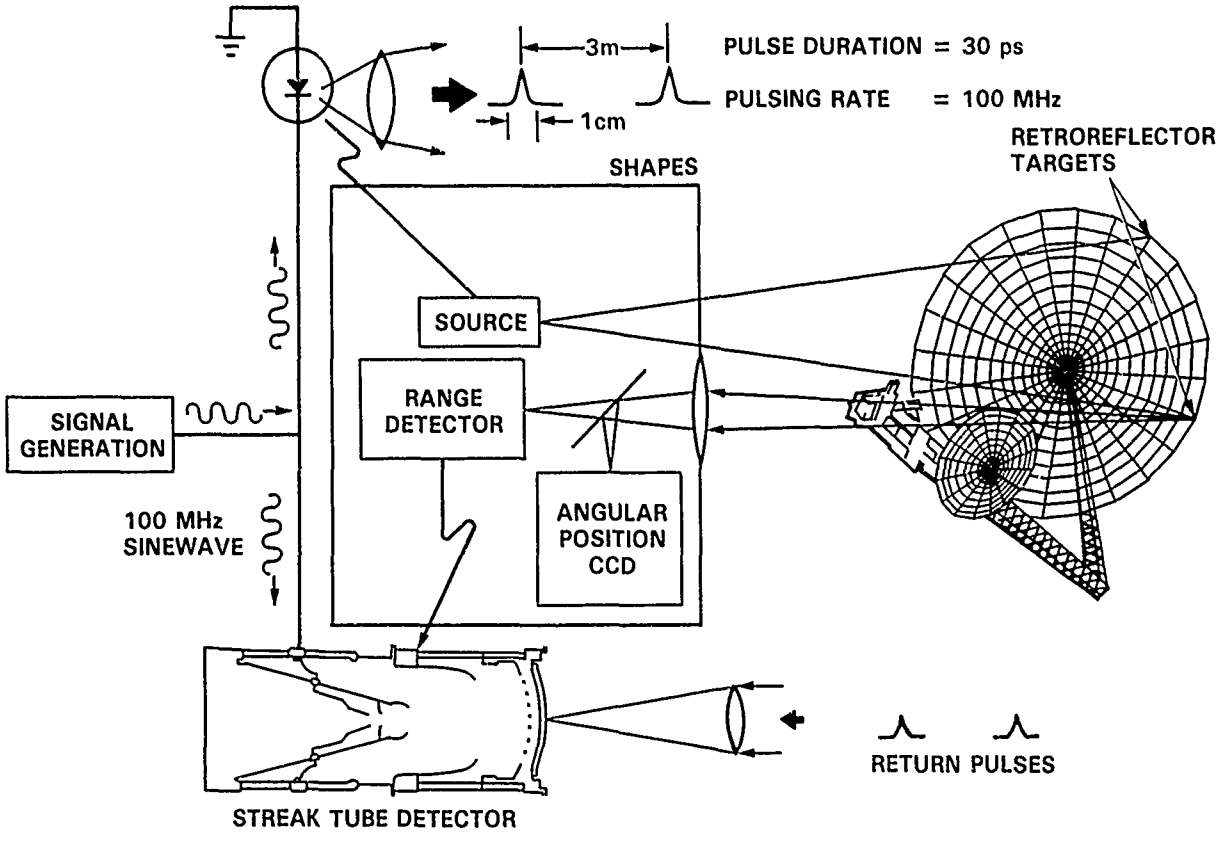

RANGE MEASUREMENT WITH A STREAK TUBE

Photoelectrons are produced at the streak tube photocathode by each returning optical pulse. The electrons are accelerated by a high-voltage grid, directed between the deflection plates by focusing electrodes and finally impinge on a phosphor screen. The fluorescent images of each target on the screen are then transferred to a CCD for readout. The deflection plate voltage is synchronized with the output laser pulse so that the electron packets formed from all optical pulses reflected from an individual target during each framing sequence will strike the phosphor at the same point. Thus each image point on the CCD is the result of the accumulation of charge from many laser pulses. This allows the use of relatively low-powered sources since it is not necessary to detect the signal from a single return pulse. A typical exposure time of 10 ms for each frame results in the integration of 10^6 pulses on the CCD.

The readout of the CCD is controlled by a microcomputer that also processes the data to determine the centroid of each spot and provide usable output. Centroids are determined to an accuracy of about 1/100 of a CCD pixel. The framing rate depends on the target exposure time per frame and the number of targets. For example, a framing rate of 10 Hz with eight targets corresponds to an exposure time of 10 ms.

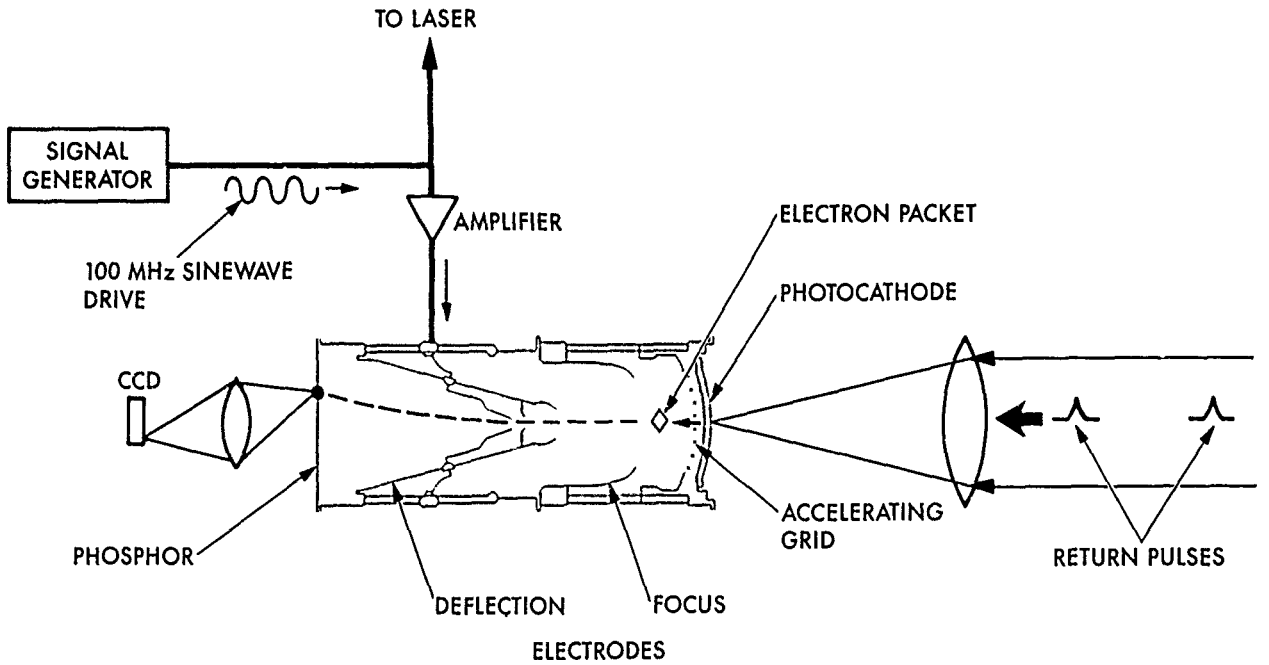

SHAPES TEST FACILITY

The SHAPES Test Facility was designed to demonstrate the sensor's capability to simultaneously track multiple moving targets with high precision. A 4-m-diameter structure was built to support the moving targets in a circular arrangement that simulates an antenna application. The SHAPES sensor was located in an adjoining room, 12 m from the target array. Shown below are an array of laser sources, a commercial streak-tube camera, and the CCD assembly. The individual components of the sensor have been separated for easy viewing. Not shown are the custom electronics used to read the CCD and the microcomputer used to control the system.

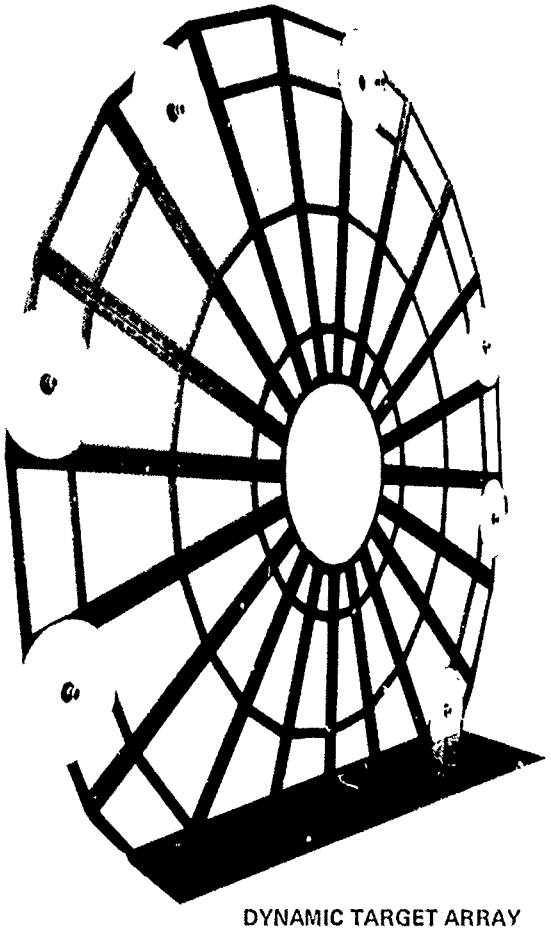

DYNAMIC TARGET ARRAY

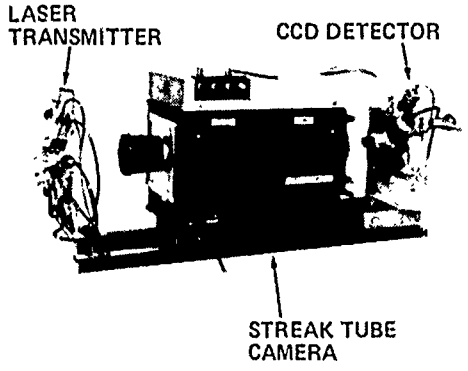

MULTITARGET DYNAMIC RANGE DEMONSTRATION

In a recent laboratory demonstration of the ranging capability of SHAPES, the range to each of eight moving targets was measured simultaneously. The targets were mounted on the 4-m-diameter SHAPES Test Facility described previously. Target motion was provided by mounting the retroreflectors on either free-swinging pendulums or on motor-driven actuators. For the demonstration, eight individual lasers were mounted symmetrically around the periphery of the collecting lens of the streak tube and pulsed simultaneously in synchronism with the streak-tube drive. Each laser was used to illuminate a single target. The data were processed to produce a plot of the target movement as indicated below. The framing rate for eight targets was 10 Hz with a relative range accuracy of 0.1 mm. This data update rate is sufficient for most control system requirements.

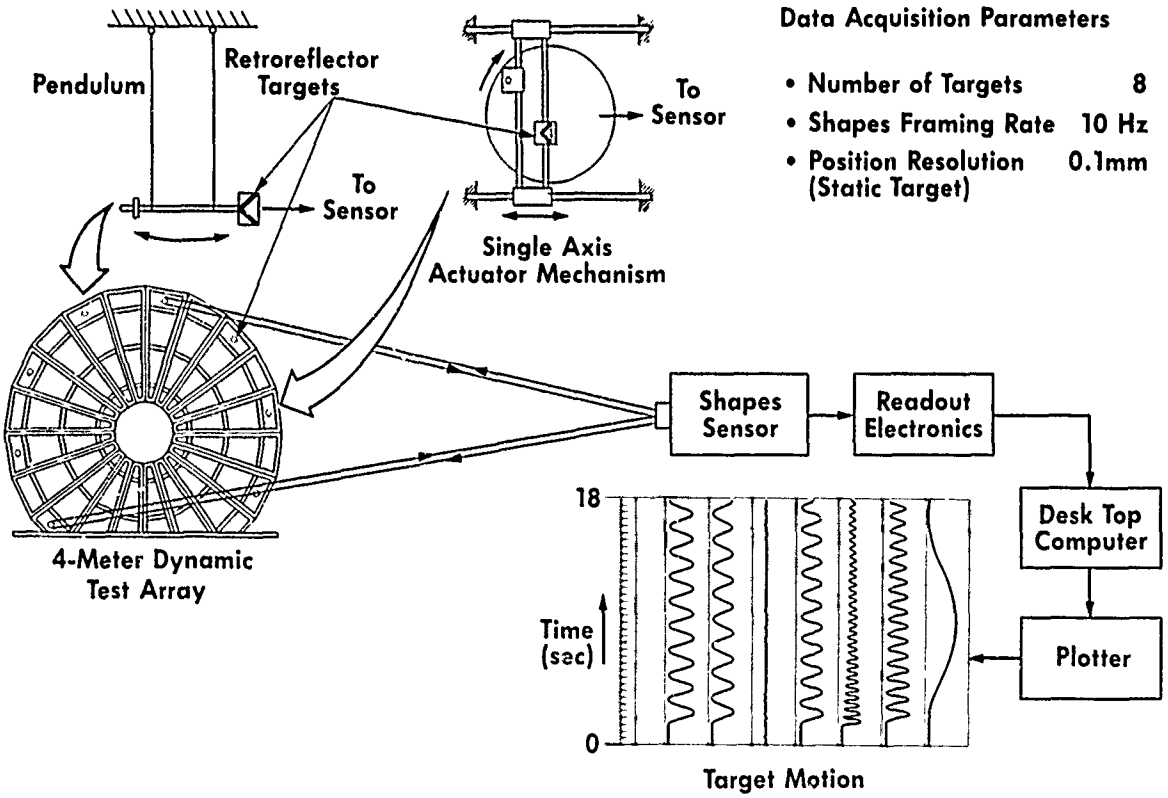

RANGE RESOLUTION

The resolution of range measurements to static targets was determined in a separate experiment. Two stationary target retroreflectors were located a known distance apart and illuminated with a single laser. The centroids of the CCD images of both targets were determined and subtracted. Based on a sample of 50 consecutive measurements, standard statistical methods were used to determine a standard deviation of 0.025 mm as indicated in the figure. The known separation of the target is used to obtain the streak-tube calibration factor.

All of the SHAPES range measurements are made relative to a reference. The reference may be provided by a calibrating target located in the sensor field of view, or it may be provided by a calibrated length of optical fiber internal to the sensor. In addition to providing range accuracy, the reference also improves the range resolution by removing much of the effects of the phase jitter and frequency drift of the drive signal that is common to the signal returns from both the reference and the target.

Experiment to Measure Range Resolution. Separation of T_1 and T_2 was Fixed at 75 mm to Obtain Streak Tube Calibration Factor.

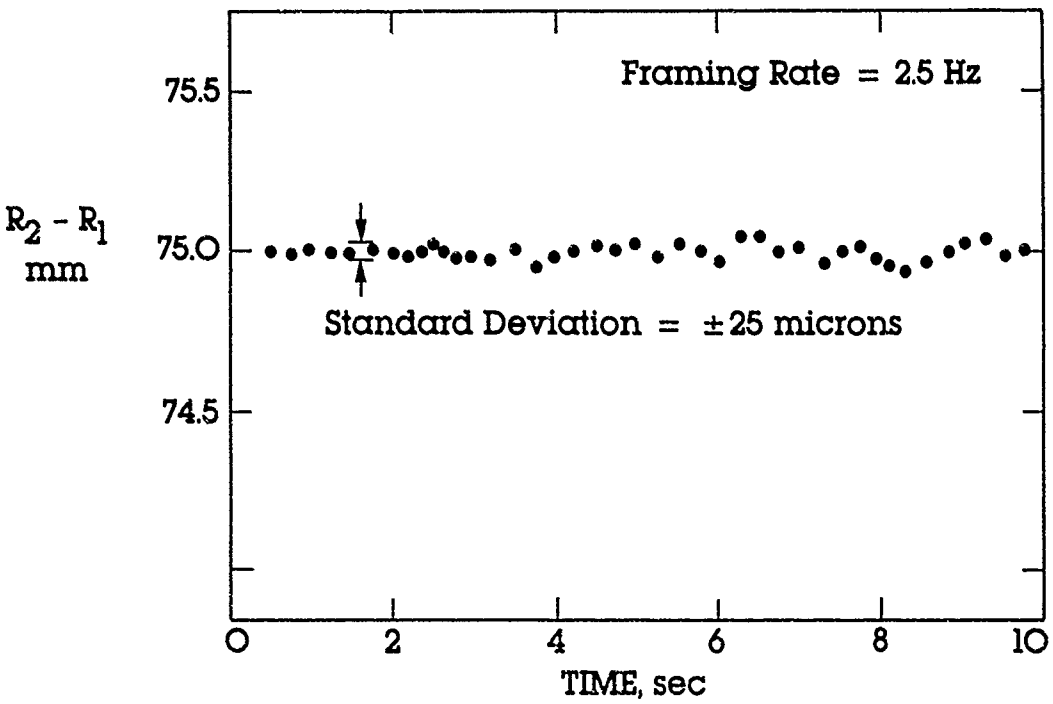

APPLICATIONS OF SHAPES

Simultaneous multitarget tracking capability is required to determine both static and dynamic in-flight characteristics of large space platforms, Space Station, and large antennas. During assembly of space structures, SHAPES measurements can be used to check static structural alignment and overall geometry during each assembly phase. After assembly has been completed, the SHAPES sensor can verify preflight structural analysis and provide the data needed to update the accuracy of models used to design attitude control and payload pointing systems. SHAPES could also be a low-cost optical system for determining absolute payload pointing from navigational base information. The center figure below shows the use of SHAPES in proximity operations where SHAPES can be used to measure relative range and attitude and their rates of change as well as the 3-D location.

The application of SHAPES to the pointing and control of a large space antenna is illustrated on the right of the figure below. SHAPES is shown operating from a central location on the bus where it is collocated with star trackers, earth sensors, or other attitude sensing devices. SHAPES is able to cover the entire antenna with a single sensor head and determine the location of many points simultaneously. This information can then be used to determine static shape, to do modal sensing and control, and, when used with the attitude sensors, to provide enhanced pointing stability and accuracy.

SPACE STATION APPLICATION OF SHAPES

LARGE ANTENNA POINTING AND FIGURE CONTROL

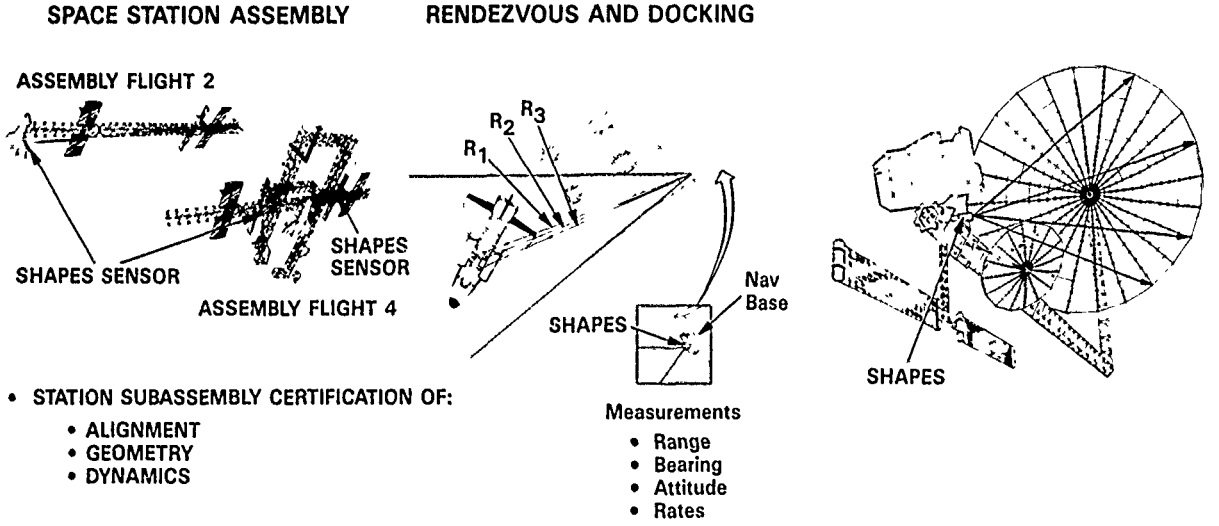

FIBER OPTIC ROTATION SENSOR

The objective of the FORS program is to develop a long life (>10 years), low cost, low weight, high reliability, navigational-grade optical gyroscope for use in future space systems. The gyroscope is being built using semiconductor lasers, fiber-optic waveguides and integrated optics waveguide circuitry for optical signal processing. The drift rate of FORS is expected to be less than .001 degrees/hr.

The operating principle of FORS is based on the Sagnac effect. A laser beam is divided on the IO chip and the two waves counter-propagated through the fiber optic coil and then recombined. Rotation of the coil results in a phase shift of one wave relative to the other. The phase shift, which is proportional to coil rotation, can be measured very accurately.

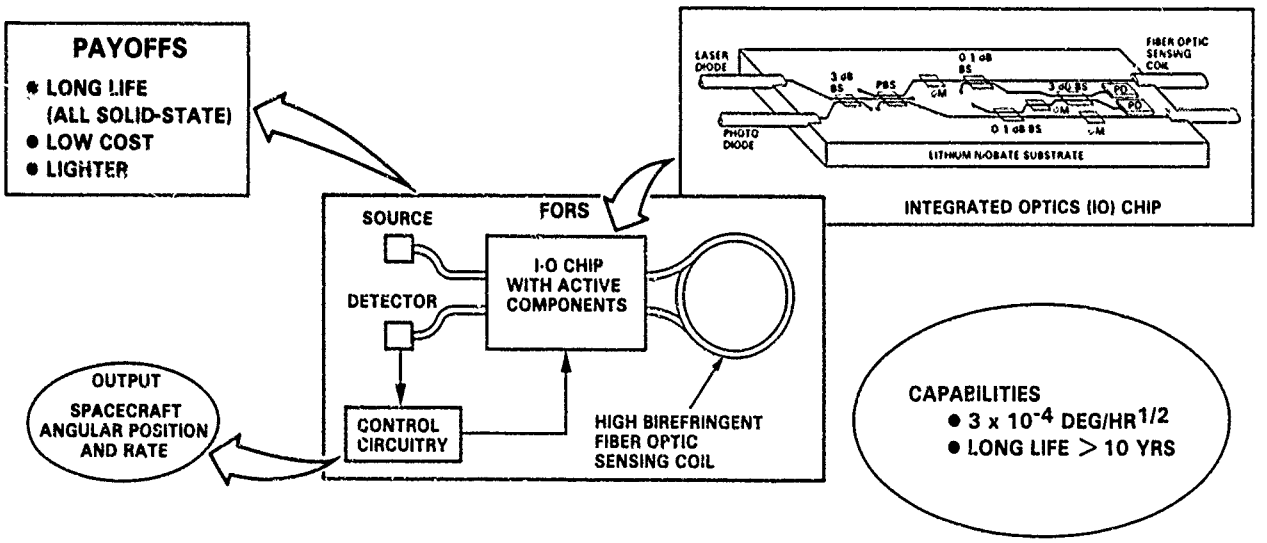

FIBER OPTIC ROTATION SENSOR WITH FULLY INTEGRATED IO CHIP

The fiber gyro design under development is shown below. It utilizes a semiconductor laser, photodetectors, fiber optic waveguide for the sensing coil, and a unique integrated optics (IO) multifunction optical circuit designed for optical signal processing. This IO configuration has an element which provides the dual function of polarizing and beam splitting (PBS). The IO chip also includes an optical phase modulator (ϕM) for use in a serrodyne closed-loop phase control providing operation over a wide range of rotation rates. The output signal is obtained by reading the optical frequency necessary for Sagnac phase nulling directly through the use of a Mach-Zehnder (M-Z) interferometer that is constructed by tapping off from the arms of the Sagnac interferometer. The M-Z interferometer provides incremental position angle by means of beats as in a ring laser gyro. In this design, utilizing the closed-loop phase nulling technique, the effect of any scale factor nonlinearity is greatly reduced and the auxiliary electronics are simplified. The complete IO circuit fits on a 5 cm long lithium niobate chip. The IO chips are under development at AT&T for JPL.

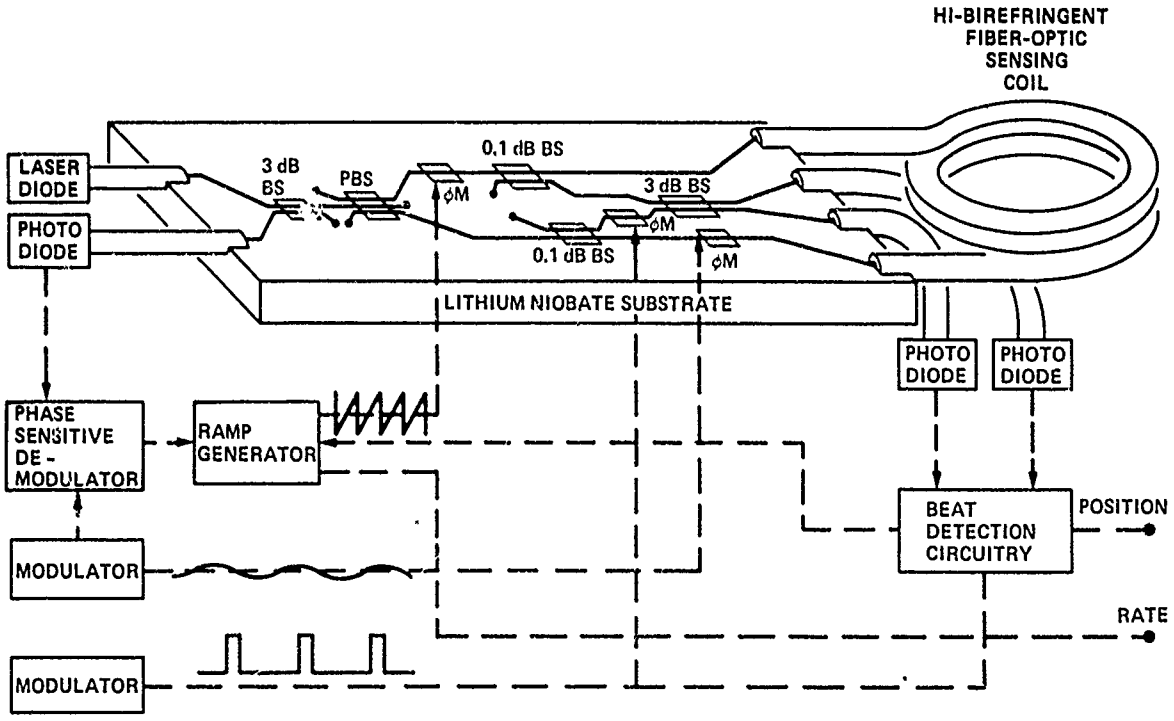

SPACE APPLICATIONS OF FORS
LONGLIFE, NAVIAGATION-GRADE IRU

The Fiber Optic Rotation Sensor is designed for inertial device applications in future space missions. The sensor can satisfy most future performance requirements while offering the potential for low weight, low cost, and long life. FORS is presently the baseline sensor for the Mariner Mark II planetary spacecraft planned for launch in 1992. For this mission, the performance requirements include drift rate of less than 1×10^{-3} deg/hr and a maximum rotation rate of 6 deg/s.

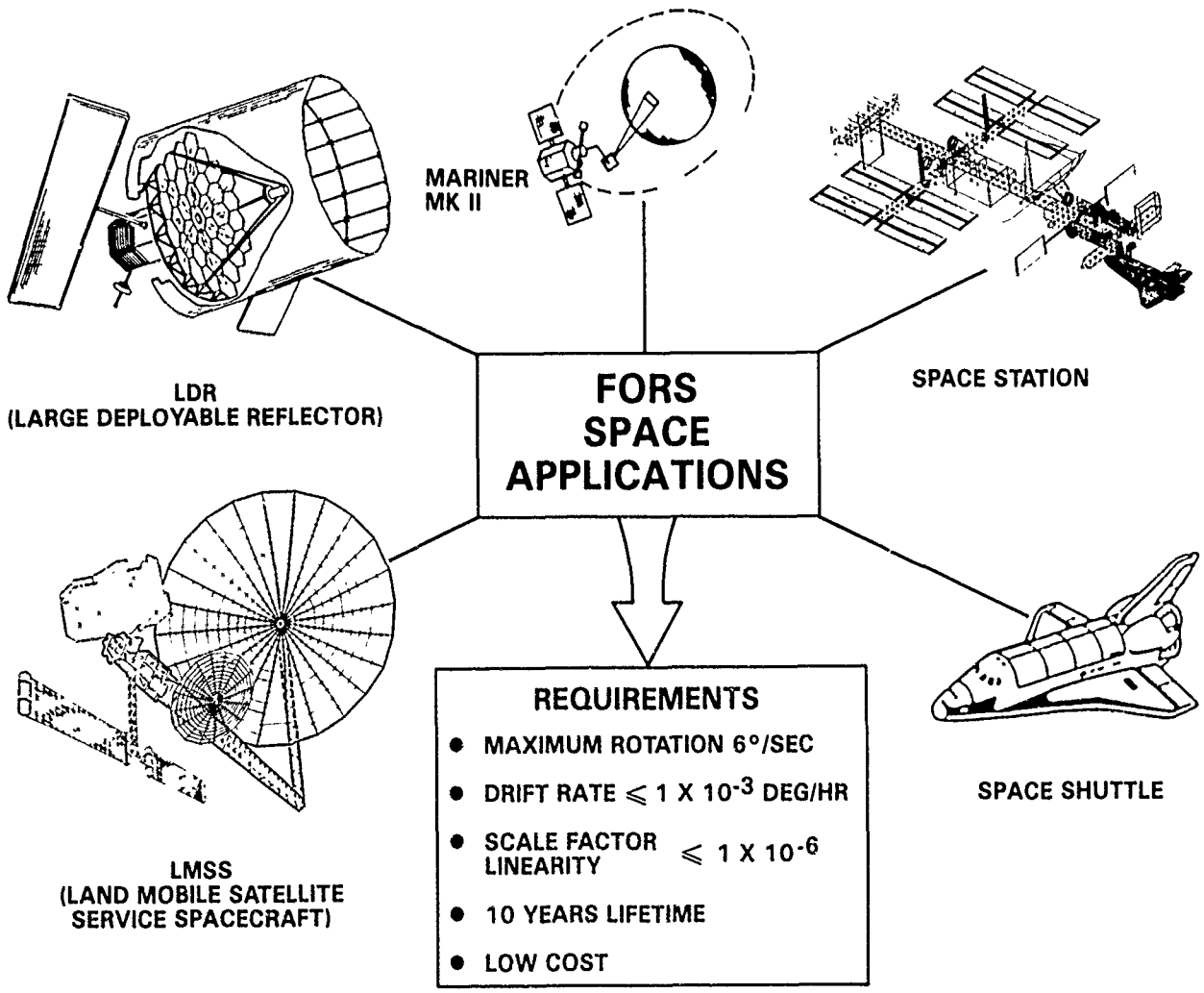

SPACE APPLICATIONS OF FORS (Continued)
DISTRIBUTED SENSING OF LARGE SPACE STRUCTURES

The FORS can be configured into a sensing system that offers the unique flexibility of placing remote miniature rotation sensing coils at many different points of a large structure. These fiber optic coils are connected with optical fibers to a central FORS sensor unit which contains the integrated optics, lasers, detectors, and required electronics to process the information. Coils as small as 3 cm in diameter are feasible. These lightweight coils, connected to the central processor, are capable of measuring angular rotation and angular acceleration of multiple remote points distributed throughout the structure and can provide a means to characterize structural dynamics and to control vibrational modes. FORS could also be used to determine the dynamics of localized Space Station payloads.

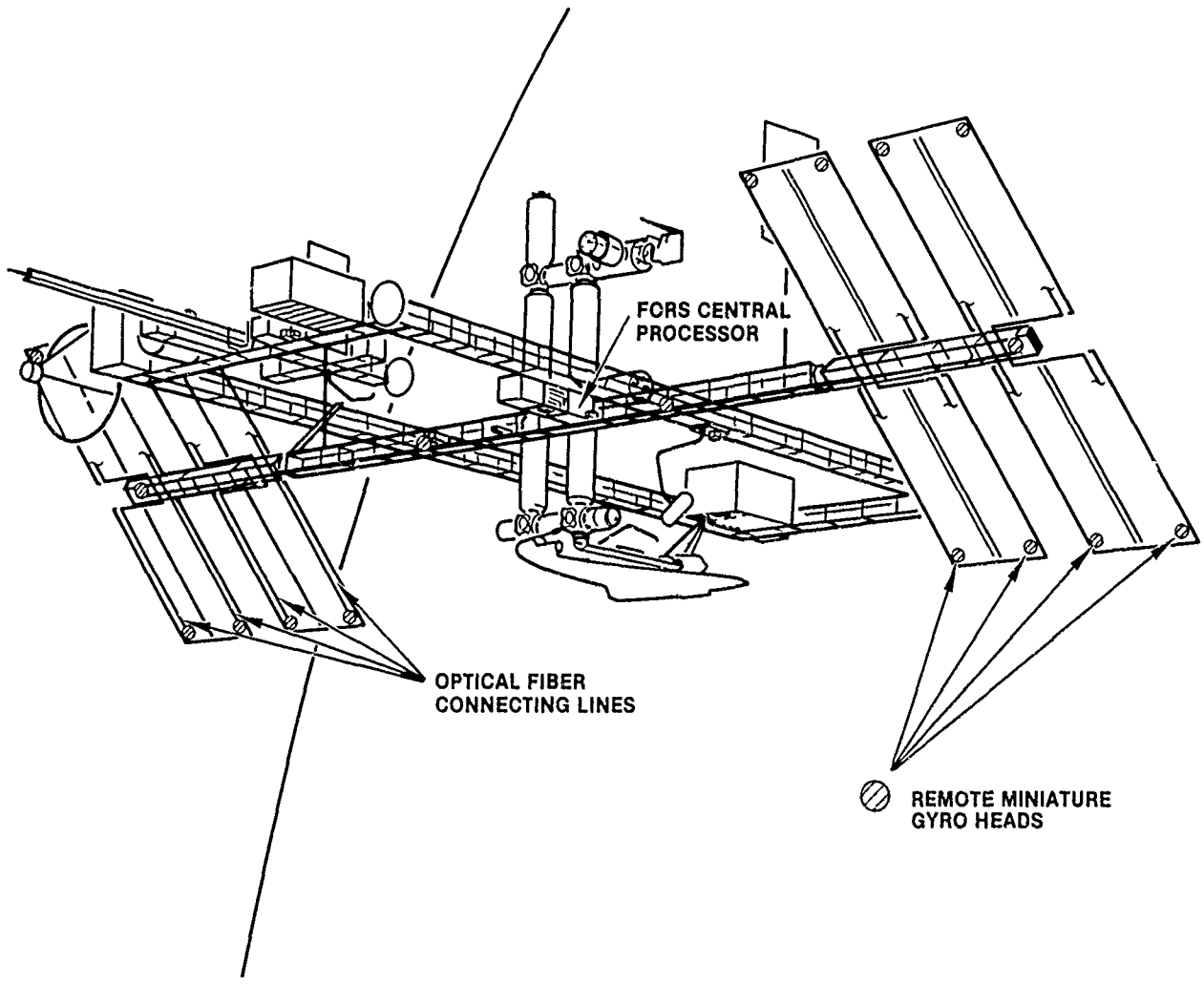

SUMMARY

This paper discussed the capability and applications of two sensors, SHAPES and FORS, for advanced missions. The multiple target, 3-D position sensing capability of SHAPES meets a critical technology need for many developing applications. A major milestone of the SHAPES task was completed on schedule on May 30, 1986, by demonstrating simultaneous ranging to eight moving targets at a rate of 10 measurements per second. The range resolution to static target was shown to be 25 microns. SHAPES scheduled technology readiness will support the sensor needs of a number of early users, some of which are listed below. The next phase in the development of SHAPES is to incorporate an angular measurement CCD to provide the full 3-dimensional sensing. A flight unit design and fabrication can be complete by FY 89.

FORS, with its significant improvement over present technology in lifetime, performance, weight, power, and recurrent cost, will be an important technology for future space systems. Technology readiness will be demonstrated with a FORS brassboard with fully integrated IO chips by FY 88. The unique capability of miniature remote sensing heads, connected to a central system, will open up new areas in control and stability of large space structures. This application requires additional study.

SHAPES

- MULTIPLE TARGET, 3-D POSITION SENSOR CAPABILITY IS CRITICAL NEED FOR MANY APPLICATIONS
- MULTITARGET RANGING DEMONSTRATED
  - EIGHT MOVING TARGETS
  - DATA UPDATE RATE OF 10 Hz
  - RESOLUTION 25 MICRONS
- SHAPES TECHNOLOGY CAN SUPPORT
  - SPACE STATION
  - COFS EXPERIMENTS
  - MSAT EXPERIMENTS
  - RENDEZVOUS AND DOCKING
  - MARS SAMPLE RETURN
  - GROUND ANTENNA POINTING

FORS

- A NAVIGATIONAL-GRADE SOLID-STATE GYRO PROVIDES SIGNIFICANT IMPROVEMENTS IN:
  - LIFETIME
  - PERFORMANCE
  - WEIGHT
  - POWER
  - RECURRENT COSTS
- HAS THE INHERENT SENSOR CONFIGURATION FLEXIBILITY OF UTILIZING MINIATURE ROTATION SENSING COILS LOCATED THROUGH A LARGE SPACE STRUCTURE
- FORS TECHNOLOGY CAN SUPPORT
  - MARINER MARK II MISSIONS
  - SPACE STATION
  - LMSS SPACECRAFT
  - ADVANCED TRANSPORTATION
  - AEROSPACE VEHICLE
  - ADVANCED ROBOTICS SYSTEMS

COFS I - Beam Dynamics and Control Technology Overview

John L. Allen
NASA Langley Research Center
Hampton, VA 23665

First NASA/DOD CSI Technology Conference
Norfolk, Virginia
November 18-21, 1986

INTRODUCTION

NASA and other Government agencies have been exploring the unique characteristics of large space systems, from large orbital antennas to manned space stations, and have initiated the development of technologies required to assure the successful performance of these next-generation spacecraft. The COFS I Project provides the invaluable opportunity to test, validate, and measure the effectiveness of theories, structural concepts, control systems, and flight certification processes for future missions through a research program focusing on multiple issues in large flexible structures, dynamics, and controls. The COFS I Project consists of a series of ground and flight activities building progressively from modeling and dynamic characterization of large space systems to the more complex issues of flexible-body control. The COFS I Project also involves the space structures and controls research community from universities, industry, and Government through a formal Guest Investigator Program in which researchers are selected to participate in all program activity phases.

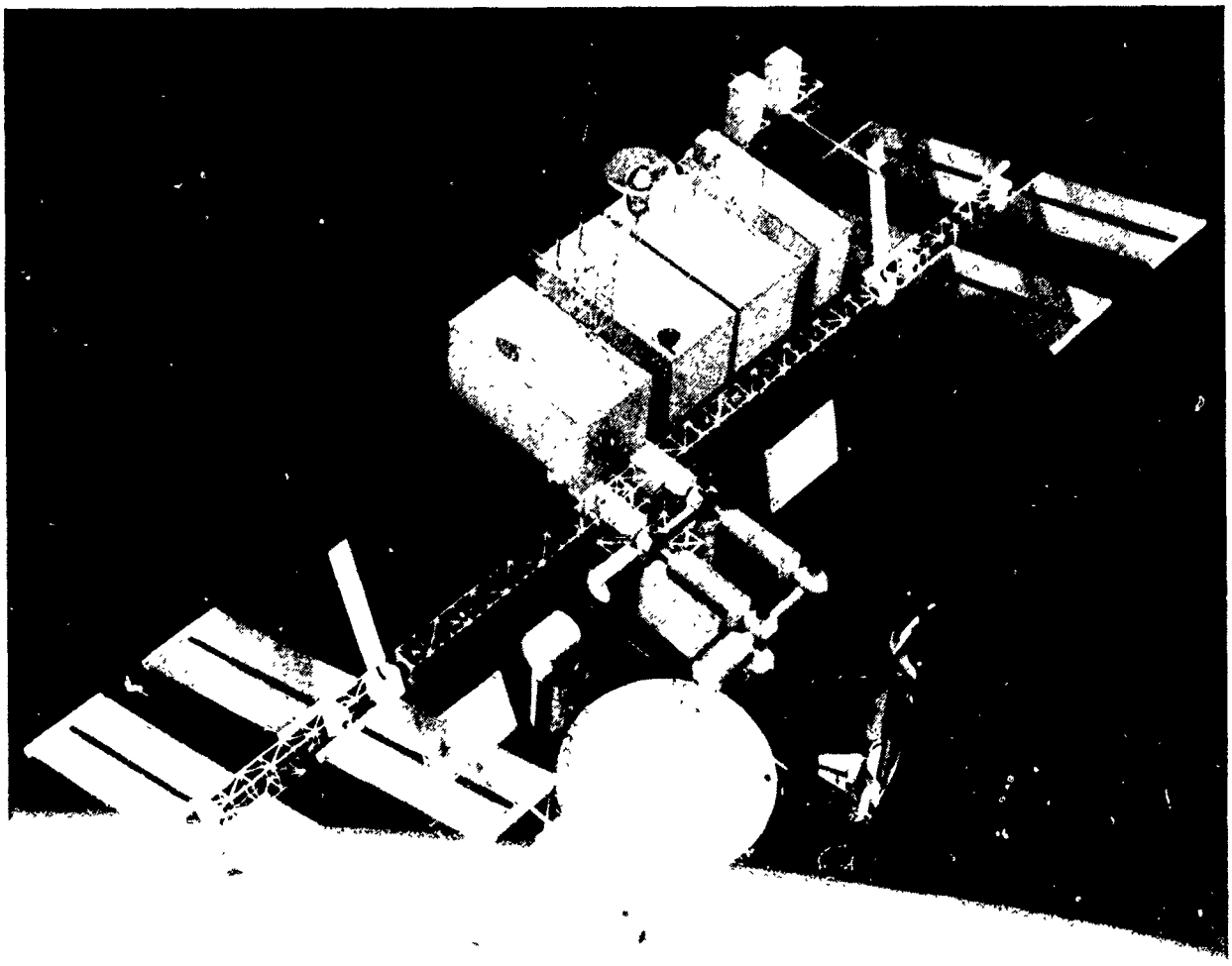

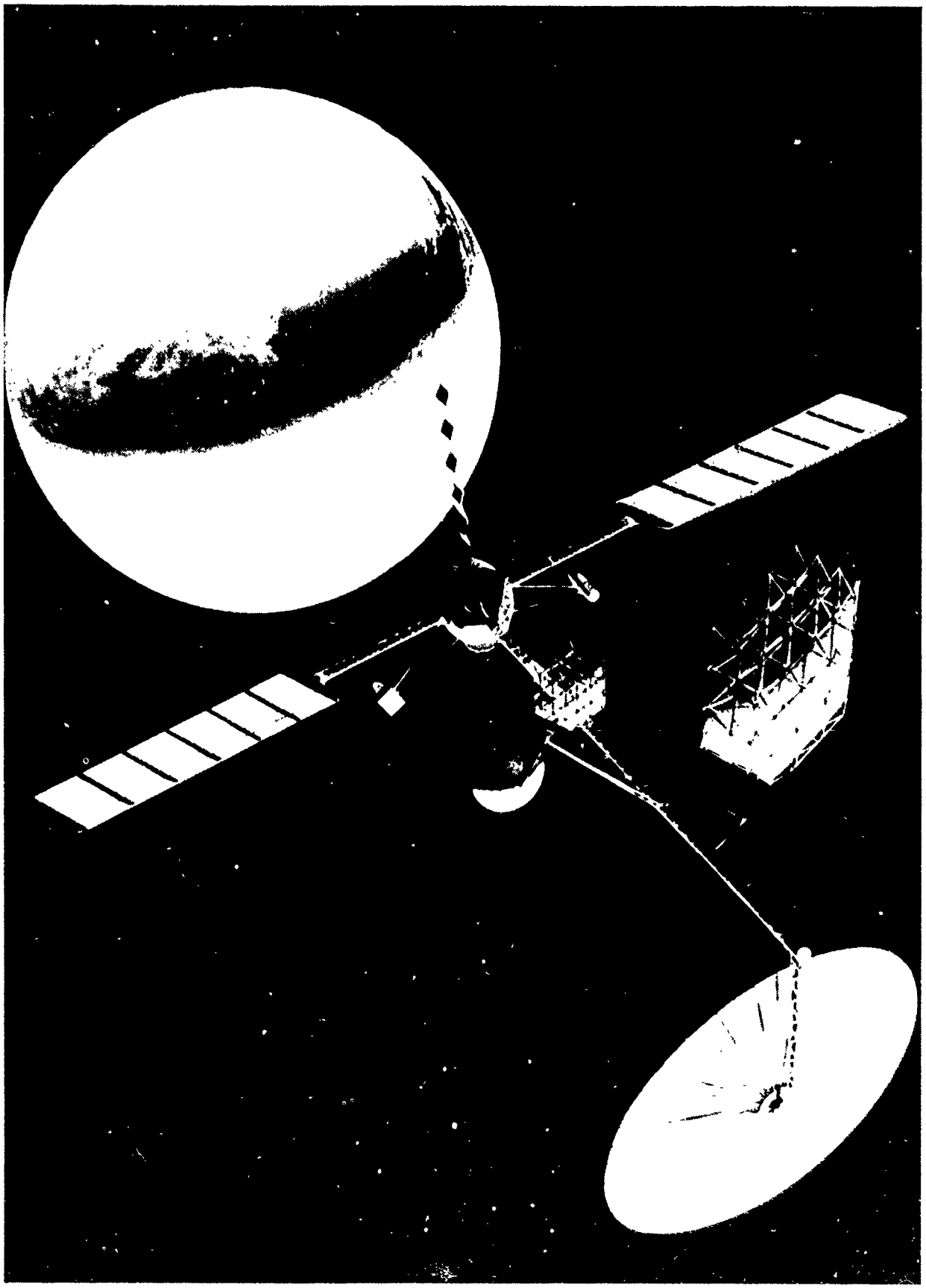

COFS I TECHNOLOGY GOALS

COFS I is the initiation of a planned series of configurations and tests that are required to achieve the overall long-range goals of the COFS program. Advanced techniques will be used to quantify the benefits and limitations of full-scale ground testing; to correlate scale model results to full-scale performance, both ground and space based; to verify robust control system design methodologies; and to identify the applicability of ground tests necessary to support future programs requiring on-orbit dynamic characterization and robust control.

- **VALIDATE GROUND TEST METHODS**
- **DEVELOP & VALIDATE IN-SPACE TEST METHODS**
- **VERIFY CSI ANALYTICAL TOOLS**
- **ASSESS SCALING EFFECTS**
- **EVALUATE DISTRIBUTED CONTROLS METHODS**

COFS I SPECIFIC OBJECTIVES

Specifically selected research objectives are tailored to attainment of COFS I technology goals and are a major constituent of the overall goals of the Control of Flexible Structures Program.

- **DETERMINE DEGREE TO WHICH THEORY AND GROUND TESTING CAN PREDICT FLIGHT PERFORMANCE OF NEXT-GENERATION LOW-FREQUENCY STRUCTURES.**
- **EVALUATE STRUCTURAL FIDELITY OF REPRESENTATIVE NEXT-GENERATION LARGE DEPLOYABLE PRECISION STRUCTURE.**
- **ASSESS MATH MODELING REQUIREMENTS FOR LARGE LIGHTWEIGHT COMPLEX SYSTEMS ON WHICH GROUND TEST RESULTS ARE QUESTIONABLE.**
- **DETERMINE DEGREE TO WHICH SCALE MODEL ANALYSIS AND TESTS CAN BE CORRELATED TO FULL-SCALE PERFORMANCE.**
- **EVALUATE SYSTEM IDENTIFICATION AND STATE ESTIMATION ALGORITHMS ON COMPLEX LIGHTWEIGHT STRUCTURES IN THE SPACE ENVIRONMENT; COMPARE ON-LINE AND OFF-LINE METHODS.**
- **EVALUATE AND VERIFY CONTROLS/STRUCTURES MODELING CAPABILITY.**
- **EVALUATE CONTROL LAWS AND CONTROL SYSTEMS.**
- **EVALUATE DAMPING EFFECTS IN MICRO-G ENVIRONMENT.**

COFS I - BEAM DYNAMICS AND CONTROLS TECHNOLOGY

The schedule shown above depicts major milestones for the significant activity areas which constitute the COFS I program. Each of these activity areas will be addressed briefly in the remainder of this presentation and the follow-on COFS I papers will provide full details of salient programmatic developments.

The Mast Flight System is being developed by Harris Corporation and is the centerpiece of the COFS I ground and flight test activities. This system, as well as the mini-Mast prototypical beam-truss and sub-scale Mast structural models, will experience extensive ground testing and correlative analysis.

A Guest Investigator Program has been established to involve all sectors of the nation's science and technology community in the COFS I research activity. Flight coding of guest investigator algorithms will be accomplished through a separate Government software contract.

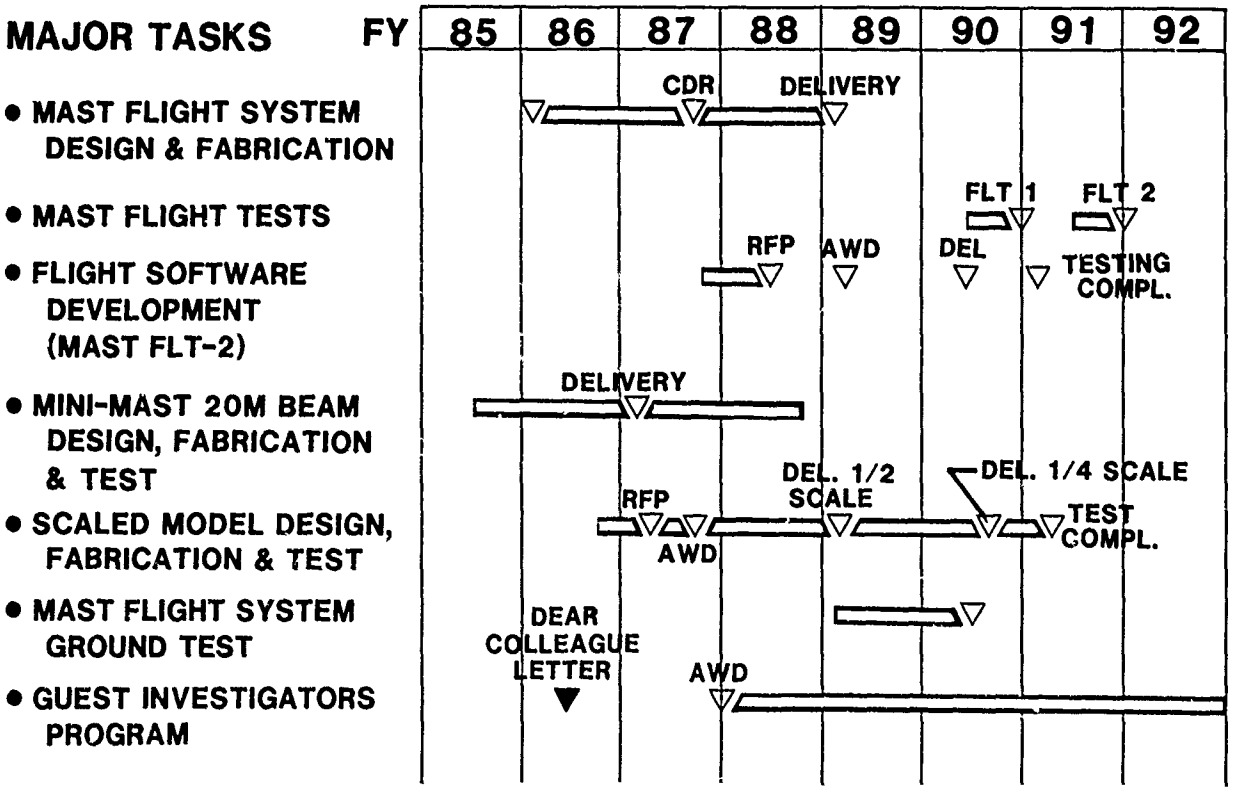

MAST FLIGHT EXPERIMENT

The approach, which has been adopted for COFS I research, centers on a flight/test structure with selected generic characteristics of large space structures. This centerpiece of the COFS I Project, the Mast flight system, contains a large (60-meters long) deployable/restowable "next-generation" truss beam attached in a cantilever fashion to its carrier (the STEP) which is, in turn, attached within the Space Transportation System (STS) Orbiter payload bay. Actuators, instrumentation, and avionics necessary for excitation, measurement, and control of the low-frequency modes of this structure are an integral part of the flight system. The beam truss also contains a Parameter Modification Subsystem (PMS) which provides the capability to change flight system physical properties, thereby altering frequency spacing and cross axis coupling between modes. The Mast flight system will be used to support two flight research missions from the STS Orbiter.

COFS I FLIGHT TESTS

The Mast Flight System, bridging the gap between ground modal verification, on-orbit modal verification, and validation of control methodologies, makes use of the same flight structure for both the ground tests and the two flight tests. As structural characteristics are identical, ground modal testing and on-orbit modal testing can be compared and evaluated. Also, as no hardware modifications are required for flight two, the structural characteristics will be the same for the distributed flex-body control experiment of that flight and the systems identification experiment of the first flight; i.e., the control algorithm will work against a system model that has been previously characterized, both on the ground and on-orbit.

Mast I. - The first flight (Mast I) of the two mission scenario basically addresses the aspects of large flexible structures and structural dynamics with rudimentary research tasks in structural damping. The Mast I experiment is dynamically excited by the subsystems of the Mast experiment at various lengths of extension, with and without modal alteration by the Parameter Modification Subsystem (PMS), and response data collected. At the conclusion of the flight test sequence, which should occupy three or four days of activity, the flight system will be restowed for the descent and landing phase. Upon return of the flight data, systems identification techniques and ground-based analyses will be conducted to structurally and dynamically characterize the beam-truss in the space environment and to establish and improve the validity of preflight ground test data and analytical models.

Mast II. - In the second flight experiment of the COFS I Project, the Mast test article will be reflown without modification of its hardware complement. During the Mast II flight, the beam structure will be excited, response data collected, and the modal characteristics determined by ground-based systems identification to verify that the structure is modally identical to that flown on the first flight. Experiments in distributed control will be conducted to evaluate performance of flex-body control algorithms operating in conjunction with a structure that has been modally characterized after launch.

GROUND-BASED TECHNOLOGY

Prior to flight mission activities, there is an extensive ground-based program to be conducted in-house to prepare for the flight phase. These activities include: (1) Utilization of prototypic full scale 20-meter truss beam segment ("mini-mast") to aid in development of structural modeling methodologies and as a preliminary test bed for examining Mast full scale dynamic characterization techniques and to evaluate flex-body control algorithms for a distributed control system, and (2) Development of one-quarter and one-half scale structural models of the Mast beam truss; complete ground-based characterization of these systems will be accomplished through modeling, testing, and analysis of the scaled components and assemblies. Prediction of Mast full scale characteristics will be developed from sub-scale model results, and correlation of these predictions with results of Mast flight system testing, ground and space-based, will be accomplished.

GROUND TEST APPROACH

GROUND TEST HARDWARE

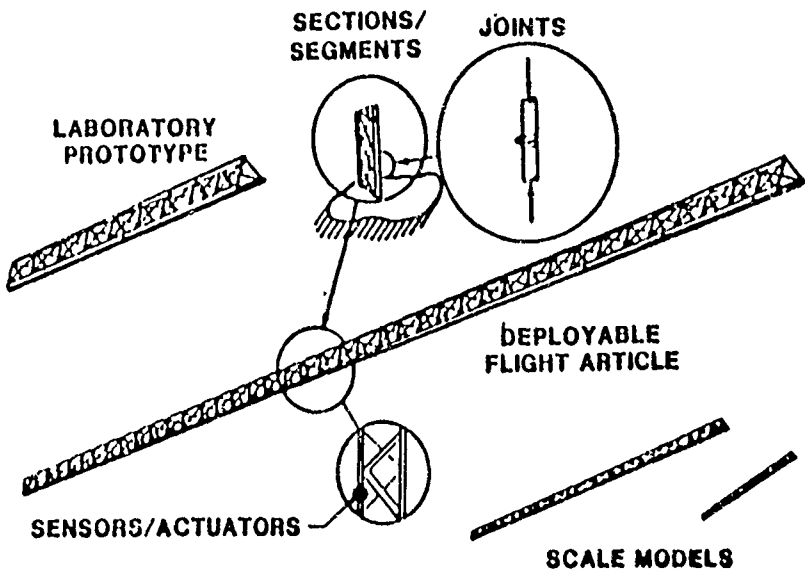

OBJECTIVES

- DEVELOP GROUND TEST METHODS AND CAPABILITY
- EVALUATE CONTROLS INSTRUMENTS
- VALIDATE CONTROL STRUCTURES ANALYSES
- EVALUATE SCALING METHODS
- EVALUATE JOINTS/ DAMPING EFFECTS
- DEVELOP STRUCTURAL DEFINITION OF FLIGHT ARTICLE

MAST FLIGHT SYSTEM GROUND TEST

The ground-based testing of the 60-meter Mast flight system will be accomplished by suspending the beam horizontally and measuring modes and frequencies to provide ground-based data by which predictions of space-based system responses may be developed. Response instrumentation and control parameters will be thoroughly evaluated. Flight performance predictions, derived from ground-based testing and advanced modeling and analytical techniques, will be assessed and ultimately correlated with zero-g Mast system flight performance data, thereby providing a quantitative measure of the ability to predict zero-g system dynamics utilizing ground-based certification methodologies.

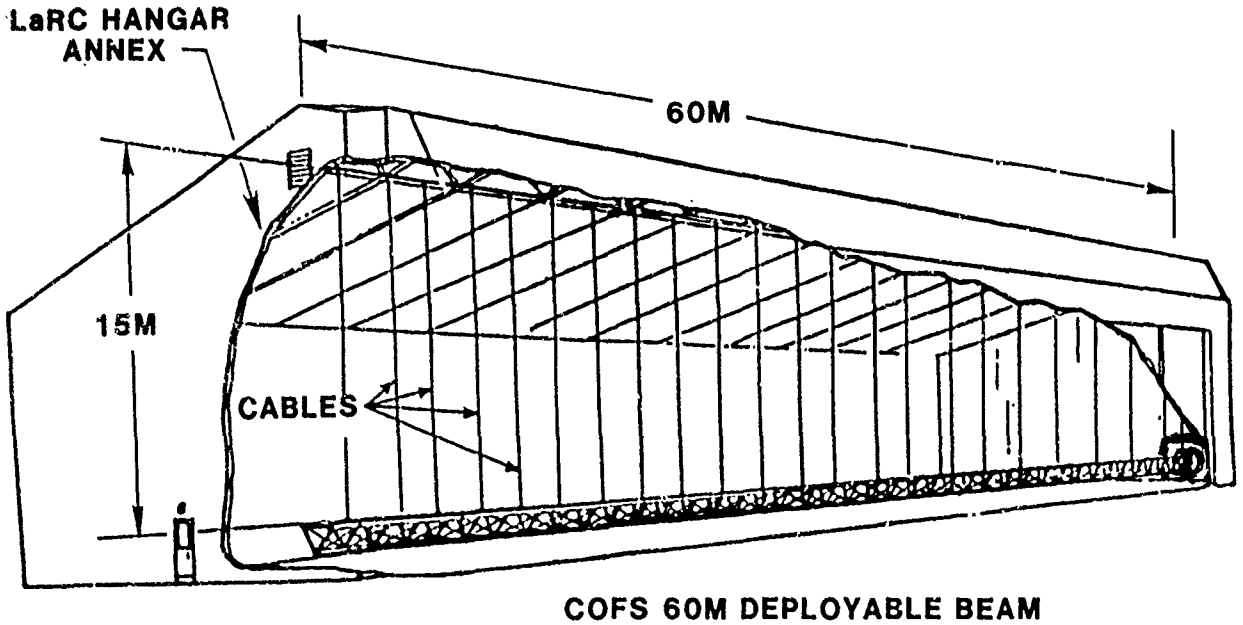

COFS 60M DEPLOYABLE BEAM

GUEST INVESTIGATOR PROGRAM

A Guest Investigator Program is being established to create a partnership with NASA, other Government laboratories, universities, and industry for direct participation in the science activities for each Mast flight and in the ground-based program. Research proposals have been solicited and received from the above community and are presently being evaluated; this process will ultimately lead to a selection of experiments by the Office of Aeronautics and Space Technology (OAST) for inclusion in the Control of Flexible Structures COFS I research program.

OBJECTIVE:

TO PROVIDE OPPORTUNITIES FOR AND PROMOTION OF GENERIC RESEARCH BOTH GROUND AND IN-SPACE AMONG INDUSTRY/ UNIVERSITY AND GOVERNMENT FOR THE DEVELOPMENT OF CONTROLS/STRUCTURES INTERACTION TECHNOLOGY

APPROACH:

ESTABLISH GROUND AND IN-SPACE FACILITIES WHICH PROVIDE FOR INDIVIDUAL AND/OR COMPANY EXPERIMENTS AT MINIMUM COST

PAYOFF:

- **BROAD BASE FOR ADVANCED CSI METHODOLOGIES**
- **DISSEMINATION OF PROGRAM DATA & FINDINGS WITHIN CSI COMMUNITY**
- **IN-SPACE RESEARCH AWARENESS**

COFS I SUMMARY

- Mast Flight System development contract has been underway for a year with delivery scheduled for late 1988.
- Ground test preparations are moving forward; the 20 meter mini-Mast test program to start soon. RFP for Scale Model Structures to be released early next year.
- Guest Investigator (GI) research proposals have been received and selection process underway leading to selection and award of GI contracts/grants in 1987.
- COFS I first flight (Mast I) tentatively scheduled for October 1990 with second flight (Mast II) a year later.

COFS I RESEARCH OVERVIEW

G. C. Horner
NASA Langley Research Center
Hampton, Virginia

First NASA/DOD CSI Technology Conference
Norfolk, Virginia
November 18-21, 1986

Control of Flexible Structures
Program Approach

The Control of Flexible Structures (COFS) program is divided into three areas of research. These three areas are controls/structures analysis development, ground test experiments, and in-space experiments.

The ground test experiments are intented to validate analyses and to confirm through hardware tests our technical readiness to successfully fly the Mast hardware. There is this close relation to the results of ground tests and analytical predictions that must be understood before flight experiments may be attempted.

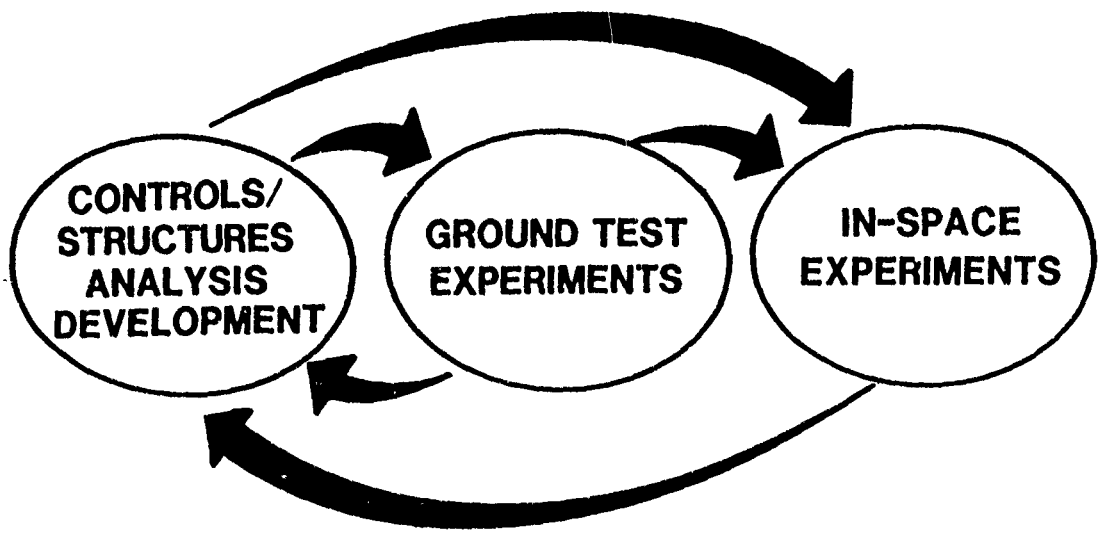

Model Validation Process

At every step of the ground test program each hardware test will be complemented by an equivalent analysis. That is, all components, subassemblies, scale models, and full scale assemblies will be tested in some fashion and the output of these tests is called measured performance. The equivalent result from the analytical models is called predicted performance. Next, the measured performance is compared to the predicted performance and the difference is an error measure.

The purpose of this process is to have a validated analytical model. Using sensitivity parameters, adjustments to the analytical model are made such that the predicted performance better predicts the measured performance.

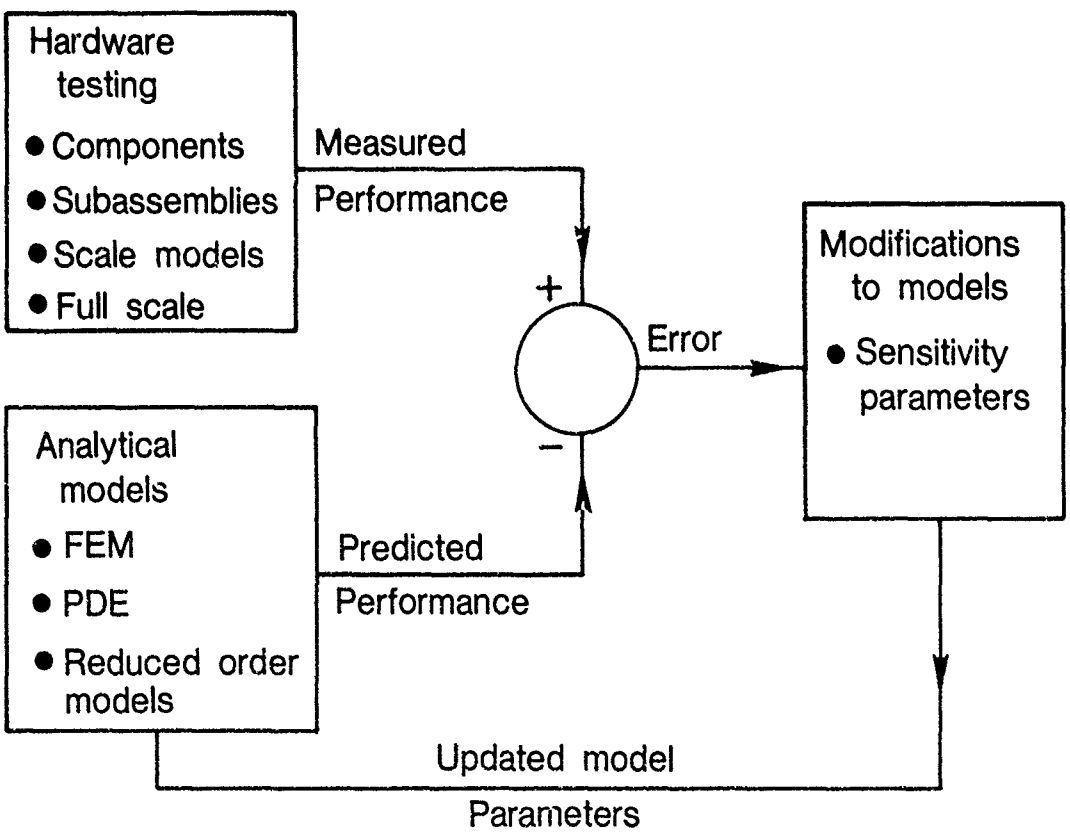

Control of Flexible Structures
Ground Test Program

The objectives of the ground test program are the development of ground test methods, evaluation of control instruments, validation of control/structure analyses, evaluation of scaling methods, evaluation of joint/damping effects, and evaluation of distributed control techniques. These tests will be conducted on components, scale models, mini-Mast, and Mast.

Ground test hardware

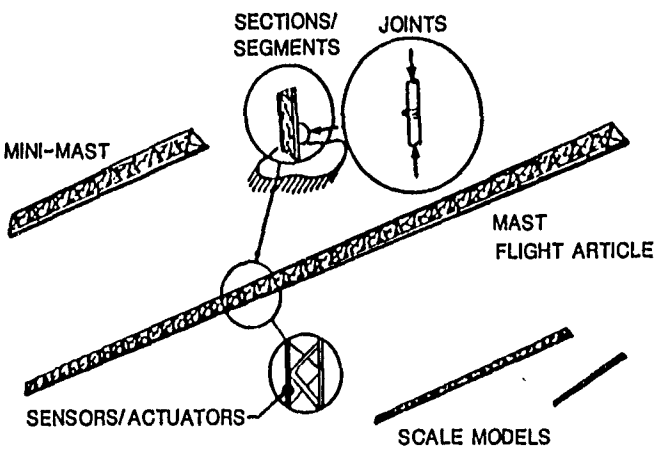

Objectives

- DEVELOP GROUND TEST METHODS AND CAPABLITY
- EVALUATE CONTROLS INSTRUMENTS
- VALIDATE CONTROL STRUCTURES ANALYSES
- EVALUATE SCALING METHODS
- EVALUATE JOINTS/DAMPING EFFECTS
- EVALUATE DISTRIBUTED CONTROL TECHNIQUES

Ground Test/Analysis Program

Examples of components that will be tested are joints that will be loaded in tension and compression to determine the joint properties such as stiffness and damping. Also, actuators will be bench tested to determine the dynamic characteristics.

Analysis

$F = k_1 x + k_2 x^3 + H.O.T.$

Component

Test

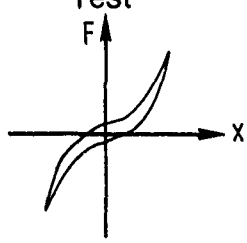

$\Sigma F = m\ddot{y}$

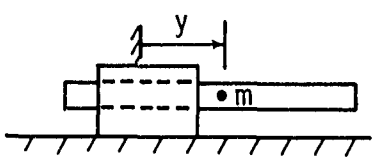

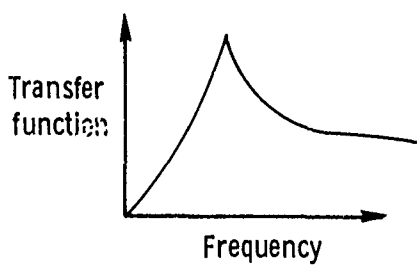

Diagonal Hinge Joint

This is a picture of a diagonal hinge joint for mini-Mast. It is shown in a test machine with a fixture to capture the joint if it should start to open.

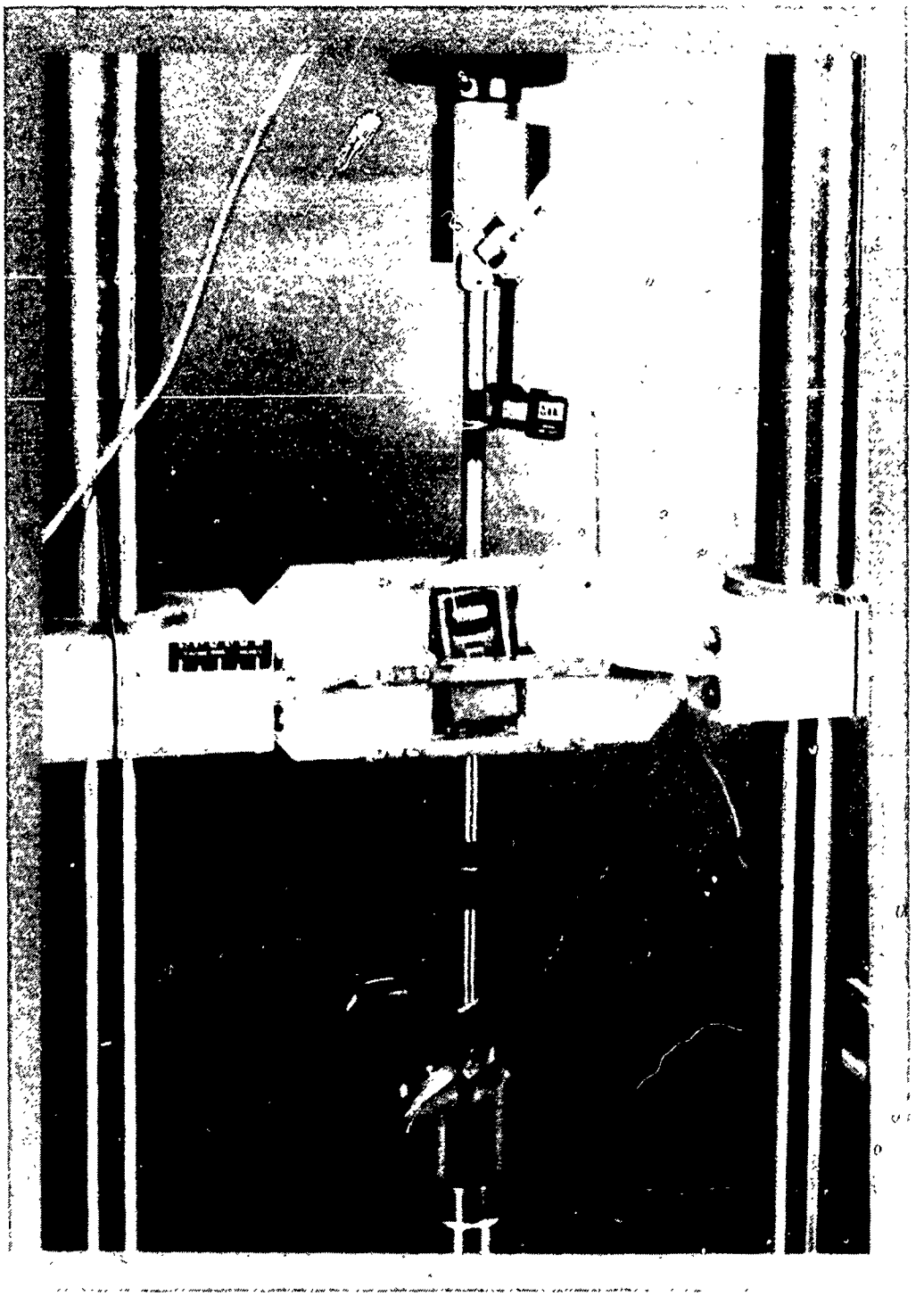

Load Deflection Data

Here are results of a joint test where the load is applied at the rate of one cycle per second which is in the vicinity of frequencies for mini-Mast. The slope of the curve is the stiffness and the area inside the curve is a measure of the damping.

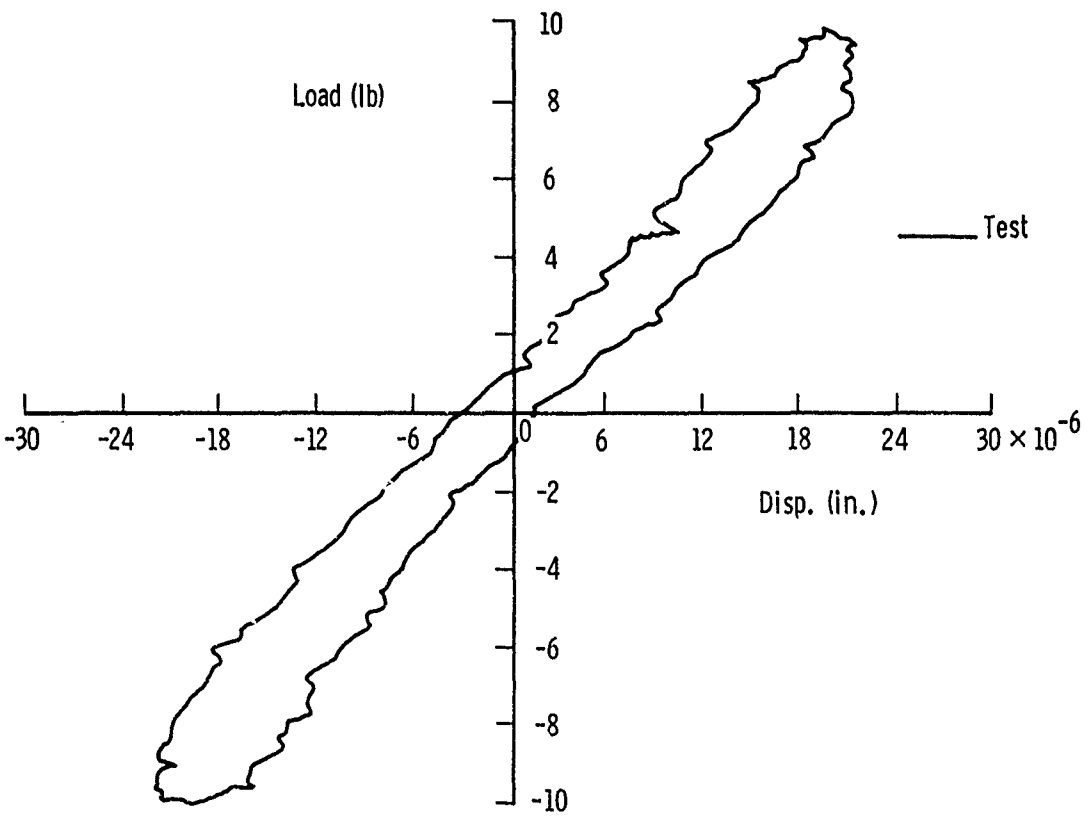

Linear DC Motor (LDCM)

This is a picture of the Harris prototype LDCM that will be tested and characterized. There will be ten actuators on the Mast flight and these actuators are the devices which apply forces to the Mast truss structure.

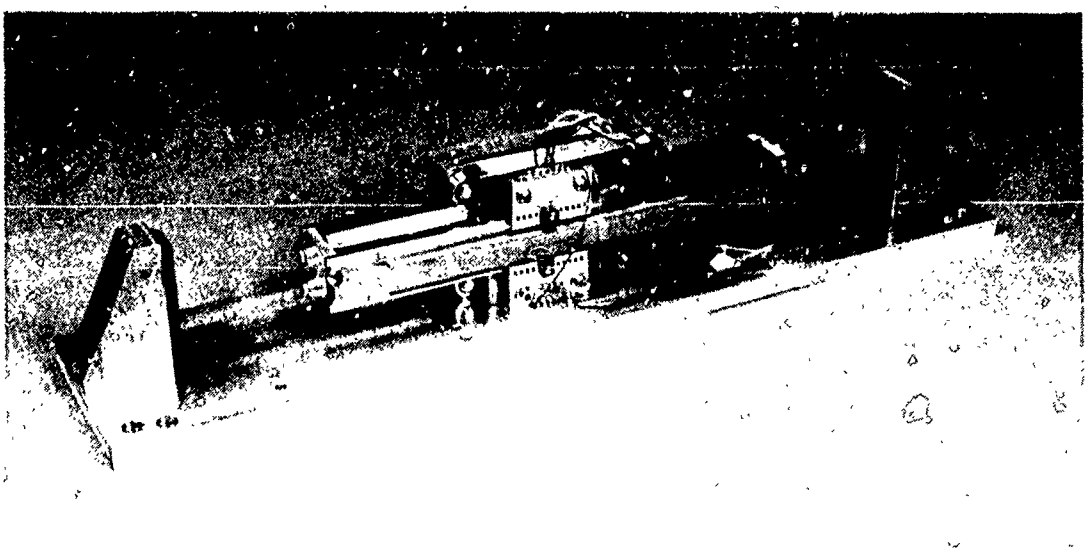

Ground Test/Analysis Program

The ground test program will progress from testing components to testing subassemblies such as the two-bay truss model shown. It is planned to static test a mini-Mast two-bay model. This is a calibration test which will be used in the model validation process to obtain a validated FEM of a two-bay model. Different test configurations, such as various loads and different boundary conditions, are planned.

Analysis

- Two-bay FEM
  $Kx = F$
- Equivalent PDE models

Subassemblies

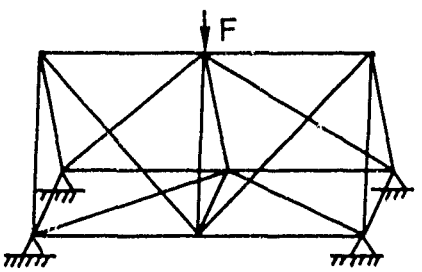

Updated FEM

Test

Static load vs deflection

- various load points
- different boundary conditions

Mini-Mast/Mast Baseline Configuration

The baseline configuration consists of three longerons, three battens, and three diagonal elements per bay.

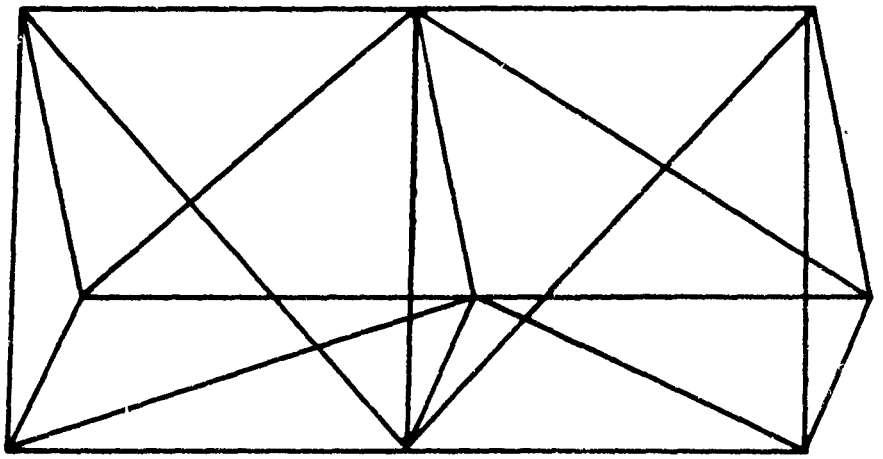

2 Bays

Scale Models

The objective of the scale model program is to study the validity of using scale models to simulate flight structures. The approach will be to procure and test four replica models. The scales of the four models are 1/2, 1/4, and 1/5. There are two 1/5 scale models planned. Also, similar ground tests and analyses programs as in mini-Mast and Mast are planned.

Objective: Study validity of scale models for simulating flight structure

Approach:

- Four replica models planned -1/2, 1/4, 1/5 (2) scale
- Similar tests and analysis programs as in mini-Mast and Mast

Ground Test/Analysis Program

The full scale testing of the mini-Mast will initially take place in the Structural Dynamics Research Laboratory. The test orientation is vertical and cantilevered from the base. In this orientation the joints should all be loaded in one direction and static as well as dynamic tests will be run. Next, the truss will be loaded in tension at the free end to load the joints in the opposite direction. The same tests will be repeated. The results of each test are run through the model validation process. It is anticipated that static test results will be used to update the stiffness matrix of the FEM and dynamics test results used to update the mass matrix.

The mini-Mast tests will be repeated with the longitudinal axis in the horizonal direction. Cables will be used to support part of the weight of the structure.

Finally, control research testing is planned for both the vertical and horizonal orientations.

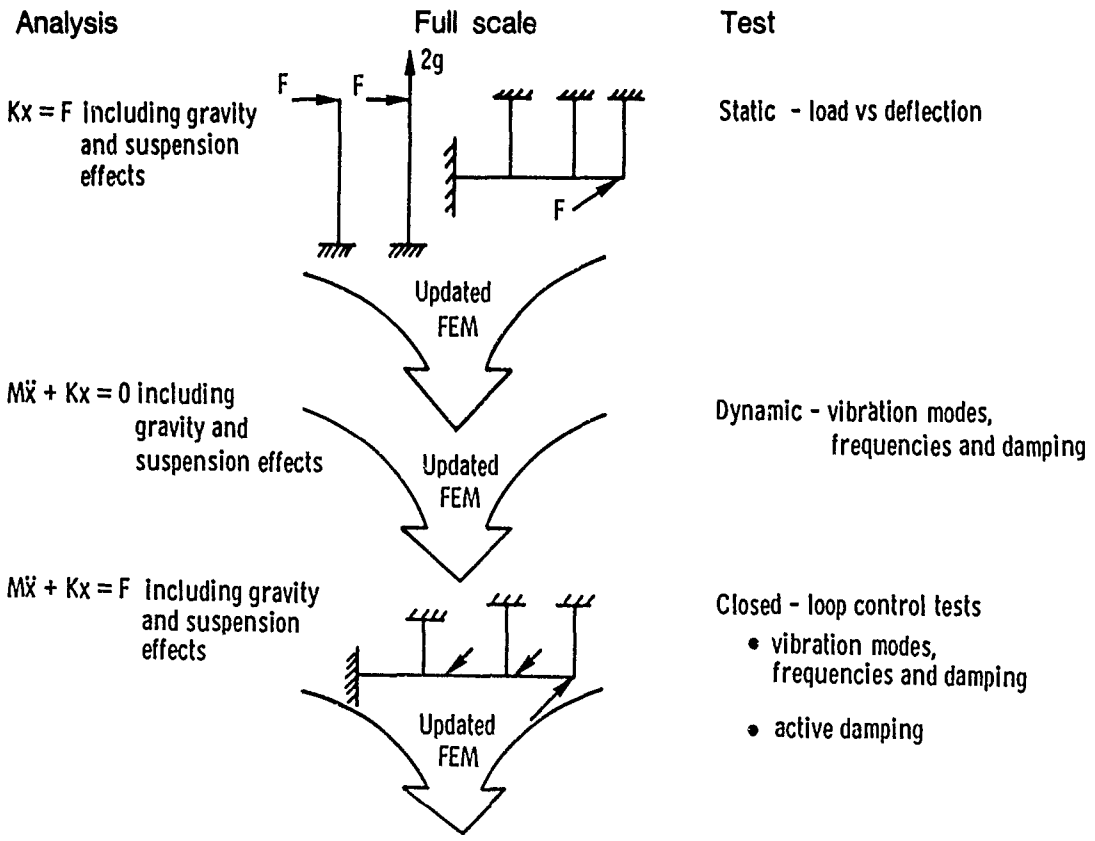

Mini-Mast Test Configurations

Test configurations A and B are the vertical orientations which will be located in the tower in building 1293B at the Langley Research Center (LaRC). Test configuration C is the horizontal orientation which will be in the hanger annex of building 1244 at the LaRC.

For test configuration A the vibration frequency spectrum from 0 to 21 Hertz is given. The lowest frequency is the first transverse bending frequency at 2.8 Hertz. The next frequency is the first torsional frequency at 11.3 Hertz.

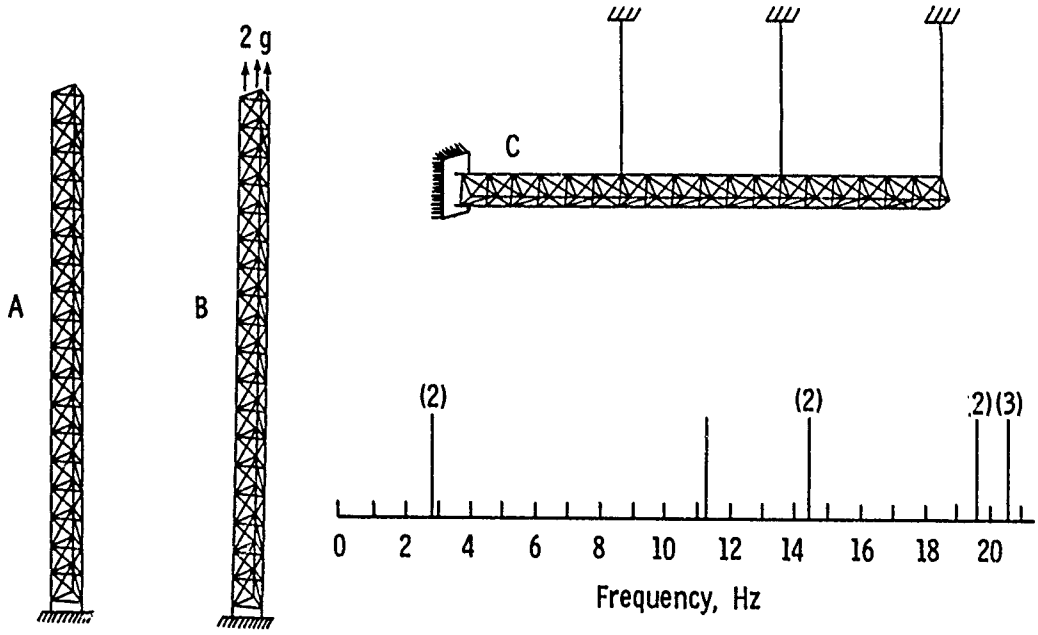

Test configuration A

Flight Test/Analysis Program

The flight test of the Mast flight system will be conducted after extensive ground testing has concluded. The result of the ground tests should be a verified mathematical model of the Mast flight system. Initial flight tests will confirm the validity of these math models. If necessary, which is likely to be the case, flight test data will be used to update and improve these math models. Both open-loop dynamics tests and closed-loop controls tests are planned.

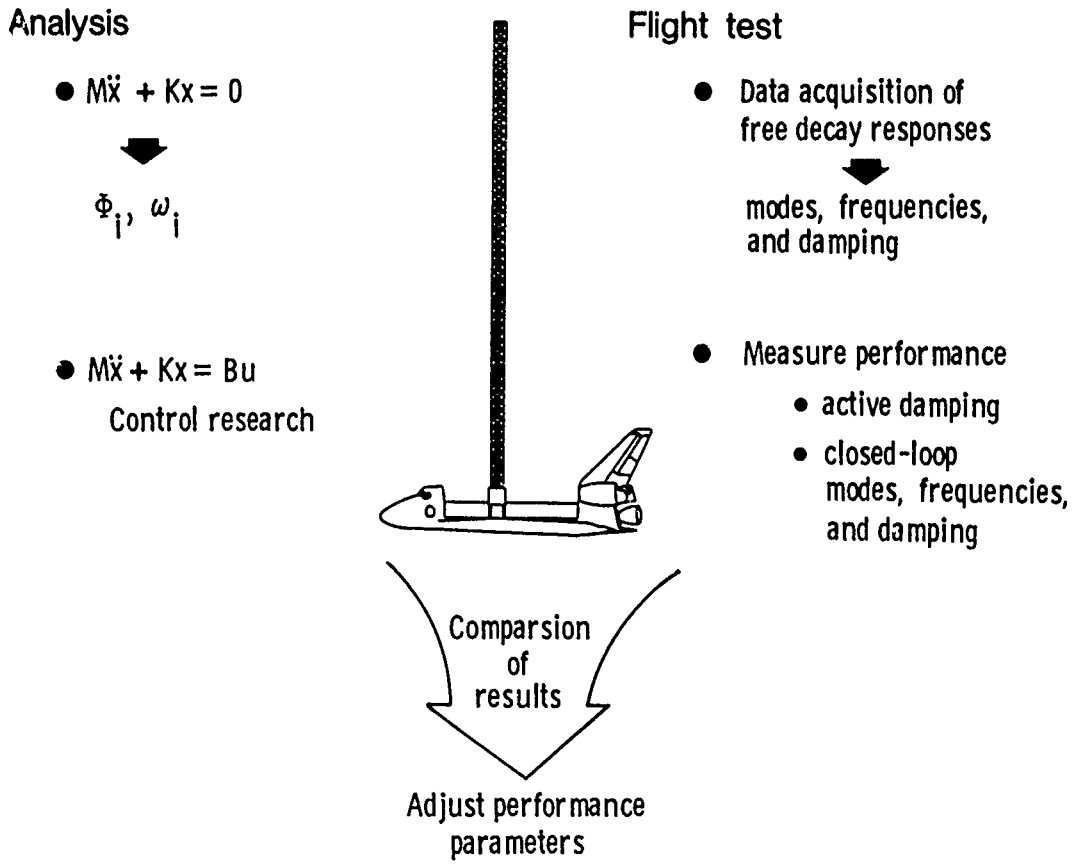

Cable Suspension Effect Study

A study of the effect of cables on the vibration frequencies and mode shapes of the cantilevered Mast truss is shown below. The major conclusions of this study are that only the first natural frequency is affected by cables. It was also concluded that cables do not affect the first mode shape and the first natural frequency is not affected by the cable arrangement.

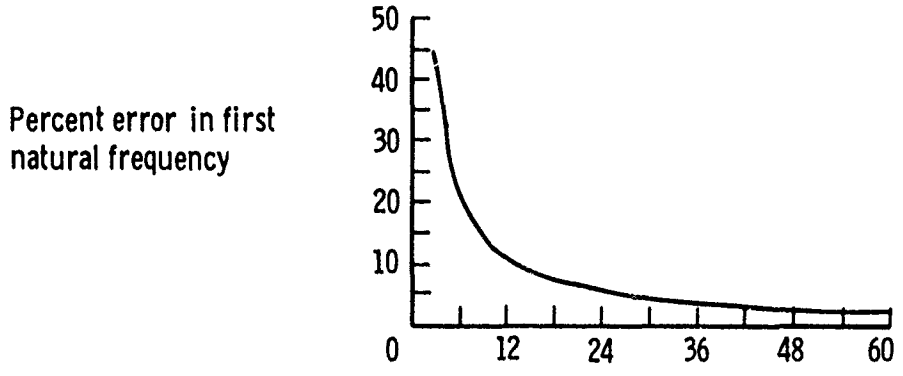

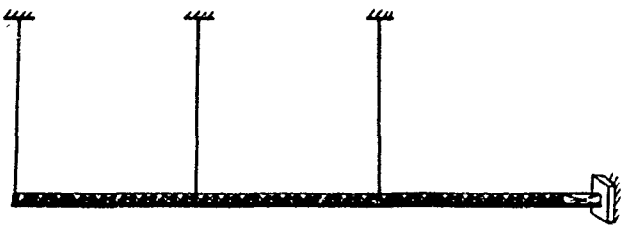

- Only first natural frequency is affected
- Cables do not affect first mode shape
- First natural frequency is not affected by number of cables.

Mast/Orbiter Vibration Frequency

A 2160-degree-of-freedom finite element model of Mast with the orbiter has been modeled in NASTRAN and EAL. The vibration frequency spectrum from 0 to 21 Hertz is shown.

The first six frequencies are the rigid body frequencies. The next two frequencies are the first bending frequencies in the fore and aft direction and the side-to-side or port-starboard direction. The next group of three frequencies consists of two second bending frequencies and the first torsion. One second bending and the first torsional frequency are at the same frequency which is one of the requirements of the structural design.

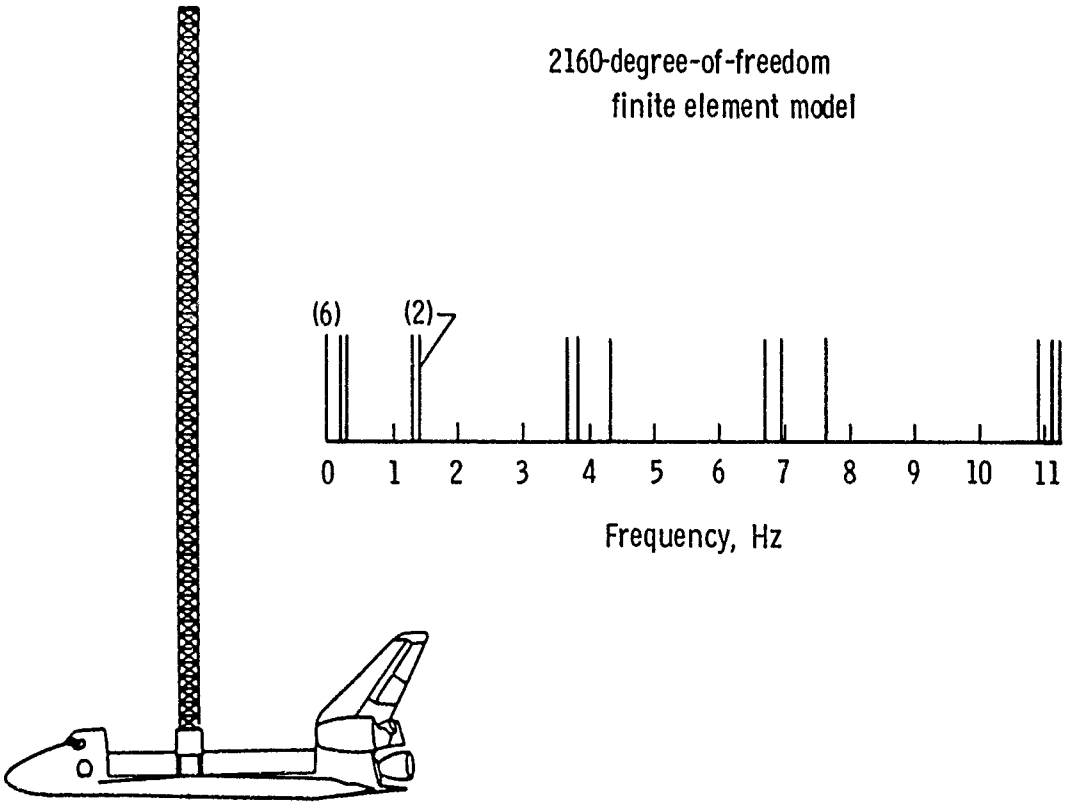

Closed-Loop Simulation Of COFS-I Flight Test

Closed-loop simulations of the Mast flight test have been conducted. The actuators have been modeled as ideal linear devices in the simulation. The curve on the left shows excitation, free vibration, and damping of the second mode. The curve on the right is only excitation of the second mode but without a spring or relative position control between the proof mass of the actuator and the structure. The results of this study indicate the need for relative position control.

COFS-I

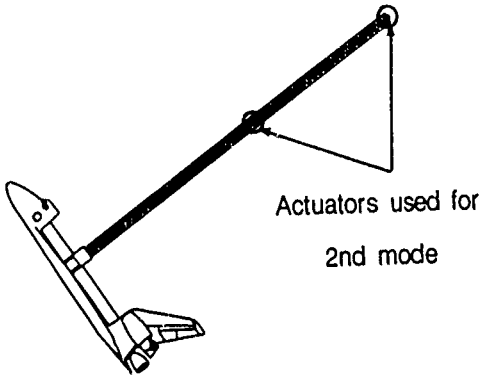

ACTUATOR MODEL

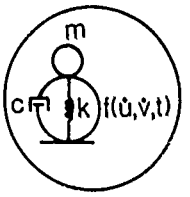

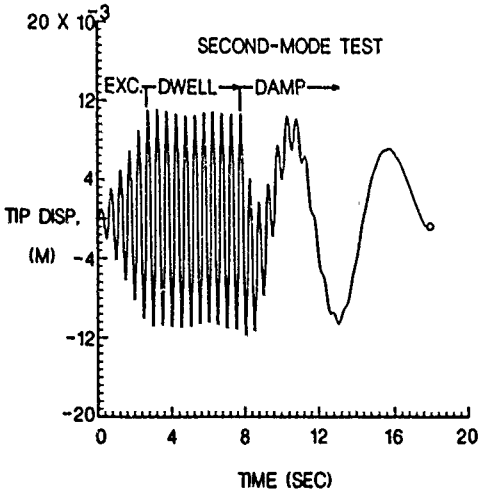

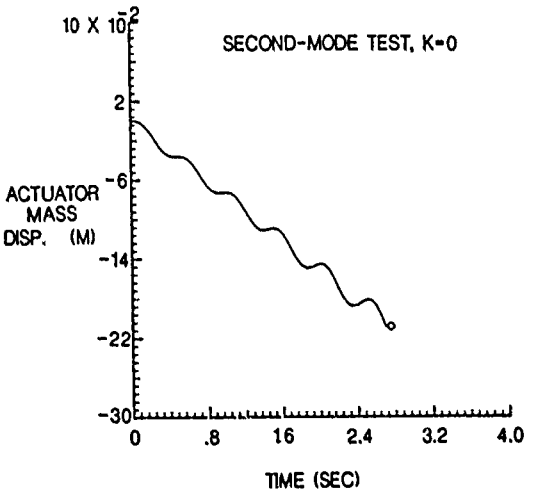

Directly Related Base R&T

The related base research and technology programs consist of analysis and scaling of joints, suspension methods for ground tests, math modeling of structures using exact element analyses and partial differential equation representations, system identification methods, and control algorithm development and tests.

- Analysis and scaling of joints
- Suspension methods for ground tests
- Exact element and PDE math modeling
- System identification methods
- Control algorithm development and tests

Research Program - Status

The mini-Mast diagonal hinge joint has been tested and results are being analysed. Mini-Mast actuators are being developed. Finite element models of both the mini-Mast and Mast have been developed. A simulation of the Mast flight tests is operational. The procurement of scale models is in preparation. Mini-Mast tests are to be conducted in 1987 with all of the above activities being supported by the base research and technology effort.

- Mini-Mast diagonal hinge joint tested
- Finite element models developed
  - Mini-Mast (1908 DOF)
  - Mast (2160 DOF)
- Mast simulation operational
- Mini-Mast actuators being developed
- Scale models procurement in preparation
- Mini-Mast tests to be conducted in 1987.
- Supported by base R&T effort.

DESCRIPTION OF THE MAST FLIGHT SYSTEM

Ronald C. Talcott
Dr. John W. Shipley
Harris Corporation
Palm Bay, Florida

First NASA/DOD CSI Technology Conference
Norfolk, Virginia
November 18-21, 1986

MAST FLIGHT EXPERIMENT FLIGHT SYSTEM CONCEPT

The Mast Flight System is composed of several subsystems. Primary among these is the Deployable Mast Subsystem (DMS) which consists of a beam assembly and an associated mechanism for deploying and retracting the beam. The beam assembly is a joint dominated graphite epoxy and titanium truss as is expected of future large space structures. Important beam characteristics are listed below. Integral to the beam assembly are actuators, sensors and associated electronics which are available for excitation and damping as desired by the experimenter. The beam structural characteristics can also be modified as desired by the experimenter using the Parameter Modification Device installed at the end of the beam. Data measured on the beam by the sensors and commands to the actuators are transmitted along the beam digitally at 150 Hz using a standard 1553 type bus. The Modular Distributed Information Subsystem (MDIS) computer functions as bus master and ensures that all experimental data is saved for future analysis. The MDIS computer also performs a safing function to prevent inadvertent overexcitation of the beam. Finally, the Excitation and Damping Subsystem (EDS) computer is available to the experimenter for implementation of control algorithms or any other numerical operations as desired. Data from all system sensors can be accessed by the EDS computer.

MAST FLIGHT EXPERIMENT FLIGHT SYSTEM CONCEPT

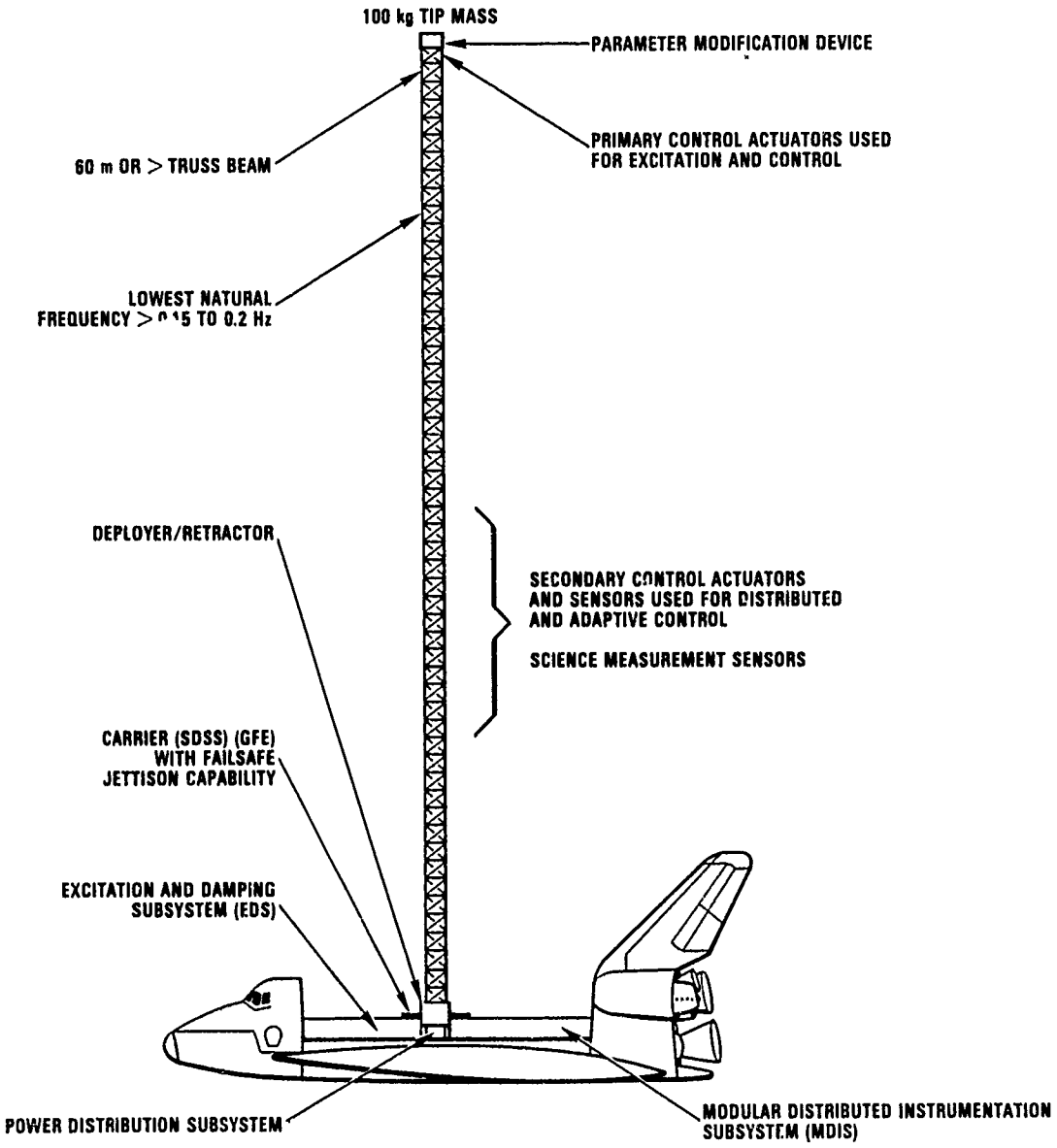

MAST (BEAM) DESIGN PARAMETERS FOR THE FLIGHT SYSTEM

DIAMETER	1.4 METERS
BEAM LENGTH, DEPLOYED	60.7 METERS
BAY LENGTH	1.124 METERS
PACKAGING RATIO	29.5 (3.4% OF DEPLOYED)
MASS PER UNIT LENGTH	4.64 kg/m
BENDING FREQUENCY*	0.239 Hz (Y-AXIS) 0.181 Hz (X-AXIS)
TORSIONAL FREQUENCY*	0.300 Hz
COEFFICIENT OF THERMAL EXPANSION	$<0.7 \times 10^{-6}\ K^{-1}$

*COUPLED TO THE ORBITER

MAST FLIGHT EXPERIMENT SENSOR AND ACTUATOR DISTRIBUTION

The actuators and sensors are mounted on platforms integral to the beam. When the beam is extended the distribution of the actuators and sensors provides excellent observability and controllability of the beam lowest ten structural modes. These include first, second, third and fourth bending in two orthogonal planes and first and second torsion. In addition a sensor complement is provided at the DMS to pallet interface so that base disturbances can be quantified and accounted for if desired.

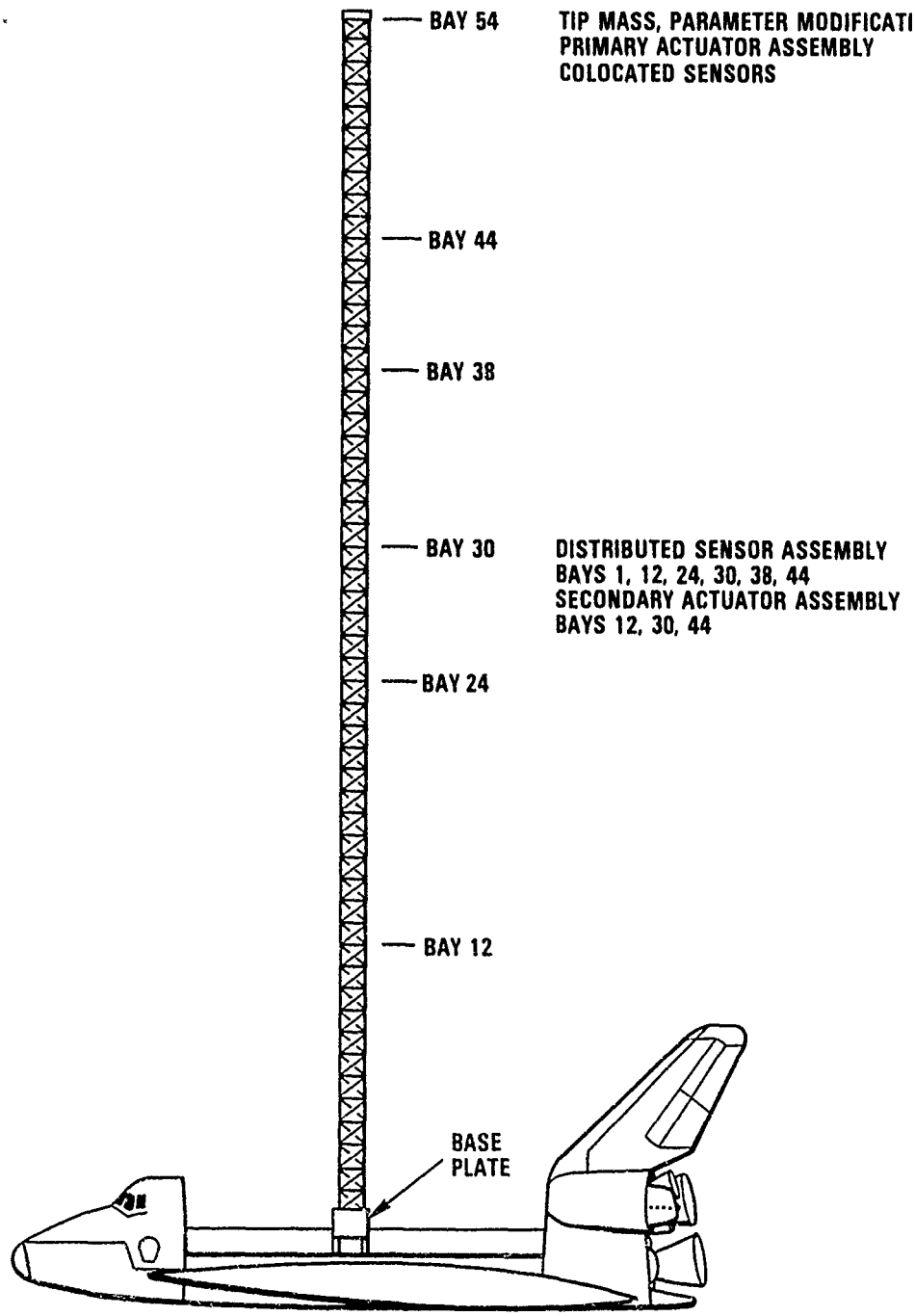

STOWED MAST FLIGHT EXPERIMENT

When not in use the system is stowed within a protective cannister inside the Orbiter payload bay. Shown below is a diagram depicting the placement of the electronic equipment platforms (remote stations) when the beam is stowed. Partially shown, for clarity, is a support structure for launch and landing loads. The system and support structure will be mounted within an enhanced MDM/STEP pallet. The MDIS and EDS computers, along with elements of the Power Distribution Subsystem, are mounted on pallet coldplates (not shown below).

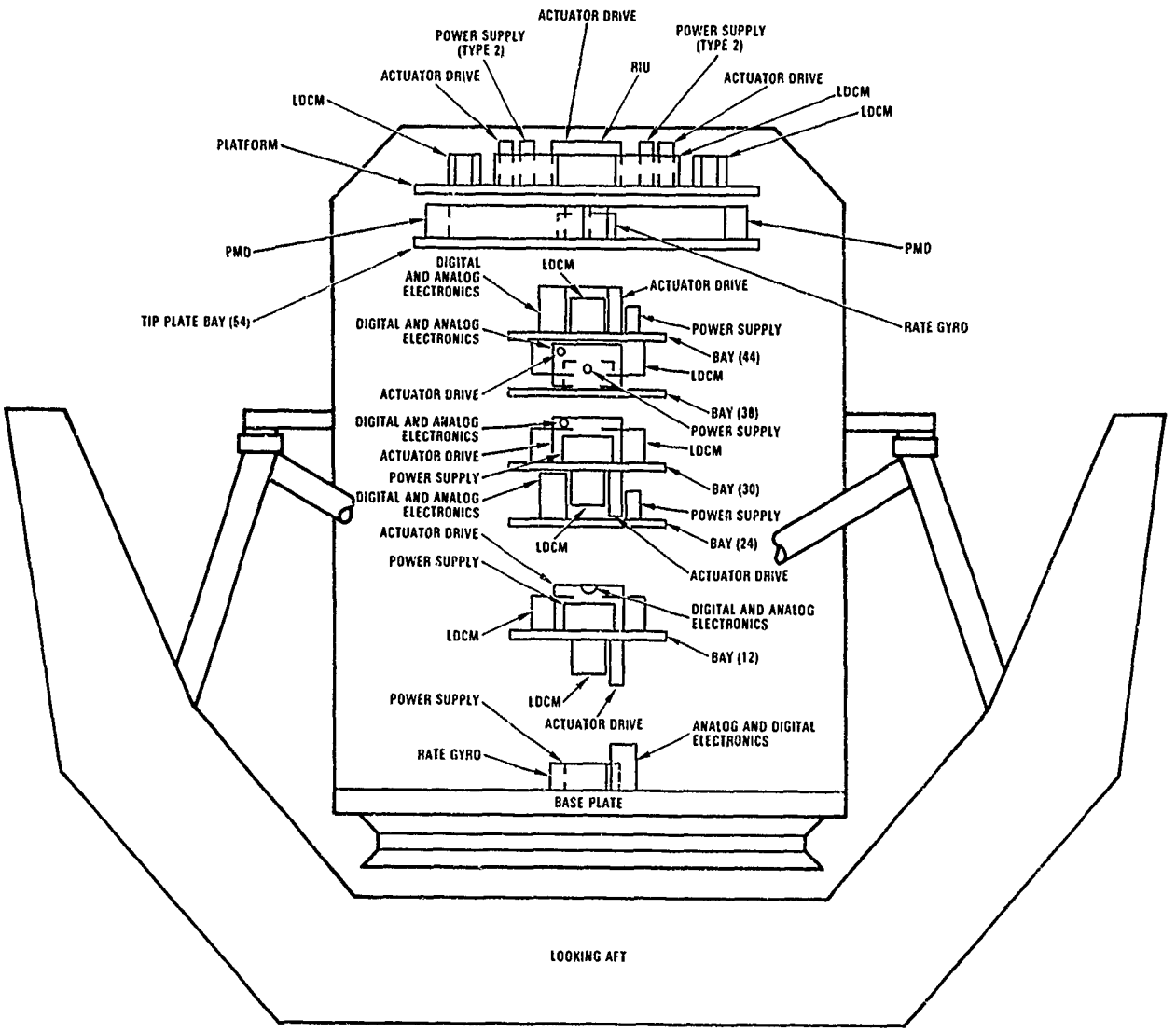

MODIFICATION OF STRUCTURAL SYSTEM CHARACTERISTICS

Beam length can be changed by the experimenter to coarsely alter beam structural characteristics. In addition, the Parameter Modification Device (PMD), located at the tip of the beam, can be used to effect fine changes in the beam structural characteristics and to cause frequency matching and coupling between either of the two beam second bending modes and the first torsion mode. The PMD functions by changing the moment of inertia of the tip station about the beam axis. Additionally the PMD can be used to move the center of gravity of the tip station creating mass coupling between the bending and torsion modes. The experimenter can move the PMD masses as desired, including a slow sweep of the PMD masses from one location to another while excitation and damping are occurring. A typical modal coupling maneuver is shown below. The beam length is first adjusted to nearly match a second bending mode and the first torsion mode (48 bays). The PMD masses are then adjusted to precisely match the torsion mode frequency with the selected bending mode frequency. The masses are then moved in the same direction to offset the tip station center of gravity and cause the oupling desired by the experimenter.

CONCEPT FOR MODAL FREQUENCY COUPLING VIA PARAMETER MODIFICATION

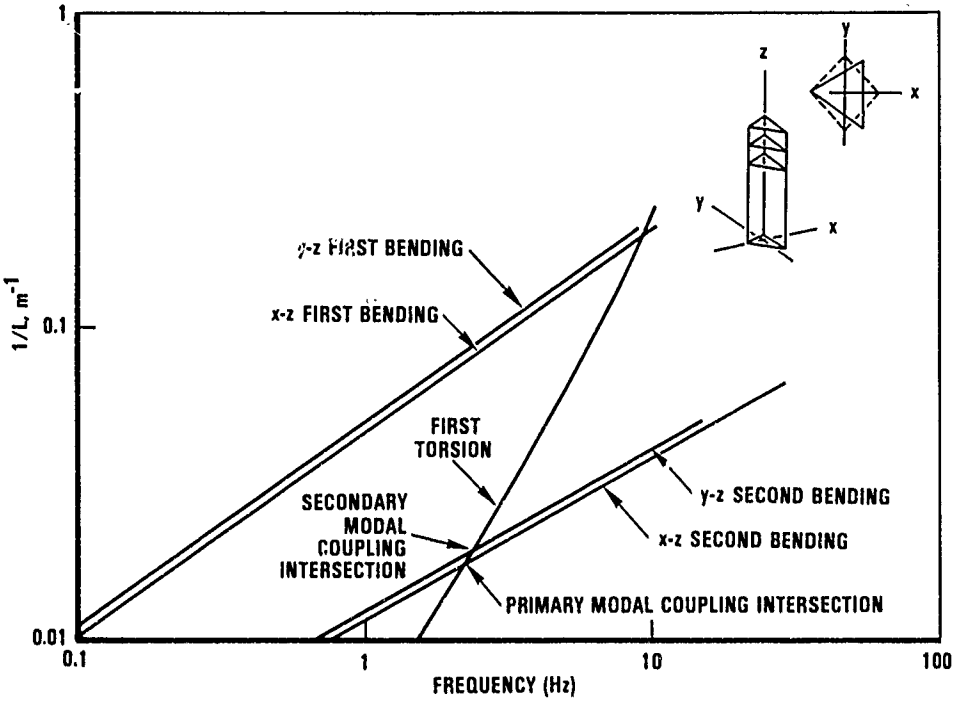

PARAMETER MODIFICATION DEVICE OPERATION

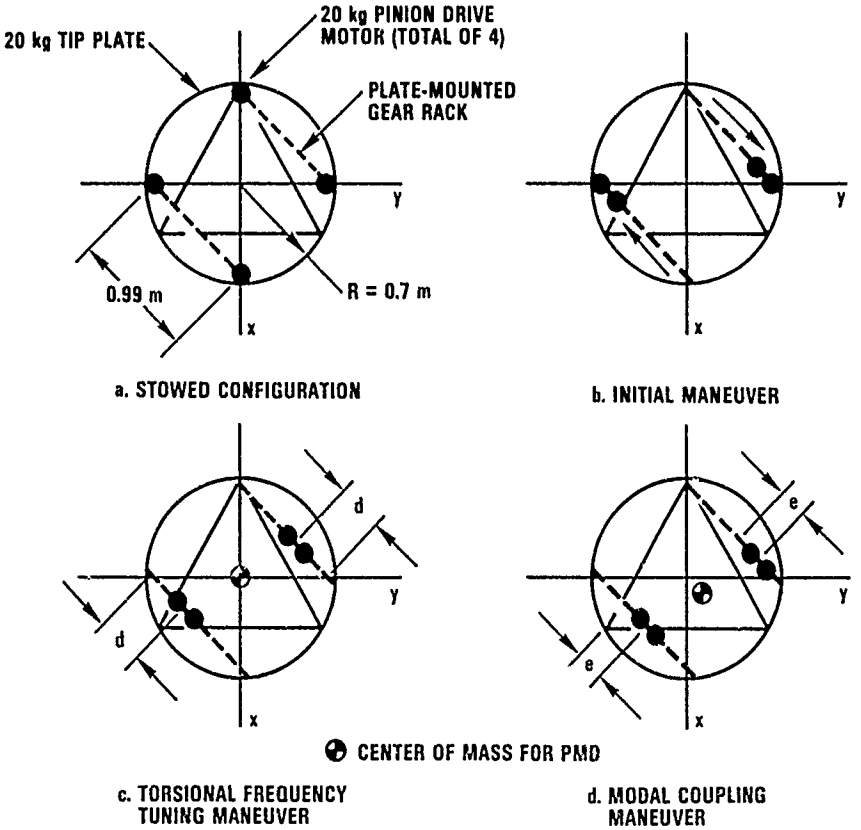

MAST SYSTEM ACTUATORS AND INSTRUMENTATION

Actuators and sensors are distributed along the beam as shown below. All sensor outputs are available to the experimenter for control or monitoring of beam performance. In addition, select accelerometer channels have dual ranges and filtered or unfiltered outputs. The filters used are two pole butterworth filters, with a 3 db cutoff at 45 Hertz, for aliasing protection. Strain gages are additionally high pass filtered to eliminate drift and thermal apparent strain. Actuators are provided at three of the intermediate remote stations and the tip. The actuators used at all locations are Linear Direct Current Motors (LDCMs). The LDCMs can be used to provide linear forces perpendicular to the beam axis (parallel to the Orbiter X and Y axes) at each remote station and torque about the beam axis at the tip remote station. Accelerometers are equipped with self calibration ports and strain gage bridges have shunt calibration circuits for pre and post experiment instrumentation health checks if desired. Select temperatures, voltages and currents are measured to provide further health and status information (not shown below for clarity).

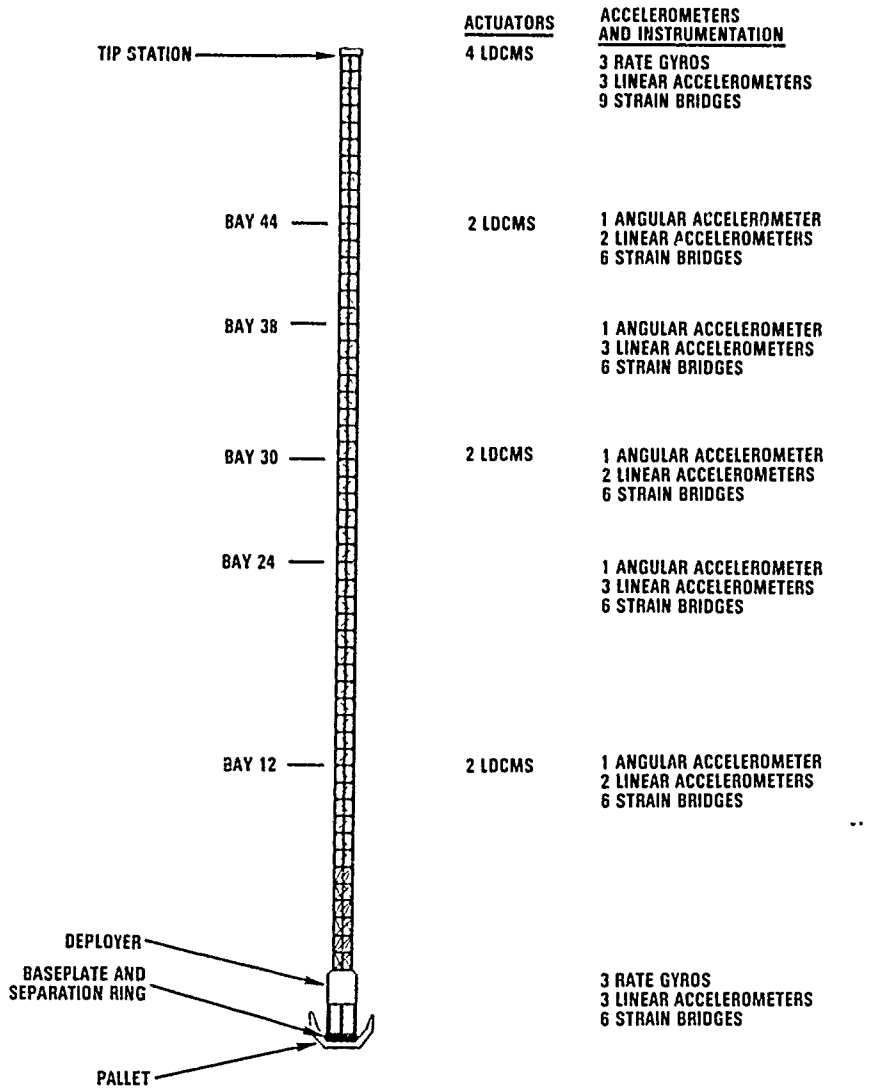

LINEAR DC MOTOR

The actuators used are direct current brushless motors. The motor has a fixed stator and a moving magnetic secondary. The secondary is used as a reaction mass. Output force is controlled by controlling motor current. In addition the motor is designed with a sensing system to provide accurate secondary position information. A position loop has been implemented to keep the secondary centered. The LDCM, including the position loop, has a straight forward two pole transfer function. Secondary position, like all other sensor data, is available to the experimenter. The figure below shows a development model LDCM. This motor is capable of a 30 Newton force output.

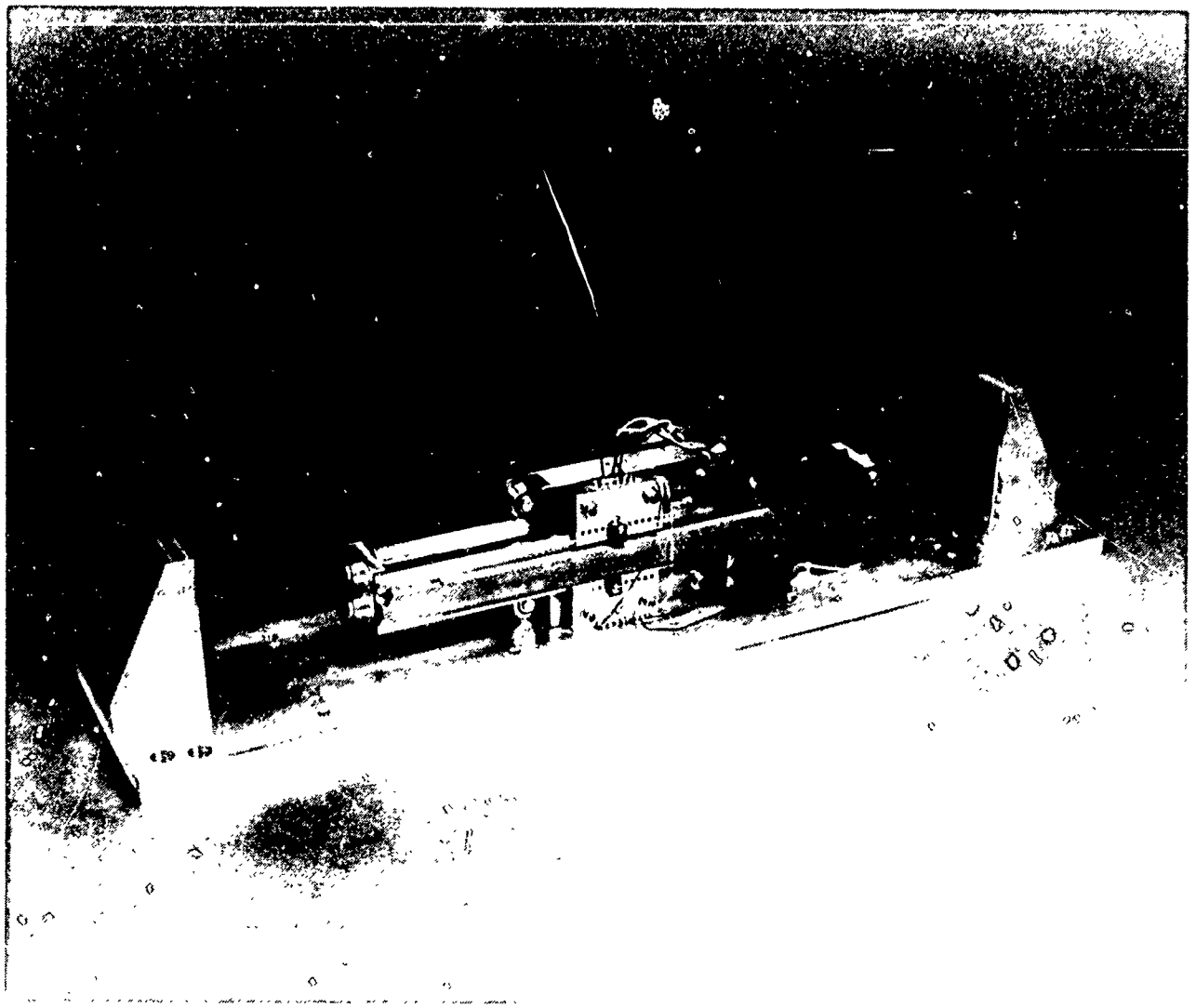

MAST FLIGHT SYSTEM BLOCK DIAGRAM

A block diagram of the system is shown below. The diagram illustrates the primary elements of the system and the provisions for experimental commands and data gathering. The mission specialist will interface to the system from the orbiter aft flight deck through the DDCU. The beam will be deployed and retracted through this interface via the MDIS computer which commands the motor controller. Experiments will also be executed through this interface via the MDIS computer. Each experimenter's software will be contained within the EDS computer. Standard system commands, such as sine sweep or broadband random actuator force and PMD commands, will be furnished with the system and can be called upon by the experimenter singly or in series.

All experimental data (as well as system housekeeping data) is passed through the HRM onto the high data rate link through TDRSS to the ground where it is stored on magnetic tape for detailed post flight analyses.

A limited amount of selectable data (limited by 2Kbps serial data link), as determined by the experimenter, can be passed to the ground during the mission for near real time evaluation to verify proper experiment conduct.

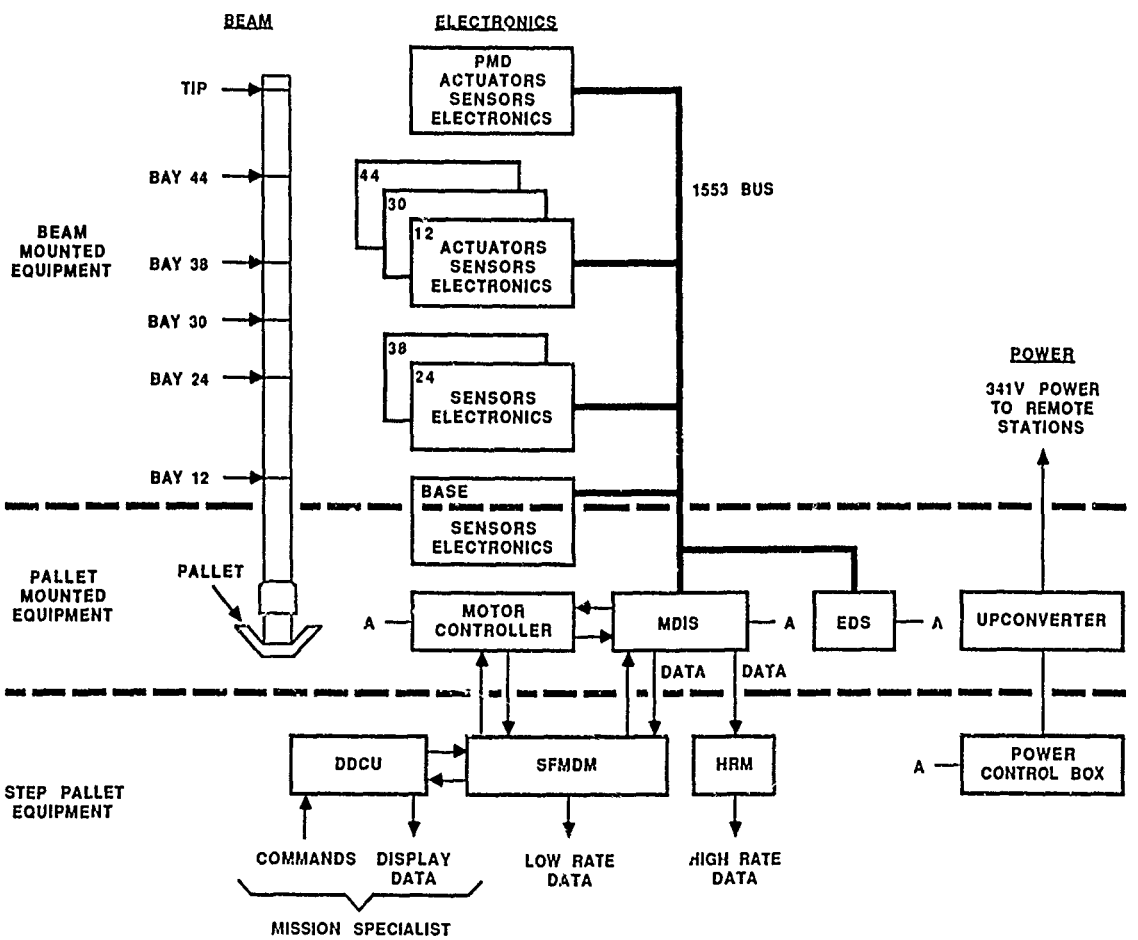

MAST FLIGHT SYSTEM
BEAM STRUCTURE
AND
BEAM STRUCTURAL PERFORMANCE

David C. Lenzi
John W. Shipley
Harris Corporation
Palm Bay, Florida

First NASA/DOD CSI Technology Conference
Norfolk, Virginia
November 18-21, 1986

MAST FLIGHT SYSTEM

The primary MAST Flight System structural component from an experimenter point of view is the beam assembly. The purpose of this paper is to provide an overall understanding of the beam assembly and data with which potential experimenters can begin to conduct analyses relevant to their experiments. The beam structure, along with the deployment and retraction subsystem, is being designed and built by the Astro Aerospace Corporation in California. A scale drawing of the MAST Flight System positioned in the Orbiter cargo bay is shown in figure 1.

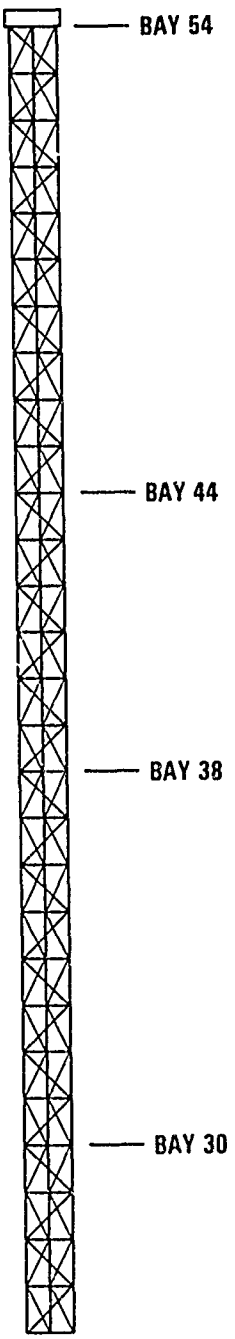

Figure 1.

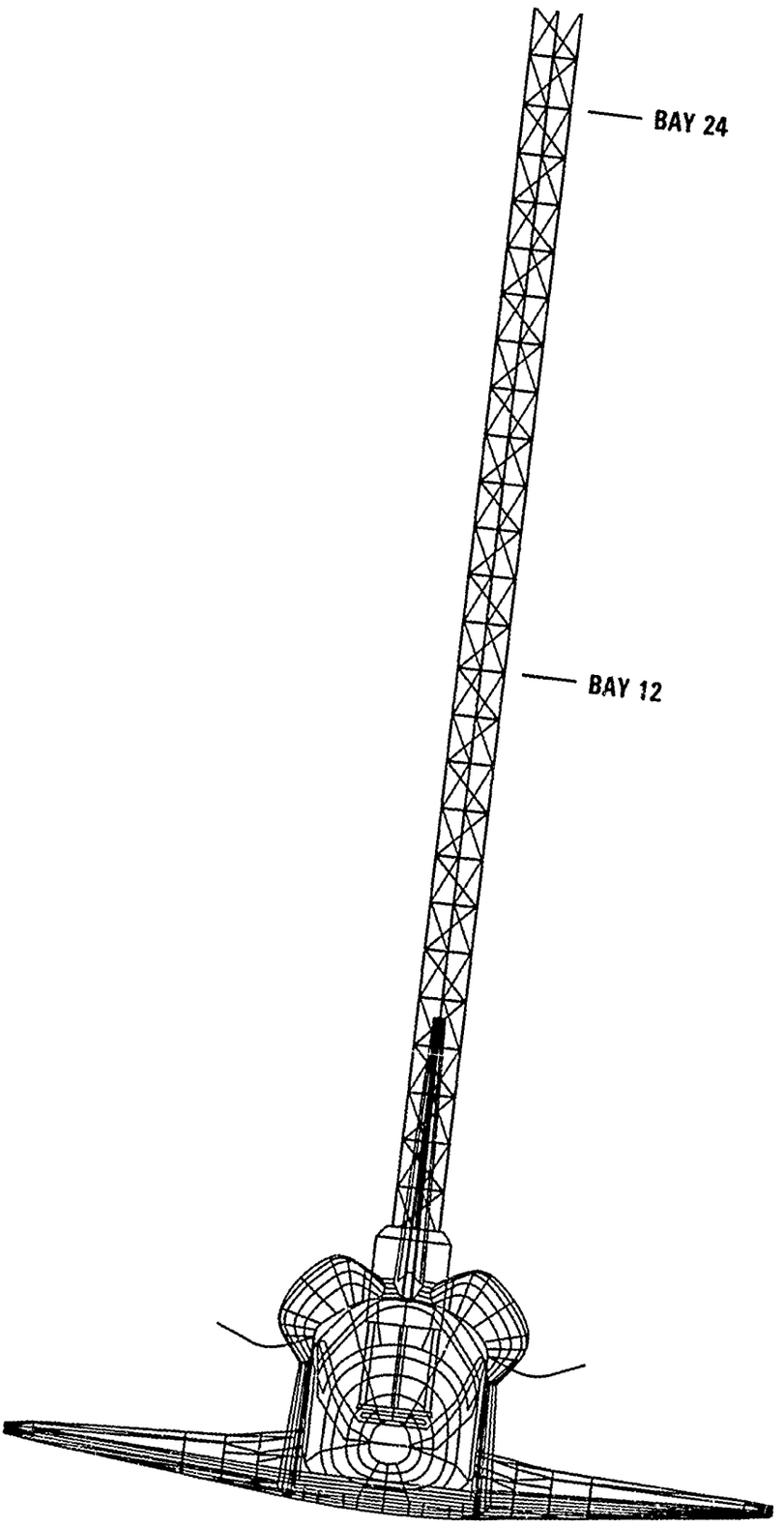

Figure 1. (Concluded)

BEAM STRUCTURAL CONCEPT

The beam structure is a statically determinate truss. Longitudinal members (longerons) provide bending stiffness and alternating diagonal members (diagonals) provide torsional and shear stiffness. Transverse members (battens) are positioned at regular intervals along the beam to assure longeron stability. The beam cross section is triangular with the longerons located at the vertices of an equilateral triangle. Each leg of the triangle is 1.212 meters long. The truss structure repeats itself in two-bay segments. There are 27 two-bay segments for a total of 54 bays. The battens at either end of a two-bay segment and all of the longerons are continuous members. All of the diagonals and the battens at the midbatten plane of each two-bay segment are hinged near the center to permit retraction. One of the three longerons has been sized slightly stiffer axially in order to provide different system modal characteristics in the x-z and y-z planes. A typical two-bay segment of the beam structure is shown in figure 2. Platforms are positioned along the length of the beam at batten planes 12, 24, 30, 38, 44, and 54 (beam tip). These platforms are used as mounting surfaces for the actuators, sensors, and associated electronics.

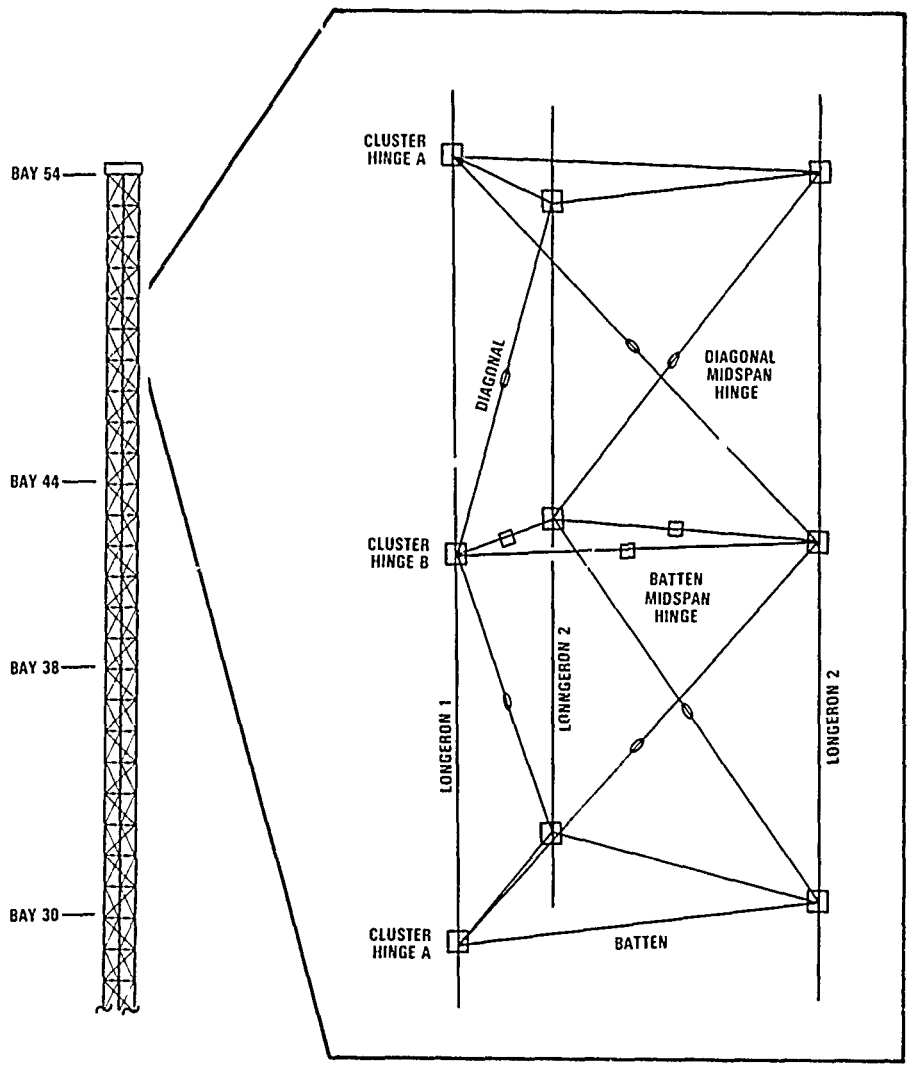

Figure 2.

TIP REMOTE STATION LAYOUT

The tip remote station is distributed on two platforms. The layout of equipment positioned on the upper platform is shown in figure 3. Four Type I Linear DC Motors (LDCM) are provided for actuators. Two of these are aligned with the x-axis and two with the y-axis. The lines of force for each actuator pair are 0.968 meter apart. Two linear accelerometers for measuring motion along the x- and y-axes and a rotational accelerometer for measuring motion about the z-axis (not shown in figure 3) are also located at the tip. Their precise positions are yet to be determined. The parameter modification device (not shown in figure 3) is to be located on the lower platform at the tip remote station.

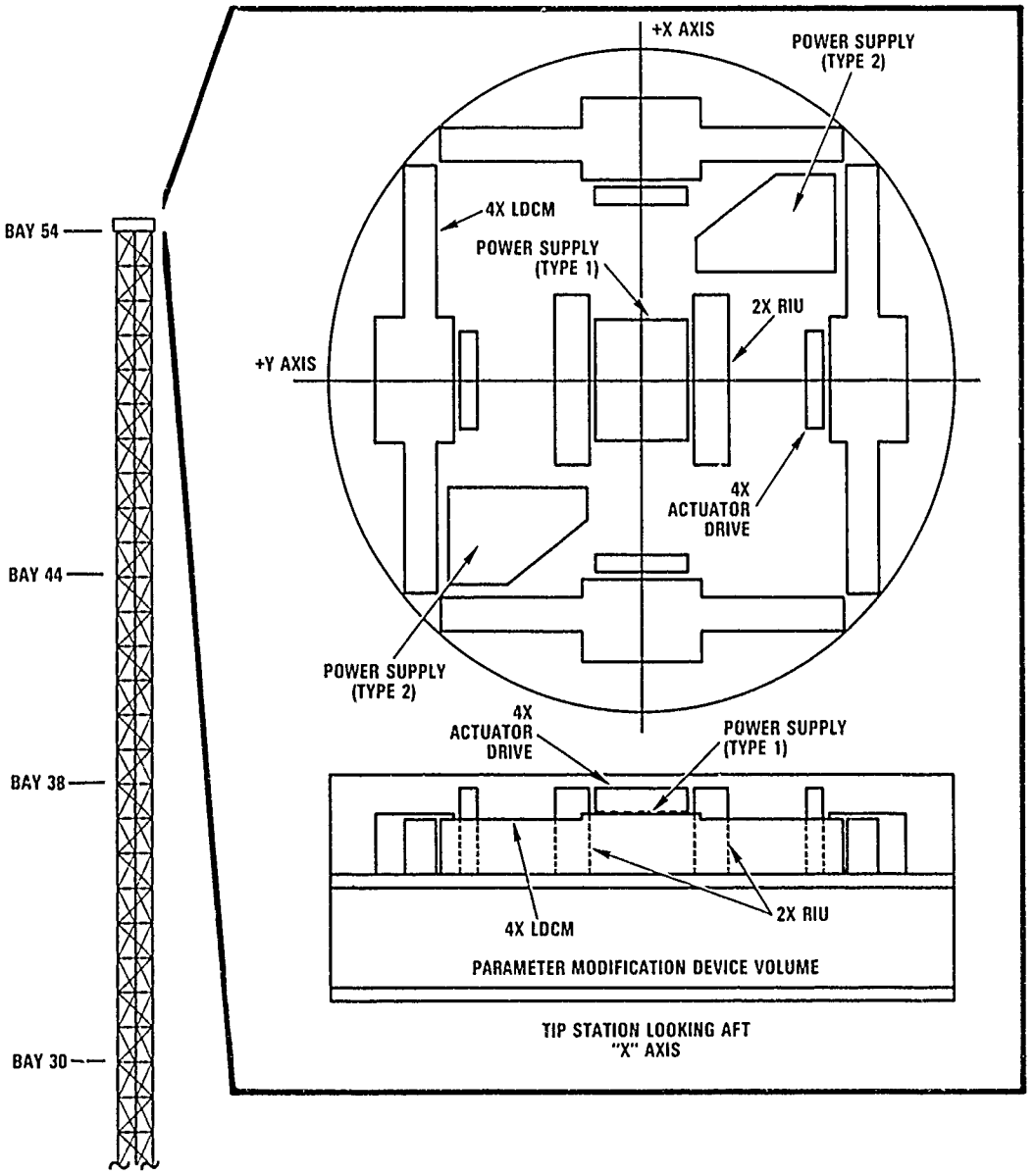

Figure 3.

INTERMEDIATE REMOTE STATION LAYOUT WITH ACTUATORS

The remote station layout for the equipment positioned at batten planes 12, 30, and 44 is shown in figure 4. Two Type II LDCMs are provided for actuators. One of these is aligned with the x-axis and the other aligned with the y-axis. The same accelerometer complement provided at the tip is also provided here (not shown in figure 4). Each linear accelerometer is mounted directly on top of its associated LDCM on the beam z-axis. The angular accelerometer is mounted on the x-axis 0.220 meter from the y-axis.

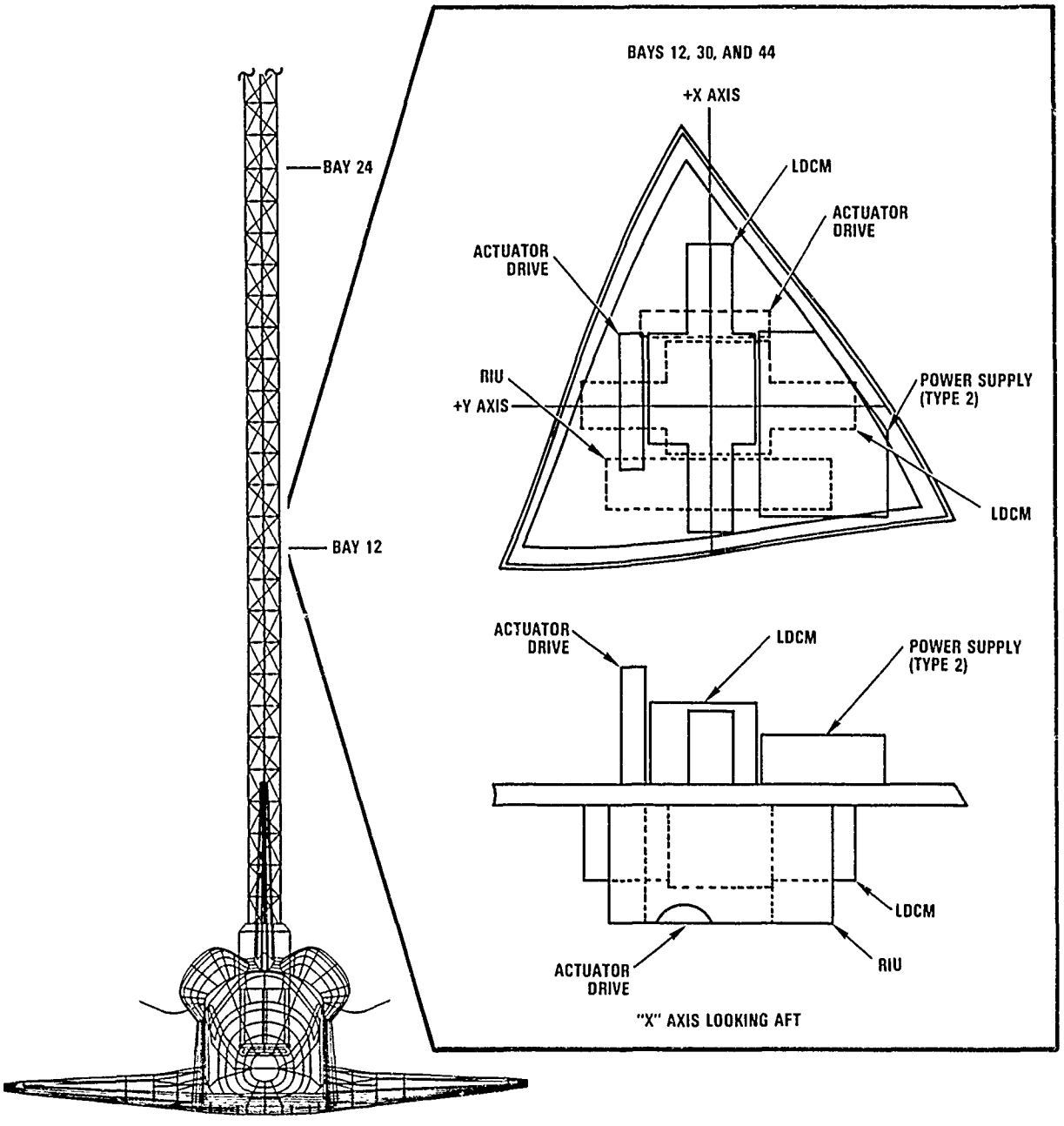

Figure 4.

INTERMEDIATE REMOTE STATION LAYOUT WITHOUT ACTUATORS

The remote station layout for the equipment positioned at batten planes 24 and 38 is shown in figure 5. No actuators are provided at these two stations; however, the same complement of accelerometers with the addition of linear acceleration along the z-axis is provided. The precise location of these accelerometers is yet to be determined.

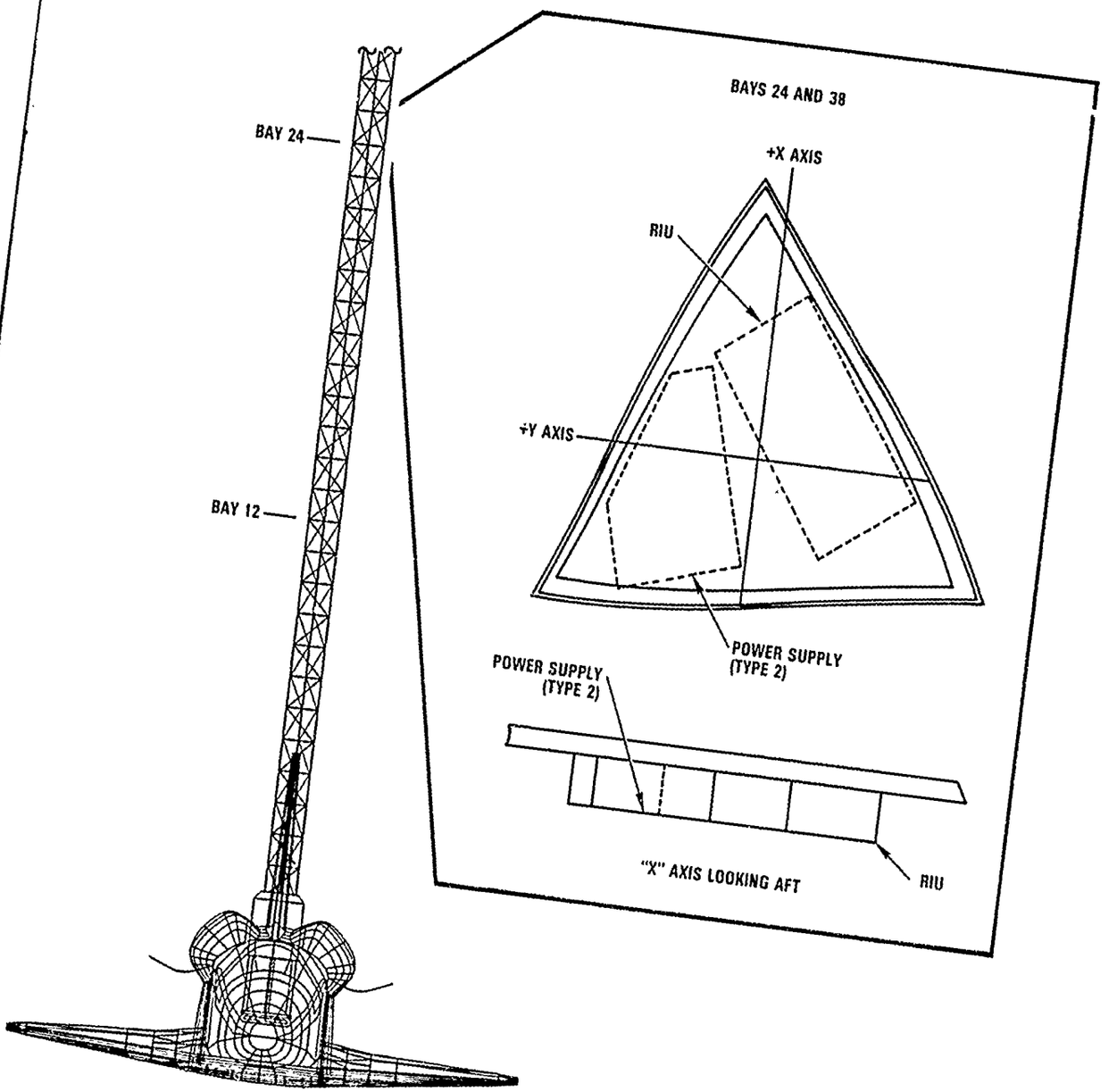

Figure 5.

BEAM ELEMENT MATERIALS

All of the beam structural elements are graphite/epoxy tubes with titanium end fittings. The lengths of the end fittings have been chosen to provide an element coefficient of thermal expansion as near zero as practical.

Longerons	Graphite/Epoxy	P-75/3501-6
Diagonals	Graphite/Epoxy	IM-6/3501-6
Battens	Graphite/Epoxy	HMS-4/3501-6
Hinges	Titanium	6AL-4V
Hinge Pins	Stainless Steel	Type 416

Lay-up details of the graphite/epoxy members are still being determined.

EQUIVALENT BEAM CHARACTERISTICS FOR SIMPLIFIED MODELING

Listed below are characteristics of an equivalent beam intended for simplified initial analyses.

Length	60.693 m
Bay Length	1.124 m
Mass/Length	4.641 kg/m
Moment of Inertia/Length	1.9 $kg\text{-}m^2/m$
EA	124.5×10^6 N
GA	2.11×10^6 N
EIx	28.63×10^6 $N\text{-}m^2$
EIy	32.39×10^6 $N\text{-}m^2$
GK	0.50×10^6 $N\text{-}m^2$

BEAM ELEMENT PROPERTIES

Detail beam element structural data for a finite element type analysis are listed below.

Element	Axial Stiffness	Effective* Axial Stiffness
Longeron 1	72.25×10^6 N	46.63×10^6 N
Longeron 2	55.35×10^6 N	38.95×10^6 N
Diagonal	4.20×10^6 N	3.86×10^6 N
Batten A	8.5×10^6 N	8.23×10^6 N
Batten B	5.1×10^6 N	4.89×10^6 N

* Member stiffness including end fitting and hinge compliance

Element	Pin-to-Pin Length	Mass
Longeron 1	1.090 m	0.372 kg/m
Longeron 2	1.090 m	0.285 kg/m
Diagonal	1.583 m	0.084 kg/m
Batten A	1.158 m	0.076 kg/m
Batten B	1.158 m	0.067 kg/m
Cluster Hinge A (including terminals and pins)		1.374 kg
Cluster Hinge B (including terminals and pins)		0.518 kg
Diagonal Midspan Hinge		0.2 kg
Batten Midspan Hinge		0.1 kg

REMOTE STATION MASS PROPERTIES

Detailed remote station mass properties for a finite element type analysis are listed below.

		Center of Gravity**			
Bay	Mass*	x	y	z	I_z
12	50.1 kg	3 mm	-7 mm	50 mm	2.8 kg-m^2
24	14.4 kg	0 mm	9 mm	-4 mm	1.0 kg-m^2
30	50.1 kg	3 mm	-7 mm	50 mm	2.8 kg-m^2
38	14.4 kg	0 mm	9 mm	-4 mm	1.0 kg-m^2
44	50.1 kg	3 mm	-7 mm	50 mm	2.8 kg-m^2
54***	147.1 kg	0 mm	0 mm	250 mm	21.6 kg-m^2

* Includes the actuator reaction mass. This mass participates in the beam dynamics only when the actuators are locked, or when they are unlocked if motion is perpendicular to the force axis of the actuator. The reaction mass of a Type II actuator at Bay 12, 30, or 44 is 7 kg. The reaction mass of a Type I actuator at Bay 54 is 11.5 kg.

** With respect to the batten midplane and center of the longeron circle.

*** Exclusive of the parameter modification device. The PMD mass is 100 kg. The PMD inertia about the z-axis can be varied from 1.8 kg-m^2 to 33.8 kg-m^2.

MAST FLIGHT SYSTEM MODAL CHARACTERISTICS

Modal data for the first 10 MAST Flight System modes are listed in the following two tables. This data includes the effect of the orbiter and pallet. Mode shapes are shown in figure 6 for reference although the pallet and orbiter have been omitted for clarity.

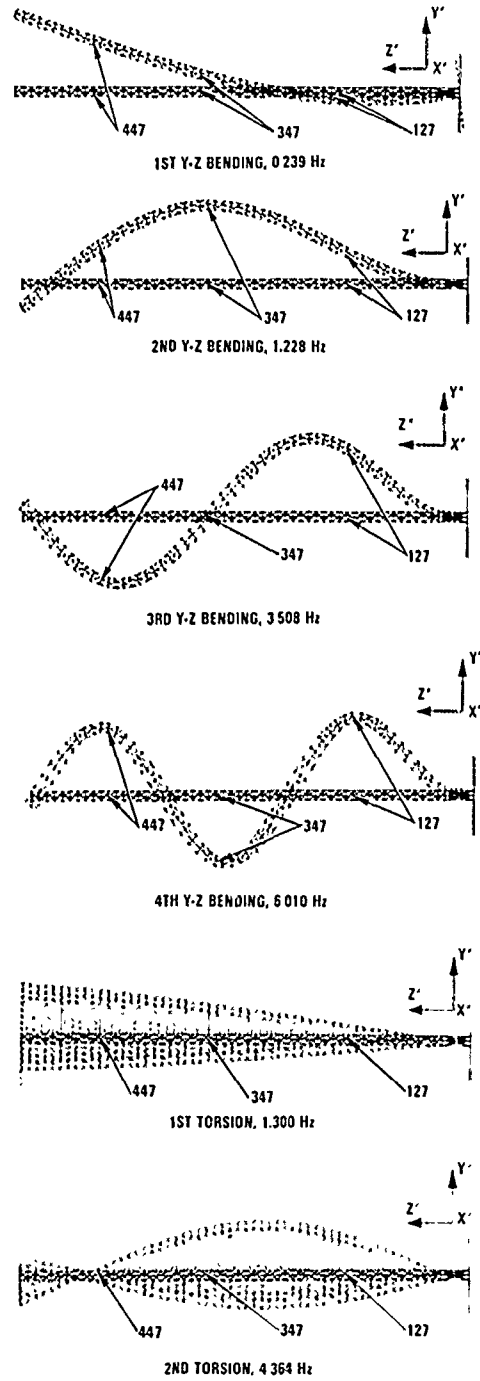

Figure 6.

MAST Flight System Modal Data (Includes Orbiter)
Beam Length 54 Bays, Maximum PMD Inertia, LDCMs Locked

BAY	COMP.	1 1st x-z	2 1st y-z	3 2nd y-z	4 2nd x-z	5 1st Torsion	6 3rd y-z	7 3rd x-z	8 2nd Torsion	9 4th y-z	10 4th x-z
12	X	.0344	.0001	.0044	.4196	.0083	.0059	.9047	.0014	-.0004	.9968
	Y	-.0007	-.1431	.3939	-.0027	-.0152	.8858	-.0052	-.0106	.9892	-.0006
	Oz	.0002	.0000	.0197	-.0124	.2686	.0190	-.0070	.7243	.0155	-.0053
24	X	.2189	-.0008	.0086	.9158	.0191	.0032	.6197	.0024	-.0006	-.5821
	Y	-.0006	.0125	.8948	-.0063	-.0355	.6240	-.0044	-.0126	-.5645	-.0006
	Oz	-.0003	.0000	.0375	-.0231	.5229	.0203	-.0064	1.0000	-.0091	.0043
30	X	.3486	-.0014	.0090	.9830	.0207	-.0006	-.0095	.0008	.0000	-.8769
	Y	-.0004	.1600	.9682	-.0075	-.0387	.0004	-.0006	-.0072	-.8642	.0000
	Oz	-.0003	.0000	.0454	-.0280	.6401	.0153	-.0046	.9090	-.0170	.0074
38	X	.5481	-.0024	.0070	.7800	.0166	-.0045	-.7236	-.0019	.0003	.2165
	Y	-.0001	.4072	.7745	-.0061	-.0316	-.7157	.0043	.0023	.2060	.0003
	Oz	-.0004	.0000	.0545	-.0338	.7810	.0617	-.0015	.5473	-.0120	.0058
44	X	.7111	-.0033	.0037	.4335	.0094	-.0044	-.7747	-.0025	.0002	.8883
	Y	.0002	.6133	.4337	-.0035	-.0187	-.7702	.0049	.0050	.8701	.0002
	Oz	-.0004	.0000	.0604	-.0376	.8743	.0003	.0008	.1687	-.0045	.0025
54	X	.9997	-.0047	-.0038	-.3883	.0080	.0016	.2212	.0006	-.0003	-.1605
	Y	.0008	1.0000	-.3807	.0031	.0120	.2187	-.0015	-.0011	-.1572	.0002
	Oz	-.0004	-.0001	.0680	-.0426	1.0000	-.0063	.0036	-.4967	.0004	-.0023
f*		0.1813	0.2387	1.2276	1.2773	1.3004	3.5079	3.6584	4.3637	6.0100	6.2370
M**		470.46	802.76	260.71	264.12	130.76	223.43	227.79	82.97	256.61	273.68

* Natural Frequency, Hz
** Generalized Mass, kg or kg-m^2 as appropriate

MAST Flight System Modal Data (Includes Orbiter)
Beam Length 46 Bays, PMD Adjusted to Match 2nd x-z Bending, LDCMs Locked

BAY	COMP.	1 1st x-z	2 1st y-z	3 1st Torsion	4 2nd x-z	5 2nd y-z	6 3rd x-z	7 3rd y-z	8 2nd Torsion	9 4th x-z	10 4th y-z
12	X	-.0115	-.0009	-.0044	.1049	-.0083	.2996	-.1573	-.0009	.6784	-.1494
	Y	-.0005	-.0830	.0176	.0096	.0891	.1595	.2880	-.0026	.1565	.6308
	Oz	-.0003	-.0020	.1075	.0038	-.0404	.0048	.0226	.3104	-.0044	.0622
24	X	.1347	-.0007	-.0284	.7427	-.0637	.9702	-.5174	.0029	.3816	-.0350
	Y	-.0022	.0212	.1294	.0735	.6851	.5284	.9539	-.0202	.0902	.3645
	Oz	-.0004	-.0020	.4231	.0183	-.1621	.0167	.0505	.9547	.0009	.0482
30	X	.2663	.0000	-.0364	.9595	-.0827	.5305	-.2807	.0024	-.3588	.1236
	Y	-.0034	.1570	.1678	.0953	.8907	.2873	.5187	-.0160	-.1311	-.5255
	Oz	-.0004	-.0020	.5693	.0250	-.2188	.0155	.0463	.9874	.0003	-.0222
33	X	.4836	.0015	-.0336	.8903	-.0770	-.5914	.3134	-.0015	-.2425	.0533
	Y	-.0053	.3955	.1558	.0887	.8302	-.3191	-.5766	.0041	-.0579	-.2306
	Oz	-.0005	-.0020	.7434	.0330	-.2870	.0079	.0244	.6606	.0016	-.0785
44	X	.6678	.0028	-.0213	.5658	-.0491	-.9478	.5019	-.0031	.4562	-.1015
	Y	-.0063	.6106	.0985	.0565	.5294	-.5123	-.9251	.0123	.1066	.4301
	Oz	-.0005	-.0020	.8561	.0381	-.3316	.0017	.0048	.2344	.0026	-.0640
54	X	.9986	.0053	.0132	-.3471	.0298	.2116	-.1119	.0006	-.0680	.0151
	Y	-.0095	.9986	-.0635	-.0344	-.3210	.1138	.2065	-.0024	-.0156	-.0640
	Oz	-.0005	-.0020	1.0000	.0446	-.3891	-.0050	-.0210	-.5518	-.0016	.0257
f*		.2162	.2618	1.585	1.594	1.606	4.606	4.613	5.191	8.555	8.577
M**		422.8	584.4	111.0	234.8	219.1	283.0	270.2	70.96	143.1	127.8

* Natural Frequency, Hz
** Generalized Mass, kg or kg-m^2 as appropriate

ALLOWABLE STRUCTURAL DEFLECTIONS

The allowable structural deflections for single mode excitation are shown in figures 7 and 8. The deflection shown is the maximum deflection of each mode. Also depicted are lines of constant signal-to-noise ratio for reference. Well over a 100-to-1 signal-to-noise ratio is available for each mode. A decrease in allowable beam second bending and first torsion structural capability has been shown when these modes are coupled to account for unexpected energy transfer between the coupled modes.

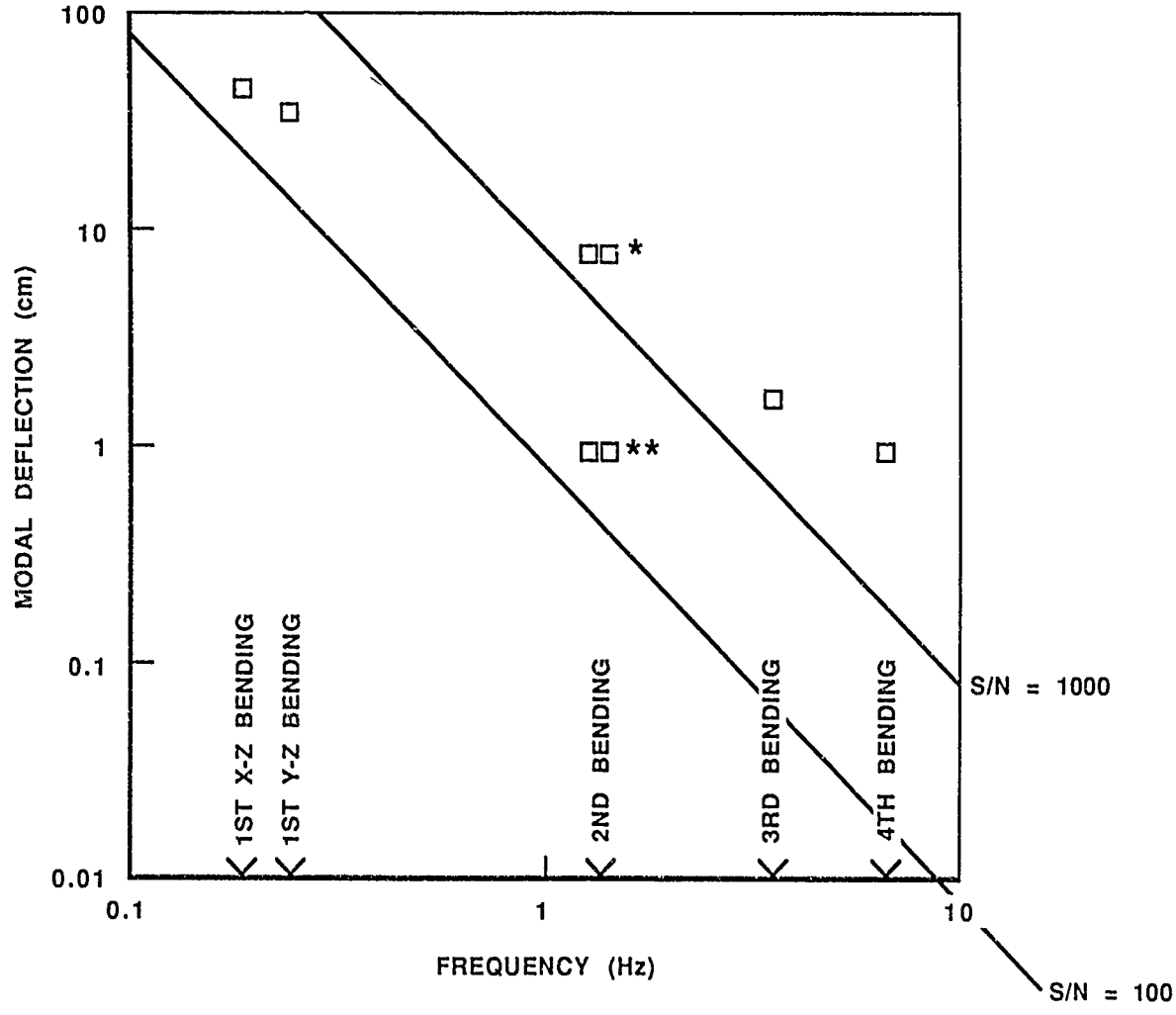

LINEAR ACCELEROMETER CHANNEL NOISE 1.5 mV_{rms}

* NOT COUPLED WITH TORSION
** COUPLED WITH TORSION

Figure 7.

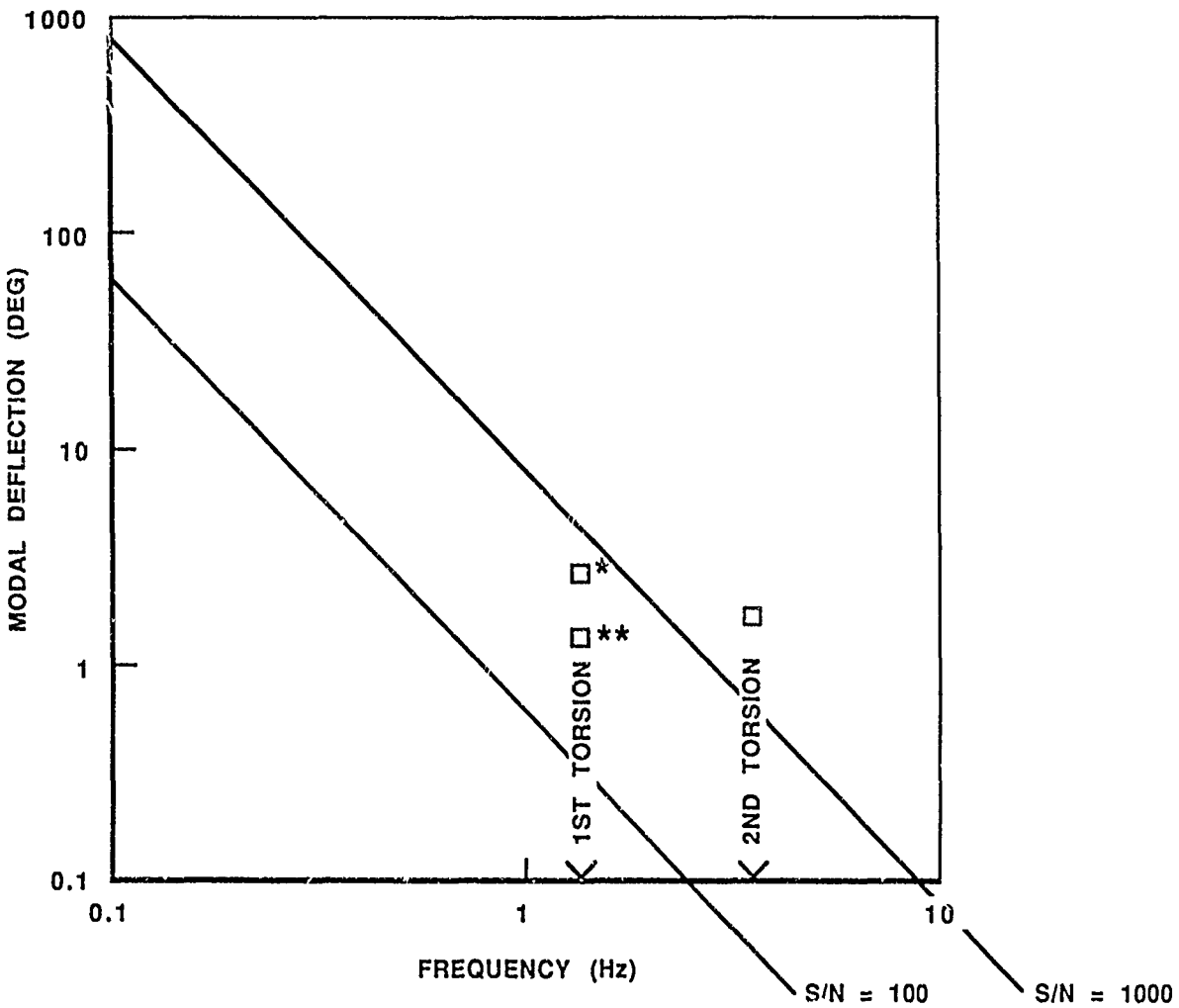

ANGULAR ACCELEROMETER CHANNEL NOISE 2.0 mV_{rms}

* NOT COUPLED WITH 2ND BENDING
** COUPLED WITH 2ND BENDING

Figure 8.

MAST FLIGHT SYSTEM DYNAMIC PERFORMANCE

L. Davis

D. Hyland

T. Otten

F. Ham

First NASA/DOD CSI Technology Conference
Norfolk, Virginia
November 18-21, 1986

This discussion focuses on the MAST Flight System as a test bed for large space structure control algorithms. After giving an overview of the whole system, four main topics will be covered: the actuators, the sensors, the control computer, and the baseline damping algorithm.

MAST FLIGHT SYSTEM DYNAMIC PERFORMANCE

1. Overview of the control system architecture
2. Placement of sensors and actuators
3. LDCM design and performance
4. Sensor performance and models
5. Computer architecture and performance
6. Baseline damping system performance

CONTROL SYSTEM ARCHITECTURE

The system to be controlled is the 54-bay mast. Sensors and actuators are placed at the various stations indicated. The control computer system communicates with the sensors and actuators via a 1553 data bus.

The actuators are Harris-designed Linear DC Motors (LDCMs). Ten of these actuators are placed at various stations along the length of the mast. The four larger, Type I actuators are placed at the tip to provide control over both the primary bending modes and the torsion modes. The remaining, Type II actuators provide good control authority over the second and third bending modes.

The control sensors consist of 18 linear accelerometers, 5 angular accelerometers, and 6 rate gyros. Sensors are collocated with the actuators and placed at additional locations to measure the motion of the structure accurately. The signal-to-noise ratio is at least 40 dB for signals to be expected during the experiment.

The control computer system samples all sensors and commands all actuators at a rate of 150 Hz. The control computations are performed in the EDS computer, while the MDIS computer handles communications both with the sensors and actuators and with the Shuttle.

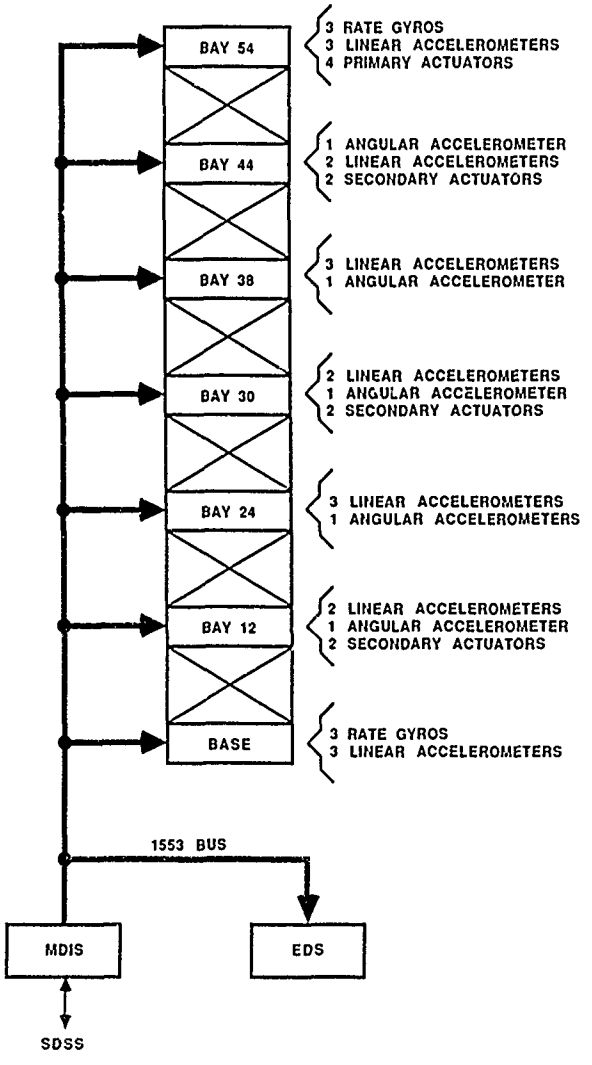

TYPE 1 LDCM

The Linear DC Motors (LDCMs) were designed by Harris to act as the control actuators for the MAST Flight System. Each LDCM consists of two pieces: the fixed primary, which houses the motor coils, and the moving secondary, which houses the permanent magnets and provides the reaction mass for the actuator.

The primary coils are rigidly mounted to the motor frame. They are switched to varying currents based on the commanded force and the position of the moving secondary as measured via the commutation vanes. The fixed coils rest between the return irons and the permanent magnets of the secondary. The eight bearings ensure that the secondary remains centered laterally while keeping friction to a minimum.

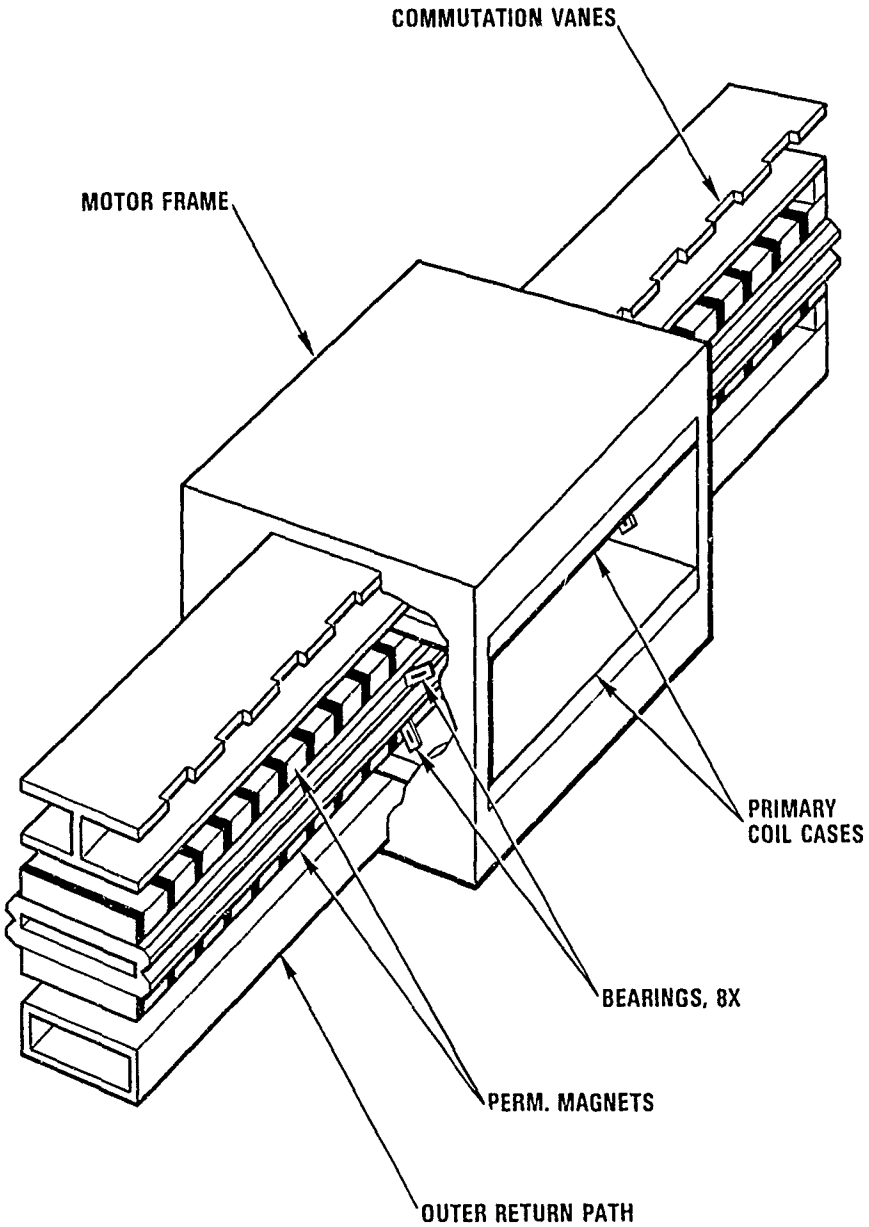

The LDCMs are compensated to provide the user full access to the capabilities of the devices while ensuring that they operate within their limitations of stroke and force.

The compensation works, in the absence of user input, to keep the LDCM secondary fixed in inertial space in spite of transient mast motion. This serves to decouple the operation of the LDCM from the dynamics of the mast. In this mode, the stroke of the actuator must be divided between the motion of the mast and the motion due to control inputs. The total stroke of the device minus the allowed motion of the mast becomes the effective stroke available for control.

The transfer function as seen by the user through the EDS command is tailored to give access to the full stroke capability at low frequencies and the full force capability at high frequencies. The limit on the user command ensures that the LDCM does not exceed these capabilities.

POSITION LOOP OPERATION

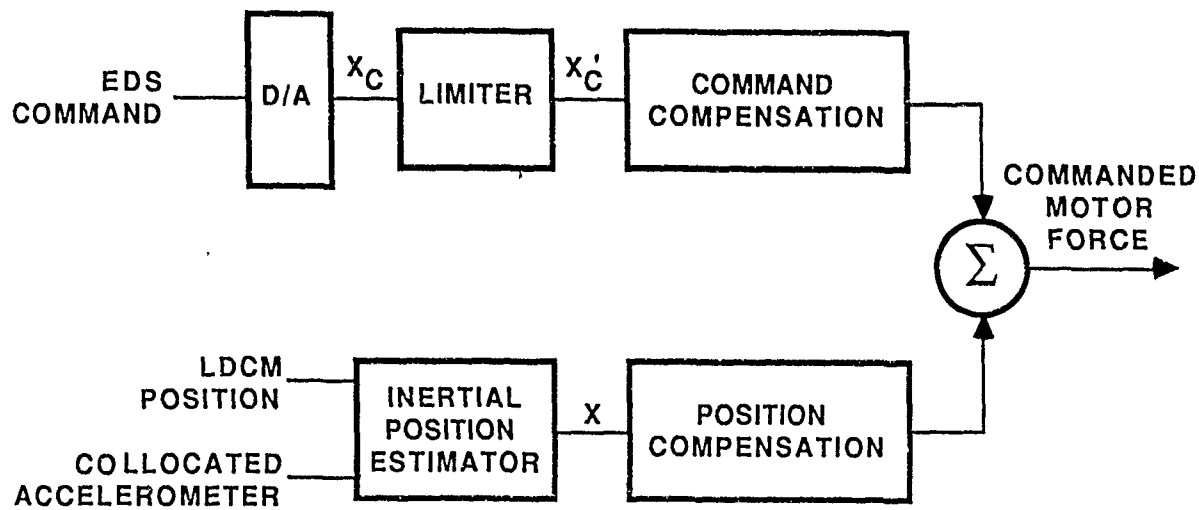

EQUIVALENT USER MODEL

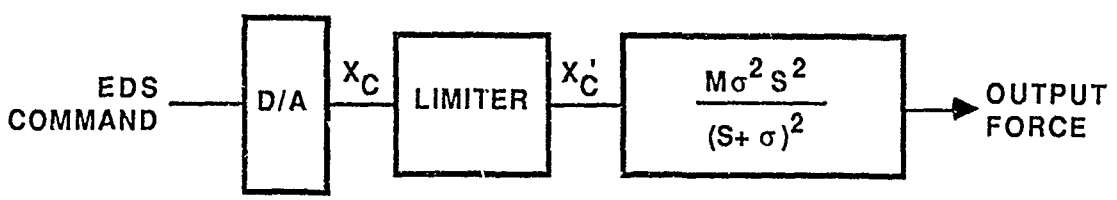

COMPENSATED LDCM SPECIFICATIONS

The overall specifications for the compensated LDCMs are shown below. The mass differential between the Type I and Type II actuators, combined with their allowed stroke limitations, combine to determine the compensated bandwidth sigma. The user command is limited by a single value such that at low frequencies the stroke is not exceeded. The bandwidth is then adjusted such that at high frequencies the force limit is not exceeded.

The user has access to the relative position of the secondary with respect to the primary of each LDCM. This accurate measurement comes from the commutation vanes of the secondary.

Accurate knowledge of relative secondary position has allowed Harris to reduce force ripple below 1% of nominal output force and additive force errors due to position feedback below 0.05 N, thus providing users with a quiet actuator for vibration suppression.

TRANSFER FUNCTION: $\frac{\text{FORCE OUT}}{\text{CMD IN}} = \frac{m\sigma^2 S^2}{(S+\sigma)^2}$

$m = 11$ kg, $\sigma = 2\pi$ RAD/SEC (TIP)

$m = 7$ kg, $\sigma = 5.5$ RAD/SEC (INTERMEDIATE)

STROKE: ±15 cm (TIP)
± 7 cm (INTERMEDIATE)

FORCE OUTPUT: ±30 N (TIP)
±15 N (INTERMEDIATE)

POSITION MEASUREMENT
RESOLUTION: ±0.48 mm

OUTPUT NOISE: RIPPLE <1% OF OUTPUT
0.05 Nt RANDOM ADDITIVE

SENSOR SPECIFICATIONS

The sensor complement has been chosen to measure the expected signals with 40 dB of signal-to-noise ratio. In some cases, the 12 bits of digital information available to the computer were not enough to reflect the accuracy of the sensor. Low ranges are used to expand the dynamic range seen by the computers.

LINEAR ACCELEROMETERS:

RANGE: +/- 1.0 G (HIGH RANGE)
+/- 0.1 G (LOW RANGE)

RESOLUTION: 500 MICRO-G (HIGH RANGE)
50 MICRO-G (LOW RANGE)

BANDWIDTH: 0-50 Hz MIN. (150 Hz MAX.)

ANGULAR ACCELEROMETERS:

RANGE: +/- 10 RAD/SEC^2

RESOLUTION: 0.01 RAD/SEC^2

BANDWIDTH: 0-40 Hz MIN. (200 Hz MAX.)

ANGULAR RATE GYROS:

RANGE: +/- 1 DEG/SEC

RESOLUTION: 0.0005 DEG/SEC

BANDWIDTH: 0-80 Hz

STRAIN GAUGES:

RANGE: +/- 7500 MICROSTRAIN

RESOLUTION: 50 MICROSTRAIN

THERMISTERS:

RANGE: +/- 100 DEG C.

RESOLUTION: 0.5 DEG C.

SENSOR MODELS

The sensors to be used for control are inertial. They conform roughly to the models shown below. The indicated noises are white, zero-mean processes. Their intensities were chosen to reflect either the resolution of the sensor or the manufacturers' estimates of rms noise amplitude, whichever was coarser. The bandwidths are the lowest available for the type of sensor under consideration.

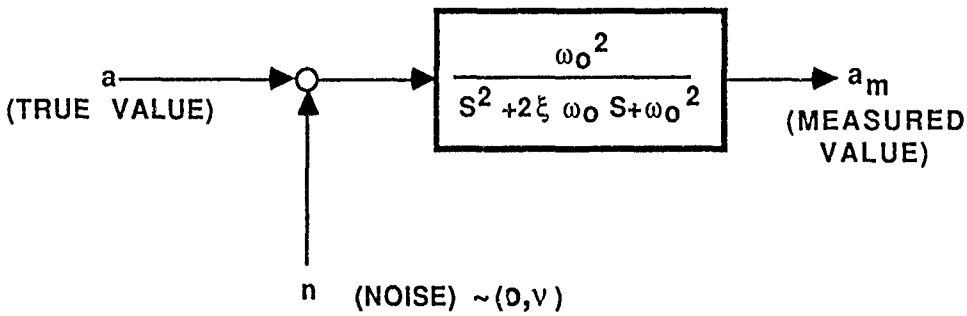

$\omega_o = 2\pi \cdot 50$
$\xi = 0.7$
$\nu = 220 \times 10^{-6}\ g^2/Hz$
} FOR LINEAR ACCELEROMETERS

$\omega_o = 2\pi \cdot 40$
$\xi = 0.6$
$\nu = 60.32 \times 10^{-3}\ (rad/sec^2)^2/Hz$
} FOR ANGULAR ACCELEROMETERS

$\omega_o = 2\pi \cdot 80$
$\xi = 0.5$
$\nu = 251.3 \times 10^{-6}\ (°/sec)^2/Hz$
} FOR RATE GYROS

CONTROL SYSTEM COMPONENTS

The control computer system has four major components: the MDIS computer, the EDS computer, the 1553 bus system, and the remote units.

The MDIS computer controls the overall operation of the system. It governs the modes of operation, the communication to and from the Shuttle, and the collection and dissemination of control data and commands.

The EDS computer performs the computations necessary to execute a user's control algorithm. It receives data directly from the remote units, processes it, and sends its commands to the remote units, all as coordinated by the MDIS.

The 1553 data bus serves as the communication link among the other parts of the system.

The remote units are located at the various bays along the length of the mast. Each unit governs the operation of the instrumentation at its own particular bay. On command, it collects data from each of the instruments, formats it, and sends it on the 1553 bus. In similar fashion it receives data from the bus, decodes it, and distributes it to the actuators.

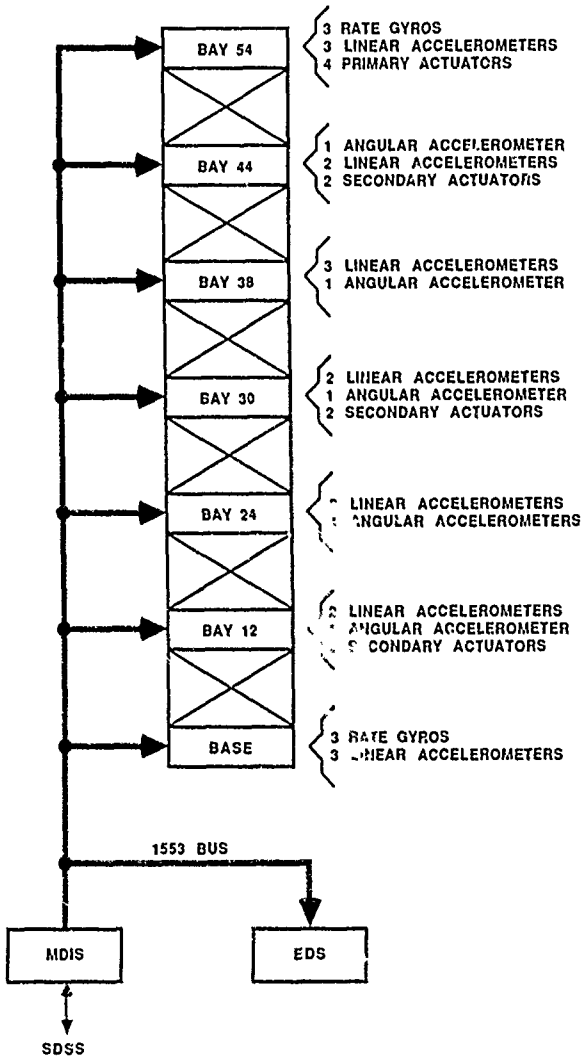

1553 BUS TRANSFER AND PROCESS INTERVAL ALLOCATIONS

The operation of the computer system during one cycle is shown below. First, data is transmitted from the EDS computer to the remote units, which then distribute them to the actuators. At the same time, the remote units collect the sensor data for the next cycle. This data is then sent back down to the EDS computer for processing. The user's algorithm is executed, and a new cycle is begun.

The computer system keeps the jitter under 30 microseconds for one cycle. This ensures clean, distortion free operation of the control algorithms.

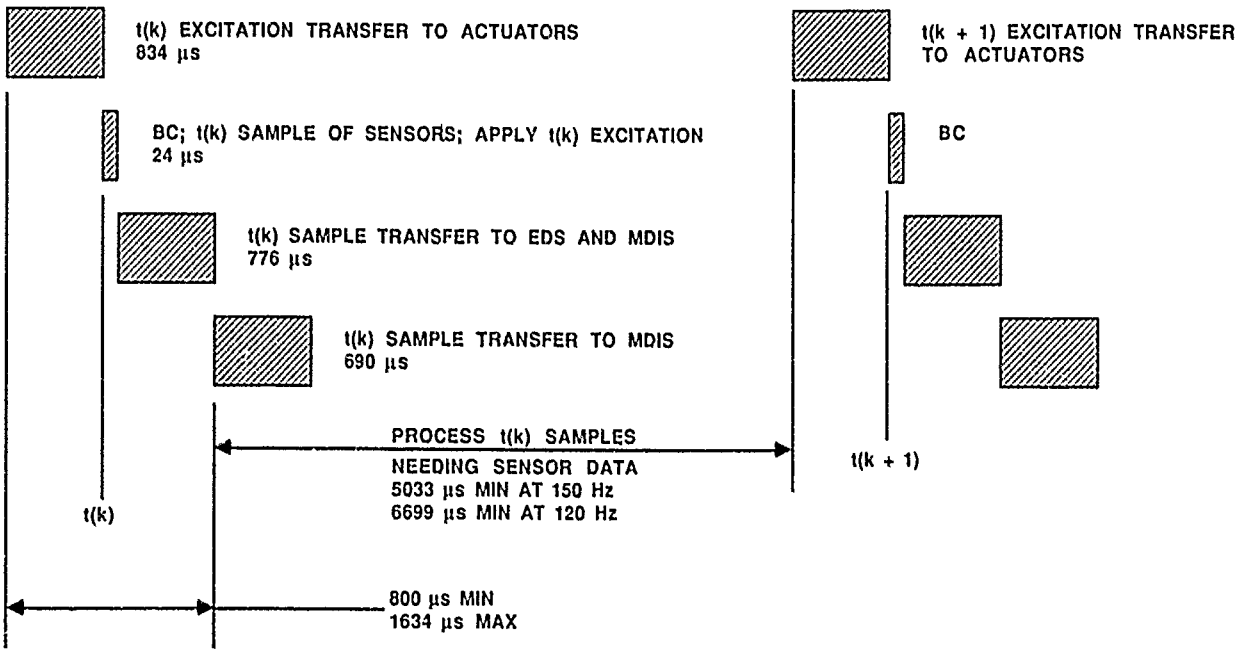

BASELINE DAMPING ALGORITHM

The MAST Flight System includes a baseline damping control algorithm. This algorithm is used as a backup in the case of user algorithm failure or between testing periods to bring the system to a quiescent state.

Harris has developed a baseline control system that is designed to damp the first 10 modes of the mast safely and reliably. It achieves the goal of 5% damping of these modes while operating within the constraints of the hardware. The decentralized approach uses the concepts of positive real design to assure that the stated goals will be achieved in spite of unexpected mission variations.

The damping system operates by first canceling the two poles of the LDCM, then introducing two additional poles: one pole cancels a zero of the LDCM transfer function, the other determines the frequency at which the damping operation of the loop begins. The parameters of the compensators at the various stations are tailored to the modes which the stations affect. Of particular interest is the trade-off between the damping achieved and the actuation level required. The parameters are adjusted to balance these two factors.

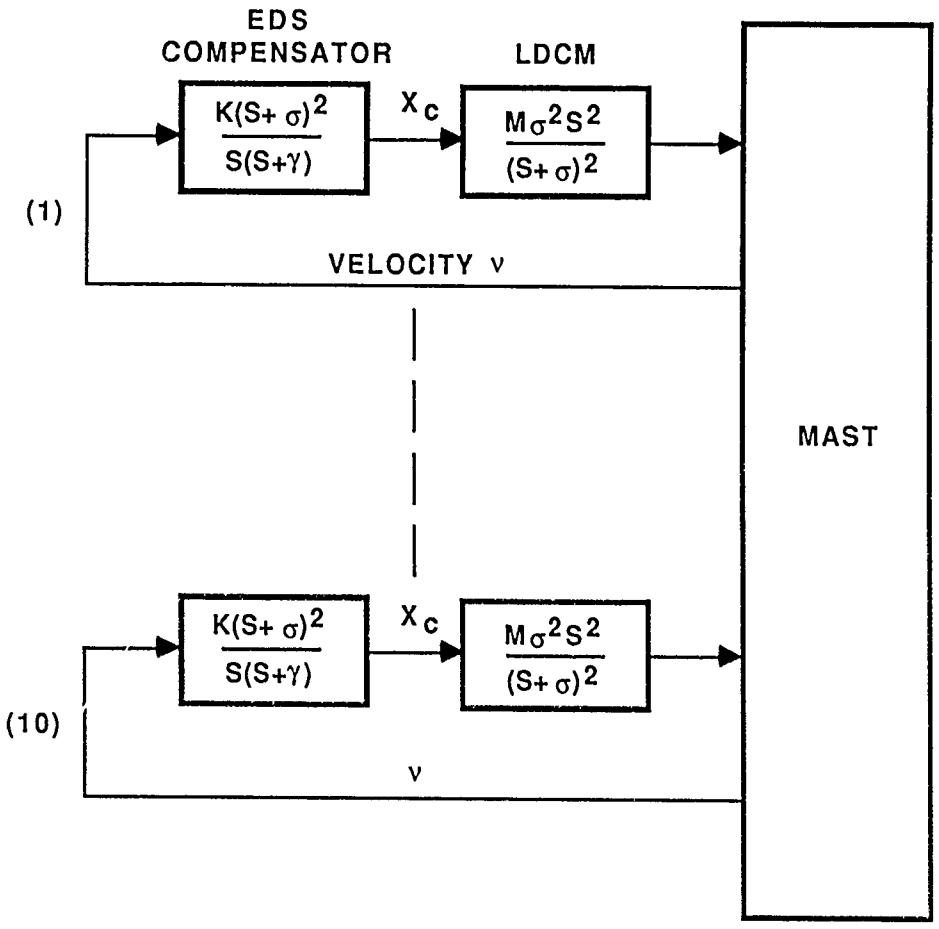

MAST FLIGHT SYSTEM MODAL DATA

The baseline algorithm was applied to the fully extended mast having the modal characteristics as shown. The modes apply to a mast connected to a simple STS model.

The units of interest are MKS. The modal coefficients are amplitude normalized such that the maximum coefficient of any degree of freedom in the model is unity. Mass normalized modes can be obtained by dividing the given coefficients by the square root of the generalized mass shown for the corresponding mode.

MAST Flight System Modal Data (Includes Orbiter)
Beam Length 54 Bays, Maximum PMD Inertia, LDCMs Locked

BAY	COMP.	1 1st x-z	2 1st y-z	3 2nd y-z	4 2nd x-z	5 1st Torsion	6 3rd y-z	7 3rd x-z	8 2nd Torsion	9 4th y-z	10 4th x-z
12	X	.0344	.0001	.0044	.4196	.0083	.0059	.9047	.0014	-.0004	.9968
	Y	-.0007	-.1431	.3939	-.0027	-.0152	.8858	-.0052	-.0106	.9892	-.0006
	θz	.0002	.0000	.0197	-.0124	.2686	.0190	-.0070	.7243	.0155	-.0053
24	X	.2189	-.0008	.0086	.9158	.0191	.0032	.6197	.0024	-.0006	-.5821
	Y	-.0006	.0125	.8948	-.0063	-.0355	.6240	-.0044	-.0126	-.5645	-.0006
	θz	-.0003	.0000	.0375	-.0231	.5229	.0203	-.0064	1.0000	-.0091	.0043
30	X	.3486	-.0014	.0090	.9830	.0207	-.0006	-.0095	.0008	.0000	-.8769
	Y	-.0004	.1600	.9682	-.0075	-.0387	.0004	-.0006	-.0072	-.8642	.0000
	θz	-.0003	.0000	.0454	-.0280	.6401	.0153	-.0046	.9090	-.0170	.0074
38	X	.5481	-.0024	.0070	.7800	.0166	-.0045	-.7236	-.0019	.0003	.2165
	Y	-.0001	.4072	.7745	-.0061	-.0316	-.7157	.0043	.0023	.2060	.0003
	θz	-.0004	.0000	.0545	-.0338	.7810	.0617	-.0015	.5473	-.0120	.0058
44	X	.7111	-.0033	.0037	.4335	.0094	-.0044	-.7747	-.0025	.0002	.8883
	Y	.0002	.6133	.4337	-.0035	-.0187	-.7702	.0049	.0050	.8701	.0002
	θz	-.0004	.0000	.0604	-.0376	.8743	.0003	.0008	.1687	-.0045	.0025
54	X	.9997	-.0047	-.0038	-.3883	.0080	.0016	.2212	.0006	-.0003	-.1605
	Y	.0008	1.0000	-.3807	.0031	.0120	.2187	-.0015	-.0011	-.1572	.0002
	θz	-.0004	-.0001	.0680	-.0426	1.0000	-.0063	.0036	-.4967	.0004	-.0023
f*		0.1813	0.2387	1.2276	1.2773	1.3004	3.5079	3.6584	4.3637	6.0100	6.2370
$\bar{M}$**		470.46	802.76	260.71	264.12	130.76	223.43	227.79	82.97	266.61	273.68

* Natural Frequency, Hz
** Generalized Mass, kg or kg-m^2 as appropriate

The pole locations shown indicate that the goal of 5% damping has been achieved. The open-loop damping reflects an assumption of 0.2% damping for the first bending modes, 0.3% damping for the second bending modes, and 0.5% damping for all higher modes.

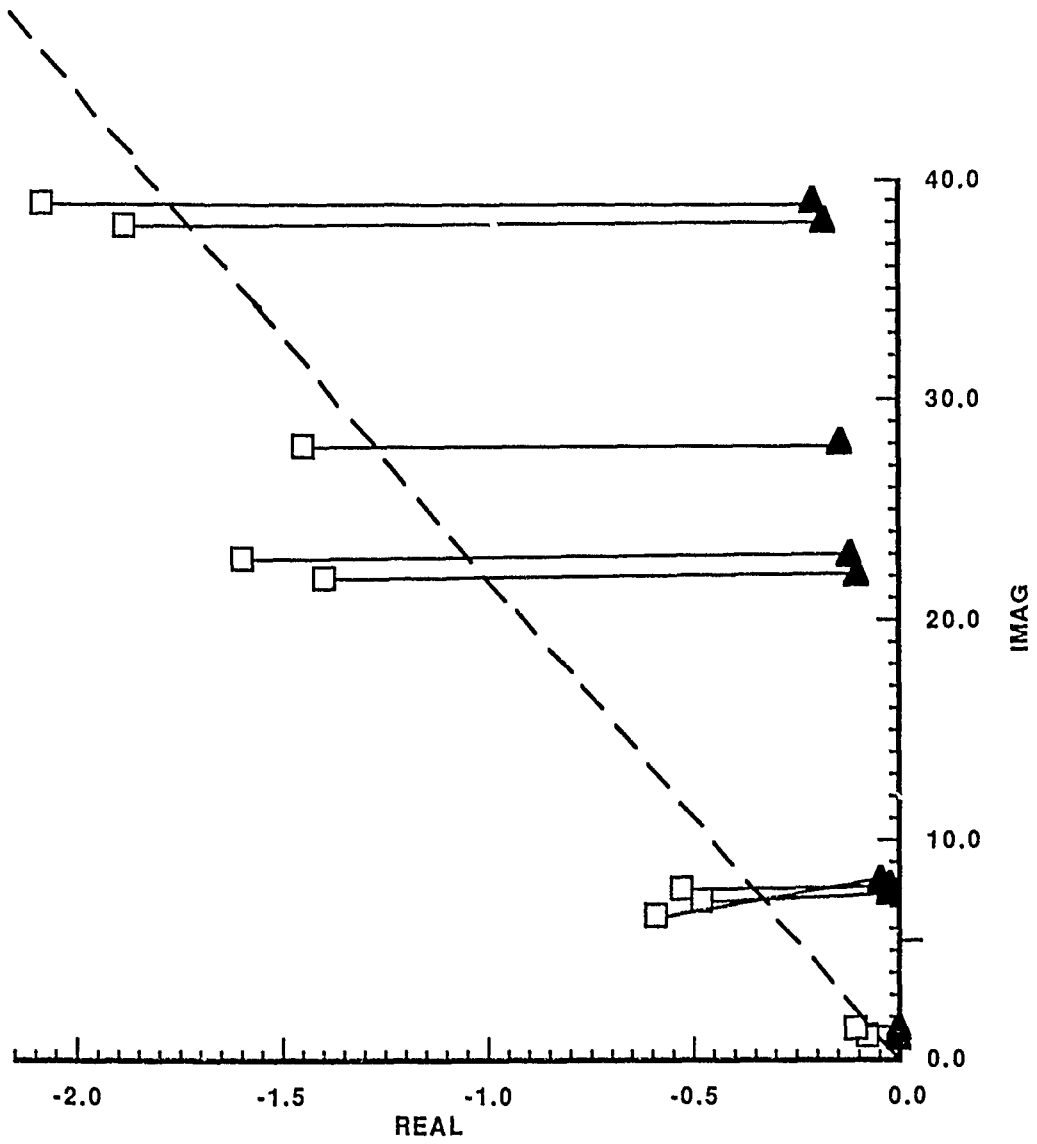

54 BAY POLE SHIFTS FOR BASELINE

DISTURBANCE PSD

Random excitation was applied at bay 44 in the x and y directions to both the open- and closed-loop systems. The other stations were used for control in the closed loop. The disturbance was as shown in the diagram. Independent disturbances were applied in the x and y directions.

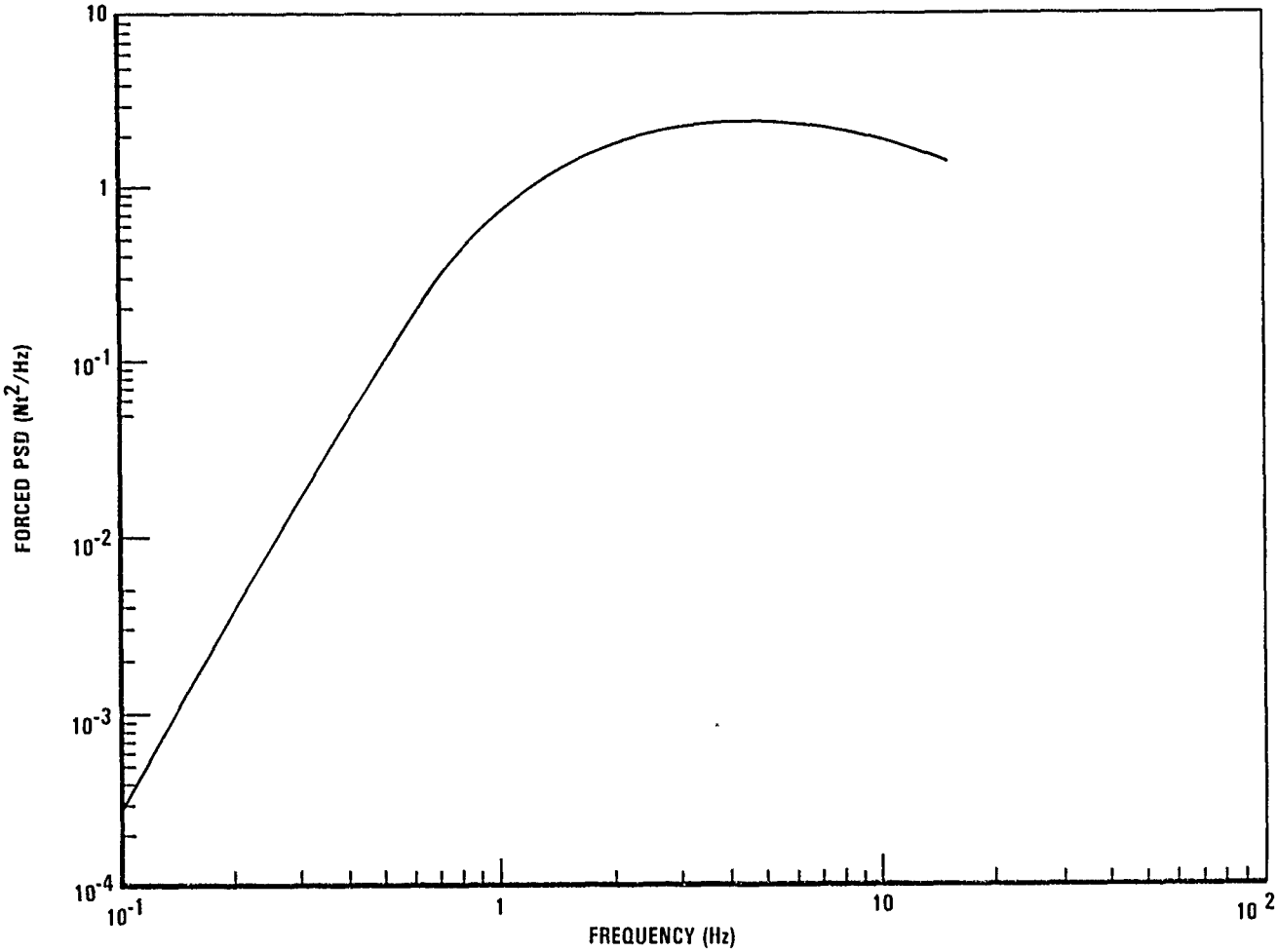

DISTURBANCE PSD (EACH AXIS)

TIP X ACCELERATIONS

The acceleration power spectral densities (PSDs) for the mast tip in the x direction are shown here for the open- and closed-loop cases. It is easy to see the marked smoothing achieved by the control system. In both cases, sufficient signal is detected to be measured by the available sensors.

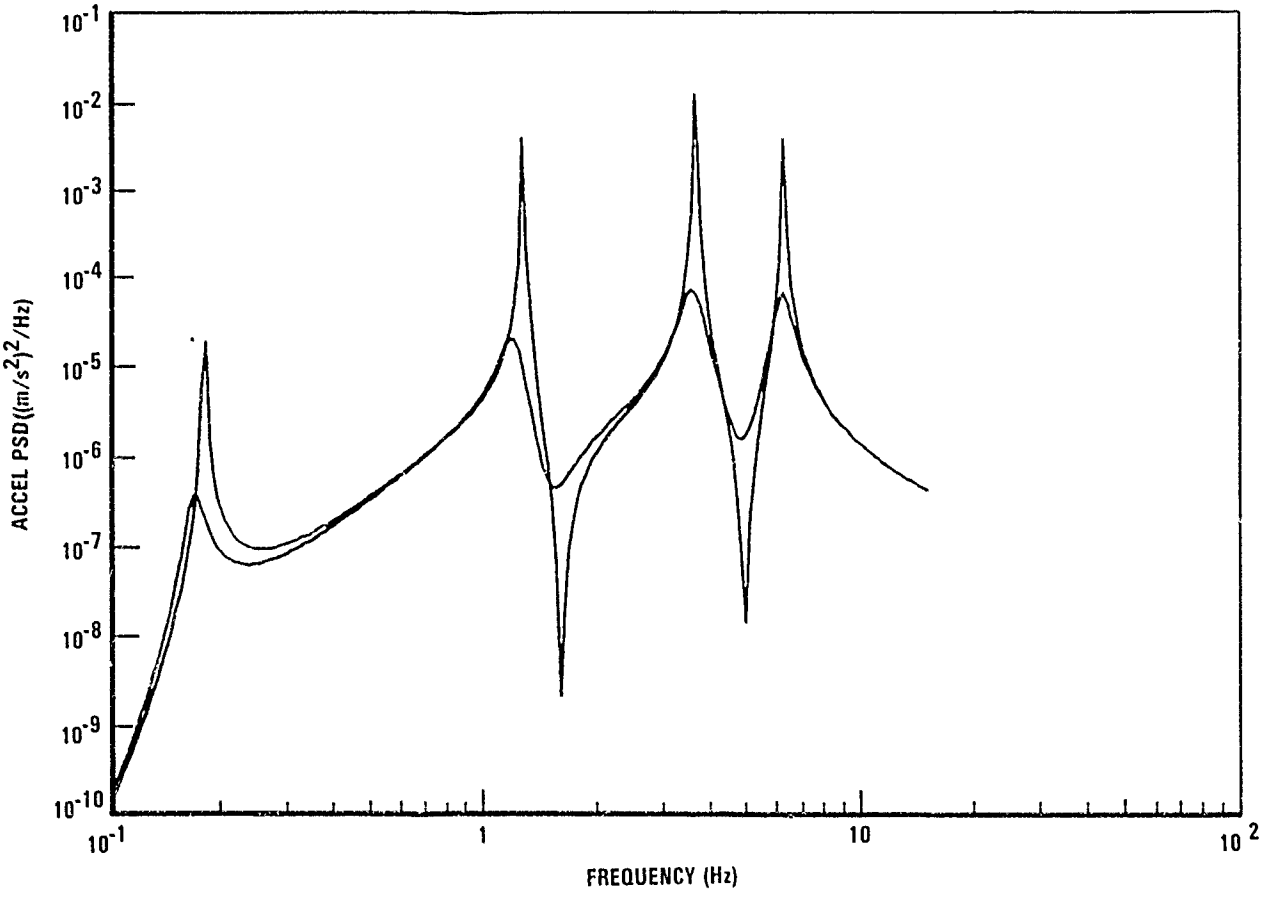

TIP X ACCELERATIONS

TIP Y ACCELERATIONS

Similar results are shown here for the y direction at the mast tip. Once again, marked smoothing of the PSD curve is indicative of the improvement in damping achieved by the control system.

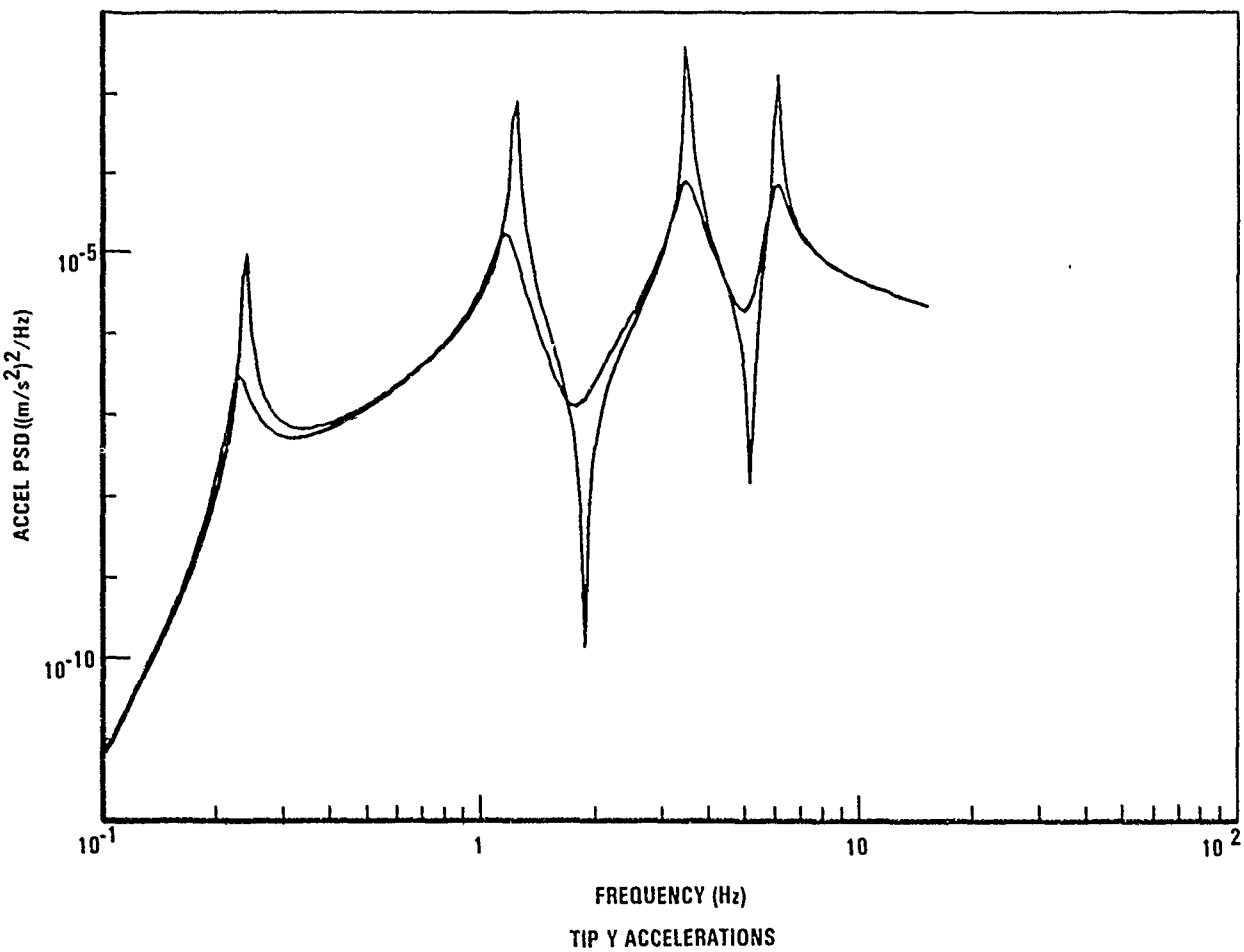

TIP Y ACCELERATIONS

TIP Z ROTATIONAL ACCELERATIONS

The torsion results shown in this diagram, while smoothed, are not as clear-cut as the bending results. This is due chiefly to the lack of direct torsion excitation by the disturbance. In this case, excitation is due to the coupling of the bending and torsion modes and to residual spillover of the control system at the mast tip.

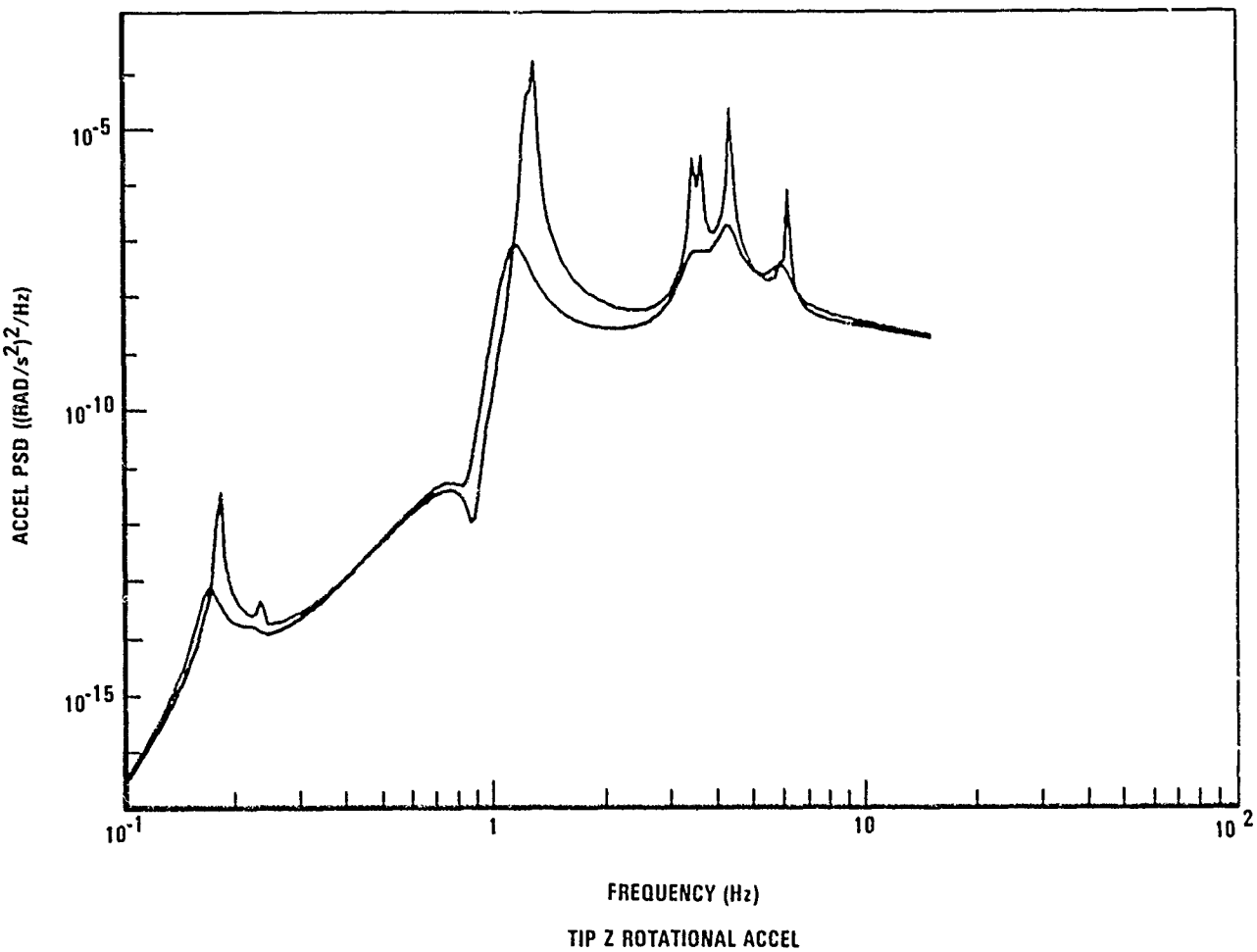

MAST FLIGHT SYSTEM OPERATIONS

M. LARRY BRUMFIELD
NASA LANGLEY RESEARCH CENTER

FIRST NASA/DOD CSI TECHNOLOGY CONFERENCE
NORFOLK, VIRGINIA
NOVEMBER 18-21, 1986

MAST FLIGHT EXPERIMENT

An artist's concept of the MAST Flight Experiment is shown in Figure 1. The Mast Flight System is a 60 meter long deployable truss structure. Detailed descriptions of the system have been given in previous papers at this conference and will not be repeated here. MAST will be mounted on a STEP/SPACELAB pallet and integrated into the Space Shuttle payload bay for orbital flight testing. It will occupy one-quarter of the payload bay space, but will require more than the standard one-quarter allocation of orbiter power.

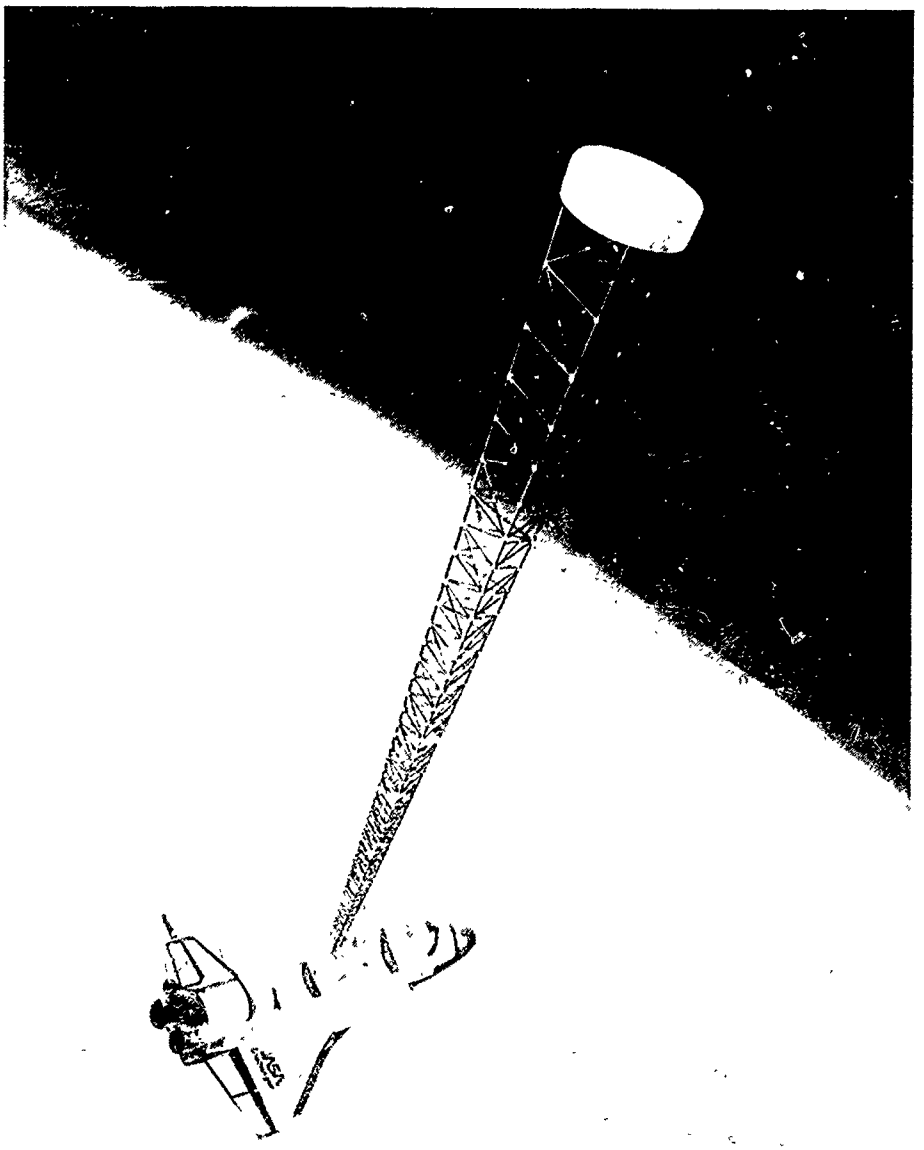

Figure 1

MAST 1 FLIGHT TEST OBJECTIVES

The first flight of MAST will emphasize structural dynamics and will be focused on determining the structural characteristics from the measured dynamic responses to controlled excitations. A major thrust will be evaluating state-of-the-art system identification techniques. In addition, the latest actuator and sensor technology will be evaluated as it can be applied to in-space testing of large, lightweight structures.

MAST I

EMPHASIZES DYNAMIC CHARACTERIZATION OF THE BEAM TRUSS

1. **TO DETERMINE THE STRUCTURAL/MODAL CHARACTERISTICS OF THE MAST FLIGHT BEAM**
2. **TO EVALUATE SYSTEM IDENTIFICATION AND STATE ESTIMATION ALGORITHMS ON COMPLEX, LIGHTWEIGHT STRUCTURES IN SPACE ENVIRONMENT.**
3. **TO EVALUATE ACTUATOR/SENSOR/MEASUREMENT TECHNIQUES APPLICABLE TO LIGHTWEIGHT, LOW-FREQUENCY STRUCTURES WITH LOW DEFLECTION/DETECTION TOLERANCES.**
4. **TO PERFORM ACTIVE DAMPING OF THE BEAM USING REAL-TIME DATA FEEDBACK.**

Figure 2

MAST 2 FLIGHT TEST OBJECTIVES

The second flight of MAST will emphasize flexible body controls experiments. A major thrust will be the use of both collocated and distributed actuators and sensors. Both the open-loop and closed-loop stability will be evaluated very carefully. Of particular interest will be the level of maturity of the various control law design methodologies and whether they provide sufficiently robust control mechanizations for large, lightweight, flexible structures. The second flight will provide the vehicle for implementing the selected guest investigator experiments. (The guest investigator program will be discussed by Mr. Anthony Fontana in the next paper.)

The remainder of this paper will focus on the flight operations planning associated with the first flight of MAST.

MAST 2

EMPHASIZES FLEXIBLE BODY CONTROLS EXPERIMENTS

1. **TO DEMONSTRATE CONTROL LAWS USING COLLOCATED ACTUATORS AND SENSORS.**

2. **TO DEMONSTRATE CONTROL LAWS USING DISTRIBUTED SENSORS AND ACTUATORS.**

3. **TO DEMONSTRATE BOTH OPEN-LOOP AND CLOSED-LOOP STABILITY.**

4. **TO PROVIDE A TEST STRUCTURE FOR IMPLEMENTATION OF GUEST INVESTIGATOR EXPERIMENTS.**

Figure 3

THE TYPICAL FLIGHT PLANNING PROCESS

The Marshall Space Flight Center(MSFC) provides the Mission Manager for the MAST Flight Experiment. This Mission Manager acts as the interface or representative between the experiment team at Langley Research Center(LaRC) and the flight planning group at Johnson Space Center(JSC). Personnel at the Johnson Space Center prepare all the flight procedures, crew checklists, flight timelines, etc., necessary to support the actual flight experiment on the orbiter. The physical integration and mounting of the flight hardware is done by personnel at the Kennedy Space Center(KSC).

The key to this whole process is an Integrated Payload Requirements Document(IPRD). To develop this document, the Mission Manager must pull in a number of different requirement documents, beginning with the Experiment Requirements Document(ERD) that is unique to the MAST experiment and is prepared at LaRC. There are a myriad of existing requirements documents that are levied on any orbiter flight experiment. The primary ones are: NHB 1700.7A - Safety Policy and Requirements for Payloads Using the Space Transportation System (STS), JSC 07700 VOLUME XIV - Space Shuttle System Payload Accommodations, SLP/2104 - Spacelab Payload Accommodation Handbook, and JA 447 - Mission Requirements on Facilities/Instruments/Experiments for Space Transportation System (STS) Attached Payloads.

The Integrated Payload Requirements Document(IPRD) develops a specific set of requirements to guide the STS integration and the flight operations, specifies a set of design and performance requirements for any unique interface hardware or software needed to accommodate the experiment system, and establishes the required verification the experimenter must perform to demonstrate that all experiment systems adequately meet all orbiter/carrier requirements. Out of the IPRD comes an Instrument Interface Agreement that governs the design and development of the interface between the experiment system and the STEP/Spacelab pallet, and an Operations and Integrating Agreement that guides the integration of the experiment/carrier into the orbiter and the orbital experiment operations.

A detailed Payload Integration Plan is developed at JSC for use in the actual physical integration at KSC and in the final flight planning. The actual crew documents come out of this flight planning process. There are many design reviews, planning meetings, flight operations reviews, flight readiness reviews, safety reviews, etc., that cannot be illustrated here, but the experiment design certification process will be described further in the next figure.

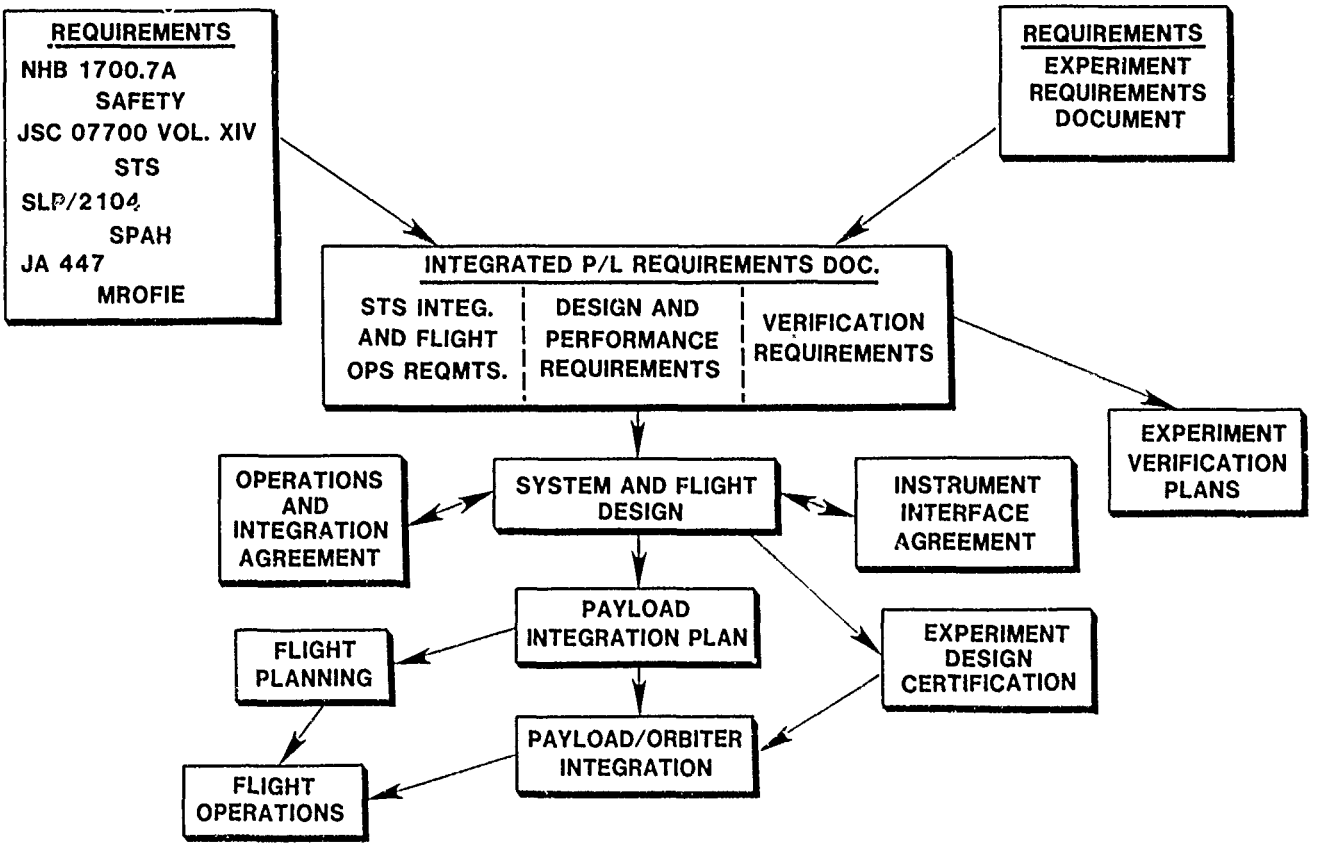
REQUIREMENTS
NHB 1700.7A
SAFETY
JSC 07700 VOL. XIV
STS
SLP/2104
SPAH
JA 447
MROFIE
REQUIREMENTS
EXPERIMENT
REQUIREMENTS
DOCUMENT
INTEGRATED P/L REQUIREMENTS DOC.
STS INTEG. AND FLIGHT OPS REQMTS.
DESIGN AND PERFORMANCE REQUIREMENTS
VERIFICATION REQUIREMENTS
EXPERIMENT VERIFICATION PLANS
OPERATIONS AND INTEGRATION AGREEMENT
SYSTEM AND FLIGHT DESIGN
INSTRUMENT INTERFACE AGREEMENT
PAYLOAD INTEGRATION PLAN
FLIGHT PLANNING
EXPERIMENT DESIGN CERTIFICATION
PAYLOAD/ORBITER INTEGRATION
FLIGHT OPERATIONS

Figure 4

CERTIFICATION

Since the primary emphasis in certification is safety, it will be referred to as the safety process. There are a number of requirements that must be met in the safety process, but the key governing documents are as follows: NHB 1700.7A (which has already been named), JSC 13830 - Implementation Procedure for STS Payloads System Safety Requirements, and JA-012B - Spacelab Project Office Payload Safety Implementation Approach. The process is coordinated by the MSFC Mission Manager in cooperation with counterparts at JSC and KSC. First, the exprimenter must prepare a set of hazard reports that identifies and describes each hazard associated with the flight hardware and experiment process. The initial preparation is soon after the experiment conceptual design review and is submitted prior to scheduling a Phase 0 safety review. Hazard reports must be maintained current and updated in keeping with the phased safety reviews so that they always reflect the current experiment configuration.
A set of safety verification plans must be developed jointly between the experimenter and the Mission Manager that specify the process by which the experimenter/integrator will verify that the payload meets all safety requirements. The hazard verification plans must also be updated and eventually contain results obtained when implementing the various test/verification procedures in the plans. Both hazard reports and safety verification plans/results become part of the safety compliance data packages submitted to support the phased safety reviews. The Mission Manager reviews all experimenter prepared documents for completeness and accuracy and assembles the official safety data packages to the appropriate safety review panels. This is an iterative process that is related to the overall experiment development and integration process. It is geared toward assuring that the payload is certified safe to fly at some time just prior to the final flight readiness review.

SAFETY PROCESSS

Governing Requirements and Procedures

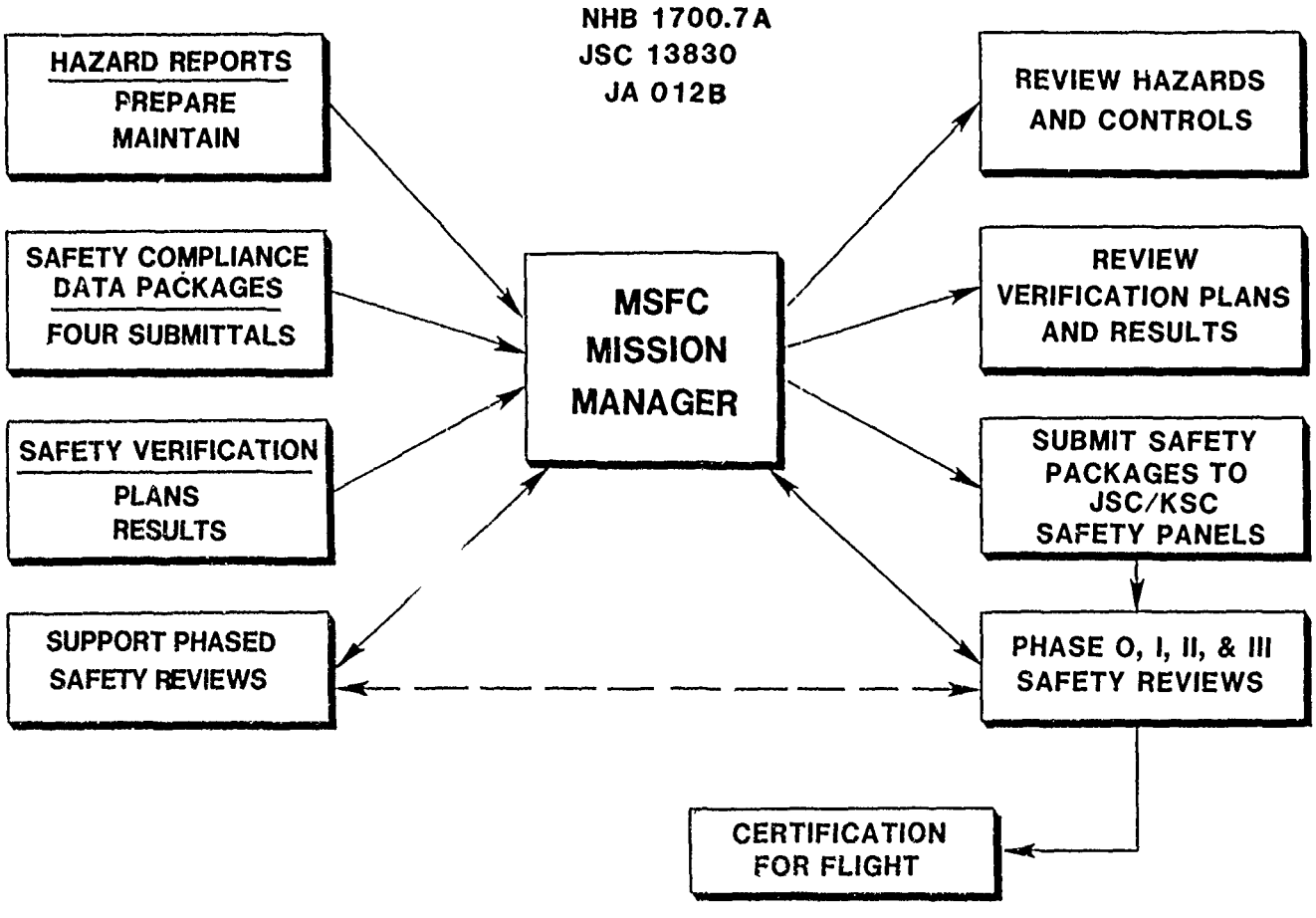

Figure 5

INTEGRATION MILESTONES

The major milestones in the experiment development and integration process are shown in Figure 6. The reader is advised that this is not the official contract schedule for development of the MAST Flight System(MFS). Rather, this is an attempt to fit a set of integration milestones into the time bounded by initiation of the program and the best estimate of the launch date. Currently, the MAST-1 flight test is scheduled for a May 9, 1991 launch. A conceptual design review(CoDR) has been held for the truss beam, and a preliminary design review(PDR) for the MAST Flight System is anticipated about the end of March 1987. Critical design review(CDR) will follow PDR by approximately 6 to 7 months. After the MAST Flight System is delivered to LaRC, there will be a period of ground testing to refine the modeling and predictions as well as validation of flight software. The MFS must then be recertified for flight before delivery to KSC.

The process of integrating the MFS with the Space Shuttle has already begun with dicussions of preliminary requirements and preparation of the initial reports identifying potential safety hazards. This is leading to a Phase Zero safety review near the end of this year. An integration requirements review(IRR) will follow the experiment PDR by some 6 to 8 weeks and will result in documentation of all the requirements that must be met in the process of integrating the MFS with the carrier pallet and then with the Space Shuttle orbiter. The actual interface (both hardware and software) between the experiment and the orbiter now starts through a design and verification process. There will be an integration preliminary design review(IPRD) and critical design review(ICDR) which will result in the necessary baseline documents and configuration control documents.

After the IPDR, the flight planning activity begins in earnest at JSC. This is an iterative process that involves the continual participation of appropriate MSFC and LaRC personnel. Numerous flight planning documents must be prepared and reviewed to establish and validate precise operational procedures for the flight. The various working groups and reviews at JSC are too numerous to detail in the figure. Some key reviews are of the MAST proposed ground operations(GOR) and flight operations(FOR) to ensure that those JSC persons that develop the details for the orbital operations thoroughly understand the experiment operations. A detailed integration readiness review(IRR) is held just before the MFS is shipped to KSC. A Space Shuttle flight operations review(SSFOR) is held to ensure that all experiment procedures, timelines, crew checklists, etc., are ready for the flight. The process of safety certification has already been described and only the phased safety reviews are shown here. The last thing is the flight readiness review(FRR) just before flight.

MAJOR MILESTONES FOR MAST-1 INTEGRATION

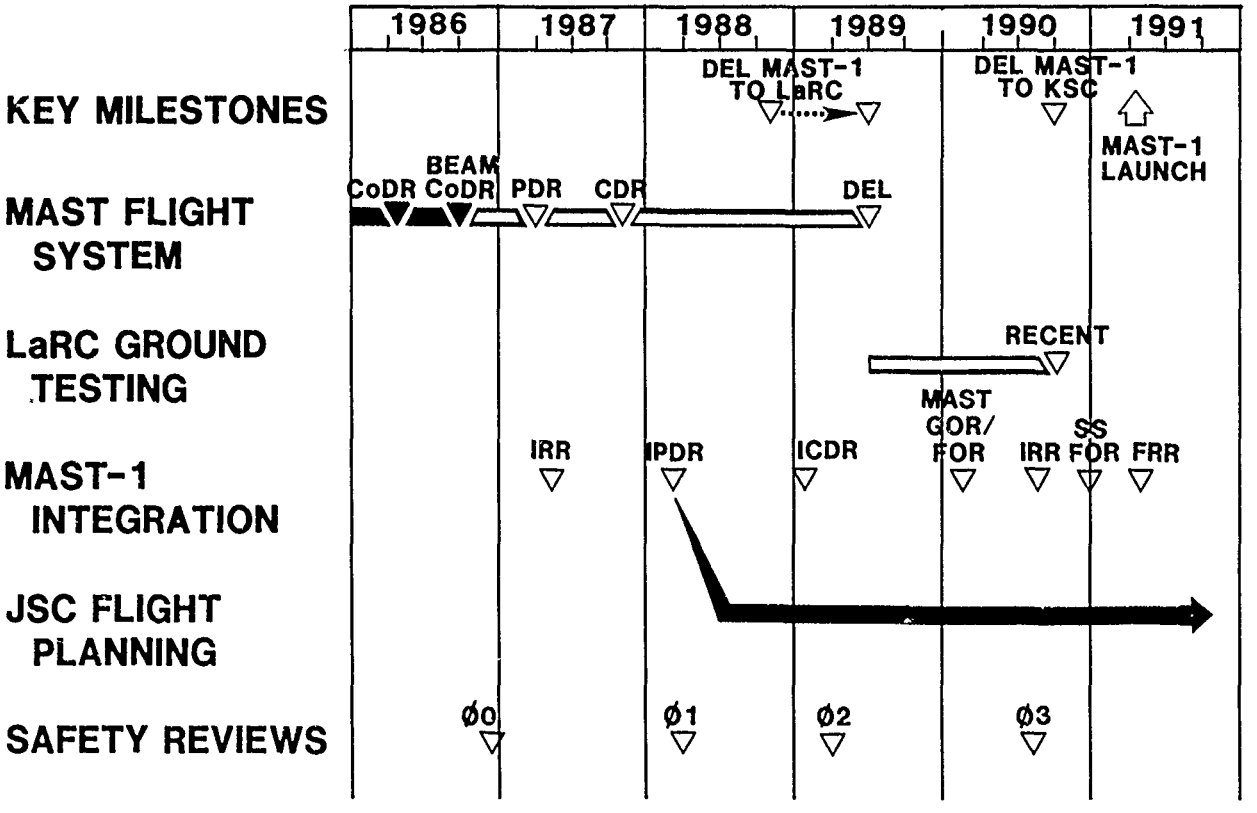

Figure 6

TYPICAL ORBITAL PLANNING

A typical day's activity is shown in Figure 7. Times shown are best estimates as of now and must be refined and fine-tuned as the experiment process is more specifically defined. This is representative of what must go into planning a day of orbital testing. Only MAST test activity is shown when in reality there are other experiments that will have activity that must be fitted into the final timeline. Every crew activity must be planned and shown in the detailed timeline as well as written into the crew checklist. (The crew checklist is a companion document to the timeline and lists the actual steps the crew implements in the performance of the orbital experiment.) This is a continuing process in which the JSC integration personnel interact with all experimenters to develop a flight timeline that accomplishes as many of the flight test objectives as possible for all experimenters on the flight. The working goal is to have the final timeline established about six months before launch.

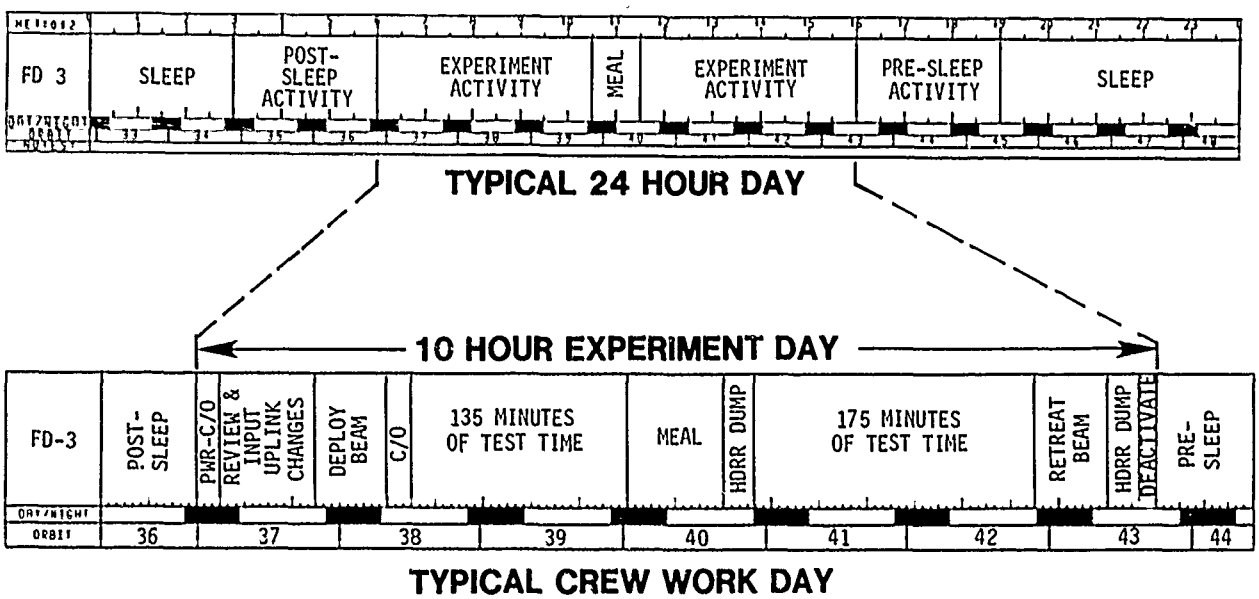

- **NEED 3 TO 4 DAYS DEDICATED TO MAST TESTING**
- **TIMES FOR INDIVIDUAL TESTS VARY ALLOWING FLEXIBILITY IN FINE-TUNING A SPECIFIC TIMELINE**
- **TIMELINE FINALIZED 6 MONTHS BEFORE LAUNCH - CURRENTLY MAY 1991**

Figure 7

TYPICAL TEST SCENARIO

The different parts of a typical MAST dynamic test are illustrated in Figure 8. Each dynamic test will require a quiescent period of as yet undetermined length prior to excitation of the beam. During this time crew motion will be restricted and all but essential orbiter operations will be suspended. A preplanned, controlled excitation of the beam will be performed using the beam mounted actuators. Termination of the excitation period begins a free-decay period in which the dynamic responses of the beam will be measured using sensors at the various beam mounted instrumentation stations. These measurements will be recorded onboard and downlinked in real time. Data would be recorded continuously from some point during quiescence to the observed end of the free-decay period. These data periods may vary from times as short as 15 minutes to as much as 45 minutes. There will be an option available to initiate an active damping algorithm after some TBD number of cycles of the dynamic response. This will facilitate reduction of the time needed for the total MAST test activity.

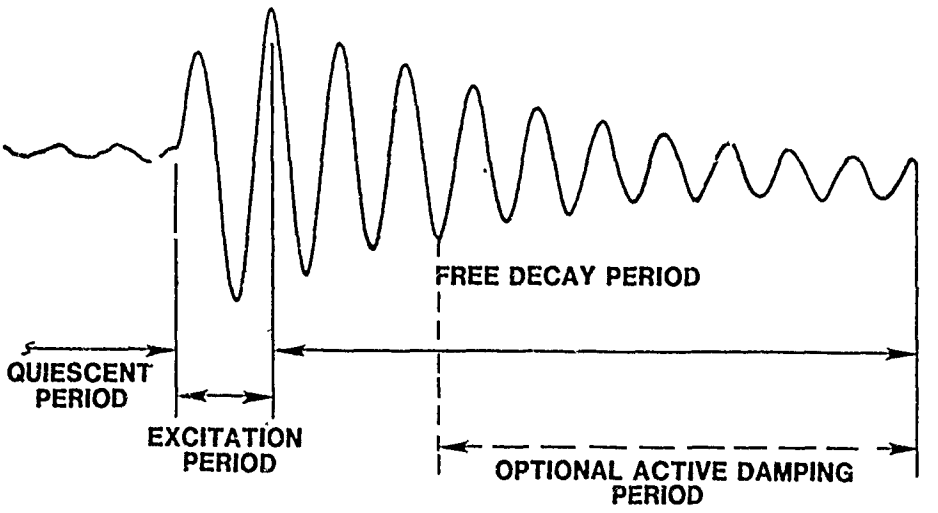

- **TOTAL DATA PERIOD COULD BE 15 MINUTES**
- **DATA RECORDED CONTINUOUSLY FROM QUIESCENT THRU EXCITATION TO END OF FREE-DECAY PERIOD**
- **DATA RECORDED ONBOARD AND DOWNLINKED**
- **CREW AND ORBITER ACTIVITY RESTRICTED FROM PRIOR TO QUIESCENT PERIOD THRU END OF FREE DECAY**

Figure 8

PLANNED ORBITAL TESTS FOR MAST 1

Numerous discussions with the principal investigators for MAST 1 have led to the preliminary list of planned orbital tests shown in Figure 9. This is not meant to be a definitive description of each actual test that will be run. It is only meant to illustrate the variety and number of tests that will be necessary to adequately identify the structural characteristics of the MAST beam truss. The actual number and specific process for each test must be developed during the integration and flight planning process. Definitive science test requirements that guide that process are still being developed.

TYPE TEST	NO. OF TESTS
1. Excitation to 25%, 50%, & 75% actuator #1 only	3
2. Excitation to 50% single actuators #9 thru 10	9
3. Excitation to 25%, 50%, & 75% multiple actuators	3
4. Parameter modifications repeat 50% multiple actuations	4
5. Increment beam length repeat 50% multiple actuations	2
6. Select beam length & param.mod.to match freq. of 1st bending & 2nd torsion modes, minimum coupling 50% excitation, multiple actuations	2
7. Param.mod.for maximum coupling repeat 50% multiple actuations	2
8. Param.mod.for 50%coupling repeat 50% multiple actuations	2
9. 50% coupling, 75% excitation multiple actuators	1
Currently Planned Tests	28

Figure 9

MAST SENSOR/ACTUATOR LOCATIONS

The locations of the MAST remote stations are illustrated in Figure 10. Details of these remote stations have been previously discussed by Mr. Ronald Talcott in an earlier paper and will not be repeated here. There are seven remote stations, one located at the tip of the beam, five at various locations along the beam, and one on the beam baseplate. Actuators are located at the tip and at three locations along the beam. Sensors and supporting power supplies and electronics are contained in all stations.

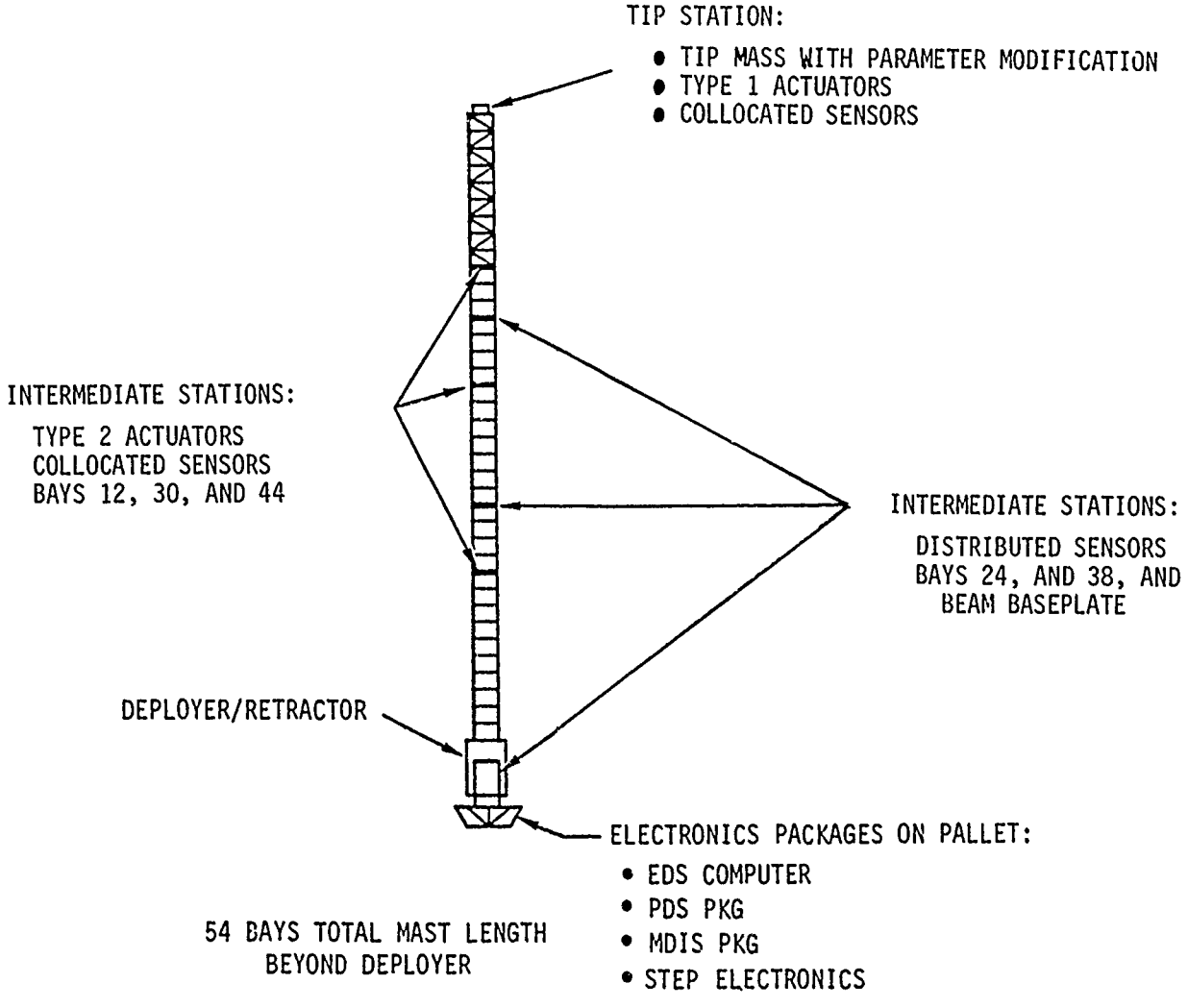

Figure 10

SUMMARY OF MAST FLIGHT SYSTEM INSTRUMENTATION

Again, details have already been provided that describe the instrumentation system and will not be repeated here. This summary is provided to illustrate the type of sensor complement from which data will be recorded and downlinked during the orbital experiment operations.

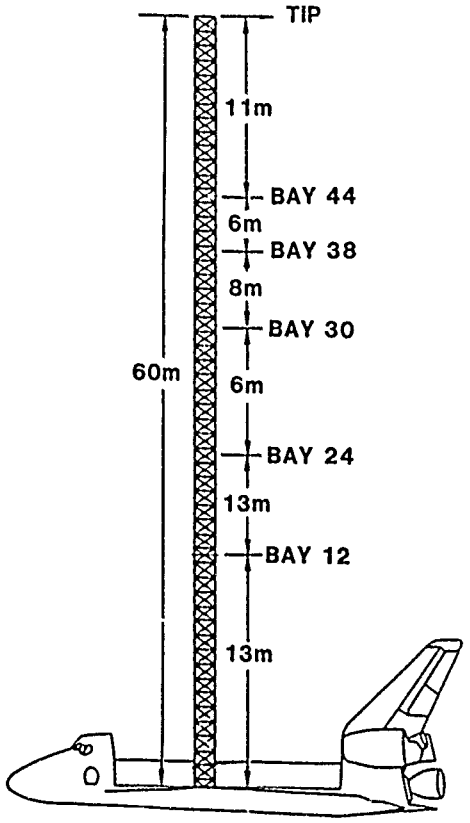

ACTUATOR	GYRO RATE	LINEAR ACCEL.	ANGULAR ACCEL.	STRAIN GAUGE	THERMISTOR
4	3	3		6	9
2		3	1	6	3
		2	1	6	3
2		3	1	6	3
		2	1	6	3
2		3	1	6	3
	3	3		6	3
10	6	19	5	42	27

Figure 11

ORBITAL DATA PATHS

The planned data flow during the MAST 1 flight experiment is shown in Figure 12. This is not a complete depiction of every instrument or interface that will be needed during the flight. Rather it only represents the various paths that data will follow in reaching the appropriate user or repository. There are two different data rates represented: a low data rate and a high data rate. The low rate data is transferred from the modular distributed instrumentation system (MDIS) computer to the smart/flex modulator/demodulator (SFMDM). This data is a subset of the high rate data and consists primarily of housekeeping data and the appropriate safety data that must be monitored by the crew in the orbiter aft flight deck. Low rate data takes two paths from the SFMDM. It is be directed via the payload data interleaver (PDI) to the S-band downlink and eventually reaches the Huntsville operations support center (HOSC). In the HOSC, data can be stripped out and routed to appropriate display instruments for monitoring by the flight support engineering personnel. Low rate data is also passed to the data display and control unit (DDCU) where it is displayed in predefined screens that are selectable by the crew. The primary interface between the crew and the experiment is through this DDCU-SFMDM-MDIS path. The crew issues appropriate commands to operate the experiment operations and tests and monitor the feedback for appropriate responses or progress. More detail on this process can be found in the previous paper by Mr. Ronald Talcott. The high rate data is transferred directly from the MDIS computer to the high rate multiplexer (HRM). This data is essentially every data sample taken by the MDIS during the expriment process. The HRM routes data to the Ku-band downlink and to the high data rate recorder. The high data rate recorder (HDRR) records all data taken by the MDIS. The data will be periodically dumped via the HRM/Ku band and satellite links to the Goddard Space Flight Center's (GSFC) satellite network data receiving and recording facilities. Master tapes of all orbital data will be made for archives and for use by the science teams for postflight data analyses. The high rate data will also be downlinked in real time for some of the earlier beam deployments and dynamic tests. This real-time downlink will be routed via satellite links to the HOSC where some combination of HOSC instrumentation and experiment ground support equipment (GSE) will be used to provide both real time display of selected data and quick-look recordings of all downlinked data. The science team will use these quick-look recordings to do preliminary analyses to verify the beam responses as compared to preflight predictions. This process will continue overnight for each test performed to provide confirmation of readiness to proceed with the next days tests. The detailed definition of these downlink paths, data formats, and display/analysis processes is still in progress.

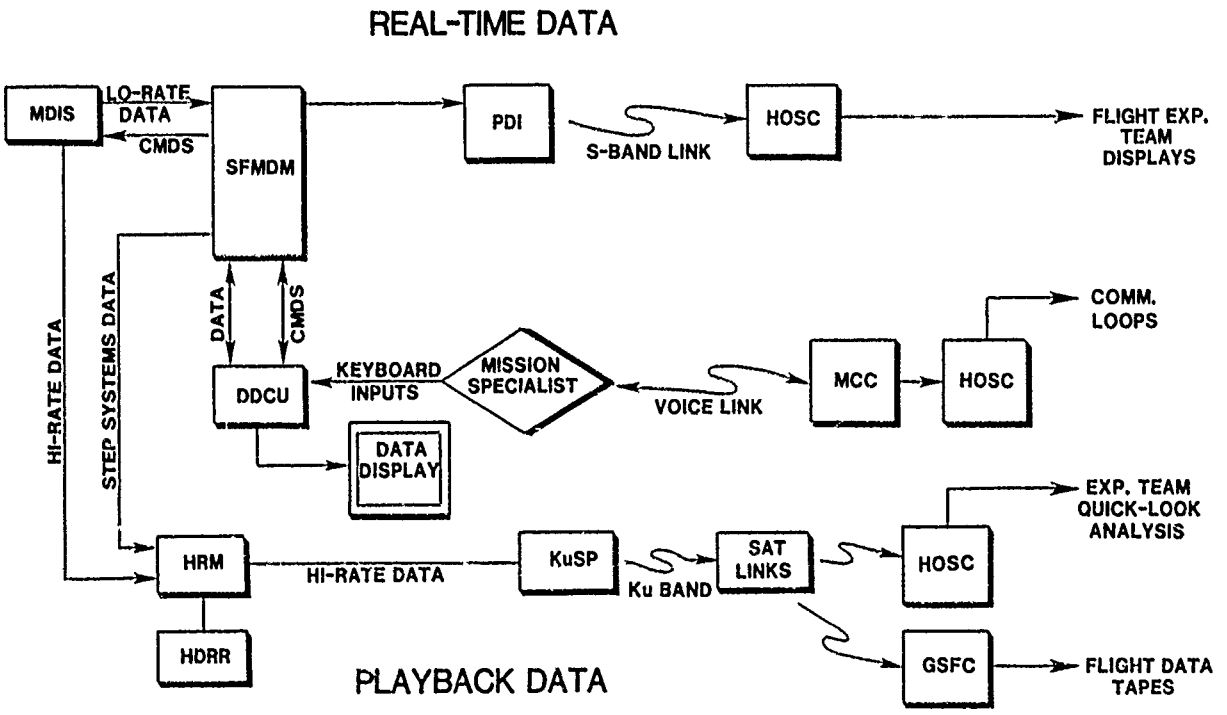
REAL-TIME DATA
MDIS
LO-RATE DATA
CMDS
SFMDM
PDI
S-BAND LINK
HOSC
FLIGHT EXP. TEAM DISPLAYS
HI-RATE DATA
STEP SYSTEMS DATA
DATA
CMDS
DDCU
KEYBOARD INPUTS
MISSION SPECIALIST
VOICE LINK
MCC
HOSC
COMM. LOOPS
DATA DISPLAY
HRM
HI-RATE DATA
KuSP
Ku BAND
SAT LINKS
HOSC
EXP. TEAM QUICK-LOOK ANALYSIS
HDRR
GSFC
FLIGHT DATA TAPES
PLAYBACK DATA

Figure 12

PLANNED DATA ANALYSIS

Figure 13 is only a cursory description of the major thrust of analysis using data obtained during the MAST flight experiment. The specific analyses and studies cannot be envisioned at this time beyond that necessary to provide the initial structural characterization, evaluate the degree to which experiment objectives were accomplished, and prepare for the second MAST flight dedicated to controls technology.

- **PRELIMINARY ANALYSIS DURING FLIGHT USING DOWNLINKED DATA TO GUIDE THE PROGRESS OF THE TESTING AND FACILITATE ANY ADJUSTMENTS TO PARAMETERS OR LIMITS THAT MAY BE DESIRED OR NECESSARY**

- **COMPLETE POSTFLIGHT ANALYSIS OF HIGH SAMPLE RATE FLIGHT DATA USING VARIOUS STATE-OF-THE-ART SYSTEM IDENTIFICATION TECHNIQUES TO DETERMINE THE DYNAMIC RESPONSE CHARACTERISTICS OF THE FLIGHT BEAM**

- **COMPARISONS AND STUDY OF GROUND TEST RESULTS AND PREDICTED DYNAMIC RESPONSES TO THE MEASURED ORBITAL RESPONSES**

Figure 13

SUMMARY

This paper has attempted to accomplish three purposes:

- To survey the integration process,
- To give brief insight into the planned orbital experiment process,
- To outline the data flow necessary to support the fight operations.

COFS I GUEST INVESTIGATOR PROGRAM

Anthony Fontana and Robert L. Wright
NASA Langley Research Center
Hampton, Virginia

First NASA/DOD CSI Technology Conference
Norfolk, Virginia
November 18-21, 1986

SUMMARY

The process for selecting guest investigators for participation in the COFS-I program is in place. Contracts and grants will be awarded in late CY87. A straw-man list of types of experiments and a distribution of the experiments has been defined to initiate definition of an experiments package which supports development and validation of CSI technology. A schedule of guest investigator participation has been developed.

COFS-I GUEST INVESTIGATOR PROPOSAL REVIEW PROCESS

Potential guest investigators have submitted approximately 60 proposals in response to the Dear Colleague Letter of February 7, 1986 which announced the opportunity to participate in the COFS-I Guest Investigator Program. The proposal review process is presented in figure 1. The Technical Merit Panel is made up of ten members from five NASA centers — MSFC, GSFC, JSC, JPL, LaRC. The Technical Reviewers are given 1 month for individual evaluation of the proposals prior to the formal meeting of the Technical Merit Panel at LaRC in October. Proposals considered responsive by the Technical Merit Panel are reviewed by the Accommodations Panel and Business Panel for implementation feasibility and cost aspects. The Technical Merit Panel reviews and approves any changes made by the Accommodation Panel or Business Panel to insure that the integrity of the experiment package is preserved. The Experiment Evaluation Board is made up of five senior members from five NASA centers. This board reviews and approves the experiment package recommended by the Technical Merit Panel. The review process is completed at NASA Headquarters by the Controls/Structures Interaction (CSI) Steering Committee with final selection for negotiations being made by the OAST Associate Administrator in early 1987. Contracts will be awarded in late CY87.

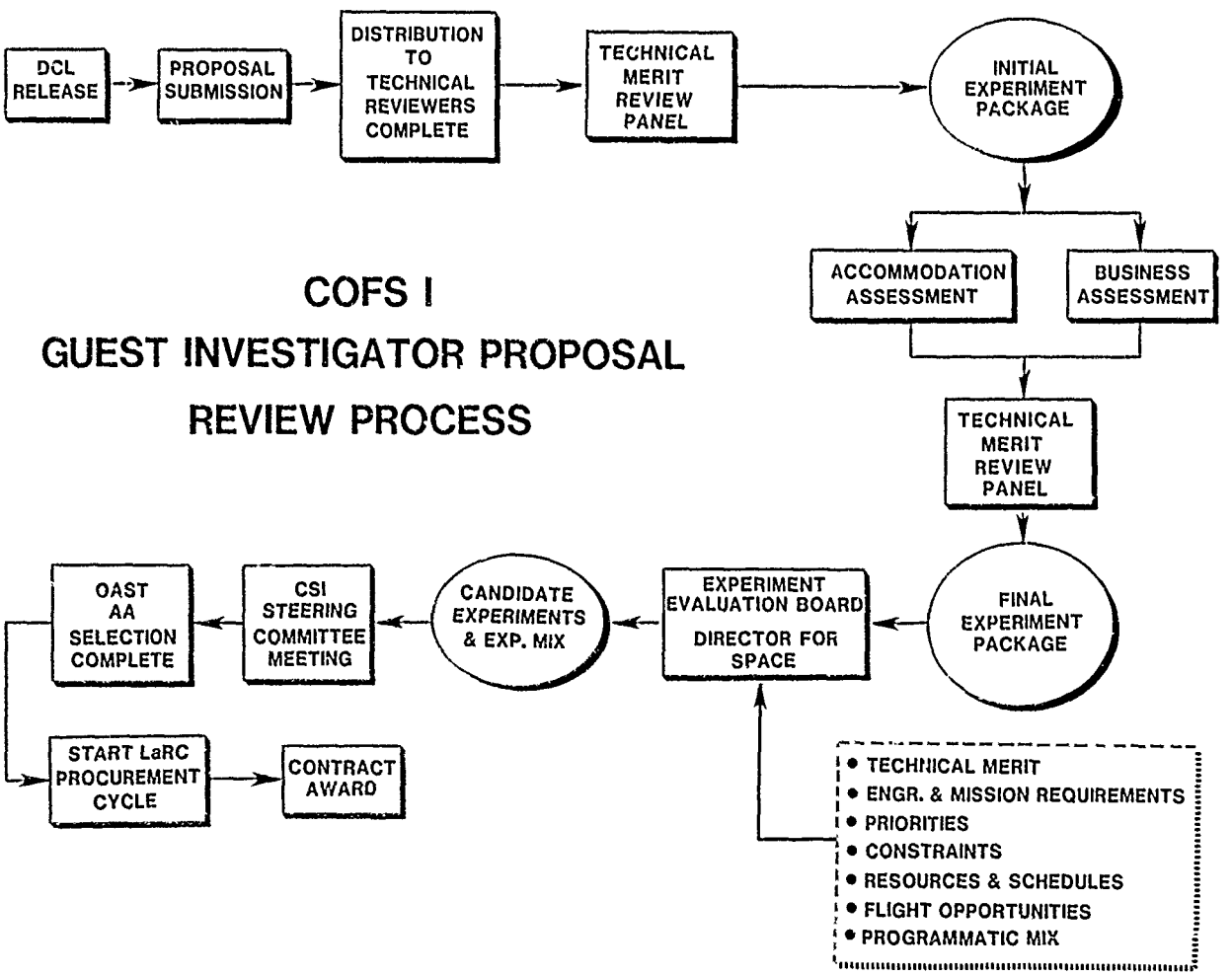

Figure 1

PANEL CHARTERS

The Charter of each panel is shown in figure 2. The Technical Merit Panel makes a technical evaluation of each proposal and assembles the best of the proposals into an integrated on-ground and on-orbit experiments package which best supports development and validation of Control/Structures Interaction (CSI) technology. The Technical Merit Panel reviews the output of the Accommodation Panel and Business Panel to insure the preservation of the integrity of the experiments package. The Accommodations Panel defines the hardware and software modifications that must be made to the Mast Flight Article in order to accommodate the proposed experiment. This Panel also establishes the feasibility of implementing these modifications and assesses the safety of each proposed experiment. The Business Panel establishes the validity of the experiment cost as presented by the proposer and the cost to NASA for implementing the experiment on the Mast Flight Article. This panel also evaluates the overall management plan presented by the proposer. The Experiments Evaluation Board reviews and approves the final experiments package recommended by the Technical Merit Panel and makes a recommendation for selection to NASA Headquarters.

- TECHNICAL MERIT PANEL
  - o EVALUATE PROPOSALS AND ESTABLISH THE TECHNICAL MERITS OF EACH
  - o RECOMMEND A PACKAGE OF PROPOSALS WHICH BEST SUPPORTS CSI TECHNOLOGY ADVANCEMENT
  - o REVIEW AND APPROVE CHANGES MADE TO THE RECOMMENDED PACKAGE BY THE ACCOMMODATIONS OR BUSINESS PANELS
- ACCOMMODATIONS PANEL
  - o DEFINE FLIGHT ARTICLE H/W AND S/W MODIFICATIONS OR DEVELOPMENTS REQUIRED FOR IMPLEMENTATION
  - o DECIDE ON FEASIBILITY OF THESE H/W AND S/W MODIFICATIONS OR DEVELOPMENTS
  - o ASSESS SAFETY OF THE PROPOSED EXPERIMENT
- BUSINESS PANEL
  - o INDEPENDENTLY ESTIMATE EXPERIMENT COST AS PROPOSED BY THE GI
  - o ESTIMATE COST OF FLIGHT ARTICLE H/W AND S/W MODIFICATIONS OR DEVELOPMENTS REQUIRED FOR NASA IMPLEMENTATION
  - o ASSESS MANAGEMENT PLAN AND INSTITUTIONAL SUPPORT
- EXPERIMENT EVALUATION BOARD
  - o REVIEW AND APPROVE THE EXPERIMENTS PACKAGE RECOMMENDED BY THE TECHNICAL MERIT PANEL
  - o MAKE RECOMMENDATIONS FOR SELECTION TO NASA HEADQUARTERS

Figure 2

STRAW-MAN LIST OF TYPES OF EXPERIMENTS

A list of potential experiment categories is presented in figure 3. Each category is defined below.

1. Deployment Kinematics and Dynamics - Prediction of beam kinematics, loads, strains, and deflections that occur during on-orbit deployment and retraction.
2. Static Linearity of Deployed Beam - Development of a sensor system for measurement of straightness of deployed beam on-orbit. Prediction of precision of straightness of deployed beam and variation of precision after disturbance.
3. Structural Characterization
   a) Design of excitation algorithms for use on-orbit for purposes of exciting the structure to produce dynamic response data containing the desired characterization information.
   b) Design of identification algorithms for use on-ground, post-flight for purposes of extracting the structural characteristics from dynamic response data taken on-orbit.
   c) Design of identification algorithms which reside in the flight article computer and are used open-loop, on-orbit to extract structural characteristics from dynamic response data.
4. Control Law Evaluation
   a) Design of non-distributed control algorithms using collocated sensors and actuators for purposes of on-orbit, real-time, disturbance suppression.
   b) Design of distributed control algorithms using non-collocated sensors and actuators for purposes of on-orbit, real-time, disturbance suppression.
   c) Design of adaptive control algorithms for use on-orbit which automatically adjust for such things as sensor/actuator failures, and changes in structural characteristics.
5. Hardware Development - Development of sensors, active actuators, passive dampers, structural members, etc. for on-orbit evaluation.
6. Other - Review of the proposals may define additional categories.

- DEPLOYMENT KINEMATICS AND DYNAMICS
- STATIC LINEARITY OF DEPLOYED BEAM
- STRUCTURAL CHARACTERIZATION
  - o EXCITATION ALGORITHMS
  - o GROUND-BASED SYSTEM IDENTIFICATION
  - o ON-ORBIT, OPEN-LOOP, SYSTEM IDENTIFICATION
- CONTROL LAW EVALUATION
  - o COLLOCATED DISTURBANCE SUPPRESSION
  - o DISTRIBUTED CONTROL
  - o ADAPTIVE CONTROL
- HARDWARE DEVELOPMENT

Figure 3

DESIRED CONTENT OF EXPERIMENT PACKAGE

The COFS-I GI experiments package should be an integrated combination of on-ground and on-orbit experiments which best supports the development and validation of Controls/Structures/Interaction (CSI) technology. The package should include experiments from each of the previously discussed categories with emphasis on structural characterization experiments and control law evaluation experiments. Ground-based system identification is technically critical and relatively inexpensive since flight quality software is not required. Therefore, a large number of these ground-based system identification experiments is justified. Other structural characterization experiments and the control law evaluation experiments are technically critical also, but the number of these experiments which can be conducted on-orbit is limited by the on-orbit test time available and the cost of developing the associated flight software. Emphasis of these experiments can be achieved by initially selecting a relatively large number of investigations with subsequent competitive reduction to a relatively small number of investigations for actual on-orbit evaluation. Competitive reduction is achieved by ground-based performance evaluations using a high-fidelity simulation of the MAST flight article.

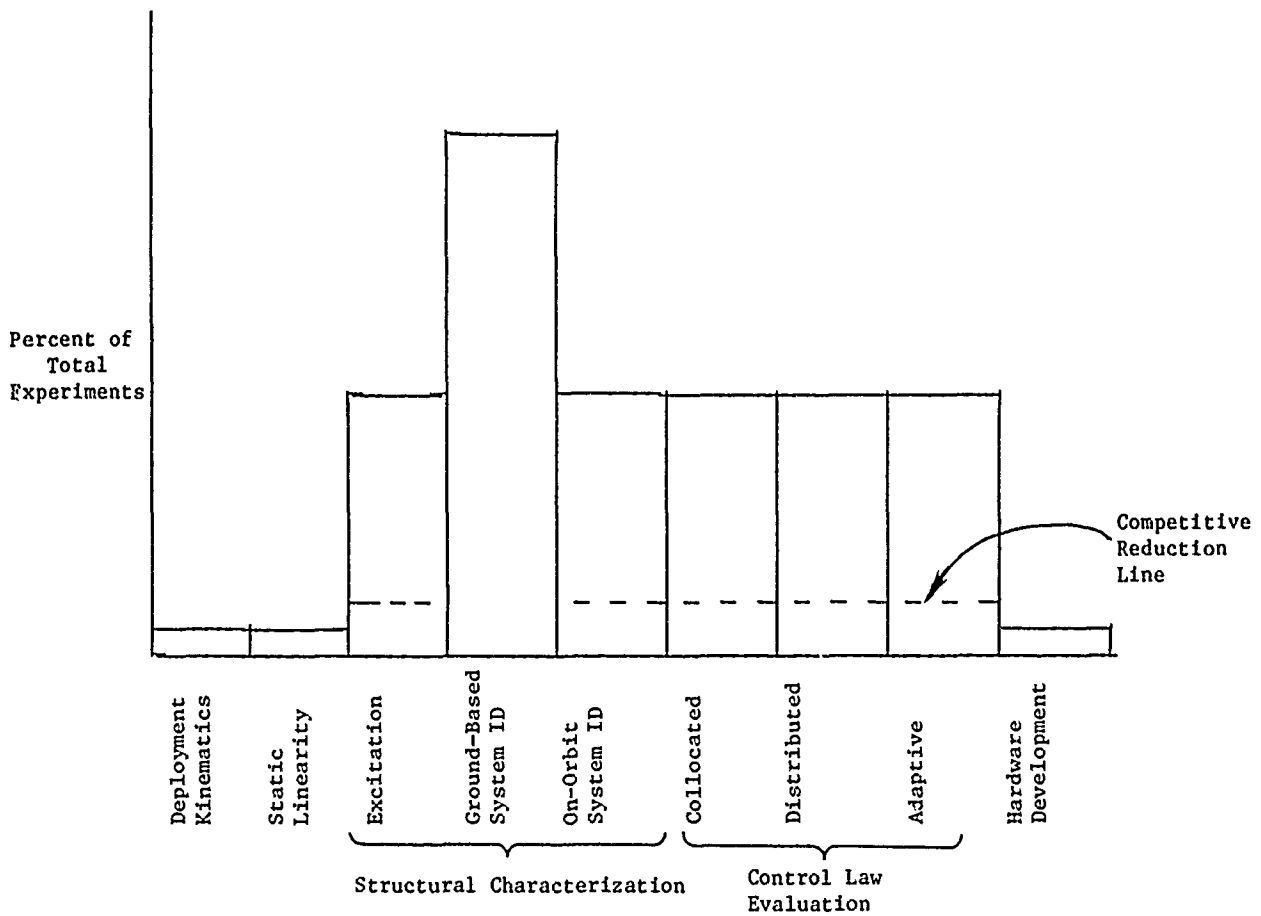

Figure 4

SCHEDULE OF GUEST INVESTIGATOR PARTICIPATION

Selection of guest investigators for negotiation will be made in early 1987 with contract and grants awarded by October 1987. Those guest investigators participating in the scaled model ground tests will have to define their test requirements by February 1988 so that timely preparation for their participation can be made by NASA. Likewise, participants in the flight article ground tests will have to submit their requirements by March 1988. Guest investigators developing algorithms for use on-orbit must submit a preliminary design by June 1988, coded in Fortran, for competitive evaluation by NASA. Development of flight software will be initiated by NASA for the best of the on-orbit algorithms. Analysis of flight data will continue for approximately 1 year after the flight tests.

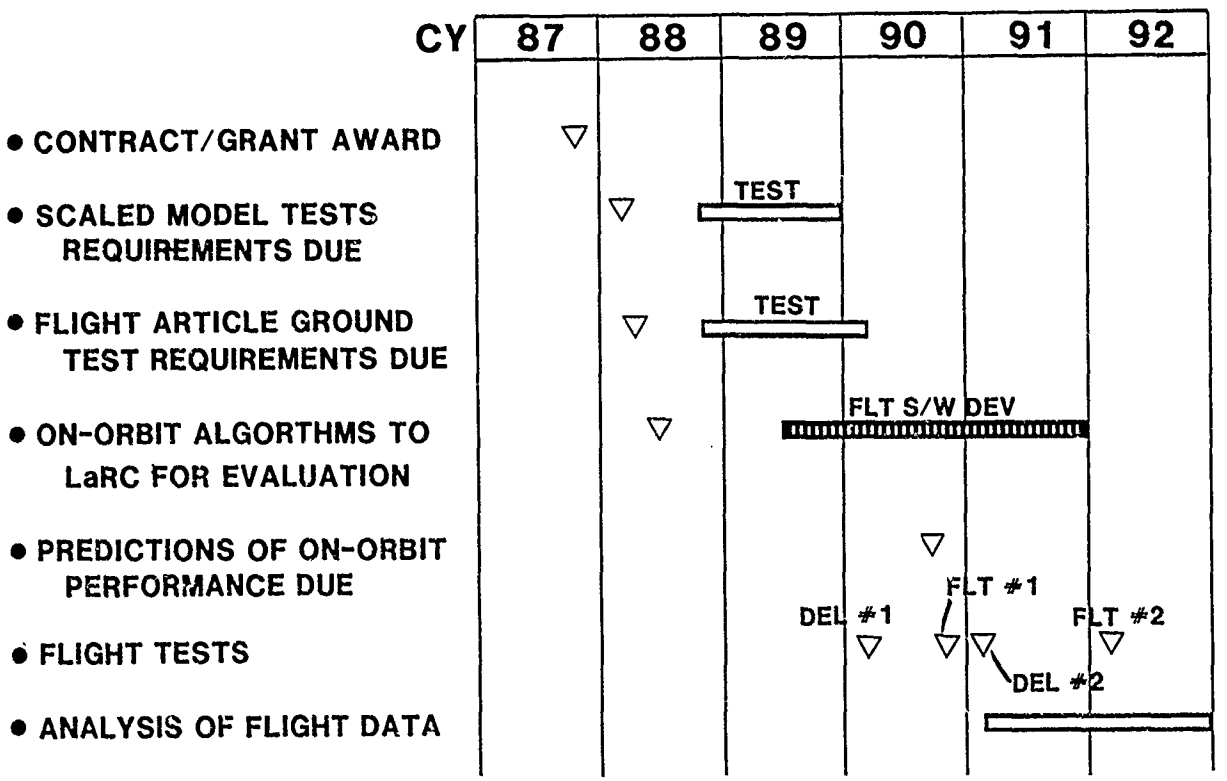

Figure 5

COFS II
3-D DYNAMICS AND CONTROLS TECHNOLOGY

Jon S. Pyle
Dr. Raymond Montgomery
NASA Langley Research Center
Hampton, Virginia

First NASA/DOD CSI Technology Conference
Norfolk, Virginia
November 18-21, 1986

INTRODUCTION

NASA has initiated a program to focus the development of Controls/Structures Interaction (CSI) technologies for the next generation of large, flexible spacecraft. This program, called "Control Of Flexible Structures (COFS)", will address critical technologies in the areas of structural dynamics and controls through comprehensive ground and flight testing of the fundamental elements of large, flexible space structures. The COFS program is a series of projects with the objective of developing a validated CSI technology data base for the suppression of inherent dynamic responses and avoidance of the undesirable interaction between flexible structures and controls in these spacecraft. The following paper discusses the current development plans for the second in this series of projects, COFS II, Three-Dimensional Dynamics and Controls.

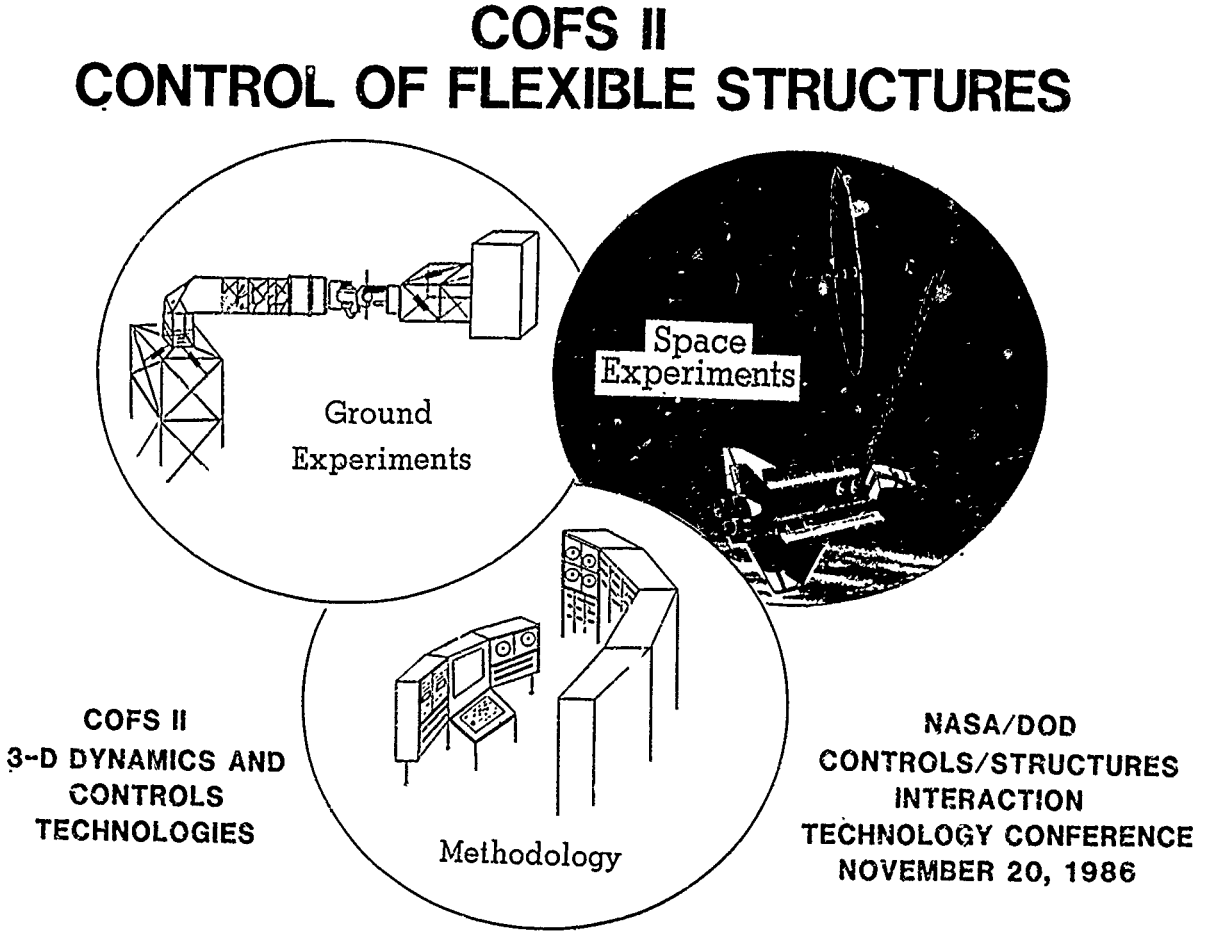

PROJECT OBJECTIVES

COFS II is the natural extension of the beam dynamics and controls experiments undertaken in the initial project of the COFS program and will advance the technology data base into the areas of three-dimensional, multibody configurations. The COFS II project will build on the ground and flight technologies developed in COFS I and will improve on the development of a multi-input/output control system for the suppression of undesired disturbances in these large, flexible spacecraft. Specifically, COFS II will evaluate prediction techniques used to define the dynamic and control characteristics of space structures through a comparison of theoretical, ground test and on-orbit test data. The project will develop advanced control techniques and on-orbit validation procedures which will lead to optimized spacecraft performance in minimal on-orbit test time. The COFS II project involves the space structures and controls community from universities, industry and government through a formal Guest Investigator Program in which researchers are selected to participate in all program activity phases.

- **DEVELOP AND EVALUATE THE METHODOLOGIES INVOLVED IN MODELING AND CONTROLLING LARGE, FLEXIBLE, 3-D STRUCTURES IN SPACE**

COFS WORKSHOP RESULTS

A Controls/Structures Interaction (CSI) workshop was held at NASA Langley Research Center on August 27-28, 1985. The purpose of the workshop was to review the proposed COFS I, Beam Dynamics and Controls project, the COFS II, Three-Dimensional Dynamics and Control project and the methods of interacting the CSI community in the experimental phases of each of these projects.

Members of the CSI community made up of individuals from major universities, related industries and government research organizations were asked to define major technology deficiencies for the next generation of large space structures. Nine critical technology needs were identified which concentrated on the control of the dynamic interaction between the parts of a multibody space structure.

The workshop attendees were also asked to identify viable flight configurations which would provide the basis for critical technology development. Most panels agreed that the configuration which included multibody beams attached by gimbals to a "realistic antenna" would provide the capability for developing the major portion of the critical technologies.

- **DEFINED CRITICAL CONTROLS AND STRUCTURES TECHNOLOGY REQUIREMENTS FOR 3-D SPACE EXPERIMENTS**

- **IDENTIFIED 3-D CONFIGURATION FOR GROUND AND ON-ORBIT TESTING**

WORKSHOP CONFIGURATION/TECHNOLOGIES

The recommended workshop configuration shown in the figure was generated utilizing the COFS I Mast beam, a deployable boom attached to the tip of the Mast by means of a gimbal, and a real antenna attached to the boom by means of a gimbal. The boom modal characteristics should be capable of combining with the structural modes of the Mast to provide interactive modal characteristics of research interest. The antenna should have a mesh surface with the capability of changing the surface shape to improve the antenna performance.

The critical technology needs for the three-dimensional configuration are primarily related to the stabilization of the multibody structure and control of that structure during repositioning. The primary dynamic characterization of the flight system will provide the basis for developing control methodologies to stabilize the structure, minimize the dynamic disturbances caused by deployment, maneuvering and articulation of the secondary boom or antenna, and pointing the antenna at a prescribed location. The successful development and validation of these primary technologies will permit further development of adaptive control techniques for more complex configurations.

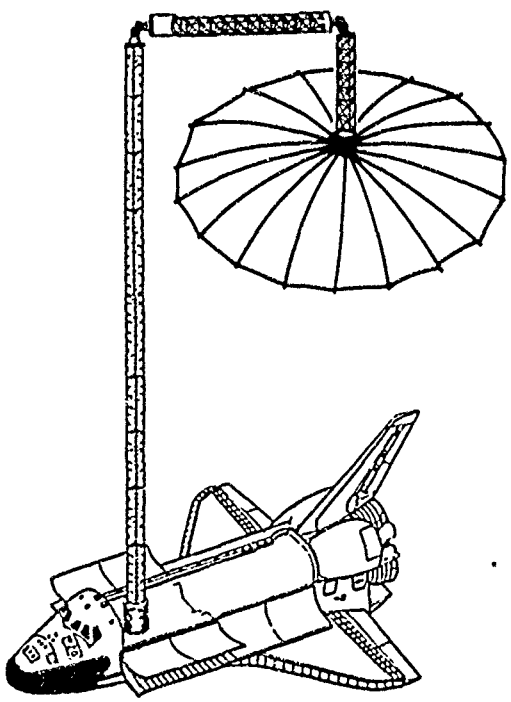

CRITICAL TECHNOLOGY NEEDS

- POINTING/AIMING
- ARTICULATION
- SLEWING
- SHAPE CONTROL
- MANEUVER LOAD
- ALIGNMENT
- SYSTEMS IDENTIFICATION
- STRUCTURAL EVALUATION
- DEPLOYMENT CHARACTERIZATION
- VIBRATION CONTROL
- ADAPTIVE CONTROL

COFS II CONFIGURATION COST OPTIONS

Estimates of the COFS II project costs were completed for various types of large, flexible, three-dimensional configurations which would satisfy the critical technology recommendation of the workshop. The results of this exercise are shown on the figure with increasing project costs as the vertical axis and increasing technology return as the horizontal axis. The COFS I project, Beam Dynamics and Control, was shown as a bench mark of the relative project development costs. Obviously, as the number of technologies and the complexity of the configuration increases, the project costs also increase. The workshop configuration provides the full development and validation of the primary technologies; however, the very high design, fabrication and development test costs for this concept preclude its utilization as the government proposed configuration. However, most of the technologies can be developed and validated through the testing of a simplified version of the workshop configuration pictured in the figure.

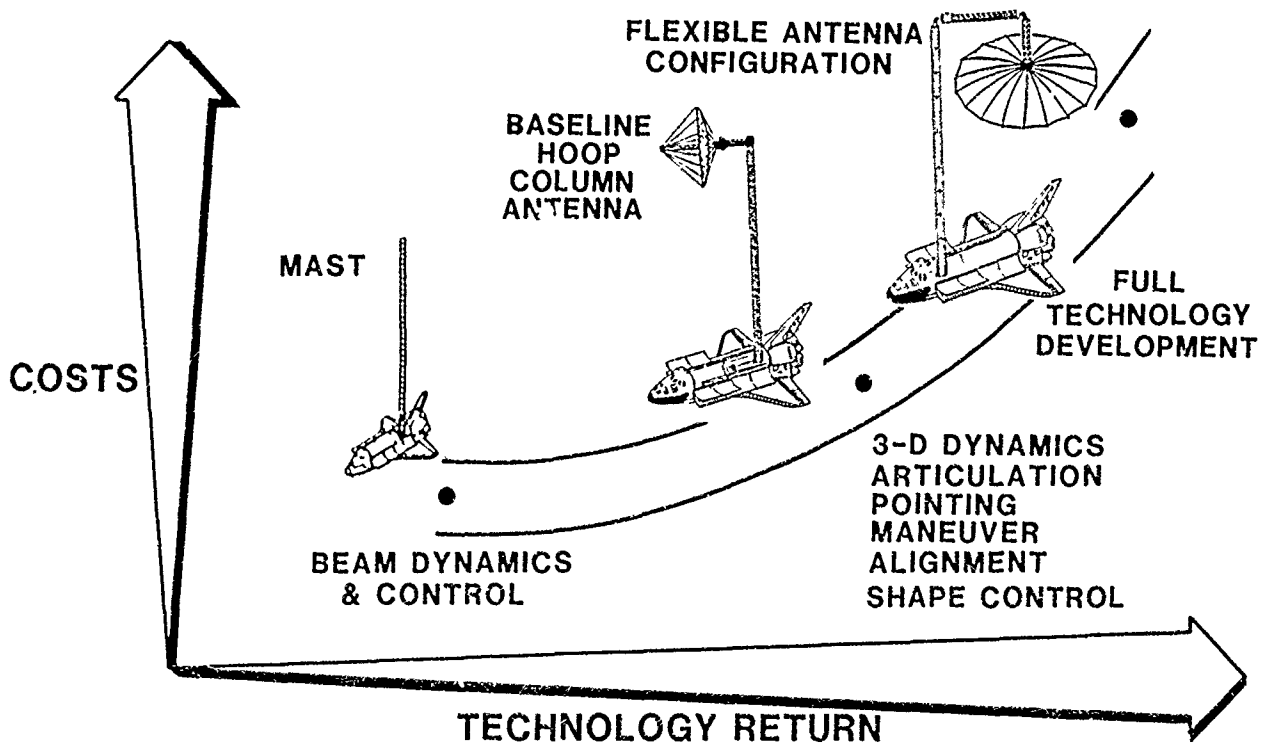

COFS II BASELINE CONFIGURATION

The simplified version of the workshop configuration shown in the previous figure is presented here as an artist's rendition. This concept includes the NASA Langley Research Center designed and developed hoop-column antenna attached to the tip of the COFS I Mast by means of a two-degree-of-freedom gimbal assembly. This concept was utilized as the study configuration for an in-house engineering analysis to determine the feasibility of attaching a realistic antenna to the Mast and to estimate the relative cost of accomplishing the desired technology development program. The antenna will be stowed in a separate canister in the shuttle bay and will be removed by the Mast during its deployment. The antenna will be deployed on command when the Mast reaches adequate height to eliminate interference with the shuttle doors and characterization of the flight system dynamics will be initiated. On-orbit validation of previously developed control algorithms will commence and will continue at various deflections of the antenna and at various beam heights. Upon completion of the flight tests, the antenna and Mast will be restowed into their respective canisters for the landing phase of the mission. Upgrading of the predicted COFS II structural characteristics based on the on-orbit test data will provide the confidence for developing and validating adaptive control techniques to be tested on the second flight of this configuration.

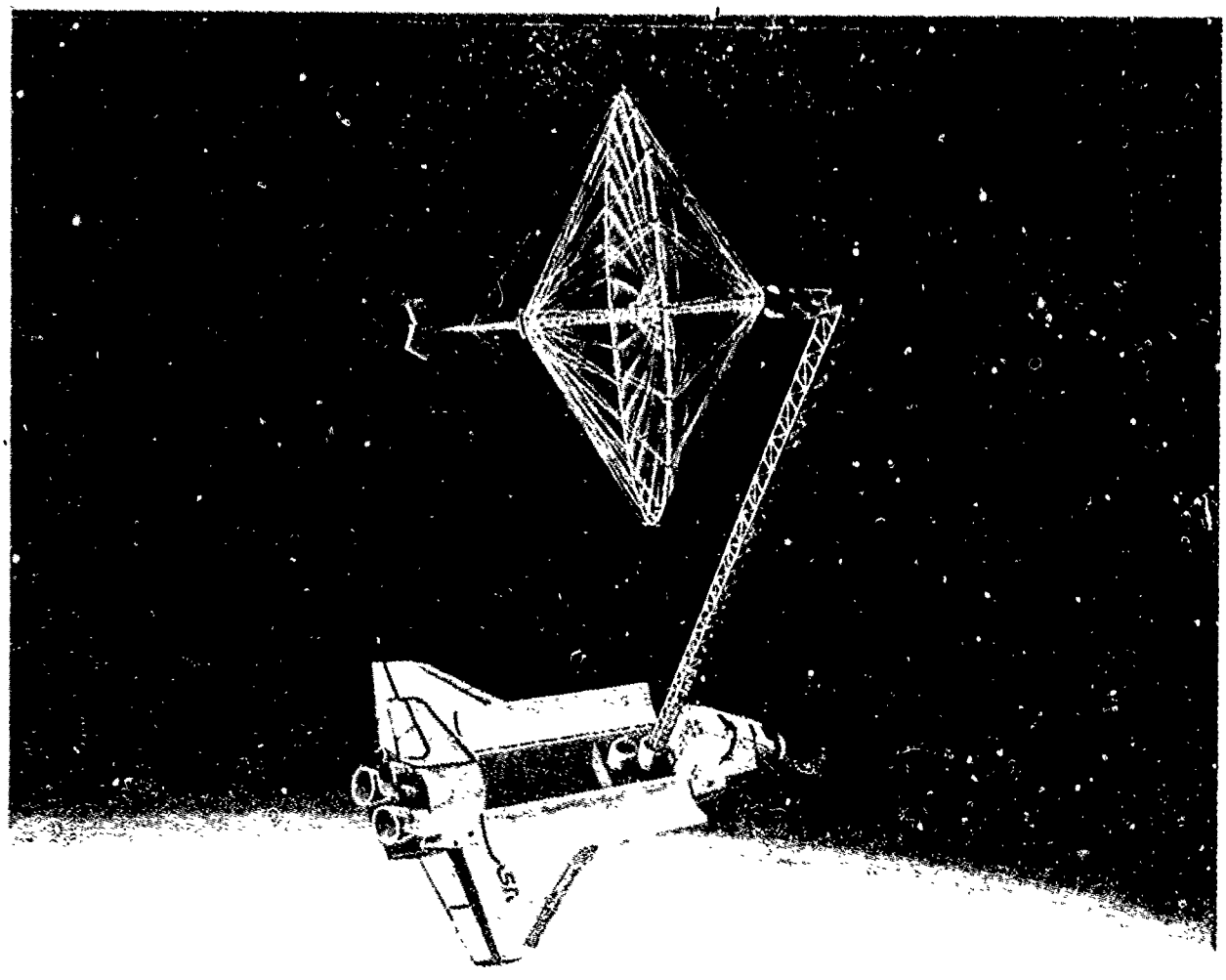

HYBRID TEST APPROACH

A major contribution of the COFS II project will be the development and validation of a hybrid test technique for the ground testing of very large, flexible, 3-D space structures. The structural characterization of the flight system will be accomplished by combining the smaller hardware components such as the baseline adapter and two-degree-of-freedom gimbal with analytical simulations of the Mast and hoop-column antenna. This hybrid system will simulate the actual flight system and provide the capability to validate experimental control algorithms, verify new control synthesis techniques, and to develop adaptive control concepts. The establishment of this testing technique through the COFS II project will be highly instrumental in the ground validation and on-orbit success of future spacecraft missions.

DEFINITION: HYBRID SYSTEM - COMBINATION OF REAL HARDWARE AND COMPUTER SIMULATION OF LARGE COMPONENTS AND/OR SUBASSEMBLIES

APPROACH:

- ACCOMPLISH LARGE COMPONENT & SUBASSEMBLY GROUND TESTS
- DEVELOP COMPUTER SIMULATION OF COMPONENTS AND/OR SUBASSEMBLIES
- COMBINE SMALL COMPONENT HARDWARE WITH COMPUTER SIMULATIONS OF LARGE HARDWARE TO CREATE FLIGHT SYSTEM SIMULATOR
- UTILIZE FLIGHT SYSTEM SIMULATOR TO VERIFY CONTROL ALGORITHMS

TEST OBJECTIVES:

- DETERMINE DYNAMIC AND CONTROL CHARACTERISTICS OF COUPLED SYSTEM AND COMPARE TO FLT SYS PREDICTIONS
- VERIFY GI CONTROL ALGORITHMS ON FLIGHT SYSTEM
- VALIDATE HYBRID TEST APPROACH FOR LARGE SPACE STRUCTURES

COFS II HYBRID TEST METHOD

The development method for the COFS II hybrid test technique is depicted in the following figure. The structural characteristics of the very large pieces of the COFS II flight system will be obtained from a combination of individual ground and/or on-orbit testing of these structures. Analytical simulations of these structures will be generated utilizing knowledge generated from basic Research and Technology development within the CSI community and in-house Langley expertise. These simulations of the large structures will be combined with the smaller articulation hardware to provide a combination of hardware and software which simulates the dynamic characteristics of the flight system in the on-orbit environment. The resultant high fidelity simulation should then provide the capability of verifying and validating developed control methodologies prior to actual flight validation.

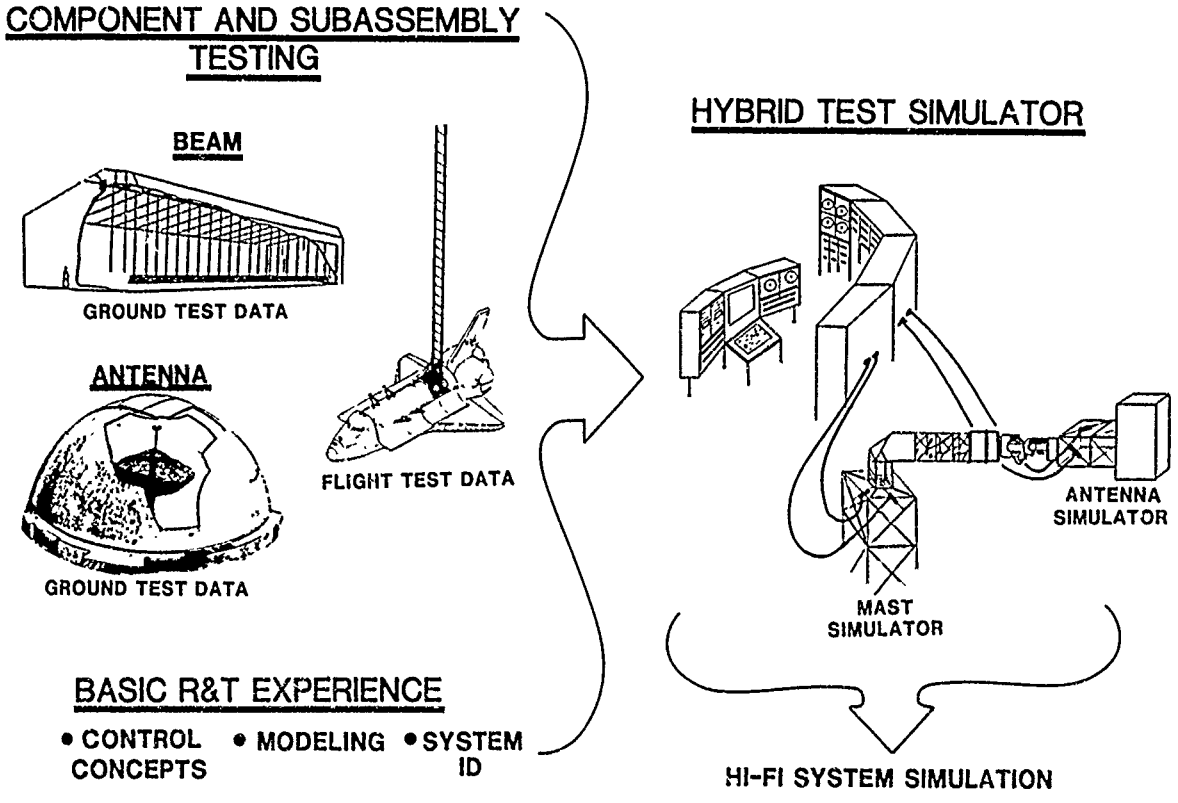

FLIGHT EXPERIMENT OBJECTIVES

The baseline COFS II configuration will provide the opportunity of developing a better understanding of the control/structural interaction characteristics of a multibody spacecraft in a zero-g environment. Techniques for evaluating deployment, structural dynamics, systems identification and possible procedures for fault detection, isolation and reorganization of sensor faults (FDIR) will be examined on the flight system during flight. Upon achieving a stable platform through alignment and vibration control, the gimbal will be used to articulate the antenna and examine pointing, slewing and articulation control algorithms previously developed and verified on the ground. Quasi-static shape control of one quadrant of the antenna will be demonstrated along with control at the hoop. Maneuver load control utilizing inputs from the shuttle will be developed and adaptive control techniques for the complex system will be evaluated. In addition, the flight results will be used to establish the viability of the hybrid testing techniques used in predicting on-orbit performance of a large, flexible, and complex structure.

- **DEVELOP AND VALIDATE ADVANCED CONTROL METHODOLOGIES ON A LARGE, 3-D FLEXIBLE STRUCTURE IN A ZERO-G ENVIRONMENT**
- **IDENTIFY AND CHARACTERIZE THE DYNAMICS OF A LARGE, 3-D FLEXIBLE STRUCTURE IN A ZERO-G ENVIRONMENT**
- **CORRELATE FLIGHT TEST RESULTS WITH GROUND TEST AND ANALYTICAL PREDICTION**
- **ESTABLISH VIABILITY OF HYBRID TESTING TECHNIQUES FOR PREDICTING ON-ORBIT PERFORMANCE OF LARGE, FLEXIBLE, AND COMPLEX SYSTEMS**

STRUCTURAL EVALUATION & SYSTEMS IDENTIFICATION

The individual technology development and validation approaches will be shown in the next series of figures. During the initial deployment of the flight experiment, its dynamic characteristics will be evaluated and compared to the predicted system characteristics generated from analytical models and the hybrid test system. This characterization will provide the validation of the predicted flight system dynamics and interaction and verify that the control algorithms developed on the ground will provide the damping and stabilization required for the flight experiments.

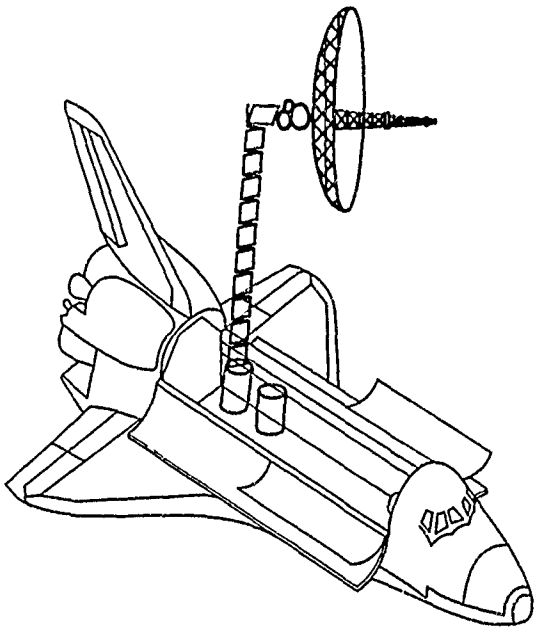

OBJECTIVES:

- CHARACTERIZE FLIGHT SYSTEM
- EVALUATE PREDICTION TECHNIQUES

APPROACH:

- DEPLOY BEAM & ANTENNA
- DETERMINE FLIGHT SYSTEM DYNAMIC CHARACTERISTICS
- COMPARE WITH GROUND RESULTS & ANALYTICAL PREDICTIONS

ARTICULATION & POINTING TECHNOLOGIES

Two of the key control technologies requiring development and validation for the next generation large space structure are controlled articulation and highly accurate pointing of the antenna-like structure. Various techniques will be developed by the Guest Investigators which will stabilize the beam structure, articulate the antenna by the two-degree-of-freedom gimbal and point it in a prescribed location. The control algorithms generated for this purpose will be verified with the hybrid simulator and then validated on the flight system in orbit on the shuttle. The flight results will then be utilized to upgrade the control techniques to provide a more efficient method of articulation and pointing of the antenna surface.

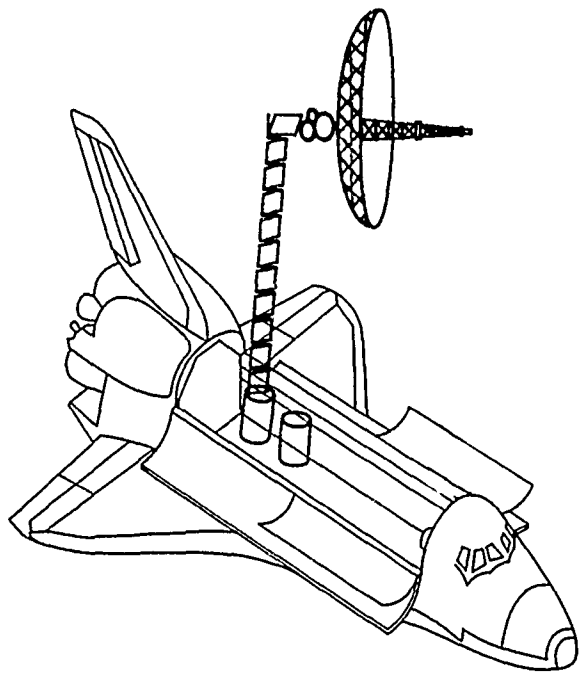

OBJECTIVES:

- DEVELOP ANTENNA ARTICULATION TECHNIQUES
- DEMONSTRATE STABLE POINTING WITH ANTENNA

APPROACH:

- SLEW ANTENNA WITH 2 DOF GIMBAL
- USE CONTROL ALGORITHMS TO STABILIZE FLIGHT STRUCTURE
- EVALUATE ANTENNA STABILITY & POINTING

SLEWING & MANEUVER LOAD CONTROL TECHNOLOGIES

When the COFS II flight system is fully deployed, it will extend between 30 and 60 meters from the shuttle bay with the tip of the antenna offset from the beam up to 20 meters. The beam, antenna and gimbal are subjected to a significant maneuver load during a sustained vernier reaction control system firing. The articulation of the antenna by the gimbal will also induce a slewing motion into the column support of the antenna and a torsional loading on the beam. Control techniques to alleviate these loads, dampen the disturbances caused by maneuver or slewing, and stabilize the flight system will be developed, verified through the ground hybrid simulator and validated on the baseline flight system during the on-orbit experimentation. These control methods will be further upgraded based on the on-orbit test results.

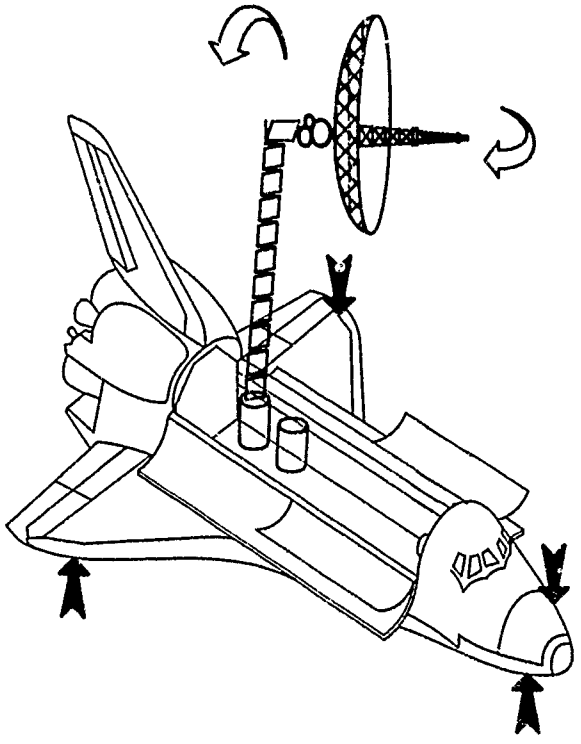

OBJECTIVES:

- ALLEVIATE SHUTTLE MANEUVER LOADS
- MINIMIZE DYNAMIC DISTURBANCES FROM INDUCED MOTION

APPROACH:

- CHANGE SHUTTLE ATTITUDE OR SLEW ANTENNA
- EVALUATE FLIGHT SYSTEM DYNAMICS
- USE CONTROL TECHNIQUES TO MINIMIZE DISTURBANCES

SHAPE CONTROL & ALIGNMENT TECHNOLOGIES

A means of determining the precise shape of the antenna surface mesh is required in order to improve the efficiency of very large, flexible antennas in space. The COFS II baseline configuration will provide the mechanism for controlling the surface shape of one quadrant of the antenna and the antenna hoop through individual actuators and sensors attached to the lanyards (hoop/surface mesh chords). Precise location of the surface mesh, the hoop and the beam structure that the antenna is attached to, will be attained through optical/digital sensors. Quasi-static control methodologies will be developed, verified and validated during the on-orbit testing of the baseline flight system. It is hoped to achieve total reshaping of one quadrant of the antenna within five minutes and to within 0.2 millimeters of a predetermined shape.

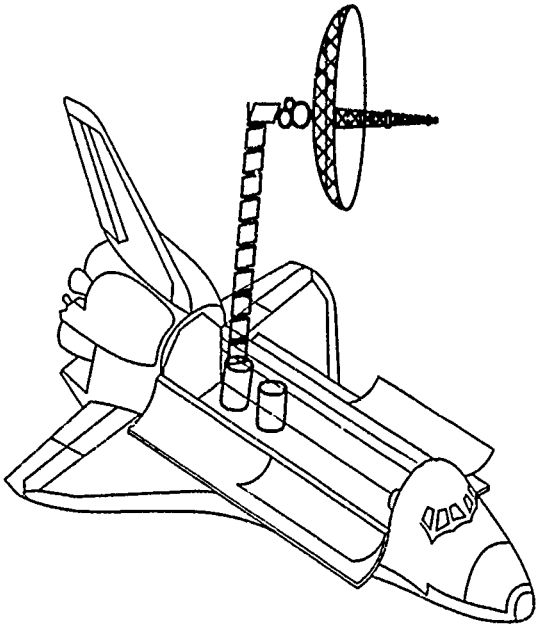

OBJECTIVES:

- DEVELOP PRECISE BEAM ALIGNMENT & CONTROL TECHNIQUES
- IMPROVE ANTENNA EFFICIENCY THROUGH CONTROL OF SURFACE MESH

APPROACH:

- STABILIZE BEAM AND ANTENNA STRUCTURE
- ALIGN HOOP & ANTENNA CENTER COLUMN
- DETERMINE SURACE MESH LOCATION
- ADJUST MESH TO OPTIMIZE SHAPE

FAULT DETECTION, ISOLATION AND REORGANIZATION TECHNOLOGY

In order to account for sensor/actuator malfunctions during long periods of space utilization of these very large structures, methods must be developed to reorganize the sensors and actuators such that alternate control techniques can be applied to manipulate or stabilize the structures. The COFS II baseline sensors and actuators will have the capability of being utilized in various groupings in order to understand and develop the techniques required to verify the FDIR technology. Simulated malfunctions of sensors/alternators will be achieved by ignoring signals from selected sensors or actuator and reorganizing the information to perform a specific control function during the flight test experimentation.

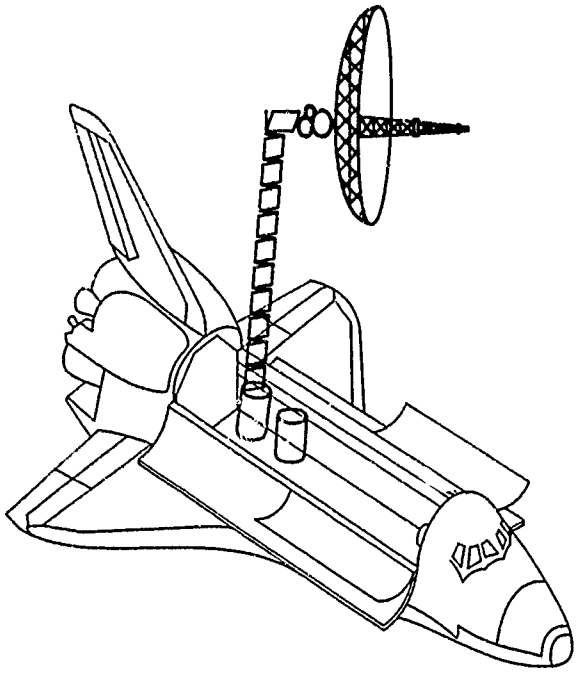

OBJECTIVES:

- DEVELOP FAULT DETECTION TECHNIQUES
- EVALUATE ISOLATION ALGORITHMS
- VALIDATE REORGANIZATION METHODS

APPROACH:

- SIMULATE AN EXPERIMENT SENSOR FAULT
- TEST SYSTEM TO ISOLATE FAULTY SENSOR
- DETERMINE ALTERNATE APPROACH TO MEASURE SYSTEM DYNAMICS
- REORGANIZE SENSOR INPUTS TO CONTINUE FLIGHT EXPERIMENT

ADAPTIVE CONTROL TECHNOLOGY

The goal of the controls community is to develop techniques which automatically compensate for all variations in the predicted characteristics of a large space structure, analyze the characteristics of dynamic inputs to the structure and eliminate vibrations, low frequency dynamics and any other destabilization factors. The COFS II baseline configuration will be utilized to evaluate preliminary concepts for adaptive controls which may lead to the anticipated goal. Control algorithms developed by the Guest Investigators will be verified on the hybrid simulator and validated on-orbit after previously discussed technologies have been fully developed and validated.

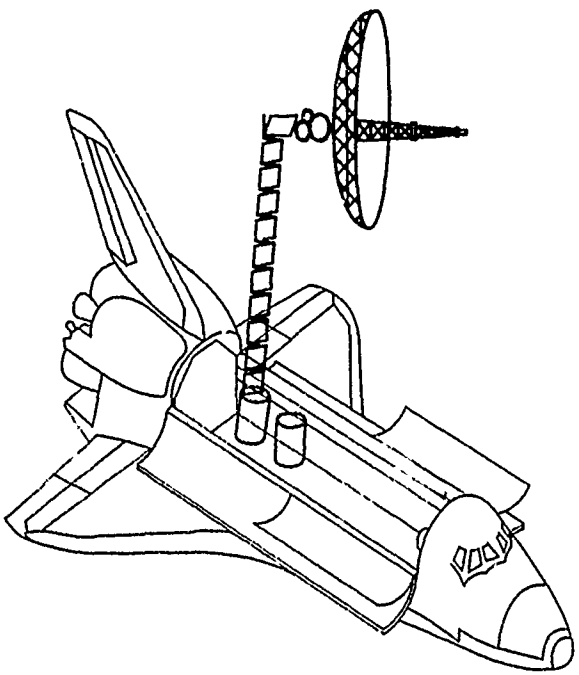

OBJECTIVES:

- ESTABLISH A CONTROL METHOD TO ACCOMMODATE VARIATIONS IN SYSTEM DYNAMICS AND UNCERTAINTIES IN SYSTEM PERFORMANCE

APPROACH:

- DEVELOP SYSTEM ANALYTICAL MODELS
- PREDICT SYSTEM PERFORMANCE
- DEVELOP CONTROL METHODS FOR REDUCING SYSTEM PERFORMANCE DEGRADATION
- VALIDATE ADAPTIVE CONTROL ALGORITHMS DURING FLIGHT

COFS II PROJECT SCHEDULE

The COFS II flight hardware development contract will be awarded early in 1989. This contract will include the design, fabrication, and testing of the flight hardware to be mounted in the shuttle bay for on-orbit testing and the prototype hardware required to construct the hybrid test system. A preliminary Request For Proposal (RFP) which identifies the primary technology goals, system specifications and specific project objectives will be released approximately 12 months prior to the official RFP. This will allow contractors adequate time to evaluate alternate hardware concepts which might provide equivalent or better technology return to the CSI community for the government investment. The current flight dates for the COFS II experiments are expected to occur in late 1993 and 1994.

The development of the hybrid simulator of the COFS II flight system will begin shortly after the award of the hardware development contract. Some of the large component and subassembly tests will be conducted within the Base R & T programs and the COFS I project prior to the initiation of the ground test task. The simulator will be constructed at NASA Langley and will be available to the hardware and software contractors and the Guest Investigators.

The software development contract will be awarded shortly after the hardware development contract and will provide the operational, baseline applications and Guest Investigator software development, the simulations of the large component dynamics to be used in the hybrid test system, and all required flight coding.

The Guest Investigator (GI) contracts will be initiated through the same procedures discussed for the COFS I project and will begin shortly after the award of the hardware development contract. Separate GI contracts will be awarded for each of the COFS II flights.

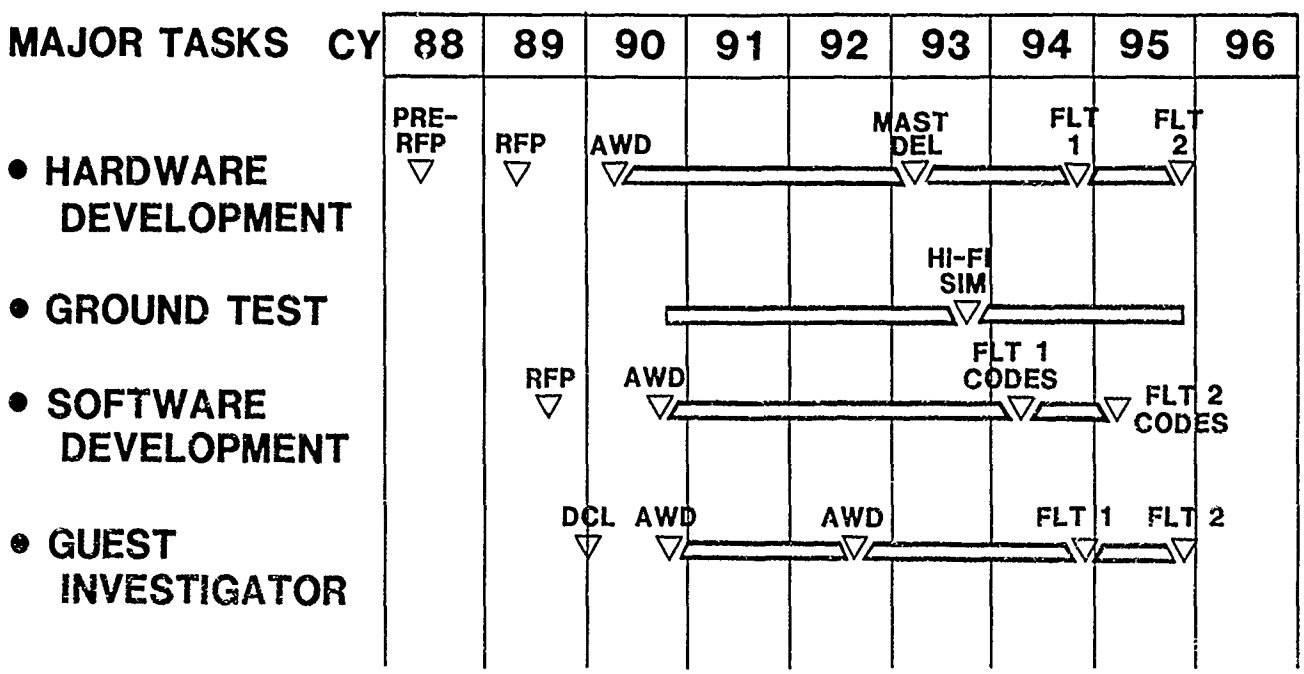

COFS II PROCUREMENT STRATEGY

The prime hardware system contractor will have the responsibility for delivering a totally integrated, operational, and flight safe system to the shuttle payload integration facility at KSC. The following options will be acceptable approaches for providing the required COFS II flight system:

(1) Baseline Configuration - The contractor will refurbish and modify the government furnished hoop-column antenna and attach it to the COFS I beam by means of a two-degree-of-freedom gimbal to provide the required technology development capability.

(2) Contractor Hardware - The contractor or a team of contractors may propose an alternate flight system utilizing contractor provided hardware which will satisfy the technical requirements of the COFS II project and provide at a minimum, equivalent technology development capability as the COFS II baseline configuration.

(3) Combined Contractor, Government Furnished Equipment - The contractor or team of contractors may propose an alternate flight system utilizing a combination of contractor provided flight hardware and government furnished equipment such as the hoop-column antenna or COFS I Mast. The resultant flight system must satisfy the technical requirements of the COFS II project and provide at the minimum, equivalent technology development capability as the COFS II baseline configuration.

The cost of options (2) or (3) must remain within the available contractual funding and funding profile or be cost shared by the contractor(s).

- **RFP WILL INCLUDE:**
  - **BASELINE REQUIREMENTS**
  - **FUNDING LIMITATION**
- **RFP WILL PERMIT BROAD INDUSTRY PARTICIPATION:**
  - **HOOP-COLUMN**
  - **ALTERNATIVE ANTENNA**
  - **OTHER COMPONENTS**

CONCLUDING REMARKS

The COFS II project is a complex and ambitious undertaking which will address several critical technology areas. Among them are modeling, structural dynamics, controls, and ground testing issues which are not only germane to this effort, but to other large space structure programs being contemplated. This effort requires the early integration of controls and structural dynamics considerations in order to achieve mission success. Several technology advances must be achieved in the areas of system modelling, control synthesis and methodology, sensor/actuator development, and ground testing techniques for system evaluation and on-orbit performance prediction and verification. This project offers a unique opportunity for the integration of several disciplines to produce technology advances which will benefit many future programs. In addition, the opportunities available to participate in the various levels in the phases of this project, e.g., analytical development and modelling, ground testing, and flight testing, permit for the involvement of a significant number of interested researchers and organizations from government, universities and industry.

- **OPPORTUNITIES FOR RESEARCH IN MANY DISCIPLINES**
- **SYNERGISTIC COMBINATION OF ANALYTICAL, GROUND & FLIGHT EXPERIMENT DEVELOPMENTS**
- **UNIQUE OPPORTUNITY FOR GUEST INVESTIGATOR PARTICIPATION AT ALL LEVELS**

COFS III
MULTIBODY DYNAMICS & CONTROL TECHNOLOGY

Robert Letchworth
Paul E. McGowan
NASA Langley Research Center
Hampton, Virginia

First NASA/DOD CSI Technology Conference
Norfolk, Virignia
November 18-21, 1986

INTRODUCTION

COFS III is the third project within the COFS program. It deals with developing multibody dynamics and control technology for large space structures. It differs from COFS I & II in two respects. First, it addresses a more complex class of structure, and second it is basically a scale model ground test and analysis program while COFS I & II feature shuttle flight experiments. The specific technology thrusts within COFS III are model sensitivities, test methods, analysis validation, systems identification, and vibration suppression.

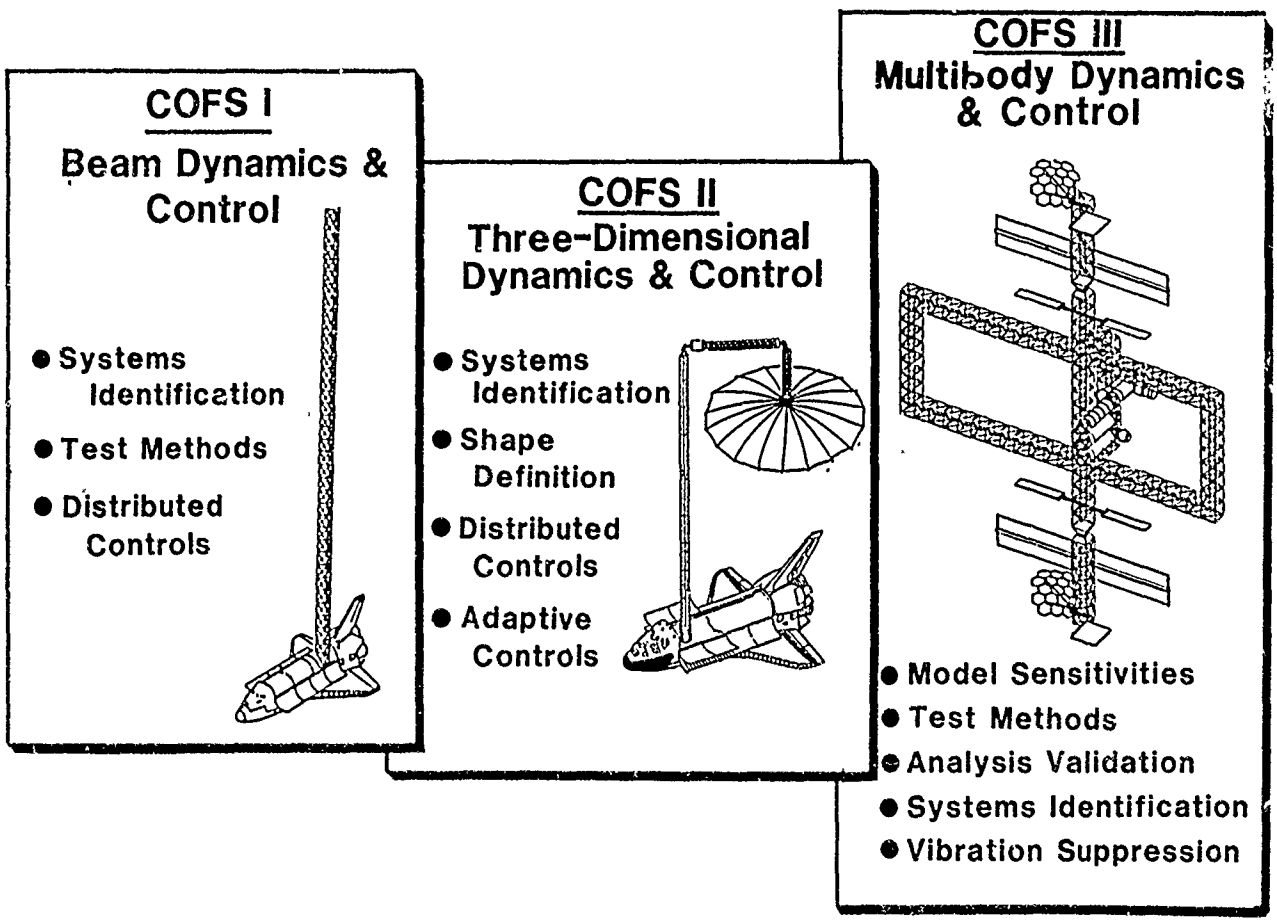

OBJECTIVE AND TECHNICAL APPROACH

The objective of COFS III is to develop a verified capability for predicting the structural dynamics behavior of multibodied, joint dominated articualted, flexible space structures, which are too large and heavy to be dynamically tested, when fully mated, in earth's one-g environment.

The technical approach for achieving this capability is to demonstrate that a combination of dynamically scaled model tests and theoretical analyses can provide a credible method for predicting the dynamics behavior of the full-scale structure and also provide a means for evaluating vibration control techniques.

OBJECTIVE:

- **VERIFIED CAPABILITY FOR STRUCTURAL DYNAMICS PREDICTION AND CONTROL OF**

LARGE MULTIBODIED, JOINT DOMINATED ARTICULATED, FLEXIBLE SPACE STRUCTURES

TECHNICAL APPROACH:

- **DYNAMICALLY SCALED MODEL TESTS**

PLUS

- **THEORETICAL DYNAMICS ANALYSIS**

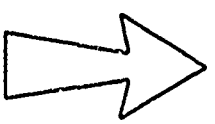

PREDICTION OF FULL-SCALE DYNAMICS & VIBRATION CONTROL

PROJECT FOCUS

COFS III is a multibody dynamics and control technology project which focuses on the Space Station structure. The Space Station was selected for several reasons. First, it is the first very large operational structure planned to be built in space. Second, it is typical of the structures of interest. Third, the Space Station will provide the first opportunity to obtain direct full-scale measurements for correlation with model tests and analysis, thereby providing for the validation of the COFS III objectives. Fourth, studying the dynamics of the Space Station is the first step in understanding and developing the technology for the growth Space Station, which is one of Langley's roles in the overall Space Station effort.

SPACE STATION

- REAL STRUCTURE
- TYPICAL OF STRUCTURES OF INTEREST
- FIRST OPPORTUNITY TO OBTAIN FULL-SCALE DATA FOR CORRELATION
  - GROUND TEST OF KEY SUBASSEMBLIES
  - ON-ORBIT FLIGHT DATA
- MEANS FOR DEVELOPING TECHNOLOGY FOR GROWTH STATION

PROPOSED LARGE SPACECRAFT LABORATORY (LSL)

This picture is an artist's conception of the COFS III model suspended in the proposed Large Spacecraft Laboratory (LSL) which will be constructed at Langley in 1988. It has been designed to provide the volume, dimensions, and suspension capabilities necessary to permit controlled ground tests of a variety of large space structures and models including the COFS III model. The dimensions of LSL are 310 ft in diameter at the base and 150 ft high.

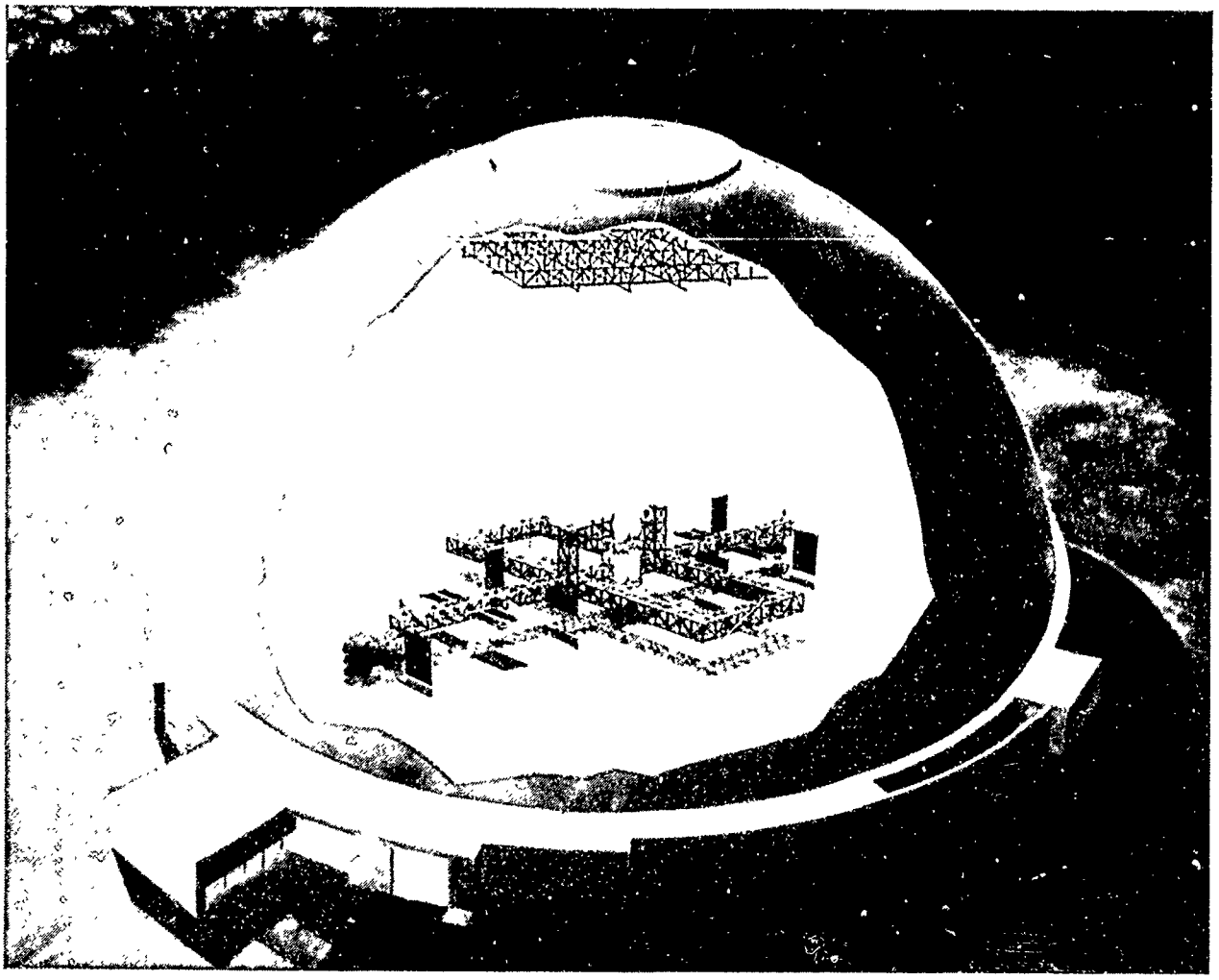

PROJECT ELEMENTS

The COFS III project elements include both contractual and in-house activities. The first contractual effort is the just-completed model definition study by Lockheed Missile and Space Company, the results of which will be added to this presentation when they are available. These results will also be used by the project office to help define the requirements for the development, fabrication, and assembly of a modular model of the Space Station. The term modular means that the model will be designed with interchangeable parts so that it can be assembled and tested in configurations identical to any of the potential Space Station assembly sequences. The contract will also require a system for suspending and testing the model within the LSL; a set of modular analytical models that will be capable of being combined to depict the structure at each stage of the Space Station assembly sequence; limited test support for model tests which will be conducted at Langley; and an option for designing and building the components required to convert the basic model into a growth configuration of Space Station. The request for proposal (RFP) for this competitive procurement is planned to be released in December with a contract award in August, 1987.

The remaining two contractual efforts, one for an active vibration suppression system and one for an advanced suspension system, will be pursued in parallel but a year or two behind the main contract.

The in-house activities include joint and member scaling and characterization studies and experiments, the actual testing and analysis of the model, and the data correlation among the test results, analysis, and full-scale on-orbit data.

CONTRACTURAL

- **MODEL DEFINITION STUDY (MAY 86)**
- **MODULAR MODEL OF SPACE STATION: DESIGN, BUILD, ASSEMBLY**
  - **BASIC SUSPENSION SYSTEM**
  - **MODULAR ANALYTICAL MODELS**
  - **LIMITED TEST SUPPORT**
  - **OPTION FOR DESIGN & BUILD OF EVOLUTIONARY SPACE STATION**

RFP: DEC 86

CONTRACT: AUG 87

- **VIBRATION SUPPRESSION**
- **ADVANCED SUSPENSION**

IN-HOUSE

- **JOINT & MEMBER SCALING/CHARACTERIZATION**
- **MODEL TESTING & ANALYSIS**
- **DATA CORRELATION**

RELATIONSHIP TO OTHER OAST ACTIVITIES

The schedule for the COFS III project shows the contract award in August 1987, the model delivery in January 1989, and the fully mated model tests beginning in May 1990 when LSL becomes operational. Component and subassembly testing will precede the fully mated model tests.

Superimposed above the schedule are those Research and Technology base activities that support COFS III, while the relevant COFS I & II activities are listed at the bottom.

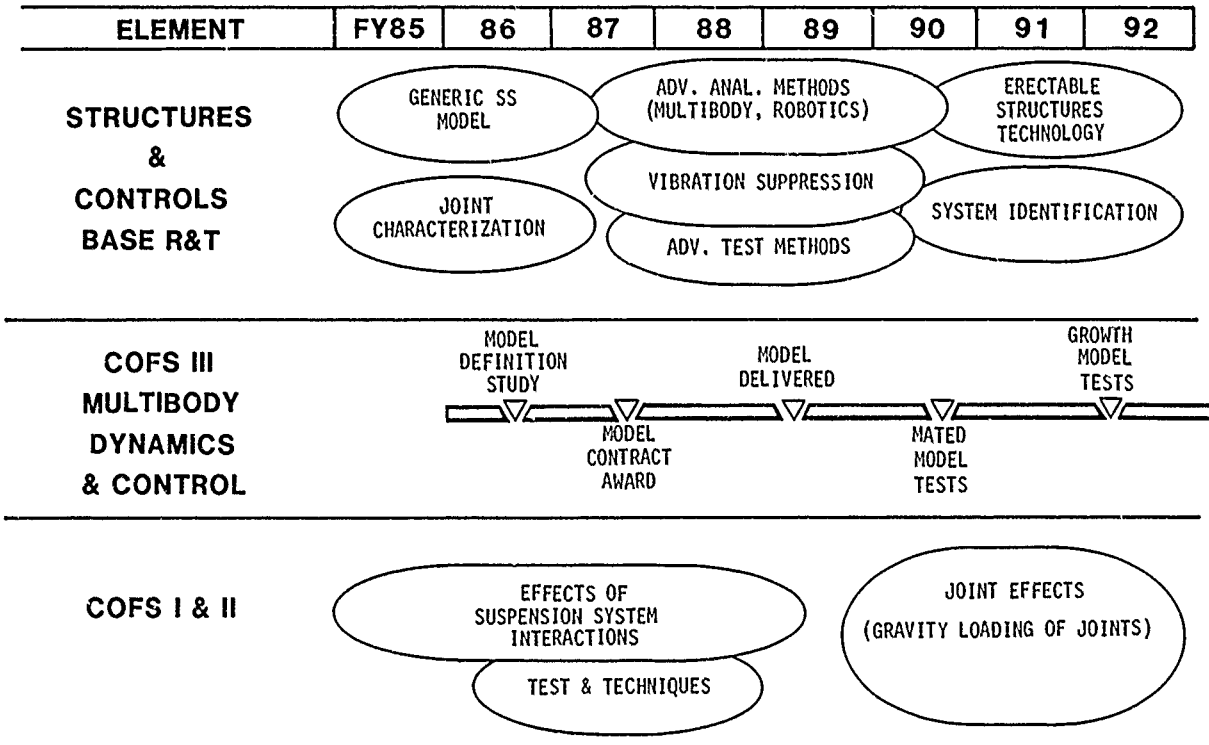

KEY TASKS

The key technical tasks required to complete the COFS III project are listed on this chart. First we must understand the sensitivities of the various model parameters in order to identify the best approaches for scaling the full-scale structure. Then, hopefully, we will be able to design and construct dynamically scaled models of both the IOC and growth configurations of the Space Station. The next step will be to conduct a comprehensive ground test and analysis program using the scaled model, the companion analytical models, and any active vibration suppression techniques developed for the model.

The final step is to validate the predictions, which were made via the analyses and model ground tests, with any full-scale subassembly ground tests that are conducted during Space Station development and with Space Station flight data when it is available.

Note that the instrumentation of the Space Station and the reduction of flight data will be provided by another activity. As a minimum, the instrumentation for the required on-orbit structural verfication of the Space Station should provide sufficient data to validate the primary COFS III objective.

- **EVALUATE MODELING SENSITIVITIES AND APPROACHES**
- **DESIGN AND CONSTRUCT A MODULAR SCALE MODEL OF SPACE STATION**
  - **ISS**
  - **GROWTH STATION**
- **CONDUCT A COMPREHENSIVE GROUND TEST AND ANALYSIS PROGRAM**
  - **ANALYSIS TOOLS**
  - **GROUND TEST METHODS**
  - **CONTROL METHODS**
- ***VALIDATE ANALYSIS VIA CORRELATIONS WITH GROUND TEST DATA AND SPACE STATION FLIGHT DATA**

* SPACE STATION FLIGHT INSTRUMENTATION AND FLIGHT DATA REDUCTION TO BE PERFORMED UNDER A SEPARATE ACTIVITY

TECHNICAL APPROACHES AND CHALLENGES

The two major challenges of this project are to (1) build as near a dynamics replica model of the full-scale structure as possible and (2) properly test the model. This chart lists four items that have a significant impact on these challenges. Each will be discussed in more detail.

- **MODEL DESCRIPTION**
- **SCALING CONSIDERATIONS**
- **ANALYSIS**
- **HARDWARE/GROUND TESTS**

DESIRED SCALE MODEL DESIGN FEATURES

This chart shows representative schematics of both the IOC and growth Space Station configurations and provides a summary description of the model using the IOC configuration shown as a baseline. The actual initial Space Station configuration is subject to change, however. In fact, as of this writing it is undergoing an extensive review. The exact configuration to be used for the COFS III model will be the one that will be identified at the Space Station System Design Requirements Review which is currently scheduled for December 1986. That configuration should be the baseline for the current configuration review.

IOC Space Station Concept

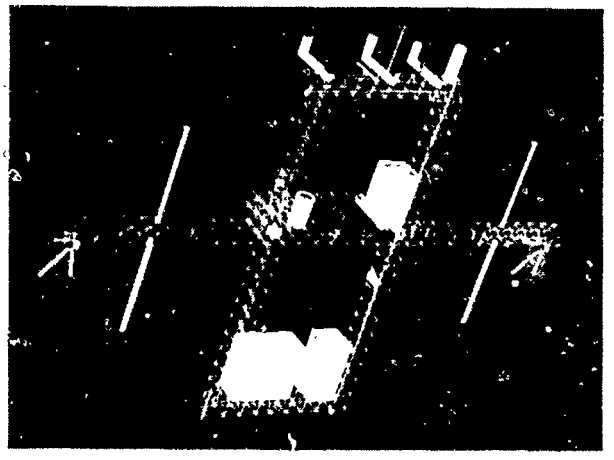

- Dynamically scaled model of 5m erectable dual-keel hybrid space station
- Modular construction for buildup stages
- Interchangeable elements
- Aluminum joints
- GR/EP structural members
- Articulating joints (manual)
- Payloads attach kinematically same as full scale

GROWTH

Growth Space Station Concept

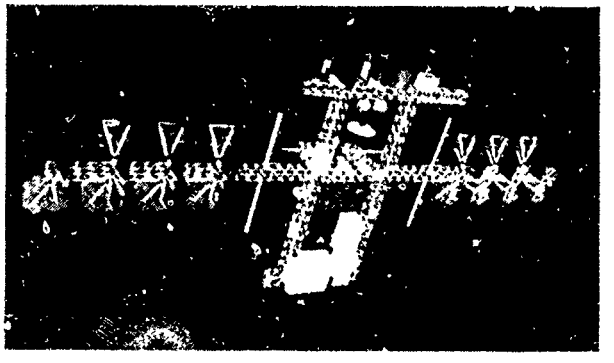

RATIONALE FOR USING DYNAMICALLY SCALED MODELS

The rationale for using dynamically scaled models to help predict the behavior of very large space structures is shown here. First, many of these structures are too large and heavy to be tested full scale. Second, the use of a model provides for a significant improvement in the analytical capability for the reasons shown. Third, in many instances the modeling of local flexibilities is overlooked when substructure synthesis methods are applied. This leads to errors or the failure to identify significant structural modes. Fourth, the model can uncover potential problems that can influence the design. Finally, the investigation of anticipated flight maneuvers and flight anomolies such as the degradation in performance from damaged, loose, or missing truss members can be accomplished.

- **MATED FULL-SCALE GROUND TESTS LIMITED BY GRAVITY & SIZE**
- **SIGNIFICANT IMPROVEMENTS IN ANALYSIS CAPABILITY POSSIBLE THROUGH:**
  - **HANDS-ON EXPERIENCE WITH REALISTIC HARDWARE**
  - **ACQUISITION OF MATED VEHICLE DATA PRIOR TO FLIGHT**
- **MODELING OF LOCAL FLEXIBILITIES OVERLOOKED IN SUBSTRUCTURES**
- **UNCOVER POTENTIAL PROBLEMS WHICH INFLUENCE DESIGN**
- **INVESTIGATION OF ANTICIPATED FLIGHT MANEUVERS AND FLIGHT ANOMALIES**

SCALE MODEL DEFINITION STUDY

A scale model definition study was initiated in May 1986 with Lockheed Missile and Space Company to help identify the scaling requirements for the COFS III model. The study was just completed in November 1986. Six key topics were addressed. First, an appropriate dual-keel hybrid Space Station configuration was selected as the baseline for the study. Second, the issue of replication versus simulation was investigated for each assembly phase, the IOC Space Station, the proposed SAVE flight experiment, and the growth Space Station. Third, the manufacturability of scaled joints and tubes was analyzed at a variety of scale factors. Fourth, the effects of a candidate model suspension system were investigated. Fifth, the impact of facility constraints was evaluated. And finally, the implications of expanding the model into a growth configuration were investigated. The results of these activities will be provided as soon as they are available.

- **STUDY TASK INITIATED MAY 86 WITH LOCKHEED MSC**

  TASK: ESTABLISH OPTIMUM MODEL SCALE FACTOR CONSIDERING THE FOLLOWING:

  - **DUAL-KEEL HYBRID SPACE STATION CONFIGURATION**
  - **REPLICATION VERSUS SIMULATION FOR:**
    - **ASSEMBLY PHASE**
    - **IOC**
    - **SAVE FLIGHT EXPERIMENT**
    - **GROWTH**
  - **COMPONENT MANUFACTURABILITY**
    - **JOINTS**
    - **TUBES**
  - **MODEL SUSPENSION EFFECTS**
  - **FACILITY**
    - **LIMITATIONS**
    - **AVAILABILITY**
  - **EVOLUTIONARY CONFIGURATION**

VARIATION OF REPLICA SCALING

The selection of the model scale factor is a trade-off since all properties scale differently. This chart shows some of these differences. The curves represent well known theoretically derived replica scaling laws. It is our initial belief that for the basic truss structure, replica scaling should be pursued to the maximum extent in order to eliminate as much uncertainty as possible. For replica scaling, accelerations and structural frequencies vary with the inverse of the scale factor, thus they increase with decreasing scale factor. On the other hand, displacements scale directly with the scale factor. Some quantities even vary over several orders of magnitude, thus small changes in scale factor can significantly alter these quantities.

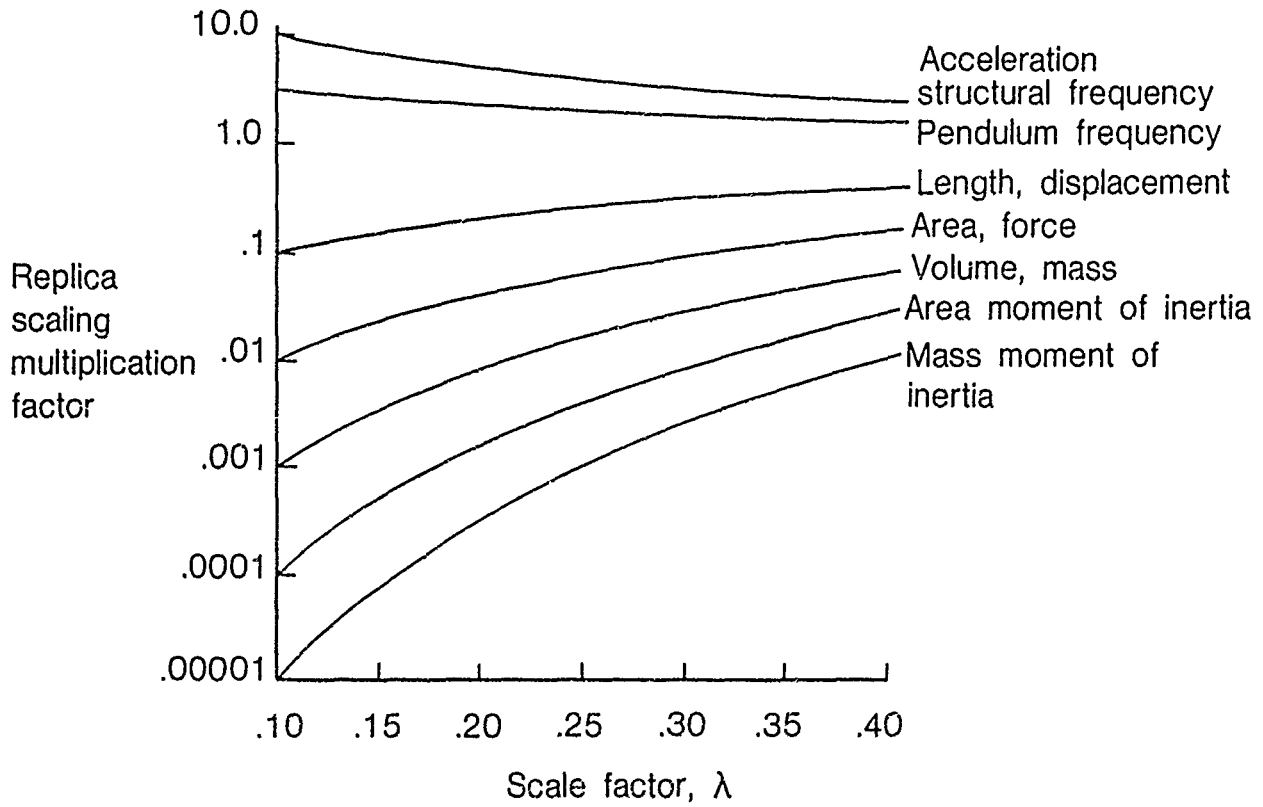

APPROXIMATE SCALE MODEL

Since the Space Station will be a large structure, sub-scale models of it will be large also. This chart shows the dimensions and weights of the dual-keel IOC configuration for scale factors from 1 to 1/4. Even a 1/4-scale model will be 155 ft x 90 ft x 29 ft which is about the size of a 727 aircraft.

APPROXIMATE SCALE MODEL SIZE & WEIGHT VS. SCALE FACTOR

Dimensions (ft.)

SCALE FACTOR	X	Y	Z	WEIGHT (KIPS)
1	115	621	361	547
1/2	57.5	310.5	180.5	68.4
1/3	38.3	207	120.3	20.3
1/4	28.8	155.3	90.3	8.5

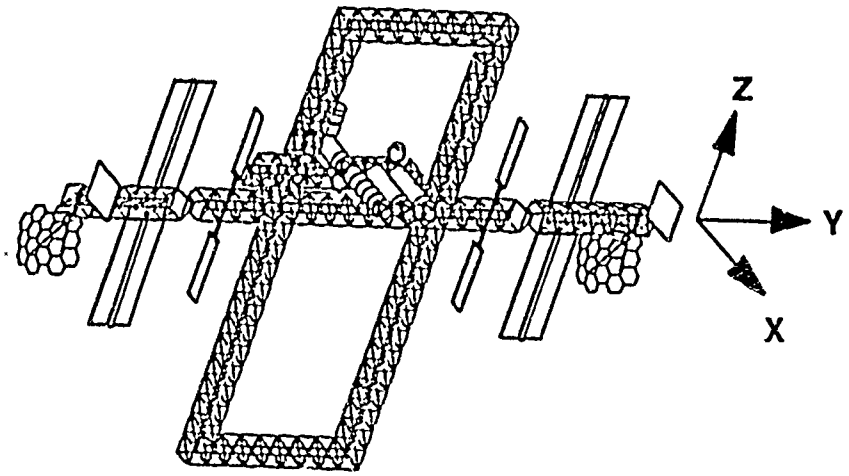

EFFECT OF SCALE FACTOR ON MODEL FREQUENCY

The size of the model test facility can also place constraints on the selection of the model scale factor. For example the LSL, which will be 310 ft in diameter at the base and 150 ft high at the center, must provide sufficient test volume and dimensions for not just the scale model but for the model and suspension system combination. In addition the suspension system should have cable lengths such that the ratio of the first model structural frequency over the suspension system pendulum frequency is a factor of 5 or greater. This minimum frequency ratio of 5 should insure adequate data quality thereby allowing the suspension system interactions to be more easily identified and removed from the test results. This boundary is shown by the vertical line on the lower figure. A scale factor of .25 is believed to be the minimum for replica scaling such that the components can be manufactured within the tolerances required while providing for their interchangeability. This boundary is also shown on the figure. Thus the upper right quadrant represents the solution space for the model, not considering test facility constraints. The diagonal line represents the constraints imposed by the LSL facility. Thus a 1/3-scale model is the largest COFS III scale model that could be tested in LSL and not violate the above constraints.

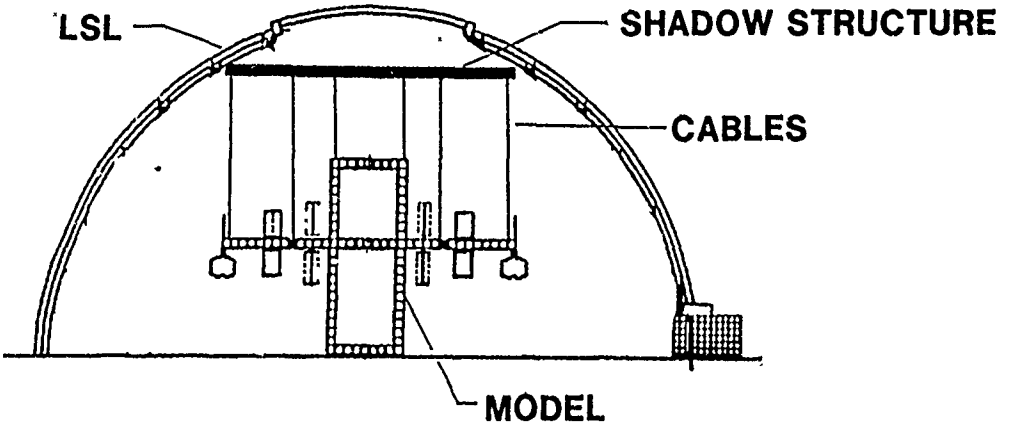

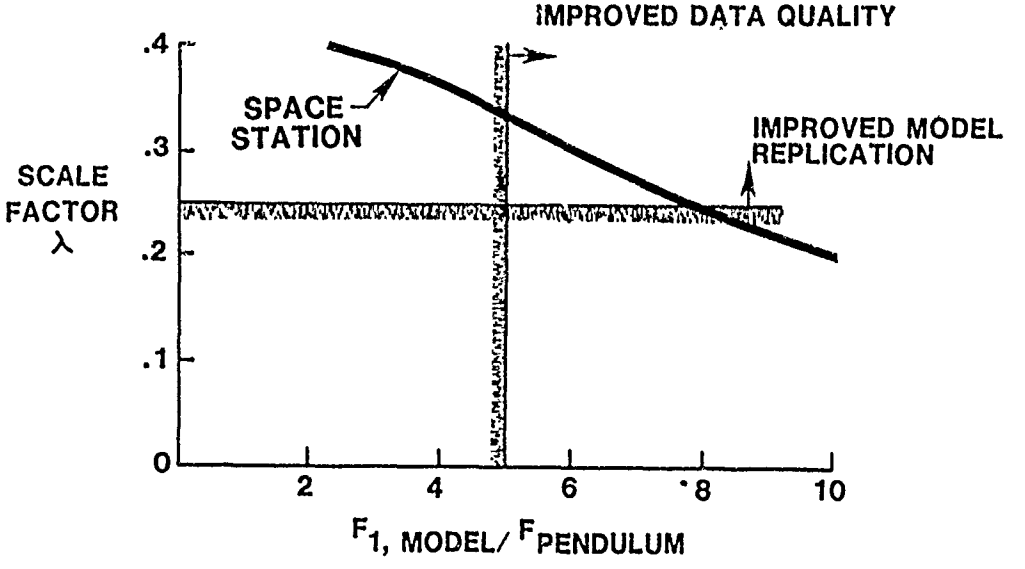

ANALYTICAL CHALLENGES

In the area of analysis, there are many challenges. Some are listed on this chart.

As was previously mentioned, the model contractor will provide modular analytical models which can be configured to represent both the model and full-scale station assembilies at each stage of the selected build-up process in space. The degree of model fidelity required for each stage will be different, with more emphasis on local effects being required in the early build-up stages while such detail may not be required for those stages approaching the fully mated configuration. How the joints will be characterized analytically is another challenge, as is the means for analytically accounting for nonlinear effects. Boundary conditions, earth conditions such as gravity effects and aerodynamic forces, and suspension system interactions created by a multiplicity of suspension cables pose unique analytical challenges. One of the main challenges will be the extrapolation of sub-scale results to credible full-scale predictions.

Some preliminary analyses and a few tests have been conducted to give some insight into these issues. These are presented next.

- **VARYING LEVELS OF ANALYTICAL MODEL FIDELITY REQUIRED FOR BUILD-UP STAGES**
- **JOINT CHARACTERIZATION**
- **NONLINEAR EFFECTS**
- **MODELING OF BOUNDARY CONDITIONS AND "EARTH CONDITIONS"**
- **SUSPENSION SYSTEM INTERACTIONS**
- **EXTRAPOLATION OF SUB-SCALE RESULTS TO FULL SCALE**

EFFECT OF JOINT AXIAL STIFFNESS

This chart shows analytically the effect of joint axial stiffness on the Space Station truss global frequencies. Specifically the variation in the truss frequency with the stiffness ratio is depicted. This stiffness ratio is the ratio of the axial stiffness of the strut to the axial stiffness of the joint. Note that for either small or large values of the stiffness ratio, the truss frequency is somewhat insensitive to small changes in this ratio; however, for intermediate values, small changes in the stiffness ratio can lead to large changes in the truss frequency. This implies the importance of accurately characterizing the joint stiffness. Typically for truss structures, the goal is to design the joint to have a stiffness ratio of approximately 2 or less so that the effective strut stiffness, including the joint, is as high as possible.

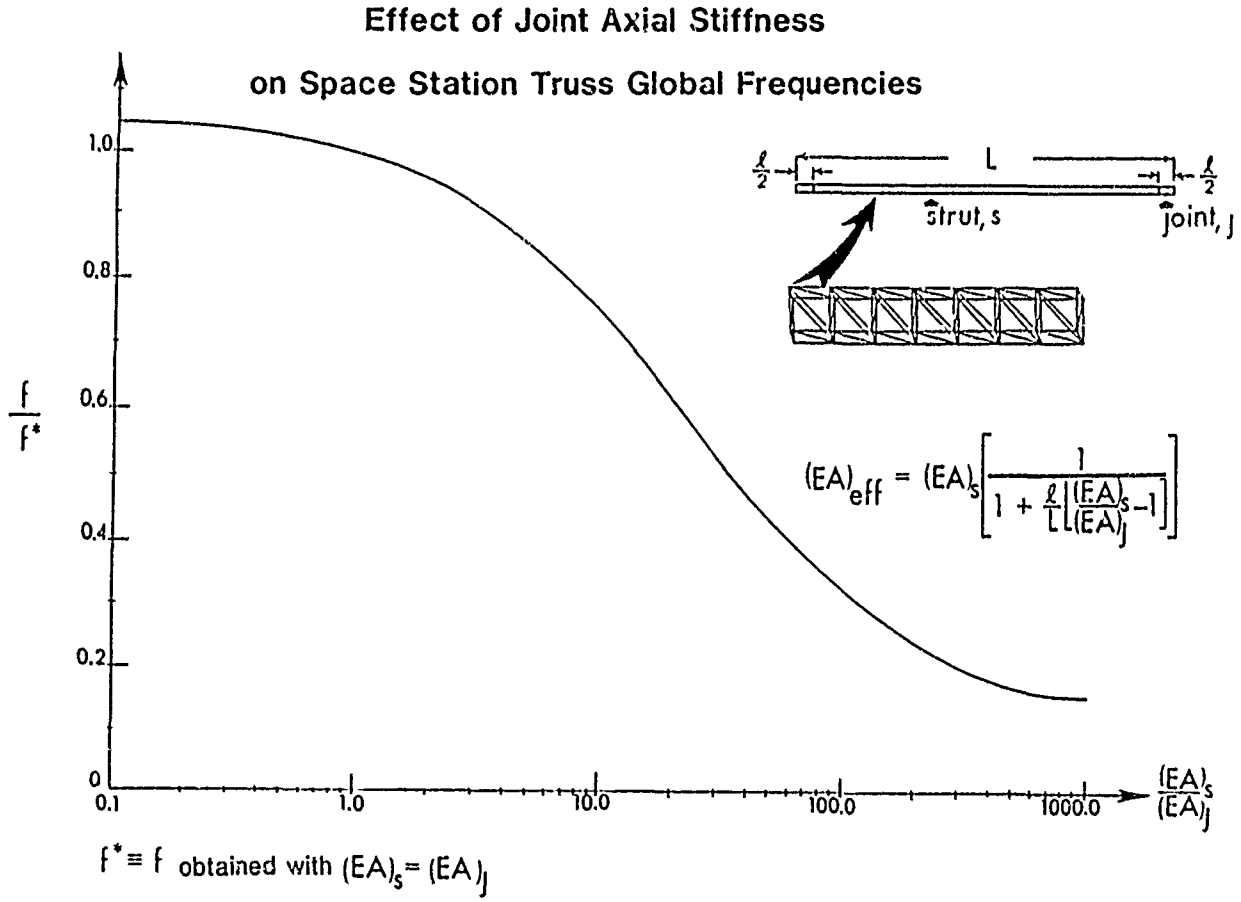

SUSPENSION SYSTEM CONSIDERATIONS

The suspension system will add an additional measure of complexity to the process of designing, testing, and analyzing the COFS III model. Some considerations for the suspension system are shown here. Since we plan to replicate the basic Space Station structure, the model will not be designed to sustain the unsupported 1-G loads of the payloads and modules. An implied requirement for the suspension system is that it should allow the model to be tested without masking the model dynamics characteristics, e.g., minimizing constraints such that coupled mode shapes can be detected over a limited operating range. Because of the large number of concentrated masses and joints, a large number of suspension cables will probably be required to support the model. Also, as previously discussed, the facility size and model scale factor determine the closeness of pendulum and model structural frequencies. Finally, a concept such as the shadow structure, depicted at the bottom of the figure, provides testing versatility, isolation from the structure of the facility, and a simple method for attaching and detaching cables.

- SPACE STATION REPLICATION IMPLIES MODEL NOT DESIGNED TO SUSTAIN UNSUPPORTED 1-G LOADS
- CABLE SUSPENSION SYSTEM DESIGN SHOULD NOT SIGNIFICANTLY ALTER MODEL DYNAMICS
- LARGE CONCENTRATED MASSES & NUMBER OF JOINTS SUGGESTS NUMEROUS CABLES REQUIRED
- FACILITY SIZE & MODEL SCALE FACTOR DETERMINE CLOSENESS OF PENDULUM AND STRUCTURAL FREQUENCIES
- "SHADOW" STRUCTURE CONCEPT PROVIDES:
  - MAXIMUM VERSATILITY IN CABLE ATTACHMENT LOCATIONS
  - EASE IN ATTACHING/DETACHING CABLES
  - PROVIDES ISOLATION FROM FACILITY

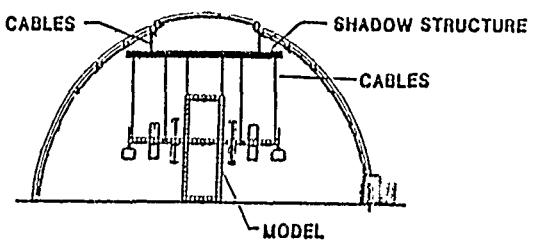

EXPLORATORY HARDWARE

Some of the exploratory hardware developed and tested at Langley which is related to the Space Station and scaled models and also to COFS III is shown on this chart. Seven bays of a full-scale 15-ft erectable structure, plus seven bays of a 1/4-scale display model of the same structure, are shown in the upper left corner. A picture of the dynamics test setup for the 1/4-scale model configured as a seven-bay truss beam is shown at the lower left. At the upper right is pictured a full-scale prototype erectable joint along with a 1/4-scale model of that joint. The picture at the lower right shows the full-scale joint undergoing static characterization tests.

The results of the tests of the seven-bay 1/4-scale model truss structure and the tests of the full-scale joints are rather interesting. They will be discussed next.

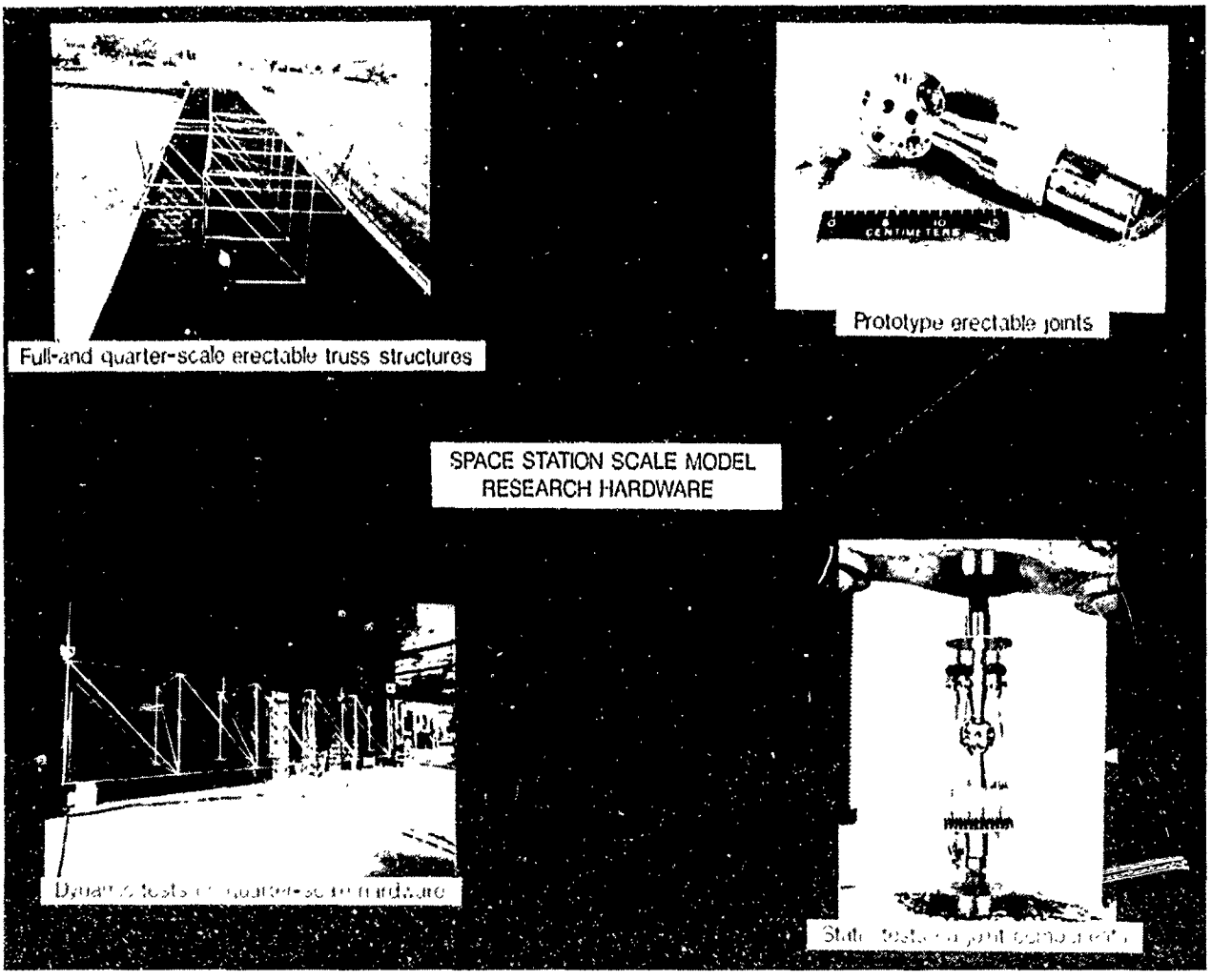

TEST AND ANALYSIS CORRELATION FOR 1/4-SCALE TRUSS

The correlation of the tests and analysis of the 1/4-scale truss revealed the importance of accounting for the local effects of the individual struts in these structures when they are lightly mass loaded. The local effects drive the global frequencies higher than a simple NASTRAN analysis predicts. A simple BUNVIS model, which is based on exact finite element technology and is equivalent to discretizing the simple NASTRAN model into smaller elements, is an improvement over the NASTRAN analysis but results in a slight overprediction. When the joint flexibilities are taken into account using estimates of the joint axial stiffness, there is an even better correlation.

As mass in the form of payloads and modules is added to this type of structure, the local effects will become less significant until at some point they will not appreciably effect the global frequencies. Exactly where that occurs has not been investigated and will probably depend on the number, masses, and placement of the payloads and modules.

Although the 1/4-scale model test results just described are encouraging, the model was not a replica of the full-scale structure. The model was built for demonstration and display purposes, not as a test article. Little attention was paid to replica scaling. Thus its dynamics properties probably do not represent the full-scale structure. But, since the model was available it provided an opportunity to obtain experience and to develop test and analysis techniques for this type structure. For these same reasons the full-scale seven-bay structure is also being tested at Langley. By testing this type of structure we will learn to account for joint effects, suspension systems interactions, and gravity effects.

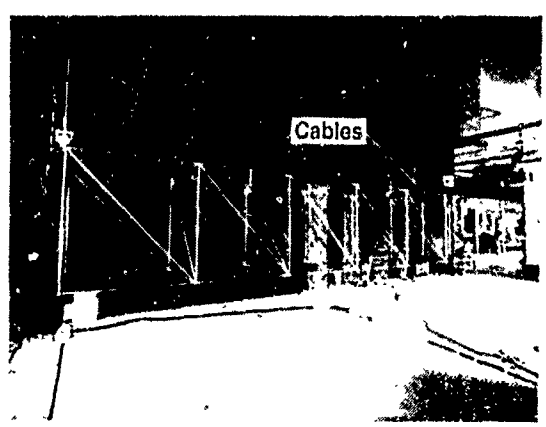

Global Mode Number	Test (Frequency, Hz)	Analysis* (Frequency, Hz)		
		Simple model		Refined model**
		Nastran	Bunvis	Bunvis
1	77.12	49.22	82.35	77.74
2	78.62	56.62	89.41	79.15
3	83.01	64.32	95.13	83.03

* 1 Element per member
** Joint flexibilities taken into account

TYPICAL FULL-SCALE SS JOINT STATIC TEST DATA

Another interesting result of Langley's exploratory development involves the testing of a typical full-scale Space Station joint. The picture at the left shows the joint/end connector assembly in the static test rig. The upper graph shows a typical joint response curve which usually describes the displacement for loads of +1000 pounds. The first conclusion would be that the response is essentially linear; however, a look at a lower operating load range of 0-40 pounds, shown in the lower graph, reveals definite nonlinearities. It will be important to characterize the joint behavior at both load levels, low levels to simulate normal Space Station operations and high levels to simulate docking and reboosts.

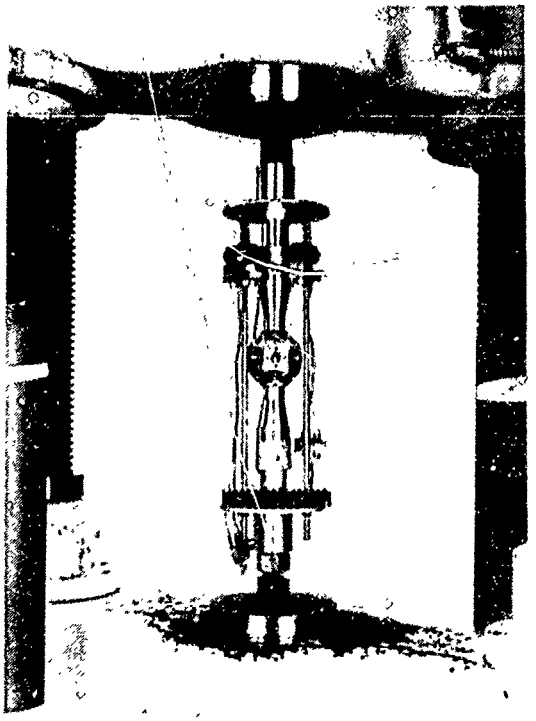

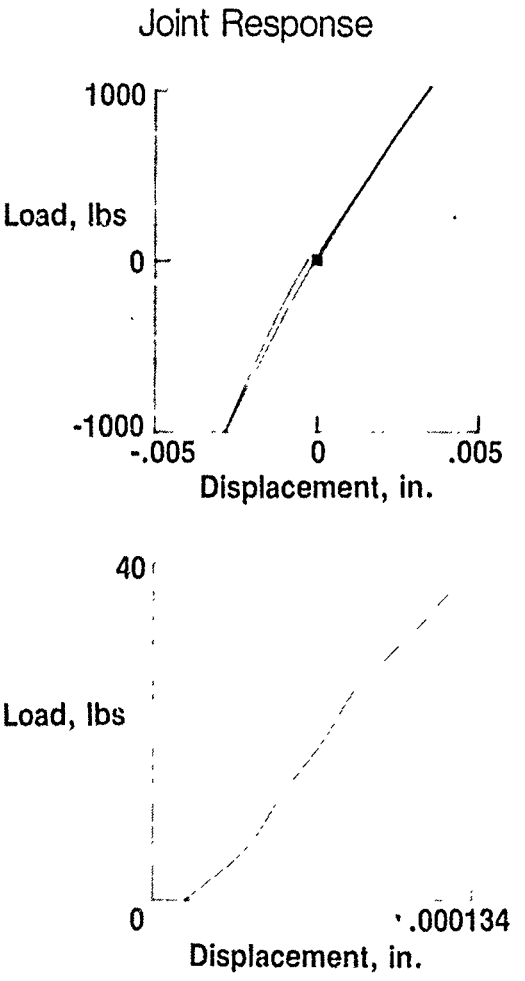

GROUND TEST SCENARIO

This chart portrays the anticipated COFS III test scenarios. We have been discussing some of the exploratory work related to the level I tests and some initial incursions into the level II test area. When the COFS III model hardware is delivered, we will be able to test a variety of subassemblies including the proposed Structures and Assembly Verification Experiment (SAVE), which is a shuttle based experiment involving a large section of the Space Station structure. In addition we will investigate various multibody configurations including the buildup stages until we finally reach the fully mated configuration. The mated configuration will be tested extensively. Subsequent tests will include alternative growth Space Station configurations and the evaluation of the dynamics interactions of various Space Station experiments.

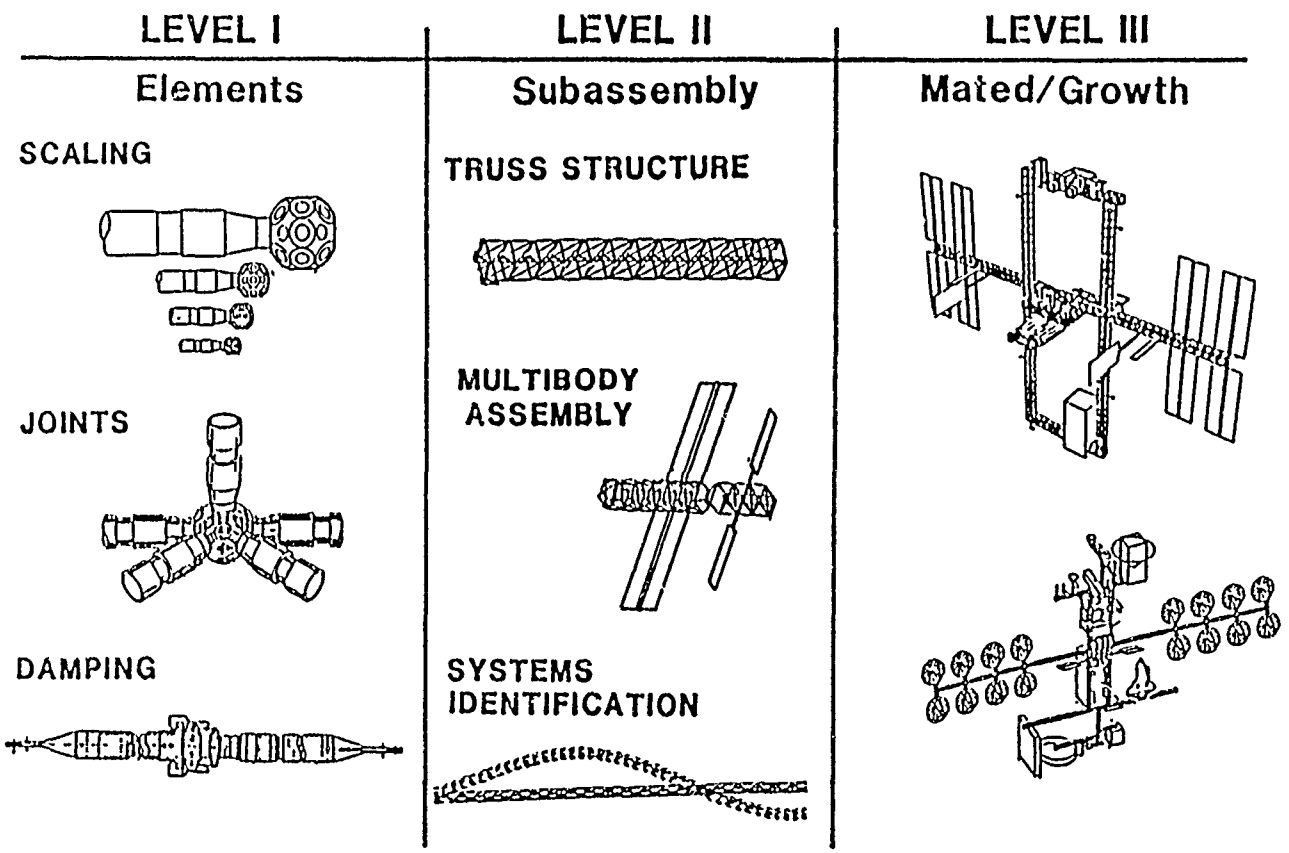

SUMMARY

In summary, the COFS III project is a technology project which will develop the methods for using dynamically scaled models and analysis to predict the structural dynamics of large space structures. The project uses the Space Station as a focus because it is typical of the structures of interest and provides the first opportunity to obtain full-scale on-orbit dynamics data. Finally it provides the means for developing the technology for growth Space Station and Space Station experiments.

- **TECHNOLOGY PROJECT**

  SCALE MODEL TESTS PLUS ANALYSIS → **PREDICTION OF FULL-SCALE STRUCTURAL DYNAMICS**

- **SPACE STATION FOCUS**

  TYPICAL STRUCTURE
  SOURCE FOR FULL-SCALE DATA

- **DEVELOPS TECHNOLOGY FOR**

  GROWTH SPACE STATION
  SPACE STATION EXPERIMENTS

CONCEPTUAL DESIGN OF POINTING CONTROL SYSTEMS FOR SPACE STATION GIMBALLED PAYLOADS

Robert O. Hughes
General Electric Space Division
Philadelphia, Pennsylvania

First NASA/DOD CSI Technology Conference
Norfolk, Virginia
November 18-21, 1986

CONCEPTUAL DESIGN OF POINTING CONTROL SYSTEMS FOR SPACE STATION GIMBALLED PAYLOADS

Robert O. Hughes
General Electric Space Division
Philadelphia, Pennsylvania

Abstract

A conceptual design of the control system for Payload Pointing Systems (PPS) is developed using classic Proportional-Integral-Derivative (PID) techniques. The major source of system pointing error is due to the disturbance-rich environment of the Space Station in the form of gimbal baseplate motions. These baseplate vibrations are characterized using Fast Fourier Transform (FFT) techniques. Both time domain and frequency domain dynamic models are developed to assess control system performance. Three basic methods exist for the improvement of PPS pointing performance: increase control system bandwidth, add Image Motion Compensation, and/or reduce (or change) the baseplate disturbance environment.

Introduction

A permanently manned Space Station (SS) is planned to be launched in the early 1990's and will orbit at about 460 Km and 28 1/2 degrees inclination. The current baseline configuration, the "dual keel" concept, is about 400 ft. long and is shown in Figure 1. The Station will orbit in a nadir pointing, gravity gradient orientation and an initial electrical power capacity of approximately 75 KW will be generated by a combination of photovoltaic solar arrays and point focusing collectors with heat engines. A central thermal heat rejection system for Attached Payloads using fluid loops and large articulating radiators is planned.

Of the approximately one hundred experiments/ instruments identified as candidate Attached Payloads for the Space Station, about forty per cent require some type of pointing capability. The accuracy requirements for these pointed payloads vary from sub-arc seconds to degrees and include several high technology solar and celestial telescopes. Most of these telescopes and other sky-viewing instruments will be mounted on the upper boom; the earth viewing payloads will be mounted on the lower boom.

Presented as paper 86-1986-CP at AIAA GN&C Conference, Williamsburg, Va., Aug. 18-20, 1986.

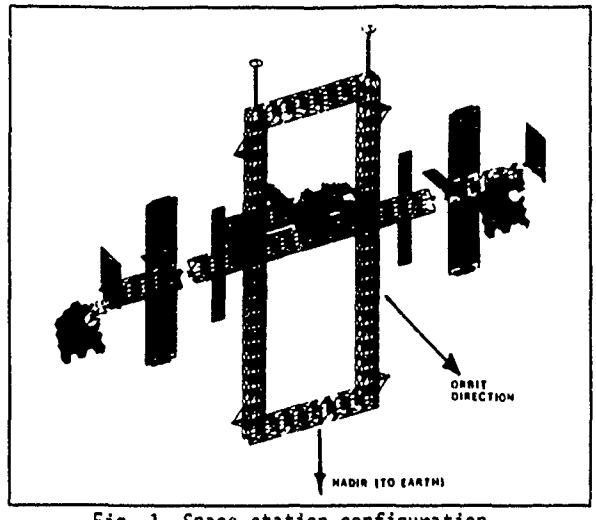

Fig. 1 Space station configuration - dual keel concept.

The Space Station attitude will be controlled by at least six large Control Moment Gyros (CMGs). Momentum build-up will be managed by off-nadir angles or Torque Equivalent Angles (TEA) generating desirable, momentum-dumping gravity gradient torques. Current estimates of the maximum nominal TEA are ± 5° in all axes with rates of .02°/sec per axis. Because the Space Station will not be stationary in its reference frame, generic and reusable pointing mounts are envisioned as the most cost-effective method of achieving most of the payload pointing requirements. These pointing mounts are called Payload Pointing Systems (PPS). Much analysis and design effort has been expended within the past decade on Shuttle based pointing mounts. Laskin and Sirlin[1] compare twelve different types of gimbal systems and perform technology assessments of actuators, sensors, isolation/suspensions systems, and control techniques. The European Instrument Pointing System (IPS) represents a type of design being considered for Space Station applications. IPS has a large payload capability (up to 7000 Kg) and has achieved in-flight sub-arc second pointing accuracies[2] during Shuttle/Spacelab quiescence disturbance periods. A major drawback of the IPS is its

end-mounted gimbal arrangement. Due to the center-of-mass offsets, this type of configuration is very sensitive to vibrational disturbances but is versatile in payload accommodation[3]. The disturbances created by normal crew activity during the Spacelab 2 mission caused pointing errors sizably larger than anticipated[4].

The Space Station as shown in Figure 1 represents a Large Space Structure (LSS). As there are no plans to either control the flexible modes (in an active distributed sense) or to estimate (observe) flexible vibrations for feed-forward reasons, non-trivial disturbances will exist at locations where gimballed payloads will be mounted. This base plate disturbance represents the major source of error for the gimbal control system. A typical CG gimbal concept is shown in Figure 2 and has a third axis of rotation which alleviates gimbal lock situations.

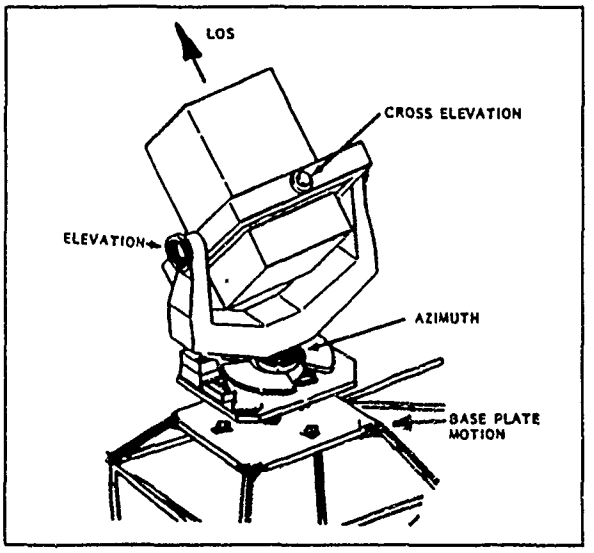

Fig. 2 CG- mount gimbal concept - 3 axes.

Disturbance Environment

Many internal and external forces will act on the Space Station causing the excitation of the lightly damped modal frequencies. The resulting vibrations at the mounting or base plate locations will be a major part of the pointing system's disturbance environment.

Disturbance Sources Smaller "ever-present" types of Space Station disturbances include: venting, slosh, machinery and pump vibrations, solar array and radiator motions, CMG torques, payload articulations, and console operations[5]. Larger disturbances occurring in a less random manner include: crew member kickoffs, nominal MRMS (Remote Manipulator) operations, tether operations, laboratory centrifuge operations, and astronaut treadmill activities. Very large disturbances occurring at very predictable and discrete points in time are Shuttle docking, RCS reboost (Station keeping via thrusters), and large excursions of the MRMS with massive payloads.

It has been determined that the maintenance of precision pointing during periods of large disturbances would not be cost-effective as the induced vibrations are more than thirty times larger than the other disturbance types. It is expected that these discrete occurrences will be coordinated with payload mission timelines in order to minimize data loss. However, payload pointing capabilities must be maintained for the two smaller disturbance levels. These levels represent quiescence or background disturbance levels.

NASTRAN Model To investigate the effects of these background sources of excitation, a NASTRAN model of the Space Station was developed. Forcing functions that modeled a "standard" crew kick-off in the pressurized module, treadmill operations, and a centrifuge with a 20 pound mass imbalance were used as model inputs. Vibration levels were assessed at various locations on the SS where pointed payloads were likely to be attached, and a representative rotational/translational case was selected. This location turned out to be at the corner of the upper boom (see Figure 1) and Figure 3 shows the rotational motion.

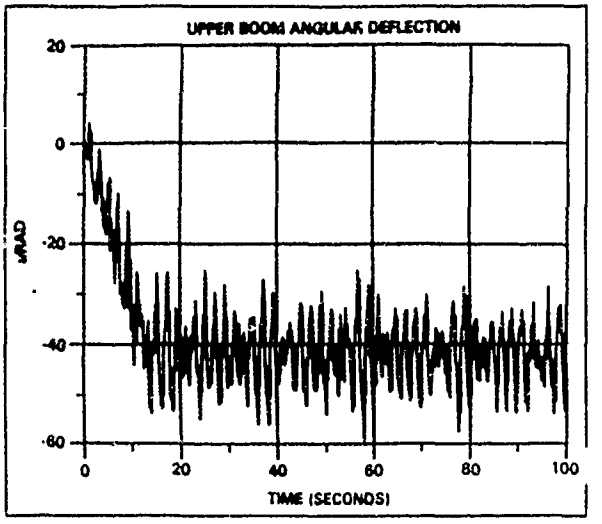

Fig. 3 Upper boom response to disturbances.

Effects of the crew kickoff causes a discernible displacement of approximately 40 microrad (8.3 arc-sec). High frequency vibrations are evident with maximum peak-to-peak variations of about 7.7 arc-sec.

Fast Fourier Transforms (FFT) The appropriate time history data files from the NASTRAN Model were processed using discrete FFT techniques[6]. The two FFT responses chosen for this study are shown in Figures 4 and 5 and represent baseplate rotational deflections and linear accelerations. The large responses at 1 Hz and 2 Hz are caused by the treadmill operation.

Control System Analysis

Models A simplified representation of the dynamic model used to assess pointing performance

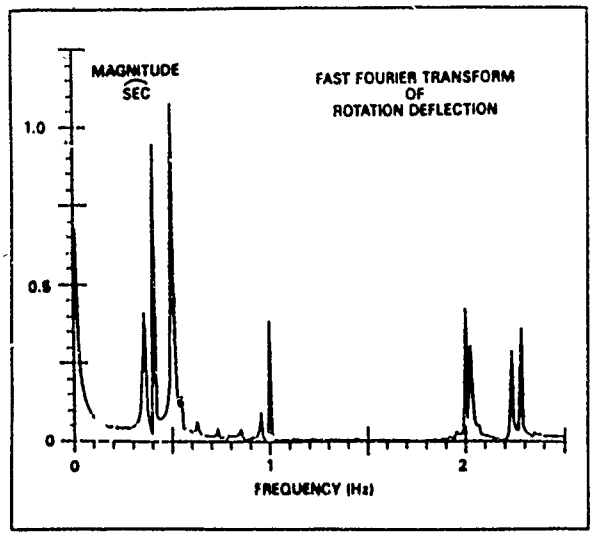

Fig. 4 Fast Fourier transform (FFT) of disturbance response - rotation.

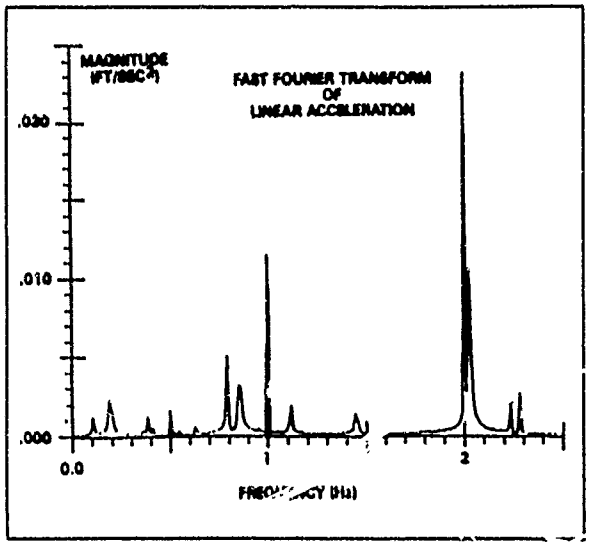

Fig. 5 Fast fourier transform (FFT) of disturbance response- linear acceleration.

of Payload Pointing Systems (PPS) is shown in Figure 6. The assumptions used in the derivation of this model include:

1) The payload was modeled as a uniform cylinder of mass M and length L. CG offsets, R, could vary from 0 (CG mount) to L/2 (end mount). The payload inertia, J, was calculated as a function of M, L, and R.

2) Frictional forces in the gimbal were modeled as a linear damping term, F. There were no non-linearities and no cable wrap-up torques.

3) The motor was modeled as a perfect torquer without time constants but with a saturation torque value of Tmax.

4) The system was noise-free and drift-free. Knowledge of the desired pointing direction was assumed perfect (implying an error-free payload sensor).

5) Only a single gimbal axis was modeled.

6) The controller was implemented in a perfect analog computer (i.e., no sampling problems).

7) The gimbal/payload was considered infinitely stiff except as noted in the flexibility discussions. No dynamic interactions with the SS were present.

8) Orbital velocity (about .06 deg/sec) was uniform, known, and used as a feed-forward input into the control system. This feed-forward technique transforms the tracking control problem into a regulator control problem[7] and results in lower problem pointing errors and increased stability margins.

Base plate vibrations represented by the two FFT responses were used as the disturbance inputs for the closed loop control system. The baseplate angular rotations (arc-sec) cause direct Line-Of-Sight (LOS) errors and must be corrected by opposing

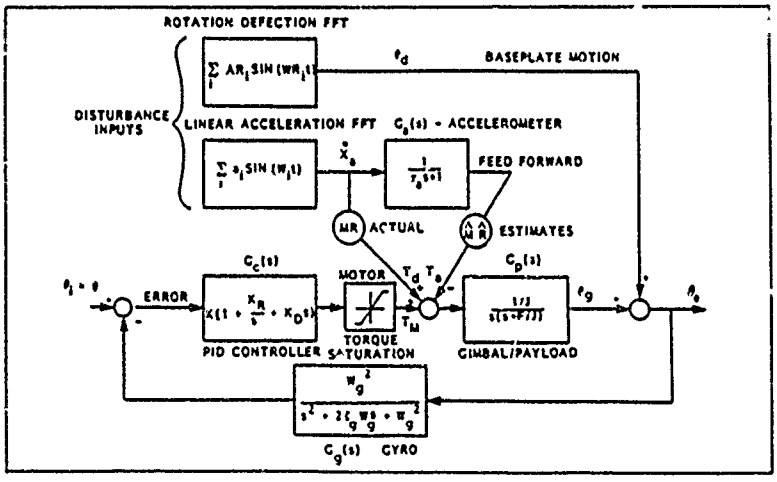

Fig. 6 Payload pointing system dynamic model.

gimbal motions. The linear accelerations $\ddot{X}_a(t)$ (ft/sec^2), act on the payload mass M (see Figure 7) through existing CG offsets, R, and cause a disturbance torque, T_d, about the gimbal axis.

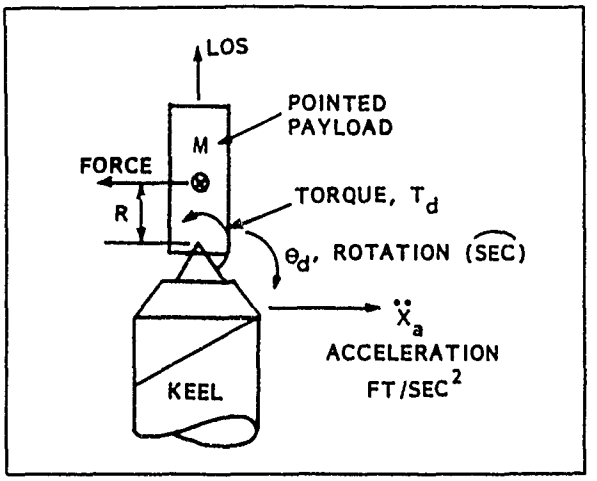

Fig. 7 Disturbance torques generated by CG-offsets.

A technique for counteracting this disturbance torque is accelerometer feed-forward compensation[8,9]. A properly oriented accelerometer with a transfer function of $G_a(s)$ measures the linear acceleration. Using estimates of payload mass, M, and CG offset, R, an opposing torque signal, T_a, is generated and used as an input to the control system. Major problems with this technique are: alignment, accurate estimates of M and R, noise, and the accelerometer's effective time constant, τ_a.

Controller Design The type of controller chosen for the conceptual design of the PPS is the classic Proportional - Integral Derivative (PID). This control design is not optimal and other techniques probably could provide higher performance; however, the PID design is well understood and provided needed versatility in the early stages of anlaysis.

To achieve a commonality in the performance assessment of various payloads, parameters, and disturbances, the pole placement technique of Guillemin-Truxal[10] was used to calculate the PID gains. That is, as various configurations and different size payloads were analyzed, the closed loop dominant poles were designed to remain in fixed positions. The three PID gains (K, K_r, and K_d) specified the locations of the two system zeros and the positions of the roots along the root locus. The controller zeros and the closed-loop poles are shown in Figures 8 and 9 for the nominal parameter values listed in Figure 10. These poles/zero locations dictate the bandwidth, stability margins, and pointing error performance of the control system.

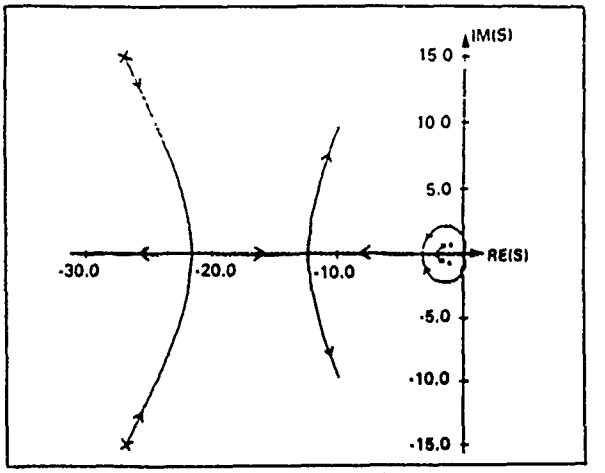

Fig. 8 Overall root locus.

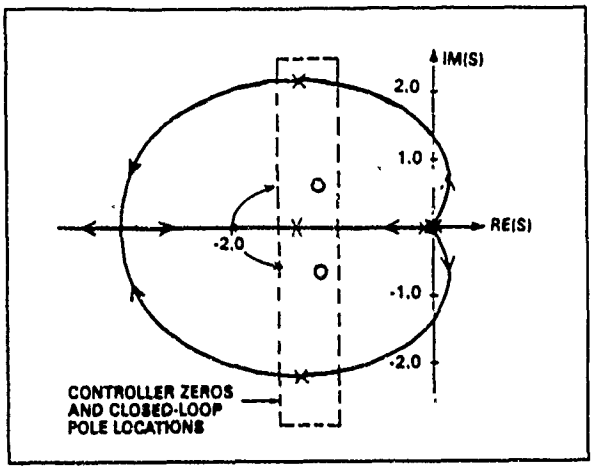

Fig. 9 Root locus-exploded view of dominant roots and controller zeros.

SYMBOL	NAME	UNITS	VALUE
M	Payload Mass	slug	3000
L	Payload Length	ft	3
R	CG Offset	ft	0
J	Payload Inertia	slug-ft^2	1108
F	Linear Damping	ft-lb/r/s	100
ω_n	Closed Loop Natural Freq.	rad/sec	2.33
ζ	Closed Loop Damping Ratio	-	.5
TMAX	Motor Torque Saturation	Ft-lb	23
ω_g	Gyro Natural Freq.	rad/sec	31
ζ_g	Gyro Damping Ratio	-	.37
τ_a	Accelerometer Time Constant	sec	.008
PL	Real Axis Pole Location	-	1

Fig. 10 List of nominal parameters.

If the gyro dynamics and the torque motor saturation function in Figure 6 are neglected, then the closed-loop characteristic equation can be expressed as:

$$1 + G_c(s)\, G_p(s) = 0. \qquad (1)$$

Using Laplace Block diagram algebra and the plant/controller parameters this equation becomes

$$s^3 + (F/J+KK_d/J)s^2 + Ks/J + KKr/J = 0. \qquad (2)$$

For the general factored form of the characteristic equation of

$$(s + c)\,((s + a)^2 + b^2) = 0 \qquad (3)$$

and using

$$\begin{aligned} a &= \zeta w_n \\ b &= w_n\sqrt{1-\zeta^2} \\ c &= PL * a \end{aligned} \qquad (4)$$

the PID gain expressions become

$$\begin{aligned} K &= J * (2 * PL * \zeta^2 * w_n^2 + w_n^2) \\ K_r &= J * (\zeta * PL * w_n^3)/K \\ K_d &= J * ((2 + PL) * \zeta * w_n - F/J)/K \end{aligned} \qquad (5)$$

where ζ is the closed loop damping ratio and w_n is the closed loop natural frequency. PL specifies the relative position of the real third pole in relationship to the real parts of the two imaginary poles. In other words, ζ and w_n specify the locations of the dominant complex poles and PL (nominally equal to unity) dictates the position of the real axis root.

Time Domain Analysis A time simulation model for the system was developed and a typical time response using the FFT disturbances and the nominal parameters (Figure 10) is shown in Figure 11 for a CG offset of 5 cm. It can be seen that the baseplate motion varies between ± 5 arc-sec while the resulting LOS error is larger. The reason for this is due to the disturbance torques being generated by the 5 cm CG offset.

Frequency Domain Analysis The PPS pointing problem is amenable to frequency domain analysis because of the sinusoidal nature of the disturbance inputs (FFTs). In general, these techniques are much faster (computationally) and more precise than those using time simulation techniques. With reference to Figure 6 and using Laplace Transform Algebra, the closed loop transfer function, derived to perform stability analyses, is:

$$\frac{\theta_o(s)}{\theta_i(s)} = \frac{G_c(s)\, G_p(s)}{1+G_c(s)G_p(s)\, G_g(s)} \qquad (6)$$

The relationship between the true LOS error and the two disturbances is:

$$E(s) = \frac{\theta_d(s) + G_p(s)(1-G_a(s))MR\ddot{X}_a(s)}{1+G_p(s)G_c(s)G_g(s)} \qquad (7)$$

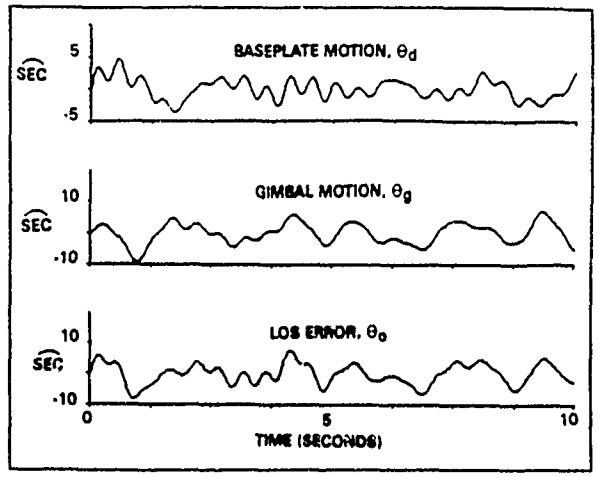

Fig. 11 PPS performance with CG-offset of 5 centimeters.

where perfect estimates of payload mass M and CG offset R are assumed. The true LOS error is

$$E(s) = \theta_i(s) - \theta_o(s) \qquad (8)$$

and is slightly different than the measured error which has been modified by the gyro dynamics. Equation (7) can also be written as the sum of two error transfer functions. That is,

$$E_T(s) = E_1(s) + E_2(s) \qquad (9)$$

where

$$E_1(s) = \frac{E(s)}{\theta_d(s)} = \frac{1}{1+G_p(s)G_c(s)G_g(s)} \qquad (10)$$

and

$$E_2(s) = \frac{E(s)}{\ddot{X}_a(s)} = \frac{G_p(s)(1-G_a(s))MR}{1+G_p(s)G_c(s)G_g(s)} \qquad (11)$$

$E_1(s)$ is the transfer function relating baseplate motion to LOS error. $E_2(s)$ represents additional error impacts due to CG offsets. Substituting jw for the Laplace variable s, the total LOS error can be calculated numerically as:

$$E = \sum_{i=1}^{N} AR_i(wr_i) * \left|E_1(jwr_i)\right| + \sum_{i=1}^{NR} A(w_i) * \left|E_2(jw_i)\right| \qquad (12)$$

where w_i and wr_i are the FFT frequencies, A_i and AR_i are the FFT amplitudes, and N and NR are numbers of FFT frequencies considered. It should be noted that equation

(12) represents a maximum worst case condition because the error contributions at each frequency are added. From a time domain viewpoint, this scenario means that the maximum error occurs when all the FFT sine waves are at their peaks (i.e., pure constructive interference).

The functions $E_1(w)$ and $E_2(w)$ of equation (12) can be termed "Control System Attenuation Functions" and they represent how well the gimballed control system can handle the disturbance sinusoids. These functions are shown in Figure 12 and are for a CG offset of 5 cm and no accelerometer feed-forward compensation. Multiplying the FFTs by their corresponding attenuation functions, weighted FFTs will result. The summing of the values of the weighted peaks is the calculation performed by equation (12).

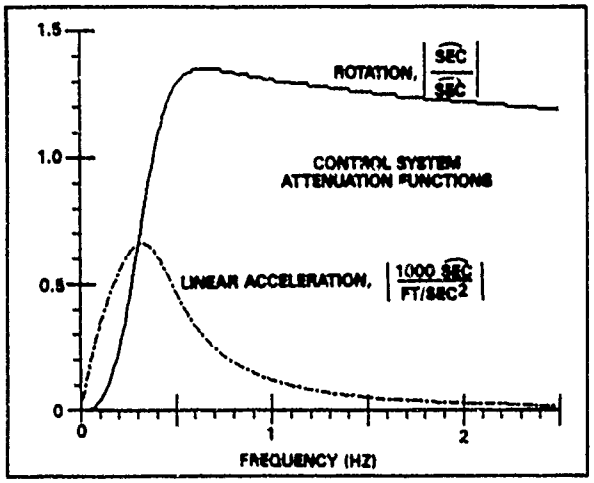

Fig. 12 Attenuation functions without feed-forward.

Bandwidth Considerations

One of the most important and descriptive parameters of a control system is its bandwidth. In general, bandwidth (or passband) is the range of frequencies that can pass through a control system. "High" bandwidth systems have fast response times and high performance factors but usually suffer from high frequency noise and reduced stability margins. "Low" bandwidth systems, while slower in reaction times, have excellent noise rejection characteristics. Laser Pointing Systems[11] have bandwidths above 100 Hz while spacecraft attitude control systems typically have bandwidths of .05 Hz and lower.

Many factors impact the bandwidth of a system[3] and include: controller design, structural flexibilities, nonlinearities, component bandwidths, component noise characteristics, and gain/phase stability margin specifications. An example of the difficulties in achieving high bandwidths was the Sperry-designed Advanced Gimbal System (AGS). Initially, an optimistic goal for a 2.4 Hz bandwidth was set. However, due to the combined effects of structural flexibility, gyro and accelerometer bandwidths, transport lags, and sampling effects, a control bandwidth of .7-1.3 Hz was achieved[12]. Bandwidths in this range appear reasonable for the PPS.

It is important to have a standard definition of bandwidth in order to compare different systems. The traditional and most widely accepted definition is "the -3db point of the closed-loop Bode Plot"[10,13]. In some systems[14], for example, the open loop crossover frequency is near the closed-loop -3db point and the two can be used interchangeably. Sometimes the natural frequency, w_n, of the dominant closed loop poles is referred to as the bandwidth. However, for the PPS system being considered herein, neither of these bandwidth definitions are correct.

Error vs. Bandwidth Variations in pointing error or stability error are shown in Figures 13 and 14 for different bandwidths, various CG offsets, and three different types of magnitude/frequency disturbance inputs. Figure 13 is the nominal case for a CG mount with small perturbing CG offsets. It is estimated that there will be a ± 5 cm CG uncertainty on orbit even with the use of an on-line mass balancing system. Without such a balancing system, an error of about ± 20 cm is estimated.

Large error sensitivities to different disturbances are seen in Figure 14. The term "8 Frequencies" indicates the nominal case of eight FFT frequencies for the rotation and acceleration disturbances. The term "3 frequencies" indicates that only the first three of the eight FFT frequencies were retained, and "1 frequency" means that only one frequency for each disturbance was used as an input. For the nominal case, the large errors which are relatively insensitive to bandwidth changes are caused by the high frequency disturbances outside the control system bandwidth. For the "3 frequency" case, bandwidth changes affect the error more strongly. The single frequency case was used to emphasize the importance of the magnitudes and frequencies FFT disturbances on pointing performance and as a verification tool. In this special configuration one frequency (w = 1.97 Hz with an amplitude of .023 ft/sec^2) from the acceleration FFT and one frequency (w_r = .51 Hz with an amplitude of 1.08 arc-sec) from the displacement FFT were used as disturbances. A pointing error of ± 3.54 arc-sec resulted and is almost a four-fold improvement in pointing performance over the nominal disturbance case. This configuration served as a verification case as the time-varying pointing error generated by the time domain simulation model was virtually periodic over the simulation time and the maximum peak-to-peak variation could be measured with accuracy. There was less than a 1% error between values calculated by the frequency and time domain techniques.

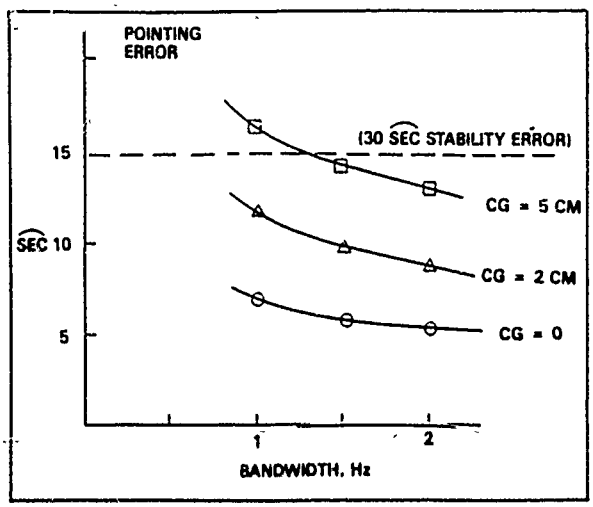

. Fig. 13 Pointing error sensitivity to bandwidth and small perturbing CG offsets.

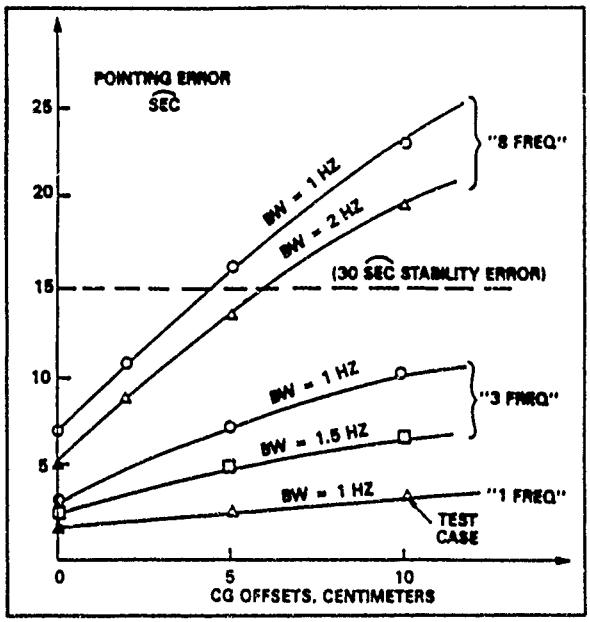

Fig. 14 Pointing error sensitivity to bandwidth, CG offset, and disturbance input.

Gyro Dynamics The dynamic characteristics of the gyro impact the overall control loop bandwidth and gain/phase margins. In Figure 15 Bode plots for three gyro natural frequencies are shown. The gain and phase margins for these cases are:

Wg (r/s)	GM (db)	PM(deg)
15	17	32
31	22	38
62	29	46

Hence, if a high gyro natural frequency (which is a measure of its bandwidth) can be realized, then higher control loop bandwidths can be achieved for the same gain/phase margins.

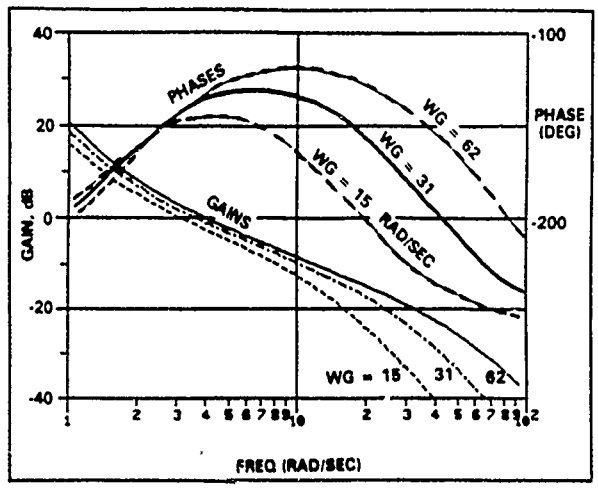

Fig. 15 Bode plots for three gyro bandwidths.

Feed-Forward Techniques Feed-forward methods can improve pointing performance without increasing the loop bandwidth. For example, if there were good predictions of the base plate motion generated by an on-board SS dynamic computer model, then these signals could drive the gimbals in phase, rather than having to wait for the sensors to detect errors.

A technique used in IPS and elsewhere is accelerometer feed-forward. Linear accelerations are sensed at the base plate and multiplied by estimates of the mass, M, and CG offsets, R. This generates a disturbance torque estimate and is used as an input to the control system. Problem areas of this technique include: noise and finite bandwidths of accelerometers, accurate mass and CG offset estimates, and sensitivity of the disturbance torques to gimbal angles. Assuming that the dynamics of the accelerometer can be approximated by a single time constant, τ_a, Figure 16 shows variations of pointing errors as functions of CG offsets and accelerometer break frequency ($1/\tau_a$). Note that for this perfect, single-axis feed-forward method, the pointing error approaches that of an ideal CG mount as the bandwidth of the accelerometer approaches infinity. This also means that the accelerometer transfer function, $G_a(s)$, approaches unity and a perfect cancellation of the induced disturbance torques is acheived.

Flexibility Effects The effects of mechanical flexibility can have major impacts on the stability, performance, and bandwidths of pointing control systems. Flexible modes that are close to the control bandwidth will reduce gain/phase margins (similar to the previous gyro analysis) and could cause instability. Sometimes an increase in system bandwidth excites flexible modes which introduces larger pointing errors than experienced with smaller bandwidths[15].

In general, it is desirable from a control standpoint to make the gimbal/yoke structure as stiff as possible, thereby ensuring high modal frequencies. For example, in the

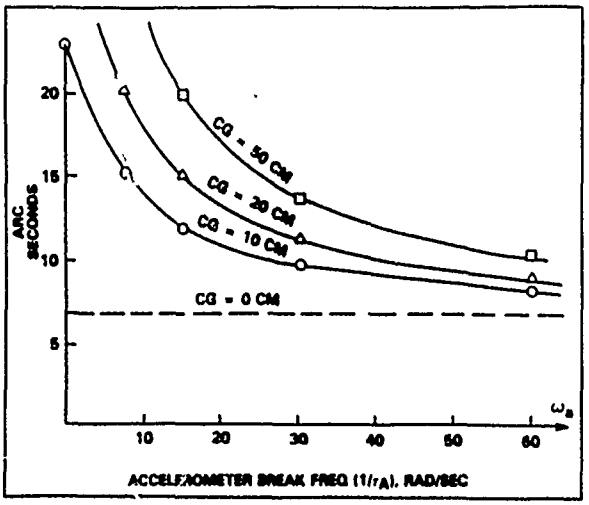

Fig. 16 Accelerometer time constant effect on pointing error.

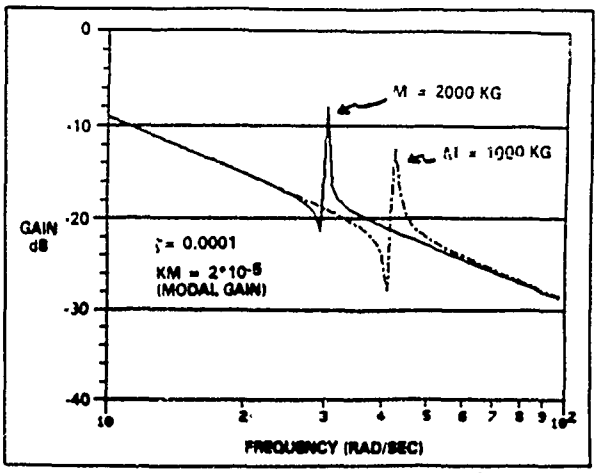

Fig. 17 Flexibility effects - open loop Bode (gain) plots.

early design phases of the AGS, a minimum frequency of 20 Hz was specified[16]. Refined numbers for structural stiffness, inertias, and damping are usually not available in the conceptual design phase of a project. Therefore, the overall control system design must be robust enough to accommodate changes in modal parameters. In the course of the IPS design, it was discovered that early stiffness estimates were too high and modifications to the control laws were necessary[17].

A general rule of thumb[18] for the design of a control system with potential flexibility problems is to choose the open-loop crossover frequency with about one-third the frequency that is not necessary to control. Another technique[8] is to design for a "minimum bandwidth" which provides for the maximum levels of margin while still meeting performance requirements.

The pole placement technique used in this study of the controller conceptual design assumed that the payload was a lumped inertia and effects of gimbal/yoke stiffness were not directly considered. Little difference in responses will be discerned for two payloads with different inertias as the loop gain, K, will increase linearly with the load inertia, J. In reality, this is incorrect as a large inertia will result in a low destabilizing fundamental frequency. Additionally, a high electrical loop gain will amplify the effects of system noise and will degrade performance. To demonstrate the effects of flexibility on loop stability, a single modal frequency transfer function was added in parallel to the payload block in Figure 6. The results of this simplified technique are shown in the open loop Bode Plot (Figure 17) for two payload masses (1000 Kg and 2000 Kg). Note that for the lower mass the resonant frequency has increased thereby providing about 6 db additional gain margin.

Options for Pointing Performance Improvement

As detailed in the previous sections the expected dynamic disturbances from the SS acting through traditional control systems with bandwidths of about 1 Hz will cause non-trival pointing errors; and, in some cases, a payload's pointing error requirement can be exceeded. The following is a discussion of several options that have potential for the improvement of pointing performance:

Controller Design Moderate improvements in pointing performance can be realized through optimal control design techniques or a more rigorous classical design approach. By advancing the state-of-the-art in sensor and actuator technologies[1], higher bandwidths can be achieved with smaller pointing errors as demonstrated in Figure 14.

Added Structural Damping An increase in the SS structural damping will decrease the amplitudes of the disturbance vibrations and a corresponding decrease in pointing error will result. Passive damping methods[19] appear promising. Active structural damping such as piezoelectric techniques are probably not cost-effective for the current SS design.

Image Motion Compensations (IMC) This proven technique is usually an integral part of an instrument's control design[20,21], but IMC also could be exterior to a payload[22]. Basically, IMC entails high bandwidth systems that control low mass actuators such as mirrors. The net effect of an IMC system is attenuation of the disturbance frequencies passed by the gimbal control system.

Disturbance Management Internal vibration sources of the space station can be managed in a fashion similiar to that of a spacecraft's traditional weight and power allocation/budget. Vibration absorbers and/or isolators can be added to equipment with offending disturbance spectra.

Payload Isolation This method attempts to isolate the pointed payload from the disturbance source which is, in this case, the entire space station. There are three isolation options to be considered: passive, active, and softmount.

Passive isolation, which typically uses springs and dampers, suffers from practical problems and does not appear feasible for the space station applications. To attenuate the > 1 Hz frequencies, an isolator frequency of .1 Hz or less would be required. For a 2000 Kg payload, this corresponds to a spring rate of 790 N/M which is likely to be softer than the power and thermal connections to and from the payload. Additionally, the gimbal system will not be able to react torques against the massive space station and this will introduce additional pointing errors. It is also likely that without any payload momentum compensation devices closed-loop stability problems will exist.

Magnetic suspension[23] and the Gimbalflex[24] are common techniques of active vibration isolation that have SS applicability. Typically, a magnetic suspension system will have six-degrees of freedom (three rotations and three translations) and will perform significantly better than passive devices[23]. The transfer of services across the isolator interface remains a problem for both types of active isolation in achieving adequate disturbance rejection.

The softmount[25] is a concept in which the payload becomes a virtual free-flyer with almost no dynamic interaction with the base body. The payload would require its own attitude control system using CMGs or reaction wheels and would be loosely connected to the space station via tethers or guy wires.

An example of how an idealized isolator in the form of a softmount could modify the error attenuation characteristics of the system considered in this study is shown in Figure 18. The example assumes: no dynamic interation between the gimbal control system and the isolator, payload pointing is controlled by CMGs with a 1 Hz bandwidth, and that all connections to the payload are such that the isolator system has a natural frequency of .1 Hz. The resultant isolator/control characteristic is similiar to that derived in a previous study[26] and provides for an order-of magnitude reduction in pointing error.

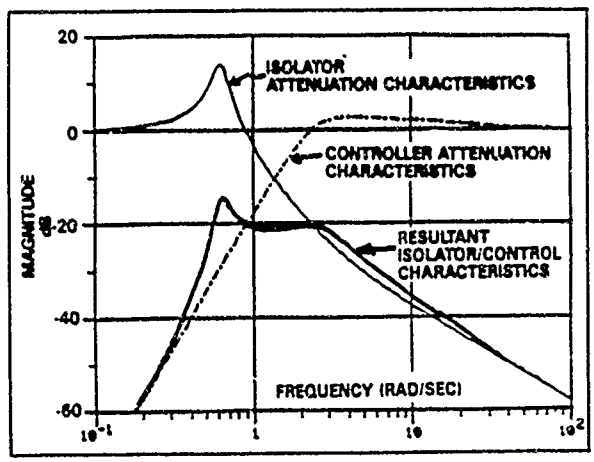

Fig. 18 Idealized isolation

CONCLUSIONS

A study of interface problems between the Space Station Structure and the Payload Pointing Control System has been completed. A major result is that the Space Station will have a disturbance-rich environment and vibration background levels will be large enough to impact the pointing performance of some payloads.

The dynamic model used to quantify the pointing performance of the conceptual design of the PPS included many simplified assumptions. It is expected that larger pointing errors will be observed when more detailed and accurate models of the PPS are developed.

End mounted gimbal systems suffer from CG offset problems and a CG mount is better from a pointing standpoint. It has been determined that at least a ± 5 centimeter CG offset will exist for a spaceborne CG mount even with an on-board mass balancing system.

To reduce the impact of Space Station vibrations on pointing performance, several design options were presented. The two most cost effective techniques appear to be disturbance management and payload Image Motion Compensation.

References

1. Laskin, R. and Sirlin, S., "Future Payload Isolation and Pointing System Technology," 1984 Position Location and Navigation Symposium, San Diego CA, Nov. 1984.

2. Hamesfahr, A., "The SpaceLab Instrument Pointing System Performance and Operations," AIAA Paper No 85-6073-CP, Shuttle Environment and Operations II Meeting, Houston, TX, Nov. 1985.

3. Hamilton, B., "Magnetic Suspension: The Next Generation in Precision Pointing," Proc. Rocky Mountain Guidance and Control Conference, Paper AAS 82-034, Feb. 1982.

4. "Spacelab 2 Scientists Fear Pictures Damaged", Aviation Week & Space Technology, p 21, Aug. 19, 1985.

5. Mettler, E., et. al., "Space Station On-Orbit Identification and Performance Monitor," paper AIAA 85-0357, 23rd Aerospace Sciences Meeting, Reno, Nevada, Jan. 1985.

6. Rabiner, L. and Rader, C., eds., Digital Signal Processing, IEEE Press, 1972.

7. Hughes, R.O., "Optimal Control of Suntracking Solar Collectors," Journal of Dynamic Systems, Measurement, and Control, Vol 101, June 1979.

8. Walton, V., "Fine Pointing Control of Orbiter Based Gimballed Payloads," Paper 77-1091, AIAA Guidance and Control Conference. Hollywood, FL, August 8-10, 1977.

9. Kösters, B, Thieme, G., and Müller, T., "Design of the IPS Control Loops," Automatic Control in Space, 8th Symposium, Oxford, England, July, 1979.

10. D'Azzo and Houpis, Linear Control System Analysis and Design, McGraw Hill, 1975.

11. Deadrick, R., "Design and Performance of a Satellite Laser Communications Pointing System," Paper AAS 85-016, Proc. Rocky Mountain Guidance and Control Conference, 1985.

12. "Advanced Gimbal System Critical Design Review," Sperry Flight Systems, April 14, 1982.

13. "Design of the Annular Suspension and Pointing System (ASPS)," Sperry Flight Systems, NASA Contractor Report 3343, Oct. 1980.

14. Åström, K. and Hägglund, T.," A Frequency Domain Method for Automatic Tuning of Simple Feedback Loops," IEEE CDC Conference, Las Vegas, NV, Dec. 1984.

15. Keckler, C.," High Accuracy Pointing for Earth Observations Experiments," Paper 84-1880, Guidance and Navigation Control Conference, Seattle, Wash., 1984.

16. Shelton, H., et. al., "Effects of Flexibility on AGS Performance," Paper AAS 82-002, Proc. Rocky Mountain Guidance and Control Conference, 1982.

17. Thieme, G., et. al., "Sampled Control Stability of the ESA Instrument Pointing System," IFAC Automatic Control in Space, 1982.

18. Nesline, F. and Zarchay, P., "Why Modern Controllers Can Go Unstable in Practice," AIAA Journal of Guidance and Control, Vol 7, No. 4., July, 1984.

19. Ashley, H., "On Passive Damping Mechanisms in Large Space Structures," Journal of Spacecraft, p 448, Sept. 1984.

20. Lorell, K. et. al., "Internal Image Motion Compensation System for the Shuttle Infrared Telescope Facility," Automatic Control In Space, 8th Symposium, Oxford, England, July, 1979.

21. Gowrinathan, S. and Gottesman, J., "Articulated Primary Mirror (APM) for the Solar Optical Telescope (SOT)," SPIE Vol. 265 Supplement, 1981.

22. Shelton, H., "Image Motion Compensation for the OSS-3/7 Telescopes," Paper AAS 83-006, Proc. Rocky Mountain Guidance and Control Conference, 1983.

23. Havenhill, D. and Kral, K., "Payload Isolation Using Magnetic Suspension," Paper 85-014, Proc. Rocky Mountain Guidance and Control Conference, 1985.

24. Osborne, N., "Gimbalflex 5-Degree of Freedom Inertially Stabilized Platform," Paper AAS-80-015, Proc. Rocky Mountain Guidance and Control Conference, 1980.

25. Sirlin, S. and Laskin, R., "Payload Isolation and Precision Pointing for the 1990's," Paper 85-010, Rocky Mountain Guidance and Control Conference, 1985.

26. Hamilton, B., "Stability of Magnetically Suspended Optics in a Vibration Environment," Sperry Flight Systems Pub 69-1554-02-00, June, 1981.

DESIGN CONSIDERATIONS FOR JOINTS IN DEPLOYABLE SPACE TRUSS STRUCTURES

Marvin D. Rhodes
NASA Langley Research Center
Hampton, Virginia

First NASA/DOD CSI Technology Conference
Norfolk, Virginia
November 18-21, 1986

INTRODUCTION

All of the structures considered for the Control of Flexible Structures (COFS) flight experiments are deployable truss structures and their response will be dominated by the structural response of the joints. To prepare for these experiments some fundamental research work is being conducted in the Structures and Dynamics Division at LaRC which will provide insight into structurally efficient and predictable deployable truss joints. This work involves generic studies of the static and dynamic response of joints as well as the development of analytical models which can be used to predict the response of a large multijointed truss. Some of this work has been documented in references 1 and 2, and additional publications are planned. In addition to the generic joint studies, the research effort encompasses the design and fabrication of a 20-meter long deployable truss beam for laboratory evaluation of its structural characteristics and correlation with developed prediction methods.

The purpose of the present paper is to present a snapshot of a limited part of this research activity and discuss some design considerations in the static behavior of joints for deployable space truss structures.

STATIC TEST EVALUATION OF TWO JOINT TYPES

The work presented in the current paper covers some recent experimental studies to evaluate the static stiffness of two joint types commonly incorporated in most deployable truss structures. These joints are a pin-clevis type and a folding linkage system described herein as a near-center latch joint. The pin-clevis joint is used in a wide range of industrial and commercial applications and there is considerable information in the open literature regarding factors that affect its static strength. However, very little information is available on the design aspects that affect the structural stiffness. The present experimental study was a limited parametric evaluation of some factors that affect the stiffness of pin-clevis joints.

The tests on the near-center latch described herein are a part of the total experimental evaluation for the 20-meter long deployable truss beam mentioned previously. This joint incorporates a spring-loaded linkage-mechanism to obtain mechanical advantage and lock the hinge in the deployed position. It has a long history of successful applications (reference 3) and has also been called an "almost-over-center latch" and a "suitcase latch". The studies conducted in this experimental program will be presented in the order shown on the figure.

- Parametric study of pin-clevis joints

- Representative tests on near-center latch joint

Figure 1

Shown on figure 2 are some structural aspects of pin-clevis joints that can affect stiffness. It is obvious that the elastic moduli of the joint components will be important. However, due to the availability of standard parts or other considerations such as cold welding, it can be expected that the pin and the joint body would be fabricated from different materials. The shear and bending deformations of the pin will directly influence joint stiffness; however,analytical characterization of their effects is difficult due to the uncertainty of the loading and support conditions on the pin. Bearing and seating conditions are also difficult to characterize for the same reasons.

All of the aspects noted above affect joint stiffness in varying degrees. The experimental study was conducted to provide quantitative information that would assist in the practical design of joints for deployable truss structures with high axial and torsional stiffness.

Design aspects that affect stiffness

- Pin and parent joint material properties
- Pin response in shear, bending and bearing
- Load path
- Pin-diameter to joint-width relation

Figure 2

TEST SETUP AND PARAMETERS

The test setup and parameters evaluated are shown in figure 3. Three plates were bolted to fixtures attached to the loading heads of a hydraulic test machine. The plates were all 1-inch wide; the center plate was 0.5-inch thick and each side plate was 0.25-inch thick. The plates had a single hole in the center of the width and the hole was reamed to fit a steel gage pin of the desired diameter. The plates were assembled and bolted lightly to the test fixture. A close fitting pin was placed in the hole and the plate set was loaded in tension to aline all of the components in the load chain. The bolts were then tightened to firmly clamp the plates to the fixture to preclude slippage during the test. The displacement across the pin connection was measured with two commercial extensometers, one on each side of the plate, while load was applied. The load was cycled slowly through tension into compression. Data from the extensometers were taken frequently during the test.

Three materials were evaluated during the test: 7075 aluminum, 416 corrosion resistant steel, and TI-6AL-4V titanium. They were selected to be representative of materials with applications in space structures and they have a wide modulus range. The specimens were all tested as sets of a given material and several sets of each material were evaluated in selective tests to determine repeatability of results. All sets were drilled and tested with a nominal 0.25-inch diameter pin. Following this test series, one set of each material was drilled and reamed to fit the next larger test pin. This process was continued with the same plate set until the width of the load-bearing section adjacent to the hole was reduced enough to cause a significant loss in the tensile stiffness of the plate. At several of the test pin diameters, the plates were fitted with pins that were slightly undersized in increments of .0010 inch to evaluate the effect of pin fit on the test results.

After varying the nominal pin diameter and determining the diameter which would yield the highest value of stiffness, the length of the plate "e" was reduced to determine the minimum plate length beyond the hole center required to give a high value of stiffness.

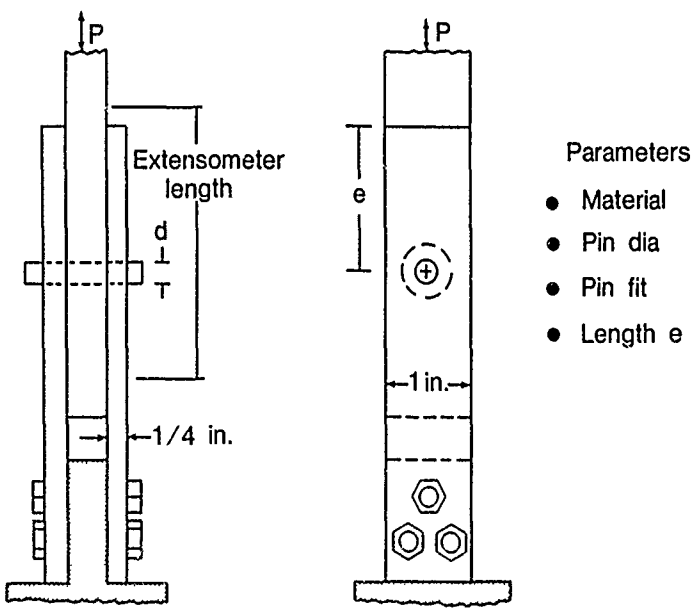

Figure 3

TESTS FOR PIN FIT

TITANIUM AND STEEL PLATES

Typical load deflection test results for a nominal 0.250-inch diameter steel pin in a titanium and a steel plate are shown in figures 4a and 4b respectively. Several test pins were used to examine the effect of pin fit on joint stiffness. It was anticipated that the effect of small changes in pin diameter and subsequent bearing area and stress distribution might affect the stiffness of the joint. However, the curves for each material are effectively parallel throughout the load range for all the diameters shown. The largest pin diameter tested (0.2510-inch diameter in figure 4a) provided a line fit with the hole (i.e., light pressure was required to insert the pin but when the pin was removed there was no evidence of substantial interference or marking of the surface around the hole or on the pin). The test results show that there was no free play between the plate and the pin. All other test results have a region of free play of approximately twice the value of the pin clearance. Therefore, hole to pin clearance should be eliminated for deployable pin-clevis joints if possible. This is especially true for truss beams and platforms that are only lightly loaded. Free play and nonlinearity in large multijointed trusses can accumulate, making accurate pointing and control very difficult to achieve. However, if the joints have interference or line fit pins, the level of interference must not be high enough to require large moments to deploy the truss. To accomplish a close hole-to-pin fit in the joint of a member that can be deployed with a reasonable moment, the diameter of the hole and pin must be accurately controlled with tolerances in the range of 0.0001 inch.

There is evidence in comparing the hysteresis in the curves of pin fit that the amount of hysteresis in the joint decreases with pin diameter. However, no measurements adequate for accurate evaluation of this effect were made.

TESTS FOR PIN FIT IN TITANIUM PLATE

.250 Nominal pin dia

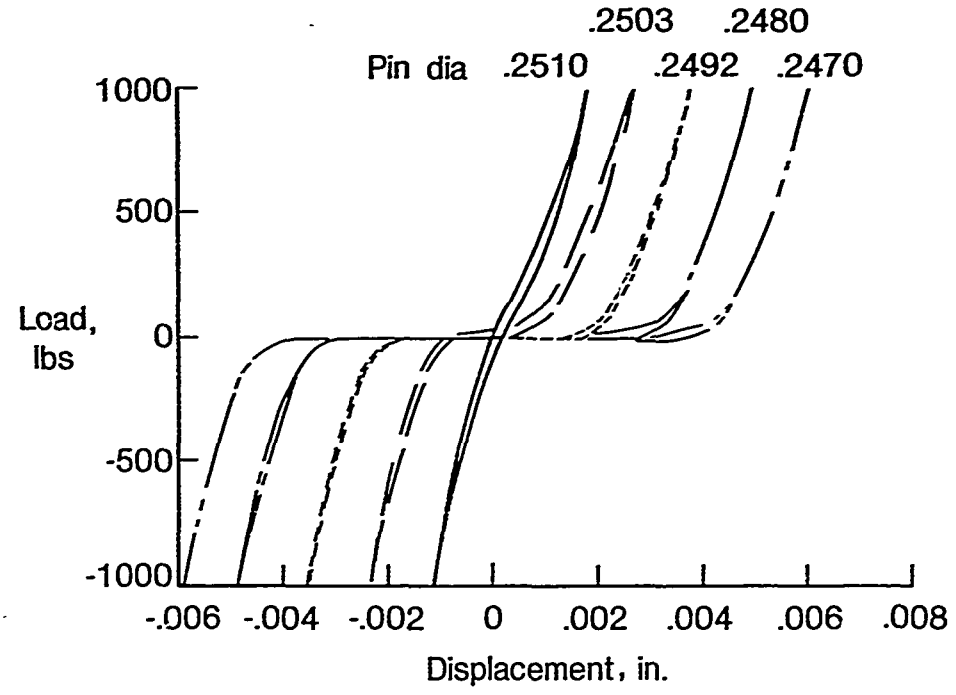

TESTS FOR PIN FIT IN STEEL PLATE

.250 nominal pin dia

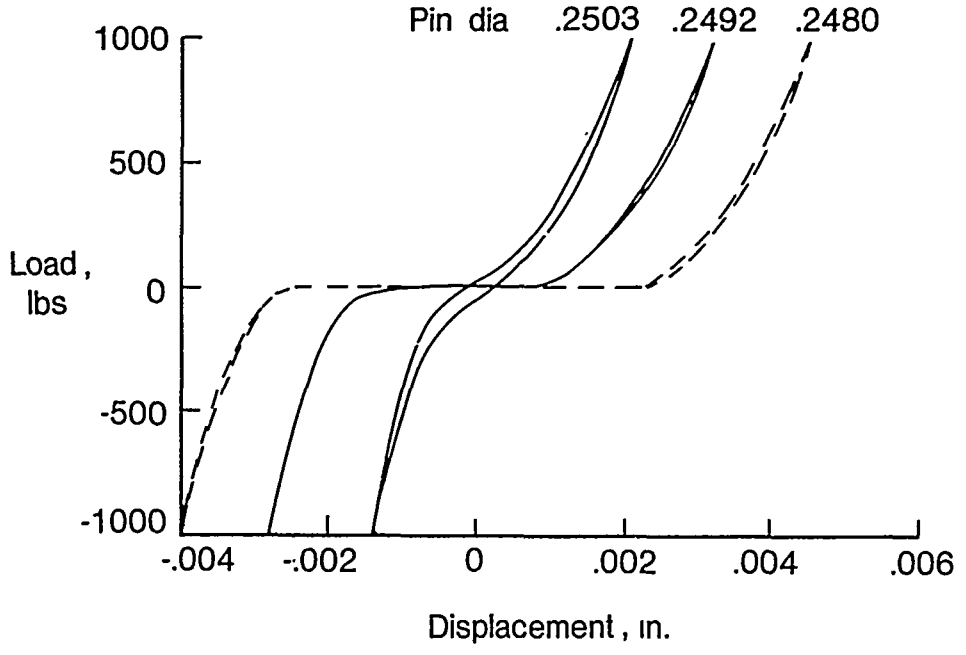

Figure 4

EFFECT OF PIN DIAMETER ON JOINT STIFFNESS

The average stiffness of the joint in the high load region (loads above 300 pounds) was determined from plotted results such as those shown on figure 4 for several nominal pin diameters. Typical stiffness results are shown in figures 5a and 5b for the steel and aluminum plates respectively. The dashed curves were faired through the points to represent the trends in the data. The stiffness for tensile loads increases in a well controlled manner with increase in pin diameter until it reaches a plateau in the range of 45 to 55 percent of the plate width. Then it decreases markedly for the largest diameter (0.63 inch) tested. However, the compression results continue to increase with pin diameter. The area reduction in the section adjacent to the pin is responsible for the loss in tensile stiffness but has no adverse effect on the compression stiffness because it is not in the compression load path. The data also indicate that the structural stiffness of a pin-clevis joint is bilinear and that the stiffness in compression will always be higher than it is in tension. This is because a tensile loaded joint has a longer load path and the net section stress level adjacent to the hole, which is in that load path, can be very high. To minimize this bilinearity, the results indicate that the pin diameter should be about 45 percent of the plate width, regardless of the parent joint material.

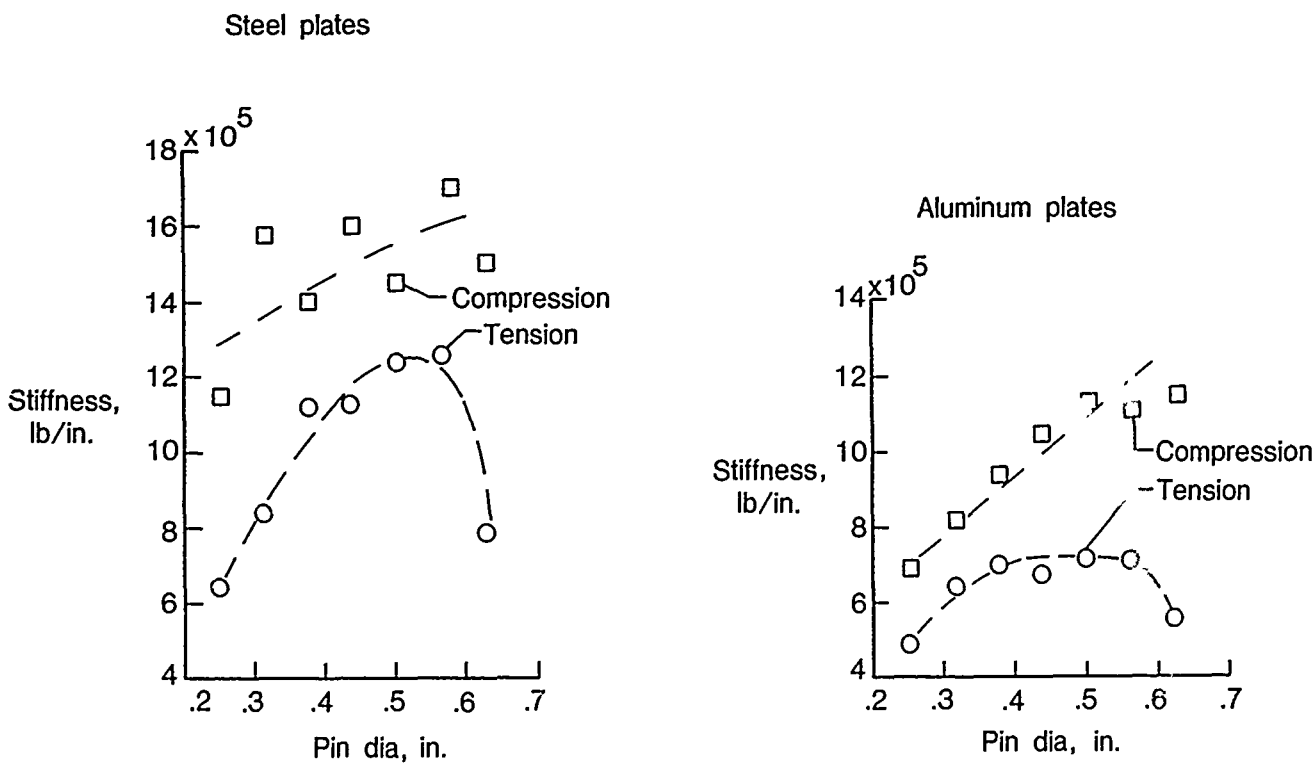

Figure 5

JOINT SECTION EFFICIENCY

Based on results such as those shown in figure 5 for all three materials tested, an estimated maximum joint efficiency was determined that may be useful in calculating the stiffness of deployable truss structures. The efficiency thus determined is shown in figure 6. The values shown are based on the maximum measured stiffness as determined from the test for a pin diameter in the range of 45 percent of the specimen width, with that stiffness normalized by the calculated stiffness of a solid bar of equivalent length. The efficiency noted on the figure for the various materials varies inversely with the elastic modulus of the plate material. Since all plates were connected with steel pins, it is apparent that the modulus of the pin contributes significantly to the efficiency of the joint.

$$\text{Efficiency} = \frac{\text{Max measured stiffness}}{\left(\frac{EA}{L}\right)_{\text{Test section}}}$$

Joint material	Efficiency	
	Tension	Compression
Steel	30%	38%
Titanium	43%	59%
Aluminum	50%	76%

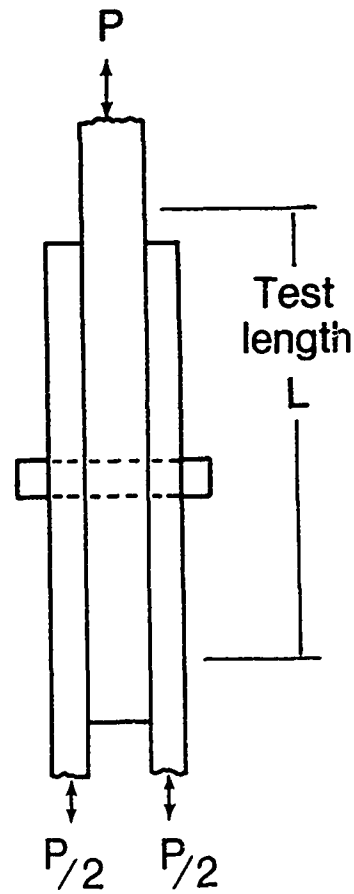

Figure 6

DESIGN RECOMMENDATIONS

Some design recommendations for pin-clevis joints are shown in figure 7. They are based on the results previously discussed and on some observations from similar work performed under the NASA sponsored contract for the 20-meter test beam model. The tests conducted in the present investigation were for only one width and thickness of plates, however, the results should be representative of a typical joint.

From the data presented in previous figures, it is apparent that a pivot pin of a high modulus material in a joint of the dimensional relations shown will result in a highly efficient joint. To minimize free play and nonlinearity, the pin should have a light interference fit with the plates, and the pin and hole surfaces should be smooth to avoid abrasion and wear. The contact surfaces may require plating or anodizing to prevent galling, particularly if aluminum or titanium materials are used in the fabrication.

Pin-clevis joints

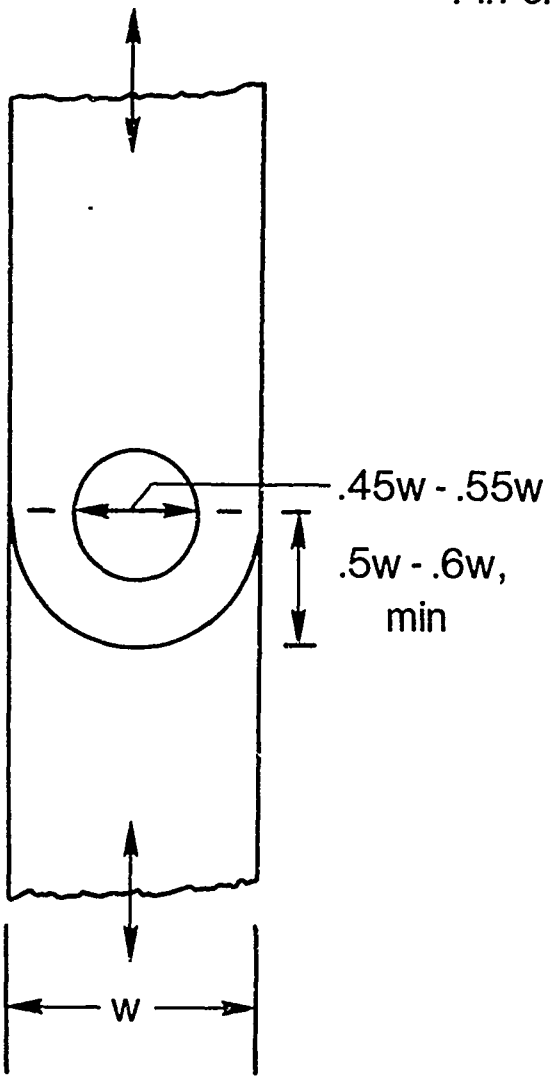

- Pin of high modulus material
- Light interference pin-to-hole fit
- Very smooth pin and hole surfaces
- Non-galling materials
- Dimensional relations shown

Figure 7

NEAR-CENTER LATCH JOINT

TEST MODEL

A photograph of the near-center latch is shown in figure 8. Joints of this type are very common in deployable trusses because they permit efficient packaging of a member and have a linkage mechanism that can carry significant axial load in both tension and compression in the deployed position. The test joint shown is a mid-length diagonal hinge for the 20-meter deployable beam that is a ground test article for COFS 1. The total test member is representative of the diagonal in that the end fittings are the same as the ones used in the beam. The length of the graphite tube has obviously been reduced to accommodate the test article in a conventional hydraulic test machine. The test joint is fairly large and more massive than would be desired for a flight test beam. This is due to the overall beam design which used the same joint to serve in two diagonal applications with slightly different hinge orientations instead of designing and fabricating a special joint for each location. Also, no significant effort was made to minimize the total joint mass.

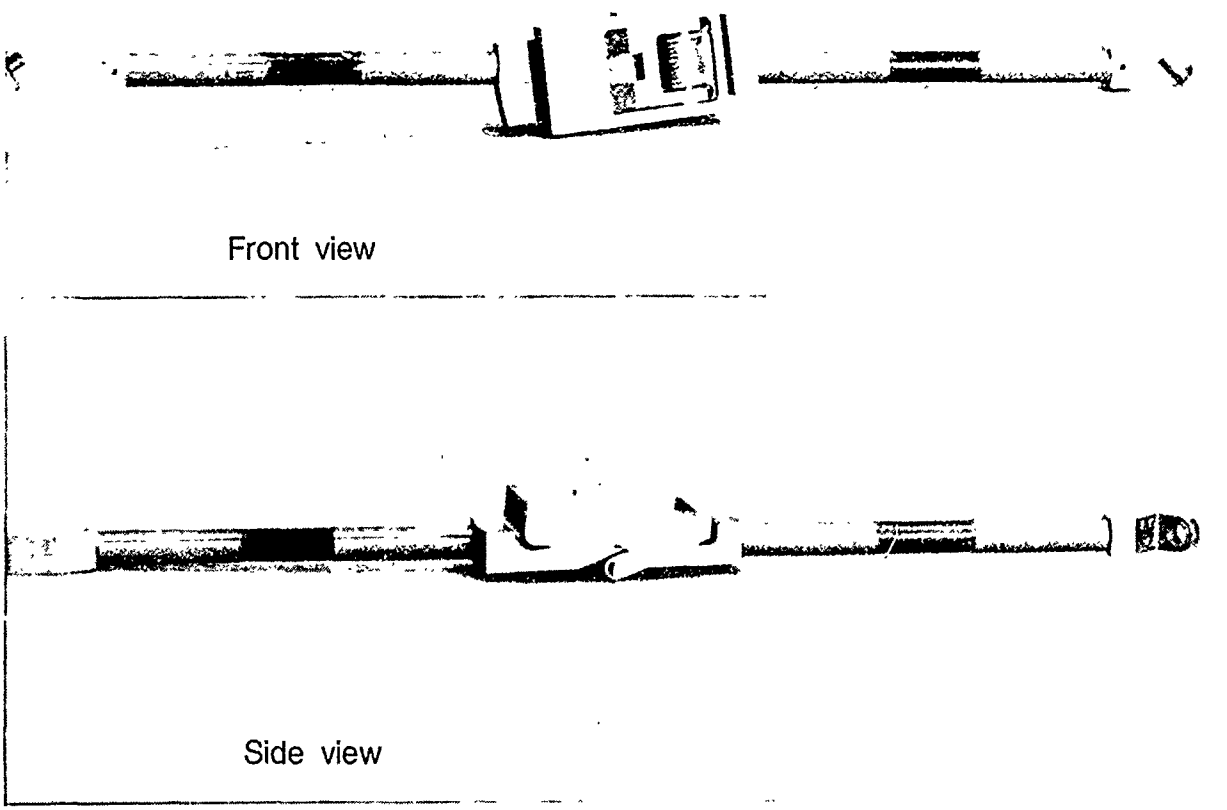

Figure 8

NEAR-CENTER LATCH JOINT

DESIGN ASPECTS

The primary design considerations for the near-center latch joint are outlined in figure 9. The parent metallic material is titanium with four hardened steel pins being used at the linkage and body hinge points. All pin holes were accurately positioned and the critical pin holes (i.e., the ones that control the closure position of the linkage mechanism) and the hinge pin hole were drilled with the parts assembled. All holes and pin diameters were sized to an accuracy of 0.0001 inch, and the assembled parts had between 0 and 0.0002 inches of interference fit. The linkage system was designed so that no member was in bending. The preload in the joint is controlled by the position of the linkage and the torsion load applied by the closure spring. The configuration was designed to have a preload in excess of 80 pounds, however, the response is very nonlinear in the closed position and the actual preload value has not been determined. Considerable effort went into the design of the joint so that a predictable and repeatable response could be obtained for a large number of units.

- Parent joint material-titanium, pin material-steel
- Linkage members in load path take only axial load
- All pins and holes have light interference fits
- Critical pin holes drilled on assembly fixture
- Interior preload of 80 + lbs

Figure 9

RESPONSE OF NEAR-CENTER LATCH JOINT

The load deflection response for the near-center latch joint is shown in figure 10. The deflections indicated in the figure were measured along an 8-inch section which included the latch only. As indicated by the symbols, data were taken at discrete values of applied load rather than continuously during the load cycle. The data points are shown connected by a faired dashed line. The response is linear over the entire 160 pound load range, indicating a preload in excess of 80 pounds. The joint has a stiffness of approximately 3.3×10^5 lbs/in. This is about the same stiffness as an 8-inch length of the graphite-epoxy tube to which the joint is attached. Although the joint is massive, its efficiency is still high in comparison with the results presented earlier for the pin-clevis joint.

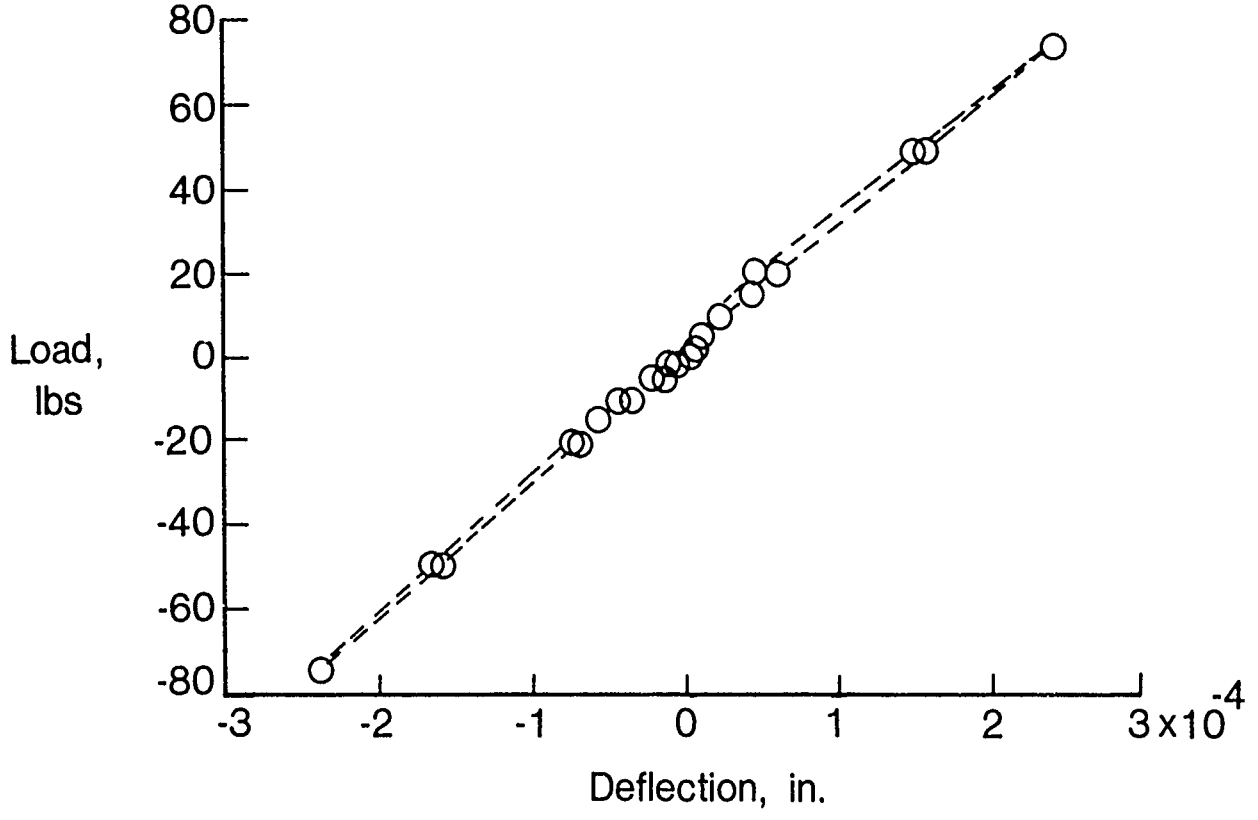

Figure 10

RESPONSE OF MEMBER WITH NEAR-CENTER LATCH JOINT

The member with the near-center latch was instrumented to evaluate the total displacement as well as the displacement across the latch shown in the previous figure. The total displacement, including that of the end attachment, is shown in figure 11. The data points on the plot were taken at the same discrete loads as those in figure 10. Also shown on figure 11, for comparison, is the curve for the latch only from the previous figure. The data shown in figure 11 are for one tension-compression cycle from the results of a three-cycle test and the data do not pass through the origin. The tension load cycle indicates a decrease in slope at a load around 20 pounds. It is suspected that this decrease in slope is due to sliding of the end tangs along their support mounting pins. Therefore, the truss member stiffness is represented by the unloading parts of the cycle. It is also apparent from the figure 12 results that the stiffness of the latch is significantly higher than the stiffness of the total member. The lower member stiffness must therefore result from bending of the end tangs. This demonstrates the significance of bending deformations in the design of high stiffness structures and the need to eliminate bending in members and connections in the load path whenever possible. However, this cannot always be accomplished. For example, the angle of the end tangs and orientation of the pivot angles for this beam were determined from a kinematic and structural analysis to minimize the internal member loads during deployment and retraction.

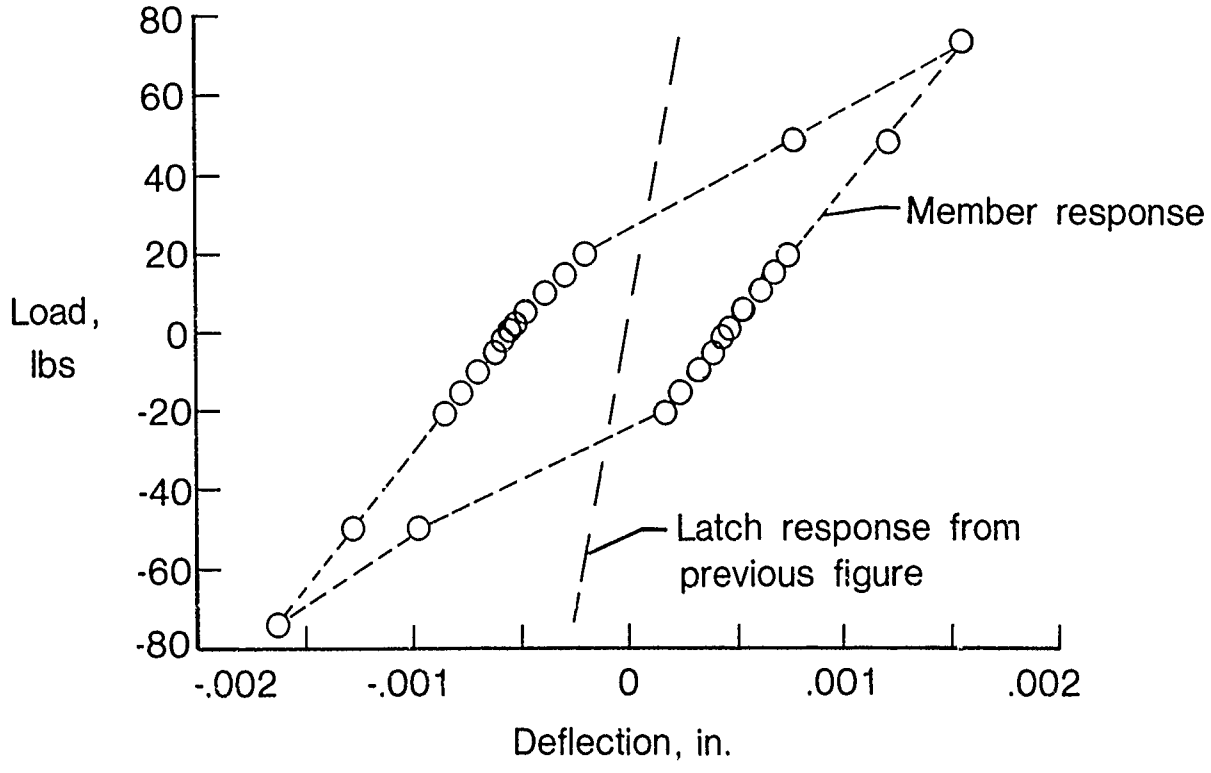

Figure 11

SUMMARY

The experimental results presented have indicated the importance of attention to detail in the design and fabrication of joints for deployable truss structures. The dimensional relations and material considerations for efficient pin-clevis joints have been outlined. The results of tests on the near-center latch indicate that joint complexity does not necessarily sacrifice stiffness. However, the test joint was fairly massive. This is undesirable for dynamic considerations, especially if the joint is in the center of a long member. Bending causes low axial stiffness and must be eliminated in the member and connecting joint if at all possible for the high axial and torsional stiffness of the truss structure to be realized.

Design recommendations formulated for pin-clevis joints

Linear load-displacement can be obtained in complex joints

Bending must be eliminated to realize attributes of well designed and fabricated joint

Figure 12

REFERENCES

1. Belvin, W. Keith: Modeling of Joints for the Dynamic Analysis of Truss Structures. Master of Science Thesis, School of Engineering and Applied Science, George Washington University, December 1985.

2. Housner, J.; Anderson, M.; Belvin, W.; and Horner, G.: Structural Dynamics Analysis. Large Space Antenna Systems Technology 1984. NASA Conference Publication 2368, Part 1, December 1984.

3. Adams, Louis R.: Stacbeam: An Efficient, Low-Mass, Sequentially Deployable Structure. Paper presented at 17th Intersociety Energy Conversion Engineering Conference. Los Angeles, California, August 1982.

COMPARISON OF MODAL IDENTIFICATION TECHNIQUES USING A HYBRID-DATA APPROACH

Richard S. Pappa

Structural Dynamics Branch

NASA Langley Research Center

Hampton, Virginia 23665

First NASA/DOD CSI Technology Conference

November 18-21, 1986

INTRODUCTION

Modal identification is the process of determining the modal parameters (natural frequencies, damping factors, mode shapes, and modal masses) of a structure from experimental measurements. In general, these parameters are not directly measurable quantities. A commonly used approach is to infer their values from a set of measured frequency response functions (FRFs). This parameter identification process, though relatively straightforward in principle, is often quite difficult and time-consuming in practice, particularly for large or built-up structures. Large structures may have many local modes in the frequency range of interest, making it difficult to determine global characteristics at nearby frequencies. And built-up structures, consisting of two or more components connected together with fasteners or joints, are often nonlinear due to imperfect load paths across the connections.

For these structures, it may be difficult to determine the true number of modes, and many of the identified mode shapes may be questionable. Identification results can vary considerably using different analysis techniques.

Many different approaches are possible for the identification of structures (e.g., Refs. 1-7). Some work has been done on comparing various techniques mathematically (Refs. 8-9). However, virtually no information is yet available on how the techniques compare in practice. Theoretical considerations, of course, form the foundation of any technique. Unfortunately, however, the performance actually observed in practice can be affected significantly by a number of factors not accounted for explicitly in most techniques. These factors include nonlinearities, unusually high modal density or damping, local modes, unmeasured excitations, large differences in modal response amplitudes, nonstationarity, sensor noise, off-axis sensor response, signal-processing biases, inconsistent data, finite dynamic range, and roundoff error, among others.

This paper discusses a new method for studying the performance of various identification techniques in practice. The procedure is analogous to using simulated data corrupted by random noise--a commonly used procedure--except now the simulated data is "corrupted" instead with a set of complex experimental data. For this study, a set of 128 frequency response functions from an erectable truss structure with high modal density and significant nonlinearity was used. These data were modified numerically by adding two artificial modes with known parameters. The resulting "hybrid data" were then analyzed using both the Polyreference technique (Refs. 10-13) and the Eigensystem Realization Algorithm (ERA) (Refs. 14-17) over a wide range of analysis orders (i.e., assumed number of modes). Identification performance is studied by comparing the identified parameters for the artificial modes with their known values. Six different cases, using distinct and then repeated eigenvalues at three different response amplitudes, were analyzed. Representative portions of the results are discussed.

CONSTRUCTION OF "HYBRID DATA"

Figure 1 illustrates the construction of a typical "hybrid" frequency response function. The top plot shows individual FRFs for each of two simulated modes. In this case (referred to later as Case 2) the modes have natural frequencies of 50 and 55 Hz, modal damping factors of 0.5 percent, residue amplitudes of 1.0, and residue phase angles of 1.571 rad.

The middle plot in Figure 1 shows a driving-point FRF measured during a modal survey test of the erectable truss structure. More than thirty resonances appear between 10 and 128 Hz. This relatively wide frequency band was chosen for the test because there are only four or five global bending and torsion modes of the structure in the interval. The remaining resonances are associated with local modes of individual members of the truss, modes of the suspension cables, rigid-body modes, and harmonics of lower frequencies arising from nonlinearities.

The bottom plot shows the corresponding hybrid function constructed by summing the top and middle functions shown in the figure. In this case the two added modes are large enough in amplitude to rise moderately above the original experimental data. Two other modal amplitudes were also used in the study: one in which both modes were ten times larger in amplitude than those shown in Figure 1, and the other in which they were ten times smaller.

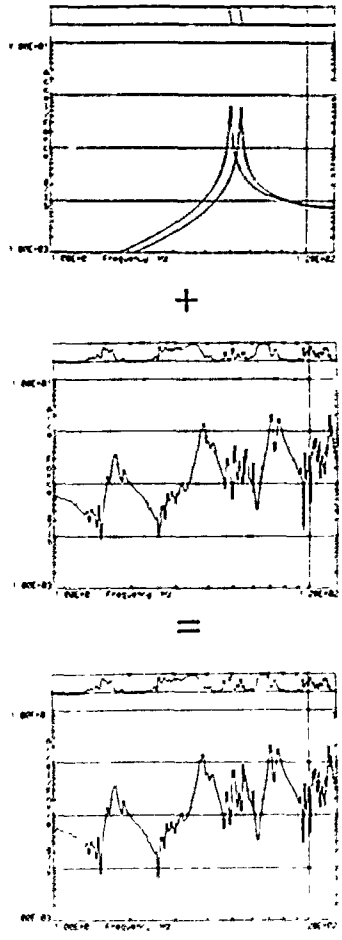

Figure 1

GENERIC 1/4-SCALE SPACE STATION TRUSS

Figure 2 shows the truss structure from which the experimental data for this study were obtained. It is a generic quarter-scale model of a configuration being considered for the Space Station. The structure is 26-1/4 feet (8.0 m) long, 3-3/4 feet (1.14 m) wide, and was suspended by two steel cables about 30 feet (9 m) long attached near the node points of the first global bending mode. The test was conducted using dual-shaker, burst-random excitation (Ref. 18), with vertical excitation applied at one end while lateral excitation was applied simultaneously at the other. Response measurements were made in the Y and Z directions (see Figure 2(b)) at each of the 32 joints using a roving set of eight accelerometers. The Hv method (Ref. 19) and one hundred averages were used in generating the set of frequency response functions.

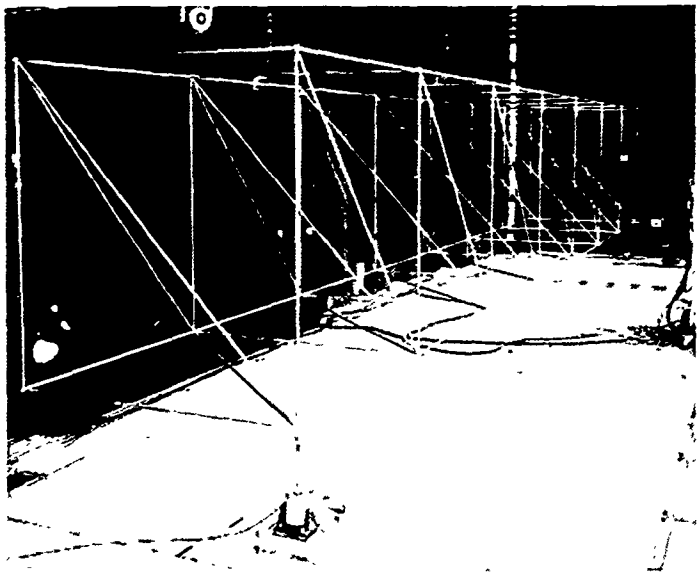

(a) Test Configuration

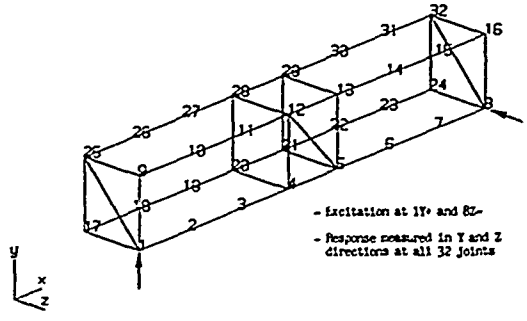

(b) Measurement Positions

Figure 2

NONLINEARITY STUDY

As mentioned earlier, the truss exhibited significant nonlinearity and high modal density. Figures 3 and 4 illustrate these characteristics. The frequency response functions shown in Figure 3 were measured at the lateral driving point using four different excitation amplitudes ranging from 0.01 lb rms at each shaker to 1.0 lb rms at each shaker. If the structure were linear, these four functions would be identical. However, considerable differences are observed. The two resonances near 70 Hz, in particular, change drastically as the amplitude is varied. Closer examination shows that most of the other resonances change as well, both in frequency and in damping level. An excitation amplitude of 0.1 lb rms at each shaker was used to acquire the data discussed in the remainder of the paper.

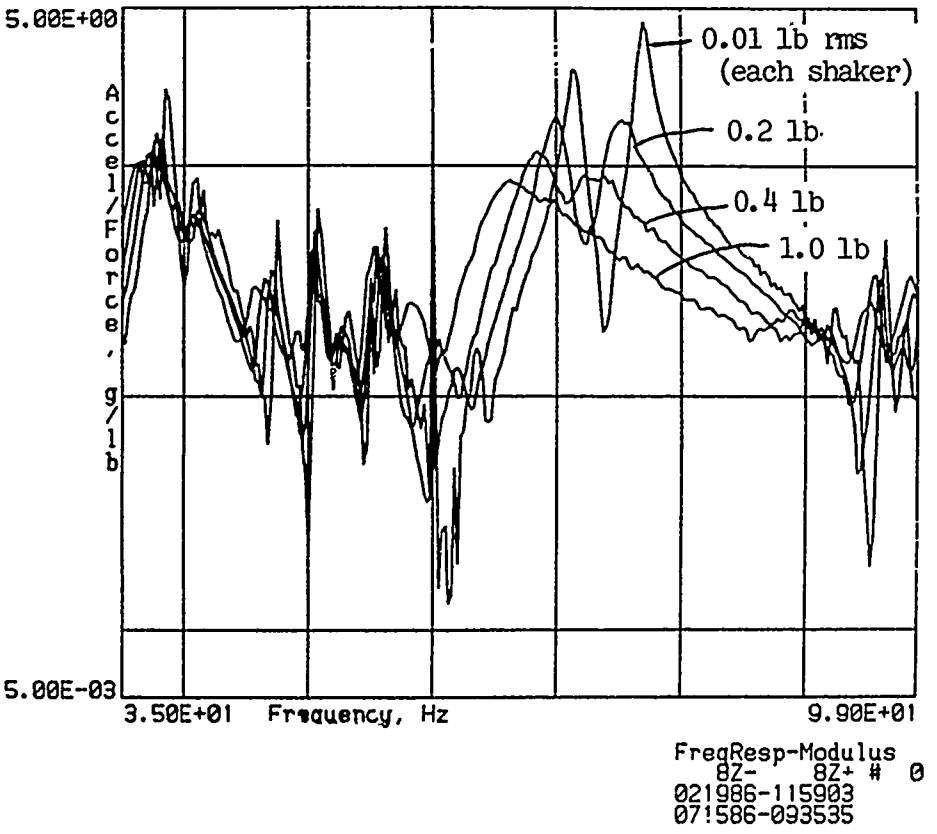

Figure 3

ESTIMATED NATURAL FREQUENCIES USING "SEARCH-FOR-PEAKS" TECHNIQUE

Figure 4 provides a quick overview of the high modal density exhibited by the truss. This plot contains 128 horizontal lines, one for each FRF which was measured. A simple "search-for-peaks" procedure (Ref. 20) was used to detect peaks occurring in each frequency response function, and the results are plotted using small tic marks. For simple, linear structures the figure would display a straight, vertical line at each natural frequency. For this data set, however, several discrepancies from this ideal behavior are observed. One discrepancy is the seemingly random scatter of peaks in the frequency interval from approximately 50 to 55 Hz. Another is that the mode near 75 Hz shifts abruptly in frequency at two different places.

The resonances between 50 and 55 Hz correspond to local resonances of the individual members of the truss. The shifts in the 75-Hz peak correspond to times during data acquisition when the eight accelerometers were moved. Whenever sensors are moved over a structure, the varying mass loading can cause frequency shifts. Miniature accelerometers were used in the test to minimize this effect, and no frequency shifting is evident except for the 75-Hz mode. It is also possible that slight variations in excitation amplitude may have occurred unintentionally during the test when the accelerometers were moved from one set of positions to the next.

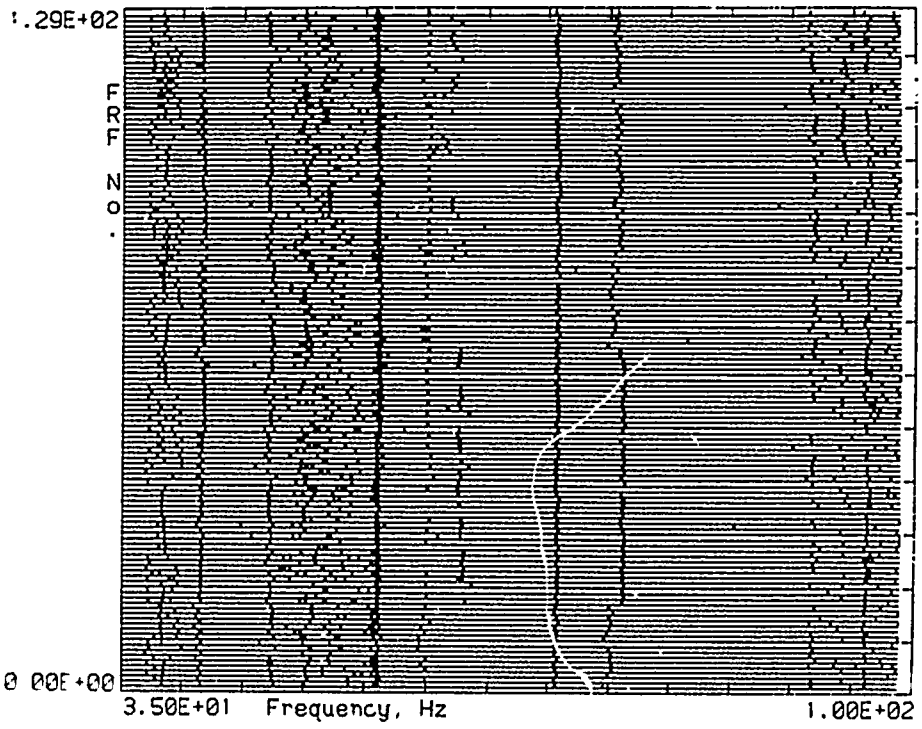

Figure 4

MODAL PARAMETERS AND MODE SHAPES FOR ARTIFICIAL MODES

The modal parameters and mode shapes used in constructing the two artificial modes, for each of six cases, are shown in Figure 5. Natural frequencies of 50 and 55 Hz were arbitrarily selected for Cases 1 through 3. The only change made in going from Case 1 to Case 3 was a reduction in residue amplitude from 10.0, to 1.0, to 0.1. The parameters chosen for Cases 4 through 6 are the same as those for Cases 1 through 3, respectively, except that the frequency of the second mode was lowered to 50 Hz. This change generated a repeated eigenvalue for these three cases.

Mode shapes for the two added modes were also arbitrarily selected. The simple alternating pattern of +1 and −1 shown in Figure 5(b) was used.

Modal Parameters, CASE 1

Label	Freq	Damping	Amplitude	Phase	Ref	Res	Mode	Flags
1	50.000	0.00500	10.00	1.571	1Y+	1Y+	1	0 0 0 1 1
2	55.000	0.00500	10.00	1.571	1Y+	1Y+	2	0 0 0 1 1

Modal Parameters, CASE 2 — Distinct Eigenvalues -- Varying Amplitude

Label	Freq	Damping	Amplitude	Phase	Ref	Res	Mode	Flags
1	[illegible]000	0.00500	1.000	1.571	1Y+	1Y+	1	0 0 0 1 1
2	000	0.00500	1.000	1.571	1Y+	1Y+	2	0 0 0 1 1

Modal Parameters, CASE 3

Label	Freq	Damping	Amplitude	Phase	Ref	Res	Mode	Flags
1	50.000	0.00500	0.1000	1.571	1Y+	1Y+	1	0 0 0 1 1
2	55.000	0.00500	0.1000	1.571	1Y+	1Y+	2	0 0 0 1 1

Modal Parameters, CASE 4

Label	Freq	Damping	Amplitude	Phase	Ref	Res	Mode	Flags
1	50.000	0.00500	10.00	1.571	1Y+	1Y+	1	0 0 0 1 1
2	50.000	0.00500	10.00	1.571	1Y+	1Y+	2	0 0 0 1 1

Modal Parameters, CASE 5 — Repeated Eigenvalue -- Varying Amplitude

Label	Freq	Damping	Amplitude	Phase	Ref	Res	Mode	Flags
1	50.000	0.00500	1.000	1.571	1Y+	1Y+	1	0 0 0 1 1
2	50.000	0.00500	1.000	1.571	1Y+	1Y+	2	0 0 0 1 1

Modal Parameters, CASE 6

Label	Freq	Damping	Amplitude	Phase	Ref	Res	Mode	Flags
1	50.000	0.00500	0.1000	1.571	1Y+	1Y+	1	0 0 0 1 1
2	50.000	0.00500	0.1000	1.571	1Y+	1Y+	2	0 0 0 1 1

(a) Parameters

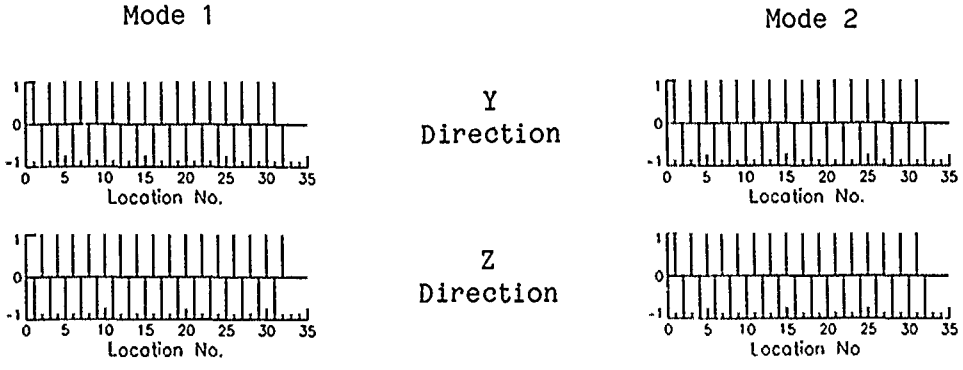

(b) Shapes

Figure 5

DATA ANALYSIS SELECTIONS

Several analysis options must be selected when using either Polyreference or ERA (see Refs. 20 and 14). It is important to recognize that considerable freedom is available to a user in choosing these analysis parameters and that the results will vary somewhat with different selections.

For this study the following choices were made: For Polyreference, a maximum mode count of 64 and a frequency interval from 35 to 99 Hz were selected; data from both references and all 64 response coordinates were accumulated into the correlation matrix; Modal Confidence Factors (MCFs) and complex residues were computed; and the assumed number of modes was incremented from 1 to 64. These selections resulted in the use of 194 time samples from each unit impulse response function.

For ERA, a block data matrix of 384 rows and 376 columns was established; data from both references (inputs) and all 64 responses (outputs) were used simultaneously, resulting in a block size of 64 by 2; time shifts of one data sample were used between all block rows, between all block columns, and between the two data matrices; a frequency interval from 35 to 99 Hz was used; and the assumed number of modes (one-half the number of retained singular values) was incremented from 1 to 64. These values were chosen so that 194 time samples were also used from each unit impulse response function.

The unit impulse response functions for both techniques were obtained by inverse Fourier transformation of the FRF data in the interval from 35 to 99 Hz (256 spectral lines).

IDENTIFICATION RESULTS

All identification results shown in this paper were generated on a VAX 11/780 computer, using Version 9.0 of Modal-Plus (Ref. 20) for all Polyreference analyses and the single-precision version of the ERA program for all ERA analyses.

To begin, the natural frequencies identified by Polyreference and ERA for Case 2 are plotted in Figures 6(a) and 6(b), respectively. These figures show all of the modes calculated by each method as the assumed number of modes (an analysis option in both techniques) was incremented from 1 to 64. The identified frequencies are indicated by short, vertical line segments. The height of each line segment is proportional to the corresponding MCF (for Polyreference) or to the corresponding Input Modal Amplitude Coherence (for ERA) calculated for the mode. Both MCF and IMAC are "accuracy indicators" used to help differentiate between extraneous eigenvalues due to noise and data distortions and the actual modes of the system. If the value of the indicator is 100 percent, the corresponding line segment is drawn as long as the distance between tic marks on the vertical axis. All identified eigenvalues are included in these plots; if the indicator had a value of zero, the corresponding mode appears as just a dot in the figure. Numbered arrows at the top of the plots indicate the frequencies selected for the two artificially added modes.

With simple, linear data these plots would also consist of straight, vertical lines located at the natural frequencies of the structure. Any data point falling off the lines would have a small accuracy-indicator value. However, as seen in Figure 6, things are not that straightforward with complex experimental data.

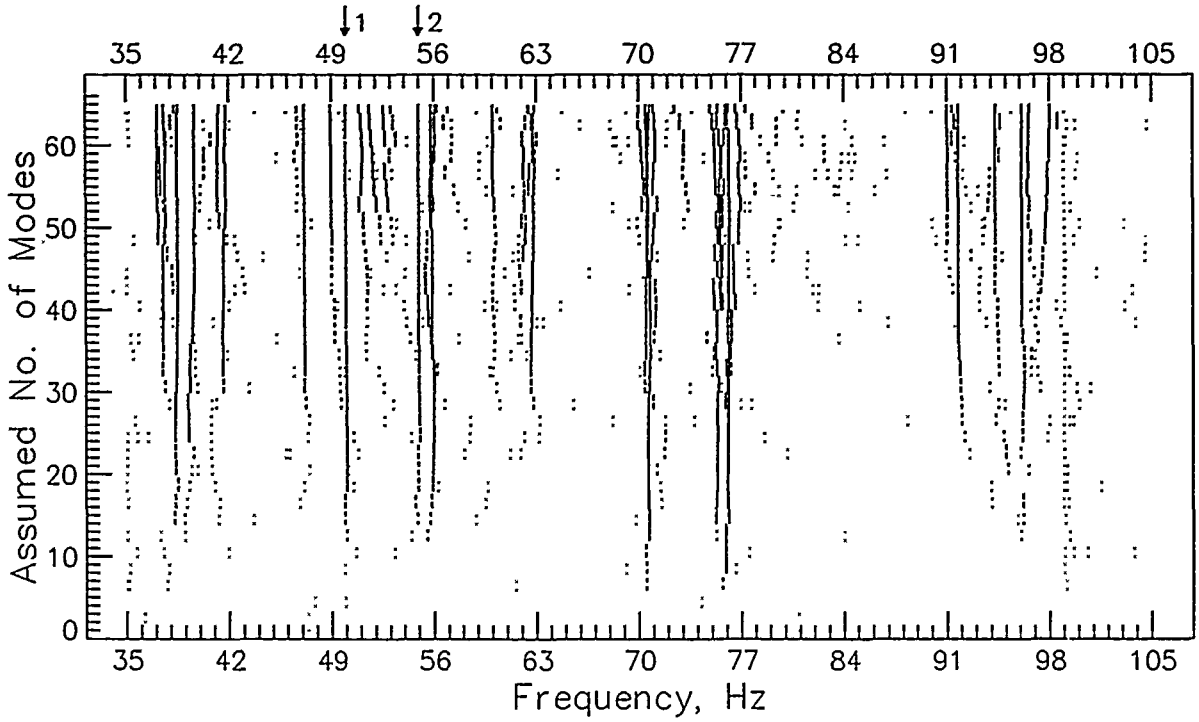

(a) Polyreference Results

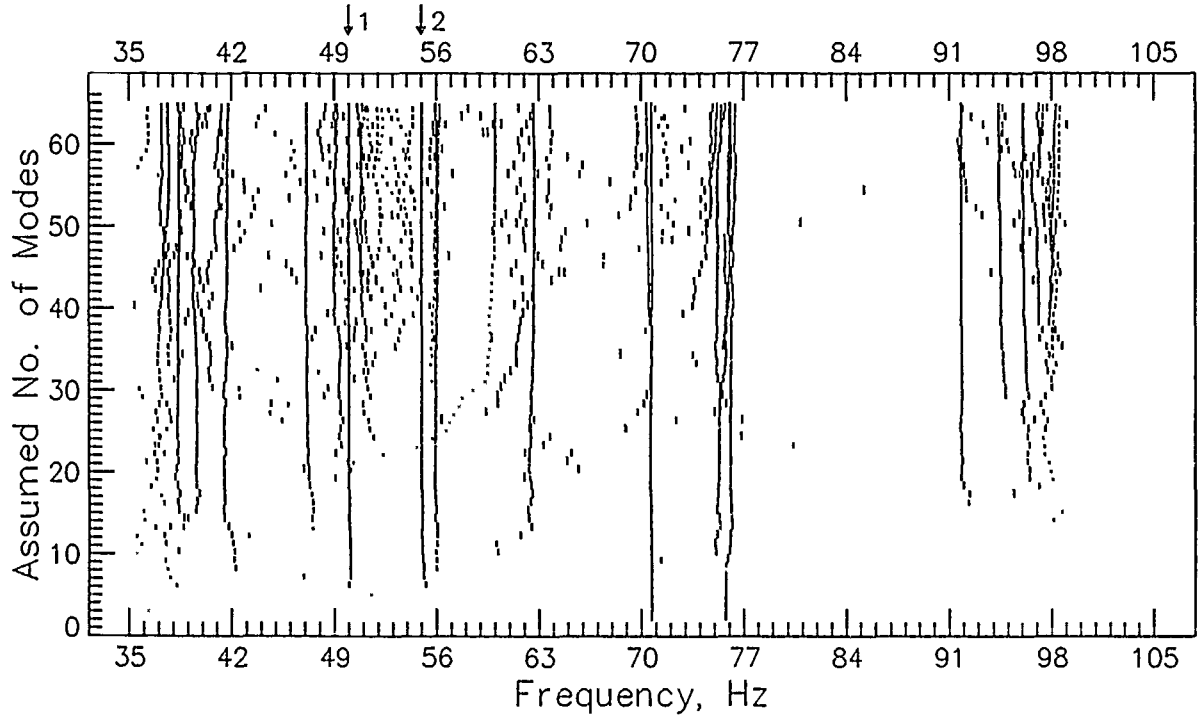

(b) ERA Results

Figure 6. Identified Frequencies for Case 2. Height of Dashed Lines Proportional to MCF (Polyreference) or Input Modal Amplitude Coherence (ERA)

Figures 7 and 8 provide a closer look at the results for Case 2 near the frequency of the second added mode (55 Hz). Figure 7 shows the Polyreference results and Figure 8 the corresponding ERA results. The identified frequencies are shown in the upper-left plots using the same format as in Figure 6. In this case, however, only the results for modes from 53 to 58 Hz are displayed to improve clarity. The five other plots in the figures provide additional, corresponding results for these modes. The true values of each parameter used for the artificial modes are again indicated by numbered arrows above the top axes. The two correlation plots at the bottom of the figures show the square of the correlation coefficient (Ref. 21) between each of the two chosen mode shapes (Figure 5(b)) and each identified shape.

A comparison of Figures 7 and 8 shows that both techniques identified the frequency, damping, residue amplitude, and mode shape information accurately for Case 2 as the assumed number of modes was increased sufficiently, although the rate of convergence is different. However, the identified residue phase angle shows a bias of approximately +15 degrees in both results. The cause of the bias is unknown at this time.

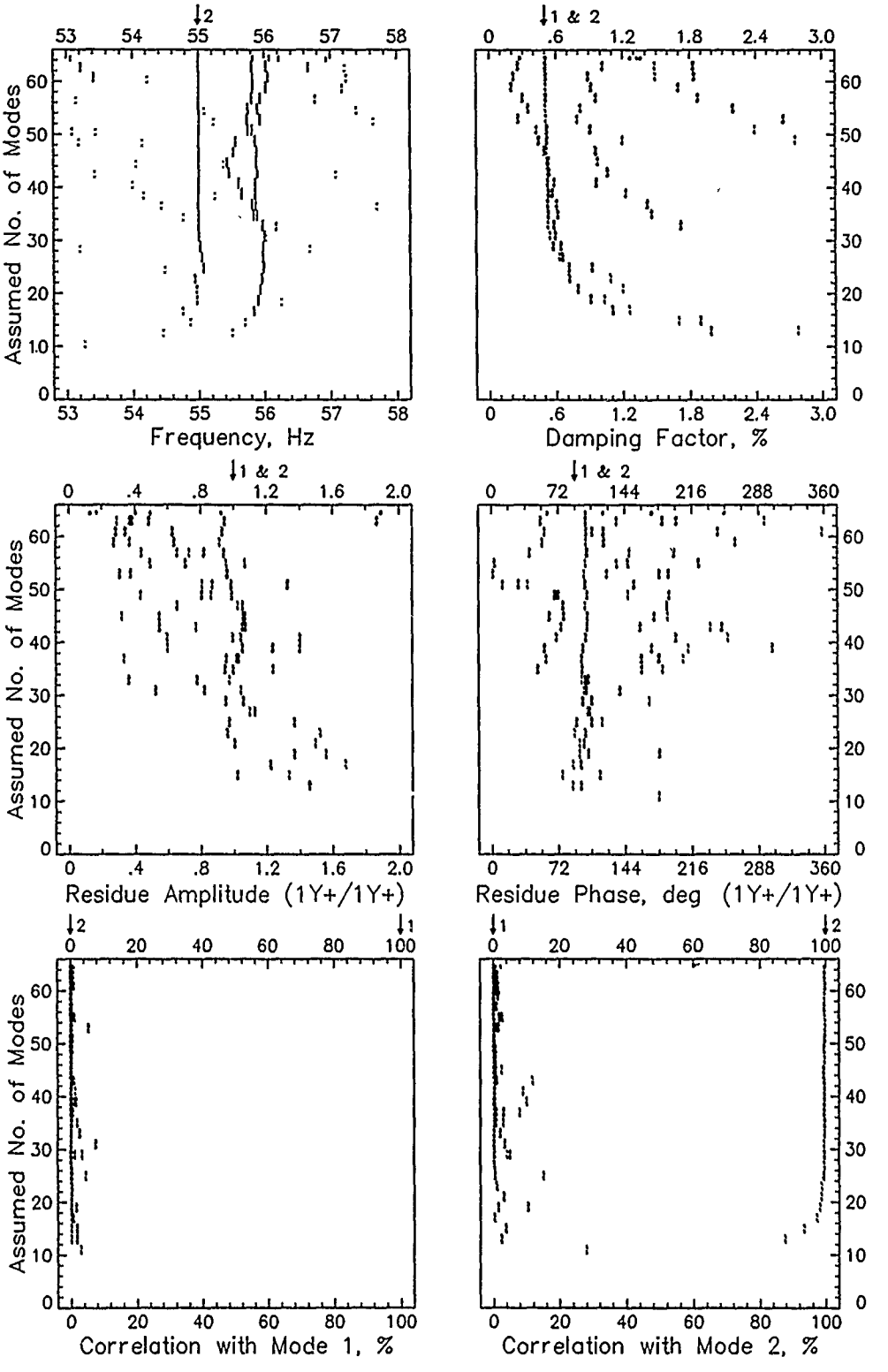

Figure 7. Complete Polyreference Results for Case 2
(Near Frequency of Second Added Mode)

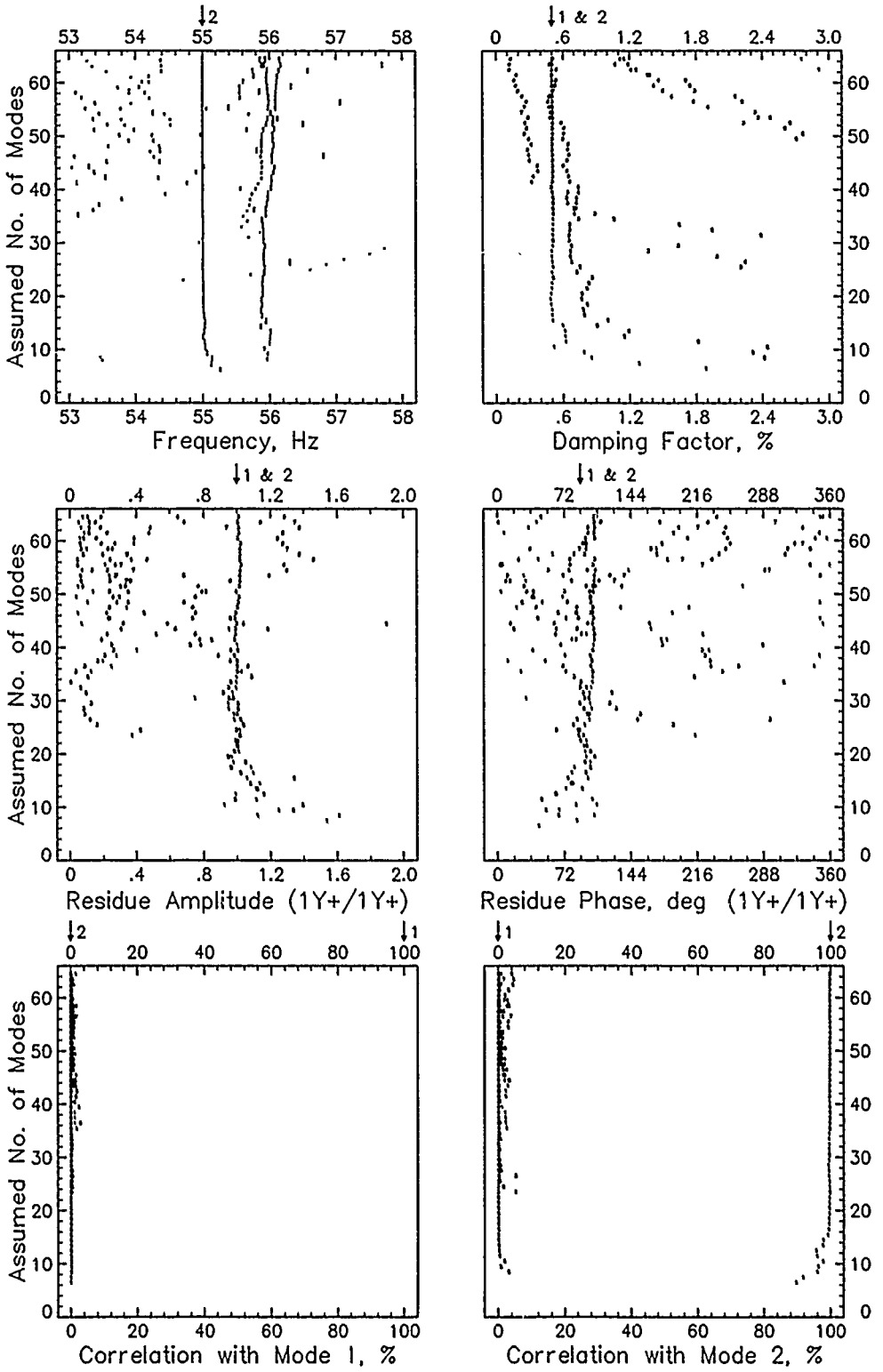

Figure 8. Complete ERA Results for Case 2 (Near Frequency of Second Added Mode)

Additional identification results are provided in Figures 9 and 10 for Cases 3 and 5, respectively. Case 3 used the same parameters as Case 2 except that the residue amplitudes were reduced by a factor of ten. At this low amplitude, the total energy in each of the two added modes is only slightly above the background noise floor. The amplitude reduction has caused the results to be uniformly less accurate than for Case 2. The residue and mode shape results, in particular, show significant deviations from their true values. Also note that the scatter in the frequency and damping results for the weak structural mode at slightly less than 56 Hz is similar in character to that for the 55-Hz artificial mode. This suggests a similar degree of inaccuracy in the identified mode shapes as well.

Figure 10 shows corresponding results for Case 5, in which the frequency of the second added mode was lowered to 50 Hz to generate a repeated eigenvalue. Both techniques successfully identified both modes. Again, however, the convergence rates are different. Note that the residue results are not determined uniquely in this case. The sum of the two identified residues, however, should equal the sum of the two true residues. Note also that the two correlation plots have been replaced by a single plot showing the total correlation between each identified mode shape and the shapes of the two added modes. The total correlation would be 100 percent for each mode for perfect identification.

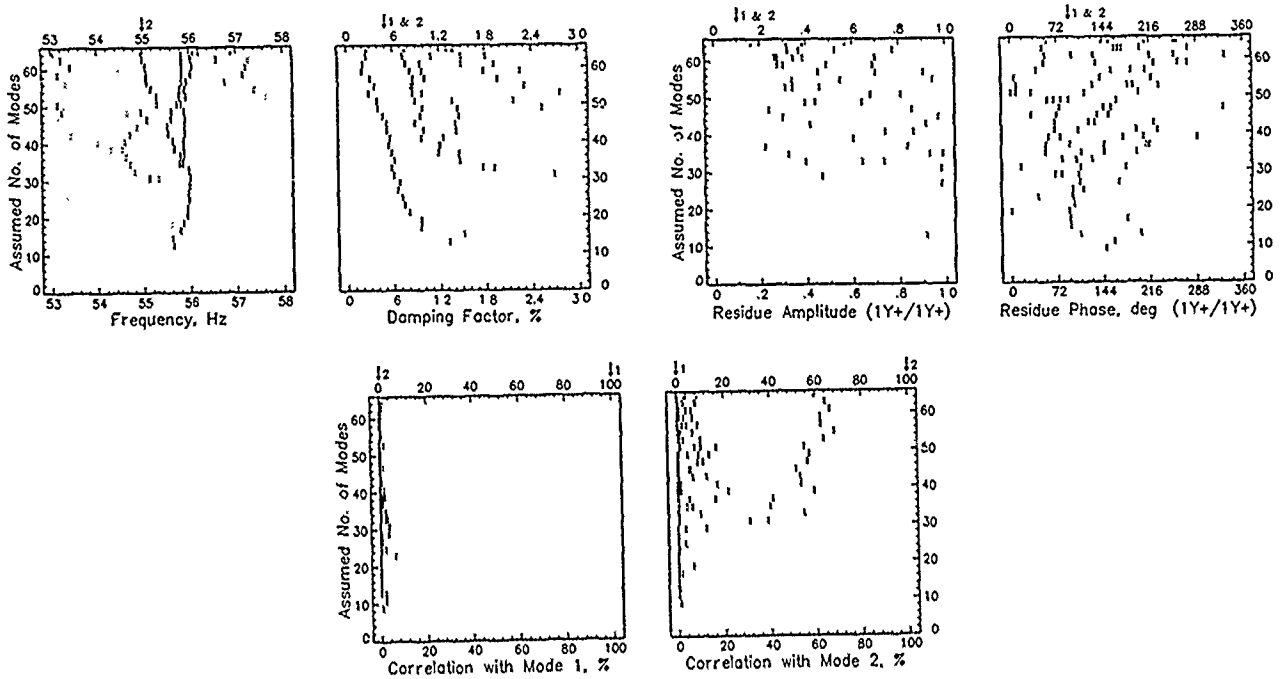

(a) Polyreference

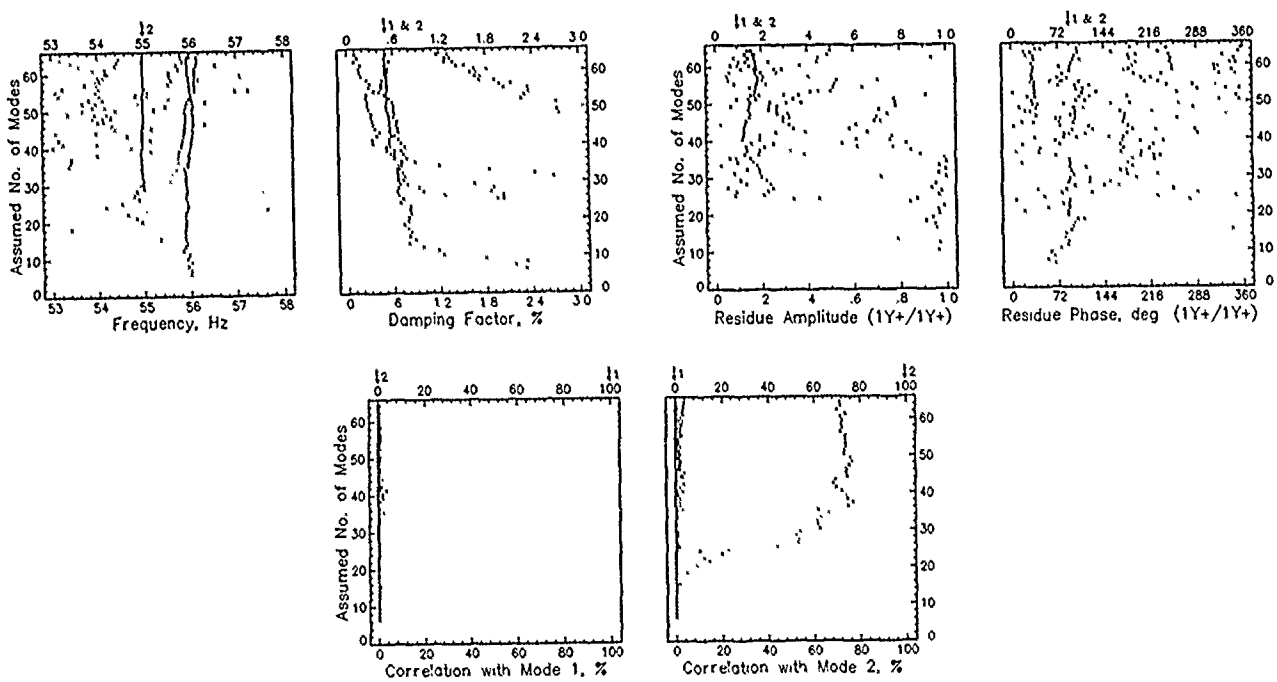

(b) ERA

Figure 9. Results for Case 3

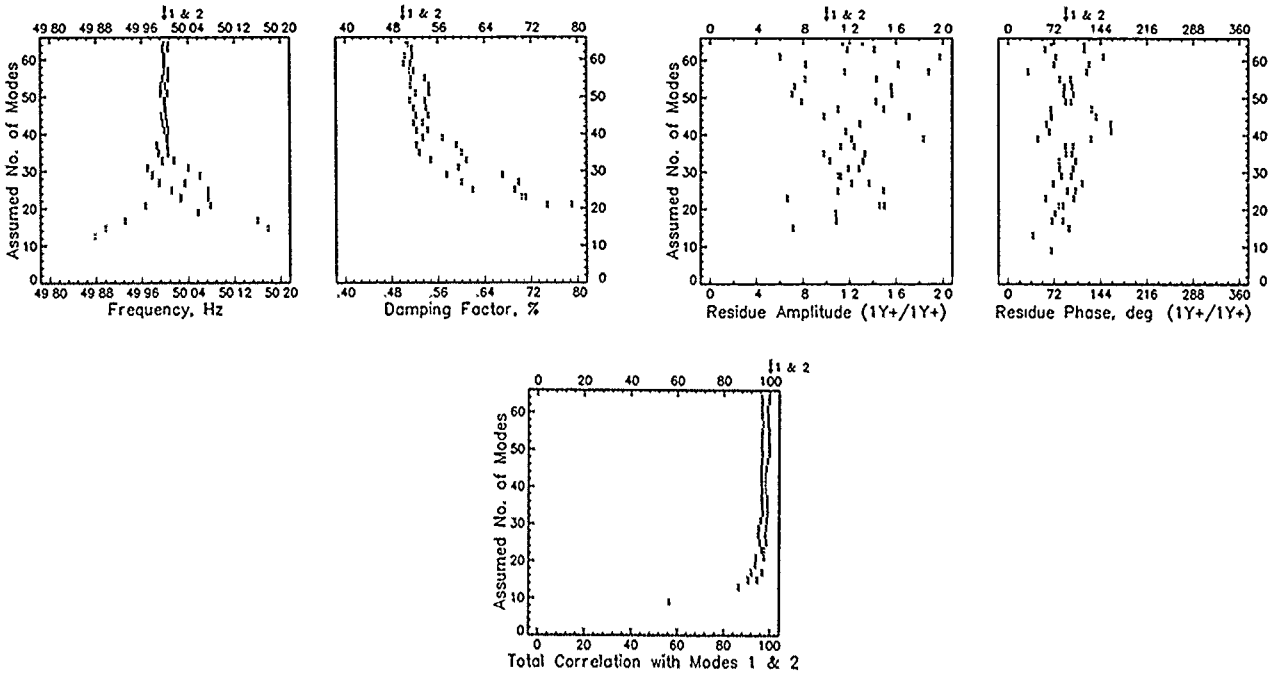

(a) Polyreference

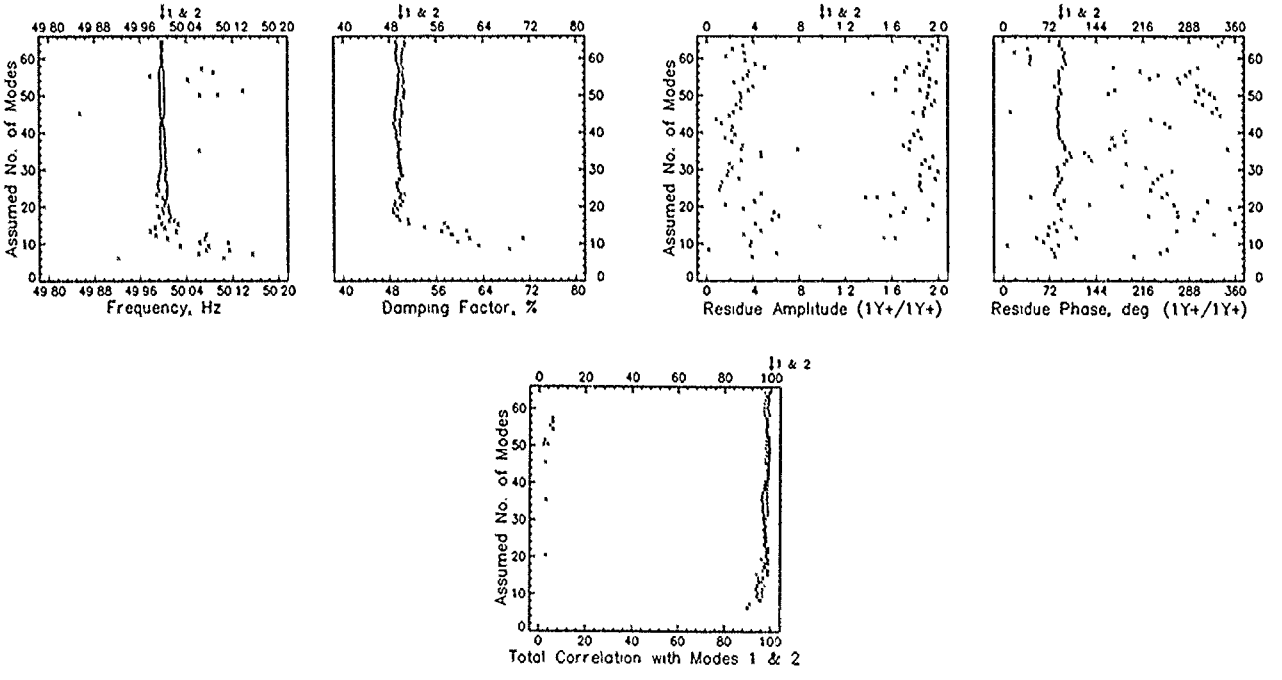

(b) ERA

Figure 10. Results for Case 5

CONCLUDING REMARKS

Modal identification of seemingly simple structures, such as the generic truss discussed in the paper, is often surprisingly difficult in practice due to high modal density, nonlinearities, and other nonideal factors. Under these circumstances, different data analysis techniques can generate substantially different results. This paper summarizes the initial application of a new "hybrid-data" method for studying the performance characteristics of various identification techniques with such data.

This approach offers new pieces of information for the system identification researcher. First, it allows actual experimental data to be used in the studies, while maintaining the traditional advantage of using simulated data. That is, the identification technique under study is forced to cope with the complexities of real data, yet the performance can be measured unquestionably for the artificial modes because their true parameters are known. Secondly, the accuracy achieved for the true structural modes in the data can be estimated from the accuracy achieved for the artificial modes if the results show similar characteristics. This similarity occurred in the study, for example, for a weak structural mode near 56 Hz (ref. Figure 9). It may even be possible--eventually--to use the error information from the artificial modes to improve the identification accuracy for the structural modes.

It must be emphasized, in closing, that it would be premature to generalize the identification results shown in this paper. More work, both numerical and mathematical, is needed to fully characterize the performance of either the Polyreference or the ERA technique with complex experimental data.

REFERENCES

1. Taylor, L. W. and Pinson, L. D., "On-Orbit Identification of Flexible Spacecraft," NASA CP-2368, December 1984, pp. 465-481.

2. Sundararajan, N., Montgomery, R. C., and Williams, J. P., "Adaptive Identification and Control of Structural Dynamics Systems Using Recursive Lattice Filters," NASA TP-2371, January 1985.

3. Mettler, E., Milman, M. H., Rodriguez, G., and Tolivar, A. F., "Space Station On-Orbit Identification and Performance Monitor," AIAA Paper 85-0357, January 1985.

4. Ewins, D. J., Modal Testing: Theory and Practice, John Wiley and Sons, Inc., New York, 1984.

5. Kurdila, A. J. and Craig, R. R., "A Modal Parameter Extraction Procedure Applicable to Linear Time-Invariant Dynamic Systems," Report No. CAR 85-2, Center for Aeronautical Research, The University of Texas at Austin, May 1985.

6. Stroud, R. C., "Excitation, Measurement, and Analysis Methods for Modal Testing," ASCE/ASME Mechanics Conference, Albuquerque, NM, June 1985.

7. Richardson, M. H., "Global Frequency and Damping Estimates from Frequency Response Functions," Fourth International Modal Analysis Conference, February 1986, pp. 465-470.

8. Leuridan, J. M., Brown, D. L. and Allemang, R. J., "Time Domain Parameter Identification Methods for Linear Modal Analysis: A Unifying Approach," AIAA Paper 84-0925, May 1984.

9. Juang, J. N., "Mathematical Correlation of Modal Parameter Identification Methods Via System Realization Theory," NASA TM-87720, April 1986.

10. Vold, H., Kundrat, J., Rocklin, G. T., and Russell, R., "A Multi-Input Modal Estimation Algorithm for Mini-Computers," SAE Paper 820194, February 1982.

11. Vold, H. and Russell, R., "Advanced Analysis Methods Improve Modal Test Results," Sound and Vibration, March 1983, pp. 36-40.

12. Crowley, J. R., Hunt, D. L., Rocklin, G. T., and Vold, H, "The Practical Use of the Polyreference Modal Parameter Estimation Method," Second International Modal Analysis Conference, February 1984, pp. 126-133.

13. Vold, H. and Crowley, J. R., "A Modal Confidence Factor for the Polyreference Method," Third International Modal Analysis Conference, January 1985, pp. 305-310.

14. Juang, J. N. and Pappa, R. S., "An Eigensystem Realization Algorithm for Modal Parameter Identification and Model Reduction," J. Guidance, Control and Dynamics, Vol. 8, Sept.-Oct. 1985, pp. 620-627.

15. Pappa, R. S. and Juang, J. N., "Galileo Spacecraft Modal Identification Using an Eigensystem Realization Algorithm," J. of the Astronautical Sciences, Vol. 33, Jan.-March 1985, pp. 15-33.

16. Brumfield, M. L., Pappa, R. S., Miller, J. B., and Adams, R. R., "Orbital Dynamics of the OAST-1 Solar Array Using Video Measurements," AIAA Paper 85-0758, April 1985.

17. Juang, J. N. and Pappa, R. S., "Effects of Noise on Modal Parameters Identified by the Eigensystem Realization Algorithm," J. Guidance, Control and Dynamics, Vol. 9, May-June 1986, pp. 294-303.

18. Zimmerman, R. and Hunt, D. L., "Multiple-Input Excitation Using Burst Random for Modal Testing," Sound and Vibration, October 1985, pp. 12-21.

19. Vold, H., Crowley, J. R., and Rocklin, G. T., "New Ways of Estimating Frequency Response Functions," Sound and Vibration, November 1984, pp. 34-38.

20. Structural Dynamics Research Corporation and CAE International, Modal-Plus Reference Manual, Version 9.0, 1985.

21. Allemang, R. J. and Brown, D. L., "A Correlation Coefficient for Modal Vector Analysis," First International Modal Analysis Conference, November 1982, pp. 110-116.

SYSTEM IDENTIFICATION AND MODELING FOR CONTROL OF FLEXIBLE STRUCTURES

Edward Mettler

and

Mark Milman

Jet Propulsion Laboratory
California Institute of Technology
Pasadena, California

First NASA/DOD CSI Technology Conference
November 18-21, 1986

LARGE SPACE STRUCTURES ACTIVE CONTROL

High performance control systems for flexible structures which provide adequate robustness require synthesis techniques that incorporate the interdependencies between performance objectives and model fidelity. Such levels of fidelity are not possible to achieve via ground testing alone. This is due to the fact that differences in ground and space environments can significantly change the measured parameters. In addition, the time-varying nature of the space environment requires real time "tracking" of key structural parameters.

An on-orbit ID function can provide the real-time knowledge of plant characteristics which greatly influence control performance, such as flex-body parameters, self-generated disturbances, shape distortions, actuation and sensing dynamics, etc. This information is then available for updating the controller plant model, and may serve as the data base from which a control function can make adjustments to autonomously tune the system performance and stability margins.[1]

In this discussion, the focus will be on those identification and modeling aspects primarily associated with large space structure dynamical control.

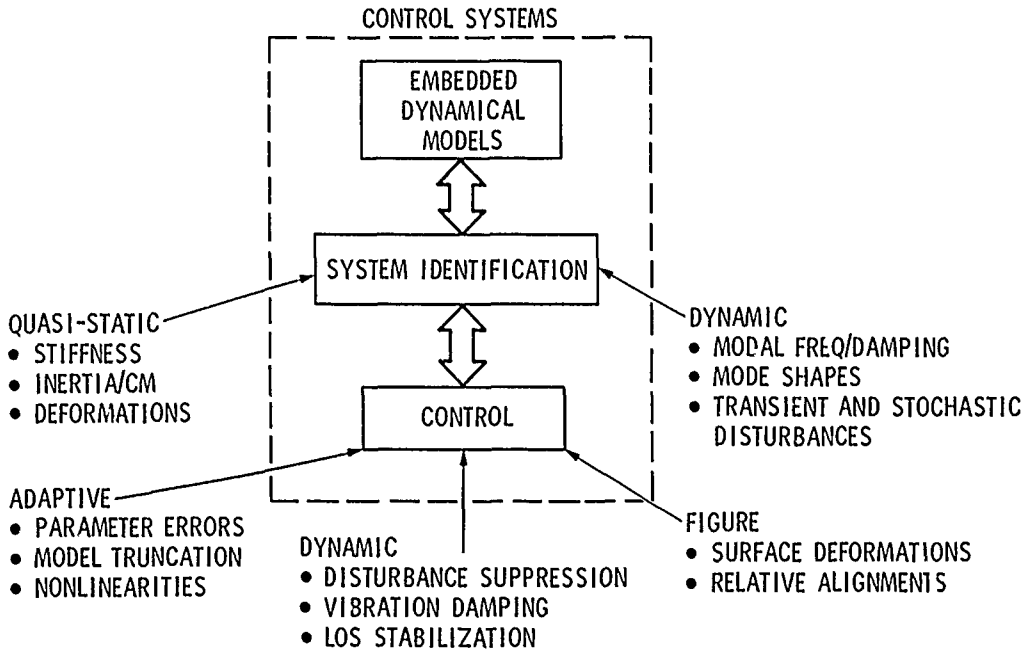

GENERAL FLEXIBLE STRUCTURE CONTROL METHODOLOGY

In general, the high frequency dynamics of LSS will not be well known and the order of the dynamics will be too large to design an effective wideband control system. New methods are required to control the low frequency modes without exciting the higher frequency dynamics inherent in the structure and to constrain the control gains from spill-over into the higher modes causing instabilities or performance loss. This area is a major thrust in the extension of modern control theory and the emerging cross-discipline technology of active structural control covers a wide range of interrelated design and system functions.

As depicted below, the general structure control methodology is to phase stabilize modes lying within the control bandwidth (in-band modes) and to gain stabilize structurally damped modes lying outside the control bandwidth. Such active control methods require very precise knowledge of the locations of the in-band modes in order to allow correct phase stabilization (such sensitivities are even more pronounced when actuators and sensors are non-colocated). Because such precise knowledge of system dynamics is not possible via ground testing alone, on-orbit system identification is required.

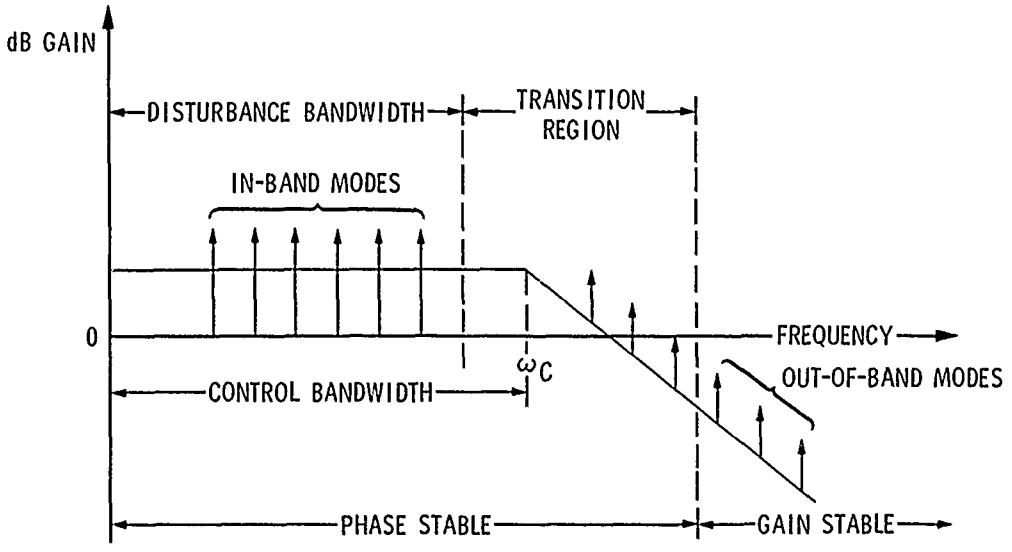

(PRECISE KNOWLEDGE OF IN-BAND MODES NEEDED FOR PHASE STABILIZATION)

DISTRIBUTED PARAMETER MODELING, APPROXIMATION AND CONTROL

Control design for distributed parameter systems introduces a number of complexities that are either not present or relatively innocuous in the design process for lumped systems. A most fundamental issue is selecting an appropriate reduced order model so that system performance objectives can be met. As is well known, a poor selection can severely degrade performance and in some cases yield closed loop instabilities. Under reasonable hypotheses on the finite dimensional approximation schemes, the distributed parameter LQG design approach utilizing a functional gain convergence criterion achieves a correct match between model order and desired performance[2]. In addition, LQG also has the desireable property that new physical objectives are easily incorporated into the design process through the state-cost functional.

We have successfully applied this distributed parameter LQG design methodology to large-scale simulations of control systems for flexible structures. The chart below contains time history plots of controller performance based on this approach. Because a functional gain convergence criterion is used, these controllers are very near optimal for the full distributed parameter system.

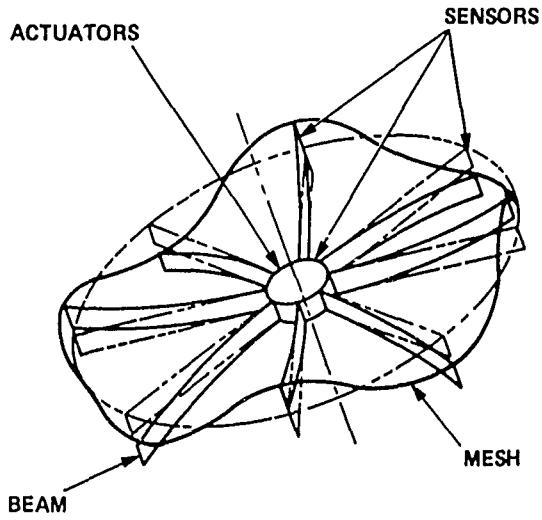

DISTRIBUTED PARAMETER ANTENNA POINTING AND VIBRATION CONTROL SYSTEM

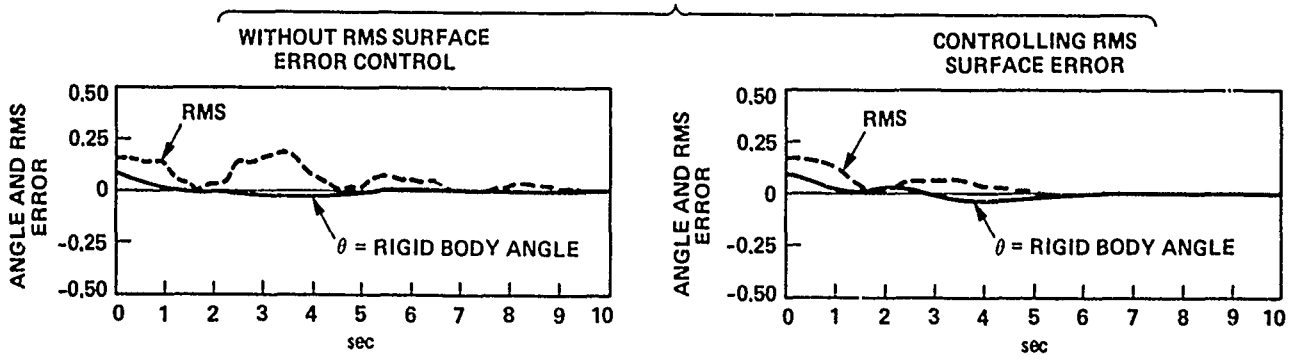

ON-ORBIT SYSTEM DYNAMICS IDENTIFICATION METHODOLOGY

The need for developing a system identification (ID) on-orbit methodology is driven by practical considerations. The post-launch changes in a physical system's characteristics must first be identified before the mission operations proceed with confidence; structural dynamics identification is essential for accomplishing active vibration control of large structures; and system characterization in space is required to verify the accuracy and adequacy of ground-based models for predicting and modifying in-flight performance.

The technical challenges involved in performing on-orbit identification are significant. As opposed to ground testing which involves elaborate test beds with virtually unlimited sensing, excitation, and computational resource, the on-orbit situation is constrained to only a few sensors, operationally viable excitations, and restricted computational resource.[3] The diagram below illustrates the integrated systems approach for on-orbit dynamics identification. The methodology involves a multi-stage identification process starting with robust nonparametric survey methods, and progressing to more refined parameter determination algorithms.

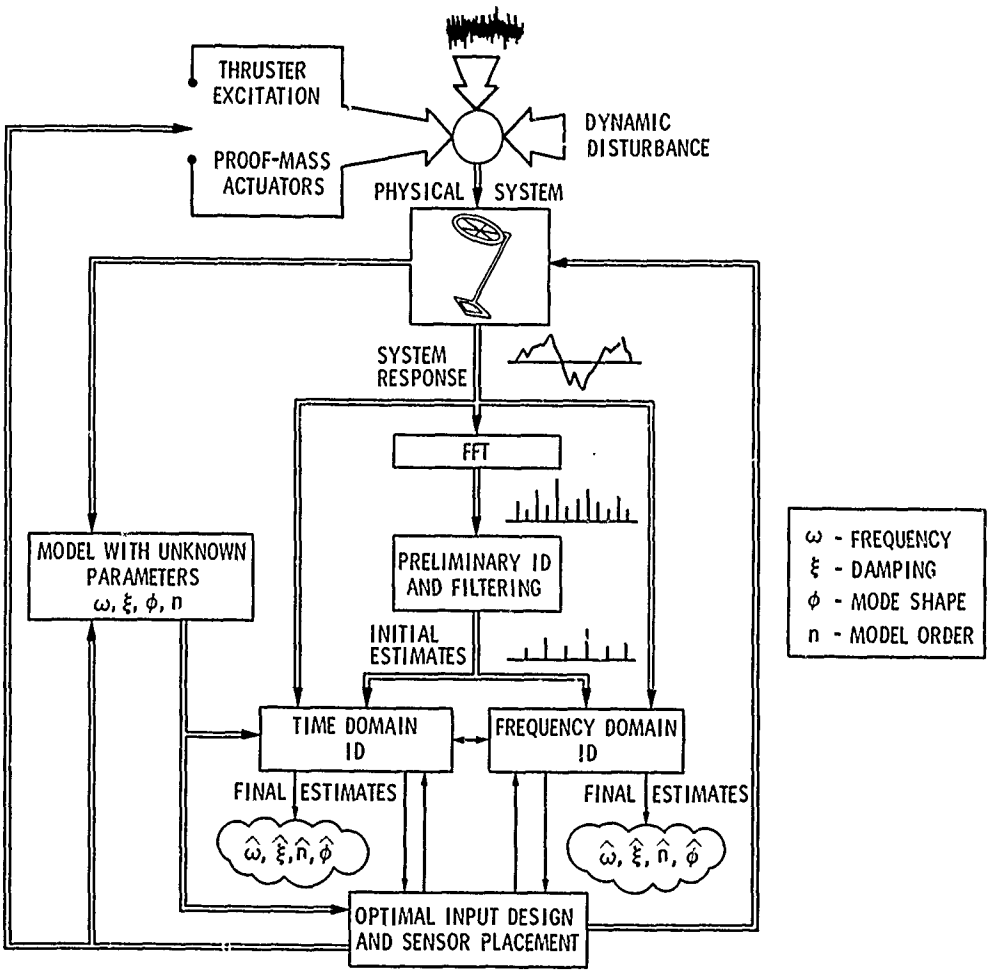

IDENTIFICATION EXPERIMENT CONSTRAINED INPUT DESIGN

On-orbit identification of modal frequencies of a 15 degree-of-freedom Power Tower model of the Space Station was considered using maximum likelihood estimation. Low frequency modes can successfully be identified by the proper application of multi-directional thruster inputs in the form of force and torques in orthogonal spaces. Higher frequency modes, however, are insufficiently excited to permit accurate estimation due to thruster power and bandwidth limitations. Among the inputs considered, it is concluded that staggered pulse sequences are superior for obtaining a more accurate estimate of the unknown parameters. When staggered thruster pulses are used the identification process may tolerate an initial parameter estimate error of up to 50% of the nominal values for the lower frequency modes. Further research is needed for the identification of modal dampings.[4,5,6]

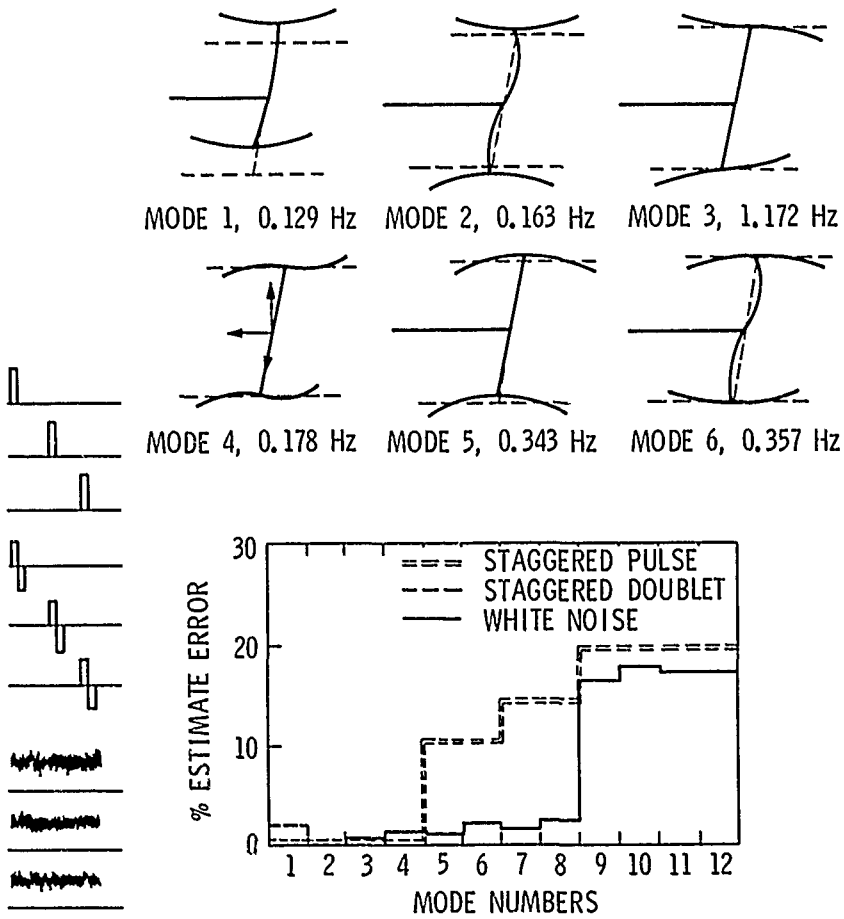

ROBUSTNESS ENHANCEMENT OF LQG CONTROLLERS

Our initial approach to control design utilizes infinite dimensional LQG theory to design compensators that are robust with respect to errors introduced by model truncation. A second error source that requires accommodation are those errors introduced by parameter error. At the present time two approaches have been developed and validated to improve the robustness characteristics of LQG compensators with respect to parameter error. The first approach synthesizes structured uncertainty and loop transfer recovery techniques to achieve a systematic process for making trades between performance and robustness[7]. In terms of synthesis, the method involves adjusting the weighting matrices in both the regulator and estimator portions of the LQG design problem in a way that reflects the structure and magnitude of the modeling uncertainties. This uncertainty information could be obtained from the covariance analysis provided by an on-line identification process. An alternative approach that has also been developed consists of a sensitivity optimization of the eigenvalues of the closed-loop system[8]. A nominal LQG compensator is used to initialize the nonlinear programming problem associated with the optimization. Constraints in the form of stability margins are imposed in the optimization to insure adequate trades between performance and robustness. On the models to which these methods have been applied, both approaches have yielded substantial improvement in robustness over standard LQG controllers.

The chart below illustrates the overall design methodology, and how the sensitivity optimization method can increase observer bandwidth in an LQG compensator and simultaneously increase its robustness properties.

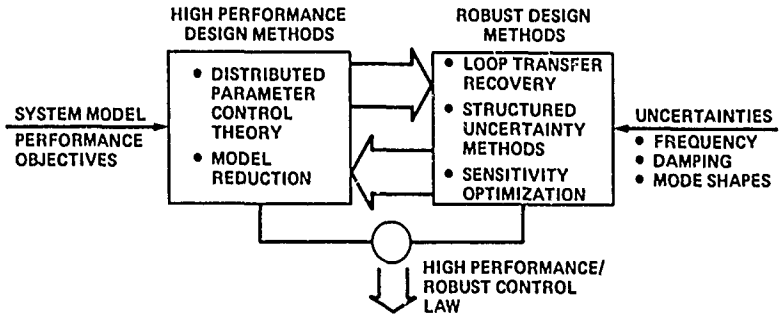

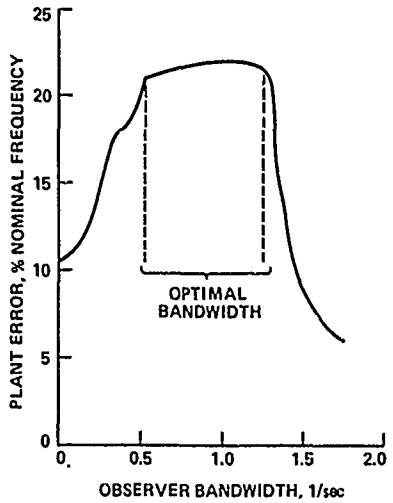

IDENTIFICATION AND CONTROL FLIGHT EXPERIMENTS

A natural progression of technology development, from analysis and simulation through laboratory physical test beds to full scale flight experiments, is basic to major CSI research initiatives. The COFS program and the ATSE (Antenna Technology Shuttle Experiment) provide the means to space test and enable application readiness of advanced identification and control technologies.

The objectives of the ATSE in identification and control have the underlying theme of an integrated system capability to support robust precision stabilization/control of the MSAT (2nd generation 20-meter dish). This can be further described by the following criteria which include operational constraints, system design limitations, in-situ performance maintenance, and synergistic use of identification/control techniques:

a) Integration of identification with active structure control for LOS stabilization
b) Identification in operational mission time
c) Design for flight system hardware limitations
d) Input design for controlled excitation[9,10]
e) Unify frequency and time domain techniques for in-flight support

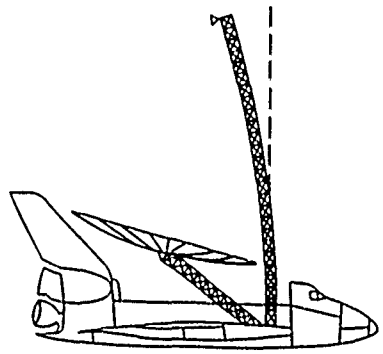

FIRST FEED-BOOM MODE (1.01 Hz)

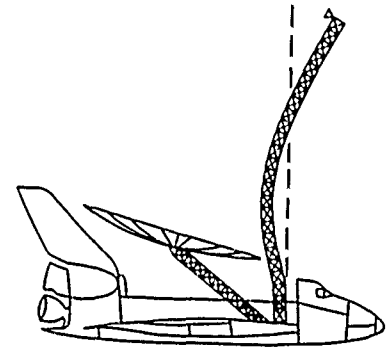

SECOND FEED-BOOM MODE (6.60 Hz)

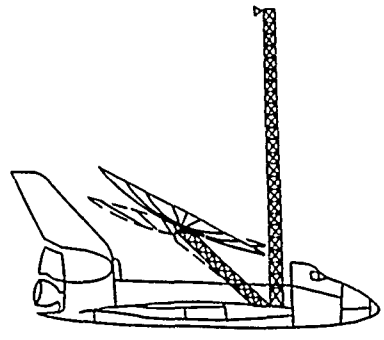

FIRST REFLECTOR-BOOM MODE (2.26 Hz)

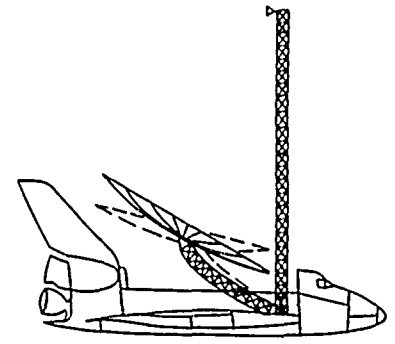

SECOND REFLECTOR-BOOM MODE (9.52 Hz)

POINTING JITTER CONTROL EXPERIMENT

The objective of this experiment is to control the dynamic motions of both feed boom and reflector boom in order to maintain precision pointing of the feed to dish line-of-sight. Distributed accelerometer signals are processed onboard by selected algorithm options to actively control boom dynamics via proof-mass actuators located at midspan and tip of each boom. Parameter updates from identification processing at the payload operations control center (POCC) are used to tune the controller-embedded reduced order plant models. Both regulation and tracking control policies are to be evaluated in a sequence of sub-experiments.

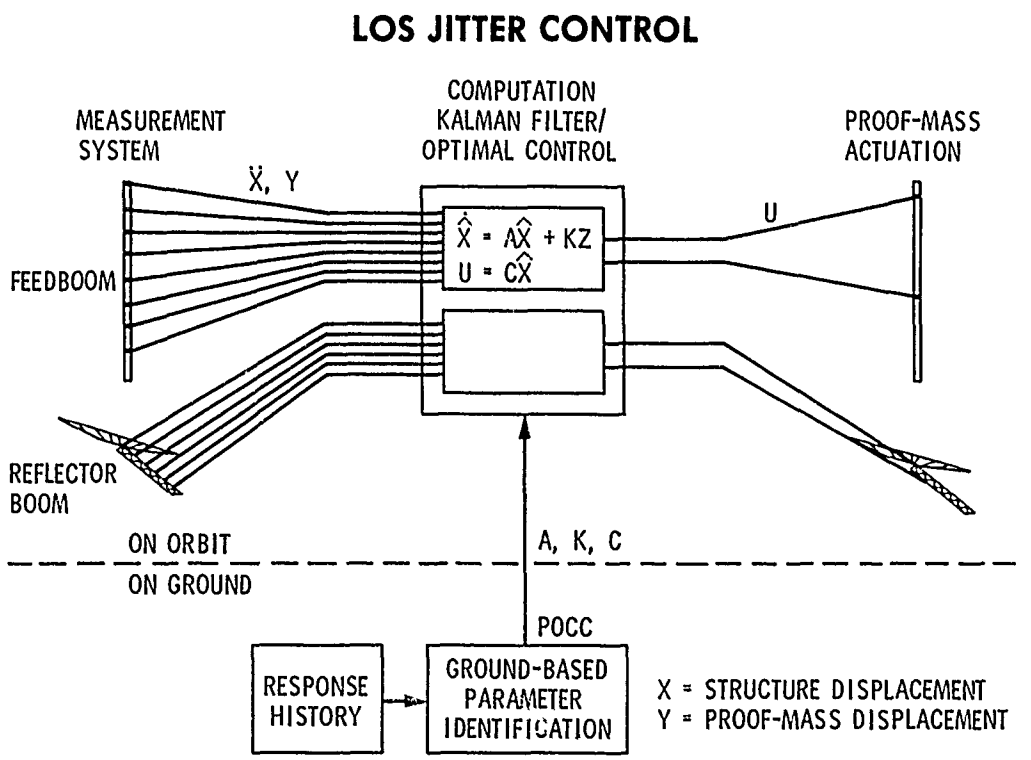

SUMMARY

We have presented the major components of a design and operational flight strategy for flexible structure control systems. In this strategy an initial distributed parameter control design is developed and implemented from available ground test data and on-orbit identification using sophisticated modeling and synthesis techniques. The reliability of this high performance controller is directly linked to the accuracy of the parameters on which the design is based. Because uncertainties inevitably grow without system monitoring, maintaining the control system requires an active on-line system identification function to supply parameter updates and covariance information. Control laws can then be modified to improve performance when the error envelopes are decreased. In terms of system safety and stability the covariance information is of equal importance as the parameter values themselves. If the on-line system ID function detects an increase in parameter error covariances, then corresponding adjustments must be made in the control laws to increase robustness. In one scenario for example, if the error covariances exceed some threshold, an autonomous calibration sequence could be initiated to restore the error envelope to an acceptable level.

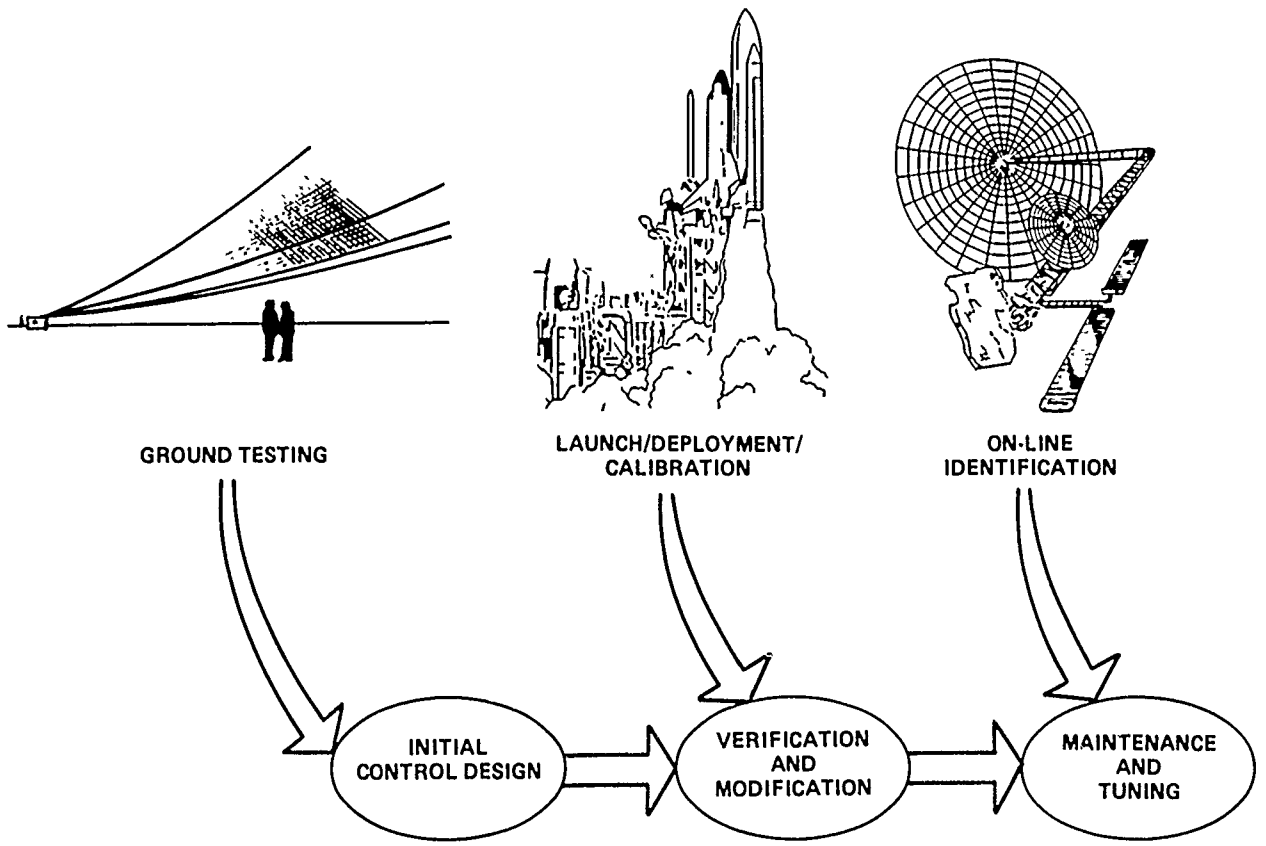

REFERENCES

1. Mettler, E., Milman, M., Bayard, D., Eldred, D.: Space Station On-Orbit Identification and Performance Monitor. AIAA-85-0357; 23rd Aerospace Sciences Meeting, Reno, Nevada, January 1985.

2. Gibson, J.S.: An Analysis of Optimal Model Regulation: Convergence and Stability, SIAM J. Contr. Opt., Vol. 19, No. 5, September 1981, pp. 686-707.

3. Bayard, D.S., Hadaegh, F.Y., and Meldrum, D.R.: Optimal Experiment Design for On-Orbit Identification of Flexible Body Parameters in Large Space Structures. Fourth IFAC Symposium on Control of Distributed Parameter Systems, Los Angeles, California, June 1986.

4. Hadaegh, F., Bayard, D., Meldrum, D.R., Mettler, E.: On-Orbit Flexible Body Parameter Identification for Space Station. Vibration Damping 1986 Workshop II, Las Vegas, Nevada, March 5, 1986.

5. Iliff, K.W. and Maine, R.E.: Maximum Likelihood Estimation with Emphasis on Aircraft Flight Data. Proceedings of the Workshop on Identification and Control of Flexible Space Structures, Vol. III, pp. 197-246, April 1985.

6. Maine, R.E. and Iliff, K.W.: Formulation and Implementation of Practical Algorithm for Parameter Estimation with Process and Measurement Noise. SIAM J. Appl. Math., Vol. 41, pp 558-578, December 1981.

7. Adamian, A. and Gibson, J.S.: Sensitivity of Closed-Loop Eigenvalues and Robustness, Fourth IFAC Symposium on Control of Distributed Parameter Systems, Los Angeles, California, June 1986.

8. Blelloch, P.A. and Mingori, D.L.: Modified LTR Robust Control for Flexible Structures, AIAA Guidance, Control and Navigation Conference, Williamsburg, VA, August 1986.

9. Nahi, N. and Napjus, G.: Design of Optimal Probing Signals for Vector Parameter Estimation. Proc. IEEE Conf. on Decision and Control, Miami, Florida, pp. 162-168, 1971.

10. Mehra, R.K.: Optimal Input Signal for Parameter Estimation in Dynamic Systems-Survey and New Results. IEEE Trans. Automat. Contr., Vol. AC-19, pp. 753-768, 1974.

DEVELOPMENT AND USE OF A LINEAR MOMENTUM EXCHANGE DEVICE

George B. Doane III
Control Dynamics Company
Huntsville, Alabama

Henry Waites
Marshall Space Flight Center
Huntsville, Aalbama

G. David Edgemon
Control Dynamics Company
Huntsville, Alabama

First NASA/DOD CSI
Technology Conference
Nov. 18-21, 1986

Program Summary

In 1981 the Marshall Space Flight Center (MSFC) began establishing an in-house facility for testing control concepts to be applied to Large Space Structures (LSS). As shown below the original concept called for a long flexible beam suspended from the ceiling by a low friction support system. The lower end of the beam was to be mounted to the Advanced Gimbal System (AGS). Analysis and system engineering soon showed that a more tenable design would be where the whole system was inverted, i.e., the AGS hung from the ceiling with the beam hanging down from it. While this configuration, augmented by a base excitation table (BET) was being built, an ASTROMAST obtained from JPL was extended, analyzed and tested. From that basic configuration has evolved the cruciform, VCOSS and ACES configurations as shown in the figure. The addition of the cruciform added low frequency nested modes and the additional instrument package at the tip contains gyros to monitor tip motion.

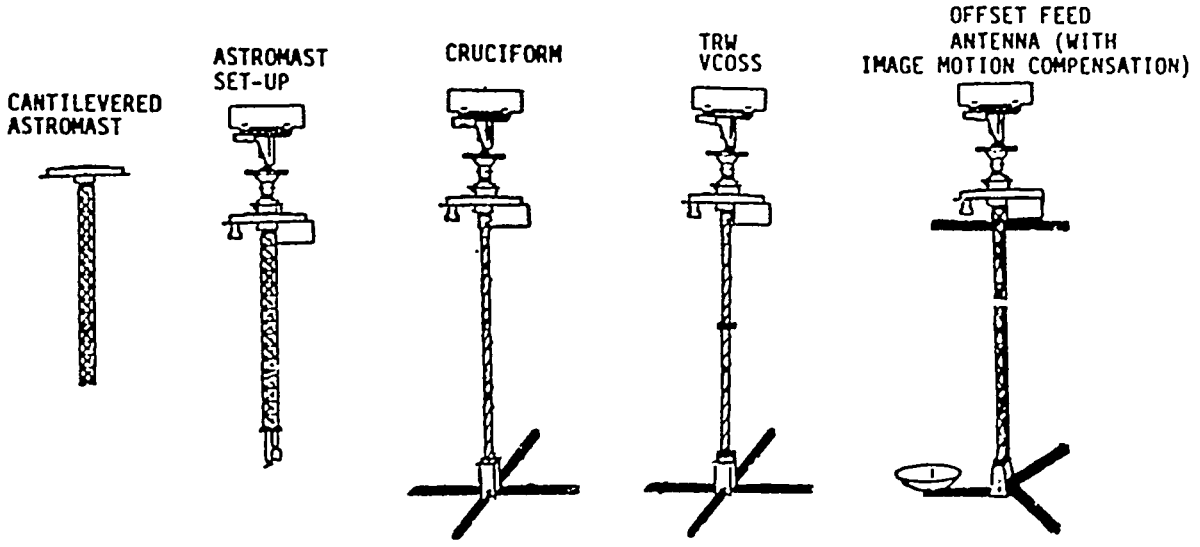

The figures below serve to show some details of the facility. The artists' figure shows the placement of the BET, the AGS (with a MSFC added third gimbal), the gyros mounted on the AGS faceplate and the beam tip instrument package. The control room, which is adjacent to the test area, contains the gimbal drive electronics, the data acquisition electronics, a Hewlett Packard 9020 computer augmented by an Analogic Vector Processor and outgoing command electronics. At the present time the system can handle 64 incoming signals and 48 outgoing channels. The present length of the beam is forty-five feet. However, the facility is capable of accommodating beams of one hundred and twenty feet in length. The photograph was taken by a camera located at the top of the beam underneath the AGS faceplate.

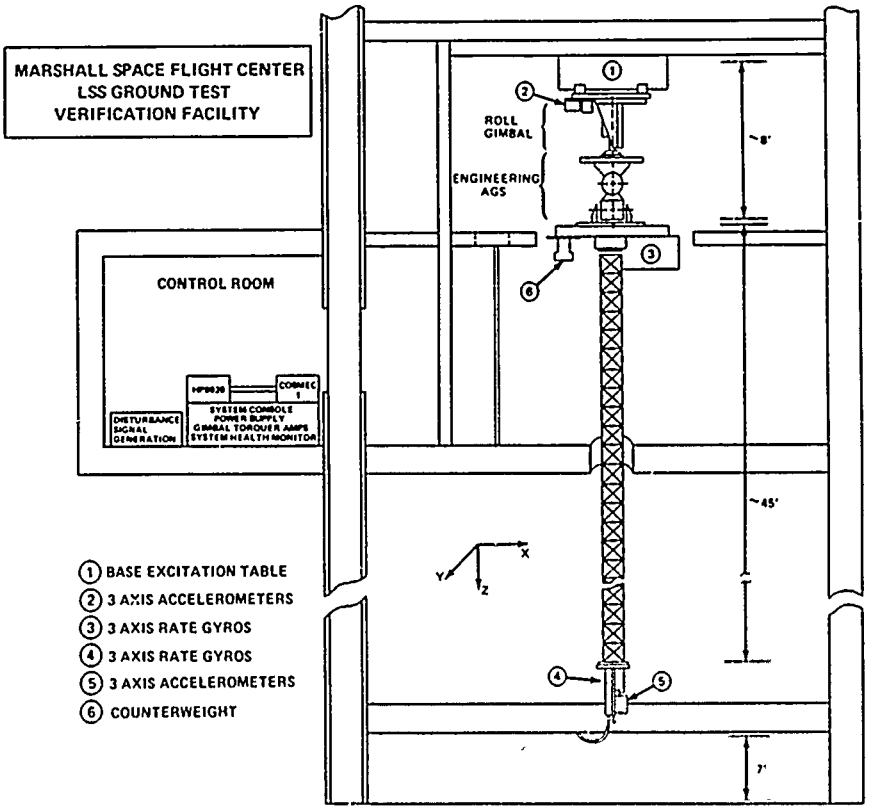

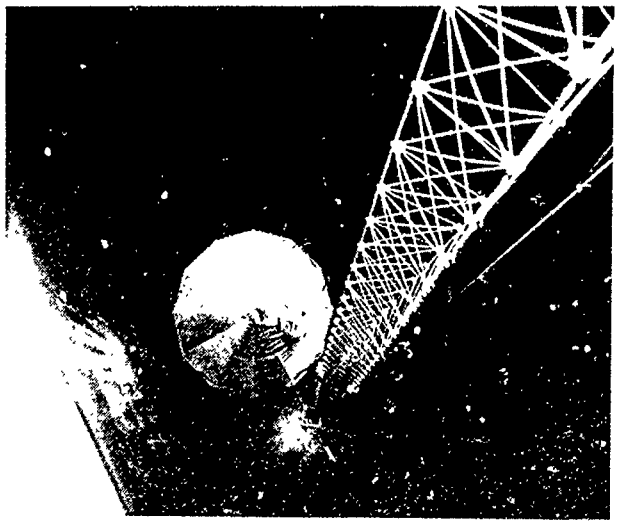

The program evolved to the point in 1985 where it was desired to test distributed sensors and actuators. An agreement was reached between the Air Force Wright Aeronautical Laboratories (AFWAL) and MSFC in which AFWAL contracted with TRW to supply four channels of linear momentum exchange devices (LMEDs). Each LMED included a collocated linear accelerometer so as to implement the sensor/actuator portion of the positivity control concept. In addition, an engineering unit, which was used as a stimulus (one channel), was supplied without an accelerometer. Additional equipment supplied under the contract included an optical measuring system to determine the beam position at each LMED with respect to the laboratory frame. The concept of the LMED is to exchange momentum between the vibrating beam and the LMED proof or seismic mass. The system energy is dissipated in the action of the electrical forcing circuitry. In the cases tried so far, the proof mass has been driven with a velocity signal derived from the collocated accelerometer. One of the pictures below shows an assembled LMED mounted to the ASTROMAST, the other shows a disassembled LMED (engineering unit).

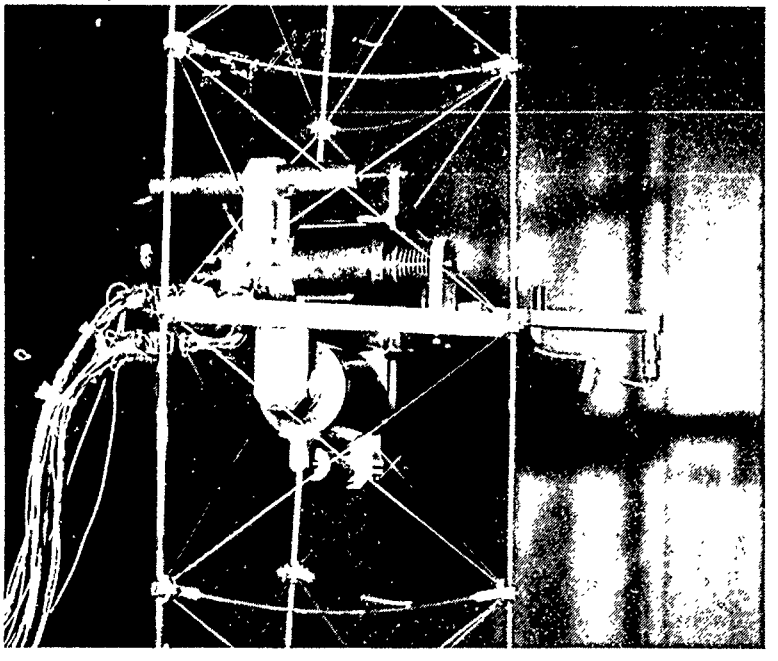

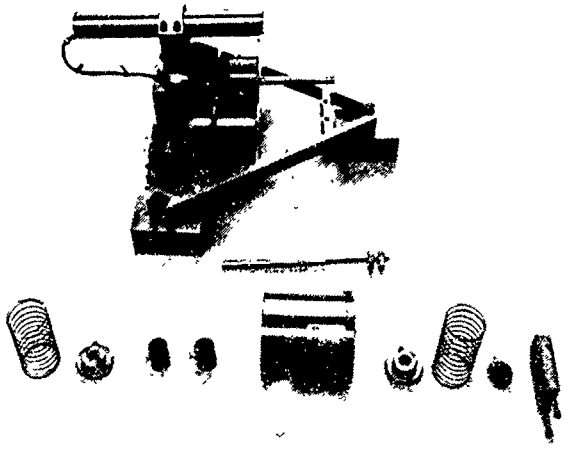

After the LMEDs were delivered, a number of component tests were run at MSFC. These tests consisted of frequency response and hysteresis curve generation tests. To generate the frequency response curves the linear motor drive amplifier was excited with wide-band noise and the resulting motion of the seismic mass was measured by the output of the linear voltage differential transformer (LVDT) that came with each LMED. This LVDT output was processed by an analyzer and produced a typical curve as shown. From this curve it can be deduced that the device's response was probably more than critically damped. To generate the hysteresis curve a sine wave was impressed on the linear motor amplifier and this voltage along with the LVDT output voltage was impressed on the x and y input channels of a recorder. A typical hysteresis curve is also shown. It was noted that as the frequency of excitation increased, the jerking or steplike characteristic of the LMED hysteresis tended to decrease.

Typical LMED Frequency Response from Volts into Power Amp to Volts Out of LVDT

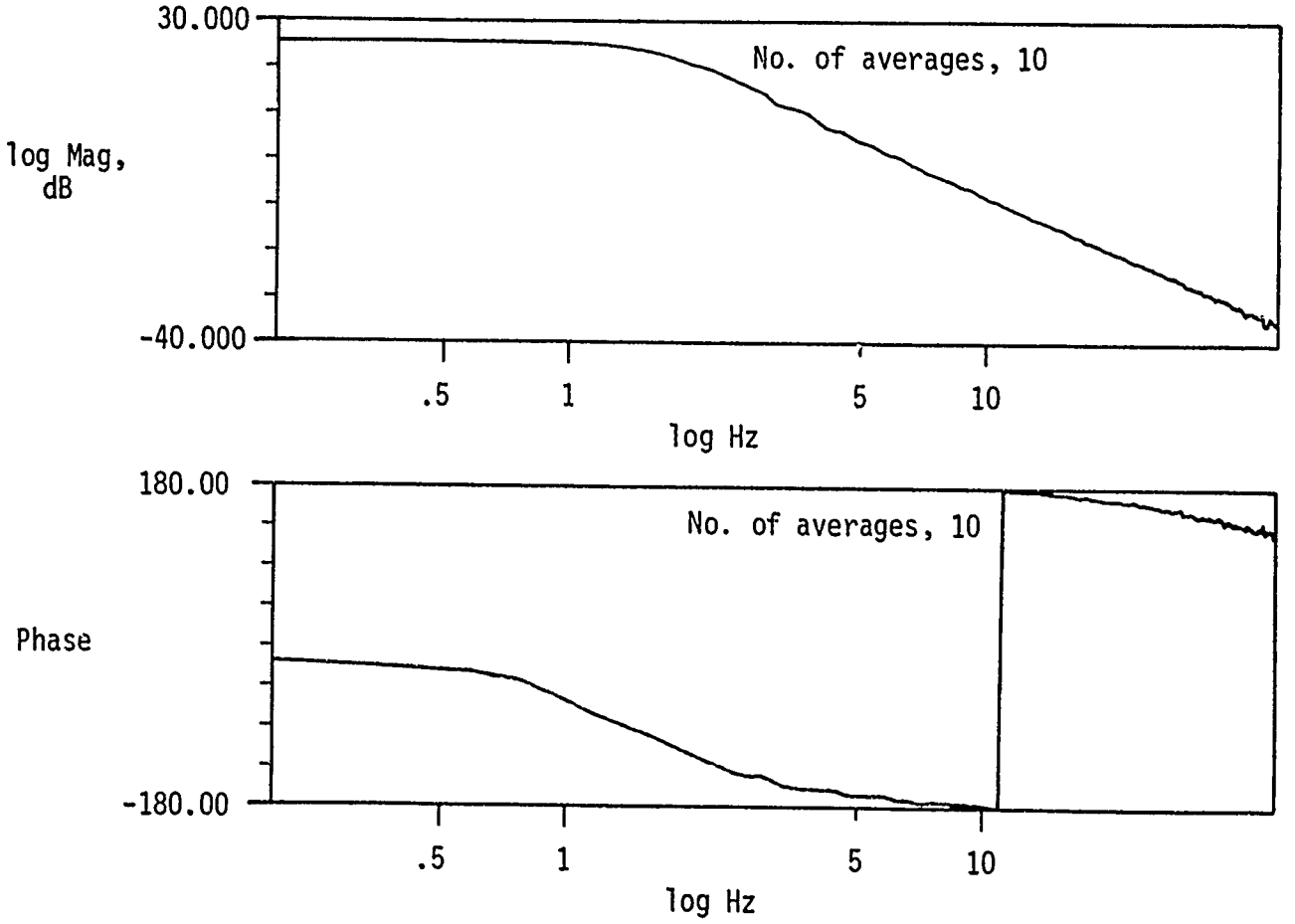

Typical LMED Hysteresis Curve

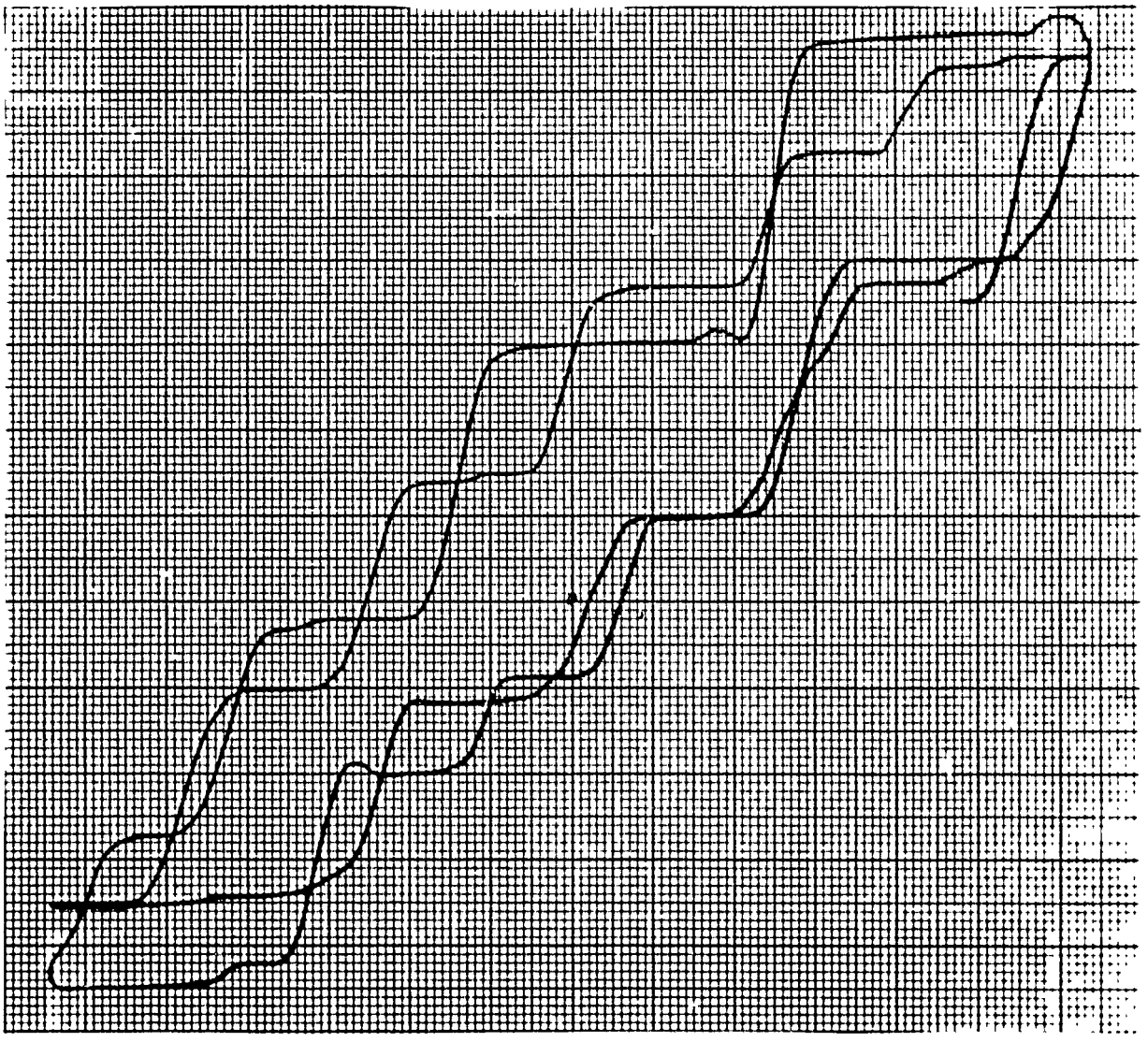

Power Amp Input 0.2 HZ Sine Wave (0.3 Volts p-p)

Study of the frequency response and hysteresis curves as well as physical inspection of the LMEDs showed that a product improvement program needed to be undertaken. Accordingly, the engineering LMED was disassembled, inspected and cleaned. This inspection disclosed that all elements of the seismic mass suspension, i.e., the shaft, springs, bearing and balls, were magnetic. It also disclosed that there were surface imperfections in the shaft. Accordingly, new matched instrument bearings were ordered as were matching steel shafts. This matched set has palpably tighter specifications than the originals even though they were a one-to-one substitution physically. While waiting for the new bearing and shaft combination to arrive from the vendor, MSFC fabricated a shaft to loose specifications. Use of this shaft with the original and new bearings confirmed that surface finish influenced highly the grabbing or steplike characteristics of the hysteresis curve. This conclusion was heightened when the new steel shaft arrived and was tried. The hysteresis was diminished greatly by constructing a hard anodized aluminum shaft to the same basic specifications as the special order steel shaft. Even though the balls were still magnetic, there was a dramatic decrease in the area of the hysteresis curve. The modification sequence is listed below.

Modification Sequence

1) original system - Thompson Super-4 bearings with polished steel shaft

2) Thompson Super-4 bearings with low magnetism stainless steel shaft

3) Barden LS4 bearing with original and low magnetism shafts

4) Thompson 4812-SS bearing with original and low magnetism shafts

5) Thompson Inst-4812-SS instrument grade bearing with matching polished steel shaft (4 micron surface finish).

6) Thompson Inst-4812-SS with anti-magnetic shaft (hard anodized aluminum, 2 micron surface finish).

At the conclusion of the modification sequence previously described, new frequency response and hysteresis curves were run. Typical results are shown. The frequency response curves show that damping has been reduced from something over critical to the neighborhood of 0.2. Going hand-in-hand with this measurement is the fact that if one displaces the seismic mass from its equilibrium position and then releases it, the mass oscillates a number of times about the equilibrium position whereas before because of friction it did not. When viewing the hysteresis curves, one has to be extremely careful of the scales. If one plots the curves corresponding to the aluminum shafts on the same scale as the original curves, they would appear to be straight lines. Some numerical feel for this may be gained by defining a gain as the ratio of seismic mass deflection to drive voltage of the linear motor. In the case of the original bearing-shaft combination a typical number might be 18. For the modified units a value of 355 is typical.

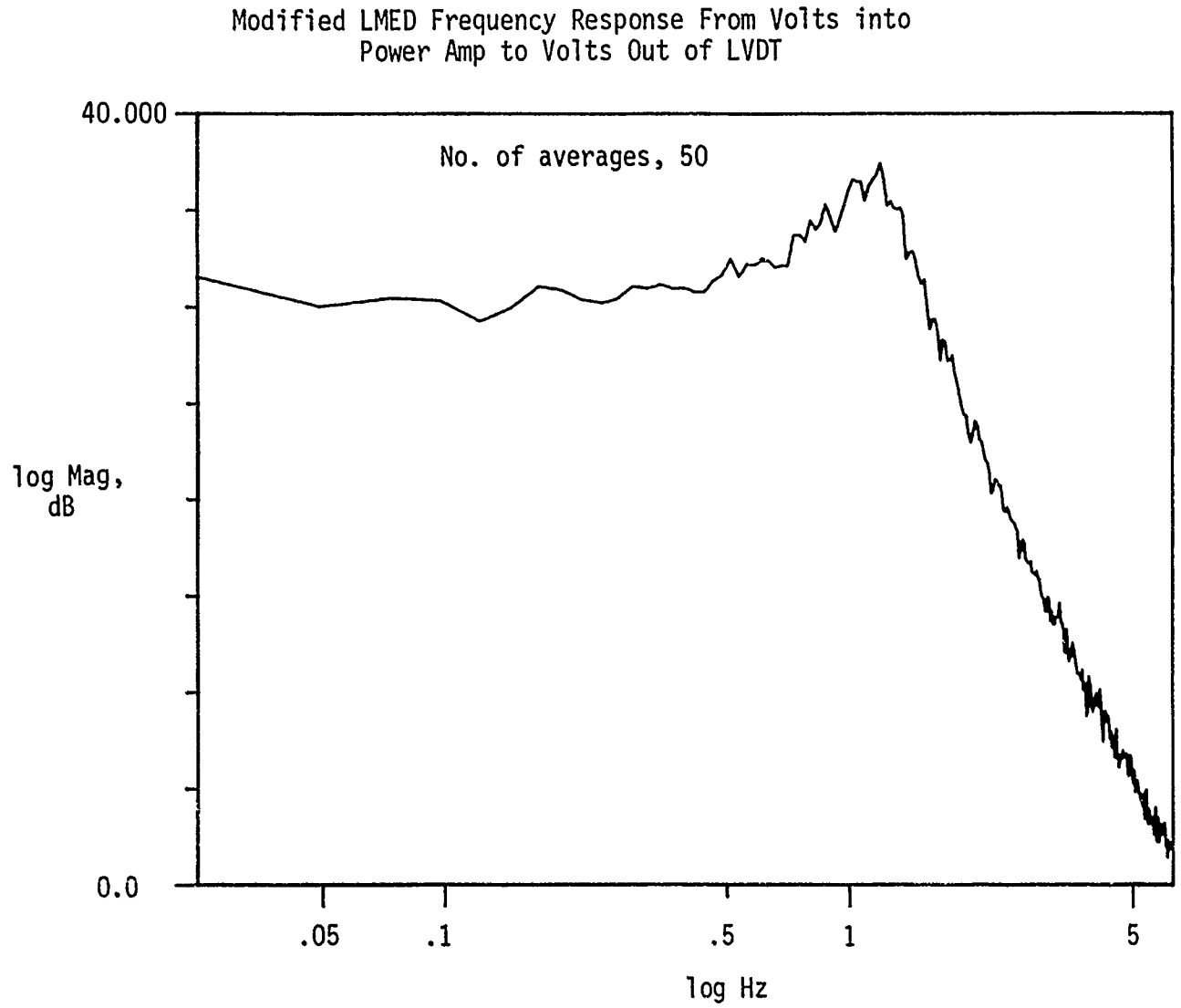

Figure 6

Modified LMED Hysteresis Curve

LVDT Output Voltage 13.5 Volts p-p Where 20 Volts= 1 Inch Displacement of Proof Mass

Power Amp Input 0.2 Hz Sine Wave (0.038 Volts p-p)

During the time period of the next AFWAL-MSFC program called Active Control (Technology) Evaluation for Spacecraft (ACES) the MSFC LSS structures/control test facility will be maintained in the ACES configuration. In this configuration the modified LMEDs as discussed above will be mounted on the structure. Also on the structure will be a laser excited beam steering subsystem incorporating a small two gimbal table for articulating the steering mirror. This configuration has a sensor complement of 6 gyro channels, 4 accelerometers (on LMEDs), 2 gimbal pickoffs on the two gimbal table and optical detector systems to measure 2 laser beam deflections and deflections of the mast at the LMED stations relative to the laboratory frame. It has 5 driven gimbals and 4 LMEDs for use as actuators. Thus, it is ready for use as a universal test bed for a number of control laws that have been developed.

STRUCTURES/CONTROLS TEST FACILITY CONFIGURATION 2

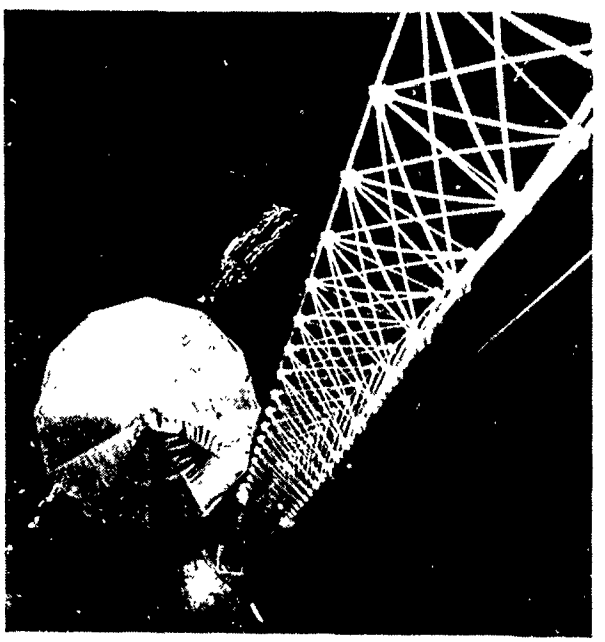

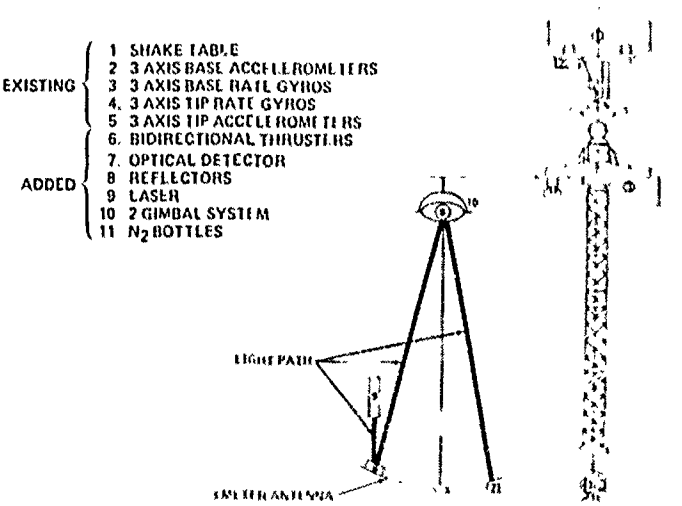

TECHNIQUES TO BE DEMONSTRATED

- ACTIVE IMAGE MOTION COMPENSATION
- VIBRATION CONTROL VIA LINEAR THRUSTERS
- EVOLUTIONARY CONTROL
- CLOSED LOOP PARAMETER ESTIMATION/CONTROL

COMPUTER-AIDED DESIGN AND DISTRIBUTED SYSTEM TECHNOLOGY DEVELOPMENT FOR LARGE SPACE STRUCTURES

Ernest S. Armstrong and
Suresh M. Joshi
NASA Langley Research Center
Spacecraft Control Branch
Hampton, VA 23665
USA

First NASA/DOD CSI Technology Conference
Norfolk, Virginia
November 18-21, 1986

CHARACTERISTICS OF LARGE SPACE SYSTEMS

Proposed large space structures have many characteristics that make them difficult to analyze and control. They are highly flexible - with components mathematically modeled by partial differential equations or very large systems of ordinary differential equations. They have many resonant frequencies, typically low and closely spaced. Natural damping may be low and/or improperly modeled. Coupled with stringent operational requirements of orientation, shape control, and vibration suppression, and the inability to perform adequate ground testing, these characteristics present an unconventional identification and control design problem to the systems theorist.

This presentation describes some of the research underway within Langley's Spacecraft Control Branch, Guidance and Control Division aimed at developing theory and algorithms to treat large space structures systems identification and control problems. The research areas to be considered are Computer-Aided Design Algorithms, and Systems Identification and Control of Distributed Systems.

- Highly flexible
- Many resonant frequencies
- Low natural damping
- Stringent operational requirements
  - Orientation
  - Shape
  - Vibration suppression
- Limited ground testing

ORACLS UPDATE

The established, tested computer-aided design system entitled "Optimal Regulator Algorithms for the Control of Linear Systems" (ORACLS) is being updated and modified so as to more easily accommodate the numerically difficult characteristics of large space systems lumped models. Modifications include greater use of LINPACK software (ref. 1) and inclusion of more robust Riccati equation algorithms (ref. 2). The ORACLS package (ref. 3) is also being expanded to allow multivariable frequency domain analysis and modern approaches to order reduction.

OPTIMAL REGULATOR ALGORITHMS FOR THE CONTROL OF LINEAR SYSTEMS

A modern control theory design package for time-invariant linear systems

- Modular construction
- Efficient numerical methods
- Unified
  - Continuous and discrete systems
  - Constant and time - varying gains
  - Deterministic and stochastic
- Quadratic synthesis methods
- Cosmic, NASA TP 1106, Marcel Dekker

FREQUENCY RESPONSE ANALYSIS

A general purpose multivariable frequency domain analysis package (FREQ) has been constructed to be compatible with ORACLS. Given a multivariable unity gain feedback loop around a cascaded design system and dynamic compensator, the FREQ package has options to compute (1) a variety of transfer matrices, with loop broken at input or output, (2) singular values and vectors for the matrices, and (3) multivariable Bode-like plots with maximum/minimum singular values plotted against frequency. Typical use of this package is in the analysis/design of compensators for spillover control.

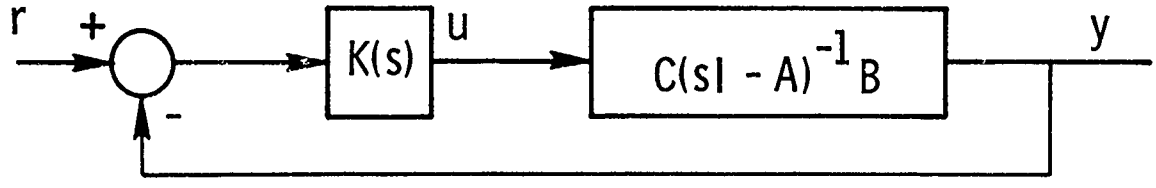

- Transfer matrices at $s = j\omega$

Loop gain	$G_0 = KC(sI - A)^{-1}B$
Closed-loop	$G_0 (I + G_0)^{-1}$
Return difference	$I + G_0$
Inverse ret. diff.	$I + G_0^{-1}$
Sensitivity	$(I + G_0)^{-1}$

- Calculates singular values/vectors
- Combines ORACLS, EISPACK, LINPACK software

ADVANCED MULTIVARIABLE ALGORITHMS

Further needs in large space structures control design have motivated other algorithm development. Algorithms for computing multivariable invariant zeros (ref. 4) and for treating controllability/observability are included since finite element models can have transmission zeros near closely spaced open-loop poles if sensors and actuators are not properly selected. High-order design models and/or high-order compensators typically occur and require order reduction techniques (ref. 5). It is anticipated that these and other algorithms will be collected into a new computer-aided design package (ORACLS II) motivated by the needs of large space structures controller design.

- Multivariable zeros and relative controllability/observability
  - Applied to sensor/actuator selection
- Multivariable frequency response package (FREQ)
  - Applied to spillover control
- Algorithms based on Hankel-Norm Theory
  - Reduced order model/compensator
- Combine algorithms into new CAD package
  - ORACLS II

SYSTEMS IDENTIFICATION AND CONTROL OF DISTRIBUTED SYSTEMS

Although there are currently many theoretical and numerical difficulties associated with control laws designed with partial differential equation models, it is felt that sensor/actuator technology and on-board computer capability will eventually be improved to the point where distributed parameter methodology can be applied to large space structures. Anticipating these developments, the Spacecraft Control Branch is supporting research into systems identification and control theory and algorithms based on partial differential equation models. The approach currently being considered is to apply spline-based Galerkin projection approximation methods (ref. 6) and multivariable identification/control theory to models generic to large space structures.

HOOP-COLUMN APPLICATION

A particular example of this research is given by the derivation of a parameter and state estimation procedure for distributed systems which was demonstrated with a model generic to the hoop-column antenna. The reflector surface of the antenna is assumed to be approximated by the static two-dimensional stretched membrane equation with appropriate boundary conditions and variable stiffness. The problem considered was to estimate the system state (u) and stiffness (E) from given applied force and displacement measurements.

- Static two-dimensional stretched membrane

$$-\frac{1}{r}\frac{\partial}{\partial r}\left[rE(r,\theta)\frac{\partial u}{\partial r}(r,\theta)\right]-\frac{\partial}{\partial \theta}\left[\frac{E(r,\theta)}{r^2}\frac{\partial u}{\partial \theta}(r,\theta)\right]=f(r,\theta)$$

Over $\Omega=[\varepsilon,R]\times[0,2\pi]$

with boundary conditions

$u(\varepsilon,\theta)=u_0$. $\quad u(r,0)=u(r,2\pi)$

$u(R,\theta)=0$

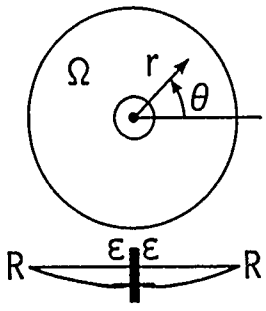

- Given $f(r,\theta)$ and measured displacements

$u_m\left(r_i,\theta_j\right)$, $(i=1,\ldots,L_r;\ j=1,\ldots,L_\theta)$, estimate

$E(r,\theta)$ and $u(r,\theta)$ within Ω

SYSTEM IDENTIFICATION APPROACH

The general approach for identification can be described as follows. After formulating a distributed model for the dynamic system, some mathematical approximation technique, such as finite elements or splines, is used to project the identification problem onto a finite-dimensional subspace. The finite-dimensional identification problem is then solved within the subspace. The approximation is successfully refined and the identification problem repeatedly solved to produce a sequence of estimates to be analysed for convergence. This approach, when specialized to the hoop-column application, is outlined below. Details of the study may be found in reference 7.

General	Hoop-column application
• Distributed parameter formulation	• Stretched membrane equation
• Project onto finite dimensional subspace	• Galerkin projection with linear spline basis functions Parameterize $E(r,\theta)$ via cubic splines
• Solve identification problem within subspace	• Output error identification technique
• Successively increase subspace dimension and solve identification problem to generate sequence of estimates	• Numerical algorithm

OPTIMAL LINEAR REGULATOR ALGORITHMS

The same general approach is being investigated for controller design. When applied to dynamic systems, the spline-based Galerkin approximation procedure produces high-order state equations. If linear quadratic regulator theory is applied for control law design, the related difficulty of solving high-order Riccati equations arises. In control applications, wherein only the regulator gain is required, direct application of the Chandrasekhar technique (ref. 8) is extremely difficult due to numerical stiffness problems. Recent results from a NASA-sponsored research grant (NAG-1-517) with Brown University have produced a new hybrid Chandrasekhar-type algorithm for approximating the steady-state gain matrix independently of the Riccati equations.

- Linear quadratic regulator problem

$$\dot{x} = Ax + Bu$$

$$J = \int_0^\infty (x^T C^T C x + u^T u)\, dt$$

$$A^T P + PA - PBB^T P + C^T C = 0$$

$$u = -Kx = -B^T P x$$

- Chandrasekhar algorithm

$$-\frac{d}{dt} P(t) = A^T P(t) + P(t)A - P(t)BB^T P(t) + C^T C, \quad P(t_f) = 0$$

$$\frac{d\,K(t)}{dt} = -B^T L^T(t)\, L(t), \quad K(t_f) = 0$$

$$\frac{d\,L(t)}{dt} = -L(t)\left[A - BK(t)\right], \quad L(t_f) = C$$

HYBRID ALGORITHM

In order to begin the hybrid algorithm, the standard Chandrasekhar algorithm is employed to obtain an initial stabilizing gain for application of the Newton-Kleinman algorithm for solving the algebraic Riccati equation. After several steps through the Newton-Kleinman sequence, enough data are obtained to rewrite the recursion equation in an alternate form giving an update formula for the gain matrix. Banks and Ito at Brown University have discovered a way to compute the gain update (K_{i+1}) without computing Z_i.

- Chandrasekhar equations give starting value for Newton-Kleinman
- Newton-Kleinman

$$(A-BK_i)^T P_i + P_i (A-BK_i) + K_i^T K_i + C^T C = 0$$

$$K_{i+1} = B^T P_i$$

- Alternate form -

$$(A-BK_i)^T Z_i + Z_i (A-BK_i) + (K_i - K_{i-1})^T (K_i - K_{i-1}) = 0$$

$$K_{i+1} = K_i + B^T Z_i$$

Can compute update without computing Z_i

HYBRID ALGORITHM (CONT'D)

Apply the (Smith) bilinear transformation to the Z_i equation. A sequential solution can then be written for the tranformed equation from which the update algorithm can be derived.

- Bilinear transformation (Smith) -

$$X = Z_i \qquad U = (I - r\tilde{A})^{-1}(I + r\tilde{A})$$

$$\tilde{A} = A - BK_i \qquad Y = 2r(I - r\tilde{A})^T D^T D (I - r\tilde{A})^{-1}$$

$$D = K_i - K_{i-1} \qquad X = U^T X U + Y$$

- Sequential solution -

$$X_{k+1} = U^T X_k U + Y$$

$$X_{k+1} - X_k = U^T (X_k - X_{k-1}) U$$

- Algorithm -

$$X_{k+1} = X_k + 2r M_{k+1}^T M_{k+1}$$

$$M_{k+1} = M_k U$$

$$B^T X_{k-1} = B^T X_k + 2r\, B^T M_{k+1}^T M_{k+1}$$

NUMERICAL RESULTS

For a distributed parameter example, consider the parabolic system below with boundary control. The control input u(t) is to be chosen to minimize J(u) subject to the dynamic equation and boundary condition constraints. After discretizing with linear splines and Galerkin projection, an Nth order linear quadratic regulator problem is obtained. The index N increases with refinement of the linear spline approximation. For N=10, CPU times are comparable between the Potter (ref. 8) and hybrid methods. However, as N increases, the hybrid algorithm excels.

- $$\frac{\partial v(x,t)}{\partial t} = \frac{\partial^2 v(x,t)}{\partial x^2}\ ,\ x \varepsilon\ (0,1)$$

$$v(0,x) = \phi(x), \frac{\partial v}{\partial x}(t,0) = u(t),\ \frac{\partial v}{\partial x}(t,1) = 0$$

$$J(u) = \int_0^\infty \left(\left| cv(t) \right|^2 + \left| u(t) \right|^2 \right) dt$$

$$cv(t) = \int_0^\infty (1+x) v(t,x)\, dx$$

	Potter	Hybrid
N = 10	0.162	0.197
N = 40	6.3	1.29

STABILITY AUGMENTATION BY BOUNDARY-FEEDBACK CONTROL

Another approach to distributed-parameter formulation of the control problem is being considered by Balakrishnan (ref. 9) for application to the Spacecraft Control Laboratory Experiment (SCOLE) configuration (ref. 10). An abstract wave formulation is developed as a nonlinear wave equation in Hilbert space. The system is shown to be controllable, and a feedback control law is developed assuming point actuators and sensors at the boundaries. The control law is shown to be strongly stable and robust to parameter uncertainties.

- $M\ddot{x}(t) + A\,x(t) + K(\dot{x}(t)) + B\,u(t) = 0$

  M: mass matrix

  A: $D \rightarrow L_2[0,L]^3 \times R^{14}$, differential operator

  K: nonlinear function

  u(t): applied moments, proof mass forces

  $$x = \Big[u_\phi(.),\ u_\theta(.),\ u_\psi(.),\ u_\phi(0^+),\ u_\theta(0^+),\ u_\phi(L^-),\ u_\theta(L^-),$$
  $$u'_\phi(0^+),\ u'_\theta(0^+),\ u_\psi(0^+),\ u'_\phi(L^-),\ u'_\theta(L^-),\ u_\psi(L^-),$$
  $$u_\phi(s_2),\ u_\theta(s_2),\ u_\phi(s_3),\ u_\theta(s_3)\Big]^T$$

  $u_\phi(s)$, $u_\theta(s)$: displacements; $u_\psi(s)$: rotation

  s_2, s_3: proof mass actuator locations

- State space form: $\dot{y}(t) = \bar{A}\,y(t) + \bar{K}(y(t)) + \bar{B}\,u(t)$
- Control law: $u(t) = -P\,\bar{B}^*\,y(t);\ P > 0$

DAMPING MODELS

The mathematical modeling of damping mechanisms is a little understood, most important aspect of systems identification of large space structures. Traditionally, damping is superimposed in linear viscous form on modal dynamic equations obtained from finite element software. Unfortunately, none of the expected forms of energy dissipation is linear viscous (ref. 11). Research employing partial differential equation dynamic models indicates that damping operators should have nonlocal structure.

- Little understood
- Recognized as most important aspect
- Linear-viscous

$$M\ddot{\hat{u}} + D\dot{\hat{u}} + K\hat{u} = \hat{f}$$

- None of expected damping is linear-viscous
- PDE damping operators can require nonlocal structure

RESEARCH IN MODELING OF DAMPING

Using the torsional beam equation to model the Spacecraft Control Laboratory Experiment (SCOLE) (ref. 10), it has been found that, for proportional damping to occur, consideration of the total beam length in the damping operator formulation is required. Future research under the Brown University grant (NAG-1-517) will consider other forms of damping operators for an Euler-Bernoulli beam model. The investigation will include damping with nonlocal interaction terms and fading memory formulations where, for example, stress is a functional of the history of deformation and prior times.

- Scale model (Balakrishnan, UCLA) for infinite beam with torsion equation

$$\frac{\partial^2 u}{\partial t^2} + 2\zeta D \frac{\partial u}{\partial t} - \frac{\partial^2 u}{\partial x^2} = 0$$

$$D\frac{\partial u}{\partial t}(t,x) = \frac{1}{\pi}\frac{\partial}{\partial t}\int_{-\infty}^{\infty} \frac{\frac{\partial}{\partial \zeta} u(t,\zeta)}{(x-\zeta)}\, d\zeta$$

gives proportional damping

- Investigating (Banks, Brown Univ.)

$$u_{xxt} - \int_{x-\delta}^{x+\delta} h(z-x)\, u_{xxt}(z,t)\, dz$$

and

$$\frac{\partial^2}{\partial x^2}\left\{ \int_0^t k(t,s)\, \Phi\left(u_{xx}(s,x)\right) ds \right\}$$

In Euler-Bernoulli beam model

REFERENCES

1. Dongarra J., et. al.: LINPACK User's Guide. SIAM, Philadelphia, 1979.

2. Arnold, W. F., and Laub, A. J.: Generalized Eigenvalue Algorithms and Software for Algebraic Riccati Equations. Computer-Aided Control Systems Engineering, M. Jamshidi and C. J. Herget (Eds.), Elsevier Science Publishers B. V., North Holland, 1985.

3. Armstrong, E. S.: ORACLS - A Design System for Linear Multivariable Control. Vol. 10, Control and System Theory Series, Marcel Dekkar, Inc., New York, 1980.

4. Emami-Naeini, A., and Van Dorren, P.: Computation of Zeros of Linear Multivariable Systems. Automatica, Vol. 18, No. 4, July 1982.

5. Glover, K.: All Optimal Hankel-Norm Approximations of Linear Multivariable System and Their L^{∞}-Error Bounds. Int. Journal of Control, Vol. 39, pp. 1115-1193, June 1984.

6. Banks, H. T. and Rosen, I. G.: Approximation Techniques for Parameter Estimation and Feedback Control for Distributed Models of Large Flexible Structures. Institute for Computer Applications in Science and Engineering (ICASE), Report 84-26, June 1984.

7. Banks, H. T., Lamm, P. K., and Armstrong, E. S.: Spline-Based Distributed System Identification with Application to Large Space Antennas, AIAA Journal of Guidance, Control and Dynamics, Volume 9, No. 3, May-June, 1986, pp. 304-322.

8. Russell, D. L.: Mathematics of Finite-Dimensional Control Systems-Theory and Design. Marcel Dekker, Inc., New York, 1979.

9. Balakrishnan, A. V.: A Mathematical Formulation of the SCOLE Control Problem: Part I. NASA CR-172581, May 1985.

10. Taylor, L. W. and Balakrishnan, A. V.: A Laboratory Experiment Used to Evaluate Control Laws for Flexible Spacecraft...NASA/IEEE Design Challenge. Proceedings of the Fourth VPI&SU/AIAA Symposium on Dynamics and Control of Large Structures, Blacksburg, VA, June 6-8, 1983.

11. Hughes, P. C.: Passive Dissipation of Energy of Large Space Structures. Journal of Guidance and Control, Vol. 3, 1980, pp. 380-382.

DISTRIBUTED CONTROL FOR COFS I

R. C. Montgomery
NASA Langley Research Center

Jeff Sulla
PRC Kentron

D. K. Lindner
VPI & SU

First NASA/DOD CSI Technology Conference
Norfolk, Virginia
November 18-21, 1986

PRESENTATION OUTLINE

This paper presents an overview of the work being done at NASA LaRC on developing the COFS-I Flight Experiment Baseline Control Law. This control law is currently evolving to a generic control system software package designed to support many, but not all, guest investigators. A system simulator is also described. It is currently being developed for COFS-I and will be used to develop the Baseline Control Law and to evaluate guest investigator control schemes. It will be available for use whether or not control schemes fall into the category of the Baseline Control Law.

First, the hardware configuration for control experiments will be described. This is followed by a description of the simulation software. Open-loop sinusoidal excitation time histories are next presented both with and without a local controller for the Linear DC Motor (LDCM) actuators currently planned for the flight. The generic control law follows and algorithm processing requirements are cited for a nominal case of interest. Finally, a closed-loop simulation study is presented, and the state of the work is summarized in the concluding remarks.

INTRODUCTION

HARDWARE CONFIGURATION FOR CONTROL

COFS I REAL–TIME SIMULATOR

OPEN–LOOP EXCITATION OF MAST USING THE TIP ACTUATORS WITH/WITHOUT LOCAL CONTROLLER

GENERIC LINEAR CONTROL ALGORITHM

ALGORITHM PROCESSING REQUIREMENTS

CLOSED–LOOP SIMULATION STUDIES WITH COLLOCATED RATE FEEDBACK

CONCLUDING REMARKS

Figure 1

COFS I REFERENCE LOCATIONS

For control experiment purposes, the COFS-I hardware consists of the space shuttle, a 60-meter statically determinant truss beam, and a tip assembly. The configuration of the experiment is shown in figure 2. Only the hardware of interest in a control system experiment is listed. The truss beam, called the MAST, has 54 sections called bays. The bays are numbered outward from the shuttle, bay 1 being nearest.

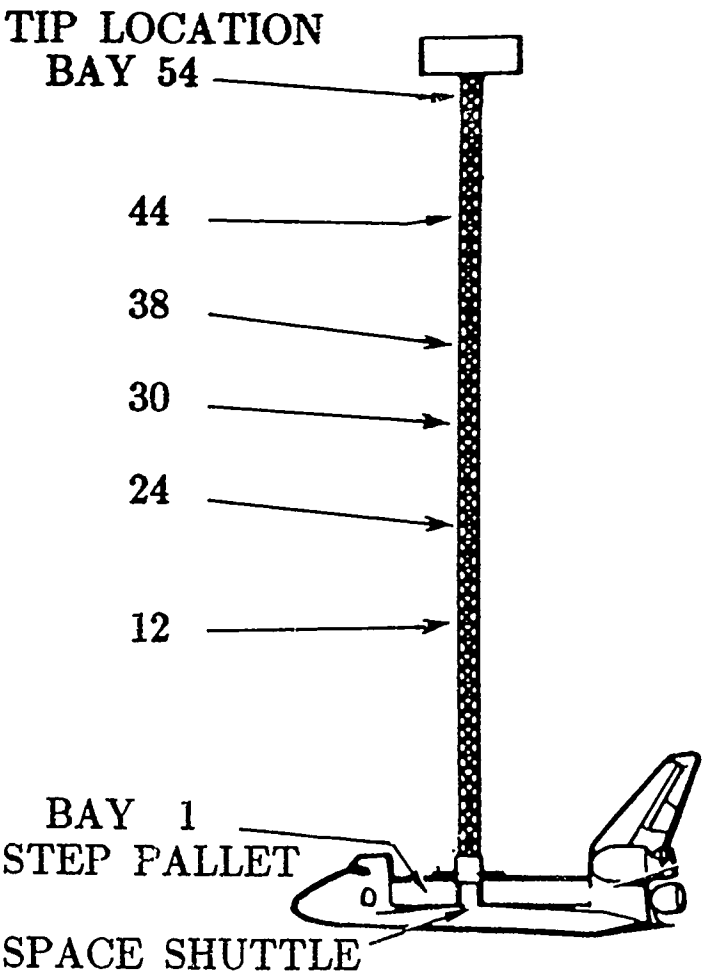

Figure 2

CONTROL SYSTEM COMPONENTS

Control law processing will be done with a digital computer located on the STEP pallet. Sensors are provided at the tip, at the STEP pallet and at five interior MAST stations - bays 12, 24, 30, 38, and 44. The types of sensor equipment provided are rate gyros and linear and angular accelerometers. The only type of actuator provided is the LDCM actuator. LDCM's are located at the tip and at three interior MAST stations. The LDCM's at the interior stations are smaller than the ones at the tip but are of the same type.

TIP LOCATION	3 RATE GYROS 3 LINEAR ACCELEROMETERS 4 LARGE LDCM ACTUATORS
BAYS 44, 30, AND 12	2 LINEAR ACCELEROMETERS 1 ANGULAR ACCELERMETER 2 SMALL LDCM ACTUATORS
BAYS 38 AND 24	3 LINEAR ACCELEROMETERS 1 ANGULAR ACCELEROMETER
STEP PALLET	3 LINEAR ACCELEROMETERS 3 RATE GYROS CONTROL SYSTEM COMPUTER 150 HZ UPDATE RATE

Figure 3

FLIGHT COMPUTER SYSTEM

The flight computer is located on the STEP pallet and communicates with it through a serial input/output data channel. The STEP pallet provides power for the MAST flight systems and also data recording. High-speed data transmission is available from the MAST flight system to the STEP pallet. All communications from the STEP pallet to the MAST flight system are through the Modular Distributed Information Subsystem, MDIS, which functions to send commands to and receive data from the Actuator/Sensor network via the MIL-STD 1553B data bus. The MDIS also interfaces with the Excitation and Damping Subsystem, EDS, which processes the control algorithms.

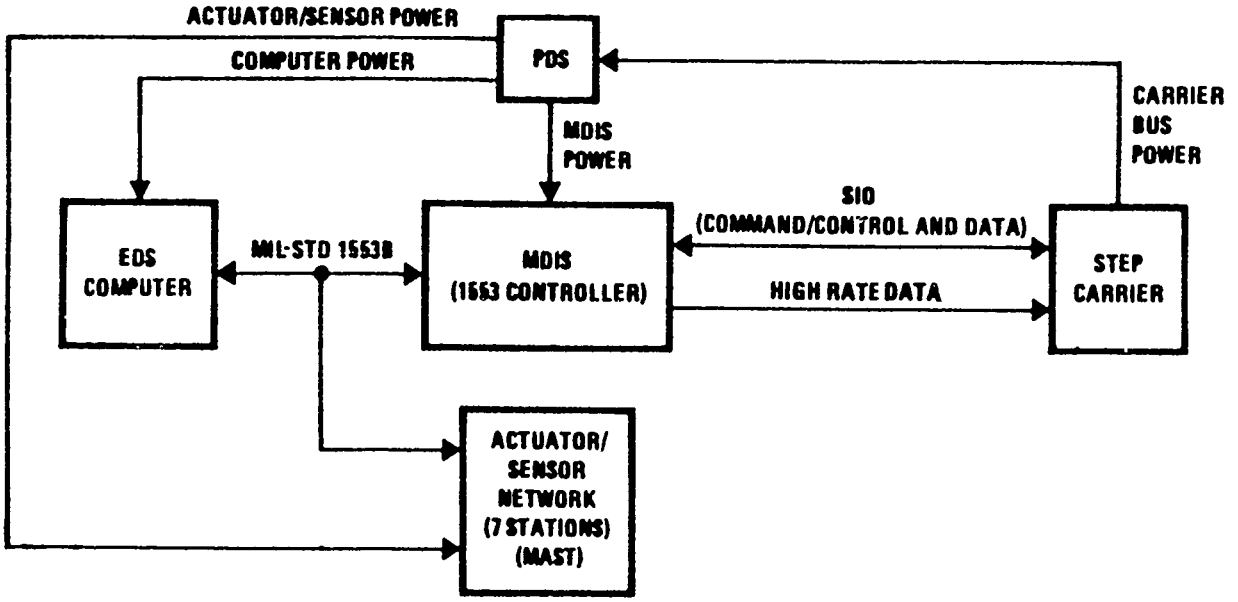

Figure 4

ALGORITHM TIMING REQUIREMENTS

The sample rate of the system is 150 samples/sec. This allows 6667 microseconds between samples. Because of projected system overheads and other necessary functions, only 5033 microseconds can be counted on for algorithm processing.

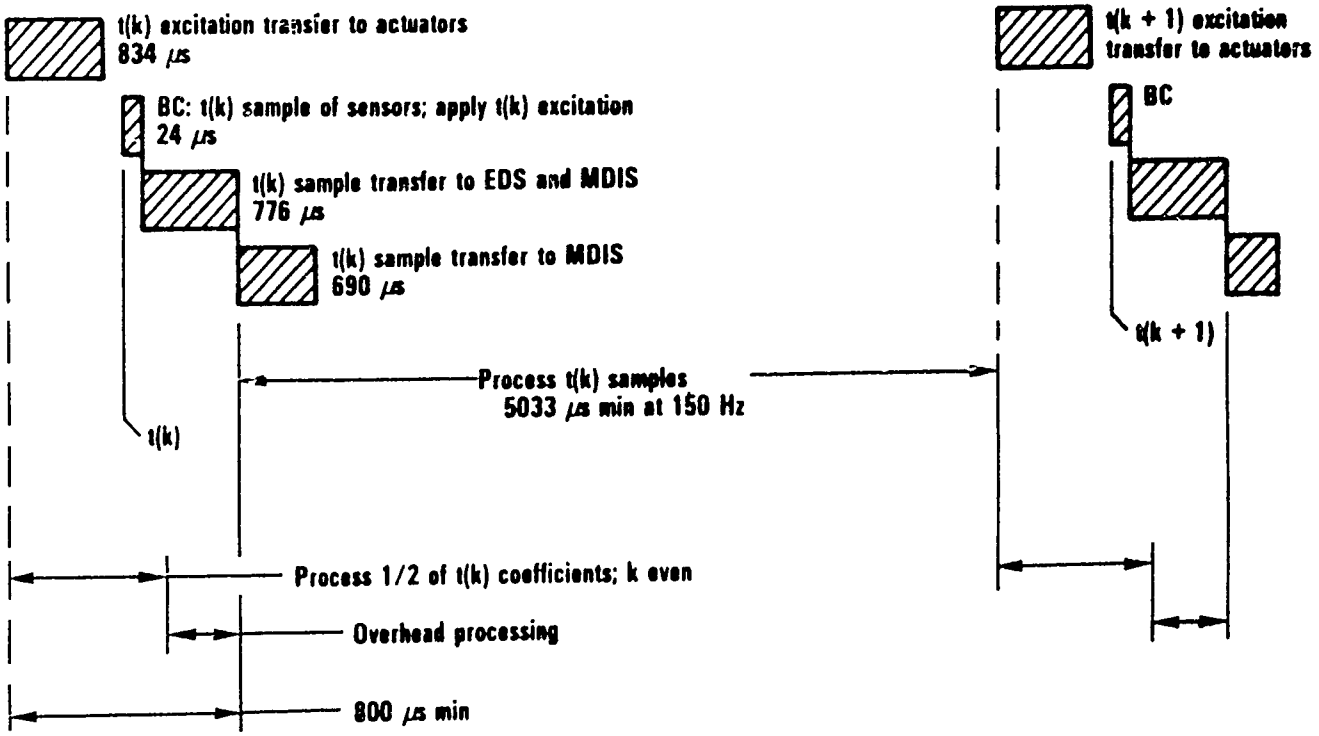

Figure 5

LDCM ACTUATOR

The LDCM actuators are currently being designed, thus, only a shetch is available. The Stator contains electrical wire windings and is hard mounted to the MAST tip. The Moving Mass contains permanent magnets and can traverse finite limits relative to the Stator. Relative force is generated between the Stator and a Moving Mass by passing electrical current through windings of the Stator, thus, moving both the Stator and the Moving Mass.

Because of travel limits, the Moving Mass is not able to store energy as would more conventional devices such as torque wheels or CMG's. Its position must at all times be a foremost consideration of the control algorithm since bi-directional control is lost at extremes. This complication is in addition to saturation which is normally considered by control analysts. At high frequencies, saturation limits the force output, but at low frequencies, force commands must be limited because of travel limits. A local controller can be designed whose frequency response is shaped according to these limits at frequencies of interest. This will somewhat alleviate the problem, but does not allow the control algorithm to ignore position management of the Moving Mass.

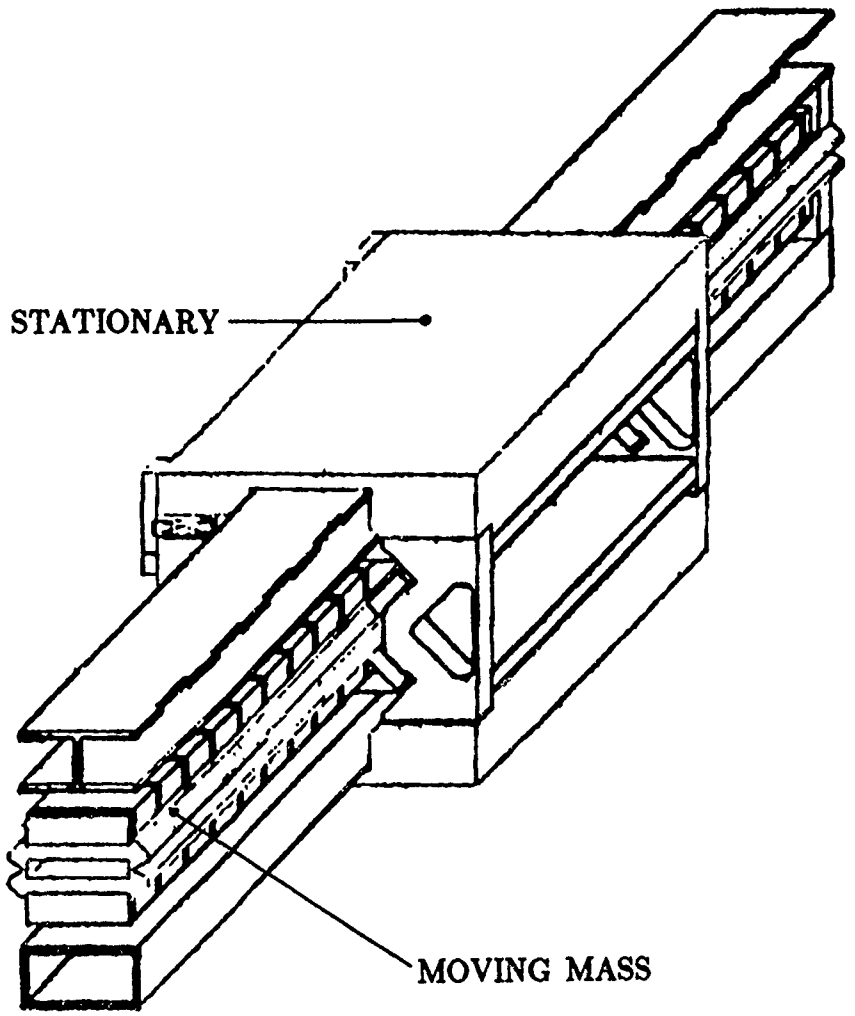

Figure 6

LOCAL CONTROLLER

Because of the problems cited concerning the use of the LDCM's, a local controller is being considered. The control computer sends commands to this controller which, based on sensor inputs from a Stator-mounted accelerometer and a sensor that measures relative position of the Moving Mass to the Stator, generates a current signal for the Stator windings.

The schematic below describes one scheme currently being considered for the local controller. Current command from the local controller is converted into a relative force, F, through a linear gain. Any nonlinearities in the conversion are modelled by f. The relative force is applied to the moving mass and in the opposite direction to the structure through transfer function Q(s). Q(s) includes the dynamics of the space shuttle, MAST, and Stator. The accelerometers mounted to the Stator respond to the MAST motion with transfer function A(s). The accelerometer output with error is twice integrated in the local controller to generate an estimate of the position of the Stator. Each integration is accomplished by transfer function I(s) which is stabilized. The sum of the estimated Stator and relative position signals is an estimate of the inertial position of the moving mass. Thus, the primary feedback of the local controller is the estimated inertial position of the moving mass.

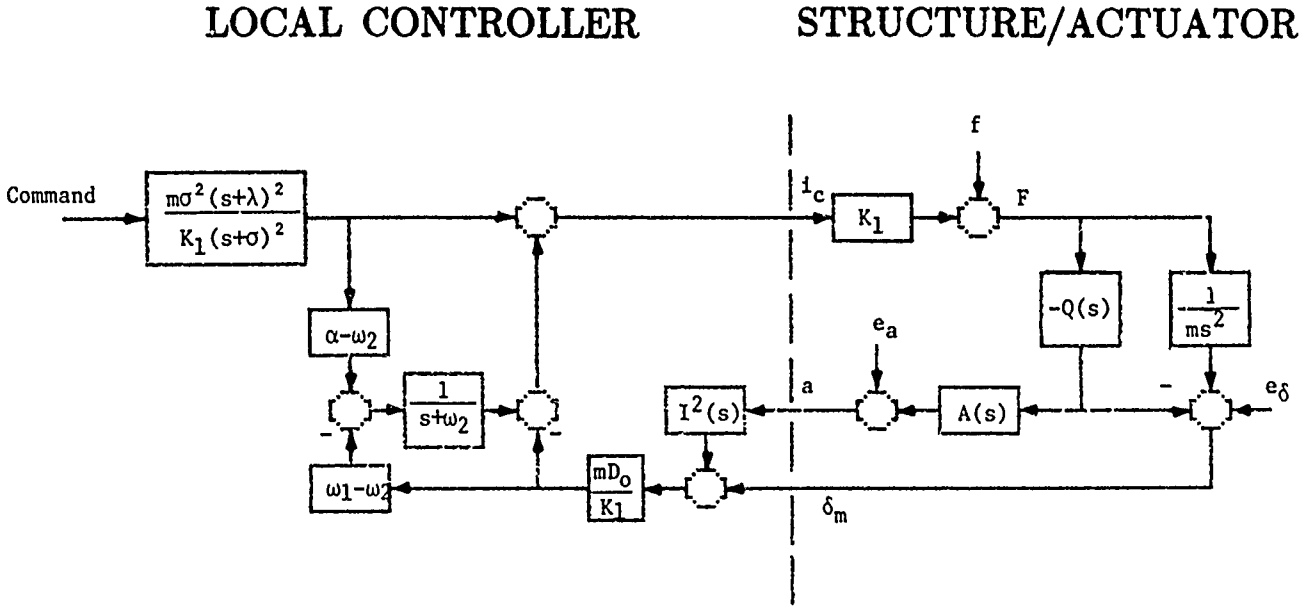

Figure 7

MODEL AND SIMULATOR

Ground tests for COFS will involve the MAST flight system, a 20-meter truss beam of similar construction called MINI-MAST, and a pendulum suspended shuttle, truss beam, and antenna apparatus called SCOLE (in support of COFS II). The ground test activities are expected to play an important role in evaluation of the guest investigator control laws for flight. A simulator has been developed for the MAST flight system and is under development for the MINI-MAST and ground test systems. For the flight system, the physical apparatus — the space shuttle, the MAST, sensor and actuators were modelled using finite element analysis techniques. The output of the finite element analysis is a set of mode shapes and frequencies that are used by the system real-time simulator resident on the LaRC CYBER 175 simulation system. The control computer is functionally simulated assuming an update rate of 150 Hz. The detailed bit manipulation, computation, and communications required by the flight system are not simulated. The number of modes used in a simulation is a variable and is typically 15 (including the 6 rigid-body modes of the system).

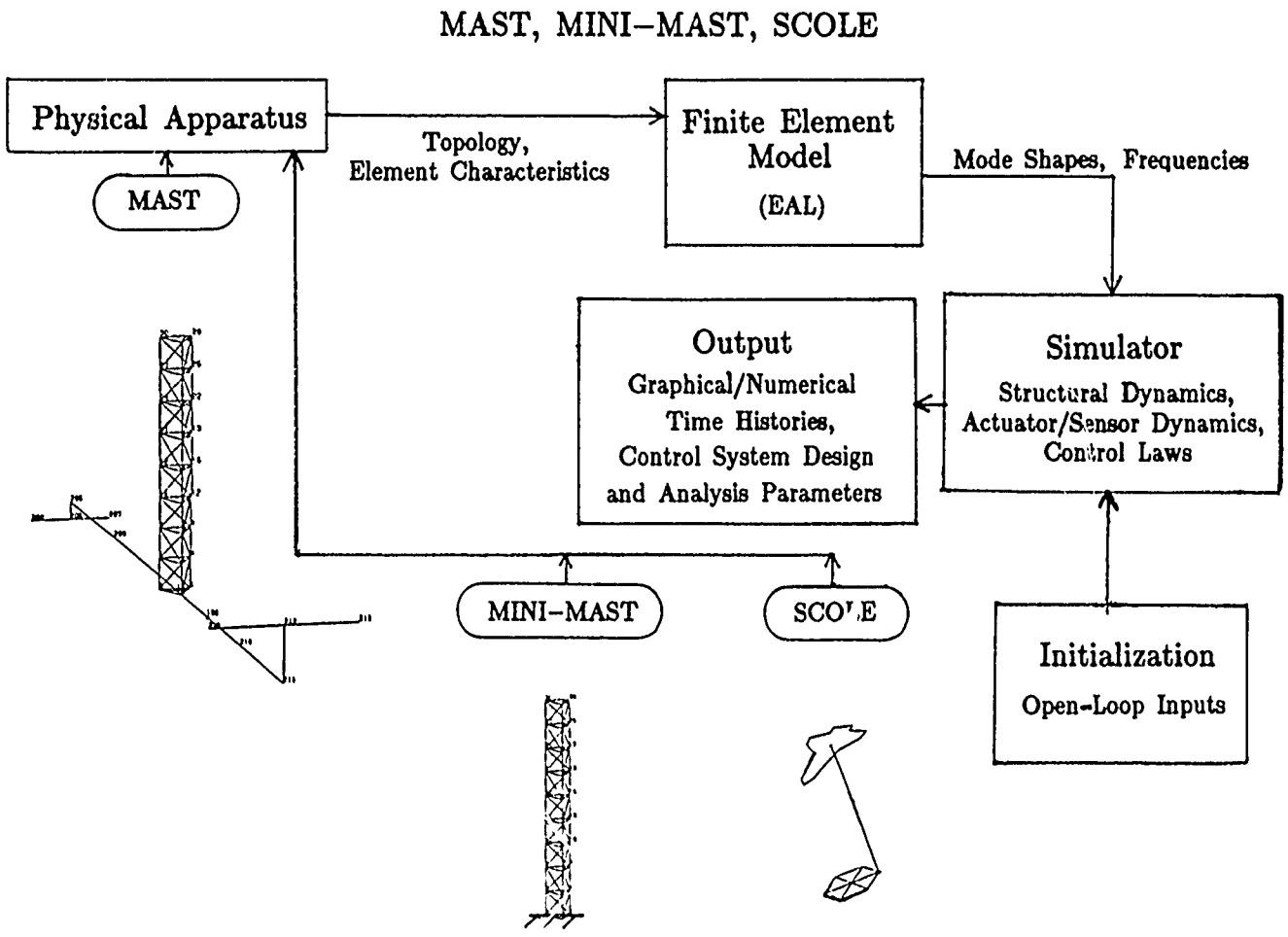

Figure 8

EFFECTS OF LOCAL CONTROLLER FIRST BENDING FREQUENCY

Figure 9 is time histories of the MAST flight system in response to sinusoidal input commands to the LDCM's to excite the first bending mode of the MAST in the direction normal to the plane of symmetry of the space shuttle. On the left are the responses using direct current command to the LDCM's. This set illustrates one fundamental problem — that the relative position of the Moving Mass continually drifts to one side. When the same simulation is conducted with the local controller engaged, the result is shown on the right. Here, the local controller corrects the drift and produces a zero steady-state response.

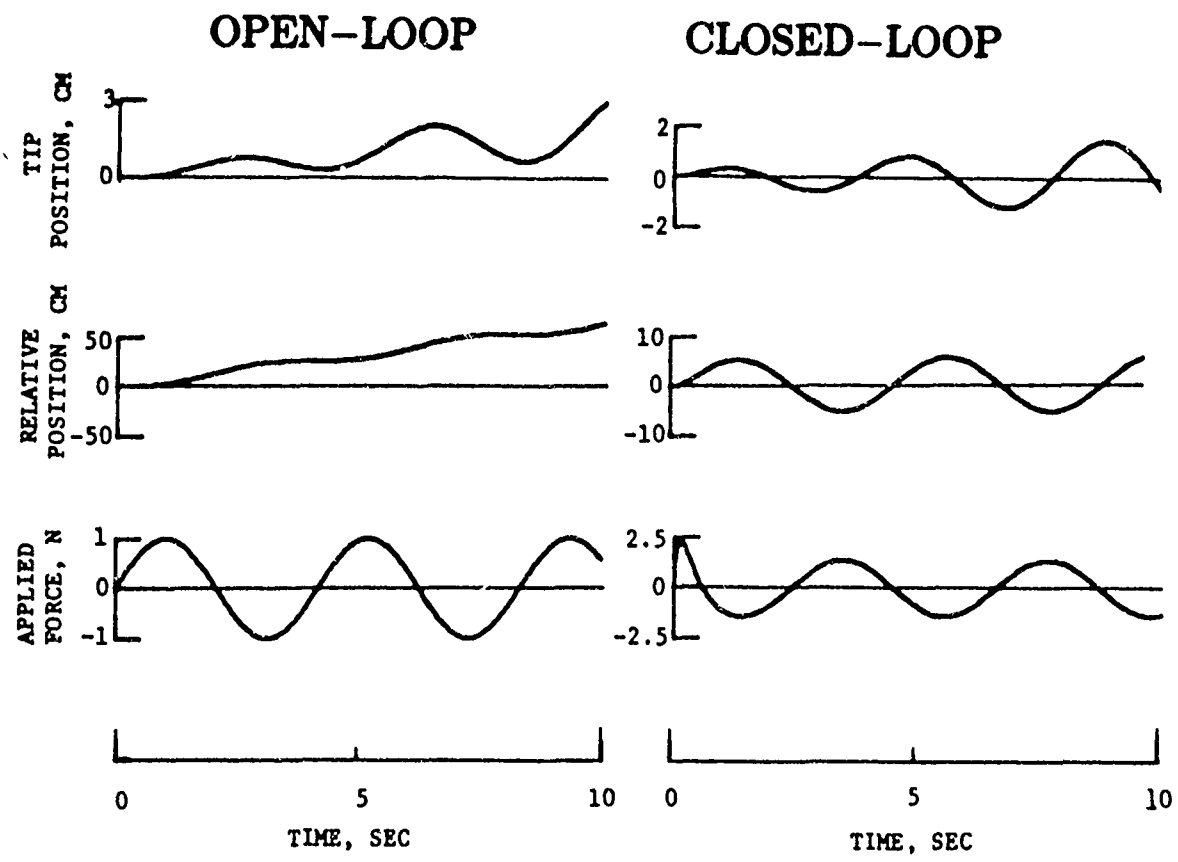

Figure 9

CONTROL EXPERIMENT SOFTWARE

The Baseline Control Law software package is envisioned to contain three subsystems. One provides excitation and disturbances, one is the control algorithm, and the last is performance evaluation.

EXCITATION AND
DISTURBANCE INJECTION SUBSYSTEM

CONTROL ALGORITHM SUBSYSTEM

PERFORMANCE EVALUATION SUBSYSTEM

Figure 10

EXCITATION AND DISTURBANCE INJECTION SUBSYSTEM

The excitation and disturbance injection subsystem will be able to generate sinusoidal inputs at a single frequency or inputs that are a finite sum of several weighted sinusoidal signals (multi-mode sinusoidal). Other input types include amplitude-limited random signals. These inputs may be used for excitation in an open-loop manner or may be used during a control law test to provide disturbances.

A necessary feature of the system is command limiting. This will be done to avoid exceeding load and deflection limits on the MAST and relative position limits on the LDCM's.

SINGLE & MULTI–MODE SINUSOIDAL

AMPLITUDE-LIMITED RANDOM

COMMAND LIMITING --
DEFLECTION AND LOAD MONITORING

Figure 11

CONTROL ALGORITHM SUBSYSTEM

The control algorithm will include variable order sensor prefilters that are of the ARMA form wherein the user provides the filter constants. These are scalar digital filters for each sensor signal used. A modest form of fault detection will be used to insure that the data passed along in the control algorithm are valid. This will include reasonability tests based on past sensor data. The primary control algorithm is linear. It is based on a state estimator followed by a control command calculation. Efficient software will be developed to take advantage of sparse matrices. The matrices in this subsystem are user supplied. The output from the control algorithm subsection is passed to scalar compensators. The compensators are also of variable order ARMA form with the coefficients user supplied. The output of the compensators is command limited prior to being sent to the MDIS.

SENSOR PREFILTERS

- SCALE FACTOR & BIAS CORRECTIONS
- ARMA FILTER FORM
- FAULT DETECTION

LINEAR ESTIMATION & CONTROL ALGORITHM

ESTIMATOR: $x_{k+1} = Ax_k + B_k + Cy_k$

CONTROLLER: $u_{k+1} = Dx_k + E_k + Fy_k$

ACTUATOR COMPENSATORS

- SCALE FACTOR & BIAS CORRECTIONS
- ARMA COMPENSATOR FORM
- COMMAND LIMITING

Figure 12

PERFORMANCE EVALUATION SUBSYSTEM

Measures of control law performance will be time histories of the sensor outputs (raw and filtered), state estimates, control commands (raw and compensated), and commands transmitted to the MDIS. This will be augmented by RMS calculations and on-line estimates of frequency and damping of selected scalar signals.

RECORDS & RMS OF

SENSOR OUTPUTS
ESTIMATED VARIABLES
CONTROL COMMANDS

ON-LINE ESTIMATES OF
FREQUENCY & DAMPING FOR
SELECTED SCALAR SIGNALS

Figure 13

ALGORITHM PROCESSING REQUIREMENTS

To get a measure of the demands the control algorithm makes on the EDS computer, calculation of the number of floation-point multiply and add operations required for a specific case has been made. The assumptions of the algorithm are that all data are processed 150 times per second. This may not be required. For example, in a modal controller, the lower frequency mode calculations may not require complete updating at 150 times/sec. The sensor outputs are assumed to be filtered by a 6th order ARMA filter. Twelve sensors are assumed. The six rigid-body and eight of the flexible modes are included in the control algorithm. This produces fully populated matrices with a state dimension of 28. Each scalar output of the linear control algorithm is passed to a 4th-order, ARMA form compensator. The time frame used in the calculation taken from a previous chart is 5033 microseconds and 20 percent overhead is used to represent operating system and logic required to process the control law. To process this algorithm under the assumptions discussed, the EDS processor must be capable of performing a multiply and add operation in 1.2 microseconds. If only the eight flexible modes are used, the processing time requirement reduces to 2 microseconds.

ALGORITHM ASSUMPTIONS:

150 SAMPLES/SECOND
12 SENSORS -- 6th-ORDER FILTERS
6 RIGID-BODY & 8 FLEXIBLE MODES
9 ACTUATORS -- 4th-ORDER COMPENSATORS

SYSTEM ASSUMPTIONS:

TIME FRAME -- 5033 μSEC
20% OVERHEAD -- LOGIC & SYSTEM

SPEED REQUIREMENT -- μSEC/MAD:
(MAD == MULTIPLY & ADD OPERATION)

1.2 μSEC/MAD

2.0 μSEC/MAD FLEXIBLE MODES ONLY

Figure 14

COLLOCATED RATE FEEDBACK
CLOSED-LOOP

One obvious control law to process with the algorithm is collocated rate feedback using estimated velocity of the Stator. Figure 15 shows a simulation run sending direct current commands to the LDCM's, i.e., no local controller. The left set of charts is the excitation phase of the simulation and the right is the controlled phase. The applied force was generated by open-loop sinusoidal force commands at the frequency of the first flexible mode. The excitation phase lasted 10 seconds. No attempt was made to limit or monitor motion of the Moving Mass. This would be required for the flight software. At the end of the 10-second excitation phase, a collocated rate feedback control law assuming perfect estimation was engaged. The collocated rate feedback gains were precalculated to produce 5 percent damping in the mode excited. The 15 lowest frequency modes of the MAST flight system were included in the simulation. The design damping was indeed obtained; however, during the experiment approximately 1.2 meters of relative motion of the LDCM's was observed. It is indeed unfortunate that their travel is projected to be only 20 CM. A study using the local controller is in the process of being made but is not available at this time. Hopefully, the local controller will produce similar results and not exceed the travel limits of the LDCM's.

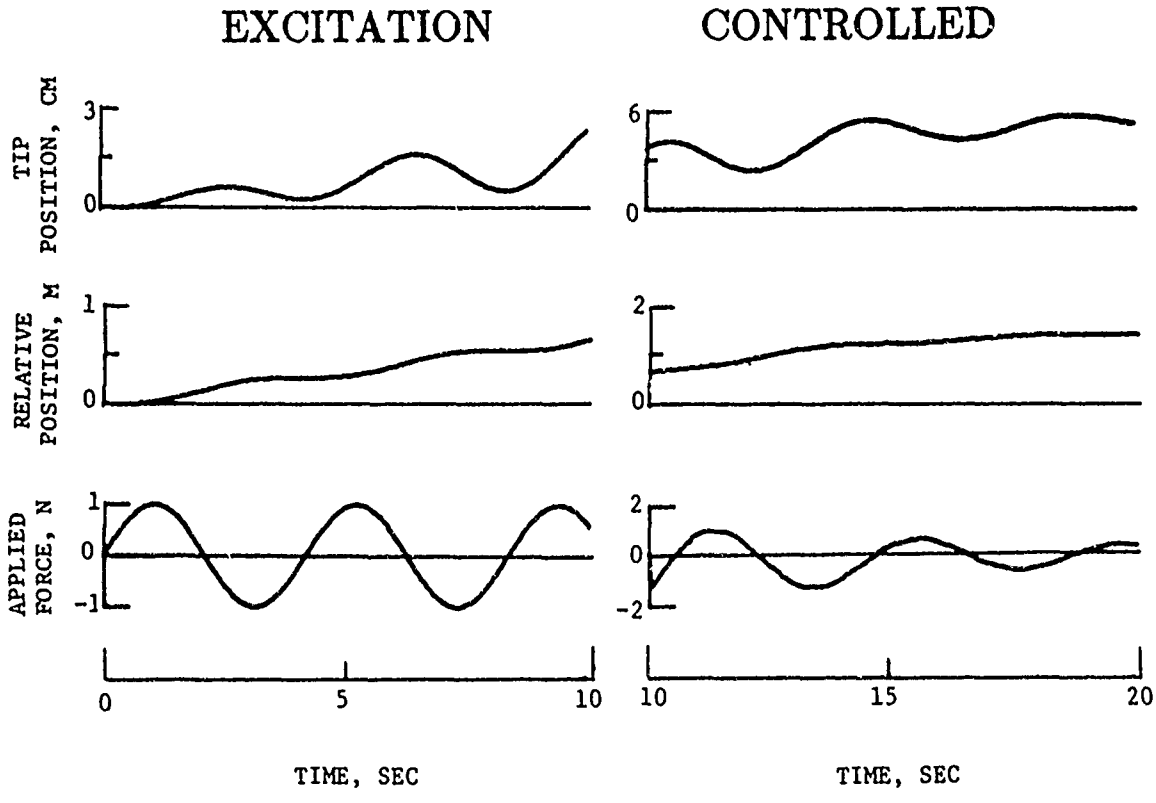

Figure 15

CONCLUDING REMARKS

This paper has proposed a Baseline Control Law software package that will, hopefully, support the research of many guest investigators. Elements of the package are an Excitation and Disturbance Injection Subsystem, a Linear Control Algorithm Sybsystem, and a Performance Evaluation Subsystem. Definition and evaluation of the Baseline is in progress, but it must be preceeded by a precise definition of the LDCM controllers. A real-time simulation of the MAST flight system is currently available at LaRC and will be used with hardware in the loop to evaluate the Baseline and software for potential guest investigators. The hardware to be used in the simulation are actuators similar to LDCM's save that they use conventional rotary DC motors to accelerate the Moving Mass. These are being developed in-house at LaRC and are expected to be available for use between January and March of 1987.

CONTROL EXPERIMENTS SOFTWARE
PROPOSED FOR COFS I

EXCITATION
GENERIC LINEAR CONTROL ALGORITHM
PERFORMANCE EVALUATION

DEFINITION AND EVALUATION IN-PROGRESS

DEPENDS ON DEFINITION OF
ACTUATOR WITH LOCAL CONTROLLER
REAL-TIME SIMULATION READY
TO EVALUATE VARIOUS LINEAR
CONTROL SCHEMES
HARDWARE IN LOOP SCHEDULED
1st QTR 1987

Figure 16

PASSIVE DAMPING AUGMENTATION

FOR

FLEXIBLE STRUCTURES

J. R. Sesak, M. J. Gronet, G. M. Marinos

Lockheed Missiles and Space Company
Sunnyvale, California

FIRST NASA/DOD

CSI TECHNOLOGY CONFERENCE

Norfolk, Virginia

November 18-21, 1986

INTRODUCTION

Many proposed future large space structure designs, including the NASA Space Station, may need to incorporate active and/or passive damping mechanisms in order to meet pointing, slewing, or microgravity acceleration requirements. Methods for implementing active and passive damping have been the subject of many studies which have indicated the merits of passive damping, either in itself or in concert with active damping.

Incorporation of passive damping for vibration suppression in the design of large space structures offers many benefits. Passive dampers require no power source, are inherently stable, and are potentially simple and reliable. Properly designed passive damping treatments can greatly reduce the settling time in transient response problems and reduce the peaks of steady-state response problems. The existence of small amounts of passive damping in an active control system can reduce active control effort such as actuator force, stroke, bandwidth, and system penalties such as the number of actuators, added mass, cost, and on-board power and microprocessing needs. Passive damping devices also provide an increased safety margin for all active control systems.

Passive damping can be added to a structure through a variety of mechanisms including constrained layer treatments, impact/friction joints, discrete viscous dampers, electromagnetic devices, fluidic devices, and tuned-mass dampers. Each of these damping treatments performs best for certain classes of damping problems. The tuned-mass damper is especially well-suited for damping large structures which are characterized by low, highly distributed, strain energy, e.g., the NASA Space Station. Although initially dubbed a large flexible space structure, the NASA IOC Station response to orbiter docking exhibits small loads and only a few inches of deflection over the distance of a baseball field. The corresponding low strains may not be enough to efficiently "work" a distributed damping material, or a damping material or device placed in the load path. The advantage of the tuned-mass damper is that it is "tuned" to draw energy from the main structure to a mechanism which works the damping material or damper. Some disadvantages of the tuned-mass damper (also termed vibration absorber) are that it adds nonstructural mass, typically provides only modest damping levels, and does not compensate for changes in the plant dynamics.

This work was supported by the National Aeronautics and Space Administration, Langley Research Center, Contract No. NAS1-17760, Harold G. Bush, Technical Monitor.

PASSIVE STABILIZATION

Tuned-mass dampers are used throughout industry in applications on ships, helicopters, cars, tall buildings, and rotating machinery. The classical two degree-of-freedom steady-state vibration absorber solution of Timoshenko and Den Hartog has been widely used to determine the optimal physical parameters for absorber designs. Much of the emphasis of recent work has been placed on developing absorber designs for use in damping responses to steady-state excitation.

The present work concentrates on the application and extension of absorber design and optimization techniques to a multimode, multi-DOF, large space structure, namely the NASA Space Station. The principal issue addressed is the optimal tuning of several absorbers for the transient response of a multi-DOF system, including the effects of modal coupling, existing structural damping, absorber placement, and absorber mass. The Space Station is subject to many transient disturbances such as docking, orbit reboost, crew motion, and payload slewing. A notable steady-state excitation source is the Science Research Centrifuge, which rotates at a frequency in the bandwidth of the primary structural modes. Because of the relatively advanced state of development of steady-state absorber design techniques, only the transient cases are considered in this study.

OBJECTIVE

- DAMP STRUCTURES CHARACTERIZED BY HIGHLY DISTRIBUTED LOW STRAIN ENERGY
  - SPACE STATION
  - ANTENNA SYSTEMS
- APPROACH: USE PASSIVE VIBRATION ABSORBER TO DRAW ENERGY TO A DAMPER. APPLY AND EXTEND ABSORBER DESIGN AND OPTIMIZATION TECHNIQUES TO MULTIMODE MULTI-DOF LSS
- SPACE STATION APPLICATION
  - LARGE CENTRIFUGE
  - SHUTTLE DOCK
  - ORBIT REBOOST
  - PAYLOAD SLEWING
  - CREW MOTION

STUDY FLOW

The optimal tuning of multiple tuned-mass dampers for the transient vibration damping of large space structures is investigated. A multi-disciplinary approach is used. Structural dynamic techniques are applied to gain physical insight into absorber/structure interaction and to optimize specific cases. Modern control theory and parameter optimization techniques are applied to the general optimization problem.

Classical dynamic models are extended to investigate the effects of absorber placement, existing structural damping, and absorber cross-coupling on the optimal design synthesis. An uncoupled dynamic optimization technique is developed which allocates the absorber mass budget over multiple absorbers in order to optimally damp the transient response.

The control design process for the general optimization problem is formulated as a linear output feedback control problem via the development of a feedback control canonical form. The design variables are expressed as control gains, and the analytical techniques of feedback control theory, both classical and modern, are applied to absorber design. A nonlinear parameter optimization method is developed and applied to an output feedback formulation of the vibration damping problem.

The techniques are applied to sample micro-g and pointing problems on the NASA dual keel space station.

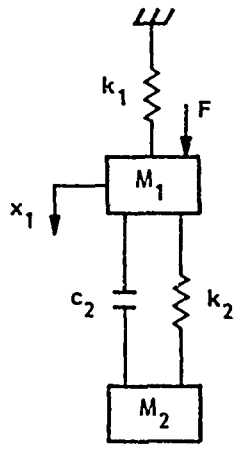

ABSORBER 2-DOF REPRESENTATION

M_1 = PLANT MODAL MASS

k_1 = PLANT MODAL STIFFNESS

- EXTEND AND APPLY PREVIOUS WORK TO TRANSIENT RESPONSE OF MULTIMODE, MULTI-DOF LSS
  - CLASSICAL - TIMOSHENKO, DEN HARTOG
  - M. CARD, J. JUANG, E. CRAWLEY (STEADY-STATE)
- DYNAMICS - MASS AND PLACEMENT OPTIMIZATION, UNCOUPLED SOLUTION
  - CLASSICAL 2-DOF VIBRATION ABSORBER SOLUTION
  - COST FUNCTION SELECTION
  - EFFECT OF STRUCTURAL DAMPING
  - EFFECT OF PLACEMENT
  - CHARACTERIZATION AND BENEFITS OF COUPLING
  - UNCOUPLED MULTIMODE MASS OPTIMIZATION
- CONTROLS - FULLY COUPLED MULTI-DOF OPTIMIZATION
  - FEEDBACK CONTROL FORM
  - ROOT LOCUS TECHNIQUES
  - MULTIVARIABLE OUTPUT FEEDBACK DESIGN FOR MULTIPLE DAMPERS
- EXAMPLES
  - SPACE STATION CRITICAL MODE SELECTION
  - COMPARISON OF RESULTS
    - POINTING
    - MICRO-G

2-DOF IMPULSE RESPONSE

Because of the variety of different Space Station disturbances and the continuing evolution of the IOC design in the Phase B program it was decided to model the transient disturbances using an impulse input. This simplification is justified by the relatively short duration of the transient pulses in comparison with the long periods of the dominant structural modes. Changes in the design evolution of the Space Station could easily alter the mix of modes which are excited. Because the impulse input excites all modes, some of the dependence of the study conclusions on a particular evolutionary configuration is removed.

The absorber parameters which are varied in this study are the mass M_2, the stiffness k_2, and the damper strength, c. Because absorber performance increases with increasing absorber mass (until a saturation point is reached), the absorber mass is selected a priori based on the available mass budget. In the analysis for the chart below, the absorber mass is assumed to be 2% of the plant modal mass. The value of δ which maximizes the absorber/structure interaction for a mass ratio of 2% is 0.98. The chart shows the impulse response envelopes (which connect the peaks of the amplitude of the sinusoidal transient response) as a function of the nondimensional damper coefficient μ. The chart shows that too high a value of μ "locks" the damper, restraining the motion across the damper and resulting in sub-optimal performance. Similarly, too low a value of μ provides too little damping. A value of μ between .086 and .11 seems desirable for this mass ratio.

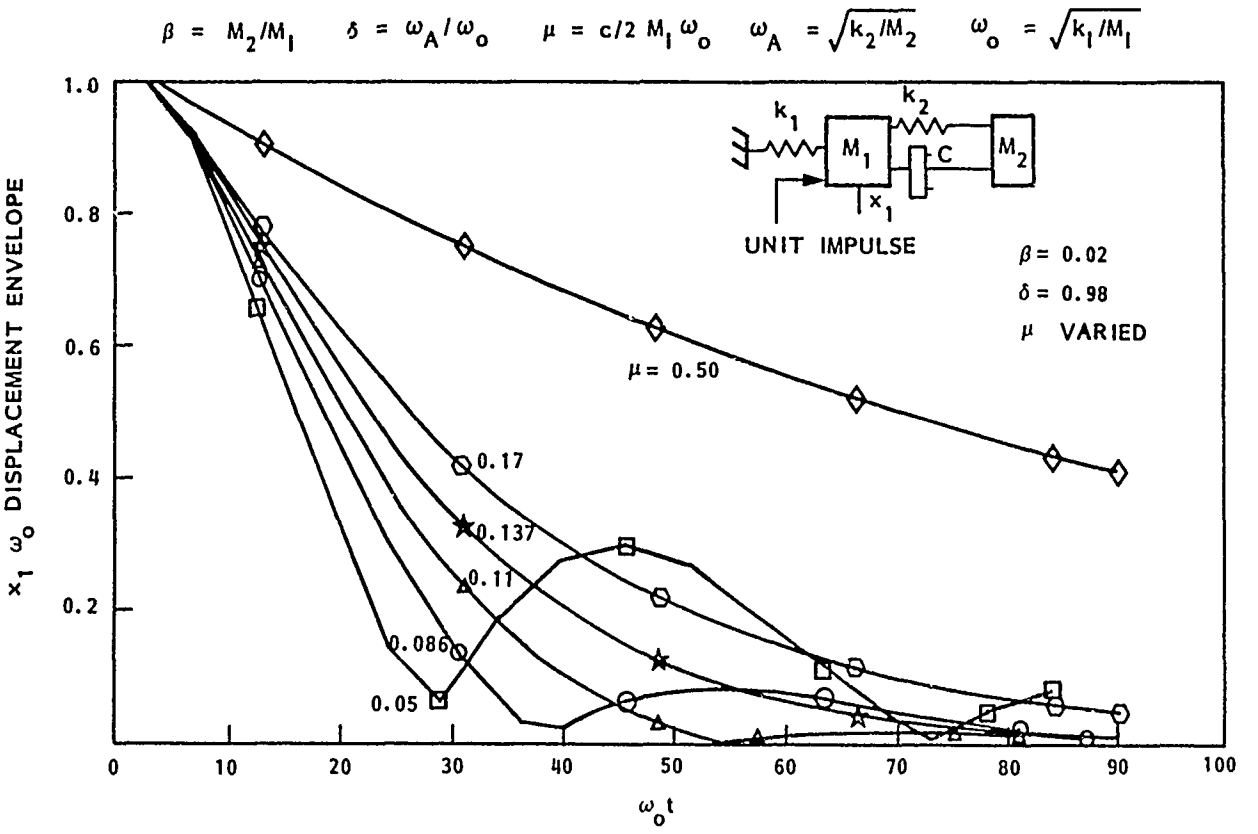

COMPARISON OF ABSORBER PERFORMANCE WITH STRUCTURAL DAMPING

The effect of inherent structural damping on absorber performance is analyzed using the two-DOF system shown in the chart. A non-zero value for c_1 is used to represent the modal damping of the original plant mode. The settling times to 20% of the peak impulse response are plotted vs. the existing structural damping for the system with and without an absorber. The results show that a 2% modal mass absorber can significantly improve the settling time of systems with less than about 5% inherent structural damping. Beyond the 5% level, the structure itself is dissipating energy so well that the absorber has little effect. Examination of the chart yields that for a 2% modal mass absorber, the response time to 20% peak is equivalent to that for the same plant without an absorber but with a structural damping level of 6%.

Similar investigations examined the effect of inherent structural damping on the applicability of the absorber tuning laws that were developed. The results indicate that the tuning laws dictate an optimal design for systems with small amounts of inherent structural damping (around 2%). Above the 2% level, the surface contours of the optimization cost function start to flatten out, indicating a reduced sensitivity of the system performance to the tuning of the absorber.

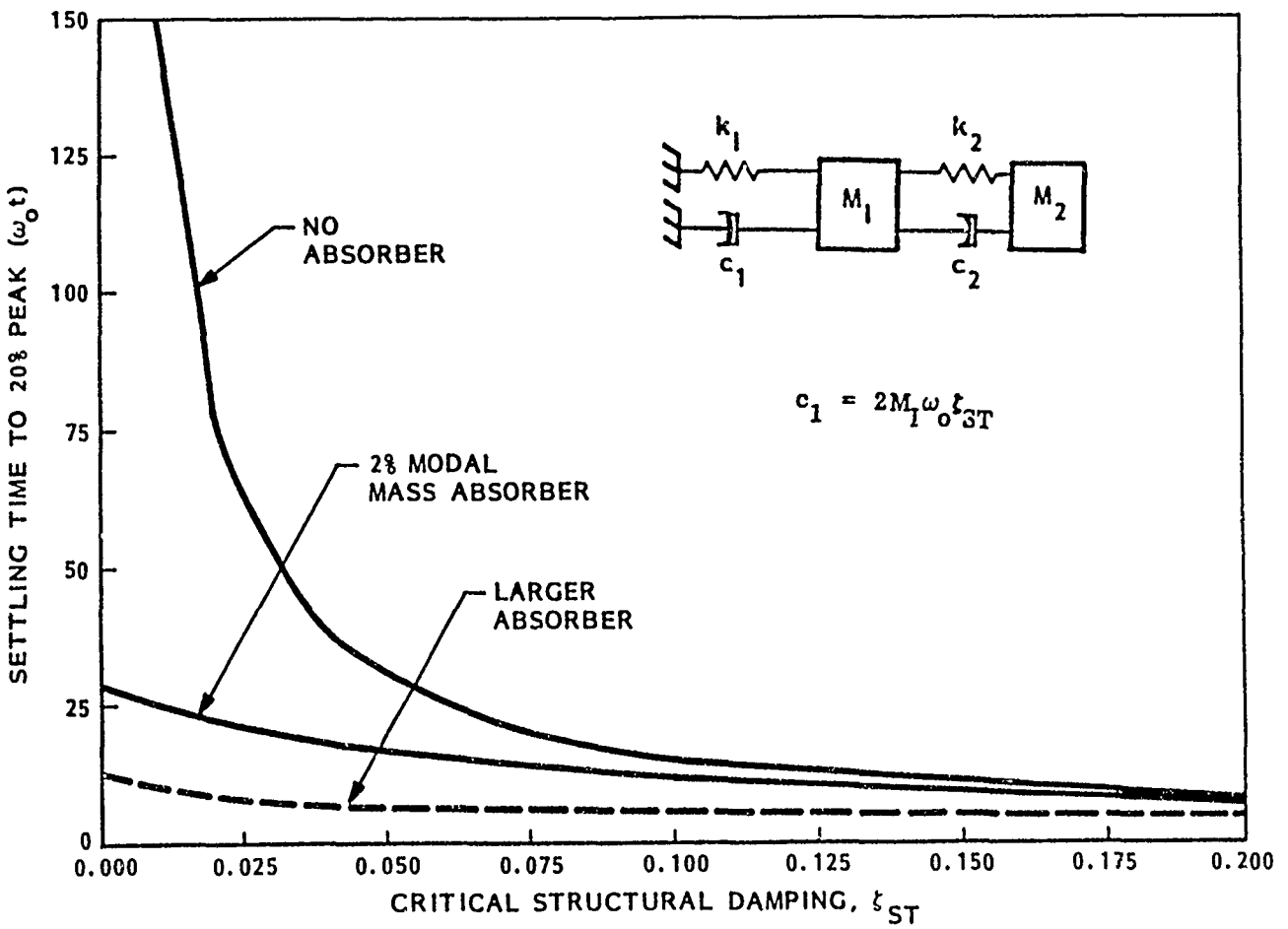

MULTI-DOF MULTIMODE ABSORBER DESIGN

Tuning laws were developed to account for the effects of absorber placement and the use of multiple absorbers to damp the same mode. Note that if the absorber is not placed at the maxima of the mode which is to be damped, the effective modal mass ratio (βeff) is reduced. This implies both reduced performance and the use of different optimal physical parameters for the absorber, based on βeff.

The equations and chart below illustrate the cost function used in the optimization, which basically minimizes the area under the impulse response curve. This cost function was selected after comparing the impulse response performance of several other penalty functions. A unique feature of this cost function is that for the impulse response case, the value of J can be expressed solely as a function of β and the existing structural damping. The good fit of the equation with the exact solution illustrates this unique feature.

EFFECT OF PLACEMENT: $\beta_{eff} = \frac{M_A \varphi_{in}^2}{M_j}$ $\quad \varphi_{in}$ NORMALIZED SO PEAK = 1.0

FOR n ABSORBERS: $M_i = M/n$, $c_i = c/n$, $k_i = k/n$

$$J = \int_0^\infty \left| 1/\omega_d \exp(-\zeta\omega_n t) \sin \omega_d t \right| dt \qquad J = \frac{1}{\zeta \omega_n \omega_d} \text{ [TERMS IN } \omega_n, \omega_d]$$

$$\text{BUT} \quad \zeta = 1/2 \sqrt{\frac{\beta}{\beta + 2}}$$

COMPARISON OF AREA EQUATION AND EXACT SOLUTION

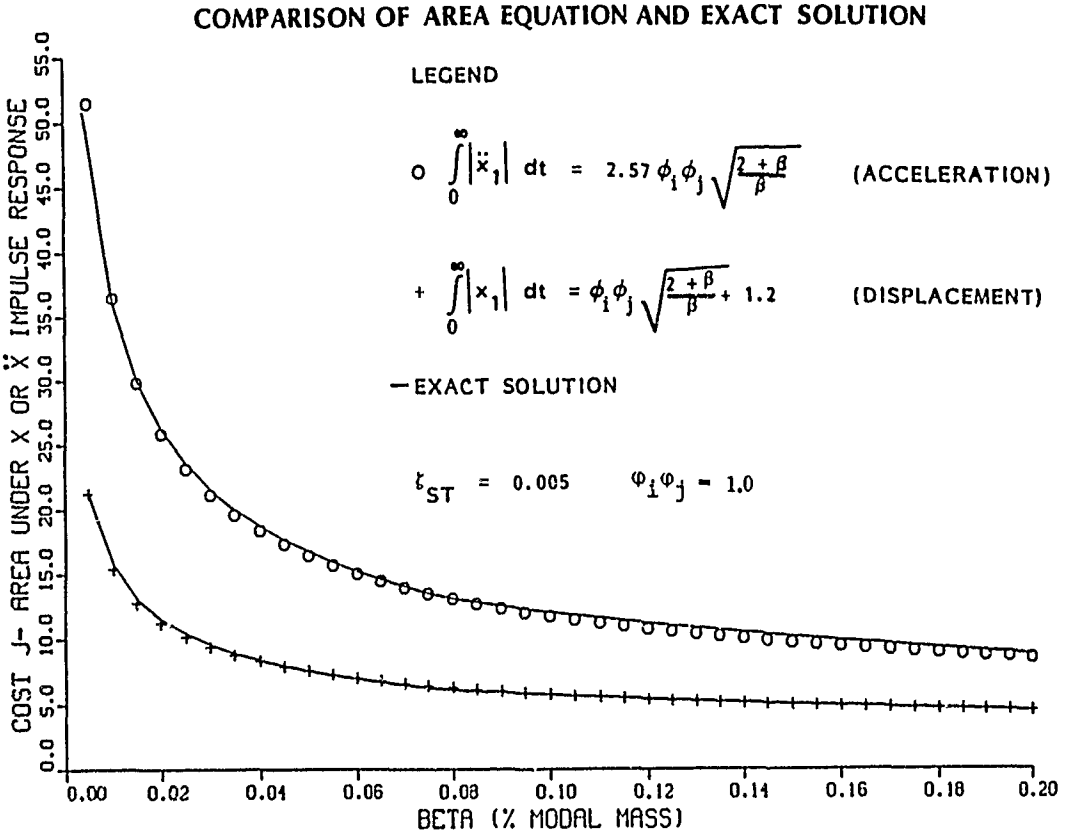

UNCOUPLED MODE ABSORBER MASS OPTIMIZATION FOR MULTI-DOF, MULTIMODE SYSTEMS

The fact that the performance index for an absorber tuned to a particular mode can be described as a function of β suggests that an uncoupled optimization can be conducted to determine the optimal allocation of the mass budget among several absorbers, each tuned to a particular mode. The procedure outlined below generalizes the performance index to include several modes. The cost function minimizes the sum of the areas under the impulse responses of all the modes. An important assumption is that the absorber on any one mode does not couple with the absorber on another mode. The amount of absorber cross-coupling depends on the spatial location of the absorbers and the frequency separation of the modes. The chart below illustrates the process whereby the cost function is minimized subject to the constraint of the total available absorber mass budget. Once the absorber mass attached to each primary mode is calculated, classical tuning laws can be used to calculate the absorber stiffness parameters, based on the value of β.

ASSUME AN ABSORBER OF MASS β_i (TO BE DETERMINED) ON EVERY PRIMARY MODE

$$\text{Min } J_T = \underbrace{J(\beta_1)}_{\text{MODE 1}} + \underbrace{J(\beta_2)}_{\text{MODE 2}} \cdots + \underbrace{J(\beta_n)}_{\text{MODE n}} = \sum_{i=1}^{n} J_i$$

SUBJECT TO CONSTRAINT $M_{A_T} = \beta_1 M_1 + \beta_2 M_{11} + \ldots \beta_n M_n$

WHERE

- $J(\beta_i) = \phi_i \phi_j \sqrt{\frac{2+\beta}{\beta}} + 1.2$ (DISPLACEMENT)
- $J(\beta_i) = 2.57\, \phi_i \phi_j \sqrt{\frac{2+\beta}{\beta}}$ (ACCELERATION)

INVOKE SIMPLE CONSTRAINED MULTIVARIATE SOLUTION:

$$\frac{\alpha J_T}{\alpha \beta_i} - \frac{\alpha J_T}{\alpha \beta_1} \frac{\alpha M_{A_T} / \alpha \beta_i}{\alpha M_{A_T} / \alpha \beta_1} = 0 \quad (i = 2, \ldots n)$$

$$M_{A_T} - (\beta_1 M_1 + \beta_2 M_{11} + \ldots \beta_n M_n) = 0$$

WHICH YIELDS n NONLINEAR EQUATIONS IN n UNKNOWNS

WHICH CAN BE SOLVED FOR β_i

ONCE β_i ARE KNOWN, USE CLASSICAL TUNING LAWS TO FIND k_{Ai}, c_{Ai} FOR ABSORBERS

CONTROL DESIGN PROCESS

The key concepts that allow application of feedback control techniques to absorber design are the placement of the design problem in a linear format, and the recasting of the combined structure-absorber dynamic equations in a feedback canonical form. This linear form is useful because most of the control-theoretic results apply to linear systems and the linear format greatly simplifies analysis and design. The feedback canonical form allows expression of the absorber parameters as controller gains and provides a convenient method for the evaluation of absorber performance. This formulation also provides needed visibility into the absorber design process.

CONVERT NONLINEAR DESIGN PROBLEM TO LINEAR PROBLEM – DO NOT LINEARIZE

- OPTIMAL SOLUTION REQUIRES ABSORBER MASS MAXIMIZATION
  - SET ABSORBER MASS AT MAXIMUM
  - ELIMINATE AS A VARIABLE
- ELIMINATE PLACEMENT AS A VARIABLE BY CHOOSING LOCATIONS OUTSIDE THE CONTROL DESIGN PROCESS
  - ASCERTAIN TROUBLESOME MODES
  - PICK LOCATIONS OF HIGHEST MODAL GAIN FOR ABSORBER ATTACHMENT
- PERFORM DESIGN WITH WELL-KNOWN READILY AVAILABLE CONTROL ALGORITHMS
  - LET ALGORITHMS DETERMINE ABSORBER FREQUENCY
  - ROOT LOCUS
  - OPTIMAL OUTPUT FEEDBACK

DYNAMIC EQUATIONS

The dynamic equations for the absorber and the system may be formulated as shown. These equations take the form of coupled second-order differential equations. System I denotes the main system, or the structure to be damped. System II denotes the absorber dynamics for the coupled equations. The main system variables and parameters are denoted by the subscripts 1, and the absorber variables and parameters by the subscripts 2. The symbol, P, represents an external force applied to the system.

$$\frac{P}{M_1} = \ddot{X}_I + \frac{C_2}{M_1}\dot{X}_I + \frac{K_1 + K_2}{M_1} X_I - \frac{C_2}{M_1}\dot{X}_{II} - \frac{K_2}{M_1} X_{II} \qquad \text{SYSTEM I (MAIN)}$$

$$0 = \ddot{X}_{II} + \frac{C_2}{M_2}\dot{X}_{II} + \frac{K_2}{M_2} X_{II} - \frac{C_2}{M_2}\dot{X}_I - \frac{K_2}{M_2} X_I \qquad \text{SYSTEM II (ABSORBER)}$$

IN MATRIX NOTATION (SYSTEM I)

$$\begin{bmatrix} \dot{X}_1 \\ \dot{X}_2 \end{bmatrix} = \begin{bmatrix} 0 & \\ \frac{-(K_1 + K_2)}{M_1} & -\frac{C_2}{M_1} \end{bmatrix} \begin{bmatrix} X_1 \\ X_2 \end{bmatrix} + \begin{bmatrix} 0 & 0 \\ \frac{1}{M_1} & 1 \end{bmatrix} \begin{bmatrix} P \\ Y_2 \end{bmatrix}; \quad Y_1 = \begin{bmatrix} \frac{K_2}{M_1} & \frac{C_2}{M_1} \end{bmatrix} \begin{bmatrix} X_1 \\ X_2 \end{bmatrix}$$

SYSTEM II

$$\begin{bmatrix} \dot{X}_3 \\ \dot{X}_4 \end{bmatrix} = \begin{bmatrix} 0 & 1 \\ \frac{-K_2}{M_2} & \frac{-C_2}{M_2} \end{bmatrix} \begin{bmatrix} X_3 \\ X_4 \end{bmatrix} + \begin{bmatrix} 0 \\ 1 \end{bmatrix} Y_1 ; \quad Y_2 = \begin{bmatrix} \frac{K_2}{M_2} & \frac{C_2}{M_2} \end{bmatrix} \begin{bmatrix} X_3 \\ X_4 \end{bmatrix}$$

MULTIPATH DIAGRAM FOR ABSORBER

This diagram demonstrates the multipath nature of the control problem. The control design gain, K, appears in two inner feedback loops, and forms the coupling matrix between the two systems. Although these gains seem to be independent and appear in different system loops, in actuality they are identical paramaters that appear simultaneously. This implies that parametric adjustment in one loop yields simultaneous adjustment in every loop containing that parameter. This property makes design difficult and illustrates a basic design limitation of the absorber. The outer feedback loop is positive in nature. Positive feedback loops are generally avoided in practice because of reduced stability margins that can cause system-wide instability. However, stability constraints are not a concern in this design process, for the entire system is guaranteed to remain stable as the passive nature of the absorber guarantees stability. The system dynamic equations are inherently stable for all physically realizable parameter values.

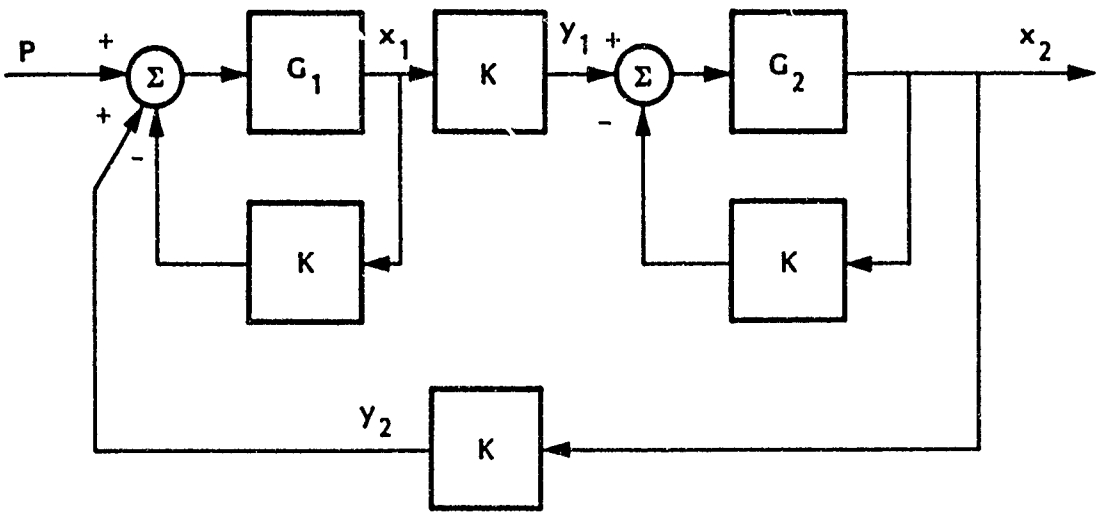

G_1 = MAIN SYSTEM (STRUCTURE)

G_2 = ABSORBER SYSTEM

K = ABSORBER COUPLING PARAMETERS
[SPRING CONSTANTS AND DAMPER VALUES = $(k_2 + sc_2)$]

P = DISTURBANCE INPUT

y_1 = SYSTEM 1 OUTPUT (DEFLECTION)

y_2 = SYSTEM 2 OUTPUT (DEFLECTION)

CANONICAL FORM FOR ABSORBER ROOTS

This system has the structure of a simple output feedback control system entailing a single feedback loop, and may be used to synthesize system gains corresponding to absorber parameters. This feedback formulation provides insight to the ability of the absorber to affect system eigenvalues. It should be emphasized that G_2, the transfer function associated with absorber, has the functional form $1/s^2$ and corresponds to the dynamics of the absorber mass without the spring and damper attached. The remaining dynamic elements of the absorber are associated with the feedback loop. The transfer function, G_1, is associated with the structure and has the functional form $1/(s^2 + \omega_o^2)$ and corresponds to a structural vibration mode. The total system may be viewed as a rigid body mode and a vibration mode that are coupled by an external feedback loop, K.

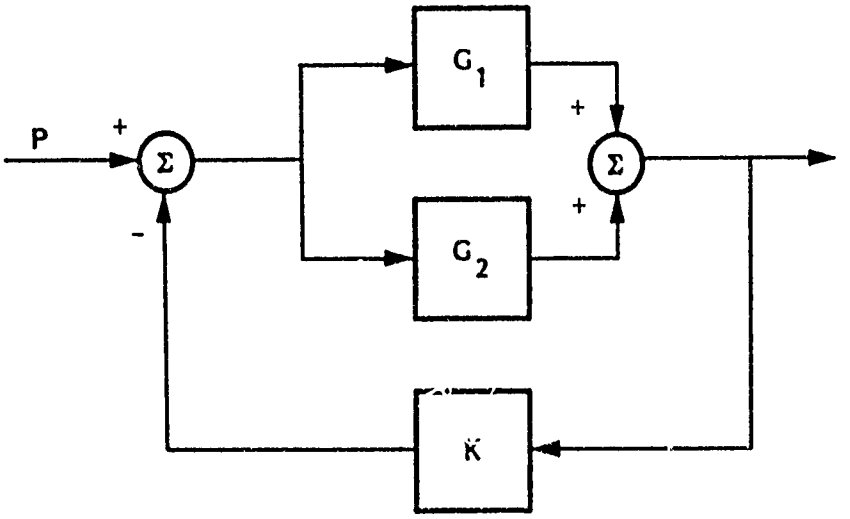

$$K = k_2 + sc_2$$

$$G_1 = \frac{1}{M_1}\left(\frac{1}{s^2 + \omega_o^2}\right) \qquad \omega_o^2 = \frac{M_1}{k_1}$$

$$G_2 = \frac{1}{M_2}\,\frac{1}{s^2}$$

ABSORBER TWO DEGREE OF FREEDOM ROOT-LOCUS PLOT

The pole-zero constellation and associated root-locus plot are shown. The poles are indicated by X's and the zeros are indicated by O's. The pole frequency at ω_o corresponds to the vibration mode of the structure with no absorber attached. A double pole occurs at the origin and corresponds to the absorber mass dynamics. The zeros occur as a result of absorber action and are located at $\pm j\omega_o/(1 + \beta)$ where $\beta = M_1/M_2$ is the ratio of the absorber mass to structural mass. A zero also occurs on the real axis at $-k_2/c_2$ where k_2 is the absorber spring constant and c_2 is the damper value. Zero placement strongly affects the locus behavior, because the closed-loop system poles tend to migrate toward the open-loop system zeros.

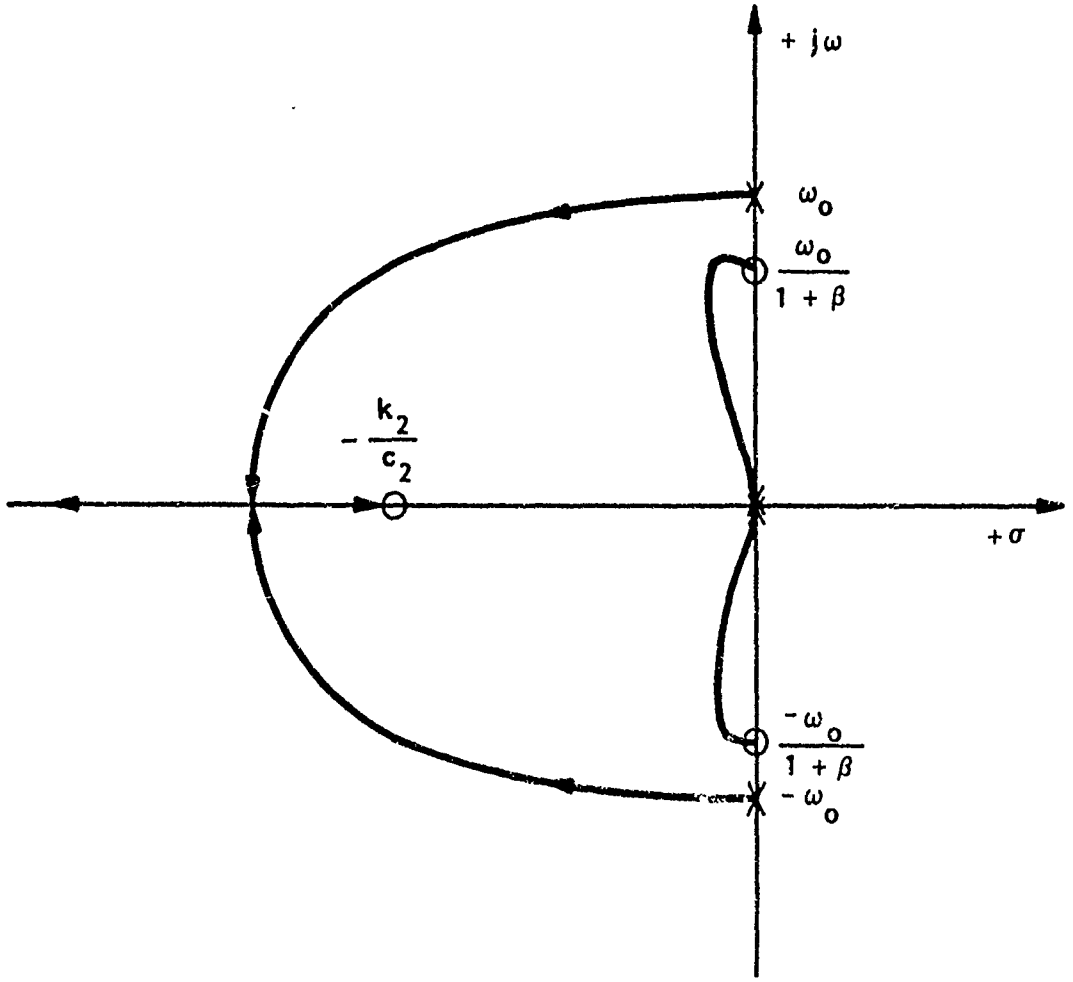

COST FUNCTIONAL FOR OPTIMIZATION

The goal of the optimization problem is to minimize some performance index which penalizes the response-displacement, velocity, or acceleration. The most common performance index applied in linear optimal control theory is the linear guadratic regulator cost functional. The positive semi-definite matrix Q and positive definite matrix R describe the weighting of the state and control variables in the performance index.

- LQR COST: $J = \int_0^\infty (\eta^T Q \eta + u^T R u)\, dt$
- MAY PENALIZE DISPLACEMENT, VELOCITY, OR ACCELERATION
- KEEPS FINITE ELEMENT MODEL 'HONEST'
- OUTPUT FEEDBACK FORM ($u = -FC\eta$)

$$J = \int_0^\infty \eta^T (Q - C^T F^T R F C) \eta$$

SPACE STATION APPLICATIONS

The optimization techniques described in the previous sections are applied to example vibration damping problems on the NASA dual keel configuration Space Station. Two example cases are considered which evaluate the capabilities of the uncoupled dynamic optimization and the parameter optimization algorithms: (1) micro-g acceleration response at the lab module, and (2) pointing response at a location on the lower payload boom. The disturbance input for both cases is a unit impulse at the habitation module. The force input at this location simulates either a shuttle docking or a crew motion disturbance, depending on the strength of the impulse. The inherent structural damping is assumed to be 0.5%.

The chart below illustrates the ICC configuration as of January 1986 which is modeled using a finite element code. Two absorbers are employed in each of the example problems, located at the maxima of the two most prominant modes in the transient response. The response locations corresponding to the two examples are also shown.

REFERENCE CONFIGURATION 5m DUAL KEEL

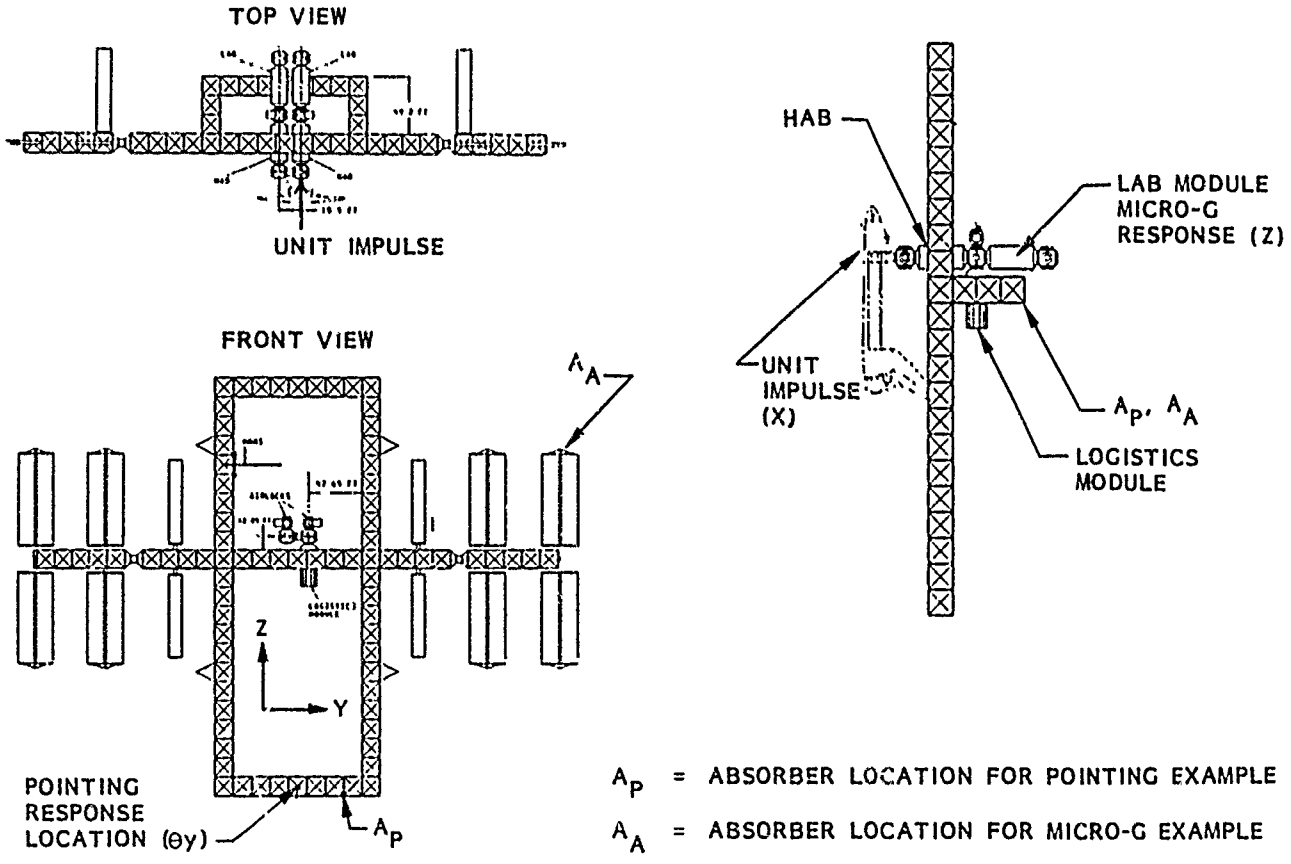

MICRO-ACCELERATION EXAMPLE RESPONSE

The chart below compares the acceleration responses at the lab module due to a unit impulse input. A total absorber weight budget of 77.2 lbs is assumed. Both techniques result in improved damping performance in comparison with the open loop case which has no absorber and 0.5% structural damping. The performance of the system tuned using the parameter optimization technique is slightly preferable. Further examination of the problem reveals that the absorbers are highly cross-coupled in this example, explaining the sub-optimal result obtained using the uncoupled dynamic optimization. The more general parameter optimization technique takes into account the effects of absorber cross-coupling.

TRANSIENT RESPONSE - PROBLEM 1

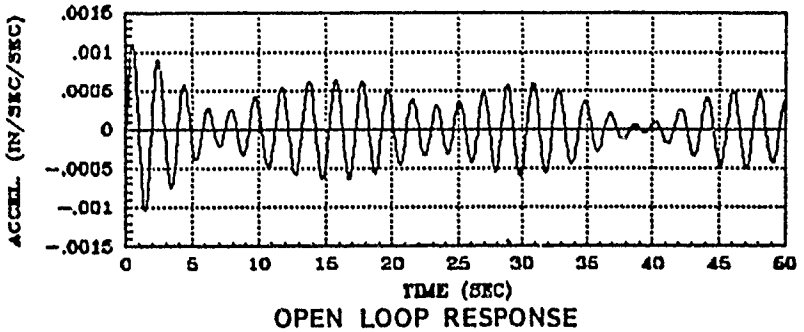

OPEN LOOP RESPONSE

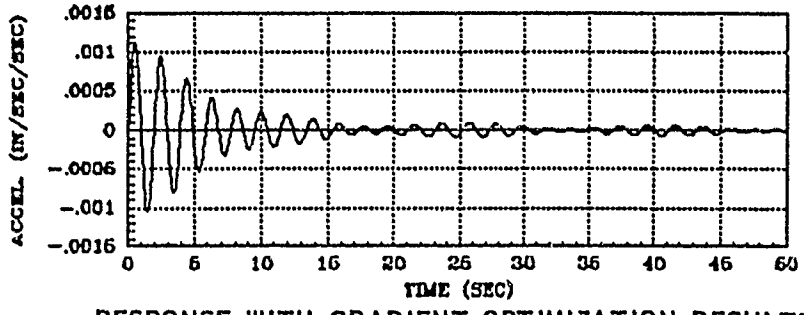

RESPONSE WITH GRADIENT OPTIMIZATION RESULTS

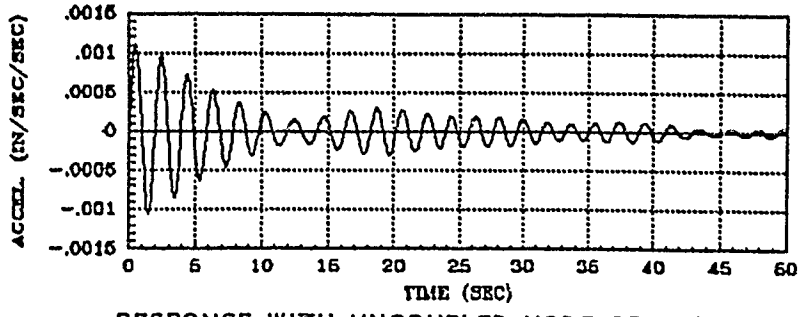

RESPONSE WITH UNCOUPLED MODE OPTIMIZATION

PAYLOAD POINTING EXAMPLE RESPONSE

The chart below compares the pointing responses at the payload boom due to a unit impulse input. A total absorber weight budget of 2,316 lbs is assumed. Again, both techniques result in improved damping performance in comparison with the open loop case. The performance of the system tuned using the uncoupled dynamic optimization is slightly preferable. Further examination of the problem reveals that the absorbers are only lightly cross-coupled in this problem. The sub-optimal result obtained using the parameter optimization technique is attributed to the fact that the averaged initial conditions on the absorbers contributed to the cost function.

TRANSIENT RESPONSE - PROBLEM 2

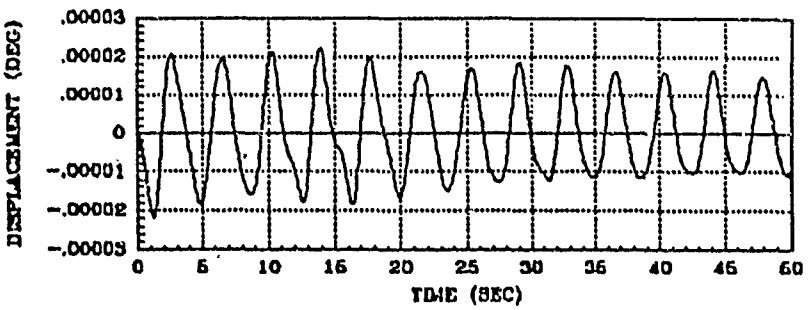

OPEN LOOP RESPONSE

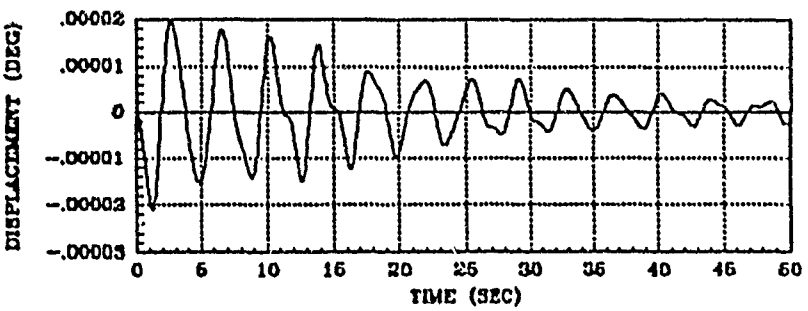

RESPONSE WITH GRADIENT OPTIMIZATION RESULTS

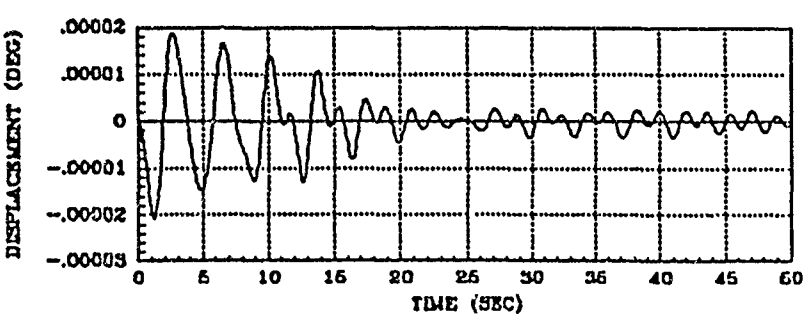

RESPONSE WITH UNCOUPLED OPTIMIZATION

CONCLUSIONS

The potential damping performance gains achieved through the use of tuned-mass dampers on lightly damped structures merits the further study of the hardware issues associated with these devices.

- DEVELOPED OPTIMIZATION TECHNIQUES FOR MULTI-DOF-MULTI-MODE ABSORBER TUNING
  - SIMPLE UNCOUPLED MASS OPTIMIZATION IS PREFERABLE FOR LIGHTLY COUPLED MODES
  - NONLINEAR OUTPUT FEEDBACK OPTIMIZATION IS PREFERABLE FOR COUPLED MODES
    - USES COUPLING EFFECTS TO ADVANTAGE
    - USES UNCOUPLED MASS OPTIMIZATION TO OPTIMIZE ABSORBER MASSES AND PROVIDE INITIALIZATION FOR NONLINEAR OPTIMIZATION

REFERENCES

1. Card, M.F.; McComb, H.G.; Peebles, S.W.: Preliminary Sizing of Vibration Absorber for Space Mast Structures. NASA TM-84488, May 1982.

2. Juang, J.: Optimal Design of a Passive Vibration Absorber for a Truss Beam. J. Guidance, Control and Dynamics, Nov.-Dec. 1984.

3. Miller, D.W.; Crawley, E.F.; and Ward, B.A.: Inertial Actuator Design for Maximum Passive and Active Energy Dissipation in Flexible Space Structures. AIAA 26th Structures, Structural Dynamics, and Materials Conference, Part 2, April 1985.

4. Miller, D.W.; and Crawley, E.F.: Development of Finite Active Control Elements for Large Flexible Space Structures. M.I.T. Space Systems Lab Report #6-85, June 1985.

5. Rogers, L.C.: PACOSS Contract Status Review. Briefing charts from review held at Martin Marietta in Denver, 10-11 April 1985.

6. Von Flotow, A.H.: Control-Motivated Dynamic Tailoring of Truss-Work Structures. Presented at the AIAA Guidance, Navigation and Control Conference, August 20-22, 1986.

7. Van de Vegte, J.; and Hladun, A.R.: Design of Optimal Passive Beam Vibration Controls by Optimal Control Techniques. ASME J. of Dynamic Systems, Measurement and Control, December 1973.

8. Van de Vegte, J.: Optimal Dynamic Absorbers for Plate Vibration Control. ASME J. of Dynamic Systems, Measurements and Control, December 1975.

MULTIDISCIPLINARY ANALYSIS OF ACTIVELY CONTROLLED LARGE FLEXIBLE SPACECRAFT

By

Paul A. Cooper

John W. Young

and

Thomas R. Sutter
NASA Langley Research Center
MS 246
Hampton, Virginia 23665

First NASA/DOD CSI Technology Conference
November 18 - 21, 1986
Norfolk, Virginia

Introduction

The COFS program has supported the development of an analysis capability at the Langley Research Center called the Integrated Multidisciplinary Analysis Tool (IMAT) which provides an efficient data storage and transfer capability among commercial computer codes to aid in the dynamic analysis of actively controlled structures. IMAT is a system of computer programs which transfers Computer-Aided-Design (CAD) configurations, structural finite element models, material property and stress information, structural and rigid-body dynamic modal information, and linear system matrices for control law formulation among various commercial applications programs through a common database. Although general in its formulation, IMAT was developed specifically to aid in the evaluation of the transient dynamic response and control of large flexible space structures. This paper contains a description of the IMAT system and results of an application of the system.

- " Integrated Multidisciplinary Analysis Tool ", IMAT, Developed at NASA Langley Research Center.
- IMAT uses executive under interactive user control and common database to store and transfer structural and controls information between commercial codes.
- IMAT development supported by the COFS program for application to large flexible spacecraft under active control.
- Application to the reference space station and a growth version of the space station will be reviewed.

Figure 1

Description of IMAT

IMAT consists of an assemblage of pre- and post- processors which, under the control of an interactive executive system, convert and transfer information between application programs through a relational database management program. A simplified schematic of the IMAT system is shown in Fig. 2. A commercial database manager, RIM (Boeing Commercial Services Inc.), forms the basis for storage and distribution of data using a database schema which accepts finite element model information, stiffness and mass matrices, linear system matrices for control studies, and analysis results such as displacements, stresses, and natural modes and frequencies. All data are stored in a generic format, which insures that the data can be shared among different application programs. These data are loaded into or extracted from the database by processors, written in FORTRAN, which format the data for specific applications programs. All input and output of data are controlled interactively by the researcher using a menu driven executive code. The executive control procedures, formulated to direct the transfer and storage of information, are complicated by the fact that the commercial applications programs involved in the creation or use of information reside and operate on computers of three different manufacturers, Control Data Corp., Digital Equipment Corp., and PRIME Inc, each with its own unique operating system. All computer systems are connected by a local area network which can transfer data at approximately 250,000 baud.

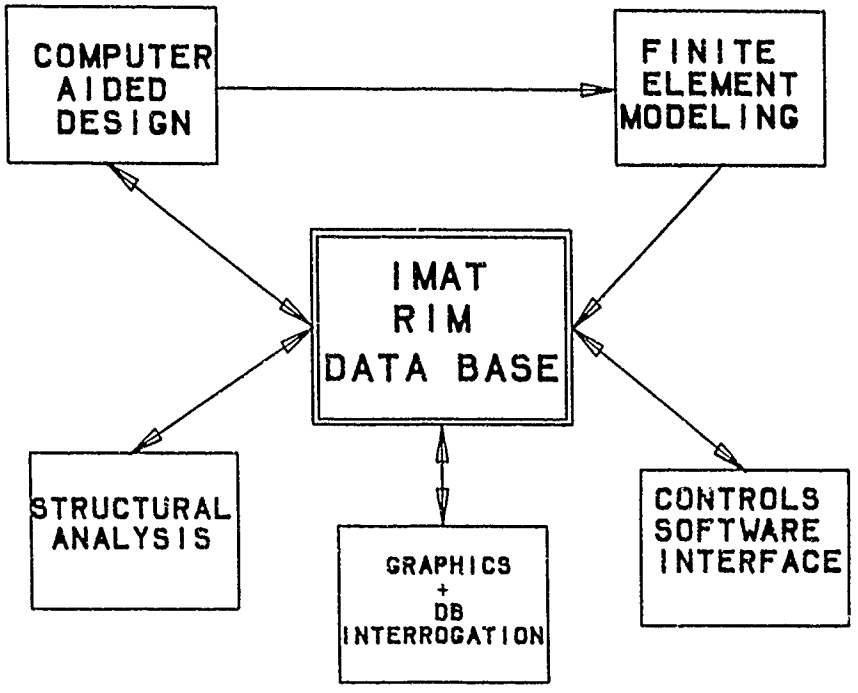

Figure 2

CAD, Finite Element Modeling and Analysis

Fig. 3 describes the codes and data paths available for computer-aided design and finite-element modeling. Wireframe geometry developed using the commercial computer-aided-design code ANVIL (MCS inc.) is converted to input for the commercial finite-element modeling code PATRAN-G (PDA Inc.). A processor stores finite-element model information from PATRAN-G in the database. The second commercial CAD capability available is the 3-D wireframe CAD system CALMA DDM (GE/CAE Inc.), which can transfer geometry information to GEOMOD (SDRC Inc.), a solid modeling code. This latter code can transfer three dimensional information to SUPERTAB (SDRC Inc.), a finite-element modeling code similar to PATRAN-G. A processor similar to that installed between PATRAN-G and the database has been developed to transfer a finite-element model description from SUPERTAB into the database. Entry into IMAT can occur at several different levels: at the CAD or modeling level or simply by loading finite- element model data prepared elsewhere through a processor into the database. Two commercial finite-element solver codes are available: MSC/NASTRAN (MacNeal Schwendler Corp.) and EAL (Engineering Information Systems Inc.). The finite-element data created by PATRAN G or SUPERTAB are stored in a generic format in the database. Processors have been developed which can create an MSC/NASTRAN bulk data input file or an EAL input file. Processors have also been developed which can convert an MSC/NASTRAN bulk data input stream to an equivalent EAL bulk-data input stream and vice-versa. Static and dynamic results obtained from the analysis codes are placed in the database, and are available for inspection or use in performing dynamic analyses or generating linear system matrices for controls analyses.

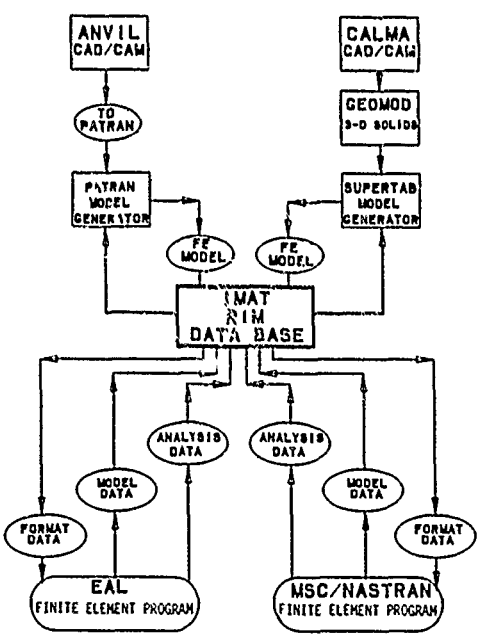

Figure 3

Linear System Matrix Generator

Fig. 4 is a schematic of the interactive capability provided in IMAT for generating linear system matrices for a controls design or analysis. The controls researcher has access to the modal, mass, inertia, and sensor and control influence information through the database interrogation capability. The researcher can use the information to evaluate the significant dynamic modes, select the modes and frequencies of interest used to define the state of the system and obtain the mass and inertia matrices necessary for development of linear system matrices. The user must provide sensor and actuator information as to type and location and must provide a modal damping value for each mode selected to define the state. A processor creates the system matrices which are then stored in the database or are fed directly to a commercial control design and analysis code called $MATRIX_x$ (Integrated Systems Inc.). The controls analyst, external to the IMAT system, develops control laws, and creates state feedback matrices which are stored in the IMAT database.

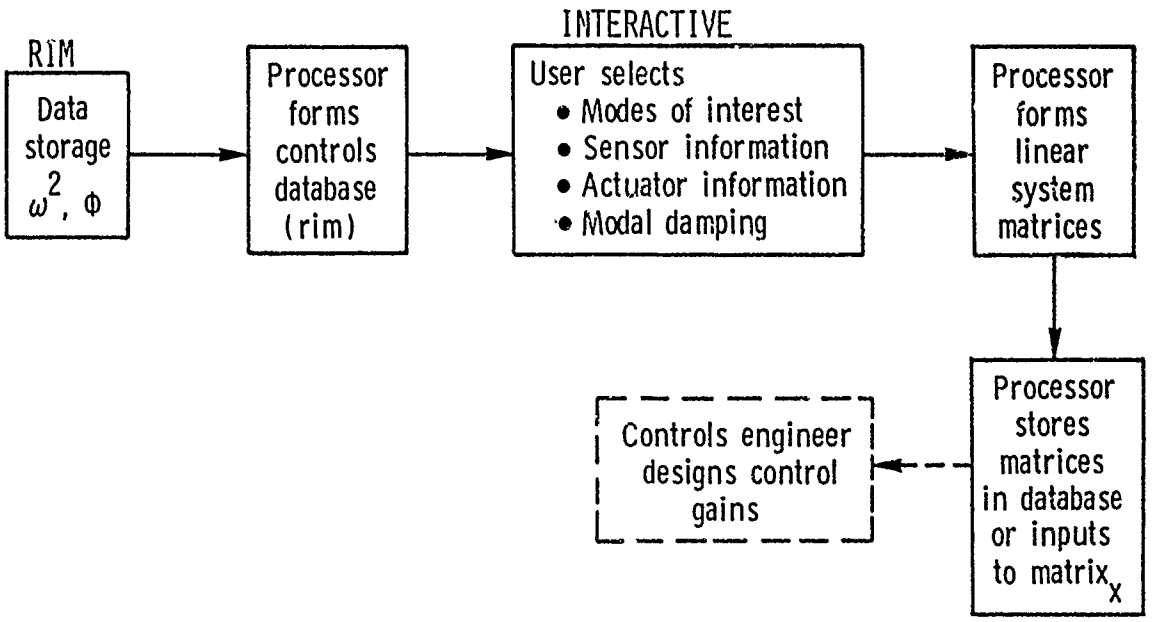

Figure 4

Dynamic Simulation in IMAT

With the control law and the natural modes and frequencies available in the database, the structural dynamicist can use the IMAT capabilities to investigate the dynamic closed-loop transient response of the structure to external disturbances and the control actuator forces. The user defines the information required for his state space matrices including disturbance locations and forces and any structural grid points of interest. The system matrices are computed and transferred to $MATRIX_x$. The time domain solution procedures of $MATRIX_x$ are exercised to solve for the state vector amplitudes as a function of time. IMAT creates a solution file and transports the file to MSC/NASTRAN. The user can then call the old problem tape with the physical model information and the solution file and use the MSC/NASTRAN output routines to compute physical information such as stress and strain as a function of time in the elements of interest.

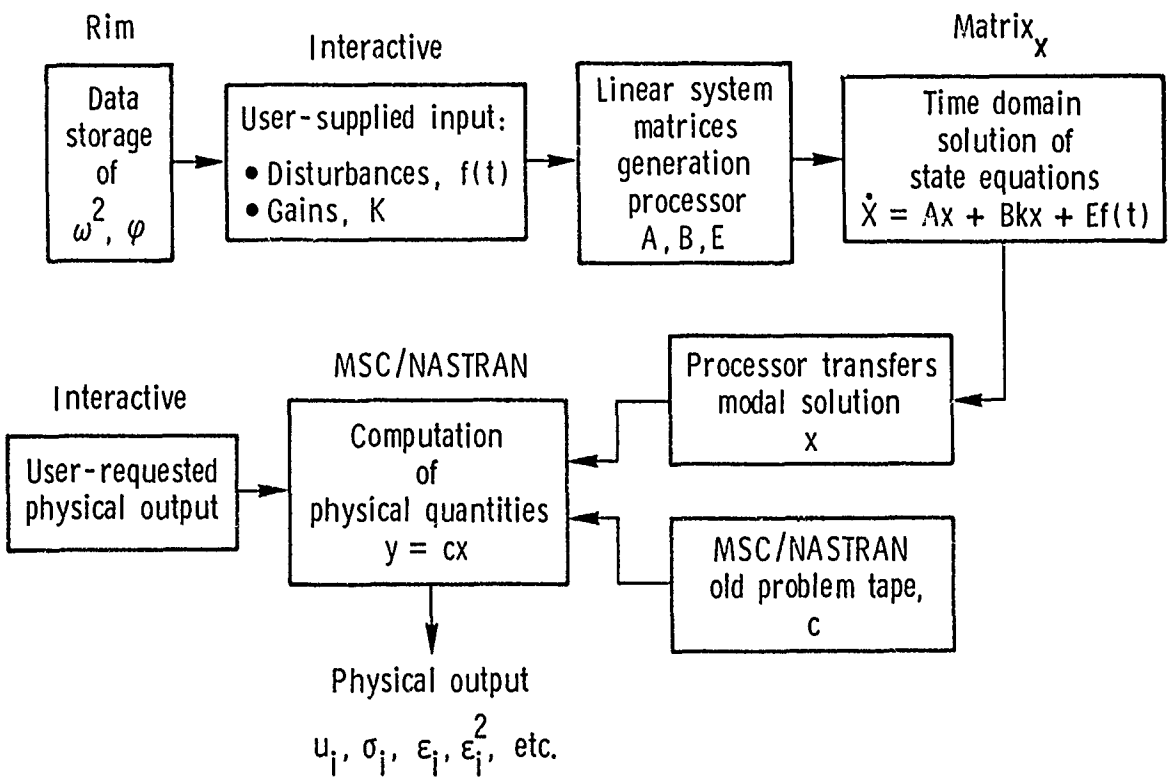

Figure 5

Application to Reference Dual-Keel Space Station

During the definition phase of the NASA Space Station program (Phase B), a reference configuration for the station was developed to serve as a baseline for investigation of the various technical criteria required to build and operate the station and for identification of system engineering and integration issues. One aspect of the phase B study was to evaluate the attitude control characteristics and the elastic dynamic behavior of the station for various expected internal and external disturbances and to investigate the possible interaction between the control system and the elastic response of the system. IMAT was used to define a finite element represenation of the station and determine and store the modes and frequencies preparatory to performing dynamic and control studies. The results of a study of the expected dynamic characteristics of the reference station, i.e. natural modes and frequencies, are presented here as an example of the application of IMAT and to present the frequency and mode characteristics of interest in the COFS 3 studies.

- **Reference station serves as a NASA baseline configuration to investigate technical criteria of the station.**
- **Our interest is to determine the:**
  - **Elastic dynamic characteristics of the station.**
  - **Attitude control characteristics with control sensors observing elastic as well as rigid body motion.**
  - **Closed-loop dynamic response of station to internal and external disturbances.**

Figure 6

Reference Dual-Keel Space Station

The reference station is a dual-keel station with a transverse boom supporting two types of solar power systems, photovoltaic and solar dynamic. The work area of the station is located at the center of the transverse boom and has four life supporting modules, the habitation, laboratory, European, and Japanese modules. The upper boom contains stellar experiment payloads and the lower boom contains earth resource payloads. Station attitude control is provided by control moment gyros located in the first bay of the port transverse boom outboard of the keel. Position and rate sensors are also located in this bay but not co-located with the gyros. Reboost control is provided by four Reaction Control System packages with nine 25 lbf jets in each package. The packages are located on the upper and lower keels.

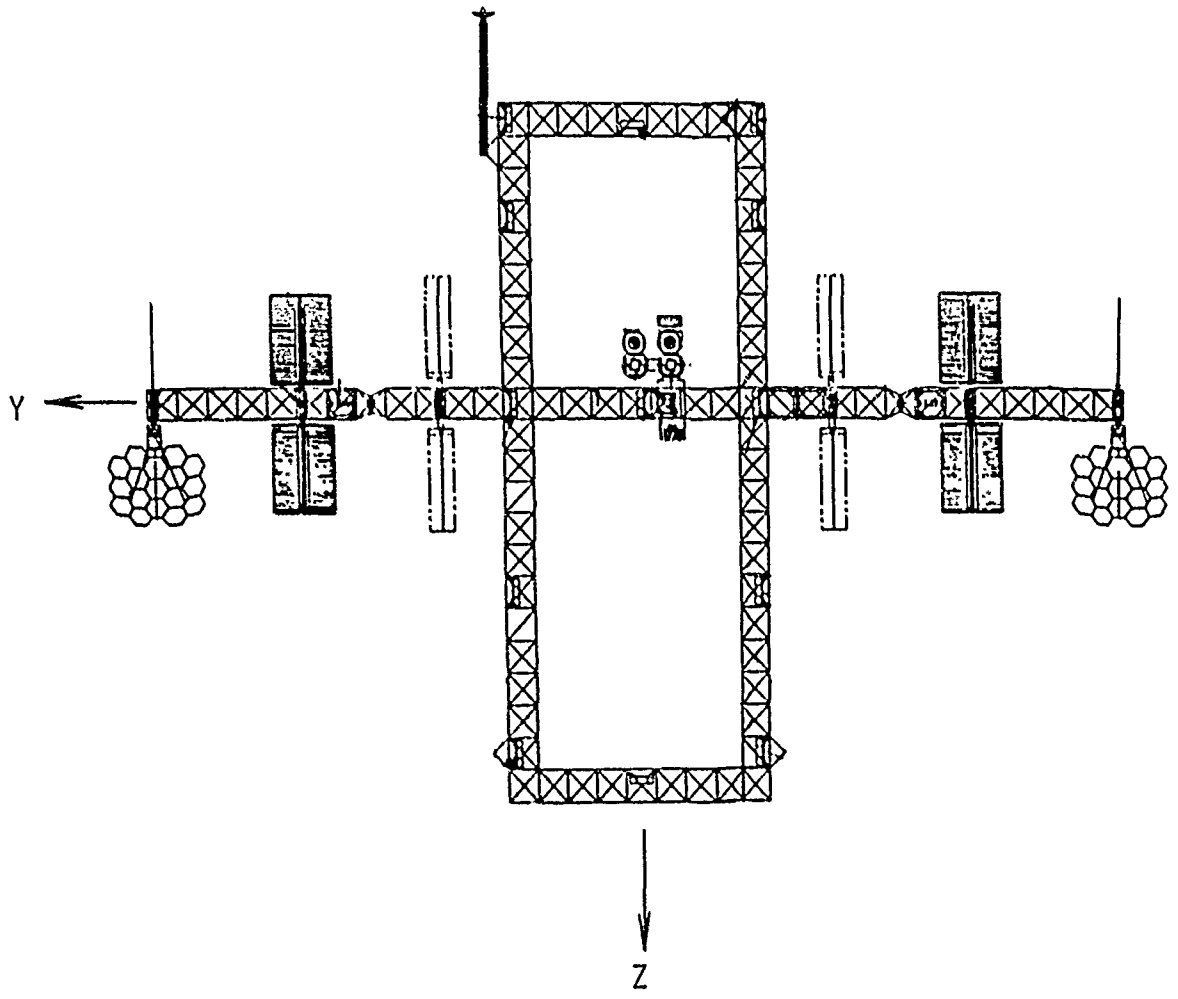

Figure 7

Finite Element Representation

The finite element model is composed of 1312 rod elements and 98 beam elements with 483 nodes and approximately 1700 dynamic degrees of freedom. Each element of the trusswork is represented by a rod element and the modules are represented by beam elements with the equivalent stiffness properties of the module cylinders and connecting components. The truss members are 2.0 inch outside diameter graphite epoxy tubes with a 0.06 inch wall thickness and a longitudinal modulus of elasticity of 40.0×10^6 psi. An approximation of the stiffness characteristics of truss joints is included in the stiffness of the rod elements by reducing the modulus of elasticity for rod element based on the length of the rod element.

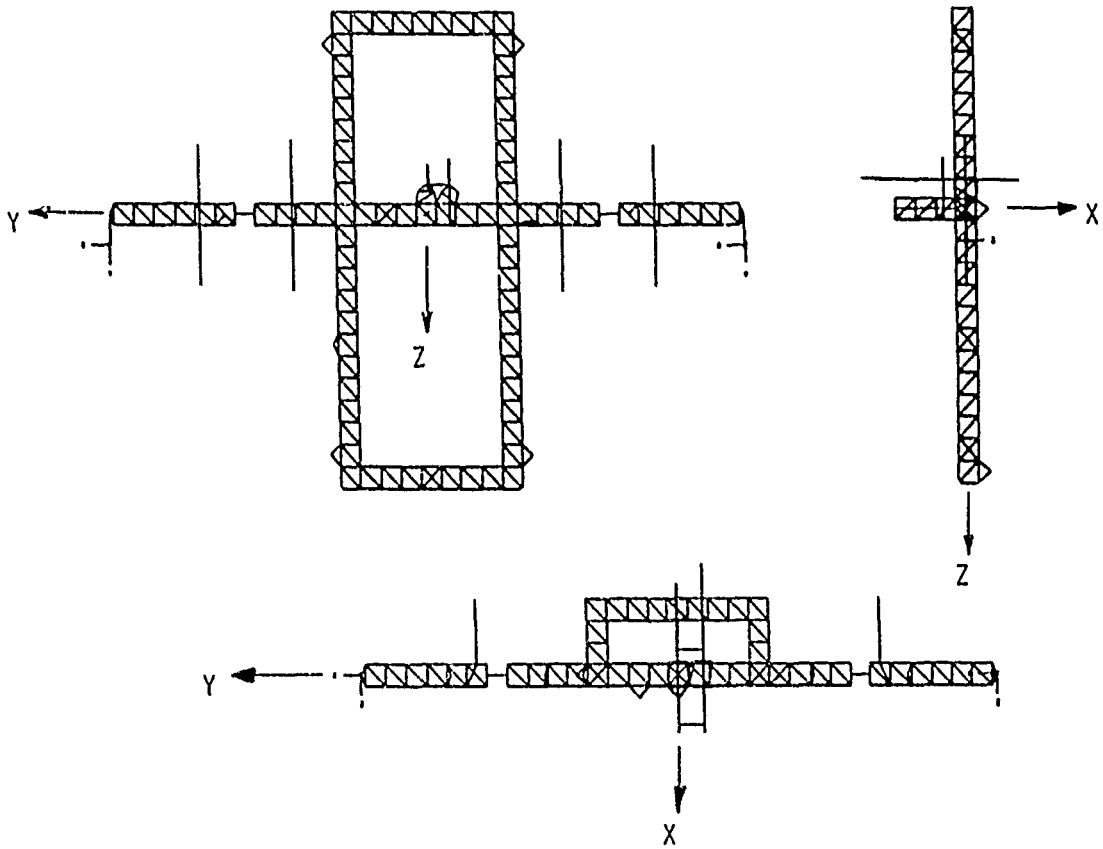

Figure 8

Mass and Inertia Characteristics of the Reference Station

The mass and inertia characteristics of the model are given in the figure. The origin of the coordinate system is located at the center of the central transverse boom between the keels and the positive x axis is taken along the flight direction as shown in figure 8.

FINITE ELEMENT MODEL

o NODES	483
o RODS	1312
o BEAMS	98

MASS AND INERTIA DATA

o TOTAL MASS 571800 LBM

o CG LOCATION

X	-117 INCHES
Y	-65 INCHES
Z	-242 INCHES

o MASS INERTIA AT BASIC COORDINATE SYSTEM OF THE MODEL

I_{XX}	1.00E12 LBM-IN**2
I_{YY}	5.61E11 LBM-IN**2
I_{ZZ}	5.63E11 LBM-IN**2
I_{XY}	1.25E10 LBM-IN**2
I_{XZ}	1.76E10 LBM-IN**2
I_{YZ}	1.71E10 LBM-IN**2

Figure 9

Modes and Frequencies

The natural modes and frequencies of the system below 2 Hz were computed using MSC/NASTRAN and brief descriptions of the modes are given in Fig. 10. Most of the modes encountered in this frequency range are appendage modes (thermal radiators and the photovoltaic power systems) and are of less interest than the framework modes in the evaluation of the overall response of the station due to external loads. The fundamental elastic mode for this model is a framework mode occuring at 0.22 Hz.

MODE	FREQUENCY (HZ)	DESCRIPTION
1-6	0	RIGID BODY
7,8	0.22	TRANSVERSE BOOM BENDING AND TORSION
9	0.25	TRANSVERSE BOOM BENDING AND TORSION
10-19	0.27 - 0.29	INBOARD RADIATORS BENDING
20	0.33	UPPER KEEL BENDING AND TORSION
21	0.36	KEEL TORSION AND TRANSVERSE BOOM BENDING
22	0.43	UPPER AND LOWER KEEL BENDING
23-30	0.45 - 0.47	PHOTOVOLTAIC BENDING
31-35	0.50 - 0.53	PV RADIATOR BENDING
36	0.64	HIGHER MODE TRANSVERSE BOOM BENDING
37-38	0.75, 0.76	ALPHA JOINT TORSION
39-42	0.93 - 1.32	COMPLEX BOOM AND KEEL BENDING AND TORSION
43-50	1.42 - 1.46	INBOARD RADIATOR BENDING
51-59	1.50 - 1.96	COMPLEX FRAME AND APPENDAGE MOTION

Figure 10

Representative Framework Modes of the Reference Station

Fig. 11A shows the fundamental elastic mode of the model which is characterized by transverse boom bending and torsion and occurs at 0.22 Hz. In Fig. 11B a higher upper keel bending mode coupled with transverse boom bending occurs at 0.33 Hz.

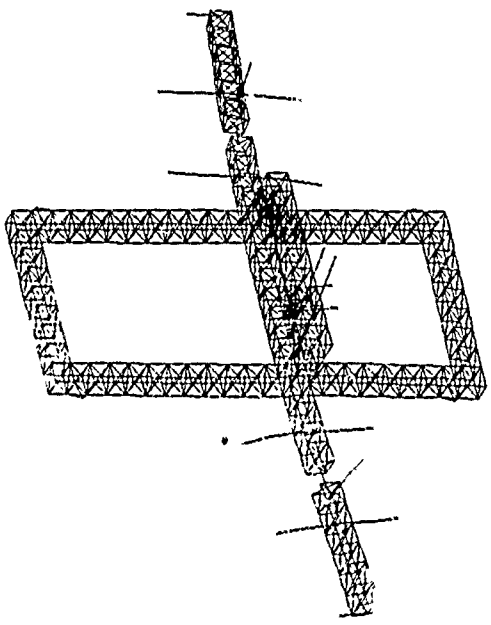

Figure 11A

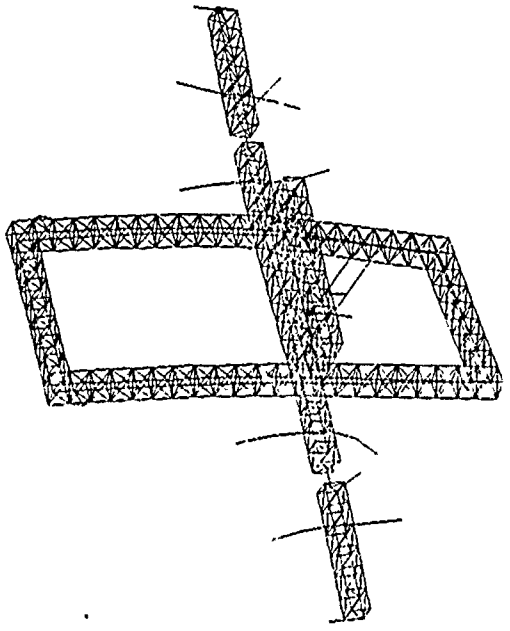

Figure 11B

Attitude Control Study of Growth Station

IMAT was used to study the control of a growth version of the dual-keel space station during an orbital reboost maneuver. Because of atmospheric drag, the space station must be reboosted periodically to maintain its desired operational orbit. This maneuver is performed using four constant-thrust reaction- control-system (RCS) jets. The purpose of the control system is to maintain station attitude during the maneuver. In the current study the stability of the attitude control system during reboost and the elastic response of the solar dynamic system sun-line axis are investigated.

- Dual-keel station has over twice the mass of the reference station.
- Study was the response of a solar-dynamic power system to reboost loads.

Figure 12

Finite Element Model of the Space Station

The growth space station configuration studied has over twice the mass of the reference station described above and is described in ref. 1 which gives a complete description of the masses and locations of the payloads, power systems, heat rejection radiators, subsystems, and the structural properties and dimensions of the truss components and support structures. The control sensors are located at the origin of the coordinate system at the center of the center bay. Four RCS jets are located on the keel structure to provide reboost propulsion and attitude control. To determine the natural modes and frequencies of the space station framework, a detailed finite element model of the station was developed using EAL. The model is shown in Fig. 13 and details of the model and the modes and fequencies are given in ref.1. The finite-element model with 735 nodes connected by 235 beams and 2110 rods had 2238 dynamic degrees of freedom.

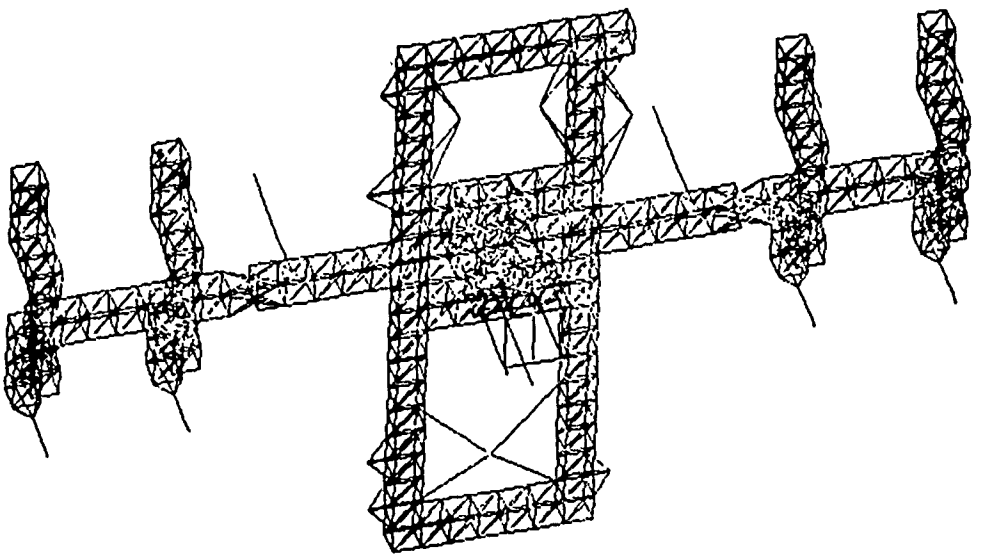

- 735 NODES
- 2238 DYNAMIC DEGREES OF FREEDOM
- 235 BEAM ELEMENTS
- 2110 TRUSS ELEMENTS

Figure 13

Reboost Control Law

Four 75-pound, constant-thrust RCS jets are located with two jets above and two jets below the center of mass of the station on the keels. The jets are aligned with the x-axis of the station so that the thrust is in the orbital direction. The upper- and lower-keel RCS thrusters are located at different distances along the y-axis from the station center of mass. Thus, a reboost maneuver with all thrusters active would produce an unbalanced moment about the y-axis, causing the station to rotate away from its vertical position. The station attitude is kept within desired limits by intermittent firing of the lower- keel RCS jets. The control logic which governs the firing of the lower-keel jets is given in Fig. 14. The logic is designed to hold the pitch attitude of the station within approximately one degree from the local vertical while applying the desired velocity increment along the flight path. The error signal (E) used to control the jet firing is a proportional-plus- differential signal consisting of pitch and pitch rate, $E = \theta_y + K\dot{\theta}_y$, measured at the sensor location. Two control studies were performed. The first study assumed that the error signal contained only rigid body motion, while the second study assumed that the error signal contained both the rigid body motion and the local flexible response at the sensor location. Following the control logic on Fig. 14, all jets are active until the control error reaches 1.0 degree plus a 0.05 degree hysteresis. At this point the lower jets are switched off and the station rotation decelerates and eventually reverses direction. When the error signal returns to 1.0 degree the lower jets are switched on and the process repeats as required.

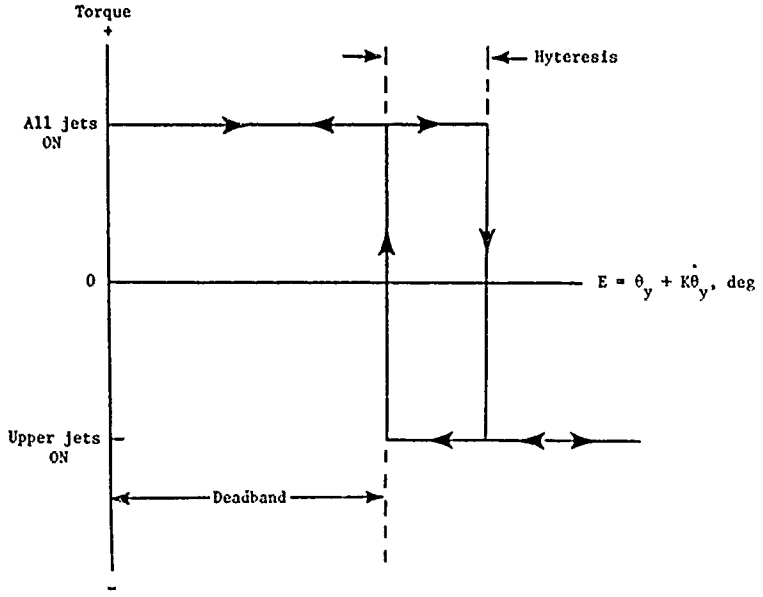

Figure 14

Control Stability

The stability of the reboost control system is illustrated on the pitch vs. pitch rate phase-plane plots of Fig. 15 considering rigid body motion only and with both rigid-body and flexible response included. The inward spiral of the plots indicates that both methods of error signal measurement lead to a stable control system during the time investigated.

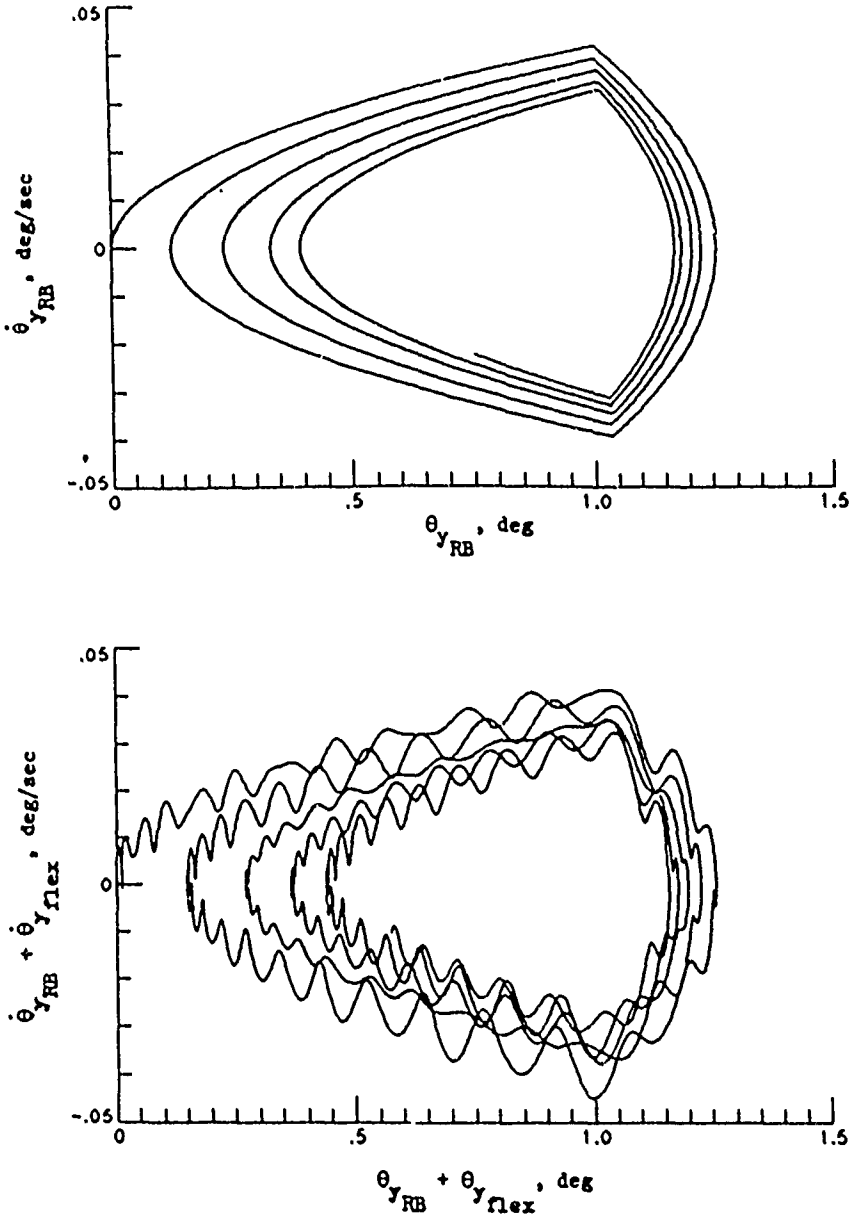

Figure 15

Solar Dynamic System

The station is powered by eight solar dynamic systems located on support structures attached to the transverse beams. A typical solar dynamic system is shown in Fig. 16. For maximum efficiency, the direction of the symmetry axis of each of the solar dynamic systems must be held to within 0.1 degree of the solar vector, even during an orbital reboost maneuver. This is done by controllers which command rotary joints located on the transverse truss and a vernier joint attached to the reflector symmetry axis. For the current study, these controllers are assumed inactive. Of particular interest in the study was the elastic response of the outboard solar dynamic system support structure and its effect on the pointing accuracy of the solar dynamic unit. Accordingly, no attempt was made to define in detail the structure of the solar dynamic system itself or to consider local dynamic response of the components of the systems. The system was represented instead by a rigid frame with the total mass and mass moments of inertia assigned on the frame at the center of mass of each system component. To simplify the problem, the sun-line vector and the x-axis are assumed to be coincident, although in actual practice the sun-line vector is continually rotating at orbital frequency.

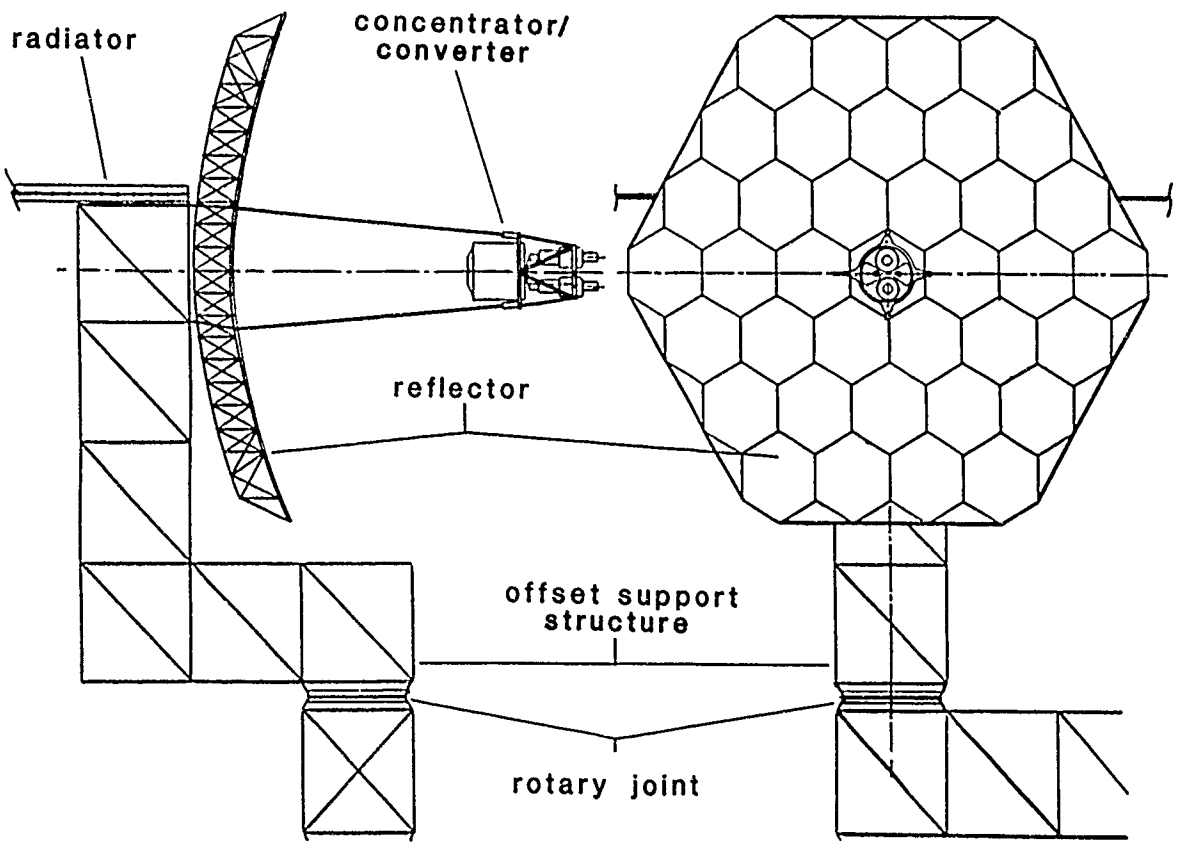

Figure 16

Solar Dynamic System Response.

Shown in Fig. 17 is the flexible component of the rotation of an outboard solar dynamic system symmetry axis during the first 500 seconds of an orbital reboost maneuver. The responses shown are for a rigid body control switching logic. Because of the one-degree deadband requirement in the control logic, the total y-axis pitch always exceeds the 0.1 degree pointing requirement. However, if the rigid body pitch angle were known, it could be nulled using the rotary joints on the transverse boom of the space station. The higher frequency flexible rotation response is well within the 0.1 degree rotation limit imposed for efficient operation of the solar dynamic system. A more complete discussion of the control analysis is given in reference 2.

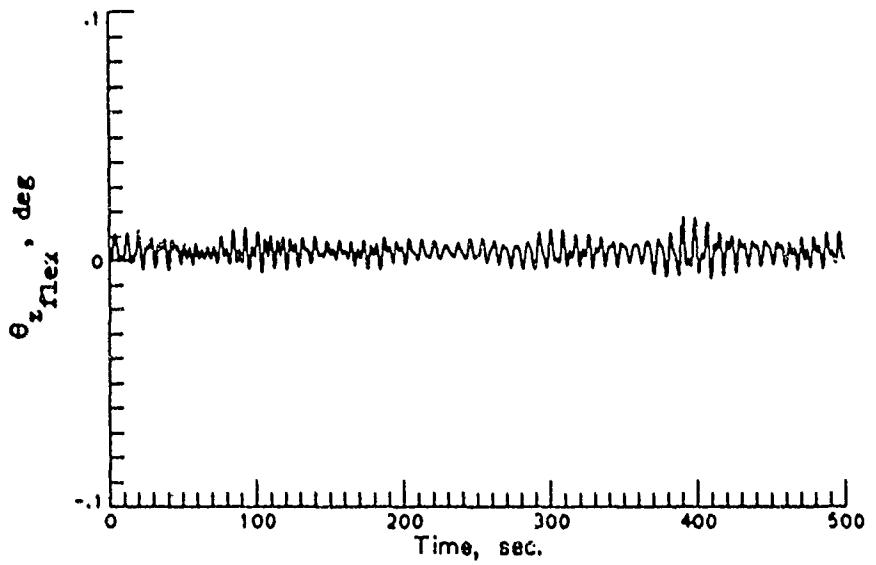

Figure 17

Concluding Remarks

The paper describes a computerized data distribution capability, IMAT, in place at the NASA Langley Research Center for the multidisciplinary analysis of the dynamics and control of large flexible space structures. The paper includes results obtained in using IMAT to investigate the dynamic characteristics of the NASA Dual-Keel Reference Space Station and the influence of structural response of the space station framework on the control of a growth version of the station during an orbital reboost maneuver. The method of control, using a proportional-plus-differential control law, led to a stable control system even with local flexible response measured at the control sensor location included as a part of the control error signal. The flexible response at the outboard solar dynamic system sun-line axis was well within the maximum rotation allowed for efficient operation. The IMAT system can be used to support the COFS program by providing an efficient means for simulating response to given linear control laws for the MAST structure in COFS I and to develop and analyze a scaled space station model for COFS III.

References

1. Dorsey, John T.; Sutter, Thomas R.; Lake, Mark S. and Cooper, Paul A.: Dynamic Characteristics of Two 300 KW Class Dual Keel Space Station Concepts. NASA TM-87680, March 1986.

2. Young, John W.; Lallman, Fredrick J.; Cooper, Paul A. and Giesy, Daniel P.: Controls/Structures Interaction Study of Two 300 KW Dual-Keel Space Station Concepts. NASA TM-87679, March 1986.

ANALYSIS AND SIMULATION OF THE MAST (COFS-1 FLIGHT HARDWARE)

Lucas G. Horta, Joanne L. Walsh, Garnett C. Horner
NASA Langley Research Center
Hampton, Virginia

and

James P. Bailey
PRC - Kentron
Hampton, Virginia

First NASA/DOD CSI Technology Conference
November 18-21, 1986

INTRODUCTION

The Control of Flexible Structures (COFS) program involves ground and flight tests of large flexible space structures such as the one shown in figure 1. The MAST (COFS-I) flight experiment is the initial phase of this program. An overview of the program is presented in references 1 and 2. The program includes the design and fabrication of 60 meter deployable truss with sensors and actuators attached at pre-selected locations. The structure will be used in a multi-flight experimental program to understand the dynamic behavior of joint-dominated structures, to supply a test bed for the implementation of modern control algorithm for vibration suppression, and to perform on/off line system identification.

This paper presents some of the in-house analysis work performed to evaluate the proposed design configuration, controller design as well as actuator dynamic modeling, and MAST/actuator dynamic simulation for excitation and damping. The MAST is modeled using the Engineering Analysis Language (EAL, ref. 3) finite element analysis program. An optimization procedure which minimizes weight while trying to maintain modal coupling is discussed. This optimization procedure facilitates incorporation of additional constraints not considered in the MAST baseline design. Mode shapes from EAL are used to construct a reduced order model of the MAST for closed-loop simulation. Details on the proposed actuator location, number, and characteristics are discussed as well as some of the alternate ways to use them. Simple rate feedback laws are implemented to show the viability of the proposed experiment. Complete simulation includes excitation and damping using the same set of actuators.

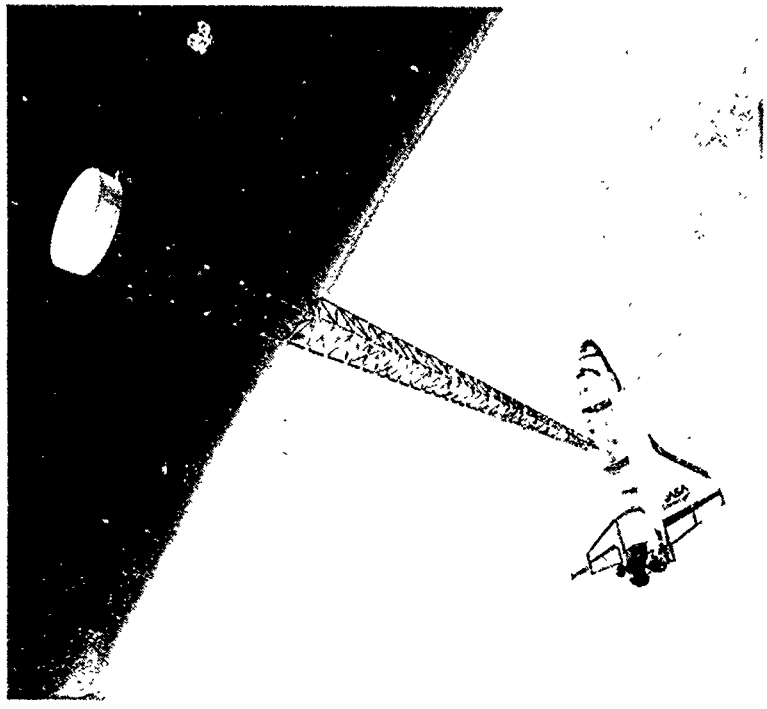

Figure 1

MAST FINITE ELEMENT MODEL

The finite element model (FEM) of the MAST is shown in figure 2. The truss beam is 60 meters long and consists of 54 bays of single-laced latticed beams. The longerons which form the vertices of the triangular cross-sections have unequal areas resulting in one strong and two weak longerons. The strong longeron is aligned with the centerline of the Shuttle axis. The longerons and diagonals are modeled using tube elements. The model includes the deployer retractor assembly, Shuttle inertia properties (modeled with beam elements), rigid platforms for sensors and actuators allocation, and a parameter modification package. There are three secondary actuator locations distributed along the beam (bays 12, 30, and 44) and one primary at the tip. Each of the secondary actuator stations contains two actuators acting in the same plane. The primary station has four actuators to impart torques as well as in-plane forces. Also included are two sensor measurement stations (bays 24 and 48) for the implementation of non-collocated control laws. At the beam tip, in addition to the actuators, a parameter modification package composed of four masses constrained to move along a track are used to vary the structure center of mass. These four masses can be independently operated to achieve high modal coupling. The FEM also contains lumped masses at each joint location and cable mass for the electronic components distributed along the beam.

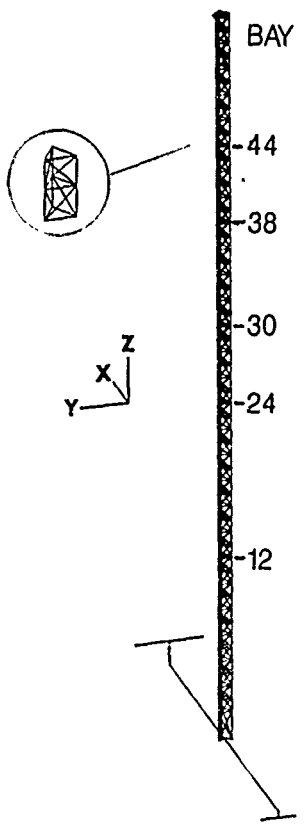

Figure 2

MAST BEAM DESCRIPTION

Table 1 shows the beam properties used in the FEM of the baseline design. Note that the longerons which form the vertices of the cross-section triangle have different cross-sectional areas in order to promote coupling between the bending and torsion modes.

TABLE 1 - FLIGHT MAST BEAM DESCRIPTION

GEOMETRY		
Diameter		1.40 m
Bay Length		1.12 m
Number of Bays		54
Strong Longeron (1)	OD/ID	0.0220/0.0104 m
Weak Longeron (2)	OD/ID	0.0229/0.0147 m
Diagonal	OD/ID	0.0191/0.0179 m
Batten	OD/ID	0.0140/0.0114 m
EFFECTIVE AXIAL STIFFNESS OF MEMBERS (EA)		
Strong Longeron (1)		39.10 E+06 N
Weak Longeron (2)		33.60 E+06 N
Diagonal		3.86 E+06 N
Batten		6.64 E+06 N
MASS SUMMARY		
Corner Joint Mass		0.9072 kg
Roll Nut (every other bay)		0.52 kg
Diagonal Mid-Hinge		0.30 kg
Cabling (distributed to each bay) Total		4.0 kg
Deployer Retractor Assembly		720.0 kg
Actuator Wts at Bays 12,30,44		18.8 kg
Tip Mass Assembly		73.0 kg
Parameter Modification Package (4 masses, 20 kg ea)		80.0 kg

Note: Data from MAST FLIGHT SYSTEM CODR held at Harris Corp, Melbourne, FLA. 4/29 to 5/4/86.

EIGENVALUES AND MODE SHAPES OF MAST FINITE ELEMENT MODEL

Table 2 shows the first ten eigenvalues of the baseline FEM without the actuator masses. The third column shows the bending axis. The corresponding first four mode shapes are shown in figure 3. The bays which contain actuators or sensors are indicated by tic marks to show how effective the actuator stations are with regard to the mode shapes. Note, for example, that for the second bending mode, bay 30 and the tip are the most effective.

TABLE 2 - FINITE ELEMENT MODEL EIGENVALUES

Mode Number	Frequency (Hz)	Direction
1	.1888	1BY
2	.2414	1BX
3	1.291	2BX
4	1.338	1T
5	1.339	2BY
6	3.686	3BX
7	3.831	3BY
8	4.303	2T
9	6.713	4BX
10	6.946	4BY

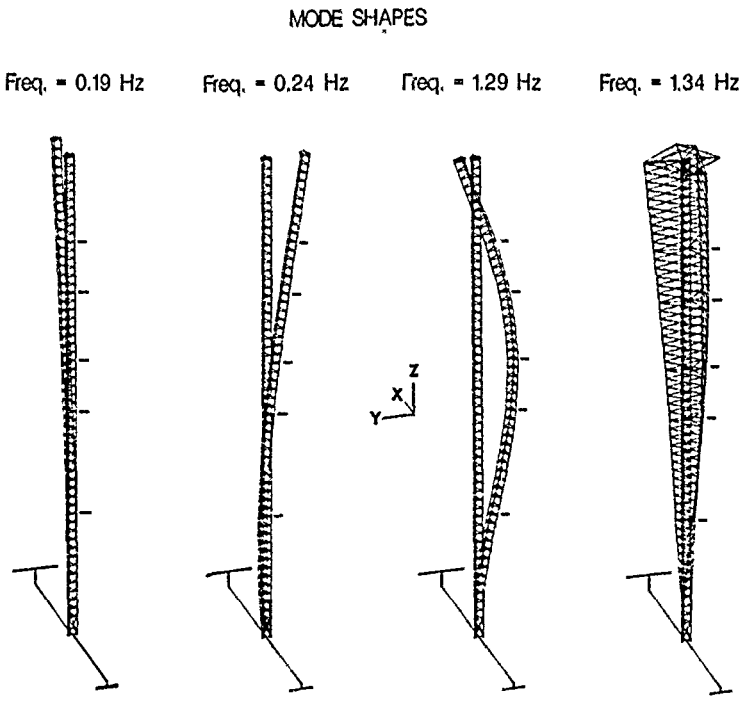

Figure 3

OPTIMIZATION FORMULATION

An optimization procedure which uses the baseline FEM has been developed in order to incorporate additional requirements not considered in the baseline design - namely, that the first bending frequency of the diagonal must be at least 15 Hz. The optimization procedure combines a general purpose optimization program (CONMIN, ref. 4) with the EAL finite element program. The problem formulation is shown in figure 4. The objective is to minimize the total mass of the system. The four design variables are the inner radii of the strong and weak longeron (R_S and R_W, respectively) and the inner and outer radii of the diagonal (R_I and R_O, respectively). The following constraints are imposed on the problem: the lowest natural frequency of the MAST must be greater than 0.18 Hz (a Shuttle requirement); the first torsion and the second bending frequencies must be within 1 percent (referred to as modal coupling); the first bending frequency of the diagonal must be at least 15 Hz (to simulate a buckling constraint); the inner radius of the weak longeron must be at least 0.25 mm larger than the inner radius of the strong longeron (to ensure that the weak and strong longerons do not change); and the minimum wall thickness of the diagonal must be at least 0.56 mm. The lower bound for all the design variables is 3.175 mm and the upper bound is 9.4 mm with the exception of the diagonal outer radius which is 11 mm.

- OBJECTIVE FUNCTION - MINIMIZE TOTAL MASS
- DESIGN VARIABLES
  - INNER RADIUS OF WEAK LONGERON, R_W
  - INNER RADIUS OF STRONG LONGERON, R_S
  - INNER RADIUS OF DIAGONAL, R_I
  - OUTER RADIUS OF DIAGONAL, R_O
- CONSTRAINTS
  - 1ST NATURAL FREQUENCY OF MAST $\geq$ 0.18 Hz
  - 1ST TORSION AND 2ND BENDING FREQUENCY WITHIN 1%
  - 1ST NATURAL FREQUENCY OF DIAGONAL $\geq$ 15 Hz
  - $R_W - R_S \geq 0.25$ mm
  - WALL THICKNESS OF DIAGONAL $\geq$ 0.56 mm

Figure 4

OPTIMIZATION RESULTS - OBJECTIVE FUNCTION AND DESIGN VARIABLES

Plots of the mass (objective function) and the design variables versus design cycles are shown in figure 5. The baseline design of the MAST is used as the initial design (design cycle = 0). Over the design process, the mass increases by 40 kg over the baseline design. The design variables associated with the longerons (R_W and R_S) decrease from the baseline design values with the inner radius of the strong longeron (R_S) reaching its lower bound. The design variables associated with the diagonal (R_I and R_o) increase from the baseline design values with the inner radius R_I reaching its upper bound. The reason for the increase in the objective function and the trends in the design variables will be discussed in the following.

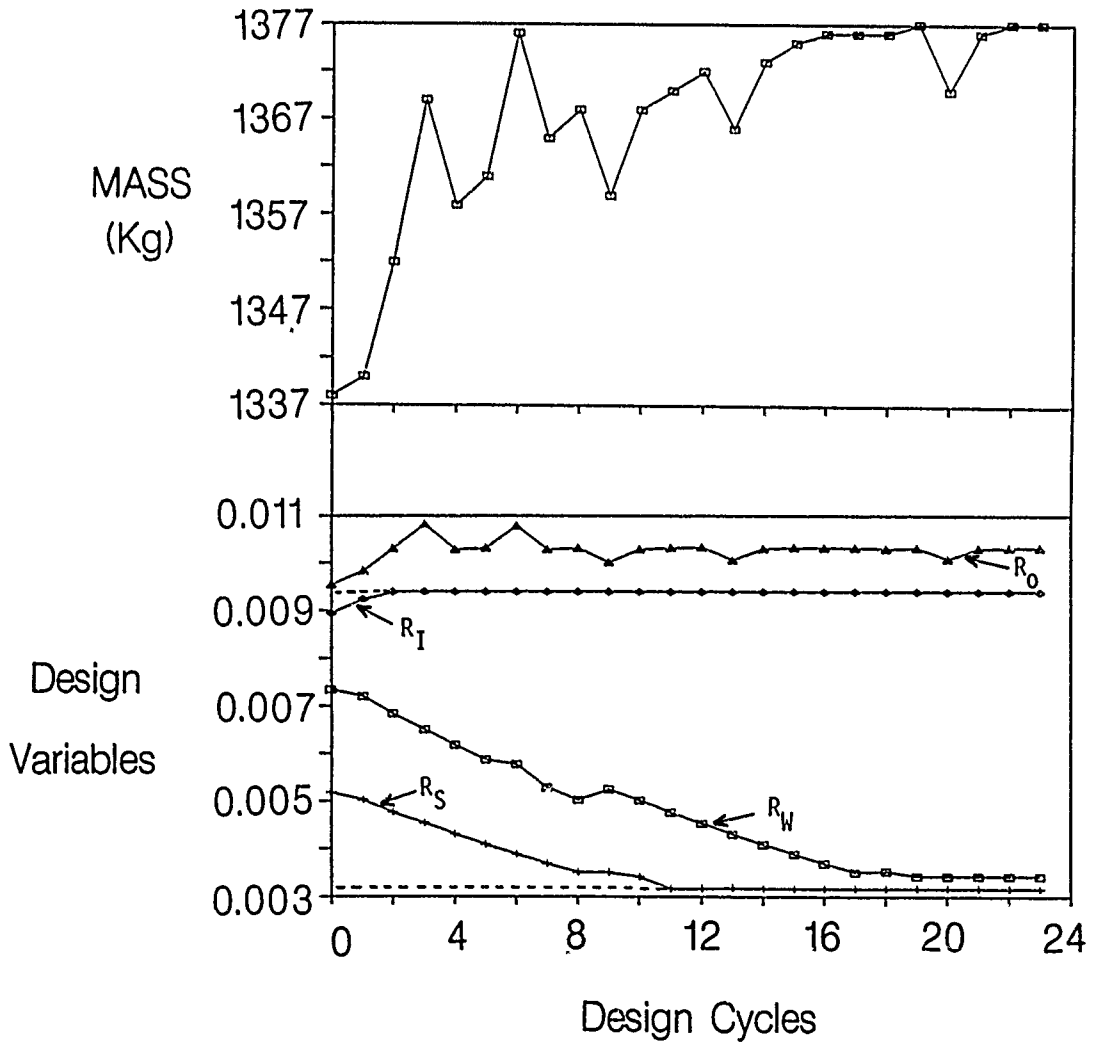

Figure 5

OPTIMIZATION RESULTS - CONSTRAINTS

As shown in figure 6, the baseline design satisfies all the design requirements except the diagonal frequency constraint (greater than 15 Hz). In general, the diagonal wall thickness (R_o-R_I, upper plot) increases as the diagonal frequency increases (middle plot). The constraints on the diagonal frequency and on the weak and strong longerons (R_W-R_S) are the active constraints causing the objective function to increase. The first torsion mode frequency is highly affected by the diagonal member stiffness. The diagonal frequency constraint is equivalent to the diagonal stiffness for small member mass changes. Thus when the diagonal frequency is increased, the torsion frequency is also increased. This causes the modal coupling and the diagonal frequency constraints to work against each other. When the first torsion and second bending frequencies are within 1 percent (lower plot), the diagonal frequency (middle plot) is less than 15 Hz (see cycles 13 and 20). When the diagonal frequency is 15 Hz, the modal coupling constraint is not satisfied. Since it is a MAST requirement to have coupled modes, alternative formulations of the optimization problem are being explored which will lead to the simultaneous satisfaction of both constraints. One formulation being investigated is to have the modal coupling as the objective function.

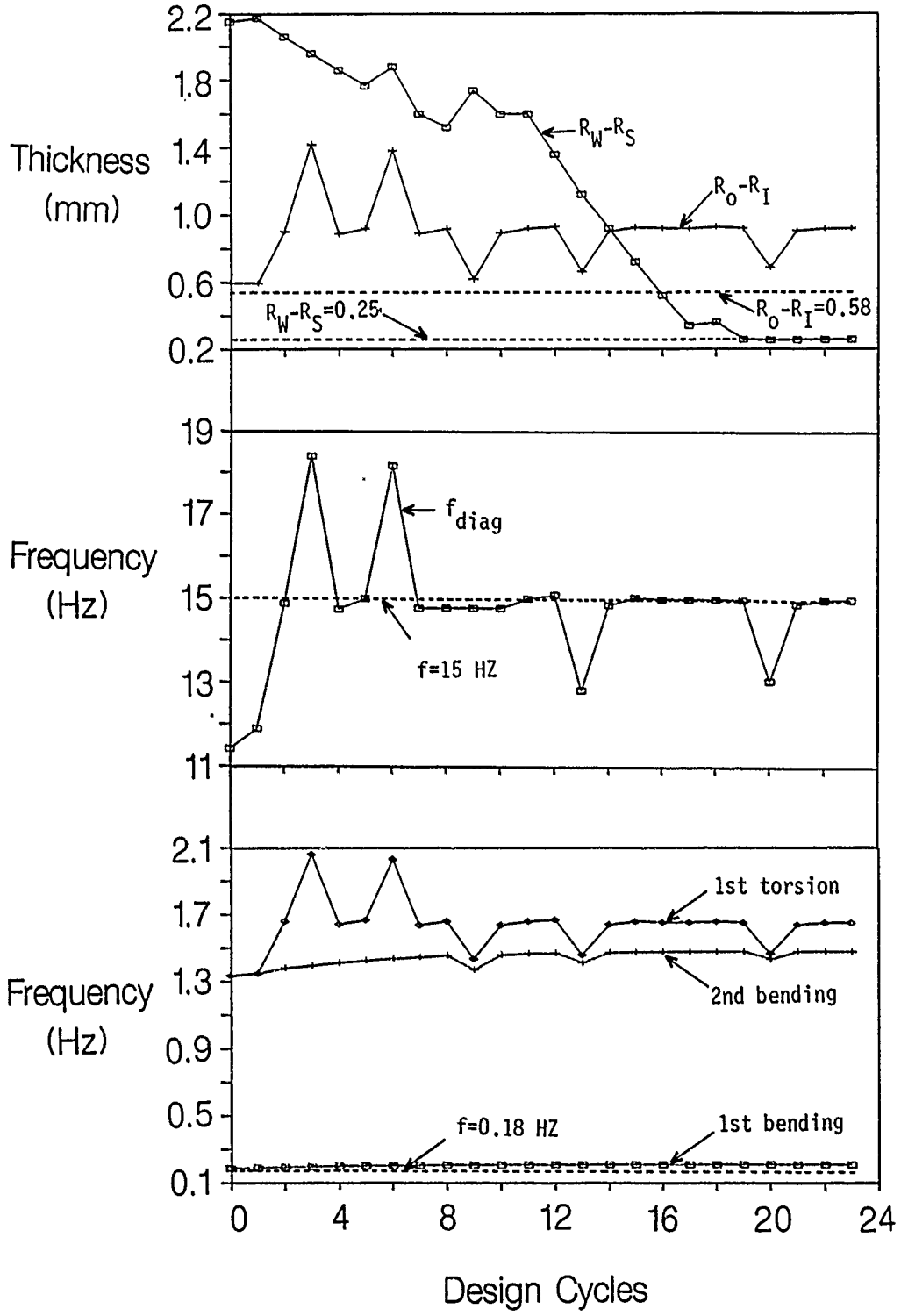
Thickness
(mm)
2.2
1.8
1.4
1.0
0.6
0.2
R_W-R_S
R_o-R_I
R_W-R_S=0.25
R_o-R_I=0.58
19
17
15
13
11
Frequency
(Hz)
f_{diag}
f=15 HZ
2.1
1.7
1.3
0.9
0.5
0.1
Frequency
(Hz)
1st torsion
2nd bending
f=0.18 HZ
1st bending
0
4
8
12
16
20
24
Design Cycles

Figure 6

LINEAR DC MOTOR (LDCM) ACTUATOR

The photograph shown in figure 7 is the prototype Linear DC Motor (LDCM) actuator built by Harris Corporation to be used on the MAST.

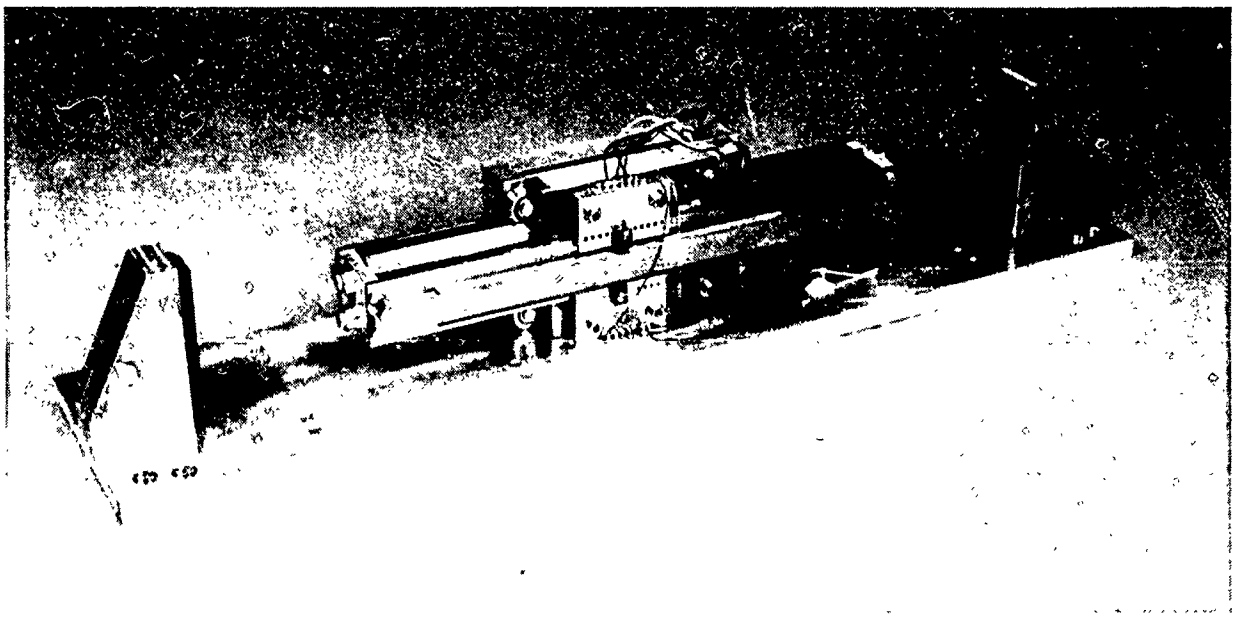

Figure 7

ACTUATOR MODELING

Actuator modeling brings out several design issues that need to be addressed. Physically, the actuator is an electromechanical device which can be commanded in a number of different ways. Using the actuator representation shown in figure 8 (the structure deflection is denoted by W whereas the actuator position is defined by Y), the equations of motion are as shown. The designer must decide how the actuators will be used and, moreover, what type of command input the actuator will require. For the system shown, Fa is the force applied to the structure which is balanced by accelerating the actuator mass in the opposite direction. When commanded a force, the actuator mass should accelerate until the desired force is achieved (assuming no stroke limits). If commanded a position, the actuator will move either relative to the structure or with respect to an inertial reference. Deciding how the actuator is used determines instrumentation needs. Moreover, deciding how it operates (position of force command) determines the actuator representation. The following work presents one of the available options.

Representation

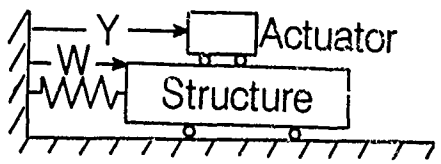

Equations of Motion

Structure

$$M \ddot{W} + k W = F a$$

Actuator

$$m \ddot{Y} = -F a$$

Issues

- Position Command
- Force Command
- Actuator Representation

Figure 8

DYNAMIC MODEL OF ACTUATOR

The dynamic model of the actuator used in this study is based on the work presented in references 5 and 6. The schematic in figure 9 shows the actuator main components. The actuator mass is denoted by m_p, stiffness K_p, damping (back EMF) c_p, and the commanded force f_g. The commanded force acts directly between the actuator and the structure. In this schematic, the structure is represented as a single spring-mass system M_s and K_s. Looking at the operation of such a device, if K_p and c_p are zero and the actuator is commanded a constant force, the actuator mass will accelerate in one direction (ideally). In this dynamic model the centering spring K_p forces the actuator mass back to a nominal position. Since such a spring does not exist, this operation is to be performed by local position feedback. The operational frequency defined as $\omega_p = \sqrt{K_p/m_p}$ divides the operational range of the actuators into two basic regions. This will be discussed in the following.

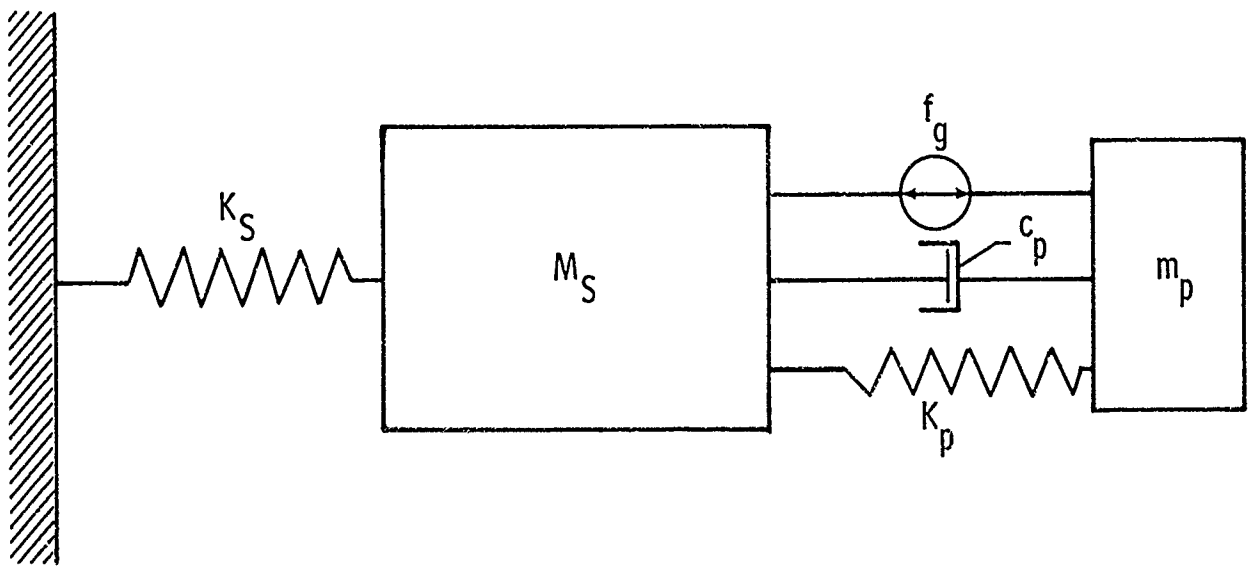

Figure 9

ACTUATOR FREQUENCY RESPONSE

The dynamic characteristics of the actuator model are better described by the frequency response plots shown in figure 10. These frequency response functions were obtained from a bench test of the actuator reported in reference 5. Although this actuator design is different from the LDCM design, they are conceptually similar. Moreover, the actuator dynamic model can be assumed the same for simulation. The upper plot shows the transfer function of the total actuator output force to the input commanded voltage. Note that the commanded voltage can be equal to any desired control. The frequency response function shown resembles that of a second-order high pass filter where above the operational frequency the response is "independent" of frequency. Moreover, above the operational frequency, defined in the dynamic model as ω_p, the output force follows the input command (see phase plot) whereas below ω_p the output is out-of-phase with the input. This is extremely important when the actuator is used for control. For example, if flexible structural modes exist on both sides of ω_p and the commanded input contains rate information from multiple modes, then in the lower modes the actuator is adding energy whereas in the higher modes it is removing energy. The operational frequency parameter is an adjustable parameter to some extent by adjusting K_p. This actuator model is used for the MAST dynamic simulation.

ACTUATOR FREQUENCY RESPONSE—MAGNITUDE

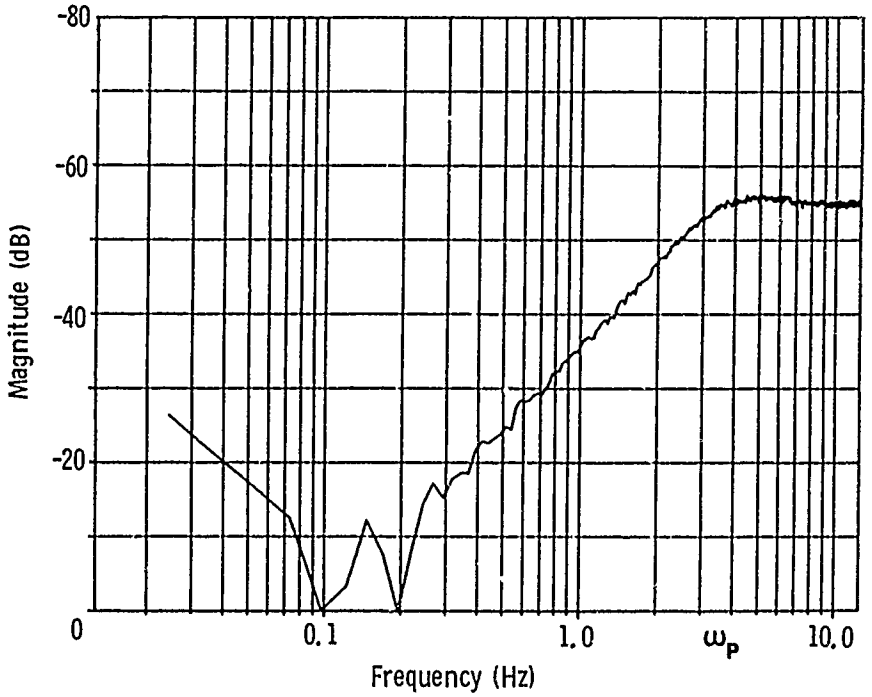

ACTUATOR FREQUENCY RESPONSE—PHASE

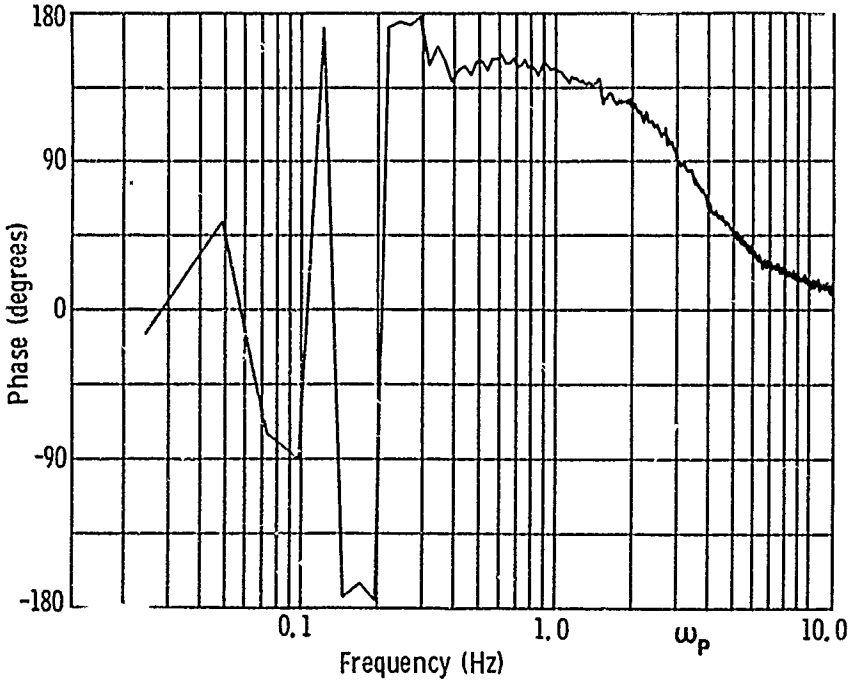

Figure 10

MAST DYNAMIC SIMULATION

The dynamic model of the actuator is incorporated into a reduced order model of the MAST. This model contains 6 rigid body modes and 10 flexible modes. A total of ten actuators are present but only the tip actuators are used in this simulation. The proposed MAST flight experiment as envisioned involves three phases - excitation, free vibration (dwelling), and control (damping). A test sequence is simulated where the same set of actuators is used for excitation and damping of the beam. For excitation the commanded force to the actuator is $f_g = \sin \omega t$. The frequency is that of the first bending mode 0.19 Hz. For control the commanded force is proportional to the beam rate $f_g = C \dot{W}$. The proportionality constant C is obtain by pole placement of the first two bending modes to achieve 5 percent modal damping. The actuator operational frequency is set to 0.1 Hz. The simulated tip response is shown in the upper plot of figure 11 and the corresponding actuator stroke output in the lower plot. A complete sequence (excitation, dwell, and damping) is presented. The excitation f_g is turned-off after a beam deflection of 10 cm is reached (t=60.4 sec). The beam is allowed to vibrate freely for 20 seconds and the control is turned-on for the last 30 seconds of the simulation.

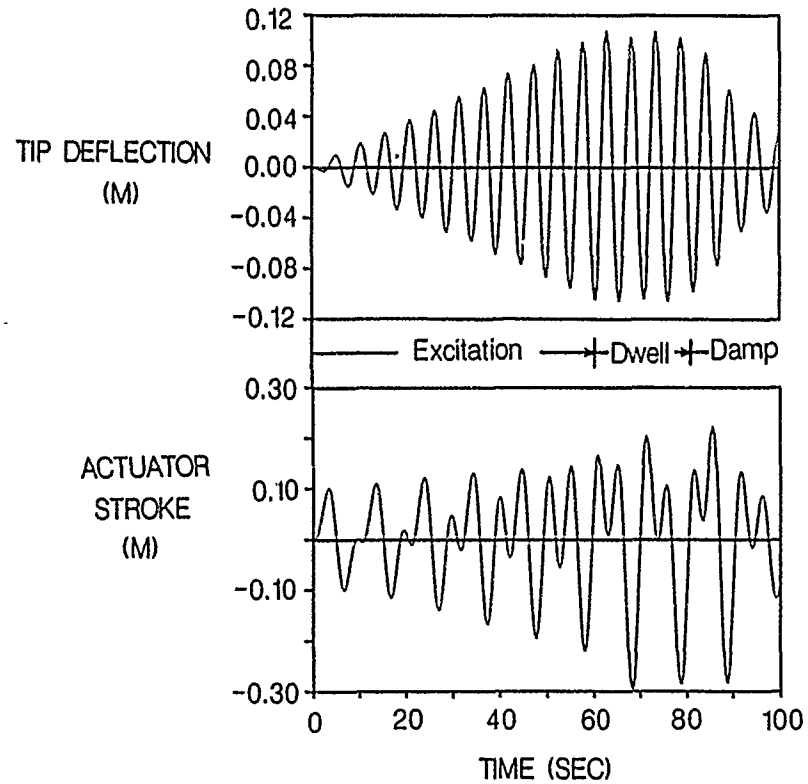

Figure 11

ACTUATOR RESPONSE

The upper plot of figure 12 depicts the force-stroke response corresponding to the excitation of the first bending mode (first 60.4 seconds). The current primary LDCM design provides a maximum force output of 30 N and a maximum stroke of 16 cm (32 cm peak to peak). This simulation shows that for first mode excitation the binding constraint is the maximum stroke. The lower plot shows the actuator force as a function of the beam tip rate during the controlled cycle (last 30 seconds of simulation). In the ideal case this plot is a line with a slope equal to the feedback gain (-6.5 m/s-N). The actuator dynamics causes this distortion.

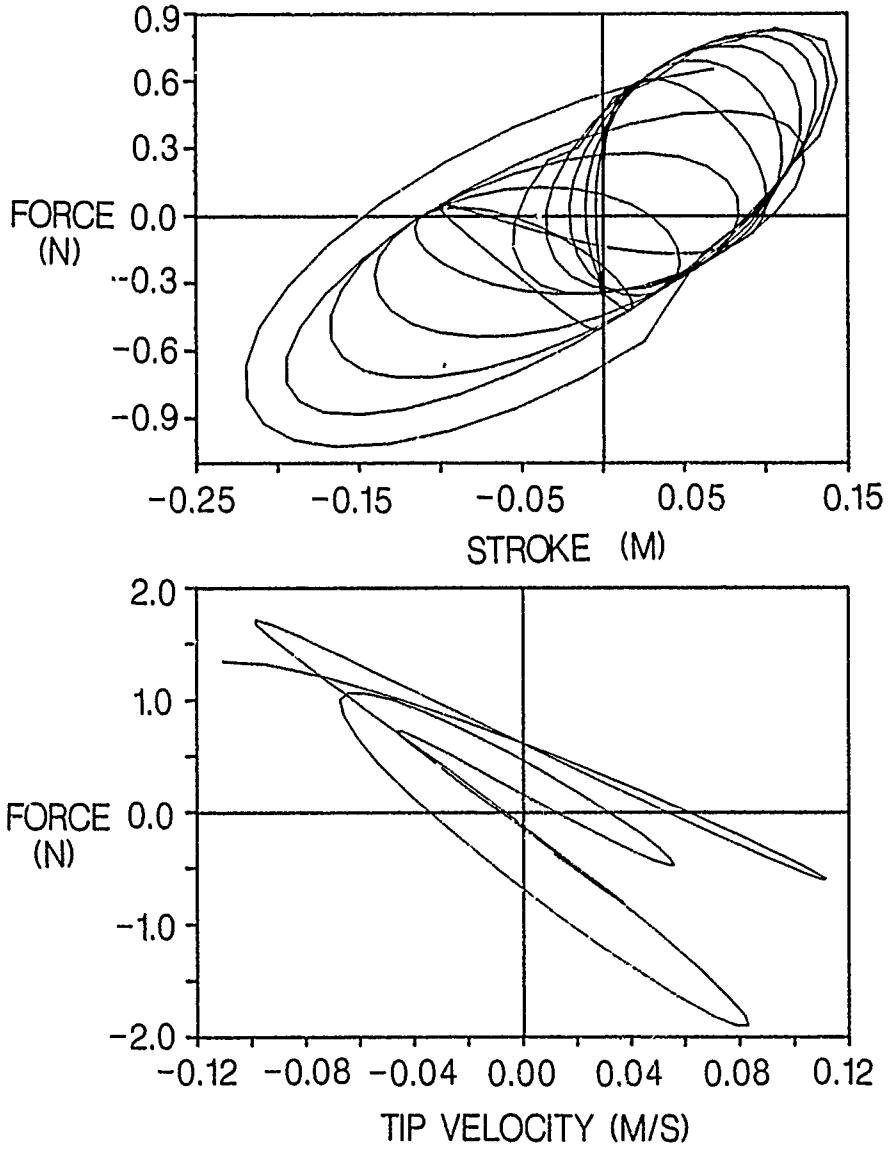

Figure 12

SUMMARY

In-house analysis work in support of the Control of Flexible Structures (COFS) program is being performed at the NASA Langley Research Center. The work involves evaluation of the proposed design configuration, controller design as well as actuator dynamic modeling, and MAST/actuator dynamic simulation for excitation and damping. A complete finite element model of the MAST has been developed. This finite element model has been incorporated into an optimization procedure which minimizes total mass while maintaining modal coupling. Results show an increase in the total mass due to additional constraints (namely, the diagonal frequency constraint) imposed on the baseline design. A valid actuator dynamic model is presented and a complete test sequence of the proposed flight experiment is demonstrated. The actuator dynamic model is successfully used for damping and the stroke limitations for first mode excitation are demonstrated. Plans are to incorporate additional design variables and constraints into the optimization procedure (such as actuator location) and explore alternative formulations of the objective function. A different actuator dynamic model to include hardware limitations will be investigated.

SUMMARY

- MAST FINITE ELEMENT MODEL GENERATED
- OPTIMIZATION PROCEDURE TO INCORPORATE ADDITIONAL DESIGN CONSTRAINTS IS DEMONSTRATED
- ACTUATOR DYNAMIC MODEL SUCCESSFULLY USED FOR EXCITATION AND DAMPING
- COMPLETE TEST SEQUENCE OF THE PROPOSED FLIGHT EXPERIMENT DEMONSTRATED

FUTURE PLANS

- AUGMENT THE OPTIMIZATION PROCEDURE TO INCLUDE PARAMETER MODIFICATION PACKAGE AND ACTUATORS
- INVESTIGATE THE PERFORMANCE OF A DIFFERENT ACTUATOR DYNAMIC MODEL

REFERENCES

1. Hanks, B. R.: "Control of Flexible Structures (COFS) Flight Experiment Background and Description," Large Space Antenna Systems Technology 1984. NASA CP-2368, Part 2, December 1984, pp. 893-902.

2. Horner, G. C.: "COFS-I Program Overview," To be presented at the First NASA/DOD CSI Technology Conference, Norfolk, Virginia, November 18-21, 1986.

3. Whetstone, W. D.: EISI-EAL Engineering Analysis Language Reference Manual - EISI-EAL System Level 2091. Engineering Information Systems, Inc., July 1983.

4. Vanderplaats, Garret N.: CONMIN _ A FORTRAN Program for Constrained Function Minimization - User's Manual. NASA TM X-62282, 1973.

5. Zimmerman, D. C.: "Dynamic Characterization and Microprocessor Control of the NASA/UVA Proof Mass Actuator," M.S. Thesis, University of Buffalo, June 1984.

6. Zimmerman, D. C.; Inman, D.J.; and Horner, G. C.: "Dynamic Characterization and Microprocessor Control of the NASA/UVA/UB Proof Mass Actuator," Proceedings of the 25th AIAA/ASME/ASCE/AHS Structure, Structural Dynamics and Materials Conference. Palm Springs, Ca. May 1984, Paper No. 84-1077.

SURFACE CONTROL SYSTEM FOR THE 15 METER HOOP-COLUMN ANTENNA

James B. Miller, Elvin L. Ahl, Jr.,
David H. Butler, Frank Peri, Jr.
NASA Langley Research Center
Hampton, Virginia 23665

First NASA/DOD CSI Technology Conference
November 18-21, 1986

INTRODUCTION

The 15-meter hoop-column antenna shown in figure 1 was fabricated by the Harris Corporation under contract to the NASA Langley Research Center. The antenna is a deployable and restowable structure consisting of a central telescoping column, a 15-meter-diameter folding hoop, and a mesh reflector surface. The hoop is supported and positioned by 48 quartz cords attached to the column above the hoop, and by 24 graphite cords from the base of the antenna column. The RF reflective surface is a gold plated molybdenum wire mesh supported on a graphite cord truss structure which is attached between the hoop and the column. The surface contour is controlled by 96 graphite cords from the antenna base to the rear of the truss assembly. The antenna is actually a quad-aperture reflector with each quadrant of the surface mesh shaped to produce an offset parabolic reflector. A detailed description of the antenna development is given in references 1, 2, and 3.

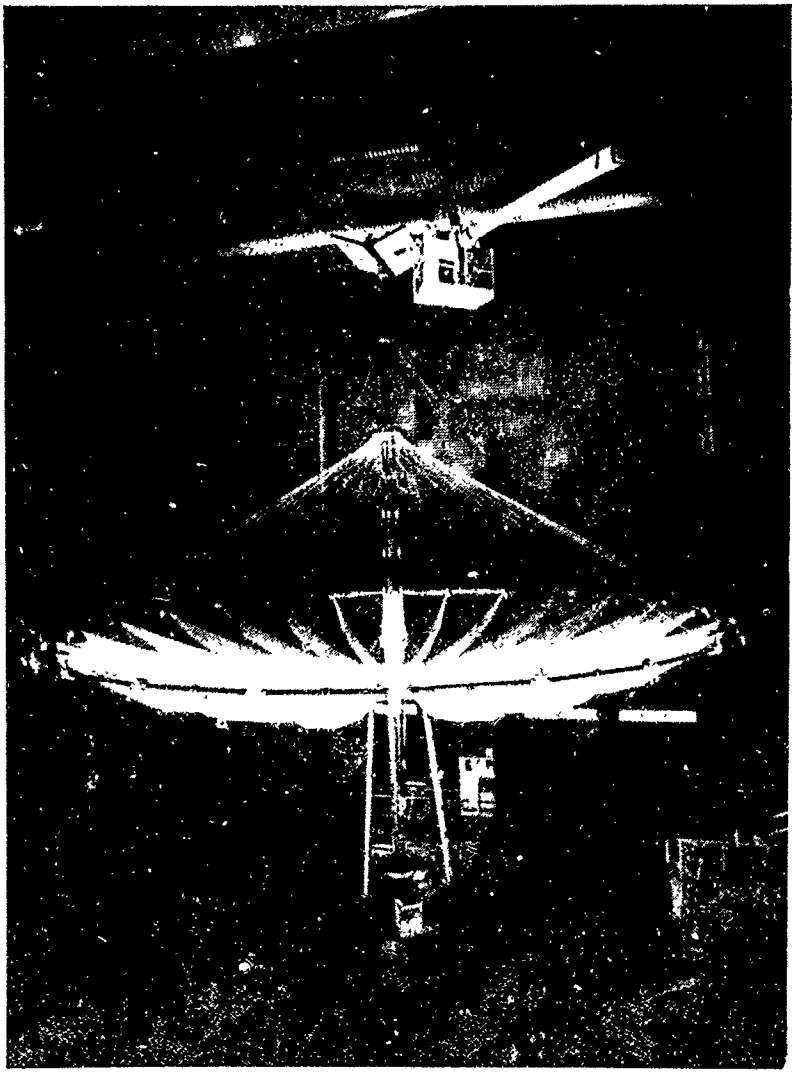

Figure 1

NEAR-FIELD AND STRUCTURAL TESTS

Tests to determine the trueness of the surface, RF characteristics, and limited structural characteristics of the antenna were conducted at the Martin Marietta Near Field Test Facility in Denver, Colorado (reference 4). Tests to more completely investigate the structural characteristics of the antenna were conducted at the NASA Langley Research Center (reference 5). The tests included adjustment of the antenna surface control cords to improve the surface quality of the reflector. This was a manual operation requiring as much as 8 hours to perform, and was limited in accuracy to approximately 0.01 inch. The time required to perform the photogrammetric measurement of the reflector surface and to perform the adjustment limited the number of adjustments which could be performed. Results of the tests indicate that: the first side lobes are dependent on the quality of the surface, large space antennas should be provided with surface adjustments, a linear approximation to the structural model provides adequate predictions for small movements of the control cords, further testing requires an improvement in both the speed and accuracy of the surface adjustment, and real time surface measurement is required.

SUMMARY OF TEST RESULTS

- Antenna performance is high.
- First side lobes are dependent on surface quality.
- RMS surface errors reduced more than 34% by control cord adjustment.
- Linear analysis adequate to predict small length changes.
- Large space antennas should be designed to permit surface adjustment.

Figure 2

A new series of CSEI tests will begin in the fall of 1987. These tests will be performed on the existing antenna with the addition of a single quadrant surface control system and surface measurement sensors. Investigations will focus on improving the reflector surface figure, the use of adaptive feed for distortion compensation, real time surface figure measurements, real time closed-loop surface figure control (reference 6).

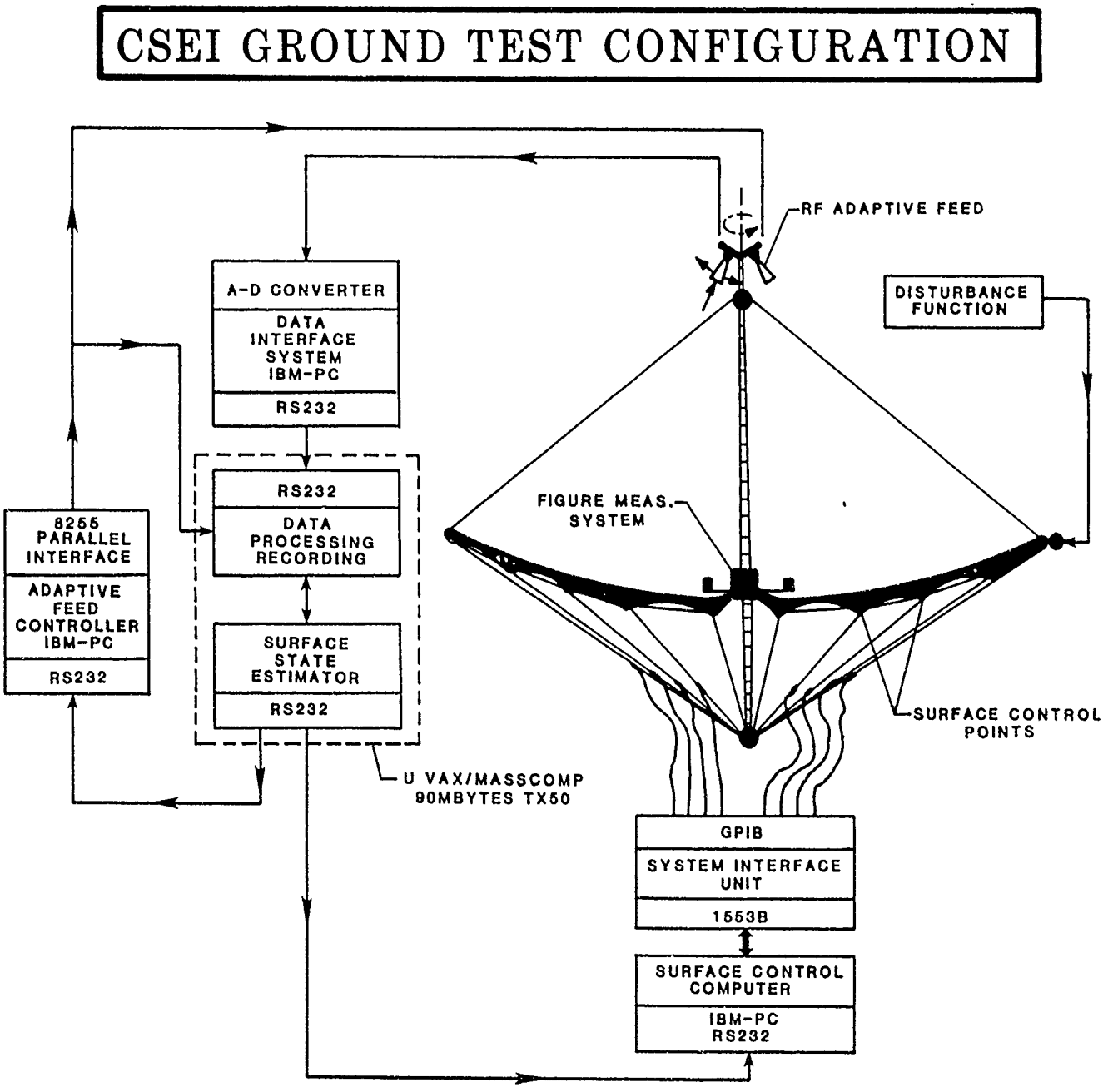

Figure 3

SURFACE CONTROL SYSTEM REQUIREMENTS

The requirements for the surface control system have evolved from the CSEI program requirements. The surface control system serves a dual role in the context of the CSEI program. It is the object of investigation in the case of surface control and control dynamics, and is a test vehicle in the adaptive feed and the real time surface measurement investigations. The primary requirement driving the design is that the surface control system must fit into the existing base structure and permit deployment and restow of the antenna. The actuator control system requirements are summarized in figure 4. The range of motion has to be maximized to the mechanical limits to permit correction for, or introduction of, large variations of the surface contour. The accuracy and resolution have been set based on the results of simulations and test results. Actuator bandwidth is being maximized to permit operation of the control actuators into the range where dynamic interactions between the surface control system and surface structural modes can be examined. System update rate has been selected to minimize the time required to make small changes in the surface contour for the adaptive feed and surface measurement tests. Load monitoring is provided for personnel and equipment safety.

SYSTEM REQUIREMENTS

- Retrofit to existing antenna base.
- Antenna must deploy and restow.
- Control one quadrant (28 cords).
- Stroke : ± 0.75″
- Load : 25 lb
- Accuracy/Resolution : ±0.002/0.0001″
- Actuator bandwidth : 4 Hz (0.50″)
  10 Hz (small signal)
- System Update Rate : 100 Hz
- Provide Load Monitoring.
- Provide a standard computer interface.

Figure 4

The surface contour of each quadrant is controlled by 28 graphite cords which are attached between the antenna base and the surface rear truss assemblies. Each of the rear trusses has 4 control cords attached to it (figure 5). The desired adjustment is achieved by controlling the length of these cords. As noted earlier, adjustment of the present manual system requires extended periods of time and is limited in accuracy to approximately 0.010 inch.

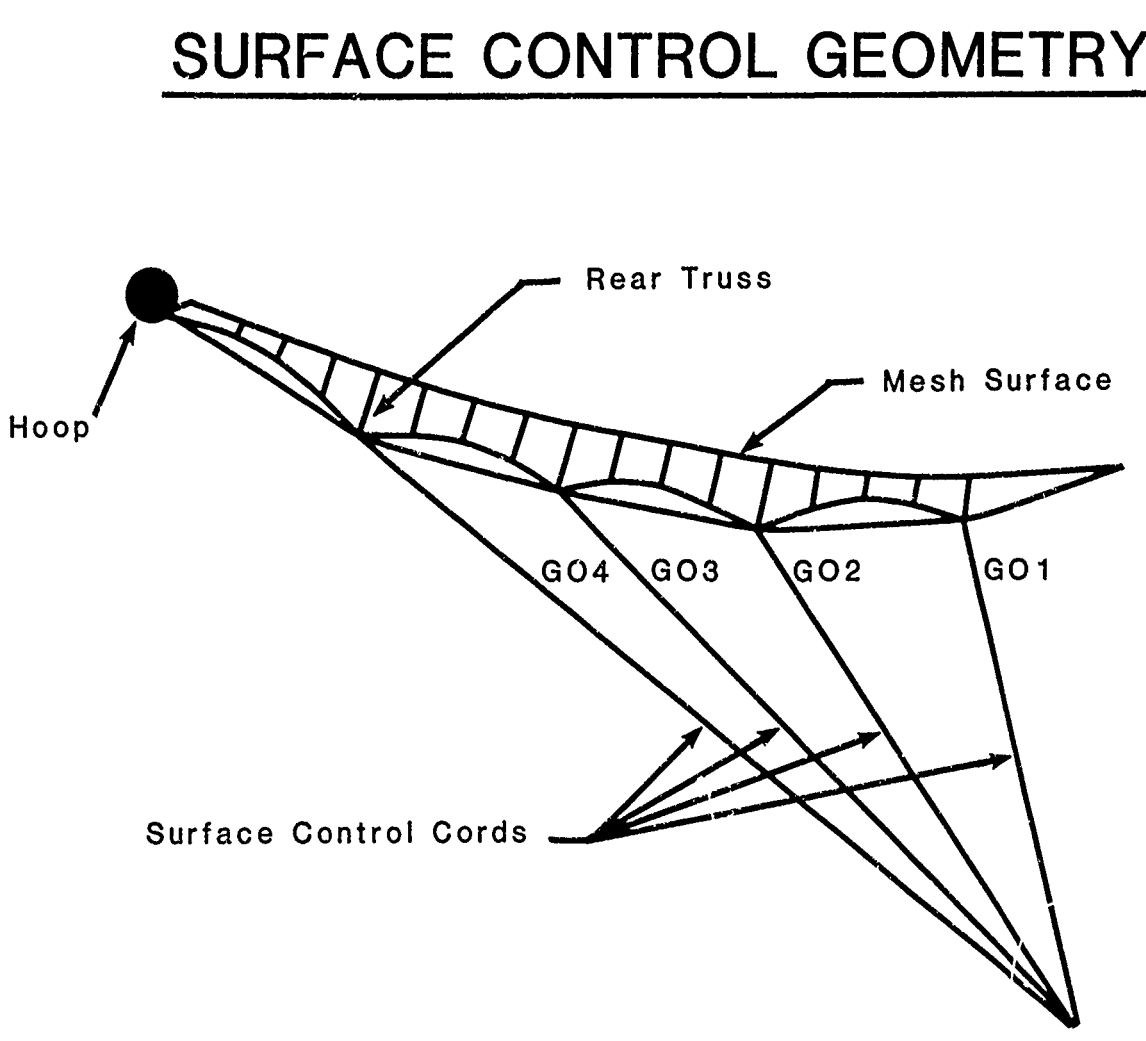

Figure 5

ANTENNA BASE AND STOP BLOCK ASSEMBLIES

Each of the surface control cords and the lower hoop cords pass through the stop blocks on the antenna base assembly (figure 6). In the stowed configuration, the cords are wound onto drums under the base plate. As the antenna is deployed, the cables unwind from the drums and feed through the stop blocks. When the cords reach full extension, a bead which is bonded to each cord is engaged in the stop block (figure 7). The space available for the automatic surface adjustment mechanism is limited to the area occupied by the stop block assemblies and the area under the base plate.

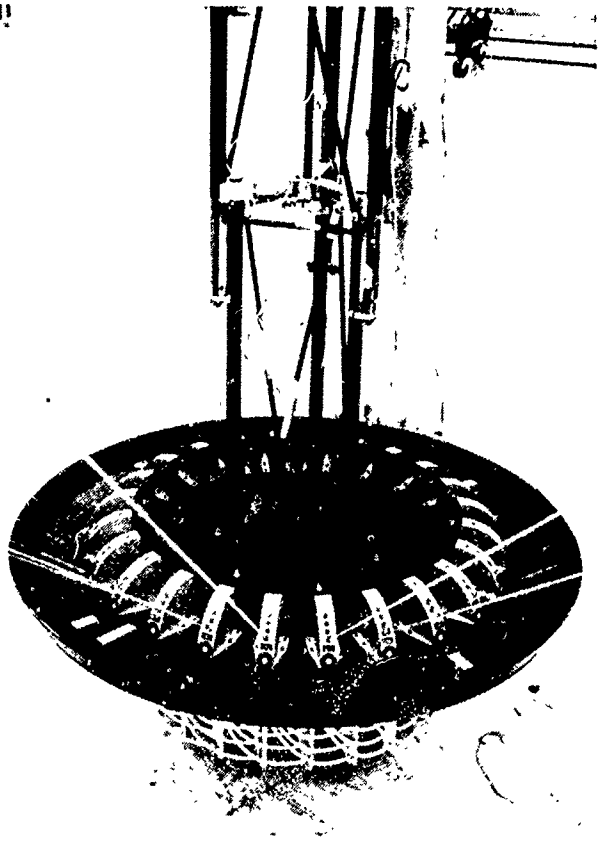

Figure 6

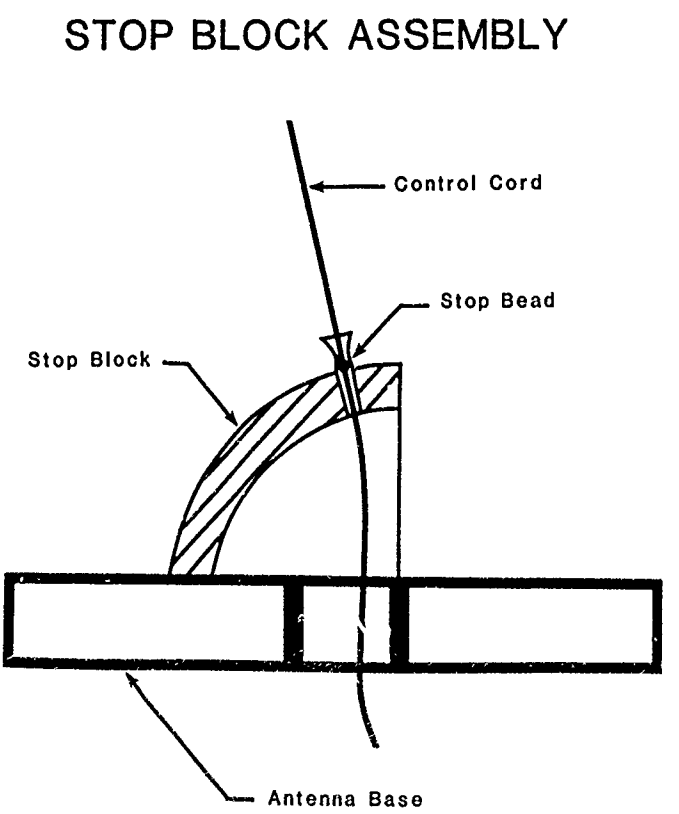

Figure 7

SURFACE CONTROL SYSTEM ACTUATOR ASSEMBLY

The surface control system consists of the 28 cord position control actuators located in 7 actuator assemblies, and the control electronics. Each of the actuator assemblies contains four motor driven actuators and a modified stop block assembly. Each actuator consists of a torque motor, gearhead, incremental encoder, brake, arcsector/encoder, actuator cable and a spring-loaded position control piston (figure 8).

Position commands from the host computer are compensated for variations in actuator cable strain and converted to arcsector position commands. The position of the arcsector is sensed by the encoder attached to the motor shaft and referenced to a simple absolute position sensor which is incorporated in the arcsector assembly. The controller drives the torque motor to position the arcsector to the commanded position. The actuator cable which is attached to the arcsector positions the spring-loaded control piston which in turn positions the actuator surface control cord. The control piston captures the surface control cord bead in the same manner as in the original stop block assembly. The brake is used to prevent back driving of the system when the torque motor is not energized.

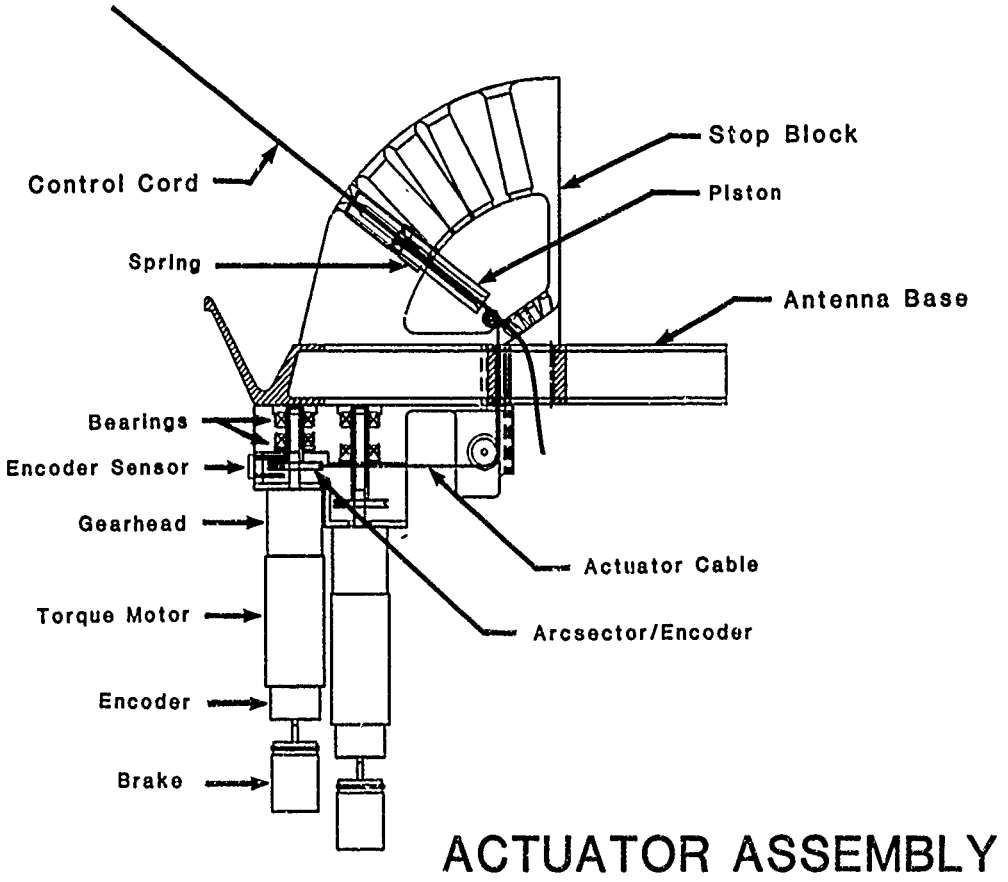

Figure 8

SURFACE CONTROL SYSTEM ELECTRONICS

The control electronics consist of seven station controllers and a system interface unit (figure 9). The system is interfaced to the host via a MIL STD-1553B serial communications bus. The seven station controllers are connected to the system interface via an IEEE-488 general purpose parallel interface bus. The dual bus structure was selected to provide ease of development, flexibility in test, upward host computer compatibility, and acceptable cost. The MIL-1553B bus provides a redundant, error detecting, noise immune interface from the antenna base to the host computer. The MIL-1553B bus requires only a dual twisted shielded pare cord, so it is ideal for large space structure applications. The IEEE-488 bus provides a simple inexpensive fast local interface to the seven station controllers which are located within a few inches of one another. The IEEE-488 bus also permits the individual station controllers to be interfaced directly to a host during development testing.

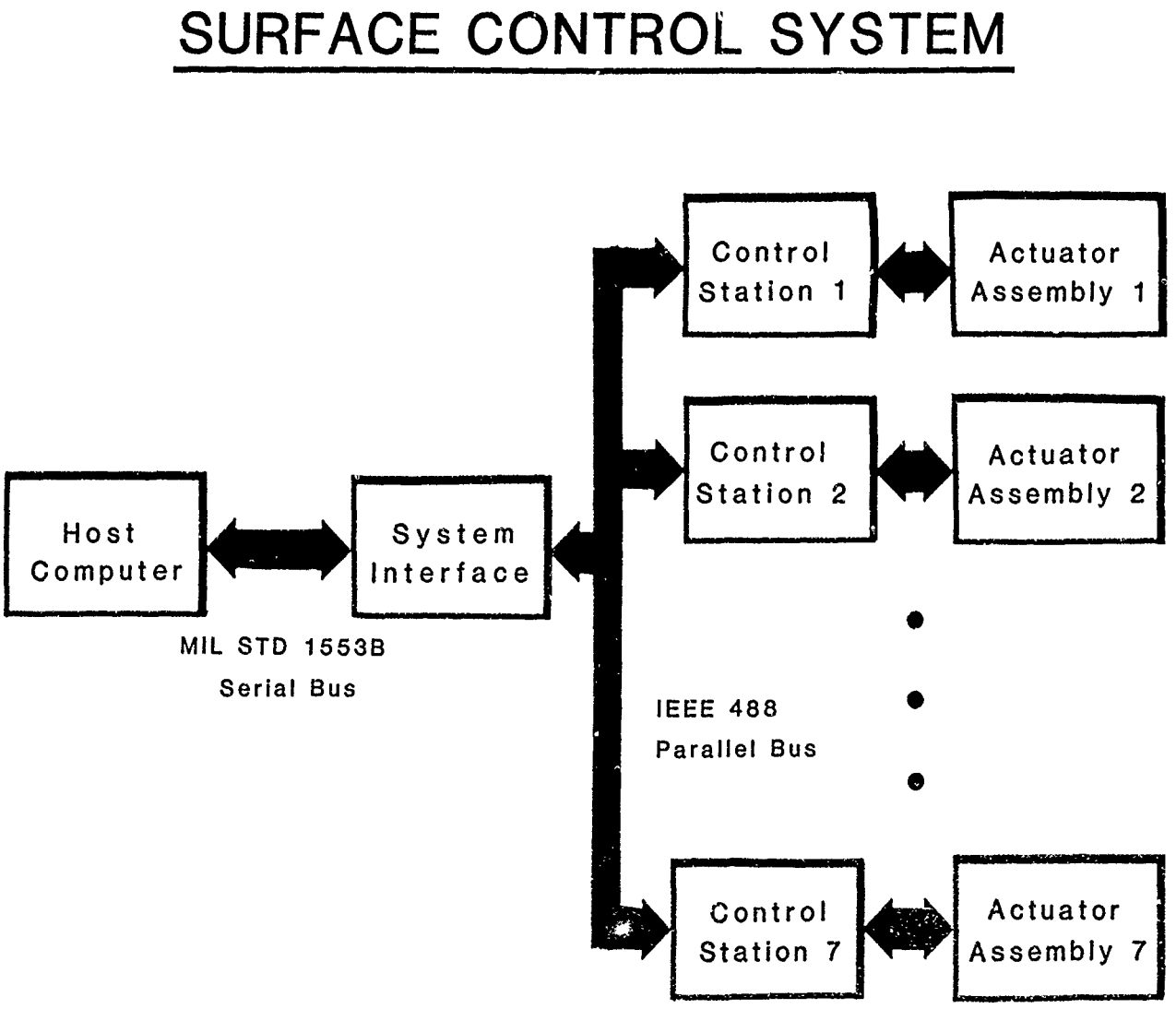

Figure 9

SYSTEM INTERFACE UNIT

The system interface unit appears to the host as a remote terminal on the MIL-1553B bus. It interprets commands and data arriving on the MIL-1553B bus and routes them to the appropriate controllers via the IEEE-488 bus. The system interface also collects data from the controllers and formats it for insertion onto the MIL-1553B bus.

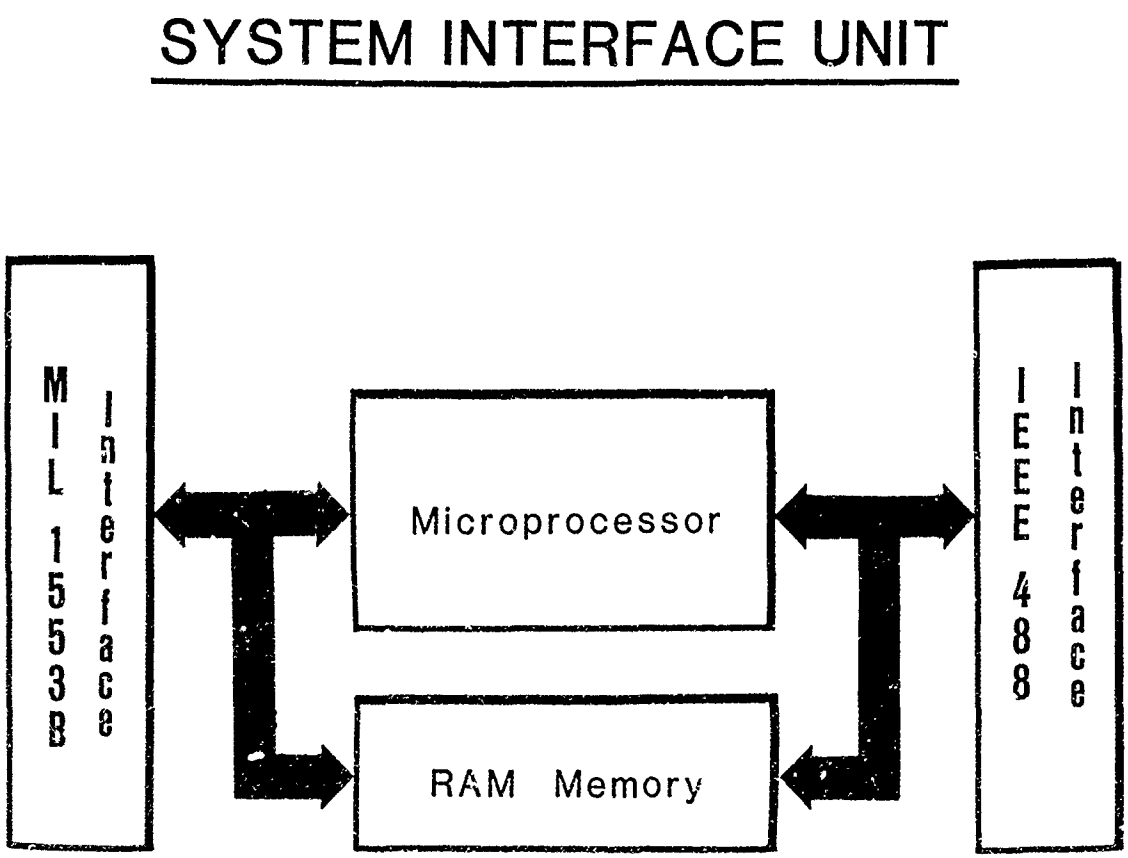

Figure 10

CONTROL STATIONS

Each control station contains an IEEE-488 bus interface, a microcontroller, four motor controllers and drivers (figure 11). The microcontroller interprets incoming commands and data, performs compensation for cord strain, collects and formats output data, controls operation of the brake, monitors the cord position and load limits, and provides operational error detection and recovery. The motor controllers keep track of the encoder position, compute position/velocity errors, compensate the error signals, and produce a pulse width modulated (PWM) drive command to the motor drive circuit. The motor drive circuit is a modified H bridge circuit which provides current drive to the motor which is proportional to the PWM command.

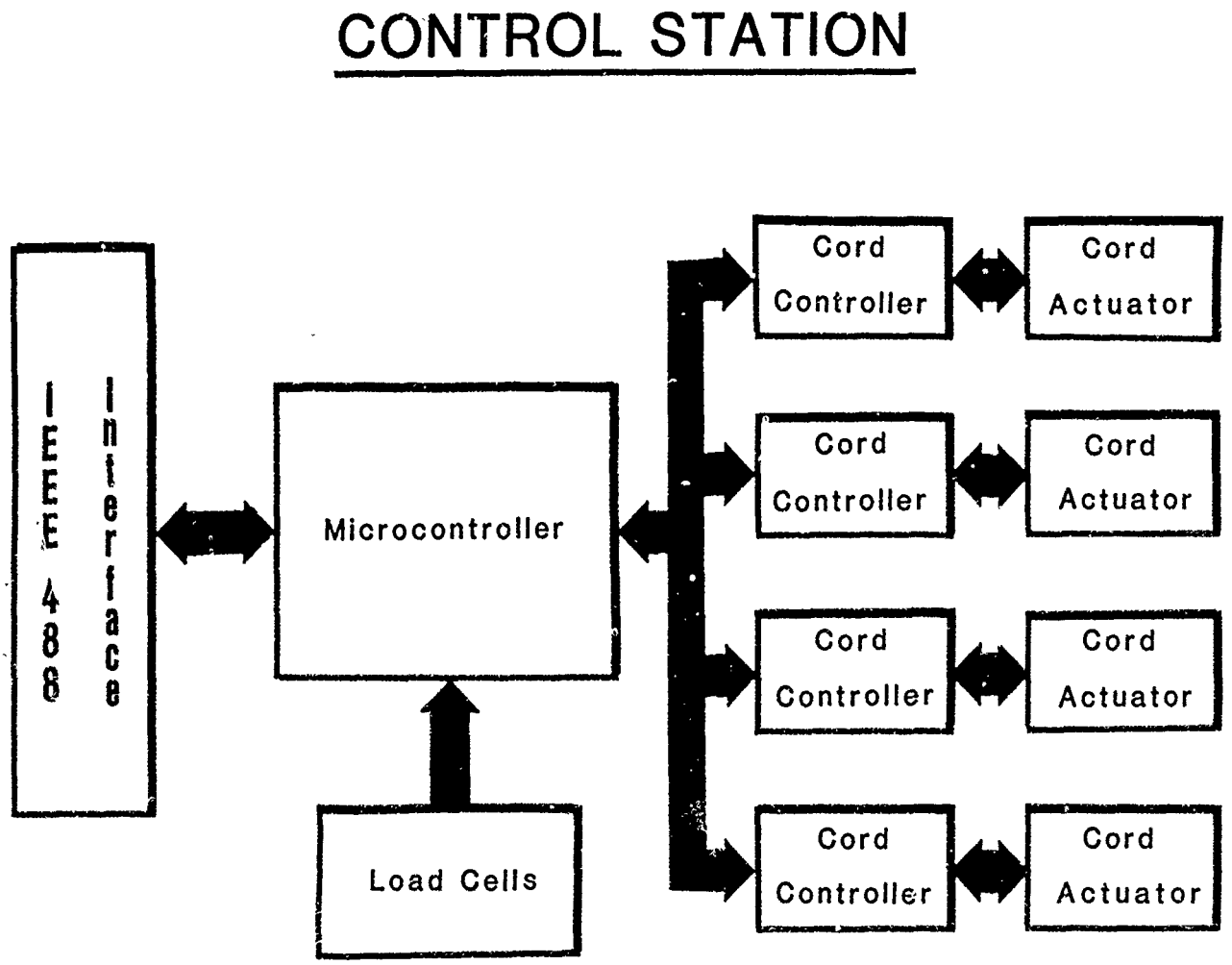

Figure 11

CONTROL CONSIDERATIONS

The surface control system actually consists of three cascaded systems (figure 12). The measurement of the surface contour in real time is in itself an area which will be investigated during the CSEI program, and could not be incorporated into the initial control system design. Thus, the position of each cord junction at the rear truss assembly is an open-loop function of the position of the control piston. Since the limited space available on the base prevented direct measurement of the cord control pistons, these, too, formed open-loop systems cascaded onto the closed-loop arcsector position controllers. To minimize the effect of the actuator cable and piston spring mass system, the piston assembly has been designed to maintain a preload on the actuator control cable, arcsector, and gearhead; and the piston assembly has been designed with a resonance more than a decade higher than the desired control bandwidth. As noted earlier, corrections are made to minimize the effects of actuator cable strain on the accuracy of piston positioning.

Analysis and simulations have been performed which indicate that the position control system, a prototype of which is presently being fabricated, will meet or exceed all of the system requirements.

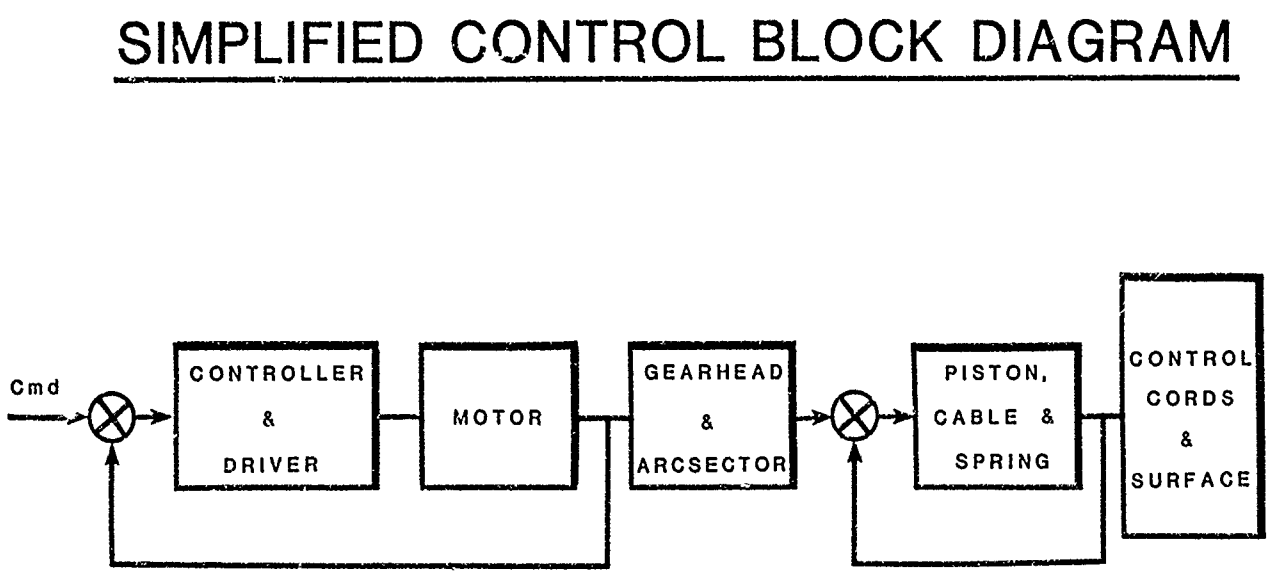

Figure 12

REFERENCES

1. Sullivan, Marvin R.: LSST (Hoop/Column) Maypole Antenna Development Program. NASA Contractor Report 3558, June 1982.

2. Campbell, T. G.; Butler, D. H.; Belvin, K.; and Allen, B. B.: Development of the 15-Meter Hoop/Column Antenna System. NASA Conference Publication 2368, December 1984.

3. Allen, B. B.; and Butler, D. H.: Hoop/Column Antenna Development Mechanism Overview. NASA Conference Publication 2371, May 1985.

4. Hoover, J.; Kefauver, N.; Cencich, T.; and Osborn, J.: Near-Field Testing of the 15-Meter Model of the Hoop Column Antenna. NASA Contractor Report 178059, March 1986.

5. Belvin, W. K.; and Edighoffer, H. H.: 15 Meter Hoop-Column Antenna Dynamics: Test and Analysis. The First NASA/DOD CSI Technology Conference, November 1986.

6. Grantham, W. L.; Bailey, M. C.; Belvin, W. K.; and Williams, J. P.: Controls-Structures-Electromagnetics-Interaction Program. The First NASA/DOD CSI Technology Conference, November 1986.

ROBUST MULTIVARIABLE CONTROLLER DESIGN FOR FLEXIBLE SPACECRAFT

S. M. Joshi and E. S. Armstrong
Spacecraft Control Branch
Guidance and Control Division
NASA Langley Research Center
Hampton, Virginia 23665

First NASA/DOD CSI Technology Conference
Norfolk, Virginia
November 18-21, 1986

ABSTRACT

Large, flexible spacecraft are typically characterized by a large number of significant elastic modes with very small inherent damping, low, closely spaced natural frequencies, and the lack of accurate knowledge of the structural parameters. This paper summarizes some of our recent research on the design of robust controllers for such spacecraft, which will maintain stability, and possibly performance, despite these problems. Two types of controllers are considered, the first being the linear-quadratic-Gaussian-(LQG)-type. The second type utilizes output feedback using collocated sensors and actuators. The problem of designing robust LQG-type controllers using the frequency domain loop transfer recovery (LTR) method is considered, and the method is applied to a large antenna model. Analytical results regarding the regions of stability for LQG-type controllers in the presence of actuator nonlinearities are also presented. The results obtained for the large antenna indicate that the LQG/LTR method is a promising approach for control systems design for flexible spacecraft. For the second type of controllers ("collocated" controllers), it is proved that the stability is maintained in the presence of certain commonly encountered nonlinearities and first-order actuator dynamics. These results indicate that collocated controllers are good candidates for robust control in situations where model errors are large.

CHARACTERISTICS OF LARGE SPACE STRUCTURES AND RESULTING CONTROL CHALLENGES

- o Large number of significant elastic modes
- o Very small inherent damping
- o Low, closely–spaced natural frequencies
- o Model errors (no. of modes, frequencies, damping ratios, mode–shapes)

▷ These characteristics make even linear design with perfect actuators/sensors difficult!

▷ There is a need for "robust" controllers

ROBUST CONTROLLERS

Robust = Maintain stability and acceptable performance, in spite of

- o Modelling errors
- o Parameter variation
- o Failures
- o Uncertainties
- o Actuator/sensor nonlinearities

ROBUST CONTROLLER DESIGN APPROACHES

The first approach considered is the LQG-type controller. In order to be practically implementable, it is usually necessary to consider only a reduced-order "design" model for synthesizing the controller. The stability of such reduced-order controllers is not guaranteed because of the control and observation "spillovers" [1,2], and because of errors in the knowledge of the plant parameters. The LQG/LTR method [3,4], which is a frequency-domain method, offers a systematic approach to robust controller design in the presence of modeling uncertainties. In this paper, the LQG/LTR method is briefly described, and the results of its application to a finite element model of the 122-meter hoop-column antenna are presented. Some analytical results on the stability of LQG-type controllers in the presence of realistic actuator nonlinearities are subsequently presented. The second controller design approach consists of "collocated" controllers which utilize actuator/sensor pairs placed at the same (or close) locations on the structure. The stability of such controllers is investigated in the presence of realistic actuator/sensor nonlinearities and also actuator dynamics.

- I. LQG–TYPE CONTROLLERS
  - LQG/LTR method (freq. domain) for robustness to modeling uncertainties
    - ▷ application to 122 m hoop-column antenna
  - Stability in the presence of actuator/sensor nonlinearities
- II. "COLLOCATED" CONTROLLERS
  - Robustly stable for any number of modes, for any parameter values
  - We investigate effect of actuator/sensor nonlinearities and dynamics

THE LQG/LTR METHOD

It was proved by Safonov and Athans [5] that the linear quadratic regulator (LQR) which employs state feedback has excellent robustness properties, namely, 60°-phase margin and infinite gain margin. However, when the complete state vector is not available for feedback and an estimator must be used, the resulting LQG-type compensator has no guaranteed robustness properties. The LQG/LTR technique [3,4] offers a method to asymptotically "recover" the robustness properties of the full state feedback controller. The LQG/LTR method basically consists of first defining a desirable "loop gain" in the frequency domain. For obtaining good tracking performance (i.e., loop broken at the output), this is accomplished by using the Kalman-Bucy filter. This loop gain is then "recovered" asymptotically using a model-based (LQG-type) compensator, which simultaneously satisfies certain stability robustness conditions, expressed in terms of frequency-domain singular values.

Basic Philosophy

- Define a "desirable" loop gain based on Kalman–Bucy filter (KBF)
- Recover that loop gain using a model–based compensator (i.e., LQ regulator and KBF) while satisfying stability conditions w.r.t. uncertainty.

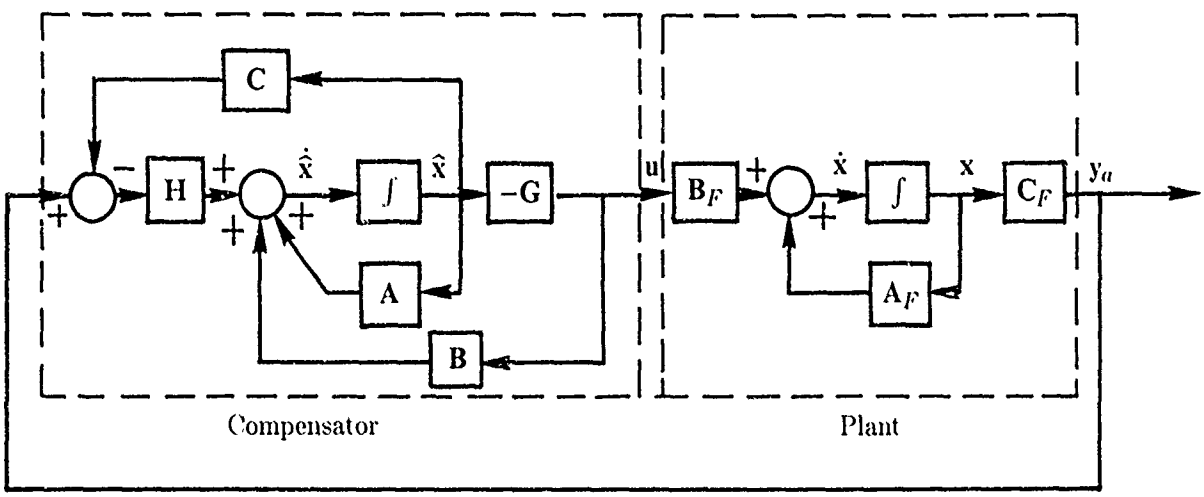

STABILITY ROBUSTNESS CONDITIONS

The modeling uncertainty can be expressed either as additive [$\Delta G(s)$] or multiplicative [$L_p(s)$]. Different sufficient conditions for stability are available for these two formulations. These are expressed in terms of the smallest or the largest singular values of the loop gain, the compensator, and the uncertainty. In the case of flexible spacecraft, all the flexible modes appear in parallel with the rigid-body modes. Therefore, the additive uncertainty model is a natural one for this problem. For satisfying the performance specifications, the $\underline{\sigma}(G_pG_c)$-curve must pass above the "performance barrier" in the low-frequency region. For satisfying the robustness conditions, the $\overline{\sigma}(G_pG_c)$-curve must pass under the high-frequency "robustness barrier" for the multiplicative uncertainty case, while for additive uncertainty, a somewhat more complicated condition has to be satisfied.

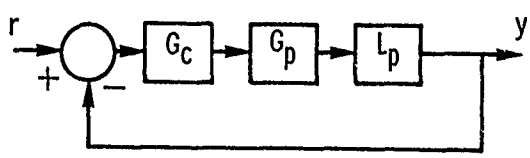

Multiplicative uncertainty

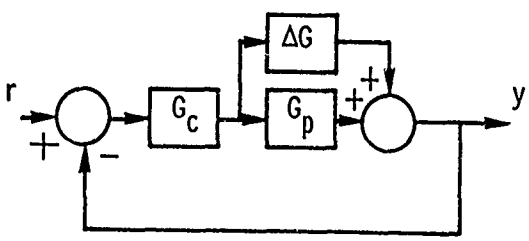

Additive uncertainty

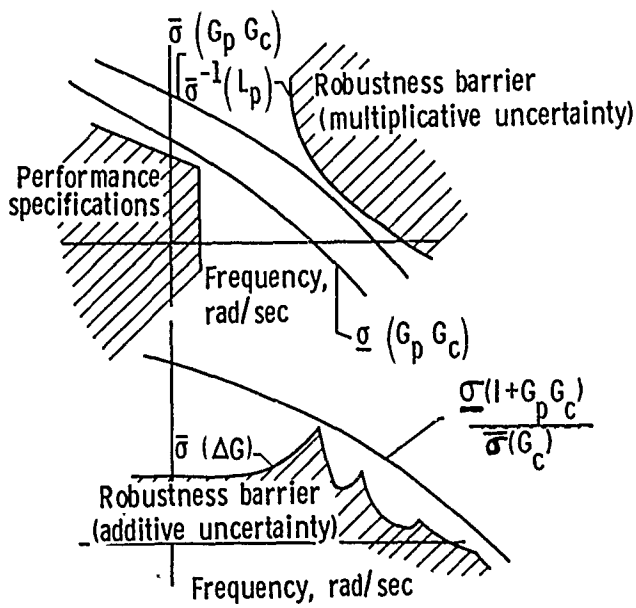

LQG/LTR CONTROLLER DESIGN PROCEDURE

The first step in applying the LQG/LTR procedure [4] is to define a reduced-order design model for the large space structure. (In this paper, a sequence of design models with increasingly higher order was considered, starting with a three degree of freedom rigid-body model.) The performance barrier is defined by using the bandwidth specification; e.g., 0.1 rad/sec for the antenna problem. The robustness barrier is defined by the unmodeled structural modes, as well as the parameter uncertainties. The second step is to obtain an "ideal" full state feedback loop gain, using the Kalman-Bucy filter equations (loop is broken at the output for good tracking performance). This loop gain should satisfy the bandwidth specifications. The third step is to design an LQ regulator so that $\sigma(G_p G_c)$ approaches the ideal loop gain in the low-frequency region, and the stability condition is satisfied in the high-frequency region. The final step is to verify the closed-loop stability and performance (eigenvalues, time-responses, etc.) of the entire closed-loop system using the "truth model."

1. Define a design model G (jω): $\dot{x} = A\,x + B\,u$
   $y = C\,x$

   o Low-freq. performance barrier (bandwidth)

   o High-freq. robustness barrier $L_p(j\omega)$
   (unmodeled dynamics; uncertainties)

2. Design a full state feedback compensator (KBF)–
   Defines "ideal" loop-gain (loop broken at output)

   KBF equations:

$$A\Sigma + \Sigma A^T + LL^T - \frac{1}{\mu}\Sigma C^T C \Sigma = 0$$

$$H = \frac{1}{\mu}\Sigma C^T \quad \Longrightarrow G_{KF} = C\,(sI-A)^{-1} H$$

   Select L and μ to achieve performance specs.

3. Design an LQ regulator to asymptotically recover the freq. response of G_{KF}.

   Compensator: $G_c = G_q\,[sI-A+BG_q+HC]^{-1}\,H$
   where

$$G_q = B^T P \text{ and } A^T P + PA - PBB^T P + q\,C^T C = 0$$

   Recovery is achieved by increasing q : $G_p(s)G_c(s) \rightarrow G_{KF}(s)$

4. Verify closed-loop stability, robustness and performance.

APPLICATION TO THE HOOP-COLUMN ANTENNA

In order to study its applicability, the LQG/LTR method was applied to a finite element model of the 122-meter hoop-column antenna [6]. The three-axis rigid-body attitude angles and the first 10 elastic modes were included in the "truth" model for this investigation. Only one three-axis torque actuator and one three-axis attitude sensor were used. An inherent structural damping of 1 percent was assumed to be present in each elastic mode.

HOOP-COLUMN ANTENNA CONCEPT

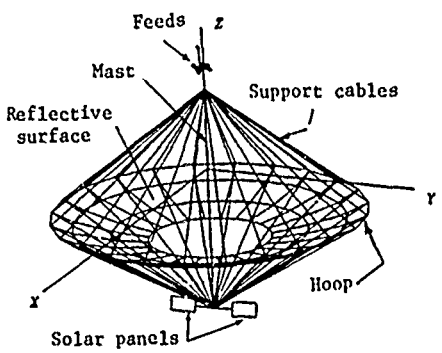

ANTENNA PARAMETERS

Mass = 4544.3 kg $I_{xx} = 5.724 \times 10^6$ kg-m^2

$I_{yy} = 5.747 \times 10^6$ kg-m^2 $I_{zz} = 4.383 \times 10^6$ kg-m^2

$I_{xz} = 3.906 \times 10^4$ kg-m^2 $I_{xy} = I_{yz} = 0$

Structural mode frequencies (rad/sec)

0.75, 1.35, 1.7, 3.18, 4.53, 5.59, 5.78, 6.84, 7.4, 8.78

Typical Antenna Mode-shapes

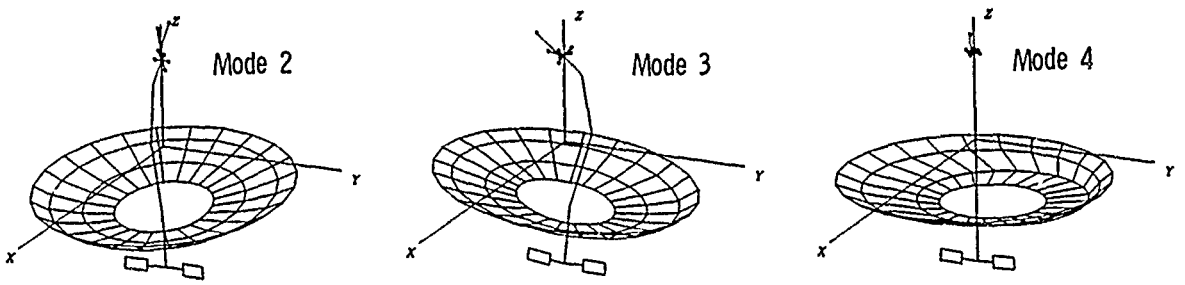

NUMERICAL RESULTS

The first design model used was the sixth order rigid-body model consisting of the three rotational modes, with all the elastic modes being lumped into the additive uncertainty. L and μ were chosen to give good performance characteristics, and the q was increased in the LQR Riccati equation to increase the bandwidth as much as possible without violating the additive uncertainty stability condition. All the computations were performed using ORACLS [7] and a new frequency-domain software package presently under development [8]. It was not possible to obtain the desired bandwidth using the rigid design model. The next step was to use the design model consisting of the rigid-body modes plus the first flexible mode, which is a torsion mode. For this case, somewhat higher bandwidth was obtained, but it still failed to meet the 0.1 rad/sec specification.

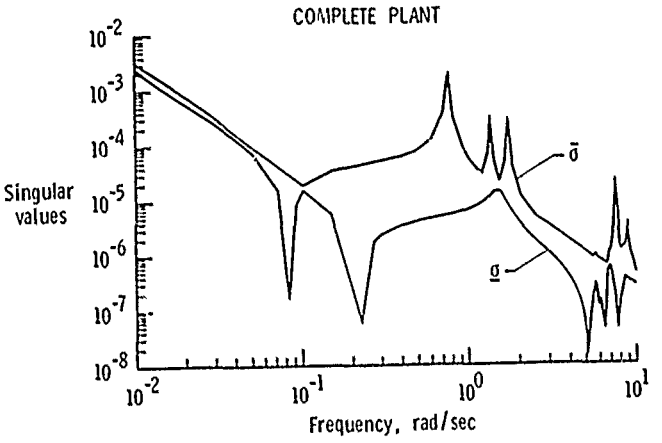

Rigid-body plus one flexible-mode design model

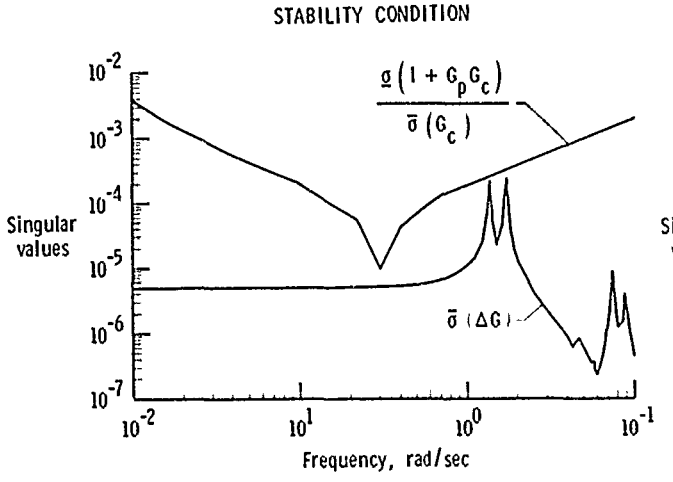

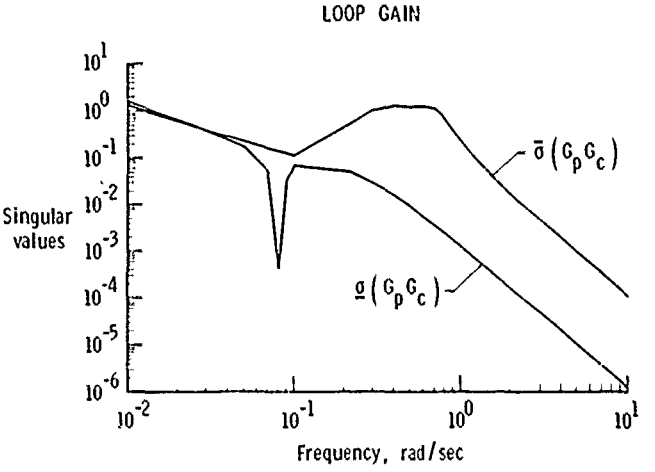

NUMERICAL RESULTS (CONT'D)

The next design model consisted of the rigid body modes and the first three flexible modes (first torsion, pitch bending, and yaw bending modes). For this case, it was possible to obtain the desired 0.1 rad/sec bandwidth while also satisfying the stability condition. However, because of the pair of invariant zeros of G_p near 0.082 rad/sec frequency, the performance is somewhat degraded, as seen by the dip in the $\underline{\sigma}(G_pG_c)$ plot at that frequency. This pair of zeros is close to the $j\omega$ axis and behaves numerically as nonminimum-phase. The frequency of the zero is determined by the sensor/actuator locations.

Rigid-body plus three flexible-modes design model

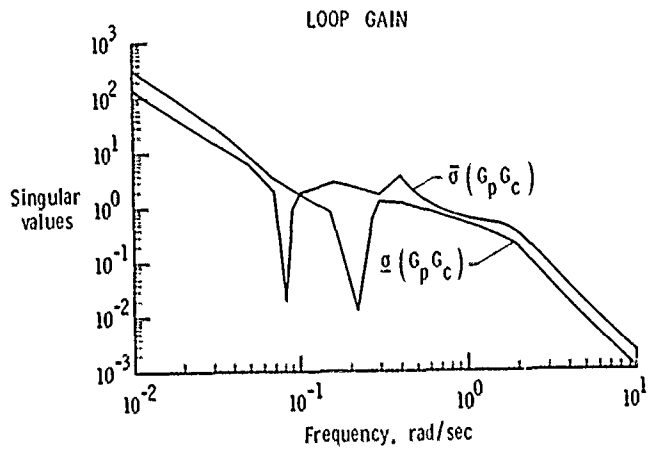

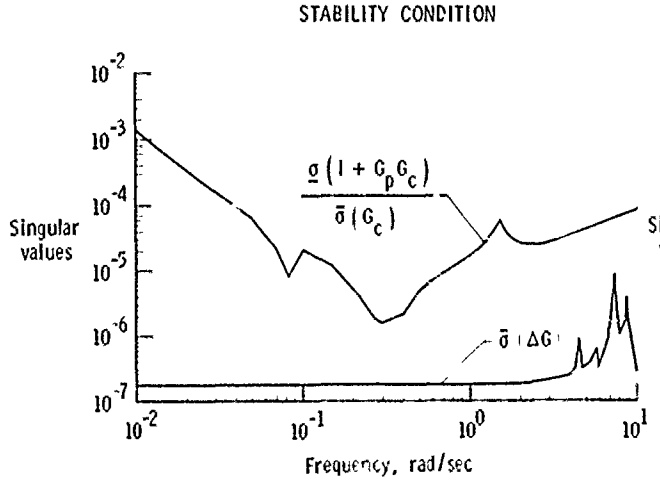

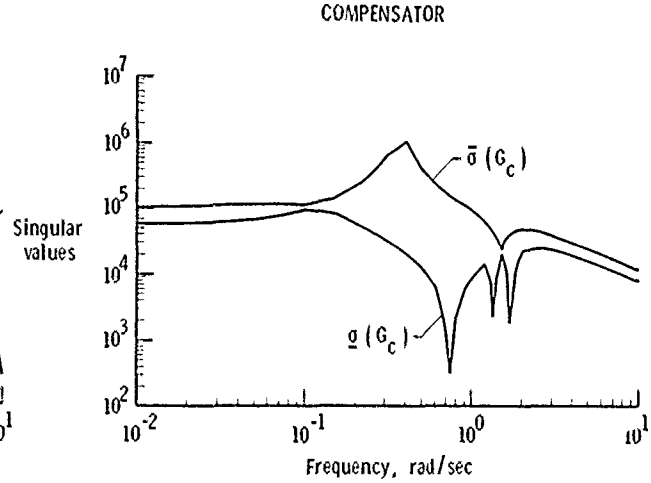

LQG/LTR METHOD-FINDINGS

The results obtained indicate that it was possible to design a robust controller using the LQG/LTR method. To achieve the required performance and robustness, it was necessary to include at least the first three elastic modes in the design model. Some degradation in performance was caused by the presence of invariant transmission zeros within the desired bandwidth. Since these zeros depend on the actuator and sensor locations, it would be advisible to consider these control aspects in the early design phase of the structure.

- LQG/LTR is a useful method for LSS control
- To meet 0.1 rad/sec bandwidth spec., the design model should include first 3 modes
- Invariant zeros present in the design bandwidth degrade the performance:
  - Zeros depend on the sensor/actuator locations
  - Therefore, control aspects should be considered in early design phase

EFFECT OF ACTUATOR/SENSOR NONLINEARITIES

Ensuring stability in the presence of unmodeled dynamics and parameter uncertainty, which was addressed in the preceding section, is only one aspect of the overall robustness problem. Other considerations include the effect of nonlinearities which are inherently present in components such as the actuators. For example, most real-life actuators have magnitude limits (saturation). Many actuators also have dead-zones, hysteresis, etc. Therefore, it is important to ensure the closed-loop stability in the presence of actuator nonlinearities.

It was proved by Safonov and Athans [5] that the LQ regulator can tolerate nonlinearities in the $[1/2,\infty)$ sector without causing instability. (A nonlinear function $N(\sigma)$ is said to lie in the $[k,\infty)$ sector if $N(0)=0$ and $\sigma[N(\sigma)-k\sigma]\geq 0$.) However, most nonlinearities encountered in practice do not lie in the $[1/2,\infty)$ sector. For example, a saturation nonlinearity lies in that sector in a neighborhood of the origin, but escapes the sector in regions away from the origin. Such (saturation-type) nonlinearities will be termed as "Type-I" nonlinearities. If Type-I nonlinearities are present, it can be proved that [9] there exists a region of attraction such that all trajectories originating in that region will converge to the origin exponentially. The expression obtained for the region of attraction, as well as the accompanying asymptotic properties, provides methods for selecting better performance function weights.

- First consider LQ Regulator (LQR) only:

Realistic nonlinearities escape the $[1/2,\infty)$ stability sector:

- Type I Nonlinearities– (saturation–type):

  –These escape the $[1/2,\infty)$ sector in regions away from the origin

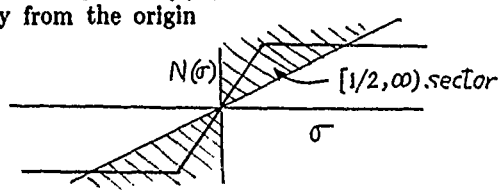

  –We prove that there exists a region of attraction (Riccati matrix P provides a natural Lyapunov function)

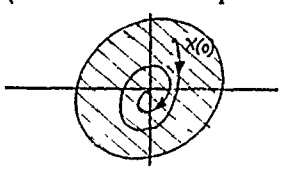

$$S_a = \{x \mid x^T P x < d\}$$

$$d = \min_{i\in[1,m]} \frac{(\ell_i R_{ii})^2}{b_i^T P b_i}$$

  – S_a can be readily determined for a given design

  – to make S_a large, increase R or decrease Q.

  – If $\mathrm{Re}\{\lambda_i(A)\} \leq 0$, $S_a \to E^n$ as $R \to \infty$.

    If not, $S_a \to$ constant bounded or semi–bounded region in E^n.

EFFECT OF ACTUATOR NONLINEARITIES (CONT'D)

Nonlinearities such as dead-zone or hysteresis lie in the $[1/2,\infty)$ stability sector in regions away from the origin, but escape the region in a neighborhood of the origin. Such nonlinearities will be termed "Type-II" nonlinearities. It can be proved that, in the presence of Type-II actuator nonlinearities, there exists a region of ultimate boundedness such that all the trajectories will enter that region in a finite time, and will remain in that region thereafter [10]. If there are any limit cycles, they will lie inside that region. The expression obtained for the region of ultimate boundedness provides methods for selecting better LQ weighting matrices.

When the full state vector is not available for feedback, a state estimate is used for feedback. Preliminary results for this case have been obtained, and will be included in a paper accepted for publication in the IEEE Transactions on Automatic Control (scheduled for December 1986). Additional work is presently in progress.

- Type II nonlinearities (dead–zone type)
  - Escape $[1/2,\infty)$ sector in a neighborhood of origin

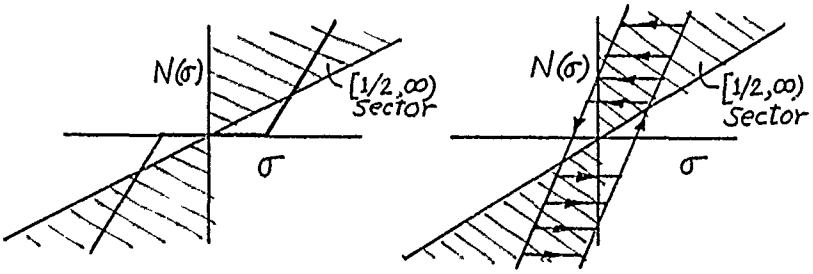

  - We prove that there exists a region of ultimate boundedness S_b:

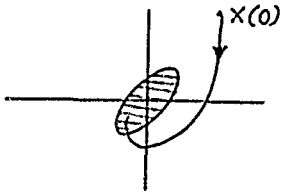

$S_b = \{x \mid x^T P x \leq h\}$

h depends on P, Q, R, α and the nonlinearities

  - Can readily determine region of ultimate boundedness for a given design
  - S_b can be made smaller by increasing α or by reducing R.

EXTENSION TO LQG CONTROLLERS

- State estimate is used instead of state vector
  Work in progress– prelim. results to appear in IEEE Trans. Auto. Contr.

COLLOCATED CONTROLLERS

This class of controllers consists of pairs of compatible actuators and sensors placed at the same (or close) locations throughout the structure. Thus attitude and rate sensors collocated with torque actuators will constitute a "collocated attitude controller". These controllers use negative definite feedback of the measured attitude and rate. The greatest advantage of such controllers is that, with perfect (linear, instantaneous) actuators, the closed-loop stability is guaranteed for any number of modes and any errors in the knowledge of the parameters. However, the actuators and sensors encountered in practice have nonlinearities and finite bandwidth, thus invalidating these general stability properties.

- Compatible actuators and sensors are placed at same locations

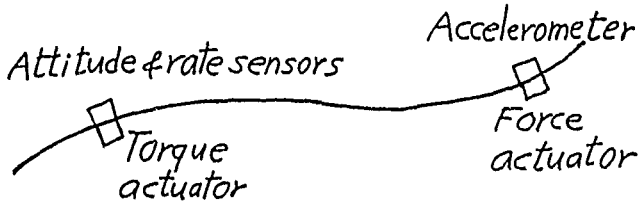

- For control of both rigid–body attitude and elastic motion

- Control input consists of feedback of measured positions and rates (rotational and/or translational)

ADVANTAGES OF COLLOCATED CONTROLLERS

- With perfect (linear, instantaneous) actuators and sensors, stability guaranteed for
  - Any number of modes
  - Any parameter errors
- Simple to implement

PROBLEM: ACTUATORS AND SENSORS HAVE NONLINEARITIES AND PHASE LAGS!

Our Contribution:– We proved that these robustness properties still hold in presence of a wide variety of realistic actuator/sensor imperfections.

COLLOCATED CONTROLLERS (CONT'D)

Therefore, we investigated the stability of collocated controllers when imperfect actuators/sensors are present. Using the Lyapunov method and function-space techniques, we proved that the stability properties of such controllers remain intact even in the presence of a variety of actuator/sensor nonlinearities and first-order actuator dynamics [11]. These results substantially increase the applicability of collocated controllers, and also identify them as good candidates for robust control especially when the modeling uncertainty is very large; e.g., during deployment, assembly, or initial operation when the parameters have not yet been identified. Investigation of stability in the presence of higher-order actuator dynamics is being planned.

OUR ROBUSTNESS RESULTS

- Robust stability for ANY parameter values and ANY no. of modes is still maintained if
  - actuator NL's are monotonic increasing and sensor NL's belong to 1st and 3rd quadrant
  - if at least one actuator and sensor per axis is functional
  - actuators have linear first-order dynamics, and

  Proportional gain < (actuator bandwidth) x (rate gain)
- With only velocity feedback (for damping enhancement), stable if all NL's belong to 1st and 3rd quadrants, and actuators have 1st order dynamics
- Research continuing for higher-order actuator dynamics and for obtaining better performance.

Nonlinearity lying in 1st and 3rd quadrants

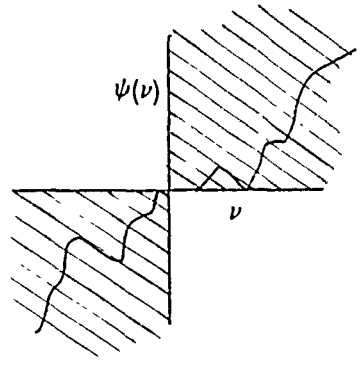

CONCLUDING REMARKS

The problem of designing robust controllers for flexible spacecraft was addressed using two approaches. The first approach consisted of an LQG-type compensator. It was found that this type of compensator can be robustified against unmodeled dynamics using the loop-transfer-recovery-(LTR) procedure. The presence of transmission zeros can cause performance degradation, and should be considered in the early design phase while selecting actuator/sensor locations. Effects of sensor/actuator nonlinearities were investigated, and expressions were obtained for stability regions. The second design approach considered utilizes "collocated" controllers, which were shown to have excellent robustness properties in the presence of not only modeling errors, but also actuator/sensor nonlinearities and dynamics. Future efforts should attempt to obtain less conservative stability regions in the presence of nonlinearities, and to develop procedures to robustify LQG-type compensators simultaneously against modeling errors and nonlinearities. For collocated controllers, efforts should be directed towards obtaining optimal feedback gains, as well as stability results with higher-order actuator dynamics.

- o LQG/LTR is a promising method
  - –Consideration must be given to transmission zeros (actuator/sensor location)
- o Collocated controllers offer highly robust control in the presence of large modeling uncertainty:
  - o Deployment
  - o Assembly
  - o Initial operation
  - o Failure modes

Directions:

- o Obtain less conservative results for LQG–type controllers with realistic nonlinearities
  - – combine with freq.–domain compensator design methods
  - – apply to realistic problem (e.g., SCOLE)
- o Study other robust control design methods:
  - – H^{∞} – methods
  - – SSV Method (Doyle, Wall, Stein, Athans)
  - – Stable factorization method (Vidyasagar)
- o Develop methods for optimizing collocated controller performance
- o Study effect of sampled–data implementation

REFERENCES

1. Balas, M. J.: Feedback Control of Flexible Systems. IEEE Trans. Auto. Control, Vol. AC-23, No. 4, Aug. 1978.

2. Balas, M. J.: Trends in Large Space Structure Control Theory: Fondest Hopes, Wildest Dreams. IEEE Trans. Auto. Control, Vol. AC-27, No. 3, June 1982.

3. Doyle, J. C., and Stein, G.: Multivariable Feedback Design: Concepts for a Classical/Modern Synthesis. IEEE Trans. Auto. Contr., Vol. AC-26, No. 1, Feb. 1981.

4. Athans, M.: Multivariable Control Systems Design Using the LQG/LTR Methodology. Lecture given at NASA Langley Research Center, 1984.

5. Safonov, M. G., and Athans, M.: Gain and Phase Margins for Multiloop LQG Regulators. IEEE Trans. Auto. Control, Vol. AC-22, No. 2, April 1977.

6. Sullivan, M. R.: LSST (Hoop/Column) Maypole Antenna Development Program. NASA CR-3558, 1982.

7. Armstrong, E. S.: ORACLS-A Design System for Linear Multivariable Control. Marcel Dekker, Inc., 1980.

8. Armstrong, E. S., and Joshi, S. M.: Computer-Aided Design and Distributed System Technology Development for Large Space Structures. First NASA/DOD CSI Technology Conference, November 18-21, 1986.

9. Joshi, S. M.: Stability of Multiloop LQ Regulators with Nonlinearities-Part I: Regions of Attraction. IEEE Trans. Auto. Contr., Vol. AC-31, No. 4, April 1986.

10. Joshi, S. M.: Stability of Multiloop LQ Regulators with Nonlinearities-Part II: Regions of Ultimate Boundedness. IEEE Trans. Auto. Contr., Vol. AC-31, No. 4, April 1986.

11. Joshi, S. M.: Robustness Properties of Collocated Controllers for Flexible Spacecraft. AIAA J. Guidance, Contr. and Dynamics, Vol. 9, No. 1, Jan/Feb 1986.

Standard Bibliographic Page

1. Report No.	2. Government Accession No.	3. Recipient's Catalog No.
NASA CP-2447, Part 1		

4. Title and Subtitle	5. Report Date
NASA/DOD Control/Structures Interaction Technology - 1986	November 1986
	6. Performing Organization Code: 542-06-11-01
7. Author(s)	8. Performing Organization Report No.
Robert L. Wright, Compiler	L-16242
9. Performing Organization Name and Address	10. Work Unit No.
NASA Langley Research Center Hampton, VA 23665-5225	11. Contract or Grant No.
12. Sponsoring Agency Name and Address	13. Type of Report and Period Covered
National Aeronautics and Space Administration Washington, DC 20546	Conference Publication
	14. Sponsoring Agency Code

15. Supplementary Notes

16. Abstract

This publication is a compilation of the papers presented at the First NASA/DOD Control/Structures Interaction (CSI) Technology Conference held at the Omni International Hotel, Norfolk, Virginia, November 18-21, 1986. The conference, which was jointly sponsored by the NASA Office of Aeronautics and Space Technology and the Department of Defense, was organized by the NASA Langley Research Center. The conference is the beginning of a series of annual conferences whose purpose is to report to industry, academia and government agencies on the current status of control/structures interaction technology. The conference program was divided into five sessions: (1) Future Spacecraft Requirements: Technology Issues and Impact; (2) DOD Special Topics; (3) Large Space Systems Technology; (4) Control of Flexible Structures, and (5) Selected NASA Research in Control Structures Interactions.

17. Key Words (Suggested by Authors(s))	18. Distribution Statement
Controls Structures Control/structures interaction Large space systems Flexible structures	Unclassified - Unlimited Subject Category 18

19. Security Classif.(of this report)	20. Security Classif.(of this page)	21. No. of Pages	22. Price
Unclassified	Unclassified	569	A24

For sale by the National Technical Information Service, Springfield, Virginia 22161

NASA-Langley, 1986